THE GEOLOGY OF THE TRALLVAL AREA RHUM, INNER HEBRIDES

Johannes Arnout Volker

B. Sc. (Hons.), Edinburgh.

Thesis submitted for the degree of
Doctor of Philosophy
University of Edinburgh
1983

EX BIBL UNIV EDINBURGH

A section through the Eastern Layered Series - Trallval from Ainshval.

I hereby declare that this thesis has been composed by myself and that the work contained is my own, except where stated otherwise.

J. A. Volker.

ABSTRACT

This thesis presents a map for the Trallval area, the last part of the ultrabasic complex of Rhum to be mapped in detail. It establishes a complex tectonic history, consisting of the differential subsidence of an approximately in situ Central Series (CS) into an irregular graben separating the Eastern (ELS) and Western Layered Series (WLS). The ELS and WLS were emplaced upward together with penecontemporaneous gabbro intrusions. The 3 layered series were not consolidated until after their juxtaposition and this is reflected in their internal structure. A number of cylindrical plugs of ultrabasic crystal mush were intruded into the consolidated complex at a later stage. Gabbros were intruded before, during and after the major tectonic events. As the layered series are thought to have an ultrabasic parent magma, this demonstrates the simultaneous injection of basic and ultrabasic magma into a small area together with the co-existence of magma chambers at different levels.

Comprehensive data are presented on lateral as well as stratigraphical variation in modal composition, size relations, mineral chemistry and micro-textures and structures of the ELS and CS, and compared with those of the ultrabasic breccias and plugs. Micro-textures suggest that the cumulates formed by in situ nucleation and growth in a boundary layer deformed by current drag until the melt-supported mush collapsed to give an uncompacted cumulate. The relative efficiency of the removal of liquid from the compacting zone below the boundary layer depended on its composition and especially its water content. Lateral variation in mineral chemistry, textures and lithology show that both the ELS and CS consist of laterally partitioned domains with vertical boundaries. This was due to local controls (uniform within each domain) over the composition and rate of cooling of the ascending intercumulus liquid.

Textures and structures in the ELS on Trallval indicate large thicknesses of uncompacted cumulate formed between the interface with magma and the chamber floor. These structures include feldspathic streamers, direct evidence for the upward percolation of intercumulus liquid expelled from the compacting zone of cumulate. The filter-pressing of intercumulus liquid is thought to be a major factor in the differentiation of magmas in sub-volcanic magma chambers.

In the CS, dunites were produced where the intercumulus liquid was removed most efficiently (by shearing of the uncompacted cumulate); the tectonic stress also opened up cracks in the cumulates, filled in by the intercumulus liquid together with entrained olivines and blocks to form the elongate breccia zones.

A study of the geochemistry of the dykes, gabbros and ultrabasic rocks suggests that they shared a similar parental magma, with evidence of extensive contamination by molten sialic crust of some of the dykes and gabbros. A microdiorite hybrid dyke on Ruinsival represents the most extreme example of this process. Contamination of the cumulates is suggested by the inclusion of xenocrysts and melt from the wall-rocks in spinel and olivine. Other, more abundant, inclusions of hydrous minerals in both spinel and olivine suggest that ascending, vesiculating intercumulus liquid may have acted as a nucleation site for both phases.

TABLE OF CONTENTS

		Page
CHAPTER 1	INTRODUCTION	1
1.1	Objectives of Research	1
1.2	Location and Fieldwork	2
1.3	History of Geological Investigation	3
1.4	Geological Setting of the Igneous Complex	4
1.5	Glaciology	5
1.6	Age Relations and Structure of the Complex	6
1.7	Previous Work	7
	1.7.1 Pre-1950 research	7
	1.7.2 Hallival and Askival	7
	1.7.3 Harris Bay area	8
	1.7.4 Central Part of the complex	9
	1.7.5 Barkeval-Long Loch area	9
	1.7.6 Unlayered ultrabasic rocks	10
1.8	Location of the Magma Chambers	11
CHAPTER 2	AN EXPLANATION OF THE MAP	14
2.1	Mapping Units	14
	2.1.1 Sandstone and acid igneous rocks	14
	2.1.2 layered ultrabasic rocks	15
	2.1.3 ultrabasic breccia zones	16
	2.1.4 intrusive ultrabasic plugs	16
	2.1.5 gabbros	16
	2.1.6 minor intrusions	16
2.2	Structure of the Ultrabasic complex	17
	2.2.1 Trallval layered series	17
	2.2.2 Central Series	18
	2.2.2.1 Ruinsival block	18
	2.2.2.2 An't Snidhe block	18
	2.2.2.3 Papadil-Trallval block	18
	2.2.3 contacts of the CS	19
	2.2.4 southern contact of the ultrabasic complex	20
2.3	Brittle Deformation	21
	2.3.1 regional faulting pattern	21
	2.3.2 Long Loch Fault	21
	2.3.3 Other faults	22
2.4	Age Relations in the Trallval Area	23
CHAPTER 3	THE ULTRABASIC ROCKS - FIELD DATA.	28
3.1	Stratigraphy of the Trallval Series	28
3.2	Stratigraphy of the Central Series	29

		Page
3.3	Distribution and Structure of the Plugs and Breccias	31
3.4	Introduction to Textures and Layering	31
	3.4.1 Textures	31
	3.4.2 Layering	32
3.5	Field Characteristics of the Trallval Series	33
	3.5.1 U8	33
	3.5.2 U9	34
	3.5.3 U10	36
	3.5.4 U11	38
	3.5.5 U12	39
	3.5.6 U13	41
	3.5.7 U14	42
	3.5.8 U15	44
	3.5.9 U16	45
	3.5.10 deformation of U14	45
3.6	Field Characteristics of the Central Series	48
	3.6.1 Dornabac Member	49
	3.6.2 Lower unit of the Long Loch Group	50
	3.6.3 Middle unit of the Long Loch Group	52
	3.6.4 Upper unit of the Long Loch Group	54
	3.6.5 Ruinsival Group	55
3.7	Field Characteristics of the Ultrabasic Plugs	57
	3.7.1 Papadil plug	57
	3.7.2 Ruinsival Plug	58
	3.7.3 Seagull Plug	58
	3.7.4 Barkeval Plug	58
3.8	Field Characteristics of the Breccia Zones	59
	3.8.1 Trallval System	59
	3.8.2 Ruinsival System	62
	3.8.3 Papadil System	67
	3.8.4 Dornabac System	69
CHAPTER 4	THE GABBROS: FIELD DATA.	106
4.1	Atlantic Corrie Gabbro	106
4.2	East Trallval Gabbro	108
4.3	West Trallval Gabbro	108
4.4	Glen Harris Gabbro	109
4.5	Other Gabbros Intruded into the CS	110
4.6	Marginal Gabbros	111
CHAPTER 5	PETROGRAPHY AND MINERAL CHEMISTRY OF THE ULTRABASIC ROCKS	120
5.1	Cumulus Textures	120
	5.1.1 dunite and dunitic peridotite	120
	5.1.2 feldspathic peridotite	120
	5.1.3 allivalite	121
	5.1.4 ultrabasic breccias and plugs	121

		Page
5.2	Textural Features and Microfabrics from the ELS and CS	121
	5.2.1 melt-supported texture	122
	5.2.2 conduit texture	123
	5.2.3 mineral lamination	123
	5.2.4 modal cumulus phase layering	122
	5.2.5 modal intercumulus phase layering	124
	5.2.6 textural layering	125
	5.2.7 graded layering	126
	5.2.8 clasts, cross-layering and convolute layering	126
	5.2.9 unlayered spinel fabrics	126
	5.2.10 exotic cumulus crystals	127
	5.2.11 intercumulus pyroxene textures	128
	5.2.12 growth interference effects	128
	5.2.13 recrystallisation fabrics	129
5.3	Mineralogy of the Layered Series	130
	5.3.1 olivine	130
	5.3.2 plagioclase	131
	5.3.3 clinopyroxene	131
	5.3.4 oxides	132
	5.3.5 sulphides	132
	5.3.6 hydrous silicates	133
	5.3.7 mineral size relations	134
5.4	Mineral Chemistry	134
	5.4.1 olivine	135
	5.4.2 plagioclase	136
	5.4.3 clinopyroxene	136
	5.4.4 histograms of compositional ranges	137
5.5	Hydrous Inclusions in Olivine or Spinel	138
	5.5.1 textural relations	138
	5.5.2 mineralogy	139
	5.5.3 variation in mineralogy through the ELS and CS	140
	5.5.4 origin of the inclusions	140
5.6	Chromitite laminae	141
	5.6.1 composition of the spinels	141
5.7	Stratigraphic Variation in the Layered Series	144
	5.7.1 techniques	144
	5.7.2 5.7.1.1 mineral modes	144
	5.7.1.2 grain-size	144
	5.7.1.3 mineral chemistry	144
	5.7.2 cryptic variation	145
	5.7.2.1 the ELS (U11 to U16)	145
	5.7.2.2 U8 to U10 of the ELS	147
	5.7.2.3 lateral variation in the ELS	147
	5.7.2.4 the CS	148
	5.7.2.5 lateral variation in the CS	150
5.8	Mineralogy of the Ultrabasic Breccias and Plugs	151
CHAPTER 6	THE PETROGRAPHY, MINERAL CHEMISTRY AND GEOCHEMISTRY OF THE DYKES AND GABBROS	211
6.1	The Dykes: Petrography	211
6.2	Mineral Chemistry of the Dykes	213

		Page
6.4	The Gabbros: Petrography	215
6.5	Mineral Chemistry of the Gabbros	218
6.6	Geochemistry of the Dykes	219
	6.6.1 classification	219
	6.6.2 major elements	220
	6.6.3 trace elements	220
	6.6.4 Sr isotope ratios and minor element patterns	221
6.7	Geochemistry of the Gabbros	223
6.8	Geochemistry of the Ultrabasic Rocks	224
6.9	Conclusion	226
CHAPTER 7	PETROGENESIS OF THE ULTRABASIC ROCKS	266
7.1	Summary of Field Observations on the ELS	266
	7.1.1 general features	266
	7.1.2 textures and structures	267
7.2	Summary of Field Observations on the CS	271
7.3	Interpretation of Ultrabasic Breccias	273
7.4	Interpretation of Ultrabasic Plugs	275
7.5	A Model for Mush Crystallisation	276
	7.5.1 boundary layer	276
	7.5.2 crystal settling	276
	7.5.3 intercumulus crystallisation	277
7.6	Microtextures of the Ultrabasic Rocks	277
	7.6.1 crystallisation of the mush	277
	7.6.2 deformation of the mush	278
	7.6.3 uncompacted cumulate	278
	7.6.4 compaction of the cumulate	279
	7.6.5 upward movement of intercumulus liquid	279
	7.6.6 deformation of the cumulate	279
7.7	Mineral Chemistry of the Ultrabasic Rocks	280
	7.7.1 parental magma	280
	7.7.2 mineral chemistry and magma composition	281
	7.7.3 compositional effects of intercumulus processes	282
	7.7.4 sub-solidus re-equilibration	283
	7.7.5 cryptic variation over the ELS	283
	7.7.6 cryptic variation over the CS	285
7.8	The Origin of the Macro-layering	286
7.9	Models for Lateral Variation	287
	7.9.1 slumping of wall cumulates	287
	7.9.2 lateral accretion	288
	7.9.3 crystallisation of intercumulus liquid	288
	7.9.3.1 in situ crystallisation	289
	7.9.3.2 thickness of the compacting zone	289
	7.9.3.3 intercumulus processes leading to lateral variation	290
7.10	The Importance of Water in the Magma Chamber	291

Page

7.11 Contamination of the Melt and the Origin of Chromitite 293

7.12 The Formation of the CS 297

7.13 Conclusion 298

APPENDIX A ELECTRON MICROPROBE ANALYSIS 300

APPENDIX B BULK ROCK X-RAY FLUORESCENCE ANALYSIS 321

REFERENCES 328

ACKNOWLEDGMENTS 337

ILLUSTRATIONS

LIST OF TABLES

		Page
2.1	Age relations in the Trallval area	24
3.1	Nomenclature of the ultrabasic rocks	71
3.2	Stratigraphic nomenclature for the CS	71
5.1	Grain-size data for the layered series	153
5.2	Representative olivine analyses	154
5.3	Representative plagioclase analyses	155
5.4	Representative clinopyroxene analyses	156
5.5	Analyses of common minerals included in spinel or olivine	157
5.6	Analyses of exotic minerals included in spinel or olivine	158
5.7	Compositions of hydrous phases in spinel vs.intercumulus phases	159
5.8	Comparison of inclusions in spinel, from different environments	160
5.9	Compositional ranges of spinels included in olivines	159
5.10	Mg-enrichment of olivines in chromitite laminae	161
5.11	Within-sample variation of olivine composition	162
5.12	Compositional ranges for the minerals in each of the units described in sections 5.7.2.1	162
6.1	Representative olivine analyses from dykes and gabbros	228
6.2	Representative plagioclase analyses from dykes and gabbros	228
6.3	Representative pyroxene analyses from dykes and gabbros	229
6.4	Representative mica, amphibole and K-feldspar analyses	230
6.6	Modal analyses of selected gabbros	231
6.7	Minor element ratios of Tertiary basaltic suites	232
6.8	Sr isotope ratios of selected dykes	232
6.9	Mixing model of Lewisian gneiss and picrite	233
6.10	Major and trace element analyses of chromitites	234
6.11	Major element analyses of the dykes	235
6.12	Trace element analyses of the dykes	236
6.13	Major element analyses of the gabbros	237
6.14	Trace element analyses of the gabbros	238
6.15	Trace element analyses of the ultrabasic rocks	239
6.16	Major element analyses of the ultrabasic rocks	241
6.17	Average trace element ratios for the major rock types in the Trallval area	242
6.18	Trace element ratios for the highly magnesian dykes	242

		Page
A.1	Analytical conditions for the microprobe	301
A.2	Precision of microprobe analysis	302
A.3	Synopsis of microprobe analyses	303
B.1	Reproducibility of discs and pellets	322
B.2	XRF analytical conditions	323
B.3	Interferences on chosen analytical lines	324
B.4	XRF - analytical accuracy	325
B.5	XRF - analytical precision	326

LIST OF FIGURES

1.1	Outline of mapping area and simplified geology of Rhum	12
1.2	Place-names and simplified structure of the ultrabasic complex	13
2.1	The internal structure of the Trallval layered series	25
2.2	The internal structure of the CS in the Trallval area	26
2.3	Fault and fracture orientation in the Trallval area	27
3.1	The stratigraphy of the ELS	71
3.2	Aereal distribution of the stratigraphic units of the CS	72
3.3	Stratigraphy of the CS	73
3.4	Aereal distribution of the stratigraphic units of the CS	74
3.5	Internal structure of the ultrabasic breccias and plugs	75
3.6	Locality map for plates and sketches of the deformation in U14	76
3.7	Diagrammatic section of the allivalite of U14	77
3.8	Field sketches of the structures in the allivalite of U14	78
3.9	Concentric layering around a troctolite xenolith	79
3.10	Loading structures along a chromitite lamina, RG1, CS	79
3.11	Field sketch of breccia zones on the slopes of Ruinsival	79
4.1	Distribution of gabbro intrusions	113
4.2	Field sketches and section of gabbro/peridotite relations	114
5.1	Location of sampling traverses	163
5.2	Histograms for compositional ranges of minerals from the ELS and the CS	164
5.3	NiO/Fo relations in olivine	166
5.4	Cr_2O_3 vs. Mg-number for pyroxenes	167
5.5	Na_2O vs. Mg-number for pyroxenes	167
5.6	Pyroxene compositions plotted on the Ca:Fe:Mg surface	168
5.7	Evolution of Ca-poor and Ca-rich pyroxenes	168
5.8	Mg-number of inclusion phase vs. that of olivine in the host rock	169

Page

5.9 Compositions of plagioclase included in spinel 169
5.10 Wt% TiO_2 vs. Mg-number of silicate phases in spinel 170
5.11 K_2O content of kaersutite inclusions in spinel 170
5.12 Al_2O_3 content of enstatite inclusions in spinel 170
5.13 Textural relations of phases included in spinel 171
5.14 Distribution of exotic silicate inclusions in spinel 172
5.15 Distribution of principal chromitite occurrences 173
5.16 to 5.18 Compositions of spinels included in olivine 174
5.19 Trivalent cation variation in chromitite spinels 177
5.21 Cryptic variation in the ELS along the W Trallval traverse 178
5.22 Lateral cryptic variation in the ELS on Trallval 179
5.23 Lateral variation in wt% NiO in olivine throughout the ELS 180
5.24 Lateral variation in Fo content of olivine throughout the ELS 181
5.25 Location of traverses along Trallval ridge 182
5.26 Lateral variation of Fo content of olivine along Trallval 183
5.27 Composite profile for the variation in olivine composition across the CS 184
5.28 Cryptic variation along the Seagull traverse 185
5.29 Cryptic variation across the Ruinsival traverse 186
5.30 Lateral cryptic variation along the DM/LLGl contact 187
5.31 Lateral cryptic variation of wt% NiO in olivine for the CS 188
5.32 Lateral cryptic variation of Fo content of olivine in the CS 189
6.1 NiO/Fo relations for olivine in dykes, gabbros and ultrabasic rocks 243
6.2 Distribution of gabbro groups 1 to 5 244
6.3 Alkali-silica plot for dykes and gabbros 245
6.4 D. I. vs. Si saturation 246
6.5 Major elements of the dykes vs. wt% MgO 247
6.6 Trace elements of the dykes vs. wt% MgO 249
6.7 Minor element ratios for the dykes 252
6.8 Normalised minor element patterns 253
6.9 Major elements of the gabbros and ultrabasic rocks vs. MgO 254
6.10 Trace elements of the gabbros and ultrabasic rocks vs. MgO 256
6.11 Minor element ratios for the gabbros and ultrabasic rocks 259
7.1 Synoptic sketches for magma chamber models of lateral variation 301
A.1 Cryptic variation traverses not illustrated in the text 313

Page

A.2 Identification key for data points on cryptic variation traverses 320

B.1 Identification key for the data points of the Harker diagrams in Chapter 6 327

LIST OF PLATES

3.1 Coralline texture, U10, ELS 80

3.2 Dendritic texture, U12 80

3.3 Cluster texture, U10 81

3.4 Harrisite pod, U15 81

3.5 Modal layering, U14 82

3.6 Chromitite layering, U9 82

3.7 Chromitite layering, U14 83

3.8 Cluster layering, U12 83

3.9 Graded cluster layering 84

3.10 Mélange of troctolite blocks in peridotite 84

3.11 Shearing and micro-faulting of allivalite, LLG3, CS 85

3.12 Flame at troctolite contact with pyroxene-rich troctolite, U14 85

3.13 Vertical pipe-like body of pyroxene-rich peridotite, U14 86

3.14 thin, resorbed allivalite, U12 86

3.15 Feldspathic streamers, U14 87

3.15 B Detail of 3.15 87

3.15 C Location of Feldspathic streamers 88

3.16 Concentric layering, U13 88

3.17 Replaced allivalite, U14 89

3.18 Troctolite blocks in peridotite with plagioclase-rich shadows 89

3.19 Ball-and-pillow loading structure, U14 90

3.20 Two lower layers of the U14 allivalite 90

3.21 General view of U14 allivalite 91

3.22 Diapiric troctolite, U14 91

3.23 Loading of peridotite into allivalite, U14 92

3.24 as above 92

3.25 Troctolite flame into peridotite 93

3.26 Detail of Plate 3.21 93

3.27 Collapsed diapiric structure, U14 94

3.28 Relic troctolite fragments of replaced allivalite 94

3.29 Relic troctolite body with flames 95

Page

3.30 Termination of the sandwiched peridotite layer, U14 95
3.31 Termination of the pyroxene-rich layer , U14 allivalite 96
3.32 Flame structures at the base of the pyroxene-rich layer 96
3.33 Trallval zone breccia 97
3.34 Parallel troctolite veinlets 97
3.35 Vertical structures, Trallval Zone 98
3.36 Pyroxene-rich matrix, Trallval Zone 98
3.37 Troctolite clasts, Trallval Zone 99
3.38 Dunitic peridotite clasts, Trallval Zone 99
3.39 Sheared breccia matrix, Trallval Zone 100
3.40 Pyroxene-rich matrix, Ruinsival Zone 100
3.41 Dendritic matrix, Ruinsival Zone 101
3.42 Giant cluster in Ruinsival Zone matrix 101
3.43 Sub-horizontal banding, Ruinsival Zone 102
3.44 Diffuse banding, Ruinsival Zone 102
3.45 Shearing in matrix at margin of Forked Zone 103
3.46 Shearing in matrix, Papadil Zone 103
3.47 Parallel troctolitic veinlets, Papadil Zone 104
3.48 Streaky matrix, Leac a Chaisteil Zone 104
4.1 Slump structure, Atlantic Corrie Gabbro 115
4.2 Flow banding, Atlantic Corrie Gabbro 115
4.3 Atlantic Corrie Gabbro brecciated by peridotite 116
4.4 East Trallval Gabbro 116
4.5 Coarse texture, Glen Harris Gabbro 117
4.6 Intrusion breccia, Glen Harris Gabbro 117
4.7 Layering in olivine gabbro on Ruinsival 118
5.1 Adcumulus texture in dunite 190
5.2 Net texture in dunite 190
5.3 Cumulus olivine in feldspathic peridotite 191
5.4 Cumulus plagioclase and pyroxene in allivalite 191
5.5 Conduit texture 192
5.7 Pyroxene fringe on olivine 192
5.8 Melt-supported texture in olivine gabbro 193
5.9 Melt-supported texture in peridotite 193
5.10 Olivine lamination in dunite 194
5.11 Lamination in anorthosite 194

	Page
5.12 Lamination of olivine in feldspathic peridotite	195
5.13 Spinel laminae in dunite	195
5.14 Spinel laminae in feldspathic peridotite	196
5.15 Spinel-rich lamina in feldspathic peridotite	196
5.16 Spinel concentrations in allivalite	197
5.17 Finely layered allivalite	197
5.18 Grain-size layering in dunite	198
5.19 Graded spinel layering in allivalite	198
5.20 Loaded allivalite/peridotite contact	199
5.21 as above	199
5.22 Channel feature in allivalite	200
5.23 Spinel geopetal in peridotite	200
5.24 as above	201
5.25 Recrystallised spinel loop	201
5.26 Localised spinel concentration in peridotite	202
5.27 Perpendicular pyroxene oikocryst in allivalite	202
5.28 Doughnut-shaped pyroxene oikocryst	203
5.29 Spinel/olivine growth interference texture	203
5.30 Micro-faulted chromitite lamina	204
5.31 Recrystallised chromitite in dunite	204
5.32 Skeletal or harrisitic olivine in protoharrisite	205
5.33 Spinel backbone in harrisitic olivine in peridotite	205
5.34 Central silicate inclusions in spinel	206
5.35 Enstatite and phlogopite included in olivine	206
5.36 as above	207
5.37 Inclusion spinel chromitite	207
5.38 Detail of 5.37	208
5.39 Spinel with silicate-inclusion-bearing rim	208
5.40 Partly recrystallised chromitite	209
5.41 Poorly sorted chromitite	209
5.42 Primary hydrous phases in plug peridotite	210
6.1 Group A quenched picrite BD1	260
6.2 Recrystallised picrite BA3	260
6.3 Peridotitic picrite BO4	261
6.4 Group B feldsparphyric basalt BB6	261
6.5 Group D spherulitic-textured basalt BE3	262
6.6 Group E microdiorite hybrid	262
6.7 Olivine gabbro E5	263
6.8 Olivine-hypersthene gabbro H5	263
6.9 Recrystallised olivine-hypersthene gabbro M2	264
6.10 Hypersthene gabbro H8	264
6.11 Zircon in phlogopite in breccia matrix B4	265

From Tiny Footprints, by Kliban, Methuen, London.

Aan mijn ouders.

CHAPTER 1

INTRODUCTION

1.1 Objectives of Research

A thick layered sequence of ultrabasic rocks, unique to Britain, is exposed on the island of Rhum, in the Inner Hebrides of northwest Scotland. It is part of a Tertiary subvolcanic complex, which also includes granophyres and felsites, emplaced within a ring fault into Pre-Cambrian country rock. This 6 km. wide intrusion forms the mountainous ground of the southern half of the island. Four doctoral theses have been completed on the more accessible portions of the ultrabasic complex, thus leaving a central, unmapped area around Trallval. This area is crucial to the understanding of the structure of the complex: it embraces at least three structurally and petrologically distinct series of layered ultrabasic rocks, as well as a number of bodies of gabbro and a score of minor intrusions, basic as well as ultrabasic. A major objective was, therefore, to present a map of the central Trallval area and to determine the structural and age relations between the layered series to the east, the west and the north. As this work completes the detailed mapping of the ultrabasic complex, started in the 1950's, it allows for the first time an overall synthesis of the geological evolution of the entire complex.

One of the fundamental problems in igneous petrology is to assess the importance of shallow reservoir magmatic processes in producing variation in extruded rock types. Differentiation in magma chambers is the most important of these processes. The separation of crystals from liquid may proceed along various paths and yield different products - cumulates and erupted residual liquids - even if the parental magma is of constant composition, depending on variations in cooling rates, depth of the magma chamber (pressure), extent of assimilation of country rock and/or meteoric water, tectonic evolution, compaction in crystal mushes, etc.

On Rhum, three distinct series of cumulates have been recognised. Two lines of investigation present themselves:

(i) To show how closely related the various series of cumulates and associated gabbros and minor intrusions are to one another and the likelihood of a common parental magma. If it can be demonstrated that

all the layered series formed from a common parental magma in shallow , intracrustal magma chambers, this leaves no alternative but to explain the differences between the series in terms of variations in magma chamber processes, such as those listed above, thus defining the second objective:

(2) To put constraints on the nature of the magma chambers under the Rhum volcano, and the processes which operated in these chambers. Recent models for these processes (McBirney and Noyes, 1979; Irvine, 1980) will be tested and refined during such an investigation.

Geochemical and petrological data for two of the ultrabasic series are presented here and used together with previously collected data (especially those of McClurg, 1982) to pursue the first objective. This includes detailed work on the petrography, mineralogy and mineral chemistry of the silicates, oxides and sulphides and whole-rock X-ray fluorescence analyses of the ultrabasic cumulates and the basic rocks. These data, field observations on the textures and internal structures, laboratory work on the microstructures and especially lateral variation in all these parameters are evaluated in the author's approach to the second problem.

1.2 Location and Fieldwork.

The island of Rhum lies approximately between the Tertiary volcanic centres of Skye and Ardnamurchan. The igneous complex covers most of the southern half of the island, an area of about 15 $km.^2$. The topography is rugged: mountains rise to 812 m., forming a double horse-shoe shaped ridge with intervening corries and glens drained by the Harris river, the Fiachanis river and the Dibidil river, respectively, for the mountain groups of:

(i) Barkeval, Hallival, Askival and Trallval

(ii) Trallval, Ainshval and Ruinsival

(iii) Askival, Trallval and Sgurr Nan Gillean.

The floors of the glens are obscured by glacial drift with a thick cover of peat and grass. The best exposure is on the glaciated lower slopes, and often reaches 100 %. Large areas of active scree and steep cliffs are compensated by superb vertical exposures higher up. The Trallval area is outlined on fig. 1.1 and overlaps with previously mapped areas to provide continuity.

Reconnaissance fieldwork was undertaken in August 1979. Much of the detailed mapping was completed in four 3 to 4 week expeditions in April, May, June and September, 1980, followed by expeditions in April, May, June and September, 1981 to finish the mapping and collecting. July and August were avoided for climatic reasons. The lodge at Harris Bay proved a practical and comfortable field base. Aerial photographs were carried in the field at all times and mapped onto directly where in conflict with the Ordnance Survey feature mapping. Due to considerable magnetic deviations in certain parts of the island, triangulation methods proved severely restricted in usefulness.

During the mapping, several topographical features, useful as reference points, have been named as follows:

(1) Seagull Loch at (GR 3515 9520).

(2) Upper Fiachanis at (GR 372 947).

These names do not appear on the Ordnance Survey 1:10,000 sheets and are shown on fig. 1.2 together with other place-names referred to in the thesis.

1.3 History of Geological Investigation.

Harker (1908) originally mapped the island, distinguishing between the basic and ultrabasic rocks. Bailey (1945) first recognised the ring fault. The acid rocks in the south were mapped by Hughes (1955) and those of the northern edge of the complex by Dunham (1962). Black (1954) mapped the granophyre to the west. This work established the younger age of the ultrabasic/basic complex and a complicated sequence of events for the formation of the acid rocks, characterised by early explosive activity.

Brown (1956) described the geology of Hallival and Askival, mapping the layered ultrabasic series as 15 macro-units, each with olivine cumulates at the bottom and plagioclase cumulates at the top. Wadsworth (1961) divided the ultrabasic rocks to the west of the Long Loch Fault into 4 much thicker, more olivine-rich units. McClurg (1982) mapped the ultrabasic rocks, both layered and unlayered, of Barkeval and the Long Loch area and presented modern geochemical work on the gabbros and dykes. Donaldson (1975) studied some of the ultrabasic breccias and interpreted them as feeders to the magma chamber from which the ultrabasic series accumulated. Forster (1980) suggested an ultrabasic parental liquid

for the layered series, based on the geochemistry of the minor intrusions of Rhum. Emeleus (1980) recently compiled a map for the whole of the island.

Detailed research on the ultrabasic rocks includes work by Wadsworth (1973) on primary sedimentary structures, by Dunham and Wadsworth (1978) on cryptic variation in the layered series, by Williams (1978) on uranium-bearing minerals in the mesostasis of the peridotite and by Henderson and so-workers (see Henderson and Wood, 1981) and Ridley (1971) on the chrome-spinels. Research in progress includes work on Sr isotopes (Palacsz, Leeds), on postcumulus processes (Butcher, Manshester), sedimentary structures in the layered series (Young, St. Andrews) and the petrology and chronology of the eastern gabbros (Faithful, Durham).

1.4 Geological Setting of the Igneous Complex.

MacIntyre et al. (1975) related the volcanism of the British Tertiary Province to the opening of the Atlantic and suggested that the main centres were located at the intersection of N-S Pre-Cambrian basement fractures and NE-SW Caledonian lines of weakness with two sets of fissures related to the opening of the Atlantic:

(1) A set parallel to the rift which developed until one fissure grew into the main rift.

(2) A set perpendicular to the free edge of the plate, propagated after initiation of the main rift.

In her thesis on the geology of the Barkeval area of Rhum, McClurg (1982) concluded that the Rhum volcanic centre may represent an aborted attempt at seafloor spreading, on the basis of the abundance of highly magnesian picrites. This episode probably preceded the formation of the main rift and the opening of the Atlantic dated at 60 m.y. (MacIntyre et al., 1975). Such an early age for the Rhum centre is supported by the similarity of the geochemistry of the late dykes on Rhum to the early lavas on Skye (McClurg, 1982).

The shape of Rhum is controlled by large-scale block-faulting, as are the shapes of the neighbouring islands of Canna, Eigg, Muck and Oigh-Sgeirr which consist mostly of Tertiary lavas (basalts, mugearites and pitchstones). The rocks on the seafloor are mainly Mesozoic sediments to the west of Rhum and Pre-Cambrian(Torridonian and Lewisian) to the east (McQuillin and Binns, 1973). The extent of the Lewisian outcrop is

thought to be limited by an extension of the Camasunary fault which runs between Rhum and Eigg.

On Rhum, a ring fault separates arkosic sandstones and shales to the north and east from the igneous complex. These sediments are of Torridonian age and dip uniformly to the WNW at 20°. Lavas, underlain by conglomerates, unconformably overlie the intrusive complex and the Torridonian sandstones and straddle the ring fault.Dyke intrusions occurred before, during and after the formation and emplacement of the central complex. Forster (1980) recognised an early NW-SE dyke swarm with a radial set superimposed on this, associated with the formation of the ring fault. Near the Long Loch Fault, dyke trends are controlled by N-S fractures in the basement. Most dykes are non-porphyritic dolerites, but feldsparphyric dolerites together with peridotitic and acidic types also occur. Inclined sheets of dolerite dip at 25° to 30° towards a focus in Glen Harris (Harris, 1908). Dunham (1962) distinguished a later set with a focus several km. further west.

A gravity survey by McQuillin and Tuson (1963) showed there is a large positive Bouguer anomaly over Rhum, which may be modelled by a cylinder of dense ultrabasic to basic rock with a cross-sectional area close to that of the exposed ultrabasic complex, and extending down into the crust to a depth of 15 km. The axis of this column intersects the surface 1.5 km. NNE of Harris Lodge.

The island is cut by a N-S fault, the Long Loch Fault, which cuts the igneous complex and which is marked along much of its length by a sharp topographic depression. Its control on the orientation of early dykes suggests the fault has a long history of movement and may be partly responsible for the siting of the Rhum central complex.

1.5 Glaciology.

Pleistocene glaciers moulded the U-shaped valleys, carved the hanging valleys, such as that of Fiachanis and the arêtes, like the summit ridge of Trallval. Large erratics, talus-slope deposits and boulder moraine also attest to their former presence. Harker (1908) reports two sets of glacial striations: a set outwards from the main mountains of Rhum superimposed on an earlier set in a WNW direction. Together with the find of mica-schist and garnetiferous gneiss at 550 m. altitude on Barkeval, this suggests the following sequence (Dunham and Emeleus, 1967):

(1) Movement of a vast ice-sheet from the mainland over the top of Rhum towards the WNW.

(2) Local glaciers centred on the mountains of the Rhum Cuillin and the hills of Orval and Fionchra.

The best striations observed during the present study in the Trallval area occur at (GR 366 926), north of Papadil, on a roche moutonnée, and conform to Harker's earlier set. Other glaciological observations include:

(1) An erratic of granitic gneiss near the top of Trallval at 630 m. altitude (GR 3730 9541).

(2) Numerous erratics of granite and quartzite on the hilly ground west of Trallval (GR 362 954).

(3) Abundant litters of erratics of felsite and explosion breccia deposited on the relatively flat ground north of Papadil (GR 362 932).

The restriction of erratics to the western slopes of the mountains also indicates westward movement of a large ice sheet.

1.6 Age Relations and Structure of the Igneous Complex.

Bailey (1945) summarised the geological history as follows:

(1) Intrusion of the acid rocks (explosion breccia, felsite and granophyre) with the formation of ring fractures, radial dykes and a set of inclined sheets.

(2) Block uplift of the acid complex along the ring fault.

(3) Intrusion of the layered ultrabasic series along ring fissures (an inner ring fault) within the main ring fault together with injection of basic magma along these fissures and subsequent subsidence of the gabbro/peridotite complex.

A feature of Bailey's model is the production of rings within rings due to repeated upheaval and collapse. Hughes' (1955) mapping confirmed the aggregate upward movement along the main ring fault and revealed extensive tilting within the fault. Dunham's (1962) mapping of two sets of cone-sheets supported Bailey's suggestion of a westward shift of activity before the emplacement of the ultrabasic complex.

1.7 Previous Work on the Basic / Ultrabasic Complex.

1.7.1 Pre-1950 Research.

Some of the earliest observations on the ultrabasic rocks of Rhum were those of Judd (1889) who noted that they were stratified at Harris Bay and became "amorphous" towards Ruinsival and Trallval: he compared the layering to the pseudo-stratification of the Mull granites. He observed the coarse contemporaneous veins in the ultrabasic rocks and considered the gabbros to be later than the granites. Geikie (1897) commented that while on Hallival the layered rocks dip to the west, they dip to the east near the Long Loch and that the general stratification becomes less marked and disappears from the head of Glen Harris and the base of Askival, i.e. well-developed layering along the northern and eastern margins surrounds a central structureless region.

Harker investigated the complex in more detail (1908), and decided that the intrusion was laccolithic, only rarely showing vertical contacts, as to the west of Trallval where gabbro breaks through the peridotite. These contacts are highly complex and commonly develop into intrusion breccias. He attributed the layering to the repeated injection of a sill underneath the previous, semi-solidified sill. An olivine-anorthite magma was thought to separate at depth into two liquids, giving rise to alternate sills of peridotite and anorthosite. Later segregation produced thin, monomineralic bands and the various concretionary and coralline growths. Harker emphasised the lenticular nature of the anorthosite layers (or allivalites) to support his ideas: allivalites, of great thickness on Hallival and Askival, die out westwards, making only two escarpments on Trallvall. The general inward dip of the allivalite sheets (towards the centre of Glen Harris) was further demonstrated by Harker. He reported irregularities, such as the steep dips near the Long Loch. He also noted the abundance of olivine west of the Long Loch Fault, although he stated that feldspathic veins are common near the fault itself and layers of almost pure olivine rock occur at the head of Glen Harris.

1.7.2 Hallival and Askival: The Eastern Part of the Complex.

The ultrabasic rocks of Hallival and Askival were the first to be studied in detail and to be interpreted as gravity cumulates at the bottom of a magma chamber (Wager and Brown, 1951). Brown (1956) subdivided the succession into 15 units, each consisting of a thick layer of peridotite, capped by a generally thinner layer of allivalite. Unit 10 was chosen as the type unit and described in detail: the peridotite consists of

60 to 70 % of cumulus olivine poikilitically enclosed by plagioclase and clinopyroxene. Variations in the texture are due to the different habits of the olivine and the clinopyroxene. For instance, bands of harrisite may occur which consist of elongate, vertically oriented olivine crystals, occasionally branching, with plagioclase in the interstices. Another peridotite variety has tabular olivines flattened parallel to (010) and to the layering. The peridotite grades into allivalite, which consists of cumulus plagioclase with subsidiary olivine and clinopyroxene (which occasionally occurs as a cumulus phase). The allivalites are finely layered on a scale of 1 mm. to 3 cm. and may include layers of slumped material; gravity stratification is rare. Chrome-spinel is concentrated towards the bottom of the unit and in some cases forms a thin seam on top of underlying allivalites. The average size of the olivine decreases from the bottom to the top of the unit. Brown (1956) also described the salient features of the other 14 units but did not mention any lateral variation. Throughout the series, no change in the composition of the olivine was detected; the plagioclase composition was shown to vary between An_{83} and An_{88} without any consistent variation with height.

1.7.3 The Harris Bay Area: the Western Part of the Complex.

Wadsdworth (1958, 1961) described the rocks from the southwest of Rhum, where they form a series of 4 units, up to 500 m. thick (the Western Layered Series) generally richer in olivine than those of the Hallival - Askival area (the Eastern Layered Series) which are not thicker than 100 m. Unit A of the Western Layered Series consists of mesocumulates (as defined by Wager et al., 1961). Layering is defined by horizons of harrisite which are, however, less common than in unit B where they form layers up to 2 m. thick, with sharp lower contacts, but irregular upper boundaries; the irregularities are progressively eliminated by succeeding layers of normal peridotite. The harrisitic olivine forms branching "trees" with many embayments which have trapped clusters of chrome-spinel and often contain an abundance of hydrous minerals. The allivalite of unit B shows streaky layering, slumping and includes blocks of olivine cumulate. Units C and D, exposed on Ruinsival, show little layering. In the Western Layered Series, cryptic variation occurs within units: olivine evolves from Fo_{88} to Fo_{85} in unit D.

1.7.4 The Central Part of the Complex.

Within 0.5 km. of the Long Loch Fault, dips are steep (40^{o} to 60^{o}) and allivalites are streaky and slumped and the rocks are disturbed by faulting, zones of igneous breccia and gabbro intrusions (Wadsworth, 1961). Bailey (1945) recorded that the dips of the allivalites define a synformal axis about the Long Loch Fault. On Ruinsival, to the east of the Long Loch Fault, olivine cumulates and allivalites dip to the west at 60^{o}, "their relationship with the rocks west of the fault being unknown" (Wadsworth, 1961). Wadsworth suggested that while it is likely that the Western Layered Series represents a lower level in the magma chamber (since these are richer in olivine, which is also more magnesian), there must be a considerable gap between the eastern and western series, as the lowest units of the Eastern Layered Series are orthocumulates and orthopyroxene-bearing, while the highest units of the Western Layered Series are adcumulates. Dunham and Emeleus (1967) presented evidence that after differential movement between the eastern and western series, they were emplaced as one solid plug. Wager and Brown (1968) emphasised that no correlation is possible between the two series as the steep dips, the slumping and the autobrecciation near the Long Loch Fault suggest that a zone of weakness had developed early in the history of the intrusion, along which the western series was emplaced just before the series as a whole was emplaced into the acid complex.

1.7.5 The Barkeval - Long Loch Area : the Northern Part of the Complex.

This study is in many ways complementary to McClurg's (1982) thesis on the geology of the Barkeval-Long Loch area. The area is similar to the Trallval area as it includes parts of all major rock units in the ultra-basic complex. She presented a revised classification (table 3.2) of the layered sequence, incorporating the allivalite of "Unit B" together with Units C and D of the Western Layered Series into a newly-named Central Series. The Central Series was shown to form a trough-like structure, elongated N-S. The Western Layered Series was redefined and included only Unit A and the peridotite of "Unit B". The Eastern Layered Series was retained as it was originally defined and was shown to have been emplaced into the acid rocks of north-central Rhum together with the Western Layered Series to form a composite, approximately oval complex. The Central Series was thought to be in situ and to have been intruded as a

number of dyke-like crystal mushes along the Long Loch Fault. McClurg documented the cryptic variation in the Eastern Layered Series, as exposed on Barkeval; the mafic minerals show consistent variation in composition with height only within a unit, but not from the lowest to the highest units. The pattern was interpreted to support Brown's (1956) claim that the sequence formed by repeated injection of fresh magma into a chamber accompanied by the eruption of the residual magma, followed by crystallisation and the formation of cumulate layers and residual magma. More layers of cumulate are formed by repetition of this cycle.

1.7.6 The Unlayered Ultrabasic Rocks.

Wadsworth (1961) described the breccias, chaotically oriented blocks of peridotite in an anorthosite matrix which pass laterally into streaky layered allivalites, and interpreted them as fault-scarp breccias. Harker (1908) attributed the breccias to intense veining of peridotite by feldspathic peridotite; this is supported by the intense veining of the blocks themselves. Donaldson's (1975) detailed work confirmed Harker's conclusions on the breccias. The breccias have vertical contacts, the blocks are not sorted by size and many harrisite blocks are only slightly rotated; a gentle stoping action is thus implied. McClurg's (1982) mapping demonstrated the intrusive origin of all ultrabasic breccias in the Long Loch area. The largest zone of breccia forms a sheath around the intrusive Central Series.

While the bulk of the ultrabasic rocks composes the layered series and associated breccia zones, a number of vertical-sided masses of un- or poorly layered peridotite pierce the sandstone outside the ring fault. These are referred to as plugs when the outline is roughly circular and tongues when it is elongate. Bailey (1945) remarked that where the peridotite presents itself in steep tongues, it often shows steep layering more or less concordant with the complications of its margins. Ultrabasic tongues along the northern margin of the igneous complex were shown by Dunham (1962) to predate the emplacement of the main ultrabasic mass, from which they differ in petrology (more magnesian olivine) and structure (vertical layering, due to the modal variation in the phases interstitial to the olivine- see McClurg, 1982). McClurg's (1982) detailed mapping of the Long Loch - Barkeval area revealed the existence of both dunite and peridotite plugs within the ultrabasic complex. McClurg regarded the plugs as intrusive offshoots from the Central Series.

1.8 The Location of the Magma Chambers.

It is clear from the previous section that layers of ultrabasic rock and crystal mushes were forming in different magma chambers at different times. These chambers did not necessarily young upwards. Donaldson (1975) suggested a depth of 1500 to 4000 m. for the Central Series chamber from the assumption of a maximum T of 1200 ^{o}C for the magma from which the harrisite layers formed (which had olivine, clinopyroxene and plagioclase on the liquidus under water-saturated conditions). A shallower depth is suggested by xenoliths of amygdaloidal basalt in some of the gabbros associated with the Eastern Layered Series before its emplacement into the acid complex (Faithful, pers. comm.). Brown (1963), from the presence of inverted tridymite in contact metamorphosed sandstone near a gabbro plug, suggested that the metamorphism occurred at a depth of less than 2100 m. from the surface. As the Central Series are thought to be in situ (McClurg, 1982) the mush crystallised very close to the surface, although the depth of origin of the mush itself is not known.

Extrapolation of the Torridonian / Lewisian unconformity from the mainland suggests that Lewisian Gneiss is less than 1 km. from the surface and is therefore the most likely lithology to make up the walls of the shallow chambers suggested by the above data. On Rhum, Lewisian Gneiss is seen only within the ring fault, associated with the acid rocks, as contact metamorphosed hornblende-plagioclase gneisses (Tilley, 1944).

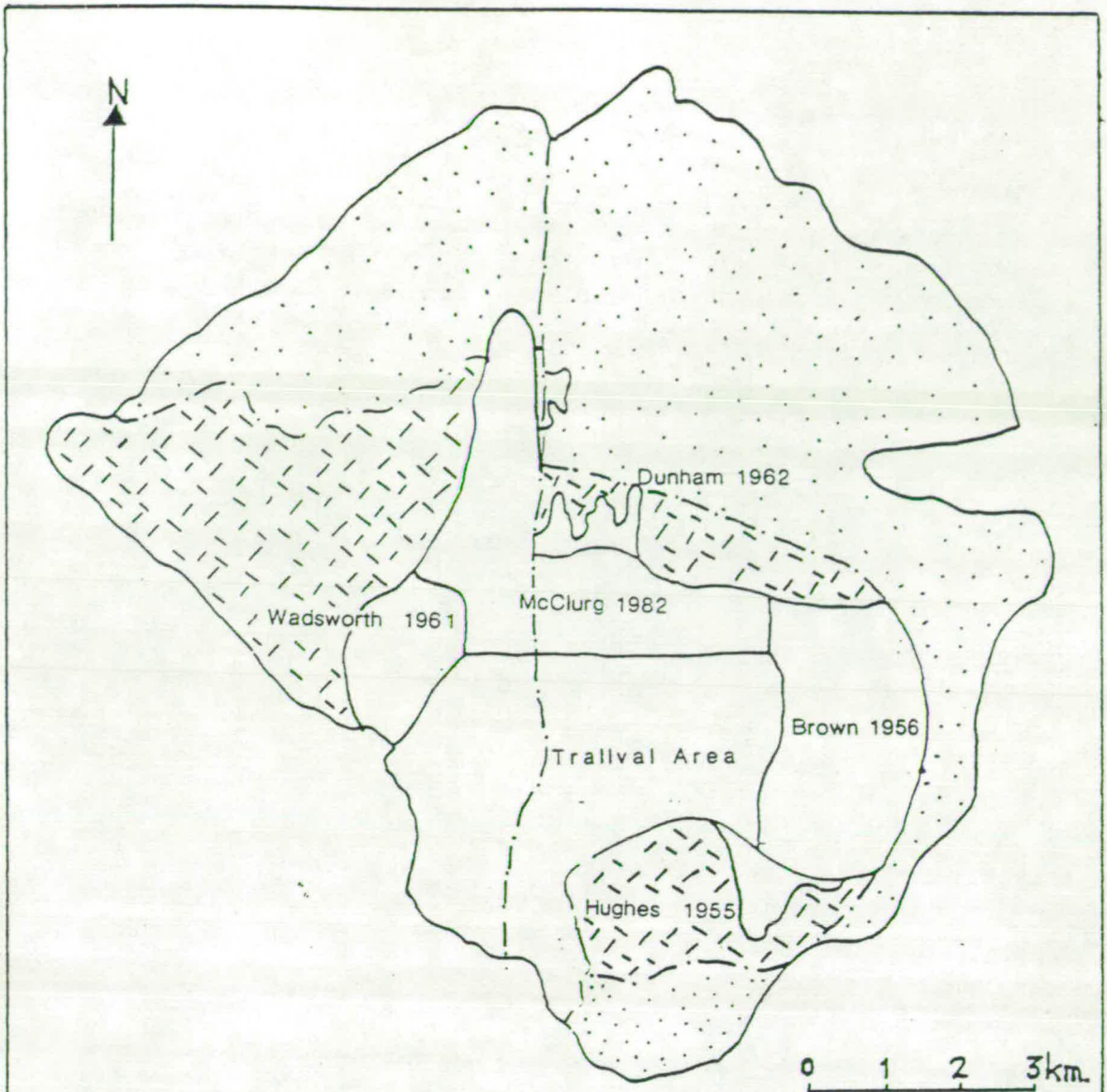

FIG. 1.1: SIMPLIFIED GEOLOGY OF RHUM. TORRIDONIAN SANDSTONE IS STIPPLED , THE ACID IGNEOUS COMPLEX HATCHED AND THE BASIC/ULTRABASIC COMPLEX IS LEFT BLANK. THE TRALLVAL AREA IS SHOWN AND AREAS MAPPED PREVIOUSLY BUT NOT REMAPPED BY THE AUTHOR ARE ALSO INDICATED.

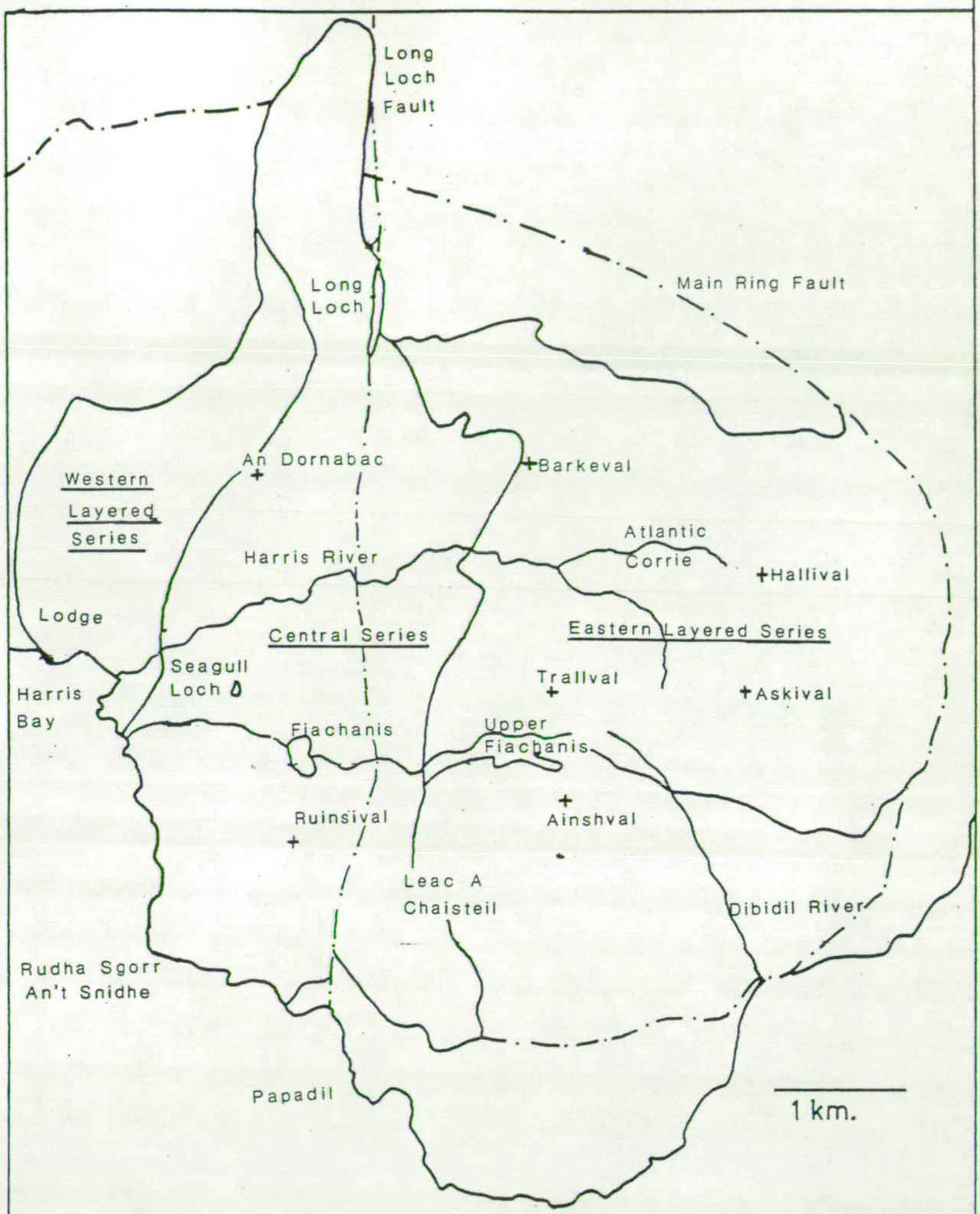

Figure 1.2 The Structure of the Ultrabasic Complex

CHAPTER 2

AN EXPLANATION OF THE MAP

The units mapped in the Trallval area (see map at the back of the thesis) are briefly described here. Their structural relations are presented in detail. The distribution and internal structures of the gabbros and intrusive ultrabasic plugs are, however, described in later chapters dealing with the individual rock units. The final section presents the age relations between the various units. To the north, east and west, the mapped area extends to, and to some extent overlaps, the areas previously mapped by McClurg (1982), Brown (1956), and Wadsworth (1961), respectively (fig. 1.1). The southern limit is the boundary with the acid rocks of the Southern Mountains complex and the Torridonian sandstone outside Bailey's (1945) main ring fault to the igneous complex. This contact is discussed in section 2.2.4.

2.1 Mapping Units

2.1.1 Sandstones and Acid Igneous Rock Types.

Hughes (1960) mapped the Southern Mountains complex. In the present study, Torridonian sandstone, granophyre, explosion breccia and felsite were all encountered while mapping along the southern boundary and the reader is referred to Hughes' account for the characterisation of these mapping units.

South of Trallval, in Sandy Corrie, about 1 km.^{2} of Lewisian Gneiss (Tilley, 1944) is exposed. As this rock type may have formed much of the wallrock to the conduits and storage chambers through which moved the magmas parental to the ultrabasic complex, the Sandy Corrie area was briefly surveyed and sampled. Both quartzo-feldspathic and hornblende-plagioclase gneisses occur- despite intense thermal metamorphism, metamorphic foliations are preserved. The foliation is generally steep and interference patterns indicate at least two folding episodes. The gneisses are cut by basic sheets which are folded and sheared into en-échelon arrays, i.e. probably of Lewisian age. Up to 20% of the oucrop consists of a pegmatitic, poorly foliated quartz-two-feldspar rock displaying granophyric texture. These sheets of granophyre are generally conformable to the foliation in the gneisses.

2.1.2 The Layered Ultrabasic Rocks.

Three series of layered ultrabasic rocks, which differ in structure and petrology have been distinguished in the field:

(1) The Trallval Layered Series, or TLS, which is correlated with the Eastern Layered Series, or ELS (Brown, 1956).

(2) The southerly extension of the layered Central Series, or CS, as mapped in the Long Loch - Barkeval area by McClurg (1982). The area west of the Long Loch Fault was mapped by Wadsworth (1961). It has been remapped here in more detail to clarify its relations with parts of the CS encountered by the author to the east of the fault.

(3) The Western Layered Series, originally mapped by Wadsdworth (1961) and redefined by McClurg (1982).

The TLS is exposed in Glen Harris, on Trallval and at the head of Glen Dibidil. It consists mostly of feldspathic peridotite alternating with subordinate allivalite layers. Over most of the area, the layering is inclined at less than 20^{o}. At or near the base, the peridotite may have laminae of dunite and/or chromitite. Fine-scale modal or textural layering is common and becomes most pronounced below the allivalite layers. The allivalite varies in structure from massive to finely layered and is often well-laminated. It is primarily a troctolite with interstitial clinopyroxene but includes lenses and layers of clinopyroxene-rich troctolite, anorthosite and peridotite. Although the TLS is isolated from the ELS by the Atlantic Corrie Gabbro, it is petrologically and structurally similar to the layered peridotites of Hallival and has been correlated with the ELS (section 3.1).

The basal member of the CS, the Dornabac Member, consists of olivine and clinopyroxene bearing anorthosites with strongly developed slumping structures,contemporaneous faults and thin peridotite horizons. Dunite makes up more than half of the overlying succession- the other main lithologies are feldspathic peridotite and chrome-spinel rich peridotite. The layering is steeply inclined, commonly dipping at more than 20^{o}. A few highly deformed layers of allivalite are interleaved with the peridotite and the dunite. Chromitite laminae are common and give an indication of layering in the otherwise structureless dunite.

The Western Layered Series consist mainly of peridotite with abundant and remarkably well-developed layers of harrisite. Its boundary with the CS forms the western limit to the area mapped in the present study.

2.1.3 The Unlayered Ultrabasic Breccia Zones.

Both members of the CS, and the TLS to a very limited degree, are disrupted by elongate steep-sided zones of breccia of layered blocks in a matrix of feldspathic peridotite. The distribution and the volumetric proportion of blocks are highly variable, and these variations, together with variations in matrix petrology, commonly define a vertical fabric (section 3.8). The breccia zones are most important to the south of Ruinsival where they are the dominant rock type. An earlier, more olivine-rich breccia has also been mapped in this area. It is distinguished from the feldspathic breccia zones by the homogeneity of its matrix and the lack of a vertical fabric.

2.1.4 Intrusive Ultrabasic Plugs.

Roughly cylindrical plugs of feldspathic peridotite intrude the layered series. These contain rare xenoliths of the layered series. The diffuse nature of the vertical layering, which parallels the plug margins, and the homogeneous, often very coarse texture of the peridotites distinguish them from those of the layered series.

2.1.5 Gabbros

All poorly layered, intrusive, medium to coarse grained plagioclase-rich basic rocks are mapped as gabbro. After the rocks of the layered series, they compose the most important lithology in the Trallval area. They occur as inclined sheets, small bosses and complex systems of interpenetrating sheets more or less conformable with the layered series. Olivine-gabbro is dominant, although olivine-free gabbros form a large stock in Papadil and also line much of the inner contact with the Southern Mountains Complex as a marginal ring dyke of variable width. Some of the thicker conformable sheets of olivine-gabbro may show layering and can be difficult to distinguish from the allivalites.

2.1.6 Minor Intrusions

Dykes up to 6 m. wide are abundant in the TLS- they are mainly of dolerite, although picrites are common in Atlantic Corrie. Within the CS, dykes are rarely seen, with the exception of a dyke of intermediate composition lining a conspicuous gully on Ruinsival. Dykes are not shown on the map but all dyke orientations measured in the field are plotted in fig. 2.3.

2.2 The Structure of the Ultrabasic Complex in the Trallval Area.

McClurg (1982) summarised the structure of the complex as follows: an elliptical, E-W oriented body consisting of Eastern and Western Layered Series, tectonically emplaced into the earlier acid complex along an inner ring fault, is disrupted and cut by the N-S elongate dyke-like mass of the CS. An account is given here of the internal structure of the TLS and that of the CS within the Trallval area, followed by a description of the contacts of each of the series and structures within the layered series close to the contact.

2.2.1 The Structure of the Trallval Layered Series.

Fig. 2.1 shows the measured inclinations of planar structures in the layered series, including modal and textural layering in the peridotite, the contacts between peridotites and allivalites, and lamination in the allivalites. Where these structures are present in the same outcrop, they are usually coplanar. However, near the summit ridge of Trallval (GR 3743 9533) the textural layering (section 3.4) in the peridotite shows an angular unconformity of about 3^{o} with the lower surface of an allivalite (section 3.5.10). A little to the west at (GR 3715 9543), one set of laminae in an allivalite dips 16^{o} more steeply than laminae elsewhere in the same layer (section 3.5.8) and is the only example of possible cross-bedding in the layered series. No measurements are shown for the obviously slumped horizons in the allivalites.

The TLS consists of 9 cyclic units, each with peridotite at the base and allivalite at the top. The mineral chemistry, together with the presence of several marker horizons also allows the correlation of the Trallval cyclic units with those of Askival, Hallival and Barkeval (section 3.1). With a few exceptions, the measured orientations of the layering in the lower 5 units follow the same pattern: the inclination of the layering varies, randomly, between 12^{o} and 30^{o}. The strike swings round from ENE-WSW in the east to E-W in the west along the outer edge of the complex (South Trallval), and, from the outer edge towards the centre of the complex (Glen Harris) the strike changes gradually to N-S. Higher units (U13 to U16) are exposed only near the top of Trallval. West of the summit ridge, the strike of the layering swings parallel to the contact with the CS and shows considerable steepening. Near the ridge, however, the layering is parallel with that in the lower units, but tends to be somewhat less steep. The maximum change in thickness for

any unit from Askival to Trallval is shown by Unit 14 (fig. 3.1) and accounts for less than 1^{o} of any decrease in inclination of its upper surface with respect to its lower surface. Other units show thickening in the opposite direction. The layering of the TLS can be approximately modelled by a set of inverted cones with a common apex near point A (fig. 2.1). The layering does not appear to shallow as the apex is approached. Those measurements which deviate from this pattern are on exposures within a few metres of gabbro contacts and are attributed to the deformation associated with the later intrusion.

2.2.2 The structure of the Central Series.

In the field, layering in the CS is difficult to measure as it is only sparsely distributed over the 1000m. of section and often poorly developed. Fig. 2.2 shows, in addition to textural, modal and lithological layering which define laterally extensive planar surfaces, orientations measured on approximately planar, isolated lenses of chromitite and on layering in thin, often disturbed horizons of allivalite. These are probably poor indicators of primary layering but may be the only clue to its strike over large areas. They are distinguished on the figure by special symbols. An idea of their usefulness can be gained by comparing the slumped layering with undisturbed layering nearby, as on the summit of Ruinsival, the slopes of Trallval and the top of the An't Snidhe fault wedge.

The CS in the Trallval area consists of 3 blocks juxtaposed by faults with vertical displacements of up to 750 m.:

(1) The Ruinsival block, to the west of the Long Loch Fault, which stretches from An Dornabac to Ruinsival and is exposed along much of the coast south of Harris Bay. It also extends into the Long Loch area.

(2) The An't Snidhe block which is wedge-shaped, on the southern slopes of Ruinsival. A number of smaller, isolated blocks are exposed elsewhere on south Ruinsival, most of which cannot be placed within the main sequence with confidence.

(3) The Papadil - Trallval block, to the east of the Long Loch fault.

Correlation from one block to another is achieved by using marker horizons such as the allivalites of the basal member, or the layers of chrome-spinel rich peridotite and by correlating variations in the mineral chemistry (section 5.6.2). Such correlation is only reliable for the larger faultblocks, exposing a section of at least 100m.

2.2.2.1 The Ruinsival Block: In the Long Loch area, the layering in the CS defines a trough with an axis near the Long Loch Fault (McClurg, 1982). This trough widens to the south and as it opens up, the layering shallows towards the centre of the trough, flattening to sub-horizontal in the upper parts of the series on Ruinsival (fig. 2.2). Layering near the edge of the trough is steep (30^{o} to 60^{o}) and invariably inclined to the SE. Between the Fiachanis river and the NW face of Ruinsival, the inclination of the layering decreases to $20\text{-}25^{o}$, while the strike changes from NE-SW to N-S. On the summit of Ruinsival, the inclination of the layering dips towards the ENE at $5\text{-}15^{o}$. From trough-like in the north, the structure becomes basin-like in the south. The anomalously steep dips of some of the chromitite lenses and the allivalites are probably due to slumping; slumpfolds verge consistently downslope. At (GR 361 954), adjacent to the Long Loch Fault, the anomalously steep dips and the change in strike are attributed to drag associated with movement along the fault (section 2.3.2).

2.2.2.2 The An't Snidhe Block: A fault-bounded wedge, 250 m. wide at the coast, of thick disturbed allivalites, interlayered with autobrecciated peridotite, which can be correlated with the basal member of the CS, occurs on the southern slopes of Ruinsival. The layering in the allivalites is consistently inclined to the NE at moderate angles (10^{o} to 30^{o}). The block may be a slice from the southern margin of the Ruinsival block. To the east, anastomosing ultrabasic breccia zones have isolated smaller areas of well-layered rocks. The dip of this layering has, in each case, a strong northerly component.

2.2.2.3 The Papadil - Trallval Block: The CS east of the Long Loch Fault shows a relatively complex structure most easily explained by the draping of layers over a highly irregular surface by drag folding upon differential subsidence of a set of semi-consolidated layers. Below Leac a Chaisteil (GR 365 940), the basal member is exposed: layering dips steeply to the west, veering round to the SW to the south of Leac a Chaisteil and to the NW north of it. Elsewhere in this tract, only the upper member outcrops. In the southern Papadil area, the layering strikes parallel to the margins of the tongue-shaped mass of the CS and defines a synformal structure with a steep NE limb (dips of ca. 40^{o}) and a shallow SW limb (20^{o} inward dip), plunging to the NW. West of Trallval, the layering dips consistently towards the NW at about $20\text{-}30^{o}$. The emergence of the basal

member at Leac a Chaisteil, the steepness of the NE limb of the Papadil synform and the rotation of the strike towards N-S as Leac a Chaisteil is approached from the north, all suggest relative uplift of that part of the Papadil-Trallval block adjacent to the Southern Mountains Complex, i.e. subsidence in the Central Series increases towards Papadil and Barkeval.

2.2.3 The Eastern and Western Contacts of the Central Series.

The contact with the ELS is exposed for about 1 km. on the north side of Trallval; it is a faulted contact lined by a sheet of gabbro of variable width (5 to 20 m.) which brecciates both the CS and the ELS, but the former much more extensively. To the north, the contact is obscured by an ultrabasic breccia zone (which also brecciates the CS and the ELS) and to the south by the Glen Harris Gabbro. The contact changes strike abruptly a number of times suggesting that fault motion along it was purely vertical. Where exposed on Trallval, it is near vertical (locally, it may have a hade of up to 10^0 to either the east or to the west) and strikes at 035 from north. The layering on both sides of the fault has suffered severe drag demonstrating subsidence of the CS relative to the ELS (figs. 2.1 and 2.2). As noted in section 2.2.1, the layering in the ELS is rotated into parallelism with the fault-plane as far away as 200m. from the fault in the higher units; this effect is much weaker in the units below U13, suggesting that the upper units (for a total thickness of 150m.) were less consolidated at the time of faulting. There is, indeed, little evidence of brittle deformation in the peridotites. The allivalites, however, are strongly bent and, closer to the contact, broken into a number of slabs as illustrated in fig. 2.1. Thus, the allivalites acted as competent layers among the dominant, incompetent peridotites and more readily displayed brittle failure on deformation.

Several thin layers of allivalite are exposed east of the contact (at GR 3717 9557 and GR 3698 9543) and have been repeatedly displaced on reverse faults striking parallel to the CS / ELS contact and dipping to the SE. This suggests that a minor compressional episode followed the tensional phase which produced the relative subsidence of the CS into the ELS and the WLS (McClurg, 1982).

The CS is bounded to the west by the WLS. The nature of this contact is more difficult to ascertain as, (i), it is intruded by an ultrabasic breccia to the west of An Dornabac and, (ii), it is not exposed to the south except at one locality (GR 3431 9507) where rocks

of the Harris Bay member of the WLS are separated from the CS by a 3m. zone of sheared feldspathic peridotite alternating with thin vertical sheets of gabbro. The strong shearing indicates that there has been considerable movement between the WLS and the CS. This is supported by the steepening of the layering in the Ard Mheall member of the WLS near the contact (Wadsworth, 1961), possibly due to drag associated with the subsidence of the CS relative to the WLS.

2.2.4 The Southern Contact of the Ultrabasic Complex.

The contact consists of three sectors:

(1) ELS against the Southern Mountains Complex.

(2) CS against the Southern Mountains Complex.

(3) CS against the Papadil Gabbro and Torridonian sandstone where it extends across the Main Ring Fault.

The first sector has been intruded along its entire length by a gabbro which shows a chill against the Southern Mountains felsite but not against the ELS. At Bealach An Fhuarain, the gabbro is brecciated over a 50m. wide zone by rheomorphic veins and sheets of felsite. This supports Brown's (1956) concept of a gabbro lubricating the emplacement of a hot (but solid) plug of ultrabasic rocks into the acid complex.

Near Papadil, at (GR 3684 9219), ultrabasic rocks are in direct contact with the Torridonian sandstone and despite the good exposure, there is no evidence of faulting. The CS extends across the Main Ring Fault and the contact is clearly intrusive. The lack of faulting does not preclude movement of the CS relative to the Southern Mountains Complex and the rocks outside the Main Ring Fault, as a zone of ultrabasic breccia intervenes between the layered CS and the contact. That the CS is also intrusive into the Papadil gabbro, and thus postdates it, was suggested by Forster (1980) on the basis of clouding of the plagioclase in the gabbro, attributed by Hughes (1955) to reheating. The contact with the Southern Mountains Complex is, however, partially lined with lenses of gabbro petrologically distinct from both the Papadil Gabbro and the Marginal Gabbro at Bealach an Fhuarain (section 4.6)

In summary, the CS is intrusive into the ELS, the WLS, the Southern Mountains Complex and the rocks outside the Main Ring Fault. It is, however, not in situ, and has subsided with repect to the enclosing rock bodies.

2.3 Brittle Deformation.

2.3.1 Regional Faulting Patterns.

Fig. 2.3 shows all faults mapped in the Trallval area, with displacements of 2 m. or more. Rose diagrams summarise the orientations of faults and dykes in each of the numbered domains and the following observations can be made :

(1) Near the Long Loch Fault (domains 4 and 6), faults and fractures are controlled by the N-S orientation of the Long Loch Fault.

(2) This is also a preferred orientation further east (domains 5 and 8). In these, however, there is a second preferred NW-SE orientation.

(3) This NW-SE orientation becomes dominant in domain 1, further east.

(4) Near Trallval, faults and fractures define a bimodal distribution with preferred orientations E-W and NE-SW; the former dominates in domain 2, and the latter in domains 3 and 9.

(5) Domain 7, to the west of the fault, is similar to domain 9.

In the Trallval area, there is therefore no radial distribution of faults or dykes, which cluster instead around NE-SW and NW-SE trends, with a N-S trend near the Long Loch Fault. This conclusion is similar to that reached by McClurg (1982) for the Barkeval-Long Loch area and Forster (1980) for dykes on Rhum outwith the ultrabasic complex. In addition there is a strong E-W preferred orientation near the centre of the complex (domain 2). In this area, the gently inclined layering in the ultrabasic rocks and the more steeply dipping sheets of gabbro strike E-W parallel to the axis of the ELS complex. These relatively superficial features locally controlled the fracturing.

2.3.2 The Long Loch Fault.

This fault maintains a N-S orientation along most of its length from the north coast of Rhum to the south coast at Inbhir Gill, except for an an eastwards bulge in Fiachanis, which sprouts splays of faults near the points of inflexion east of Ruinsival summit and west of Trallval. From the stratigraphy of the CS, minimum vertical displacements of 200 m. and 450 m. (downthrow to the west) can be inferred for the Long Loch area and the Ruinsival area (fig. 3.4). Right-lateral motion of 750 m. is evident from the displacement of the Main Ring Fault in central Rhum (Dunham and Emeleus, 1967). Lateral movement cannot be precisely estimated in the Trallval area, due to the large vertical displacement and the lack of reliable markers. The displa-

cement on the approximately vertical ultrabasic breccia zones does suggest a minimum dextral motion of 600 m. (correlating the Papadil zone with the Ruinsival Forked Zone and the Leac a Chaisteil zone with the Fiachanis zone, see fig. 3.5). On the surface, the Long Loch Fault usually forms a deep gully except where covered by moraine as in Fiachanis. To the southeast of Ruinsival summit, the fault is exposed as an area of cataclased, highly serpentinised dunitic peridotite about 60 m. wide. Carbonate veins suggest hydrothermal activity occurred along the fault.

2.3.3 Other Faults.

On Trallval and Ruinsival, there are numerous faults subsidiary to the CS / ELS contact and the Long Loch Fault, respectively. Neither transverse nor vertical displacements exceed 20 m., and the direction of downthrow is in the same sense as that of the related major faults. The consistency of this faulting pattern on Trallval strengthens the case for the subsidence of the CS. The An't Snidhe faults are an independent major couple, bounding a wedge which has been relatively upfaulted some 500 m., based on the stratigraphical offset within the CS. Rotation of the layering within the wedge (fig. 2.2) suggests that there has been slightly greater uplift along the northwestern brach. The rotation of the layering correlates with the vergence of the slumps within the wedge. The latter may therefore be syntectonic, i.e. the An't Snidhe faults predate the final consolidation of the ultrabasic rocks.

2.4 Age Relations within the Trallval Area.

Table 2.1 is entirely based on cross-cutting relationships observed in the field and those deduced from the map patterns. The contact relations for individual rock units are discussed in detail in the relevant chapters.

GENERALISED SEQUENCE		SEQUENCE OF EVENTS FOR INDIVIDUAL AREAS					
		BARKEVAL	EAST TRALLVAL	WEST TRALLVAL	RUINSIVAL	SOUTH RUINSIVAL	PAPADIL
late evolved dykes	basic dykes		Chilled tholeiitic andesite dyke	chilled dolerite dyke	microdiorite hybrid dyke		dolerite dykes
plugs		plug		plug	plug		plug and olivine gabbro
gabbros				Glen Harris olivine gabbro	olivine gabbro	olivine gabbro	
picrites		picrites	picrites	picrites			
ultrabasic breccia zones (UBM)		UBM		UBM	UBM	UBM	UBM
gabbros				W Trallval gabbro	olivine gabbro		
Central Series				Central Series	Central Series	Central Series	Central Series
Olivine-free gabbro			marginal olivine-free gabbro	olivine-free gabbro			olivine-free gabbro
Gabbros		olivine gabbro	olivine gabbro	olivine gabbro			
Eastern Layered Series (ELS)		ELS	ELS	ELS			

TABLE 2.1 AGE RELATIONS IN THE TRALLVAL AREA.

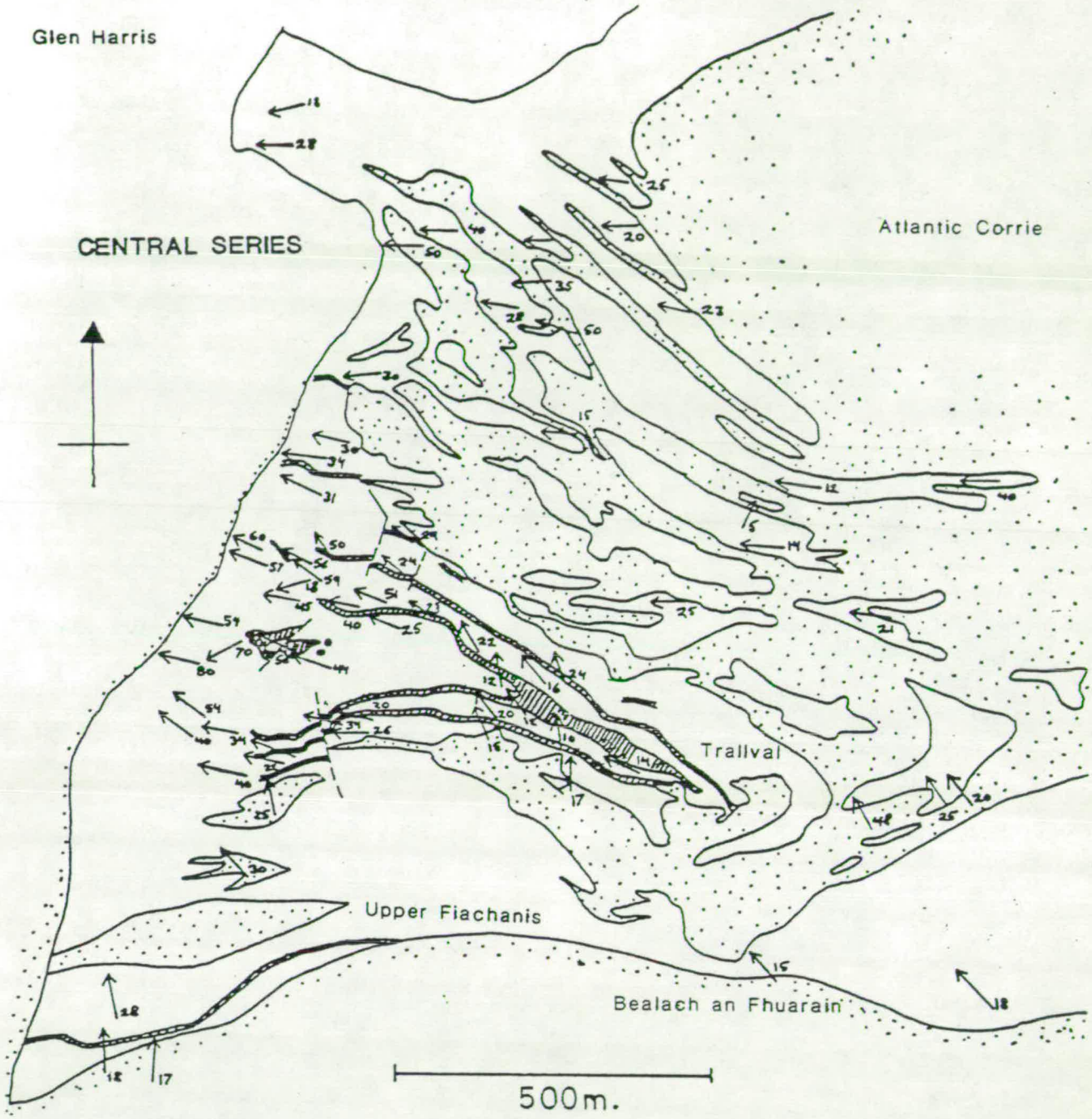

FIG. 2.1 The internal structure of the Trallval Layered Series. Gabbro is stippled and the main allivalites are cross-hatched. Arrows indicate the dip of the igneous layering in degrees. The Trallval Layered Series form that part of the Eastern Layered Series within the author's study area, the Trallval area (see fig. 1.1).

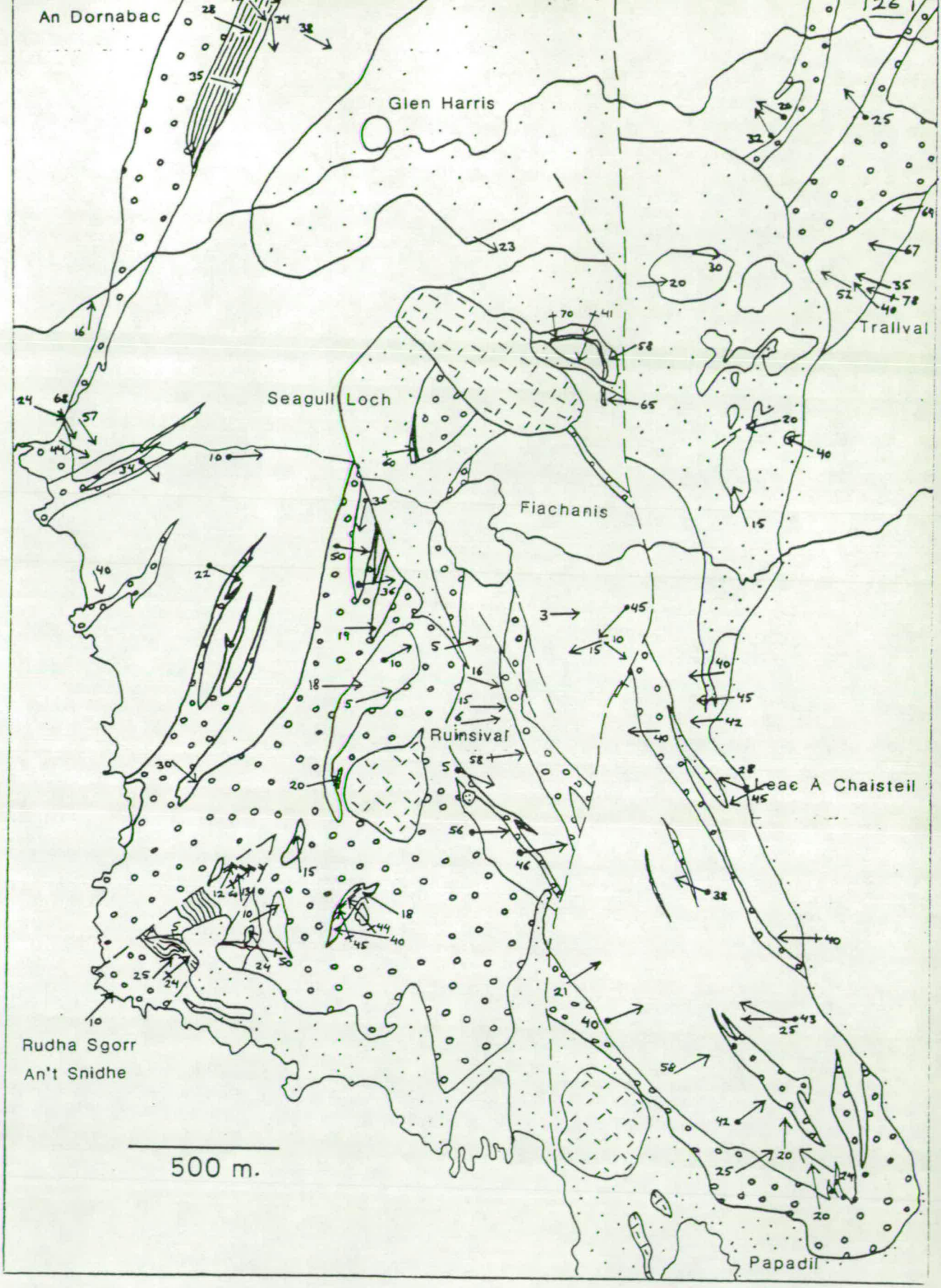

FIG. 2.2 The internal structure of the Central Series in the Trallval area: gabbro (stippled), intrusive ultrabasic plugs (hatched), ultrabasic breccia (circles), allivalite (lined) and peridotite (unornamented) are distinguished. Igneous layering is shown for peridotite (plain arrows), allivalite (crossed arrows) and chromitite (dotted arrows).

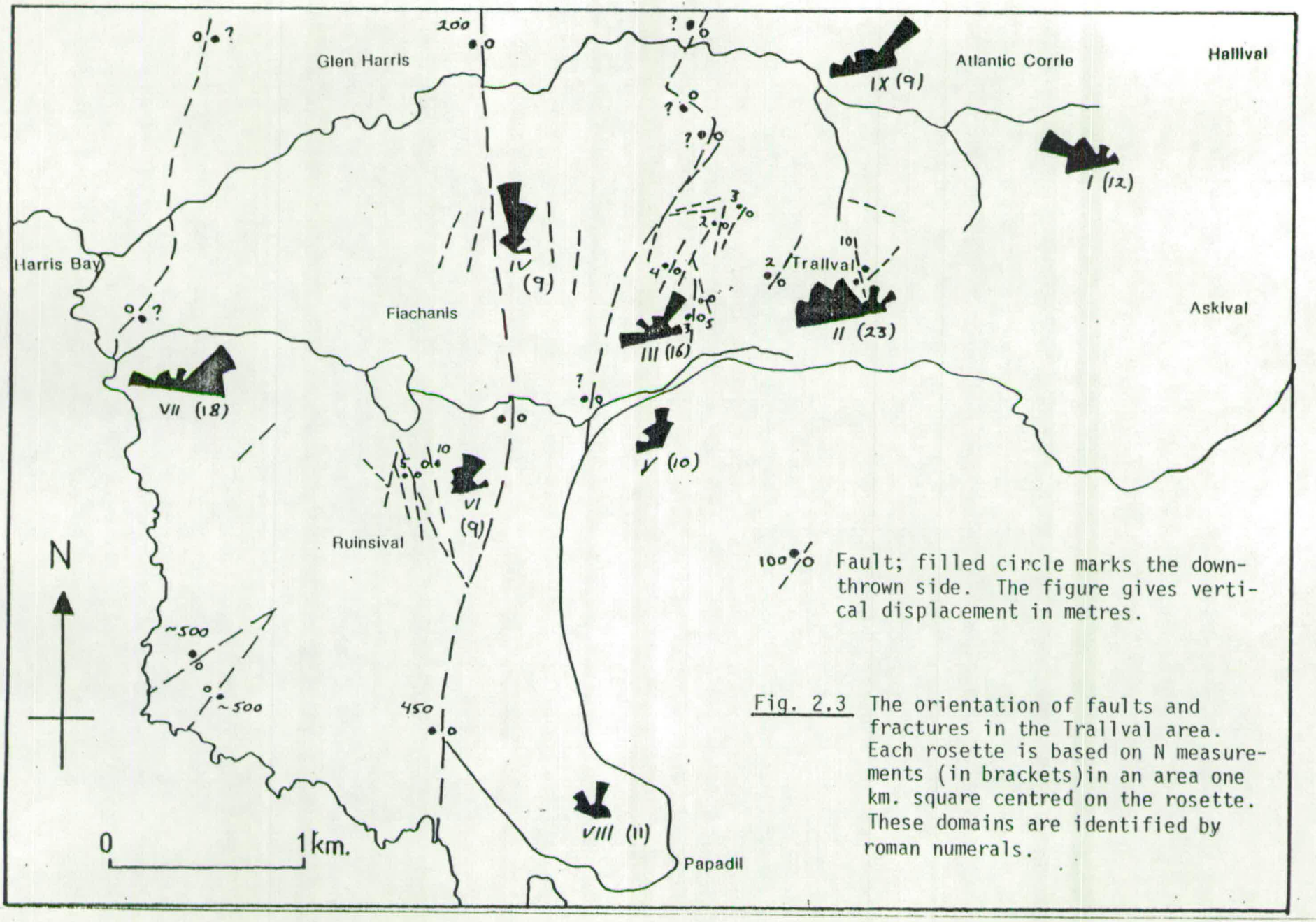

Fig. 2.3 The orientation of faults and fractures in the Trallval area. Each rosette is based on N measurements (in brackets)in an area one km. square centred on the rosette. These domains are identified by roman numerals.

CHAPTER 3

THE ULTRABASIC ROCKS - FIELD DATA.

The stratigraphy of the layered series is presented first, together with an account of the distribution of the ultrabasic plugs and breccia zones. The layered series is then compared with the intrusive plugs and breccias in terms of textures and structures observed in the field.

The nomenclature adopted here is similar to that recommended by Irvine (1982) is his review of the terminology for layered intrusions. The essential minerals of the Rhum ultrabasic rocks are olivine, plagioclase, clinopyroxene and spinel; accessory minerals, such as mica and amphibole rarely exceed 1-2 modal %. For each rock, these can be separated into, (i), at least partly and, (ii), entirely intercumulus phases (Wager et al., 1960). Most of the peridotite layers in the ELS, for instance, have cumulus olivine and spinel and postcumulus plagioclase and clinopyroxene. More than half of the cumulus fraction of the allivalite layers consists of plagioclase. A strict scheme of classification is suggested in table 3.1. In addtion, rocks with 50% or more chrome-spinel are called chromitite and those with more than 30% cumulus clinopyroxene, clinopyroxene-rich troctolite which grades into gabbro. The peridotites of the plugs and breccias commonly have much plagioclase which looks partly cumulus (see section 5.2.2). These are usually classified as feldspathic peridotite and where the plagioclase forms 40 to 50 % of the rock, as highly feldspathic peridotite.

3.1 The Stratigraphy of the Trallval Layered Series.

Seven complete and two incomplete macro-rhythmic units (average thickness: 65 m.) of peridotite capped by a thinner allivalite form a 500 m. thick succession on Trallval (fig. 3.1). The succession has been repeatedly intruded by thick sheets of gabbro and isolated from the ELS on Askival by the Atlantic Corrie Gabbro. Though texturally and structurally similar to Brown's (1956) units, the layered series on Trallval has much thinner allivalites. The correlation proposed in fig. 3.1 is based on the following features:

(1) Allivalite thickness. Whereas the 5 lower allivalites on Trall-

val are less than 1 m. thick, the top 3 vary in thickness from 4 to 8 m. On Askival, U13, U14 and U15 have allivalites 28 to 54 m. thick while lower allivalites vary from 4 to 8 m.

(2) Unit thickness. Correlation of the two thickest units on Trallval with the thickest on Hallival and Askival (U10 and U11) gives an identical result to the correlation based on relative allivalite thickness.

The Trallval units are thus tentatively correlated with units 9 to 15 fo the ELS on Hallival and Askival. In addition, part of the peridotite layer of a newly defined unit, U16, caps the succession. The geographical distribution of each unit is shown in fig. 3.2. Several marker horizons confirm the above correlation:

(1) On Askival, the allivalite of U14 is the most strongly deformed by slumping (Brown, 1956 and the author's own observations). On Trallval, it, too, is the most disturbed allivalite. Both on Hallival and Trallval, the allivalite of U13 is also slumped.

(2) On Barkeval, cumulus pyroxene appears in U8 and U9, and in U8, U9, U10 and U14 on Hallival. On Trallval, cumulus pyroxene is found in U8 and U14.

(3) Chromitite laminae occur at the base of U8, U12 and U15 in the Hallival - Barkeval area (Brown, 1956; McClurg, 1982), and within the peridotite of U8, U10, U11 and U14. Basal chromitites only occur locally in U12, U13 and U15 on Trallval (the base of U8 is not exposed) and discontinuous chromitites within the peridotite of U9, U10, U11, U14 and U15.

The correlation is further corroborated by the correlation of cyclic units, as defined by the cryptic variation in mineral chemistry. Nevertheless, it is clear from fig. 3.1 that there are remarkable, though progressive changes in unit thickness and lithology from Hallival to west Trallval, via Askival and east Trallval. If there has been no vertical faulting between Askival and Trallval, the correlation suggested above implies an average westward dip of the igneous layering of less than 5^{o}.

3.2 The Stratigraphy of the Central Series.

As Fig. 3.3 shows, there is more extreme macro-unit and allivalite thickness variation (average unit thickness: 150 m.) within the CS,

which has a maximum thickness in excess of 1100 m.. McClurg (1982) proposed a stratigraphy for the CS on the basis of her mapping in the Barkeval - Long Loch area. This scheme is revised on the basis of new information (Table 3.2):

(1) The Outer Breccia Member is here considered a marginal breccia partially lining the outer contact of the CS as it does not bear a consistent stratigraphical relationship to the layered units of the series. Such a marginal breccia also occurs at Papadil, where it is in contact with the Long Loch Group. Adjacent to other exposures of the Dornabac Member it may (as at Rubha Sgorr an't Snidhe) or may not be present (as at Leac a Chaisteil).

(2) The Dornabac Member is retained as defined by McClurg (1982)- it corresponds to Wadsworth's (1961) Dornabac Series.

(3) The Long Loch Member is renamed Long Loch Group , as it consists of three macro-rhythmic units of peridotite followed by allivalite. As the lower two allivalites are not seen in the Ruinsival section, the group is taken as the mapping unit, though variations in mineral chemistry allow correlation of the Ruinsival section with the lithologically defined units to the north (section 5.7.2.5).

(4) The Ruinsival Member, as mapped on Barkeval, is re-interpreted as an intrusive peridotite plug. The heterogeneous feldspathic peridotite with poorly developed, vertical layering is quite unlike the succession of dunite, chromitite and sub-horizontally layered dunitic peridotite on Ruinsival.

The Ruinsival Group consists of two macro-rhythmic units and corresponds to Wadsworth's (1961) Upper Ruinsival Series. The vertical traverses in Fig. 3.3 are correlated on the sharp contact between the distinctive streaky allivalites of the Dornabac Member and the dunitic peridotite of the Long Loch Group; this is correlated with the contact between feldspathic peridotite and dunitic peridotite at Leac a Chaisteil on the basis of the sharp regressive change in the mineral chemistry across this contact (section 5.7.2.5). The regular thickness and uniform dunitic composition of the lower member of the Long Loch Group with its persistent allivalite (only absent in the Ruinsival section) supports this correlation. Fig. 3.4 shows the distribution of the subdivisions of the CS over the mapped ground.

3.3 The Distribution and Structure of the Intrusive Plugs and Breccia Zones.

Donaldson (1975) noted that the five elongate zones of ultrabasic breccia mapped at the time converged on a point near the Long Loch. Fig. 3.5 shows all breccia zones mapped by the author. The breccia zones are almost entirely restricted to the CS (a zone about a metre wide and 30 m. long occurs near point X in the ELS). Their axes of elongation converge on one of four points. The set of zones converging on a single such focus are here described as a system; all breccia zones are thus conveniently separated into four systems. The zones which make up the Dornabac system are not shown on the figure as they do not appear on McClurg's (1982) map, although she does state that intrusive breccias are common between An Dornabac and the Long Loch Fault. Fig. 3.5 suggests the zones represent radial fracture systems, the breccia forming the infill of the fractures. The orientation of the flow-banding in the breccias often parallels the margins of the zones (as in the Trallval system). In some cases, however, it is consistently oblique to these, especially in the Papadil system (section 3.8.3).

Ultrabasic plugs in the Trallval area all occur within 1.5 km. of the Long Loch Fault The mean diameter of the plugs varies from 210 m. for the Ruinsival plug to 610 m. for the Barkeval plug. Smaller ultrabasic plugs occur further away from the fault, within the complex (McClurg, 1982; Butcher, pers. comm.). Where it can be measured, the steep layering consistently parallels the margins of the plugs. The distribution of the two lithologies of the Papadil plug also follows a concentric pattern. All plugs appear distinctly on aerial photographs.

3.4 An Introduction to Textures and Layering.

Subtle variations in the distribution of the postcumulus phases in the peridotites has produced an astonishing diversity of textures, generally succeeding one another in layers closely paralleling the lithological peridotite/allivalite layering.

3.4.1 Textures

Nearly all textural varieties are found both in the layered series and in the plugs and breccias. Examples of the main textural types are illustrated in Plates 3.1 to 3.4 and briefly described below. All textural types reach varying degrees of coarseness.

Coralline Texture: olivine-enclosing clinopyroxene oikocrysts and/or clusters of olivine are enclosed by an interconnected framework of plagioclase oikocrysts (Plate 3.1).

Dendritic Texture: the plagioclase oikocrysts form discrete entities or clusters (Plate 3.2). The name derives from the commonly radiating or branching morphologies of these clusters, which differ from the macro-spherulo-poikiloblastic texture (Donaldson et al., 1973) in that each clump consists of a number of intercumulus oikocrysts rather than a single one. With an increase in the density of the plagioclase, the texture grades into coralline texture.

Cluster texture: cumulus feldspar forms the node of the clusters (Plate 3.3). With an increase in the content of cumulus feldspar, and in the density of the clusters, peridotite may grade into troctolite (Plate 3.9).

Harrisitic Texture: peridotite with a distinctive hopper or skeletal olivine morphology, ascribed to supercooling (Donaldson, 1974) forms two types of layers (Wadsworth, 1961) :

(1) Harrisite, forming flat-bottomed and wavy-topped layers of elongate, skeletal ("harrisitic") olivines (up to 2 m. high) oriented perpendicular to the layering.

(2) Irregular harrisite, consisting of "harrisitic" olivines, 2 to 20 cm. long in a random orientation (Plate 3.4).

A complete gradation exists between irregular harrisite and normal peridotite as the size of the olivine and the complexity of its shape approach that of granular olivine. This trend correlates roughly with modal decrease in postcumulus plagioclase. Layers with the intermediate type of olivine (0.5 to 2.0 cm. long) are described as protoharrisite.

3.4.2 Layering.

Monomineralic layers are rare on Rhum; even dunite and anorthosite almost always have a small amount of postcumulus pyroxene, plagioclase or olivine. Cumulus phase layering involving, (i), olivine and, (ii), olivine + feldspar produces the peridotite/allivalite layering. Some of the minor layering within allivalites is due to the appearance and termination of cumulus clinopyroxene. Contacts are usually sharp (plate 3.5). Modal, textural and grain-size layering are ubiquitous in the peridotite of each unit, while modal layering dominates in the allivalite. The most common types of layering are described in

detail for each unit in sections 3.5 and 3.6, and illustrated in Plates 3.6 to 3.9. The term banding is used to distinguish diffuse, laterally impersistent, often undulating layering typical of the ultrabasic plugs from the planar, sharply defined, continuous layering, typical of the layered series, where banding is only rarely seen (see Irvine, 1982). Layering is often modified by subsequent processes such as brecciation, slumping, shearing, diapirism, loading, replacement and the percolation and expulsion of intercumulus liquid (Plates 3.10 to 3.15).

3.5 Field Characteristics of the Trallval Series.

The Trallval Series is best exposed on the northern and southern slopes of West Trallval (traverses 6 and 7 on Fig. 3.1; GR 373 954). It is from this area that the type section of each unit is described. Other exposures of the unit are examined in reference to the type section Unless stated otherwise, layers are about 0.5 to 2.0 m. thick, and laminae less than 5 cm. thick.

3.5.1 Unit 8.

This unit is poorly exposed as it outcrops on the floor of the glens and is intensively intruded by sheets of gabbro.

Type Section: 82 m. of peridotite, 2 m. of allivalite.

The lowest part of the unit is feldspathic peridotite with coarse, coralline texture, layers of protoharrisite (1 m. thick or less) and some of dunitic peridotite. About 20 m. up, layers of protoharrisite up to 3 m. thick, often with flattened ellipsoidal patches of irregular harrisite (each consists of a number of sheaves of parallel olivines up to 6 cm. long, randomly oriented and separated by coarse interstitial plagioclase and pyroxene) alternate with layers of harrisite (less than 1 m. thick) and feldspathic peridotite, some of which have irregularly shaped pods of protoharrisite. In Glen Harris, there is considerable internal brecciation, with blocks of the above lithologies and fragments of chromitite (ca. 5 cm. across) in thick layers of feldspathic peridotite. The brecciation is often local, being restricted to patches about 1 m. across, with a high content of postcumulus feldspar. About 50 m. up, feldspathic peridotite with modal layering alternates with coralline-textured pyroxene-rich feldspathic peridotite. Where the underlying layer is brecciated, the micro-layering is intersected by vertical streamers (section 3.5.7). The alliva-

lite is underlain by ca. 2 m. of feldspathic peridotite, with chromitite layering, which overlies about 5 m. of heterogeneous feldspathic peridotite with pods of irregular harrisite, small lumps of chromitite and slivers of allivalite with partial rims of spinel. The contact between the well-laminated, plagioclase-rich allivalite and the peridotite below is partly resorbed: it is sharp with upward incursions (fingers) of peridotite which truncate the allivalite lamination and indicate replacement of allivalite by peridotite. The allivalite has a 10 cm. thick anorthosite layer near the top.

The Unit Elsewhere:

- In Glen Dibidil, the allivalite is only 15 cm. thick, but equally rich in plagioclase.
- In East Trallval, the allivalite is fragmented, and immersed in feldthic peridotite which has modal banding, oblique to a 5 mm. spinel horizon (GR 3830 9567).
- In South Trallval, the allivalite has streaky layering, some pyroxene-rich laminae, and shows slumping structures. Locally, it is fragmented, the blocks sitting in a feldspathic peridotite matrix with chromitite lumps (GR 3686 9478).

3.5.2 Unit 9

The distribution of this unit is similar to that of U8 and it is equally heavily injected with sheets of gabbro, obscuring layering and stratigraphy.

Type Section: 50 m. of peridotite, 2 m. of allivalite.

The unit has a basal chromitite lining 1 or 2 crystals thick. The lower 5 m. consist of micro-layered feldspathic peridotite layers irregularly alternating with uniform peridotite with pods, 0.2 to 1.0 m. across, of protoharrisite and irregular harrisite. The uniform peridotite also includes 4 to 10 cm. thick layers and lenses of dunite. The micro-layering is persistent, slightly undulating, and due to laminae with coarse olivine and a high intercumulus feldspar content grading up into a finer grained peridotite. A beautifully developed chromitite zone forms the next 15 to 20 m. Chromite and intercumulus feldspar enriched laminae weather out strongly (Plate 3.6) and form regular and continuous ribs in groups of 3 to 6, with variable spacing forming a layer about 0.5 m. wide. These layers are repeated at 2 to 6 m. intervals. One of the laminae is a 1 cm. thick chromitite (GR

3753 9607). Vertical, pipe-like bodies of pyroxene-rich peridotite, with oblique offshoots, replace the feldspathic peridotite locally, but do not affect the chromitite which continues as a plagioclase-free lamina. Coralline feldspathic peridotite overlies the chromitite-layered zone, although it has a 3 cm. thick lamina of disseminated spinel with some fragments of chromitite, 3 m. up; this lamina shows loading features (GR 3689 9483). Above this, several layers, 2 to 3 m. thick, of protoharrisite, which have coarse olivine at the bottom (in one layer 5 cm. long on average) fine upwards to granular peridotite over the top 30 cm. The protoharrisite is succeeded by a thin sequence of grain-size and modally layered coralline feldspathic peridotite, in which coarse, feldspathic laminae (olivine ca. 1 cm. across) alternate with granular peridotite (olivine less than 2 mm. across) with only scattered coarse olivine. About 35 m. up, peridotite with large, isolated clusters (up to 1 m. across, Plate 3.3) shows textural layering: thin layers of clusters alternate with thin layers of merging clusters.

The 2 to 3 m. below the allivalite consist of layered, coralline, highly feldspathic peridotite; much of the feldspar is cumulus, forming about 30 % of the rock, while olivine only forms about 35 %. The allivalite is 1.8 m. thick and consists of mafic troctolite with a 10 to 20 cm. thick, discontinuous cap of anorthosite. Near the bottom, it has 5 to 10 cm. long clasts of peridotite, a discontinuous layer of feldspathic peridotite and a zone of folded anorthosite clasts about 1 m. up. At (GR 3758 9592), the allivalite, just above a sheet of gabbro, is strongly folded and has a 20 cm. sheath of structureless peridotite around the convolutions of its upper surface, which cuts the layering in the overlying unit.

The Unit Elsewhere: the peridotite is not well enough exposed to demonstrate lateral variation, however, on the western slopes of Askival, the allivalite consists of 6 m. of mafic troctolite and has a layer of peridotite near the middle. Near the bottom, the upper contact of a layer of mafic troctolite in olivine-poor troctolite shows well-developed flames.

3.5.3 Unit 10

This thick unit is dissected into separate masses by the Atlantic Corrie Gabbro and veined by thinner sheets of gabbro throughout its outcrop (Brown, 1956, noted the abundance of coarse pyroxene-plagioclase veins in this unit on Hallival).

Type Section: 89 m. of peridotite, 2 m. of allivalite, a subsidiary allivalite at 70 m.

Locally, a basal chromitite lining about 5 crystals thick underlies a 10 m. layer of coralline, highly feldspathic peridotite with modal layering and a few 50 cm. layers of protoharrisite. Then, over 30 to 40 m., the peridotite is massive, feldspathic, coralline with a few angular blocks of peridotite and troctolite, followed by an abrupt transition to regularly layered dendritic feldspathic peridotite (the layering is partly modal, partly due to variation in the coarseness of the texture). After about 5 m., there is a return to the homogeneous, coralline peridotite, with, however, some pods of protoharrisite, for another 20 m. or so.

Below the lower allivalite, there is about 5 m. of felspathic peridotite with sharp, regularly spaced, slightly undulating chromitite layering and a few thin layers of protoharrisite. Between the ribs enriched in plagioclase and spinel, the layers are graded from feldspathic peridotite at the bottom to dunitic peridotite at the top. The top metre is grain-size layered: layers with coarse olivine and elongate pyroxene oikocrysts alternate with layers coarsening upwards from fine-grained peridotite to protoharrisite.

The lower allivalite is 20 cm. thick and lined along its lower, fingered contact, by a sprinkling of chromite. It is well-laminated and has anorthosite laminae. The peridotite sandwiched between the two layers of allivalite, or sandwich peridotite, is highly feldspathic and well-layered with anorthosite laminae parallel to the modal layering, and scattered fragments of troctolite. The contact with the upper allivalite is highly irregular: at (GR 3736 9577) a pendent of allivalite slumps 1.5 m. down into the peridotite. The upper allivalite (of variable thickness, 0.2 to 1.5 m. across) is poor in olivine, laminated, and has thin anorthosite layers along the top and bottom. The topmost anorthosite has a thin chromitite within

it (the allivalite of U10 on Hallival has much coarse spinel according to Brown, 1956). The upper contact is interleaved with lenticular layers of peridotite.

The Unit Elsewhere:

- Along the northeastern wall of Atlantic Corrie, the peridotite differs mainly in having occasional layers of harrisite, 0.5 m. thick with olivine up to 10 cm. long, near the middle, and thicker and more abundant layers of protoharrisite below the allivalite. The allivalite is 3 to 5 m. thick, has pyroxene-rich laminae, anorthosite layers near the top, a feldspathic peridotite layer about 2 m. up, an interleaved upper contact and a partly resorbed lower contact.
- Below and to the west of Askival, the peridotite has layers of dunitic peridotite near the bottom and fragments of chromitite in the chromitite-layered zone near the top. The allivalite has a partly resorbed lower contact and consists of a lower layer, and intervening peridotite, and an upper layer, respectively 6 m., 4 m. and 2 m. thick. The lower troctolite is rich in cumulus pyroxene in 1 to 6 cm. thick laminae which may bifurcate, thicken or peter out. The top allivalite has internal anastomosing shear zones (sub-horizontal) separating unlaminated troctolite lithons. Near the top, it has thin anorthosite laminae and some slump folds. Further south, the lower allivalite degenerates into trails of anorthosite clasts, 1 to 2 cm. across, which locally aggregate into elongate lenses, 0.05 to 1.50 m. at most, at (GR 3873 9512).
- Chromitite layering also occurs to the east of Hallival over 6 m. near the top of the peridotite. Harrisite layers are common, while the allivalite is much thicker (24 m.) but also has anorthosite layers near the top, much coarse chromite and an interleaved upper contact.
- In East Trallval, protoharrisite patches occur in the lower layer of uniform peridotite and well-developed banks of harrisite in the upper uniform layer together with layers of protoharrisite, several of which have chromitite laminae (one is 4 cm. thick but rapidly splits into 3 thinner laminae). Troctolite fragments occur at various levels in the peridotite and near the top. These occur in a zone with several chromitites which line some of the troctolite fragments. Cumulus pyroxene in 3 to 6 mm. thick laminae occurs near the top of the peridotite.

3.5.4 Unit 11.

Sheets of gabbro are scarce in West Trallval. To the east, however, thick bodies of gabbro have stoped through most of the unit. U11 is well exposed on the eastern wall of Atlantic Corrie.

Type Section: 82 m. of peridotite, 1 m. of allivalite.

Coralline feldspathic peridotite with excellent modal layering forms the first 30 m. of the unit. About 5 m. down from the top of this layer, a 3 m.-long, pillow-shaped mass of peridotite, possibly detached from the overlying layer as a ball-and-pillow structure, sits in the feldspathic peridotite and does not disturb the layering. Four m. from the bottom, the coralline peridotite has a lens of cumulus pyroxene, 20 cm. across. The middle part of the unit consists of 5 to 10 m. thick layers of layered dendritic peridotite with a 2 to 3 m. zone of chromitite layering, and subsidiary layers of massive coralline peridotite. The top 10 m. of peridotite are highly feldspathic, with good modal and chromitite layering. There is a layer of heterogeneous peridotite with both angular and shapeless fragments of troctolite 5 m. below the allivalite. The allivalite itself is streaky and consists of ca. 10 cm. thick, sheared, lenticular layers of troctolite, often folded and even convolute, in a feldspatic peridotite matrix.

The Unit Elsewhere:

- The Atlantic Corrie section starts with 20 m. of massive, coralline feldspathic peridotite, followed by alternating irregular harrisite and peridotite layers, each grading into the other: some harrisite layers (ca. 1 m. thick), flat-bottomed, pass up into dunite via a wavy transitional zone; coarse pyroxene and plagioclase (similar to the interstitial material in the harrisite) fills cracks extending down into the underlying dunite. About 70 m. up, unlayered coralline peridotite is interbedded with 1 cm. laminae of protoharrisite. Vertical pipes of wehrlite (15 to 20 cm. across) with 5 cm. thick feldspathic peridotite margins, cut the layering and are constricted at the protoharrisite laminae (GR 3900 9656). There is no correlation between the coarseness and the thickness of the harrisite layers. The unit has three thin horizons of allivalite.

The lower is highly variable in thickness:from a string of thin anorthosite lenses, it thickens to an 8 m. thick mass of slumped troc-

tolite about 1 km. to the south, where it has peridotite clasts near its base. The troctolite is mafic, with a 15 cm. lenticular layer of anorthosite and its upper contact overlain by chromitite up to 3 cm. thick which is continuous even where the allivalite is not, and may line the lower, the upper or both surfaces of thin allivalite lenses (less than 30 cm. thick).

The middle allivalite is a similarly discontinuous layer with a continuous chromitite and merges with the lower allivalite to the south of Godfrey's Gulch (GR 3893 9675) which gives good exposures of the allivalites and chromitites. The lower and middle allivalite are separated by 6 m. here and it is another 5 to 10 m. up to a 1 to 2 m. thick layer of mafic troctolite with several 10 cm. thick layers of peridotite at the bottom and a top half with low-angle planar cross-lamination. The peridotite between the allivalites is feldspathic with some layers of protoharrisite.

- On Askival, the basal massive layer seen in Atlantic Corrie is reduced to 6 m. Only the lower of the 3 allivalites continues this far south. It is 2 to 3 m. thick, has a 5 cm. capping of anorthosite and is generally mafic, with a locally resorbed contact.
- A double allivalite reappears in East Trallval in a 5 m. zone with 2 or 3 chromitites. Layers of protoharrisite and of feldspathic peridotite with protoharrisite pods are common in the lower 60 m. of peridotite. There are layers of dunite, but none of harrisite. At several levels in the upper half of the peridotite, there are vaguely defined layers of uniform feldspathic peridotite with fragments of poorly laminated troctolite.

3.5.5 Unit 12

This is the lowest unit which shows signs of steepening close to the faulted contact with the CS, and the highest unit to be extensively intruded by gabbro.

Type Section: 51 m. of peridotite, 2 m. of allivalite.

The basal 10 m. of dendritic feldspathic peridotite is discontinuously layered on a small scale and passes up into texturally layered feldspathic peridotite (alternating coarse and fine dendritic texture), with some internal brecciation. From 20 to 30 cm. up, coralline feldspathic peridotite is interlayered with olivine-rich peridotite with flattened pods of feldspathic peridotite and , near the top of the

layer, pods of harrisite and protoharrisite. The top 20 m. have the best examples of dendritic clusters and cluster-layering in the ELS: the sequence consists of a rhythmic succession of layers with clusters along the top and a plagioclase depleted lower part (Plate 3.8). High in the sequence, layers of isolated, drooping clusters alternate with layers of densely packed, flattened clusters. The transition may be accompanied by an increase in the size of the individual clusters. Plate 3.9 shows a texturally graded sequence: clusters increase from 4 cm. to 40 cm. across, eventually yielding a thin sequence of amalgamated clusters, or troctolite. The cluster-layered sequence also includes some layers of modally layered dendritic peridotite (Plate 3.2).

The allivalite consists of two thin layers of coralline peridotite with troctolite schlieren (Plate 3.14), with a 6 m. thick sandwich peridotite. The schlieren are at most 25 cm. thick. The lower layer is 40 cm. thick, whereas the upper layer is only 20 cm. thick, includes schlieren of anorthosite, 5 to 10 cm. thick, and passes laterally into layered dendritic peridotite (GR 3714 9518). The disposition of the schlieren-bearing layers reflects relic slump or loading structures, presumably within a (now partially replaced) sequence of allivalite and peridotite layers.

The Unit Elsewhere:

- Below Hallival and Askival U12 has a continuous basal lamina of chromitite. On Askival, fragments of chromitite occur about 5 cm. up into the overlying peridotite which has harrisite layers near the top. The allivalite, a 4 m. layer of massive mafic troctolite, has a few laminae of anorthosite.
- In East Trallval, zones of mélange (fragmented troctolite in a matrix of dendritic peridotite) occur at the bottom, where the mélange also has fragments of chromitite and pods of protoharrisite. One mélange zone, at (GR 3775 9535) is a direct extension of a tongue of troctolitic gabbro protruding into the peridotite. The fragments here, at the bottom of U12, are thickly coated with chromitite rims up to 10 cm. thick. Some of the matrix peridotite in the mélange zones has modal banding, undisturbed by the fragments. In coralline peridotite around a troctolite block, at (GR 3794 9513), concentric and planar modal layering is developed in response to the presence of the fragment as

no layering is observed elsewhere in the area (Fig. 3.9). The allivalite is locally coherent, up to 5 m. thick, mostly mafic troctolite and poorly laminated.

3.5.6 Unit 13

Although the exposure is not continuous, gabbro intrudes only a small fraction of the outcrop area. To the west, however, the steepness of the layering suddenly increases with attenuation of the allivalite and disordering of the internal structure of the peridotite. This may be due to mobilisation of the unit as a drag effect resulting from the subsidence of the CS (section 2.2.3).

The Type Section: 38 m. of peridotite, 4 m. of allivalite, subsidiary allivalite at 22 m.

A chromitite, 5 mm. thick, forms the contact between the anorthosite at the top of U12 and the dunitic peridotite in SW (but not in NW) Trallval. Clusters of feldspathic peridotite, downward radiating, extend into the 2 to 3 m. dunitic layer at its upper contact with dendritic feldspathic peridotite, which has both modal and textural layering (due to a variation in cluster size). Layers of dunitic peridotite alternate with modally layered feldspathic peridotite and dunitic peridotite with isolated 50 cm. clusters from 10 to 25 m. up. The higher part of the unit is regularly layered with 1 cm. laminae of dunitic peridotite alternating with laminae of coralline feldspathic peridotite. The layer contacts undulate with a wavelength of 2 to 4 m. (amplitude 5 to 10 cm.), and are dimpled on a 2 to 3 cm. scale. Approximately 16 m. below the allivalite, there is a zone of fragmented troctolite in dendritic peridotite, which occurs on the southern slope of Trallval only and becomes a coherent, laminated layer of troctolite to the west, 20 to 30 cm. thick. At 32 m., a peculiar textural phenomenon occurs in the form of concentric shells of dendritic peridotite alternating with olivine-rich peridotite to form huge balls, up to 6 m. in diameter, and slightly flattened (Plate 3.16; GE 3743 9527). The modally controlled layering surrounds a core of dunitic peridotite.

The allivalite is 3 to 4 m. thick; the entire layer has convolute laminations forming slump structures, outlined by pyroxene-rich laminae and thin layers of feldspathic peridotite. The top 10 cm. has several planar intercalations of peridotite. Folded, single laminae can be traced from near the top to near the bottom of the layer, indi-

cating that the layer has been deformed as one unit. The allivalite has a discontinuous 20 cm. thick anorthosite layer.

The Unit Elsewhere:

- 150 m. east of the CS contact, the allivalite and the layering in the peridotite rapidly steepen to 40 to 50°, and the allivalite is only 1 to 2 m. thick.
- In East Trallval, the basal chromitite horizon is undiminished in thickness and locally splits into a doublet with 5 cm. of intervening dunitic peridotite; the lamina vanishes westwards. The feldspathic peridotite above the dunitic peridotite has pods of harrisite and protoharrisite. Layeres of protoharrisite also occur near the middle of the unit. The allivalite breaks up into a mélange from west to east over 200 m. along strike, but where coherent, the troctolite is rich in plagioclase, includes an anorthosite layer with 3 to 5 cm. thick lenses of pure plagioclase rock, has a locally resorbed contact and thin peridotite layeres at the top.
- On Askival, harrisite layers are common within the 10 m. of peridotite. In the succeeding 26 m. of allivalite, a 1 m. layer of peridotite occurs 7 m. from the top and many anorthosite lenses 13 m. from the top.

3.5.7 Unit 14

This is by far the best exposed unit on Trallval and can be followed along strike for nearly 2 km., 90% of it exposed, though some parts are inaccessible due to the steepness of the terrain.

The Type Section: 35 m. of peridotite, 8 m. of allivalite, a subsidiary allivalite at 20 m.

Immediately above the allivalite of U13, feldspathic peridotite is modally layered over 2 m. Higher up, the layering is more widely spaced, with an average interval of 1 to 2 m. Feldspathic streamers, perpendicular to the layering are abundant and regularly distributed; they are up to 5 m. high, tend to broaden upwards from 10 to 50 cm. across and are composed of finely dendritic highly feldspathic peridotite. Most of them clearly cut plagioclase-rich laminae, appear to vanish across plagioclase-poor layers, then re-appear in the succeeding plagioclase-rich layers (Plate 3.15). Surfaces parallel to the layering show circular features, indicating their pipe-like nature. Nowhere are streamers developed as conspicuously as in this unit (GR 3728 9529). A 10 m. thick chromitite-layered zone of feldspathic

peridotite (Plate 3.7) follows the dendritic peridotite. In chromitite layering, the thickness of the intercumulus feldspar-rich lamina varies independently of the thickness of the included chromite-rich horizon, though it is usually thicker. The layering is somewhat undulating, and locally replaced by shapeless pods and pipes of plagioclase-poor peridotite (Plate 3.13), which extend further along plagioclase poor laminae in the layered peridotite. The pipes vary from 10 cm. to 8 m. across and the larger pipes may include partly resorbed blocks of feldspathic peridotite. They may be as much as 15 m. high, appear to be rootless and have numerous offshoots, oblique to concordant to the layering. The dendritic feldspathic peridotite above the chromitite zone has scattered chromitite fragments and extends up to the subsidiary allivalite in a texturally layered sequence, including cluster-layering (clusters vary from 15 to 60 cm. across in a few layers).

The subsidiary allivalite is underlain by a 40 cm. thick layer of protoharrisite. The allivalite is well-laminated over the top half, with thin anorthosite lenses; it is extremely irregular in thickness, which does not exceed 60 cm. (Plate 3.17) and flames line the upper contact with texturally layered peridotite. A coralline layer 2 to 3 m. thick is followed by a finely dendritic layer and then a layer of peridotite with feldspathic clusters (30 to 40 cm. across), cluster-layered, underlies the main allivalite. The lower part of the allivalite has a layer of anorthosite, but it is mostly mafic troctolite and highly deformed; it consists of a layer of allivalite mélange which thickens rapidly to the east, and a strongly folded layer of laminated troctolite. The upper part of the allivalite is relatively undeformed, has a locally developed layer rich in cumulus pyroxene (Plate 3.5) and merges with the lower part to the west, where the intervening layer of banded feldspathic dendritic peridotite thins and stops. The deformation of the lower part is the subject of a separate section (section 3.5.10). The upper half is strongly laminated, plagioclase-rich, with many pyroxene-rich laminae and pockets and lenses of anorthosite oblique to the foliation.

The Unit Elsewhere:

- The Askival section only has 16 m. of feldspathic peridotite, which includes layers of harrisite. Chromitite is common along the upper or

lower surfaces of the harrisite and within the peridotite. The top 8 m. of peridotite is dendritic, highly feldspathic and modally layered over 1 m. just below the allivalite. After 4 m. of laminated troctolite, there is a 15 cm. peridotite layer which has a locally resorbed contact with mafic allivalite which includes anorthosite clasts. There are another 4 layers of peridotite within the 70 m. of allivalite, at 6 m., 12 m., 29 m. and 31 m. The top 22 m. is strongly slumped and individual layers can be followed along their convolutions over a stratigraphical interval of up to 8 m. Cumulus pyroxene is abundant.

- In East Trallval, after a basal layer of coralline peridotite, the entire unit consists of a mélange of mostly angular blocks of troctolite in uniform, unlayered or banded feldspathic peridotite. Blocks are scattered throughout this layer, but more densely concentrated in the upper 10 m., probably corresponding to the whole or part of the allivalite as exposed to the west, which is described above.

- At (GR 3726 9545), to the west of the type section and 200 m. away from the CS contact, the 6 m. thick allivalite plunges downwards, achieving a 20^{o} dip increase over 20 m. and thinning to 3 m. There is a clear break after another 30 m. and the allivalite reappears along strike as a 50 m. long, undulating slab, 2 to 3 m. thick, with laminae rich in pyroxene and anorthosite lenses in the top 1.2 m. The slab is surrounded by undisturbed, structureless peridotite.

3.5.8 Unit 15.

The outcrop is limited to the top NW corner of Trallval. Together with U13, U14 and U16, it is strongly affected by drag along the faulted contact with the CS up to 200 m. away from the contact.

The Type Section: 41 m. of peridotite, 5 m. of allivalite.

At the base, the peridotite is heterogeneous with locally developed coralline texture, lensoid masses of protoharrisite, streaky fragments of troctolite (grading into feldspathic peridotite at the edges) and fragmented chromitite. A 2 m. thick protoharrisite layer overlies this 3 to 5 m. thick disturbed zone; it is overlain by modally layered feldspathic peridotite and some thin protoharrisite layeres which grade up into olivine-rich peridotite via feldspathic peridotite. About 30 m. up, there is a 6 8 m. thick layer of irregular harrisite (olivine reaches 3 cm. in length) with 20 cm. pods of harrisite (Plate 3.4), which forms the dip slope conspicuous as an inclined flat shield on

the west flank of Trallval (GR 3730 9540). Feldspathic peridotite underlies the allivalite, which is fully exposed only within the disturbed zone close to the contact with the CS (see below), where it is 3 to 4 m. thick and has a lower dimpled contact. The lower half of the allivalite is mafic troctolite and exhibits a planar cross-lamination, with a 16° angular discordance; the lamination consists of alternating troctolite and anorthosite laminae about 2 to 5 mm. thick. Laminae and lenses rich in pyroxene and pods and dykelets of anorthosite which may bifurcate or terminate abruptly are common in the upper half.

The Unit Elsewhere:

- In the disturbed zone to the west, coherent slabs of finely layered feldspathic peridotite and of attenuated allivalite are set in an extremely coarse, coralline textured feldspathic peridotite (plagioclase-poor patches up to 2 m. across), in places poorly modally banded except in a 1 to 2 m. wide sheath above and below the allivalite slabs where the peridotite is finely layered. The modal layering mimics the undulating outline of the slab. An allivalite slab at (GR 3713 9549) is 7 m. long, 85 cm. high and has a layer of finely layered feldspathic peridotite 13 to 18 cm. about 50 cm. above the allivalite, cut by feldspathic streamers up to 40 cm. high.

3.5.9 Unit 16 (Minimum thickness: 8 m.)

Several metres of peridotite with wispy lenses of allivalite near the bottom overlie the least disturbed exposure of the U15 allivalite. It is dendritic texturally-layered feldspathic peridotite with a discontinuous 10 cm. layer of dunite. To the west, coarse, structureless peridotite envelops near-vertical slabs of streaky allivalite, of layered feldspathic peridotite, disrupted chromitite and shapeless fragments of dunitic peridotite from which branching clusters of troctolite extend up to 1 m. away from the block, as in some of the intrusive breccia zones of the CS (section 3.8.2). The slabs of layered peridotite are up to 50 m. long and approximately in situ, though there are a few zones about 5 m. wide, where it has been thoroughly brecciated (with rotation of the clasts) by the structureless peridotite.

3.5.10 The Deformation of Unit 14.

Fig. 3.6 is a sketch-map of the outcrop of the allivalite, the eastern half of which forms the summit ridge of Trallval. From west

to east, the change in the style of deformation is such that the structures are best described by splitting the outcrop into 4 sectors; for each of these, a diagrammatic section is given in Fig. 3.7.

Eastern Sector. Length: 310 m.

Nowhere in this sector is the allivalite coherent: it forms a horizontal layer of breccia, or mélange, of troctolite blocks in a feldspathic peridotite matrix. Furthest east, the mélange is a chaotic mixture of angular blocks in an unlayered matrix (Plate 3.10). Blocks are concentrated at certain levels; where blocks are scarce, there is a shadow zone above the blocks in which the peridotite is more feldspathic and of a finer texture than elsewhere (Plate 3.18). The width of the shadow corresponds precisely to the maximum horizontal dimensions of the block. Further west, the troctolite fragments are organised into layers. The lower layers are highly sheared, with aligned schlieren of troctolite and the occasional angular block. Modal layering is developed in the peridotite above the zone of schlieren mélange, continuous through some of the blocks, cut by feldspathic streamers (more concentrated above accumulations of blocks) and pipes of pyroxene-rich peridotite and deformed into fluid escape structures (Fig. 3.8 A). Pillows of block-free peridotite, 5 to 10 m. across, with concentric modal layering near the margins, sit within the mélange layers (Plate 3.19).

Ridge Sector. Length: 110 m.

The upper allivalite - eroded from the summit ridge east of this sector - forms a regular, coherent layer with some peridotite veins in the east. Of the mélange layers to the east, the lower ones terminate and the upper mélange passes into a sequence of thin alternating layers of peridotite and troctolite with pillows of peridotite. The 1 m. thick, schlieren-rich mélange layer underneath passes westwards into a coherent layer of mafic troctolite with clasts of troctolite and anorthosite; it is underlain by unlayered peridotite with an irregular lower contact, which cuts the layering in the peridotite below. These three troctolite layers persist over the entire sector, with only a thin layer of feldspathic peridotite (less than 1 m. thick; Plate 3.20) between the lower and middle layers and one about 3 m. thick between the middle and upper layers (Plate 3.21).

The lower layer has subangular clasts of plagioclase-rich troctolite in its lower part and, above this, is itself plagioclase-rich, with diapiric mounds which bend the layering in the uppermost 10 to 20 cm. (Fig. 3.8 B; Plate 3.22). Flames are sporadically developed at the upper contact with peridotite, up to 80 cm. high. The layer thickens to the east, by an underplating process: the westwards inclination of the cluster-layering in the feldspathic peridotite below is slightly steeper than that of the lower surface of the allivalite; close to the allivalite, clusters are flattened and merge to form a thin plaque of troctolite, which underplates the allivalite.

The layered middle troctolite has pillows and more irregularly shaped masses of peridotite throughout (Figs. 3.8 C and D). The sinking of the peridotite (Plates 3.22 and 3.24) is complemented by the rising of the troctolite and anorthosite layers as flames and diapirs (Plate 3.25). The combination of the two processes produces complex interference patterns, suggesting a sequence of inflation and collapse of the diapiric structures (Plate 3.26). These complex structures are truncated along a planar surface by the overlying feldspathic peridotite, which has feldspathic streamers in its lower half, and a layered upper half; even within the convolute troctolite layer, the folded and sheared troctolite ribbons are sharply truncated by thin tongues of peridotite which follow the more coherent plagioclase-rich slabs (Plate 3.27). The upper troctolite layer is regular in thickness, and has a good planar lamination.

Cliff Sector. Length: 90 m.

The sandwiched layers of peridotite terminate at the western end of this sector, only exposed in the steep cliffs to the south and north of the ridge. The lower troctolite is continuous over most of the sector, except near the middle where it breaks up into a series of round-nosed slabs. The middle layer is gradually resorbed and replaced by feldspathic peridotite, with wehrlite patches and feldspathic streamers, westwards, as the two sandwiched peridotite layers merge and between them reduce the troctolite to a few, widely scattered, resorbed relics over 30 to 50 m. (Plate 3.28 and Fig. 3.8 E). The replacement is gradual, and more extensive along the layers of mafic troctolite, while the plagioclase-rich top of the layer, isolated from the lower part of the layer by merging peridotite pillows (Fig. 3.8 C),

continues as an array of relic lumps throughout the sector. The lower part vanishes totally, although it sprouts beautifully developed flames before it does so, both in the northern and the southern exposures (Figs. 3.8 F and G). It is above these flames that feldspathic streamers are best developed in the peridotite. The upper troctolite layer still maintains a fairly regular thickness. Thin dykelets of peridotite with sill-like offshoots penetrate as much as 1 m. down into the allivalite from above. Pyroxene-rich laminae pick out slump structures in the troctolite, which are truncated by planar modal layering (Fig. 3.8 H). At the western end, the middle layer reappears, with flames along the top (Fig. 3.8 I), spectacularly truncated by the peridotite (Plate 3.29). Further west, the peridotite layer thins and stops, enclosing folded slabs of troctolite near its termination (Plate 3.30). A lens of magnetite and cavity-filling zeolites associated with pegmatitic pyroxene forms a pocket below a fragmented slab of troctolite in the most extensively replaced part of the allivalite.

Western Sector. Length: 120 m.

The middle and upper troctolite layers merge to form the totality of the 3 to 5 m. thick allivalite, as the lower layer of brecciated anorthosite in mafic troctolite breaks up into fragments and terminates. At the junction between the middle and upper layers, a pyroxene-rich lens of extremely irregular thickness (Plate 3.31), with a sharp lower and a gradational upper contact, has good troctolite flames along its base (with upward coarsening texture, lamination parallel to the margins of the flame and truncation of the planar lamination in the pyroxene-rich rock, Plates 3.32 and 3.12) and scattered troctolite fragments (less than 3 cm. across) which locally collect into lenses up to 10 cm. thick. The lower 1 to 2 m. of the upper layer has many pyroxene-rich laminae and lenses, while the upper metre is strongly laminated and rich in discordant anorthosite layers and lenses. Further west, the allivalite is bent downwards and thins to 3 m., enclosing peridotite lenses in its lower metre, and eventually breaks up into isolated, sligthly undulating slabs (section 3.5.8).

3.6 Field Characteristics of the Central Series.

As no single traverse does justice to all of the groups, only those characteristics applicable to a layering unit as a whole are

noted without further comment. Local phenomena and lateral variation are described in their geographical context.

3.6.1 The Dornabac Member.

Maximum thickness: 25 m. of brecciated peridotite, 120 m. of allivalite.

The best exposures are on An Dornabac, where the member was described by Wadsworth (1958) as allivalites similar to those of Hallival with uneven, streaky layering and well-developed slump structures, forming stacks of slumped layers 1 to 2 m. thick alternating with 1 to 2 m. thick layers of unslumped material. Blocks of peridotite are common throughout, the troctolite is rich in cumulus pyroxene and poor in spinel

The member thins southwards to less than 1.0 m. thick at the coast. The peridotite of the blocks in the underlying breccia is olivine-rich and modally layered with chromitite laminae. The lower and upper 10 m. of allivalite consist of poorly laminated mafic troctolite. The streaky cumulates in between consist of lenticular layers of troctolite and feldspathic peridotite. Contemporaneous faults are ubiquitous. Over 5 to 10 m., the feldspathic peridotite may be dominant over troctolite, which is often fragmented into slabs discordant to the layering in the feldspathic peridotite. Where the troctolite dominates , the peridotite occurs as sheared blocks forming sigmoidal lenses.

The outcrop at Rubha Sgorr an't Snidhe (GR 346 932) is correlated with the An Dornabac exposures on the basis of the thick, slumped layers of troctolite, the abundance of pyroxene and on the mineral chemistry and its variation with height (section 5.7.2.5). There are two layers of allivalite, 20 to 25 m. thick, separated by a 40 m. thick zone of breccia.

The lower allivalite consists of alternating layers 10 to 30 cm. thick of strongly contrasting feldspathic peridotite and mafic troctolite. The layering in the troctolite is lenticular and often convolute, with common recumbent folds. Individual slumps are up to 3 m. thick and include blocks of peridotite as much as 2 m. across which deflect the layering above and below. The dendritic feldspathic peridotite is both modally and texturally layered and has some layers with a squat variety of streamer, perpendicular to the layering, which consist of columns of plagioclase, one oikocryst thick. The peridotite below the

lower allivalite has 20 - 50 cm. thick reverse graded layers, with cumulus plagioclase concentrated at the sharply defined bottom of each layer.

The upper allivalite is rich in pyroxene and includes layers of gabbro which alternate with thin anorthosite, troctolite and feldspathic peridotite layers. The feldspathic peridotite includes small (less than 3 cm. across), rounded troctolite clasts in regular laminae, which sometimes show size grading.

The outcrop at Leac a Chaisteil of feldspathic peridotite with 4 thin allivalite layers is correlated with the Dornabac Member on the pattern of mineral chemistry variation and its structural position in the CS. The allivalites are 1 to 2 m. thick with lenticular, streaky layering, slumping in the lowest layer and two anorthosite laminae in the second layer; the two higher layers have lenses rich in cumulus pyroxene and are finely laminated with planar cross-lamination in the upper layer which also has numerous sheared sigmoidal lenses of feldspathic peridotite. This layer is oblique to the textural layering in the overlying feldspathic peridotite. Below the upper allivalite, massive, coralline peridotite forms most of the exposed section; higher up, the peridotite is texturally layered with alternating 1 to 3 m. thick layers of dendritic and cluster-textured peridotite and some fine-scale modal layering close to the allivalite.

3.6.2 The Lower Unit of the Long Loch Group.

Maximum thickness: 100 m.

This unit maintains a fairly constant thickness over the whole outcrop of the CS and with its persistent allivalite forms a reliable marker band which has been identified in the screens of peridotite between the wide breccia zones of South Ruinsival. Layer thicknesses increase to the south and downdip (as observed in the field at GR 3434 9505). About this unit, Wadsworth (1958) wrote that it is conformable with the Dornabac Member and in tectonic contact with the Harris Bay Member of the WLS. The following description is for the section where the unit reaches its maximum thickness, along the SW coast at Harris Bay.

Within the basal metre, the dunitic peridotite, which forms most of the unit, has clasts of troctolite from the Dornabac Member. Two metres up from the contact, a 2 m. thick layer of feldspathic perido-

tite grades up into dunitic peridotite, followed by a 1 m. layer also grading up into dunitic peridotite from a lamina of protoharrisite at its base which persists over 2 km. and is locally underlain by a 5 to 10 mm thick lamina of chromitite. The overlying sequence of dunitic peridotite with reverse, graded modal layering includes two 30 cm. thick layers of dunite, a layer of protoharrisitie at 7 m. (with pods of harrisite) and at 12 m., folded, disrupted chromitite lenses up to 10 cm. long along the upper contact of protoharrisite layers or within the dunitic peridotite. At 60 m., the dunitic peridotite yields to uniform peridotite with layers of coralline peridotite, protoharrisite and some 3 mm. laminae of feldspathic peridotite. Another 20 m. up, coralline peridotite forms a massive sequence with faint modal layering and a 1 m. thick layer of protoharrisite with harrisite pods. No allivalite occurs at Harris Bay.

On An Dornabac, the peridotite is only 65 m. thick, and, above the 2 to 10 m. transition zone with clasts of troctolite and folded chromite lenses (up to 25 cm. by 7 cm. at GR 3535 9683) along the top, consists of layers of dunitic peridotite with a few thin layers of protoharrisite and coralline peridotite. The basal 3 to 10 cm. of the dunitic peridotite layers may have a lamina of disseminated chromite 1 to 3 cm. thick, followed by a lamina of protoharrisite which grades rapidly into dunitic peridotite with a decrease in intercumulus plagioclase content. The dunitic peridotite is capped by a thin (0.5 m. thick) fragmented allivalite, underlain by 2 to 3 m. of feldspathic peridotite.

The lower part of this unit at Rubha Sgorr an't Snidhe is completely brecciated. The coherent top 15 m. consist of cluster-textured feldspathic peridotite, with a few layers of reverse modally graded peridotite (feldspathic at the bottom, dunitic at the top) below anorthositic troctolite with sigmoidal peridotite lenses. Exposures of the unit in the peridotite screens to the east are also limited to the upper half, structurally overlying breccias with blocks of dunitic peridotite including chromitite laminae. The exposed sequence starts with dunite followed by 3 m. of peridotite with undulating chromitite layering and lenses of protoharrisite and chromitite (GR 3538 9353). The layered zone is overlain by 5 m. of dunitic peridotite with pods of harrisite (olivines more or less vertical, up to 10 cm. long and chromite along the bottom), coarsely coralline, feldspathic peridotite,

EDINBURGH UNIV. EX BIBL.

a 3 m. layer of dunitic peridotite with a lenticular discontinuous layer of feldspathic peridotite and, underlying troctolite, 1 m. of dunitic peridotite with wispy lenses of troctolite. The allivalite consists of a number of sharply truncated slabs of troctolite, which vary in thickness from 3 to 6 m. , separated from one another along strike by 5 to 20 m. of feldspathic peridotite with cluster texture. The troctolite is well laminated, slumped, with anorthosite pods and lenses oblique to the lamination and some sheared lenses of dunitic peridotite. At Leac a Chaisteil, the unit consists of massive peridotite with a disrupted chromitite lamina 15 m. from the top and a fragmented layer of anorthositic troctolite.

The exposures on Trallval are brecciated by both feldspathic peridotite and gabbro. The brecciated peridotite is mainly dunitic peridotite, with layers of protoharrisite, texturally layered and chromitite-layered feldspathic peridotite. An anorthositic allivalite at (GR 3658 9484) has a 1 to 3 cm. thick chromitite lining along its lower surface, and overlies chromitite-layered peridotite. Anorthositic allivalite is also exposed 1 km. to the north, where it is 6 m. thick and includes 2 mafic layers of troctolite with wispy dunitic peridotite lenses. The entire layer has recumbent slumpfolds, and is underlain by dunitic peridotite with chromite along the base, which overlies feldspathic peridotite.

3.6.3 The Middle Unit of the Long Loch Group.

Maximum thickness: 260 m.

This is the highest unit exposed in the Barkeval - Long Loch area (McClurg, 1982) and it underlies much of the Trallval area. The only continuous exposure is along the SW coast, where, like the previous unit, it lacks an allivalite, the boundary with the overlying unit being cryptic. The basal layer is a distinctive, massive 10 m. thick dunitic cumulate of black, lustrous olivine, which Wadsworth (1958) also described from the An Dornabac area, noting that the rest of the unit consists of peridotite with an increasing proportion of cumulus feldspar towards the top. The black layer is followed, at Harris Bay, by 80 m. of unlayered peridotite with pegmatitic patches of plagioclase and pyroxene which grades upward and to the north into dunitic perdotite with planar lenses of both chromitite and pure chromite. The overlying 170 m. consists of homogeneous dunitic peridotite with rare,

folded pods of chromitite, 5 cm. across at the most.

From An Dornabac to Seagull Loch, the unit is poorly exposed but, above the black olivine layer, it consists of massive dunitic peridotite, except for the top 15 m.: a 10 m. layer of coralline peridotite is followed by a heterogeneous zone of highly feldspathic peridotite with a discontinuous cap of anorthositic troctolite (at most 20 cm. thick), another 2 m. of modally layered feldspathic peridotite, and then a 50 cm. thick allivalite with a locally resorbed lower contact.

The basal black layer is not exposed elsewhere, but a thick section from the middle of the unit is exposed in a NW plunging syncline of dunitic peridotite to the north of Papadil. The lower layers have some scattered, coarse black olivines, followed by layers of dunite grading up into dunitic peridotite. The layers are straight and regular in thickness (10 to 40 cm.), but the transition from dunite to dunitic peridotite forms a 2 to 5 cm. thick wavy contact. This is the best exposure of layering in dunitic peridotite on Rhum (GR 3685 9244). Some of the dunite layers have a chromitite at the bottom, one of which is traceable for 10 m. and folded on top of itself. About 60 m. up, layers of dunite 10 to 50 cm. thick alternate with layers of dunite with pods of dunitic peridotite up to 4 m. thick. Twisted, disrupted chromitites occur commonly at this level, and can be divided into two types: (i), concentrations of chromite crystals wedged between olivines, forming a pure chromite-olivine rock, and, (ii), chromite with interstitial plagioclase forming a chromitite lens or lamina. Thin laminae of the latter, type II, variety form a triplet in a layer of dunite at (GR 3659 9303); the laminae degenerate laterally into horizons of thicker, discontinuous, folded chromitite lenses. The top 20 m. at Papadil consist of homogeneous peridotite.

At Leac a Chaisteil, the unit consists of dunitic peridotite with scattered lenses of chromite (type I). In the area to the west of Trallval and north to Barkeval, the basal peridotite is also dunitic with a layer with large, poikilitic pyroxene and is overlain by 60 to 100 m. of homogeneous, unlayered dunite and dunitic peridotite with disseminated coarse chromite, occasionally concentrated into laminae from one crystal to 2 cm. thick, often disrupted and folded into separate lenses, up to 20 cm. long and 5 cm. thick (type I concentrations are most common and form recrystallised aggregates, e.g. at GR 3680

9590). The top of the unit is not exposed here.

3.6.4 The Upper Unit of the Long Loch Group.

Maximum thickness: 360 m.

This unit is only exposed to the west of the Long Loch Fault. Despite its thickness, little of it is seen due to intrusions of ultrabasic breccia zones and gabbro. It has a thick allivalite which persists even into the Ruinsival area, but is best exposed NE of Seagull Loch. The peridotite is best exposed along the coast and on the western slopes of Ruinsival. A 130 m. sequence of dunitic peridotite with some dunite layers up to 5 m. thick near the top and a 1 m. thick layer with folded lenses of types I and II chromitite in dunitic peridotite, grades into peridotite with some pegmatitic pyroxene-plagioclase pods about 150 m. up. A return to dunitic peridotite at 290 m. with thick layers of dunite, is marked by numerous planar lenses of type I chromitite in dunite and contorted lenses of type II chromitite in dunitic peridotite. A double lamina of type II chromitite appears at the base of a layer of dunitic peridotite overlying dunite (GR 3540 9449). This chromitite zone is about 20 m. thick (the proportion of chromitite to peridotite is about 1 to 1000). Over the top 40 m., the dunitic peridotite grades into peridotite with more feldspar. In screens 10's of m. wide, between the anastomosing breccia zones, allivalite occurs at (GR 3548 9443) and at (GR 3485 9360) about 1 km. to the SW. While the latter exposure consists of streaky troctolite wisps, ca. 10 cm. thick by about 1 m. in length in a 1 m. thick layer of peridotite, the former, to the south of Loch Fiachanis, consists of a thin, discontinuous, streaky troctolite underlain by 2 m. of cluster-layered feldspathic peridotite.

The allivalite is also exposed north of Loch Fiachanis, where it overlies dunitic peridotite with thin layers of feldspathic peridotite, and consists of 20 m. of pyroxene-rich troctolite interlayered with troctolite and olivine-rich troctolite. Sheared blocks of dunitic peridotite are common, while a few undeformed blocks deflect the steep layering. Wadsworth (1958) described slumps and gravity-layering in this sequence and also correlated it with the allivalite NE of Seagull Loch, the deformation of which he attributed to tectonic movements after the consolidation of the cumulate. About 20 m. below the allivalite NE of Seagull Loch, dunitic peridotite passes up into feldspathic peri-

dotite via a 1 m. layer of peridotite with clusters. The overlying feldspathic peridotite has streakily distributed cumulus plagioclase which forms discontinuous laminae and some thick lenses which sometimes have cumulus pyroxene, too. The feldspathic peridotite occurs in lenticular layers and displays both slumping and internal brecciation. The 16 m. thick allivalite is rich in pyroxene, and highly deformed: contemporaneous faulting and incipient boudinage by plastic flow under shear stress are conspicuous (Plate 3.11). Lenticular and sigmoidal peridotite lenses are included in the troctolite at most levels. The top 5 m. are poor in olivine. The lower parts of the allivalite are partly replaced by tongues of peridotite which truncate the lamination and the shear fabric.

3.6.5 The Ruinsival Group.

Maximum thickness: 250 m.

Two macro-cyclic units compose the group. The relationship of the units is not clear due to a thick intrusion of gabbro at the critical level and extensive brecciation of the upper half of the Ruinsival Group. The entire group is therefore treated in a single section. Wadsworth (1958) noted that the cumulates on the NW face of Ruinsival are layered sub-horizontally with chromitites in the lower part and rhythmic layering in allivalite with cumulus pyroxene near the summit of Ruinsival. The group is, indeed, most continuously exposed on the NW face where a thin allivalite marks the top of the underlying group. Where this is absent, the base of the Ruinsival Group can be recognised by the basal 65 m. of peridotite layered on a scale of 20 to 200 cm. Each complete layer has a lamina of wehrlite along the bottom, followed by dunitic peridotite (20 to 40 cm. thick) which has a wavy contact with peridotite (0 to 160 cm. thick) which may have 2 to 5 cm. thick type I chromitite lenses 2o to 30 cm long. Some layers lack the wehrlite and/or the chromitite. In the top 20 m. of the layered peridotite, the peridotite layers are up to 5 m. thick and are locally enriched in interstitial plagioclase, forming internal brecciation pockets up to 100 m^3 in volume, which are fed by a dendritic vein system from the surrounding plagioclase-poor peridotite. A distinctive chromitite zone forms the top 25 m. of the peridotite in this unit. It can be traced laterally for more than 1 km. On the NW face, it consists of two 20 to 30 cm. thick chrome-spinel-rich layers

(with about 10 to 15 % chromite) separated by 5 m. of peridotite and overlain by 15 to 20 m. of heterogeneous feldspathic peridotite with several, fragmented, thick (3 to 10 cm.) chromitites of type II near the top, parts of which have foundered as much as 10 m. into the coralline peridotite (Fig. 3.10). The 20 to 30 cm. spinel-rich layers both have chromitite-layering. The lower layer has some concentrated chromite laminae and the upper layer includes subangular clasts of dunitic peridotite, 2 to 5 cm. across. The chromitite zone lies below a body of gabbro which includes some 3 m. thick slabs of well-layered troctolite with thin, undulating anorthosite and feldspathic peridotite layers . Slabs 0.4 to 1.2 m. thick are exposed in the ultrabasic breccia to the south. A similar slab at (GR 3550 9420), 50 cm. thick has modally layered troctolite sandwiched between protoharrisite laminae, with underlying cluster-layered feldspathic peridotite. The lower part of the second unit is only exposed as blocks in ultrabasic breccia, which consist of dunitic and feldspathic peridotite in about equal proportions. Coherent peridotite reappears about 230 m. above the base of the group, where it is interlayered with feldspathic peridotite and passes up into coralline feldspathic peridotite with laminae of mafic troctolite, bearing clasts of anorthosite.

On the NE shoulder of Ruinsival, only the upper part of the lower unit occurs. It consists of dunitic peridotite overlain by thick layers of peridotite with a few layers of troctolite forming a 10 m. sequence underlying a layer of heterogeneous feldspathic peridotite with 5 cm. thick, widely scattered troctolite lenses up to 1 m. long, often with a rim of chromite, which in one case reaches a thickness of 20 cm. The mafic troctolite is sometimes modally layered and one block has an anorthosite lens. About 6 m. higher, in the lateral equivalent of the chromitite zone on the NW face, lenses of coarse, type I chromitite up to 10 cm. thick by 20 cm. long are restricted to one layer of peridotite, 5 m. thick (GR 3605 9432). Another 200 m. to the east, the chromitite zone is still about 5 m. thick, and has laminae continuous over 10 m., 1 to 2 cm. thick and abundant planar to contorted lenses of both types of chromitite. The zone is again underlain by 6 m. of heterogeneous peridotite with troctolite clasts. Above the chromitite zone, the 150 m. of unlayered peridotite has a single continuous chromitite about 20 m. up, but otherwise shows little variation, although,

in the top 60 m., there are layers of uniform peridotite, a few of mineral-laminated peridotite and some pods of feldspathic peridotite strung out at about the same stratigraphical level to produce a poor variety of layering. The junction between the lower and upper units, which must lie near the bottom of this sequence, is cryptically defined (section 5.7.2.5) as the lower unit here lacks an allivalite cap.

The top of the lower unit is also exposed to the SE of Ruinsival summit, where it consists of feldspathic peridotite, capped by a thin, streaky, mafic allivalite. The upper unit has dunitic peridotite with a layer of feldspathic peridotite which passes laterally into a layer of strongly slumped, poorly laminated, mafic troctolite. About 10 to 20 m. of texturally-layered feldspathic peridotite overlies the thin allivalite and may be a part of a third unit.

3.7 Field Characteristics of the Ultrabasic Plugs

These cylindrical peridotite bodies are characterised by a general coarseness and homogeneity of texture, rare, rounded xenoliths and concentric, vertical banding, best developed close to and parallel to the intrusive contact.

3.7.1 The Papadil Plug.

This composite plug is situated just outside the CS and has:

(1) An outer sheath of olivine-gabbro, 1 to 40 m. wide, in contact with a breccia zone in the CS to the north and with 2-pyroxene gabbro elsewhere.

(2) A core of feldspathic peridotite, roughly circular in plan, a little off-centre, containing uniformly distributed clasts of mafic troctolite. The clasts are sub-rounded, with resorbed margins and, where elongate, do not appear to be aligned with the banding. Locally, the peridotite has impersistent, undulating to convolute, steep, inward-dipping modal banding, best developed near the contact with the enclosing peridotite, where bands are spaced at 3 to 5 cm. Small fragments of chromitite with coarse spinel occur sparsely.

(3) The bulk of the plug consists of coralline peridotite, rich in poikilitic pyroxene (ca. 20 %), with a texturally coarse outer facies and a zone about 80 m. wide, around the feldspathic core, of finer texture. Banding is sporadically developed, except near the margin, where it is steep, inward-dipping and parallels the locally sinuous contact with the gabbro. Bands of feldspathic peridotite 1 to 4 cm. wide grade into the peridotite away and towards the contact and also laterally.

3.7.2 The Ruinsival Plug.

The plug consists almost entirely of feldspathic peridotite with a coarse coralline texture transitional to cluster texture of remarkable homogeneity; a finer textural variey is locally developed, where the peridotite includes a few rounded blocks of dunitic peridotite and fragments of chromitite. Angular blocks of dunitic peridotite occur near the inward-dipping margin and vertical banding is developed in the marginal zone, especially strongly where the plug cuts gabbro. At the SE corner, the plug includes blocks up to 10 m. long of the adjacent, distinctive breccia zone and thus postdates it. At (GR 3527 9387), the coralline peridotite shows a dramatic textural chill from a cluster-textured rock (clusters 0.5 to 1.0 m. across) 5 m. away from the contact to finely coralline peridotite at the contact. Some banding is developed in the interior, sub-vertical and concentric. Locally, sub-horizontal to upwards curving bands, more or less normal to the plug's axis, are developed as offshoots from the vertical bands, extending up to 0.5 m. towards the core of the plug. Rootless, wispy veins of anorthosite which can only be followed for 5 to 20 cm. are common throughout the plug.

3.7.3 The Seagull Plug.

A plug of olivine-rich peridotite composition, it sharply truncates allivalite layering and the gabbro / CS contact to the east along a sinuous boundary, which is paralleled by vertical modal banding in the plug. Banding is not developed elsewhere; an irregular distribution of plagioclase gives rise to dunitic and coralline feldspathic peridotite patches (some of the dunitic areas may be highly resorbed blocks of dunitic peridotite). The plug has a few angular blocks of dunitic peridotite near the contact and rare, subrounded blocks within, with diffuse outlines and no more than 30 cm. across. The wispy, thread-like, impersistent anorthosite veins are ubiqutous.

3.7.4 The Barkeval Plug.

This is the largest and most heterogeneous plug. It is homogeneous in the upper 100 m., which consist of coralline or cluster-textured (clusters 10 to 20 cm. across) peridotite with an 80 m. wide marginal zone of feldspathic peridotite, which includes angular xenoliths up to 15 m. from the intrusive contact. At the contact

between the outer, feldspathic ring and the olivine-rich peridotite core, modal banding is well-developed, as is textural banding with dendritic bands and some bands which are graded from a fine coralline texture to a coarse texture inwards. The core of the plug has more widely spaced, poorly developed, steep, inward-dipping, modal banding and subrounded blocks of dunitic peridotite (about 20 cm. across on average). Where it is exposed on the southern slopes of Barkeval, and also in its eastwards extension, the plug contains slabs of troctolite up to 6 m. thick. The slabs may be in a sub-horizontal to a sub-vertical position in a heterogeneous feldspathic peridotite matrix. In its lowest reaches, the plug includes gabbro and dunitic peridotite with breccia zones in blocks 10 to 50 m. across. Close to the contact with the gabbro at (GR3663 9700), the peridotite includes blocks of gabbro, of gabbro with xenoliths of hornfelsed peridotite from the layered series, and of hornfelsed peridotite, the latter often with a thin coating of spinel.

3.8 Field Characteristics of the Ultrabasic Breccia Zones.

All breccia zones are clearly intrusive, yet the textures in the peridotitic matrices closely resemble those in the layered series and the same terminology is applied here. The matrix of the breccias varies from pyroxene-rich (up to 30 to 40 % pyroxene), to olivine-rich matrices with 50 % or more of olivine, via feldspathic peridotite (Plate 3.33). The latter are most common. The internal structure of the breccias is complex; numerous internal intrusive contacts, anastomosing systems of peridotite dykes, shear zones and modal banding give the breccias a strong, generally vertical fabric. The orientation of this fabric usually follows the zone trend, which is defined by the elongation of the zone and similar to (though not the same as) the trends of the other zones in that breccia system (Fig.3.5).

3.8.1 The Trallval System.

Over much of its outcrop, the easternmost zone is well exposed, while the zones to the west are seen only in streambeds and several small bluffs. The eastern, or Trallval, zone is set in isotropic dunitic peridotite of the Long Loch Group, which provides a strong contrast with the feldspathic peridotite of the breccia matrix. As Fig 3.5 shows, the zone has a continuous western channel with verti-

cal structures which follow the breccia trend, and a bulge to the east with a subhorizontal to inclined fabric. The bulge is located at a sharp kink in the boundary of the CS, and has an upper sub-horizontal contact with the CS, which thus forms a roof to the bulge. A number of subsidiary breccia zones, vertical sheets which follow the trend, cut the dunitic peridotite west of the channel; these are 1 to 5 m. wide, matrix-supported, with angular slabs of the local peridotite set in feldspathic peridotite. Along strike, the thinner zones may pass into a set of parallel veins of feldspathic peridotite with one or both margins rimmed by anorthosite or troctolite. Over most of this 50 m. wide strip, the dunitic peridotite is riddled by parallel, closey spaced, thread-like veinlets of anorthosite (Plate 3.34) which impart a moderate schistosity to the rock. The veinlets increase in density and thickness towards the zones of intrusive feldspathic peridotite and occur up to 15 m. away from the Trallval zone and less from the subsidiary zones.

The Western Channel.

The western contact of the Trallval zone is sharp and vertical. The matrix peridotite includes thin tabular slabs of dunitic peridotite (long axes parallel the breccia trend) rimmed by troctolite, up to 5 m. away from the contact. These slabs are only slightly rotated: at (GR 3696 6915), a double chromitite in the dunitic peridotite can be traced from block to block, maintaining a sub-horizontal orientation. The western channel, about 50 m. wide, consists of coralline feldspathic peridotite with about 10 volume % of angular dunitic peridotite blocks, varying in size from 1 cm. to 4 m. across, with an average size of 5 to 10 cm. The matrix has vertical, streaky modal banding, anastomosing sheets of highly feldspathic, block-free peridotite with rounded dunitic peridotite clasts 10 cm. across. Around (GR 3702 9621), the feldspathic peridotite has large blocks of gabbro (similar to the Glen Harris Gabbro) and one of regularly, texturally layered feldspathic peridotite (similar to that of the ELS), all 5 to 10 m. across, and cut by thin (5 to 20 cm. wide) sheets of feldspathic and olivine-rich peridotite (Plate 3.35).

The Eastern Bulge.

The bulge shows bewildering variety in matrix composition, block lithology and orientation of structures. It is exposed on a gently

sloping plateau, which falls off steeply to the north and abuts onto the cliffs of Trallval to the south, where a roof-zone to this breccia is exposed. To the east, the breccia follows and then cuts across the contact with the ELS. To the north, the bulge rapidly contracts to a few feldspathic peridotite dykes, 1 to 5 m. wide, cutting the ELS. A zone of large blocks of dunitic peridotite, up to 25 m. across, form a partly brecciated screen between the channel and the roof. A block at (GR 3700 9590) has 2 parallel chromitite laminae with a gentle dip to the NE, which demonstrates that there has been no rotation of this block with respect to the CS outside the breccia zone. Small blocks with this chromitite doublet are found in an array extending 5 m. to the east and 2 m. up, decreasing in number with distance from the mother block. Immediately to the east of this screen, thin, tabular slivers of dunitic peridotite, elongate in the plane of the breccia trend, often folded back on themselves with downward-pointing noses, suggest relative movement of the highly feldspathic matrix upwards relative to the screen. At the eastern contact, the ELS peridotite lacks the closely spaced parallel veinlets but does have a few irregular anorthosite veins up to 3 m. away from the contact. To the south, the contact rapidly flattens and then veers to the west to underlie dunitic peridotite of the CS. Structures in the breccia below this contact, such as matrix banding and alignment of clasts, are also sub-horizontal.

The bulk of the eastern bulge consists of a pyroxene-rich feldspathic peridotite matrix (Plate 3.36) enclosing blocks of gabbro and peridotite: there is no size sorting of the blocks and the matrix has no persistent fabric. Vertical zones up to 20 m. wide with a well-developed tectonic fabric, each with a matrix of distinctive clast lithologies, form the remainder of this bulge. Size sorting of clasts is good in some of the zones which contain a single clast lithology (Plate 3.37). In other zones, blocks of mixed lithologies occur in tightly packed clusters of a dozen or so blocks. Most clasts are of dunitic peridotite- other lithologies include feldspathic peridotite, plug peridotite (see below), troctolite, anorthosite and a block of the distinctive streaky allivalite of the lower Long Loch Group. All these rock-types occur <u>in situ</u>, bordering the breccia zone. The larger blocks (1 m. or more) are invariably veined by feldspathic peridotite and anorthosite which generate small pockets of breccia

at their intersections within the block; some of the wider cracks are filled by breccia matrix with small clasts and a fabric often at high angles to the crack edges. Peridotite blocks are usually angular, though many of the smaller blocks are rounded (Plate 3.38). Some of the dunitic peridotite blocks have partial rims of troctolite which fill in irregularities along the edge of the block and tend to be much thicker (up to 10 cm. across) on the NE side of the blocks. Troctolite also lines the margins of many of the vertical sheets with a well-developed fabric. Small (5 to 20 cm. across), elongate, aligned clasts of anorthosite impart a strong fabric to the matrix where it swirls round some of the larger clasts as at (GR3710 9588; Plate 3.39), around a block, circular in plan, with a 15 m. diameter, of coarsely textured feldspathic peridotite with rootless, wispy anorthosite veins (similar to the Ruinsival plug).

The subsidiary zones between the main breccia zone and the Long Loch Fault have vertical internal structures (olivine foliation, sheets of block-free peridotite, contacts between breccias with modally contrasting matrices) which follow the breccia trend. The clasts are locally derived, apart from troctolite fragments (5 to 20 cm. across). Troctolite also lines the margins of the more olivine-rich block-free sheets of peridotite. Generally, the matrix peridotite is highly feldspathic.

3.8.2 The Ruinsival System.

More than half of the 3 to 4 km.^{2} of the ultrabasic outcrop south of the Fiachanis River consists of ultrabasic breccia zones. The Ruinsival system is composed of three main prongs extending northwards from a huge mass of intrusive peridotite in S Ruinsival. Ruinsival may be described as a mega-breccia, with blocks over 100 m. wide; the rotation of some of these blocks within the breccia may explain the anomalous attitude of their internal layering (section 2.2.2). Subsidiary zones flank the main breccia mass. Wadsworth (1958) described the central prong of the main mass as the Ruinsival breccia zone: the zone dips steeply to the east, as does the streaky layering within it, the matrix is not of a uniform modal composition and the zone was interpreted as a fault-scarp breccia. Donaldson (1975) examined the Harris Bay breccia, a subsidiary zone to the west, which was described as an upward-closing body with vertical structures,

wispy banding in the matrix (sometimes continuous through the blocks) and without any size or density sorting of the blocks, some of which are embayed.

The Massive Breccia of South Ruinsival.

The breccia zones on Fig. 3.5 postdate an earlier episode of brecciation, seen only on the southern slopes of Ruinsival. The earlier episode produced a homogeneous mass of structureless peridotite with blocks of dunitic peridotite,usually sub-rounded with diffuse margins. Contacts with the CS are gradual, the proportion of matrix to blocks increasing from 1 : 4 to 10 : 1 over 50 to 100 m. Where the matrix is subordinate, it dissects the peridotite into a mosaic of sub-horizontal, tabular slabs. The matrix has a finely developed uniform, dendritic texture of remarkable homogeneity. In the main body of the breccia, the clasts are well sorted, 20 to 30 cm. across, rounded and show little variation in composition. In some places, the breccia matrix grades smoothly to dunitic peridotite and the hint that this early breccia may be a lateral equivalent of the Long Loch Group, underlying Ruinsival, is re-inforced by the presence of several 10 m. blocks of a similar olivine-rich breccia with only a few rounded blocks at (GR 3555 9432), at the northern foot of Ruinsival.

A strong, vertical fabric is not always developed in the later generation of breccia zones either, especially in the south, but t... these do have sharp contacts with the country rock, are much richer in feldspar and include blocks of gabbro, of troctolite and of the earlier breccia, besides blocks of dunitic peridotite. The feldspathic breccias form a system of interconnected sheets which generally thicken to the south and downwards (see map) where they merge to form a body, at least 500 m. across, of massive, coralline to cluster-textured highly feldspathic peridotite with only occasional blocks of peridotite; clusters are up to 1 m. across. Near contacts with gabbro, the texture is heterogeneous, streaky and the peridotite includes rounded fragments of gabbro. Within the stock, at (GR 3540 9313), there is some modal plagioclase banding developed in the breccia matrix sympathetic to the outline of a sub-horizontal 30 m. long by 3 m. thick slab of layered feldspathic peridotite, probably derived from a feldspathic horizon in the CS. Clasts of peridotite are often

sliver-shaped and many are veined; small fragments of chromitite, up to 5 cm. across, also occur. Some blocks have a shell of feldspathic peridotite with outward radiating clusters; at (GR 3570 9286) such a shell forms a spherical feature 1.4 m. across.

The transition from the massive body in the south to the system of converging sub-vertical sheets to the north consists of a stockwork of sub-horizontal and sub-vertical sheets of breccia which isolate tabular, often sub-horizontal slabs of dunitic peridotite; oblique sheets of breccia are common,too, but tend to be thinner (Fig. 3.11). This transition is not well defined and is spread over 500 m. Thin, block-free sheets of the highly feldspathic matrix peridotite cut the tabular peridotite bodies in swarms, and occasionally swell to brecciate the peridotite in pockets 3 m. across or so. Larger sheets usually do carry peridotite blocks. Troctolite appears as clasts in the breccias and the matrix around some peridotite blocks is enriched in pyroxene.

The Vertical Zones of the Ruinsival System.

Many features of the Ruinsival system are similar to those of the Trallval system, such as strongly developed vertical, internal structures, veinlets in the adjacent peridotite, the development of a breccia trend and bulges with sub-horizontal structures. Several features are unique to the Ruinsival system, however, and some of these may be due to the larger scale of the brecciation processes on Ruinsival. The zones and prongs composing this part of the system will be described starting with the westernmost one at the mouth of the Fiachanis River and progressing eastwards.

The Fiachanis Rivermouth Zone: this breccia has coarse olivine in the matrix and an intricate contact with a large body of gabbro, which it postdates as it includes numerous xenoliths, including schlieren, and trails of xenocrysts of plagioclase as well as shapeless patches of plagioclase enrichment which may represent partly assimilated gabbro. At (GR 3416 9474), the xenoliths of gabbro are coated by a chromitite of variable thickness (up to 5 cm.). Blocks of peridotite are rare in this breccia, but it has 2 prongs which cut the dunitic peridotite to the NE as 60 cm. thick dykes.

The Harris Bay Zone: The matrix of the breccia, described by Donaldson (1975), is rich in pyroxene and has some harrisitic olivine. The

blocks are extremely varied in composition and include gabbro similar to the Fiachanis Rivermouth gabbro, coarse pyroxene-rich gabbro, streaky troctolite, feldspathic breccia matrix with peridotite clasts, dunitic peridotite and dunite. Some gabbro clasts disaggregate into trails of xenocrysts at the edges. The outer contacts are vertical and, apart from vertical slivers of peridotite at the contacts, the marginal 1 to 3 m. of the body is block-free, strongly modally banded, while the largest blocks are found near the centre of the zone; it does narrow upwards and northwards, although it continues to the NE as a sheet of variable thickness.

The Ruinsival Zone: The frequency and intensity of the following features in the country rock peridotite increase steadily as the zone is approached:

(1) Vertical sheets less than 1 m. across of highly feldspathic peridotite, along the breccia trend, with angular blocks of local peridotite. The adjacent peridotite is intensely veined and the sub-parallel anorthosite veinlets often converge on one another in dendritic fashion and drain into (or out of) the sheet of breccia.

(2) Pegmatoid patches of pyroxene and plagioclase, 10 to 20 cm. across.

(3) The content of interstitial plagioclase and pyroxene in the peridotite.

(4) 1 to 2 cm. thick, coarse pyroxene / plagioclase veins.

(5) Zones of veined peridotite, 1 m. across, not flanking a sheet of breccia.

The Western Prong: consists of streaky, highly feldspathic peridotite with blocks and boulders of troctolite and gabbro which deflect the modal banding in the matrix. Many large blocks have wedge-shaped shadows free of banding to the NW, suggesting that there is a lateral component to the relative motion between blocks and matrix. The prong is ill-exposed inland and rapidly dwindles to a plexus of thin sheets of feldspathic peridotite with blocks of dunitic peridotite only. Parallel veining becomes yet more intense towards the central prong , the veinlets often converging and disaggregating the peridotite into individual olivine crystals to form thin sheets of feldspathic peridotite.

The Central Prong: described by Wadsworth (1958), is closely connected to the eastern prong by a number of linking channels. They are

themselves composite intrusions, the individual anastomosing sheets being separated by screens of peridotite. The matrix is generally highly feldspathic with banding, angular clasts of dunitic and feldspathic peridotite, slumped troctolite (GR 3524 9380), and of earlier sheets of breccia. Locally, the matrix has concentrations of poikilitic pyroxene (Plate 3.40). Near Loch Fiachanis, the breccia also has fragments of chromitite, blocks of gabbro, the early uniform, olivine-rich breccia and slabs of layered feldspathic peridotite. Blocks of feldspathic peridotite have a plagioclase-free rim, the thickness of which varies indepently of the size of the block.

The Eastern Prong: well exposed near the top and down the north face of Ruinsival, this zone has massive textures, with the development of coralline (Plate 3.41) and giant cluster texture: at (GR 3530 9403), clusters are up to 1.5 m. across (Plate 3.42). Near the summit of Ruinsival, the matrix is, however, strongly sub-horizontally banded with deflections around angular blocks of country peridotite and rounded troctolite fragments (Plate 3.43). The banding is modally controlled (some bands are nearly anorthositic) but diffuse and irregular compared to modal layering in the country peridotite (Plate 3.44). This strongly banded, highly disturbed facies is also adjacent to a gabbro which it cuts. The internal structure of the breccia assumes a vertical attitude to the north and downwards with alternating block-free and block-bearing sheets. Some of the latter are characterised by a fairly uniform size of clasts (10 to 20 cm.) while others have a chaotic mixture of clast sizes, with blocks up to 5 m. across. To the north of Loch Fiachanis, the eastern prong appears in a number of enclaves within the late Glen Harris Gabbro. Anorthosite clasts are abundant and even thin, subsidiary zones without peridotite blocks carry fragments of anorthosite into the parallel-veined country rock. Within the main zone, peridotite blocks are strongly sheared, parallel to the breccia trend and may have a selvage of anorthosite on their northern side. Anorthosite blocks, too, are often elongate and aligned with the breccia trend.

Trachytoid Sheets: at numerous localities dispersed over the entire area of outcrop of the Ruinsival System and restricted to it, thin sheets of block-free peridotite cut all other structures in the breccias. They vary in thickness from 10 to 80 cm. and have a characte-

ristic texture: plagioclase oikocrysts form elongate, isolated clusters up to 5 mm. long, which are aligned parallel to the walls of the sheet, giving a strong impression of flow, similar to trachytic texture. These trachytoid sheets appear to be the latest injections in the area, except on the southern slopes of Ruinsival, where they are cut by troctolite sheets and anorthosite veins (both have less than 10 % pyroxene), of ultrabasic composition (section 6.8), neither of which follows the breccia trend, however.

Zones East of the Ruinsival Zone: In this area, most of the peridotite is poised on the brink of brecciation: anorthosite veinlets are ubiquitous, forming converging (or radiating) systems which feed (or are supplied by) 1 to 10 cm. thick veins of feldspathic peridotite or anorthosite. The larger veins are usually vertical and along the breccia trend but may merge and brecciate the peridotite in pockets about 1 m. across. The thicker feldspathic peridotite sheets often have marginal strips or cores of anorthosite. One major zone, the Forked Zone, occurs in this area: it is named after its surface expression on the Ruinsival-Ainshval col. It is a breccia with a streaky, vertically banded, highly feldspathic matrix and chiefly notable for the clear evidence of micro-faulting and shearing near the margins, where anorthosite lenses are sheared in a sense indicating downward movement of the breccia relative to the walls: the sigmoidally deformed lenses occur in en-échelon arrays to form a vertical shear layer, 1 to 3 m. thick, parallel to the western margin (GR 3579 9424; Plate 3.45). The vertical eastern contact is exposed at (GR 3585 9406) and shows the classic igneous intrusive features of peels of country rock peridotite and short, thick apophyses of breccia matrix. As the zone is traced up the northern face of Ruinsival, it widens by 3 to 5 m. for every 20 m. of height. At the top of the scarp, internal structures flatten out to become sub-horizontal.

3.8.3 The Papadil System.

The Papadil system intrudes a layered dunite / dunitic peridotite sequence. The overall steep dip of the layering (30 to 50^{o}) explains the discrepancy between the strike of each breccia sheet and that of its internal structures (Fig. 3.5). This discrepancy is only rarely displayed elsewhere in the CS where dips of the layering are more shallow (0 to 30^{o}). The system consists of a major branching zone in the

south, the Papadil Zone, and the Leac a Chaisteil Zone in the north, with several subsidiary zones.

The Papadil Zone: The longest branch of the Papadil Zone forms a marginal breccia, 30 to 150 m. wide, along the SW contact of the CS with the Papadil Gabbro. Intense shearing and micro-faulting occur over 5 to 20 m. from the contact. The sense of shear indicates subsidence of the ultrabasic complex relative to gabbro (Plate 3.46). The clasts include sheared slivers of peridotite, the matrix is poor in olivine and has lenticular anorthosite bands which dip steeply inwards and strike parallel to the contact. In from the contact, the breccia matrix has a coarse, coralline to cluster-textured fabric and carries blocks of dunitic peridotite, fragmented chromitite and highly irregular, forked or cruciform segments of vein troctolite. At (GR 3668 9247), near the contact with the peridotite, which here has several chromitite laminae, the breccia has large blocks of feldspathic peridotite with protoharrisitic olivine, partly coated by chromitite up to 10 cm. thick. Further to the east, blocks of protoharrisite have rims of anorthosite. Parallel veinlets along the breccia trend are well displayed in the adjoining dunitic peridotite. They are subvertical and concentrated into 5 to 20 cm. wide zones, with an anastomosing fabric and may be found up to 10 m. away from the contact (Plate 3.47).

In the very SE, the breccia transgresses the Main Ring Fault of the igneous complex and is in direct contact with Torridonian sandstone; it forms a body of coarse feldspathic peridotite with patchy coralline texture and an occasional 5 to 10 m. block of dunitic peridotite. A northern branch off this stock, with several offshoots to the west, lines the eastern contact with the Southern Mountains Complex.

The Leac a Chaisteil Zone: this breccia follows and brecciates an allivalite in the CS, belonging to the lower unit of the Long Loch Group. Near the scarp at (GR 364 939), it also has blocks of gabbro, dunitic peridotite and troctolite. It is vertically structured with screens of peridotite and gabbro parallel to the margins, includes a large body of troctolite and has the following internal structures, which all parallel the breccia trend:

(1) Marginal zones 5 m. across, block-free apart from a lining of angular peridotite blocks and strips at the contact itself.

(2) Streaky modal and grainsize (plagioclase) banding in the block-free and block-poor, coarse, highly feldspathic, dendritic-textured peridotite matrix. Plate 3.48 illustrates the steakiness of the fabric.
(3) Within the central 50 to 80 m., zones of concentrated blocks alternate with clast-poor matrix. The blocks of dunitic peridotite are rounded, and close to 20 cm. across.
(4) Later 10 to 50 cm. thick sheets of a more olivine-rich, block-free feldspathic peridotite which cut through both the earlier matrix and its clasts.
(5) Coarse 1 to 10 cm. thick veins of pyroxene and plagioclase.
About 800 m. to the south and 80 m. higher, the zone thins to 5 m. of streaky, highly feldspathic peridotite with tabular slabs of dunitic peridotite and thin pancake-shaped ones of anorthosite. Subsidiary zones 0.4 to 2.0 m. thick flank the main breccia zone and are separated by veined country rock. The coarse olivine (up to 2.5 cm. long), in the feldspar and pyroxene rich matrix of these sub-zones is foliated often at an angle to the margins, as is the modal banding. Blocks of dunitic peridotite rarely exceed 20 cm. in diameter

3.8.4 The Dornabac System.

The one zone in the system examined in this study is a marginal breccia west of the Dornabac Member of the CS, the Lag Sleitir Zone of Wadsworth (1958). It is continuous from An Dornabac to Harris Bay, thinning from 170 m. to 10 m. At Harris Bay, the Lag Sleitir Zone has a feldspathic peridotite matrix, with faint vertical banding, sub-angular blocks of dunitic peridotite up to 30cm. across and strips of troctolite. Only the peridotite to the east (part of the CS) is parallel-veined. The breccia is also exposed along the banks of the Harris River, where it consists of a number of sheets up to 10 m. wide, separated by screens of peridotite. They have blocks of harrisite (from the Ard Mheall member of the WLS) and dunitic peridotite in a feldspathic matrix cut along the breccia trend by anastomosing sheets of pyroxene-rich peridotite . Some sheets have a few rounded dunitic peridotite clasts. The sheets merge to the north to form the Lag Sleitir Zone, as described by Wadsworth (1958).

TABLE 3.1 Nomenclature for the ultrabasic rocks of the Trallval area.

Ratio of cumulus olivine to cumulus feldspar:

>1 = peridotite				<1 = allivalite		
Modal content of dominant cumulus mineral: (in %)						
> 95	95 - 85	85 - 70	< 70	< 70	70 - 95	> 95
dunite	dunitic peridotite	peridotite	feldspathic peridotite	mafic troctolite	troctolite	anorthosite

TABLE 3.2 Stratigraphical division of the Central Series. Rock units included within the layered series by each author are underlined.

WADSWORTH (1958)	MC CLURG (1982)	THIS STUDY
	Ruinsival Member	Late ultrabasic plug
Upper Ruinsival Series		Ruinsival Group (RG1, RG2)
Lower Ruinsival Series	Long Loch Member	Long Loch Group (LLG1, LLG2, LLG3)
Dornabac Series	Dornabac Member	Dornabac Member
Lag Sleitir Breccia	Outer Breccia Member	Lag Sleitir Breccia Zone

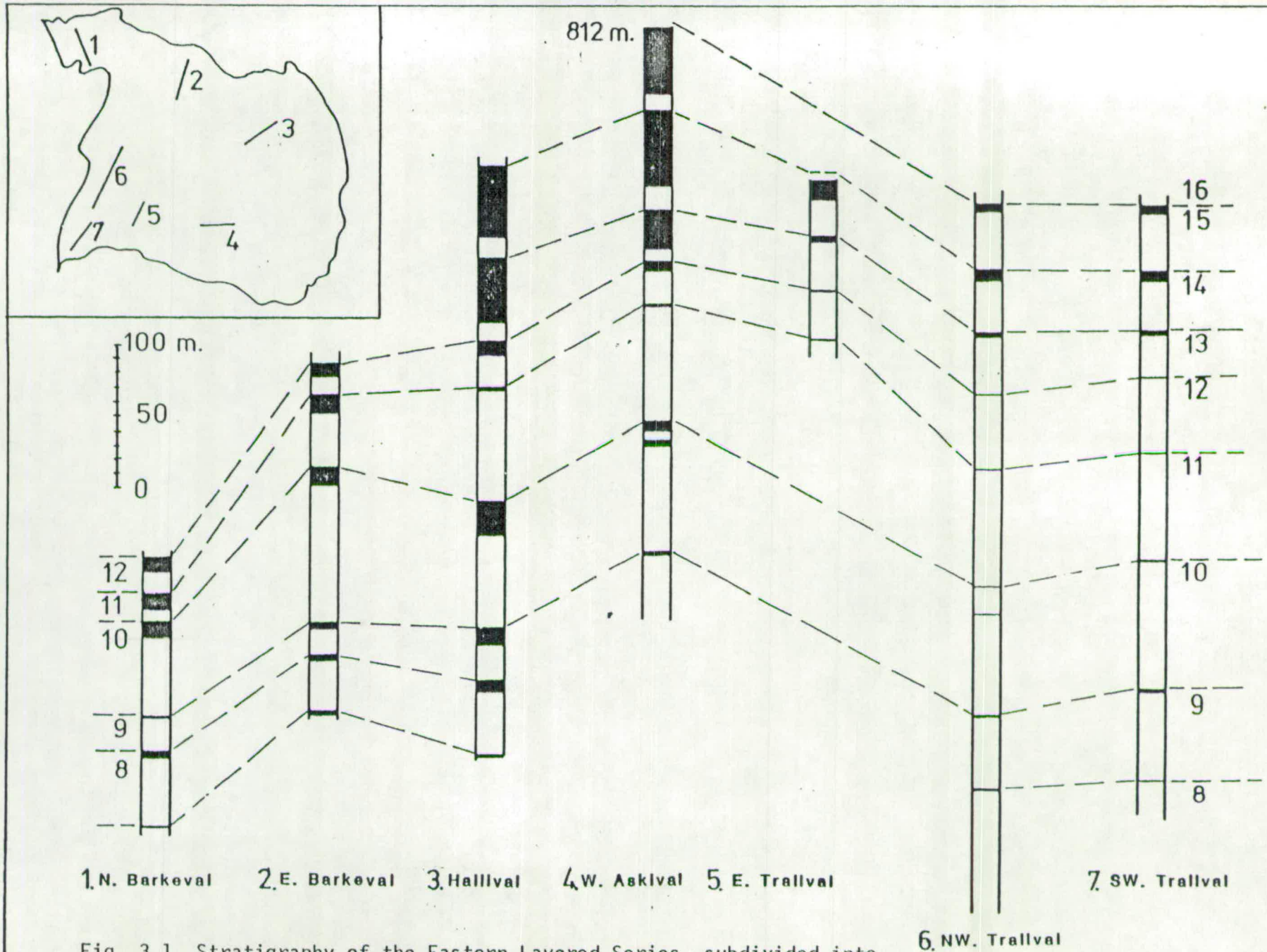

Fig. 3.1 Stratigraphy of the Eastern Layered Series, subdivided into units (numbered). Allivalite is shown in black, peridotite unornamented. Inset showslocation of sections on the outcrop of the ELS.

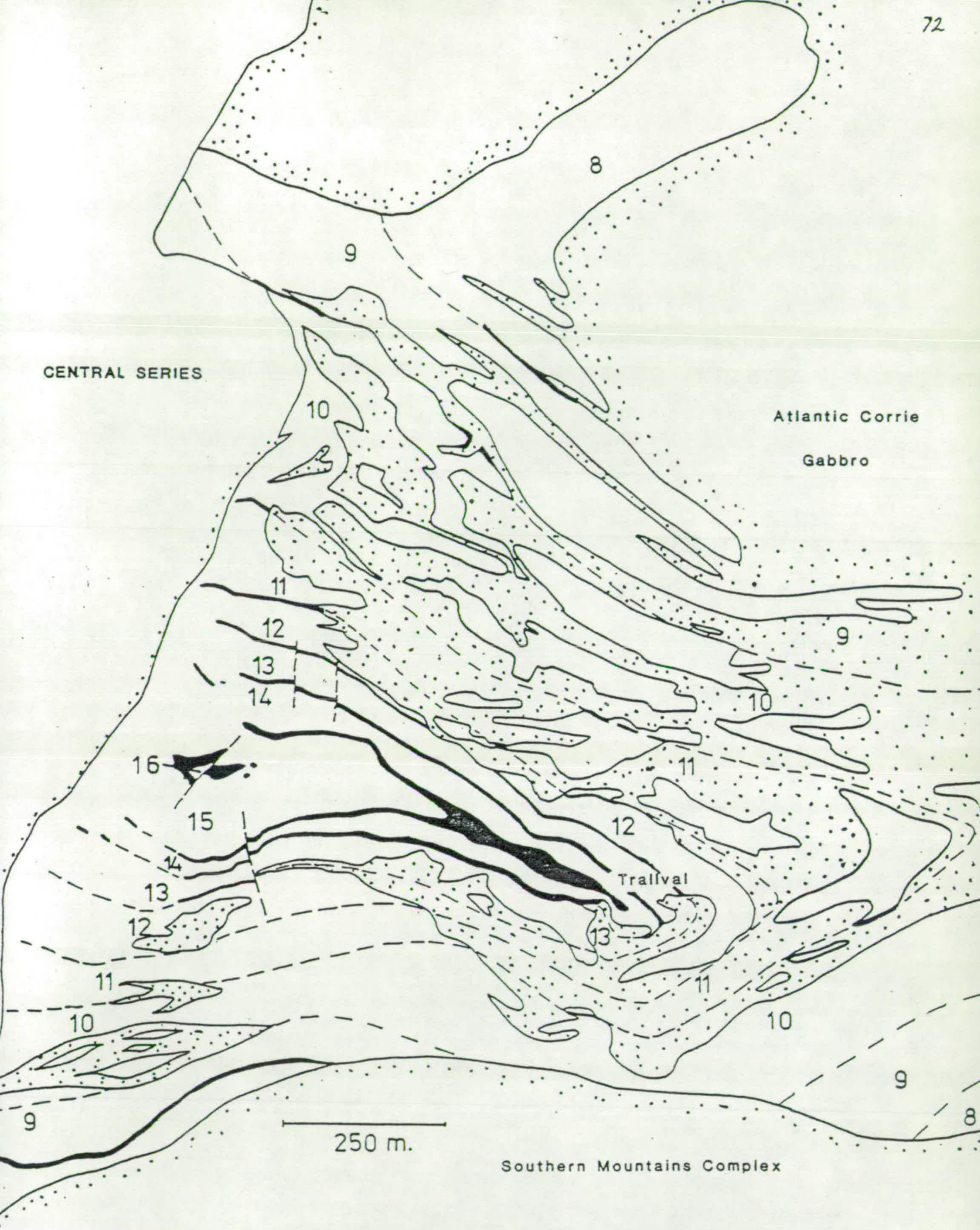

FIG 3.2 The distribution of the numbered stratigraphic units of the ELS in the Trallval area. Gabbro is stippled, peridotite unornamented and alliv alite shaded.

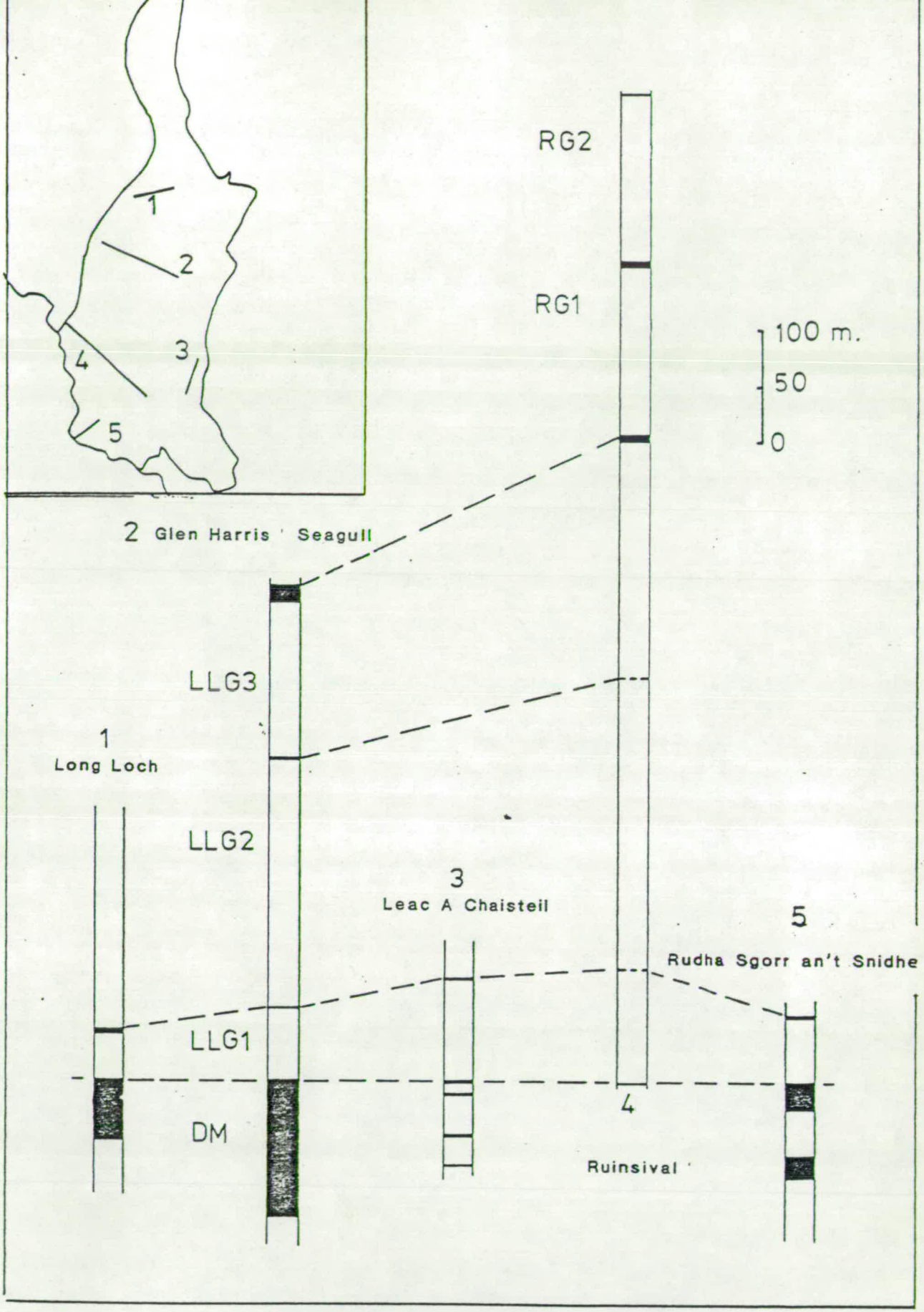

FIG. 3.3 The stratigraphy of the Central Series, subdivided into lettered and numbered units, and correlation of sections over the outcrop of the CS in the Trallval area. Allivalite black, peridotite unornamented.

FIG. 3.4 The distribution of the lettered and numbered units of the Central Series over the Trallval area. Area of breccia zones, plugs or gabbro are stippled near the contact with the Central Series. Allivalite is shaded in black.

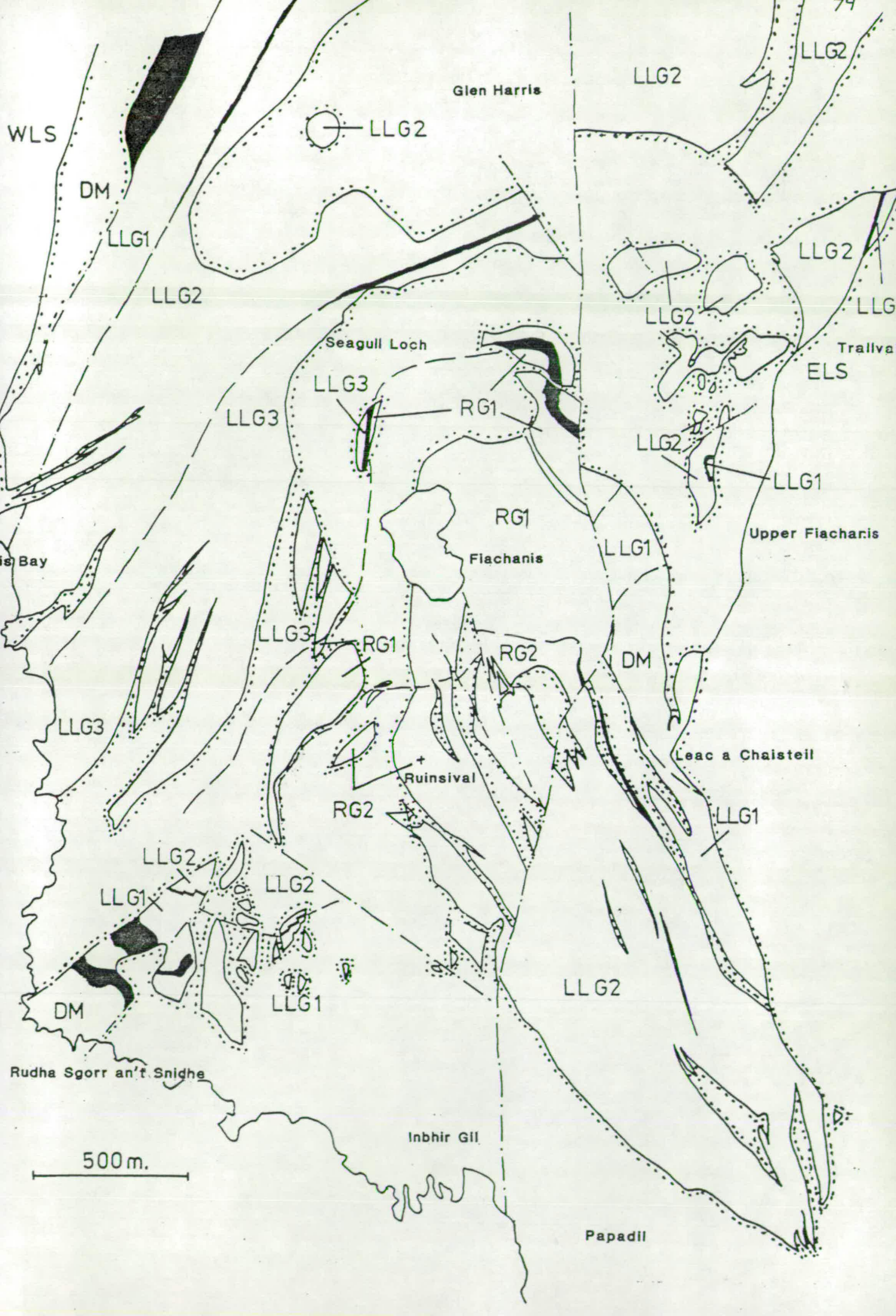
WLS
DM
LLG1
LLG2
Glen Harris
LLG2
LLG2
LLG2
LLG2
LLG2
LLG
Tralliva
ELS
Seagull Loch
LLG3
LLG3
RG1
LLG2
LLG1
RG1
Upper Fiachanis
Fiachanis
LLG1
is Bay
LLG3
RG1
RG2
DM
LLG3
Leac a Chaisteil
Ruinsival
RG2
LLG1
LLG2
LLG2
LLG1
LLG2
DM
LLG1
Rudha Sgorr an't Sniche
Inbhir Gil
500 m.
Papadil

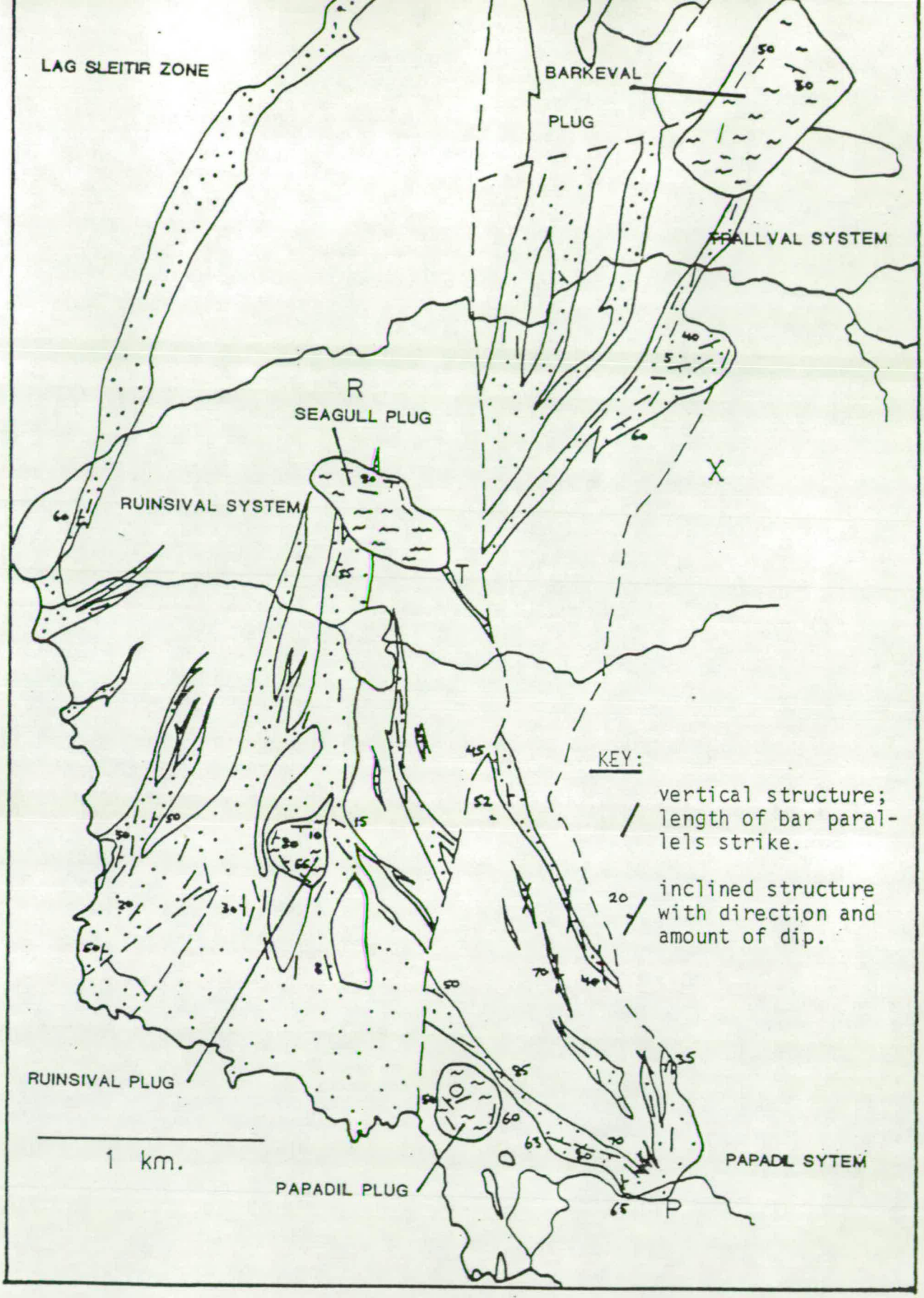

FIG. 3.5 The distribution and internal structure of the ultrabasic breccia zones (stippled) in the Trallval area. Later gabbros are omitted for clarity but ultrabasic plugs are shown (ripples). There is a small breccia zone in the ELS at X. Other initials indicate points of convergence of the individual zones within the system denoted by that initial.

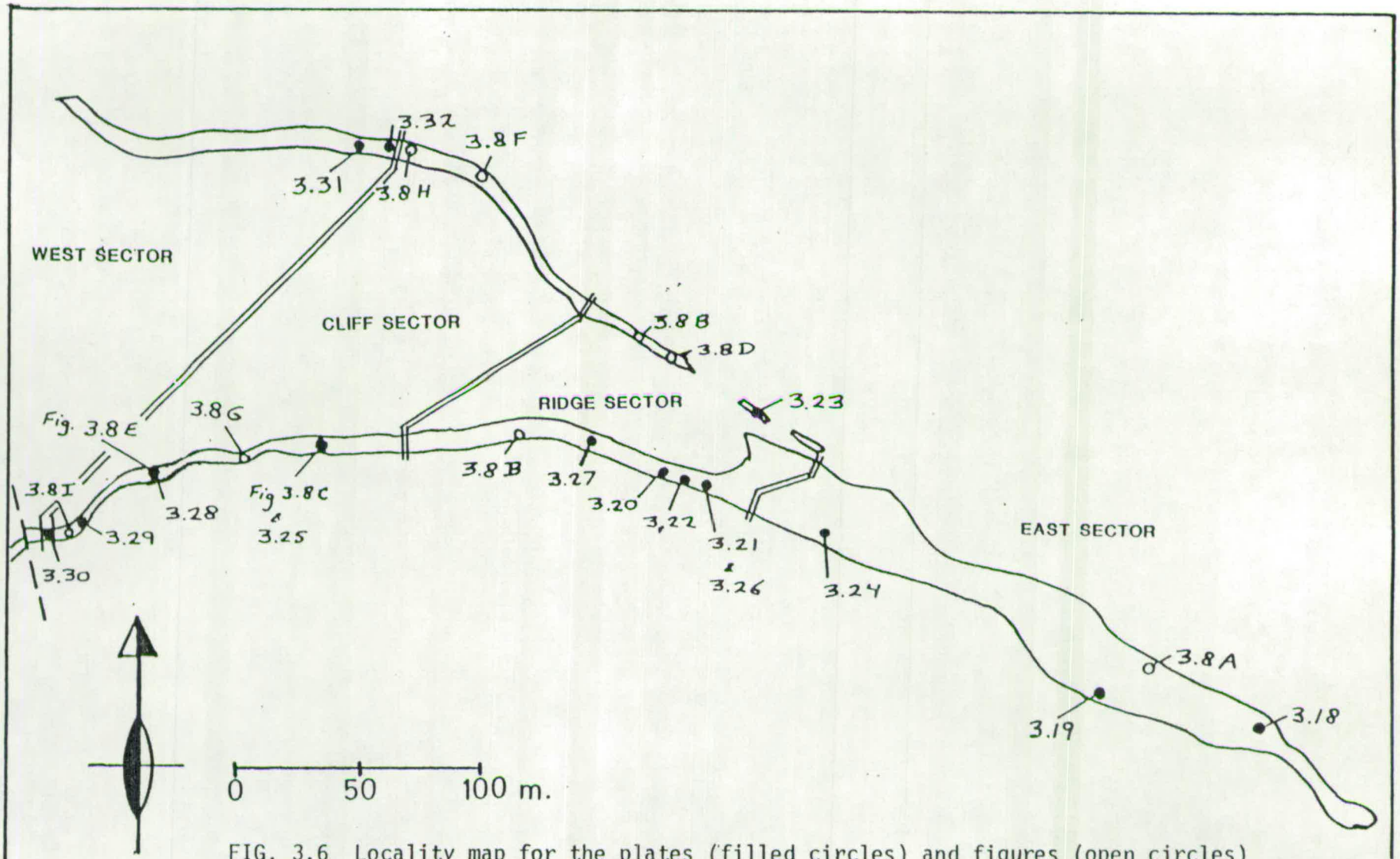

FIG. 3.6 Locality map for the plates (filled circles) and figures (open circles) illustrating the deformation of the allivalite of Unit 14 (section 3.5.10), along the summit ridge of Trallval.

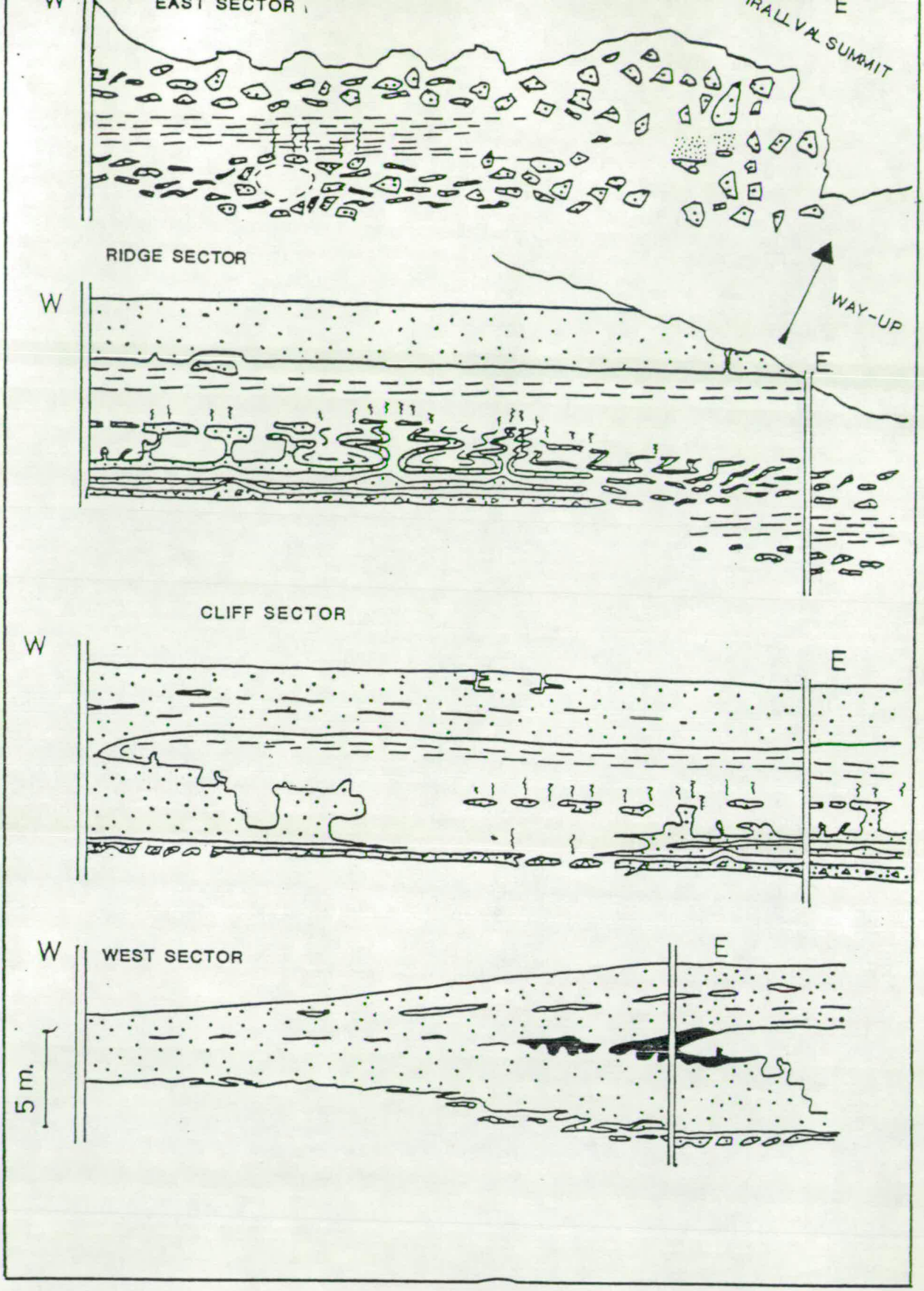

FIG. 3.7 Diagrammatic sections of the troctolite (stippled) layers along the summit ridge of Trallval. Pyroxene-rich troctolite is black, peridotite unornamented and the wiggles indicate feldspathic streamers. Layering in peridotite is shown by hatched lines.

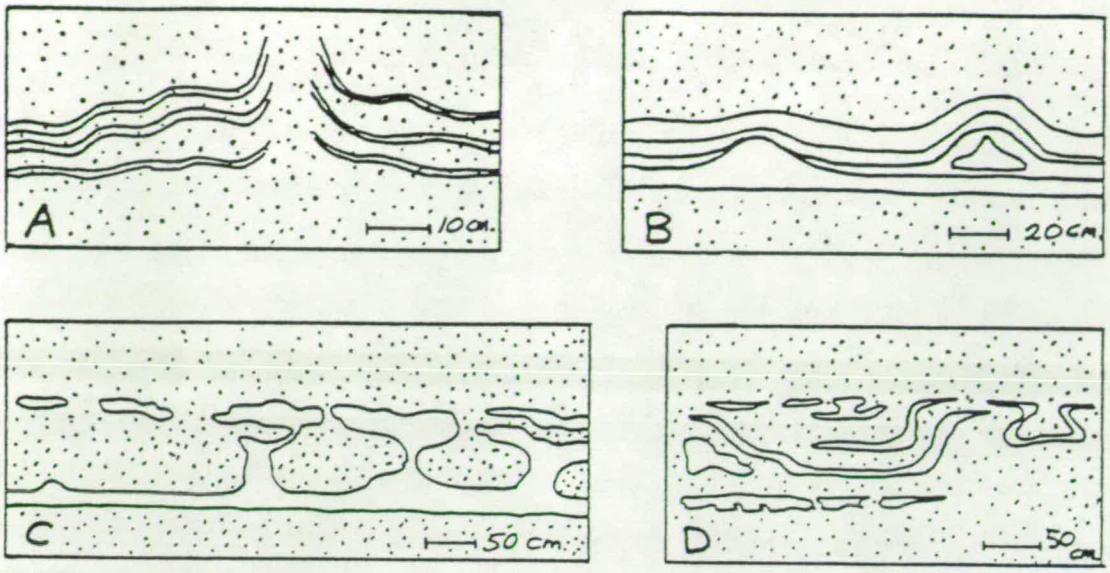

A- Deformed modal layering in peridotite

B- Deflection of layering in allivalite above diapiric mound and a clast.

C- Merging peridotite "pillows" replace troctolite.

D- Relic loading structures in allivalite.

E- Partly resorbed troctolite block.

F- "Flames" at a troctolite/peridotite contact with streamers.

G- Flames at a troctolite/peridotite contact.

H- Slumped layering truncated by planar layering in troctolite.

I- Flame of troctolite with anorthosite lamina and thin peridotite lenses.

FIG. 3.8 Field sketches of the structures in the allivalite of Unit 14.

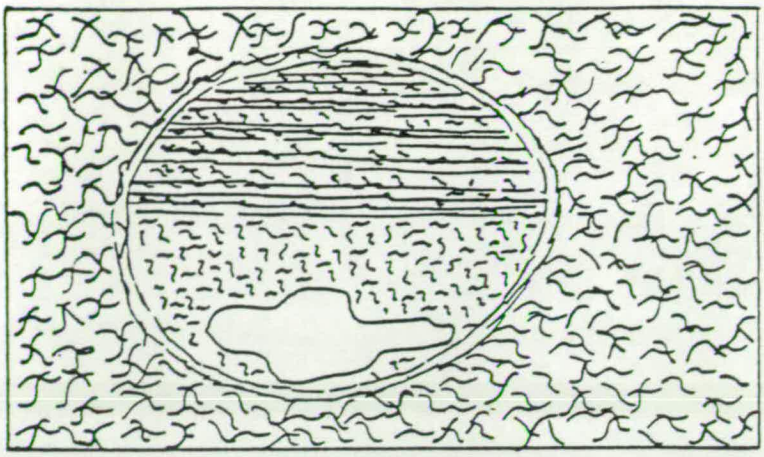

FIG. 3.9 Planar and concentric layering developed around a troctolite xenolith in the otherwise unlayered peridotite of Unit 12, East Trallval.

20 cm.

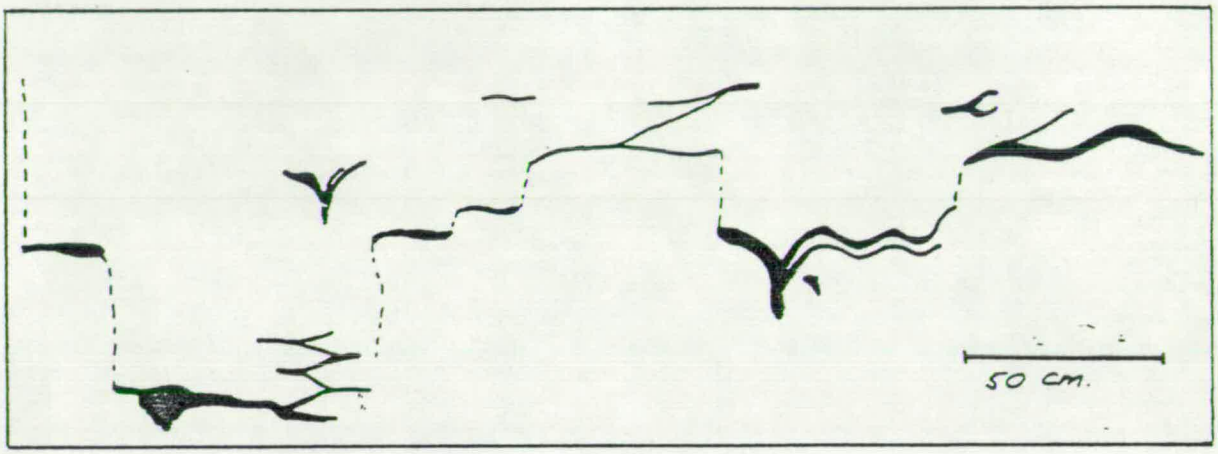

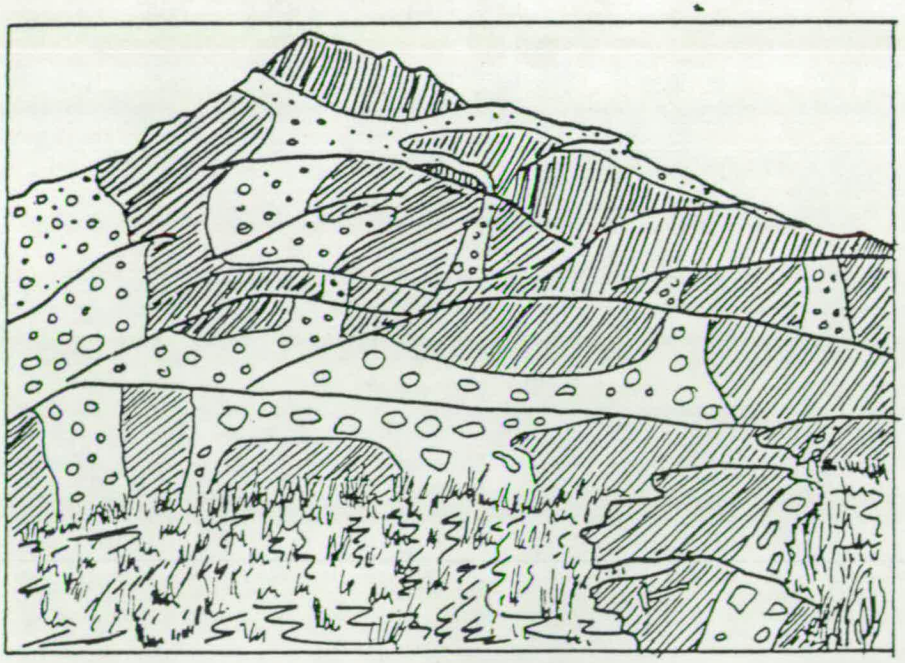

FIG. 3.10 Loading structures along a chromitite lamina in Unit RG1 of the CS, NW Ruinsival. Peridotite below the chromitite is less feldspathic than the peridotite above.

FIG. 3.11 Field sketch of breccia zones on the southern slopes of Ruinsival. The skyline is about 1.5 km. long.

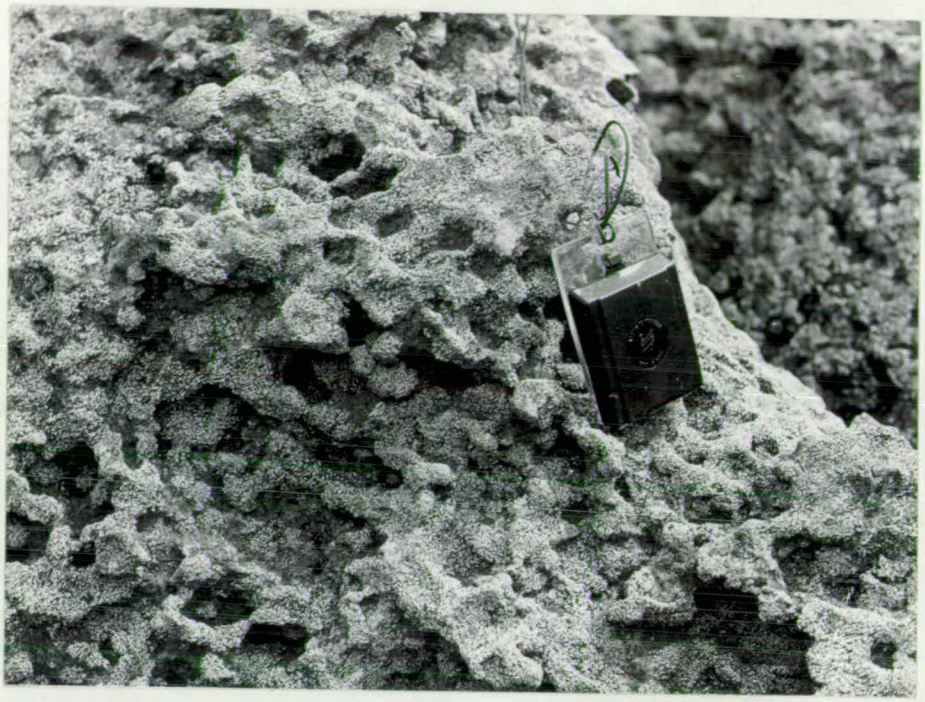

PLATE 3.1 Coralline texture, U10 peridotite, NW Trallval. Pale mineral = plagioclase oikocrysts, dark crystals = cumulus olivine, pyroxene oikocrysts weather in. length of compass: ca. 10 cm.

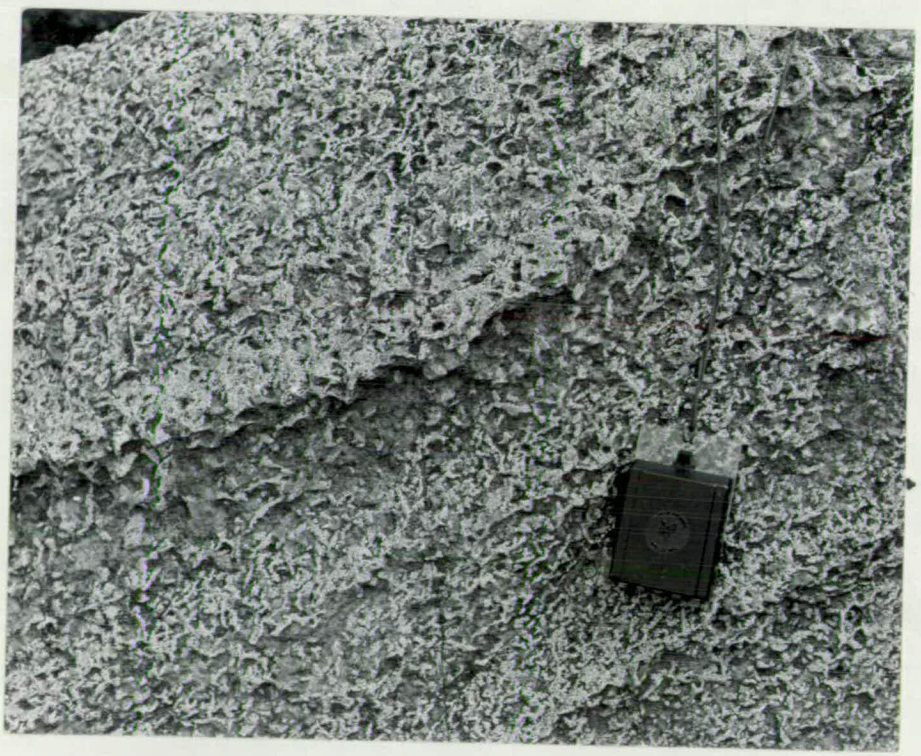

PLATE 3.2 Modal layering in dendritic-textured feldspathic peridotite, U12, NW Trallval. Pale mineral = plagioclase, large dark patches = pyroxene oikocrysts with olivine inclusions, small dark spots = cumulus olivine.

PLATE 3.3 Cluster texture on dip surface, U10 peridotite, NW Trallval. Pale, branching clusters of plagioclase oikocrysts with dark intervening areas of pyroxene oikocrysts. Both pyroxene and plagioclase include cumulus olivine. Length of notebook: ca. 15 cm.

PLATE 3.4 Harrisite pod in U15 peridotite, W. Trallval. Elongate, skeletal mineral = olivine. Other minerals as in Plate 3.2.

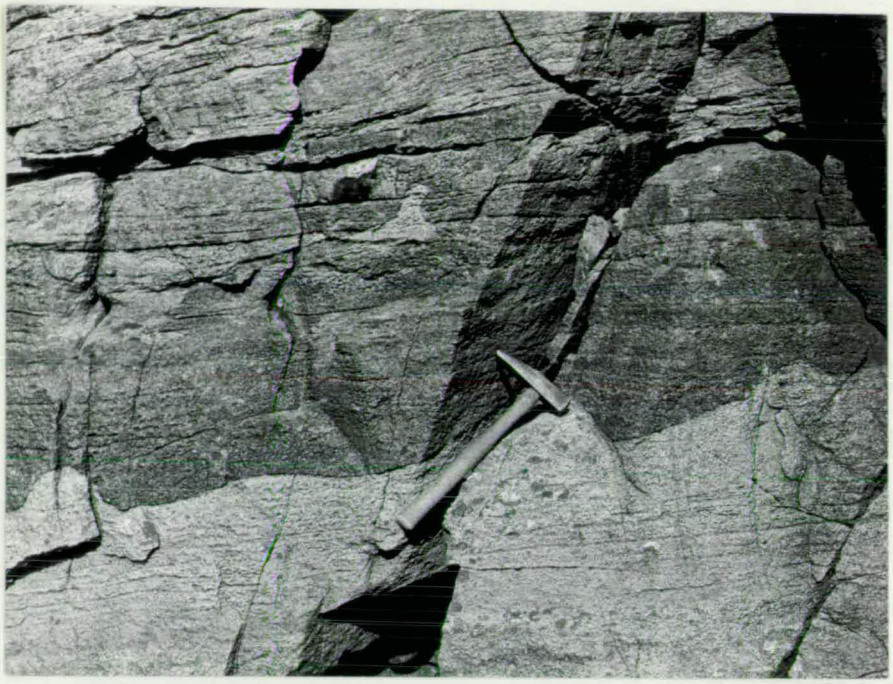

PLATE 3.5 Modal layering of cumulus pyroxene and plagioclase in allivalite. U14, NW Trallval. The upper, dark layer is rich in pyroxene. Hammer length : ca. 35 cm.

PLATE 3.6 Spinel-rich laminae stand out in this weathered, chromitite-layered peridotite; NW Trallval. The arrows indicate the spinel-rich laminae.

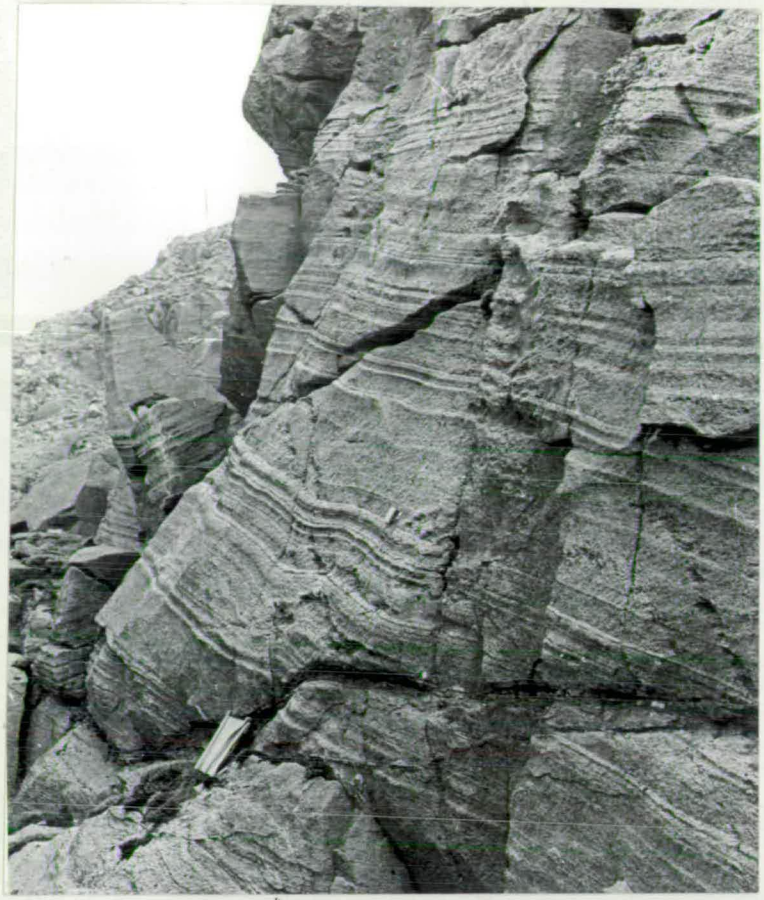

PLATE 3.7 Chromitite-layering in feldspathic peridotite, U14, NW Trallval. Rhythmically repeated pale layers have concentrations of spinel and intercumulus plagioclase.

PLATE 3.8 Cluster-layering in peridotite, U12, NW Trallval. Arrows parallel the layering.

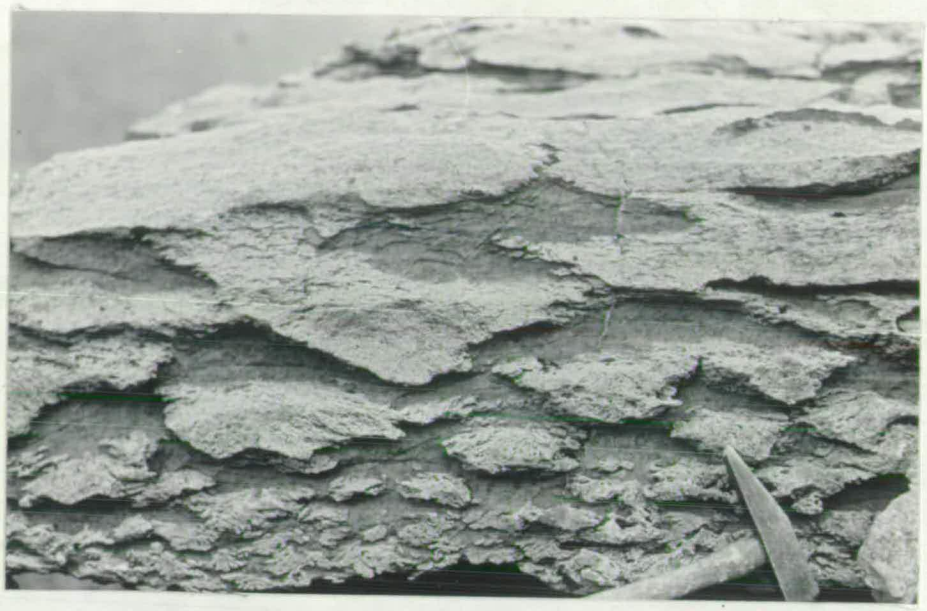

PLATE 3.9 Graded cluster sequence: a gradual transition from peridotite to troctolite, U12, NW Trallval. Length of hammerhead: ca. 10 cm.

PLATE 3.10 Melange of troctolite blocks in feldspathic peridotite, U14, SW Trallval.

PLATE 3.11 Shearing and micro-faulting in the allivalite of unit LLG3 of the CS, near Seagull Loch.

PLATE 3.12 Flame along the troctolite/pyroxene-rich troctolite contact of plate 3.5. Note the coarsening of the texture towards the top of the flame. U14, NW Trallval

PLATE 3.13 Vertical, pipe-like body of pyroxene-rich peridotite replaces primary chromitite layering in peridotite, U14, NW Trallval. Tripod height: ca. 60 cm.

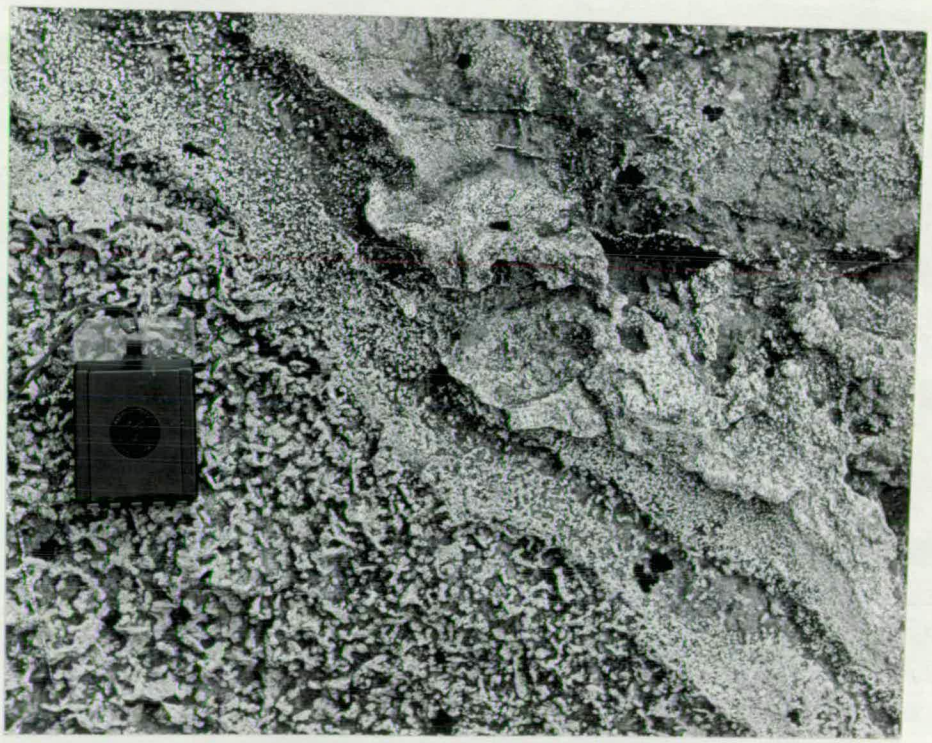

PLATE 3.14 Largely resorbed thin allivalite underlain by dendritic peridotite, U12, NW Trallval.

PLATE 3.15 A Feldspathic streamers, perpendicular to modal layering, developed at the base of U14, SW Trallval.

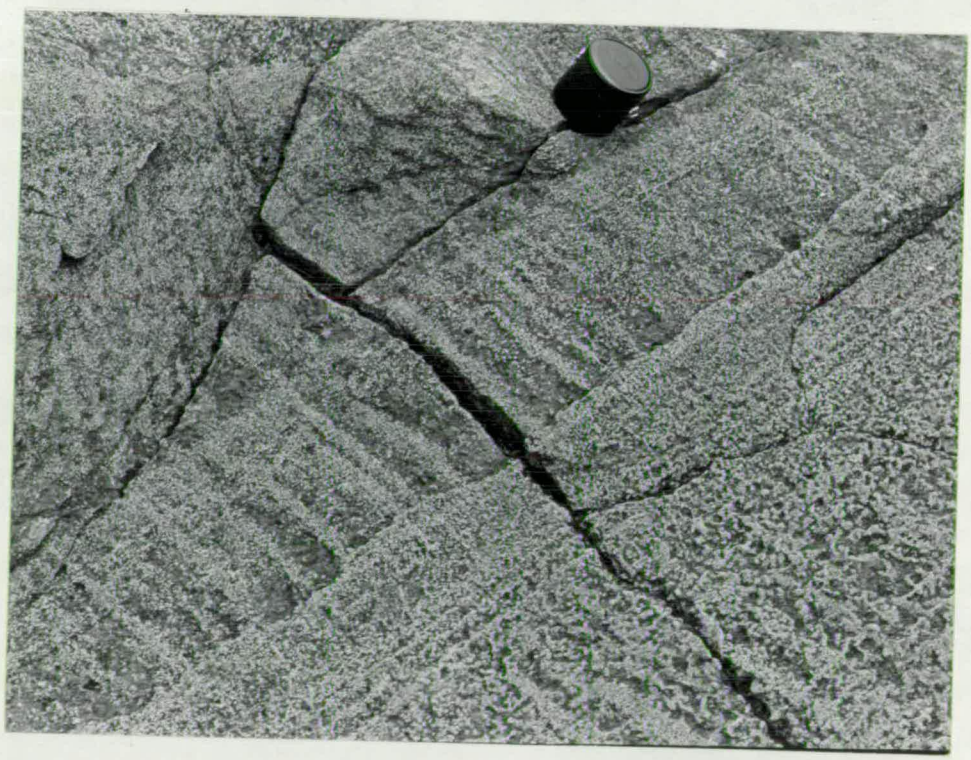

PLATE 3.15 B Detail of above.

PLATE 3.15 C The south face of West Trallval, exposing a 170 m. section through the ELS (also see frontispiece). The feldspathic streamers are well-developed above the lower pale layer (the allivalite of U13). The higher allivalite layer is that of U14, with the deformation structures described in section 3.5.10.

PLATE 3.16 Concentric layering around a plagioclase-free peridotite core, U13, SW Trallval. Knapsack (lower left) gives the scale.

PLATE 3.17 Partly replaced subsidiary allivalite in U14 peridotite, SW Trallval.

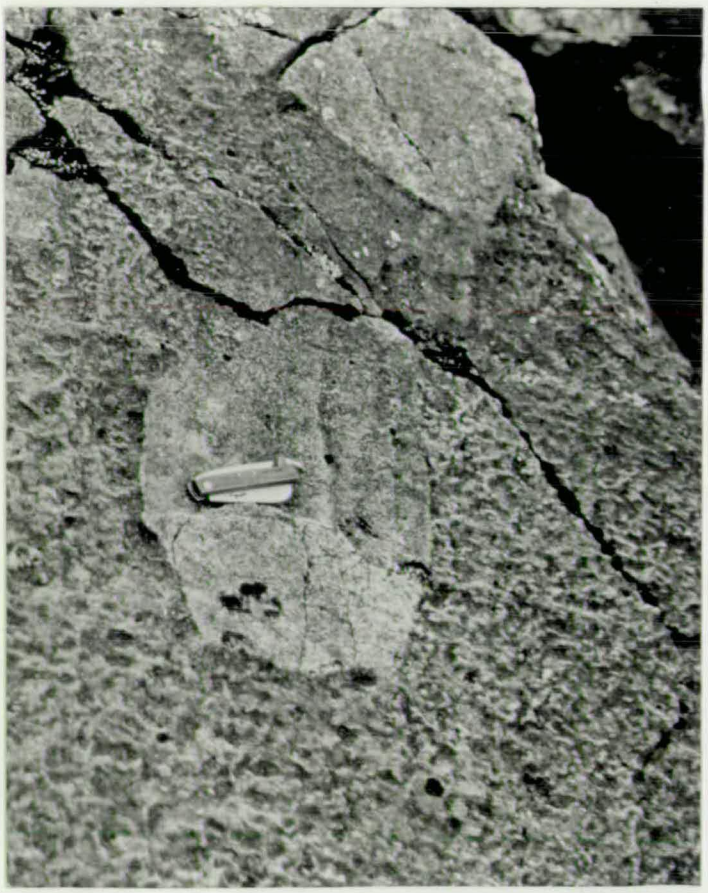

PLATE 3.18 Peridotite brecciating a layer of troctolite. A "shadow" of peridotite enriched in plagioclase is developed above each block, attributed to the redistribution of plagioclase by the upward expulsion and flow of intercumulus liquid. U14, Eastern sector, Trallval summit ridge. Knife length: ca. 10 cm.

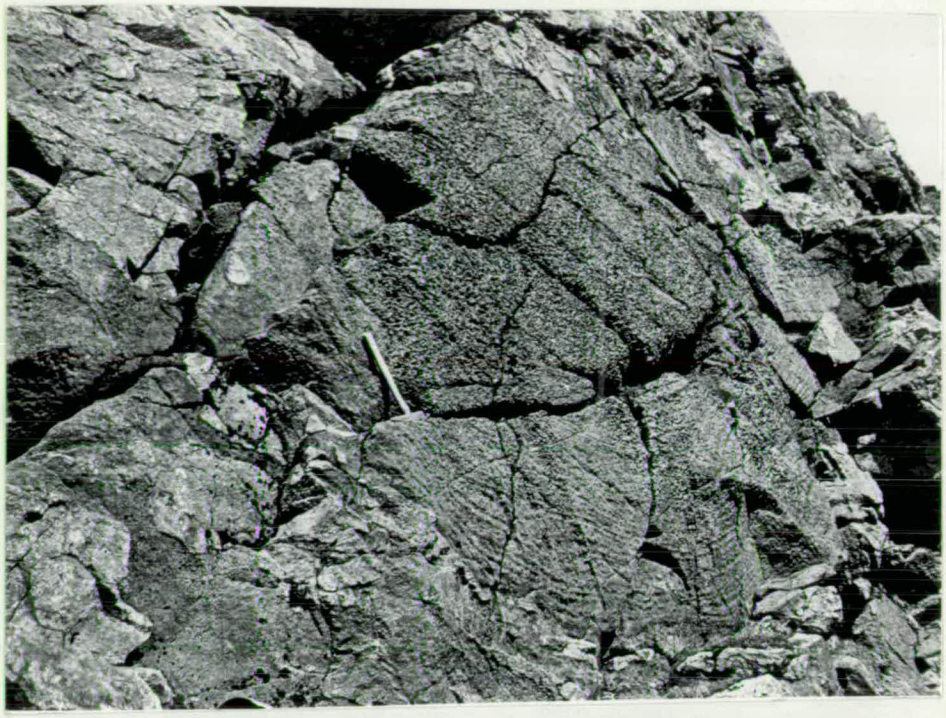

PLATE 3.19 "Ball and Pillow" loading structure of block-free peridotite which settled downwards into a troctolite mélange. The marginal, modal banding in the peridotite developed after loading occurred. U14, Eastern Sector, Trallval summit ridge.

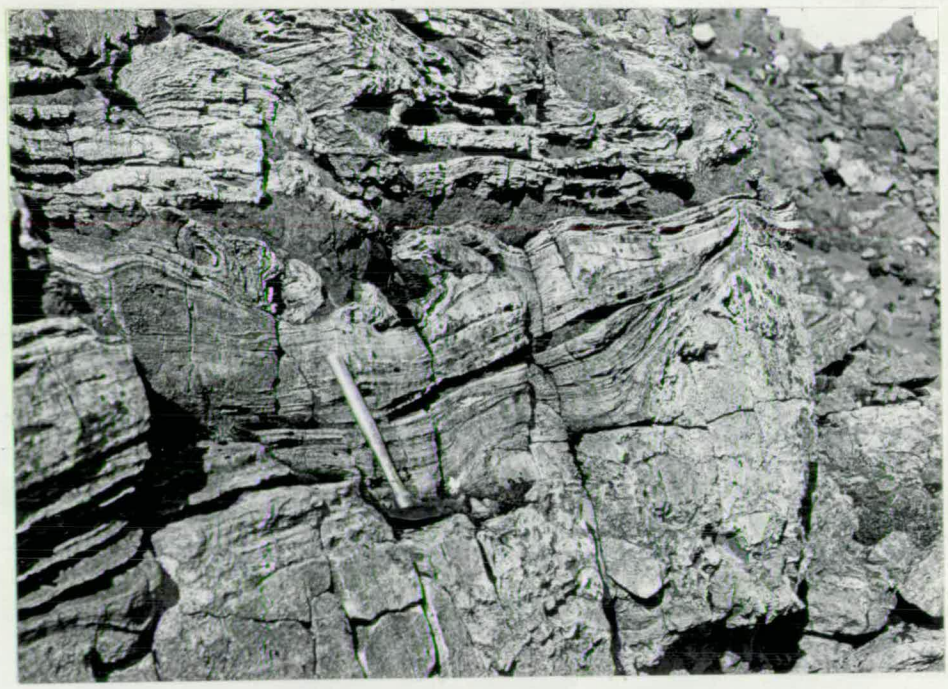

PLATE 3.20 Contact between the lower and middle layers of the U14 allivalite, with the thin, intervening peridotite. Ridge Sector, Trallval summit ridge.

PLATE 3.21 Deformation structures in the lower 2 troctolite layers of the allivalite of U14. The upper layer, above the layer of "sandwich" peridotite, is unaffected by the deformation. Ridge Sector, Trallval summit ridge.

PLATE 3.22 Diapiric structure at troctolite contact with overlying interlayered troctolite/peridotite sequence. U14, Ridge sector, Trallval summit ridge.

PLATE 3.23 Deformation in layered troctolite produced by sinking of peridotite "pillow" (in shadow, lower left). U14, Ridge Sector, NW Trallval.

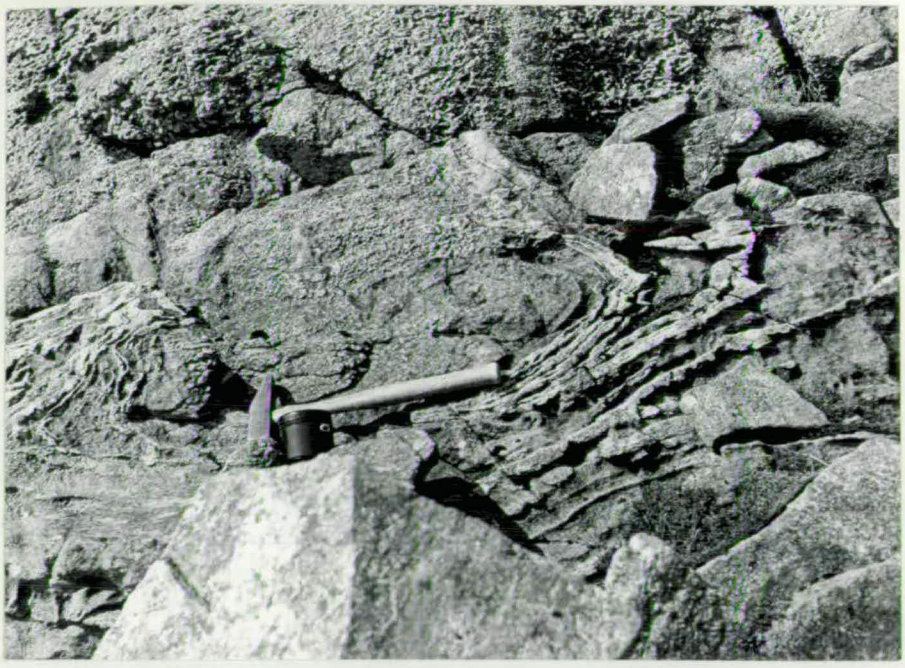

PLATE 3.24 Ball-and-pillow loading structure at lower contact of peridotite layer in U14 allivalite, East Sector, Trallval summit ridge.

PLATE 3.25 Troctolite flame into feldspathic peridotite, U14 allivalite, Cliff Sector, Trallval summit ridge. Note subsequent modal banding in peridotite.

PLATE 3.26 Detail of plate 3.21, showing the lower clast-bearing layer and the middle, convoluted layer (see text of section 3.5.10).

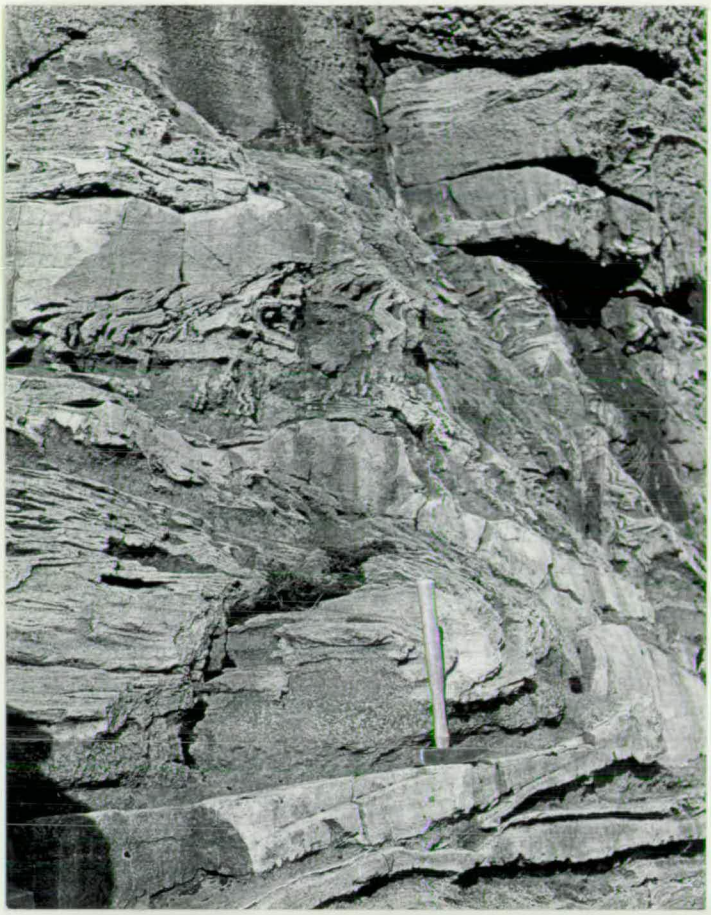

PLATE 3. 27 West side of a collapsed diapiric structure in the middle troctolite layer, allivalite of U14, Ridge Sector, Trallval summit ridge. Note the termination of folded troctolite laminae and their chemical replacement by peridotite.

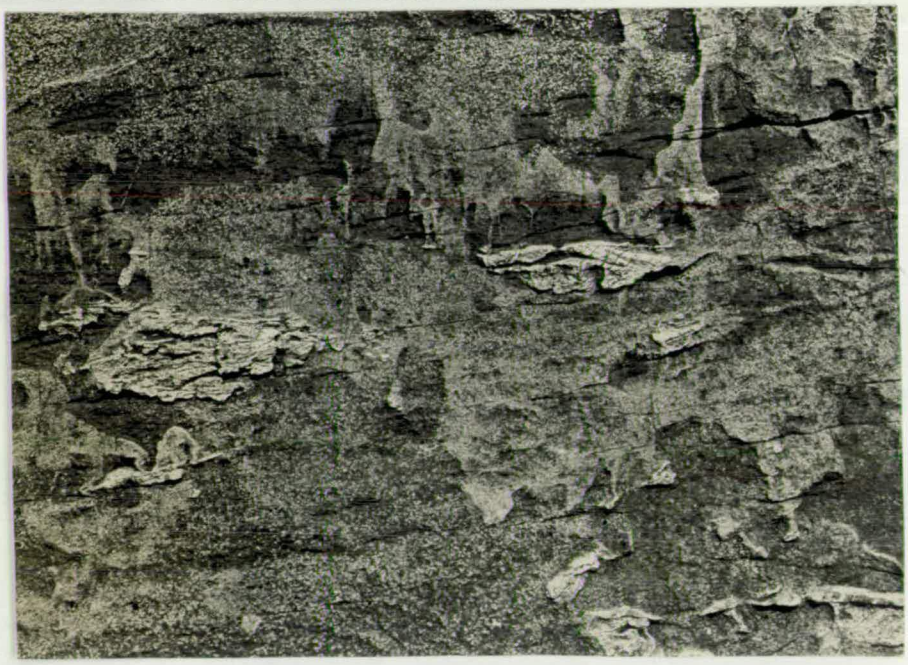

PLATE 3.28 Largely replaced allivalite with relic troctolite fragments. Cliff Sector, U14 allivalite on Trallval summit ridge.

PLATE 3.29 Relic troctolite body, with flames along the top, completely surrounded by peridotite. U14, Cliff Sector, Trallval summit ridge.

PLATE 3.30 Western termination of the sandwich peridotite in U14. Folding of the troctolite layering and inclusions in the peridotite suggest injection of the sandwich peridotite into the allivalite. Cliff Sector, Trallval summit ridge.

PLATE 3.31 Western termination of the dark pyroxene-rich troctolite layer, with its flame-lined lower contact, in the allivalite of U 14. West Sector, Trallval summit ridge. The photograph juxtaposes the west-facing scarps of 3 separate bluffs jutting out to the north.

PLATE 3.32 Flame structures at the base of the pyroxene rich layer of plate 3.31.

PLATE 3.33 Breccia of dunite and troctolite blocks in a dendritic-textured feldspathic peridotite matrix. Trallval zone, NW Trallval.

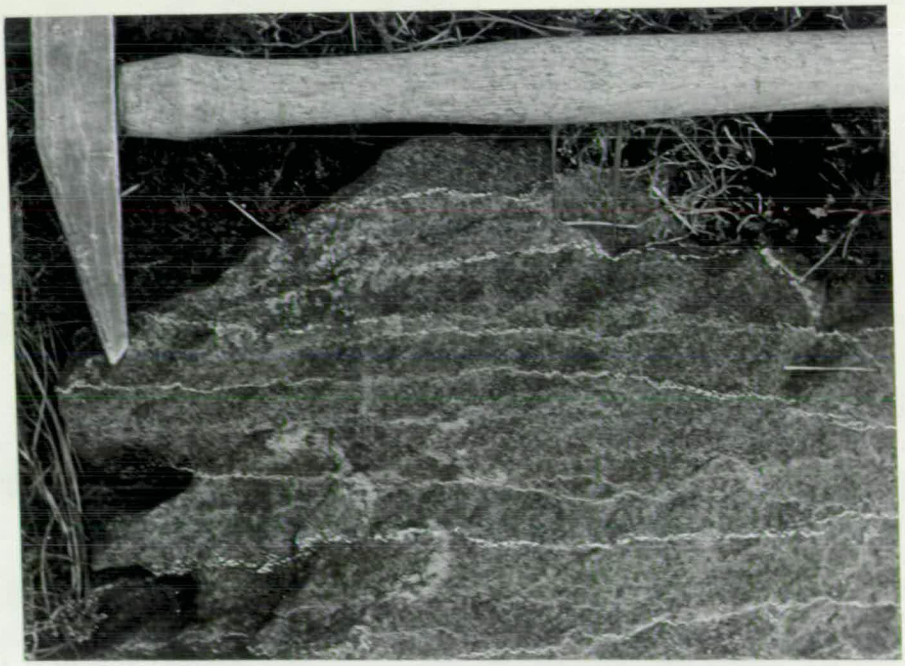

PLATE 3.34 Parallel troctolitic veinlets injected into CS peridotite, adjacent to and parallel with the Trallval Zone of breccia. Plan view, NW Trallval.

PLATE 3.35 Vertically structured breccia with blocks ofperidotite (dark) and gabbro (homogeneous, pale rock) and late dykelets of olivine-rich peridotite which cut both the gabbro and the peridotite. Plan view, Trallval Zone, Glen Harris.

PLATE 3.36 Pyroxene-rich, block-free breccia matrix. Pyroxene forms the large, spherical crystals. Eastern bulge of Trallval Zone, NW Trallval.

PLATE 3.37 Well-sorted, subangular troctolite clasts in feldspathic peridotite matrix, Trallval Zone, NW Trallval.

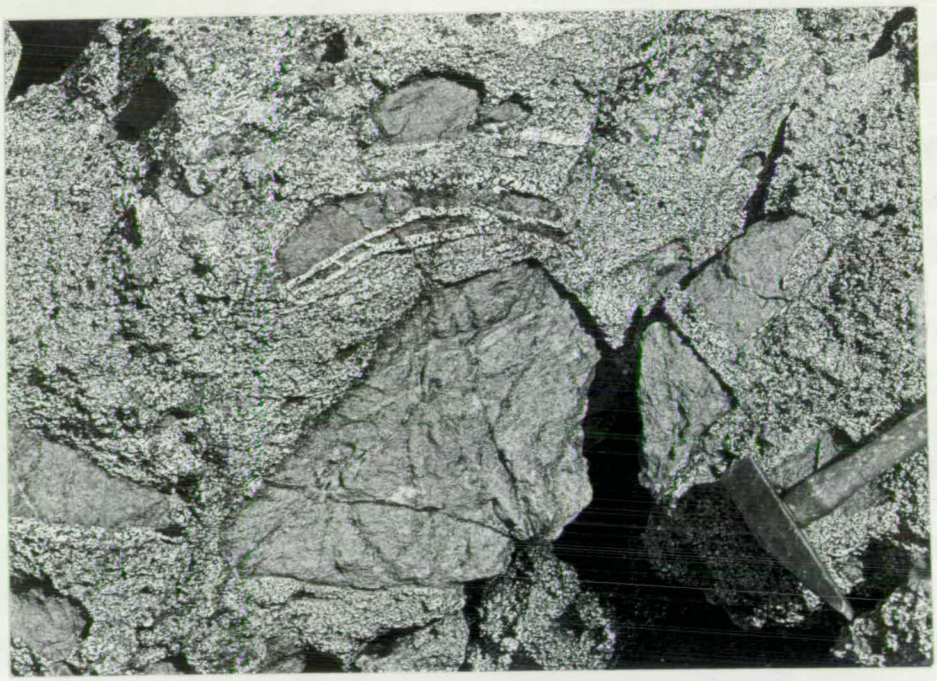

PLATE 3.38 Dunitic peridotite blocks (one with early troctolite veins) in highly feldspathic peridotite matrix, Trallval Zone, NW Trallval.

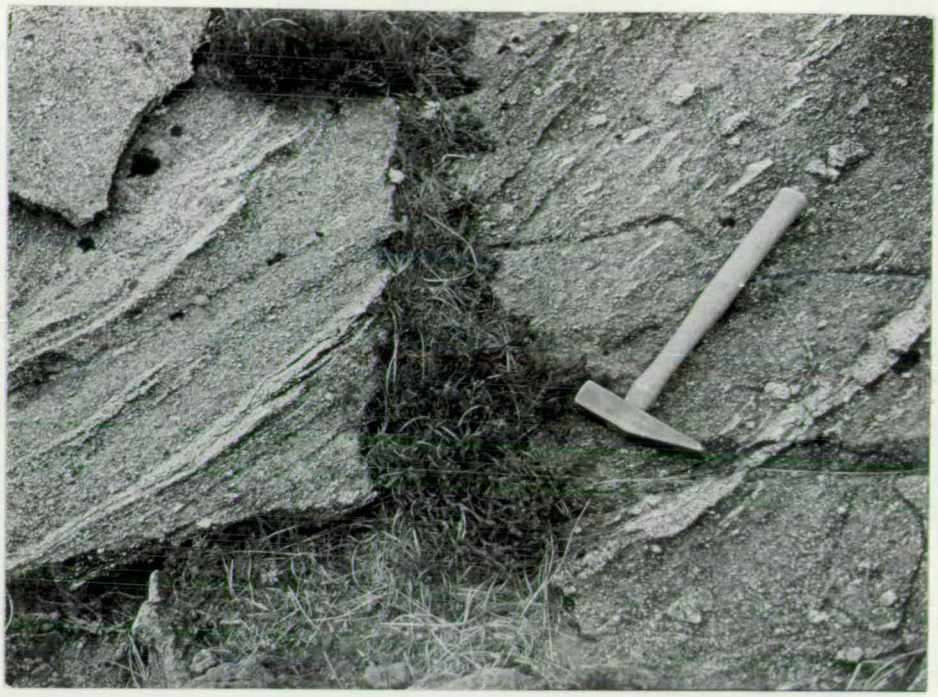

PLATE 3.39 Sheared breccia matrix and clasts of troctolite and anorthosite. Near "roof" contact of Trallval Zone, NW Trallval.

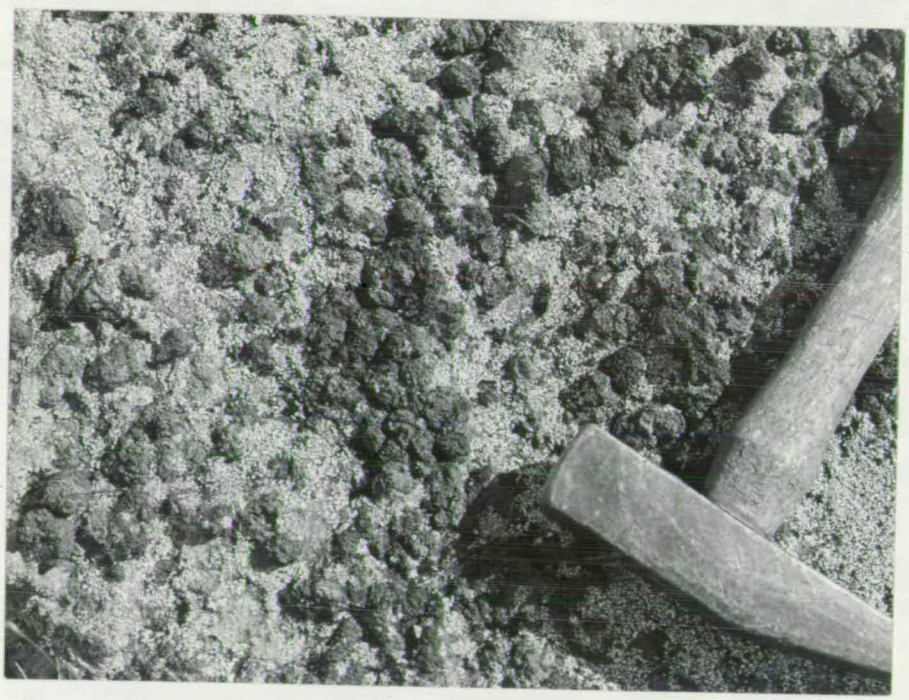

PLATE 3.40 Pyroxene-rich, highly feldspathic peridotite in breccia matrix of Ruinsival Zone. Pyroxene forms the bulbous crystals. SW Ruinsival.

PLATE 3.41 Heterogeneous, dendritic-textured matrix, Ruinsival Zone, NW Ruinsival.

PLATE 3.42 Giant, plagioclase-rich cluster in breccia matrix, Ruinsival Zone, central prong, NW Ruinsival.

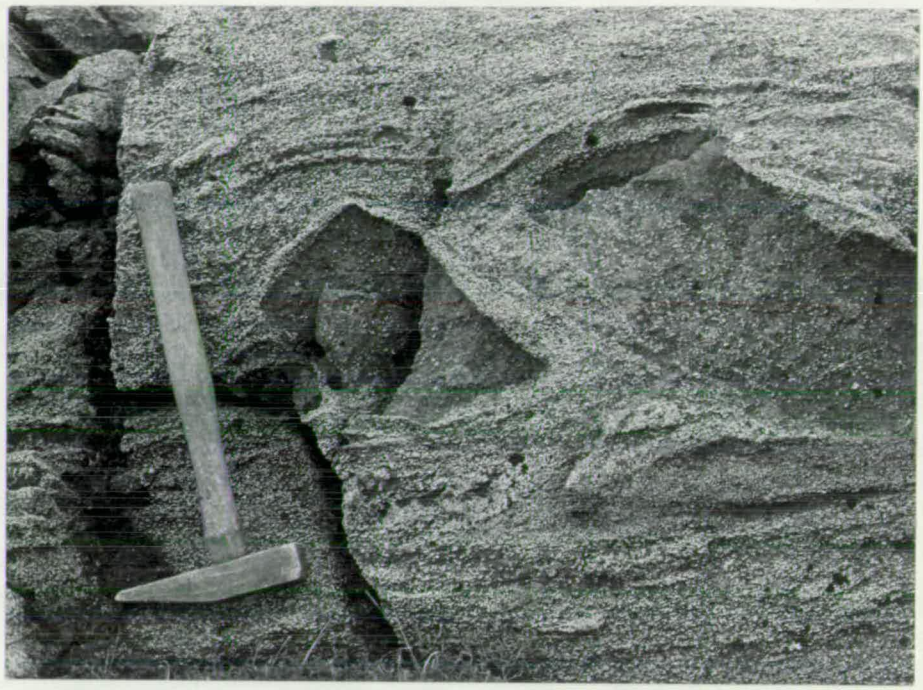

PLATE 3.43 Sub-horizontal banding deflected by peridotite blocks near roof contact of the eastern prong of the Ruinsival Zone, Ruinsival summit.

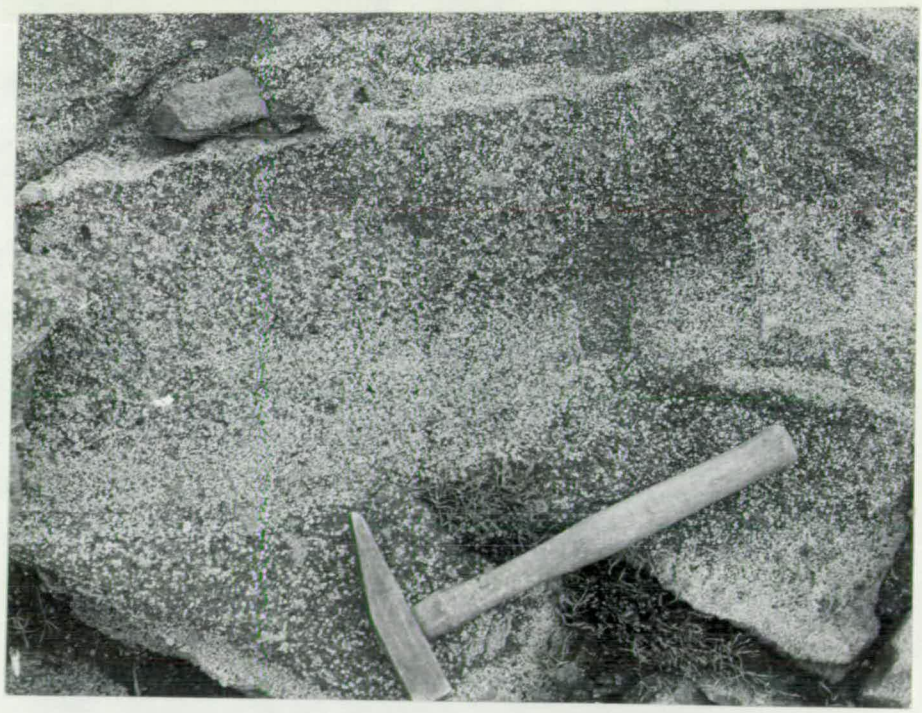

PLATE 3.44 Diffuse, modal banding in the matrix of the Ruinsival Zone of breccia, eastern prong, Ruinsival summit.

PLATE 3.45 Shearing of the breccia matrix near the western margin of the Forked Zone, N Ruinsival.

PLATE 3. 46 Marginal shear layer in the Papadil Zone of breccia, Papadil.

PLATE 3.47 Parallel troctolitic veinlets adjacent to and parallel with the Papadil Zone, Papadil. Grade 1 egg for scale.

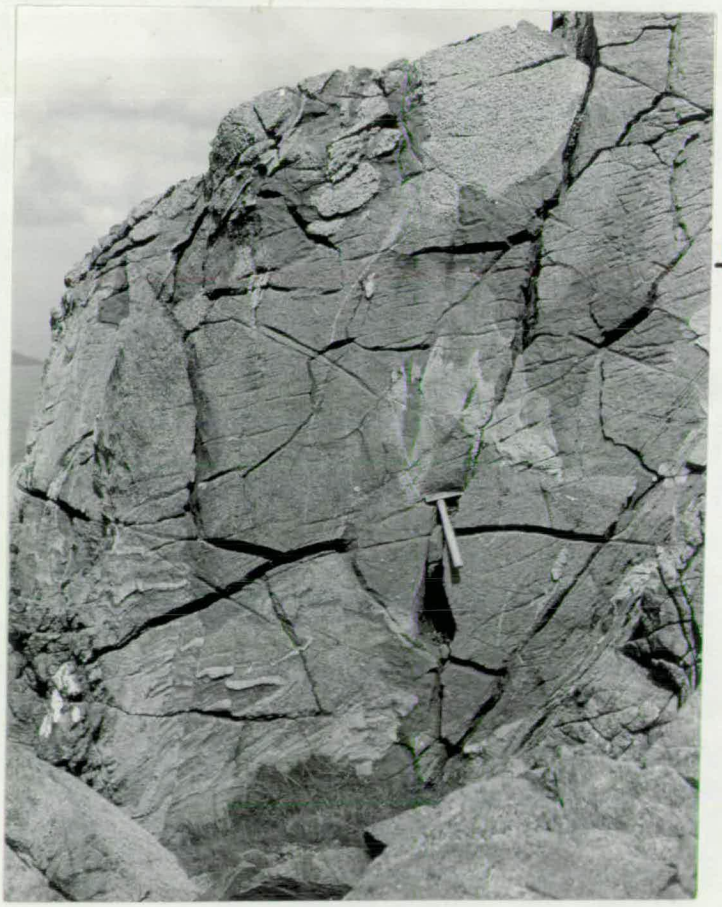

PLATE 3.48 Streaky textures in the matrix of the Leac a Chaisteil Zone of breccia, Leac a Chaisteil.

CHAPTER 4

THE GABBROS: FIELD DATA.

The field relations of fine-grained sheets are presented in Chapter 6. All other basic bodies intruded into the layered ultrabasic sequences have been mapped as gabbro and are shown in Fig. 4.1. The two major bodies are the Atlantic Corrie and the Glen Harris Gabbro intruded, respectively, into the ELS and the CS. Smaller, petrologically distinct gabbros occur within both areas. While the ELS has a continuous dyke-like gabbro along its southern contact, only sporadic pockets of gabbro have been emplaced along the contacts of the CS. A marginal gabbro partly sheathes the Papadil peridotite plug (section 3.7.1).

4.1 The Atlantic Corrie Gabbro.

Harker (1908) described the gabbro as a laccolithic eucrite mass, consisting of separate injections, with prevalent layering and much mica at the Trallval - Askival col. McClurg (1982) noted its petrological similarity to allivalite.

Form: a 520 m. thick, laccolithic system of confluent sheets, sometimes conformable to the layering in the ELS.

Field Characteristics:

Despite its modal heterogeneity, the rock weathers to dark-grey, characteristically smooth surfaces. Steeply inclined slabs are often wet, unlike peridotite faces, due to the lack of fracture and the lesser permeability of the gabbro. Etching by peaty water allows field identification of its component minerals and their textural relationships. Well-laminated plagioclase forms 50 to 90 % of the rock, oxides are scarce, subhedral olivine is an essential constituent, the texture is granular and the grain-size fine to medium (1 to 5 mm. crystals). Biotite is locally abundant in vertical zones 1 m. thick, pyroxene varies in grain-size (it is sometimes phenocrystic) and is unevenly distributed, being often concentrated in clusters, lenses, layers and pure-pyroxene laminae, coplanar with the plagioclase lamination, which impart an inconspicuous, undulatory banding to the gabbro an a scale of 5 to 20 cm. The banding is strongest near con-

tacts with peridotite and paralleled by layers with fragmented, often hornfelsed, peridotite and blocks of a finer facies of a similar gabbro.

As Fig. 4.1 shows, the layering, sub-horizontal near the centre of the intrusion, steepens towards its margins, reaching 30 to 40° near the summit of Trallval. The sheets which make up the composite body, with brecciated peridotite and gabbro along the lower and upper surfaces, can be idealised as a pile of saucer-shaped intrusions, thickest near the centre (up to 80 m. thick) where they merge, being interleaved with coherent peridotite only over the outer 700 m. of the body, 3 km. in diameter. The centre of the mass is well-exposed in Atlantic Corrie, and one 25 m. thick sheet is well-layered, including layers of olivine-free anorthosite, pyroxene-free troctolite and plagioclase-rich layers with poikilitic pyroxene (GR 3793 9624). Slump structures are common in the overlying sheets (Plate 4.1), which is also strongly layered (Plate 4.2). Some of the thicker sheets have a coarse facies in this area.

Contact Relations with the Peridotite.

These are best exposed on the northern slopes of E Trallval, where the gabbro sheets intrude and stope the peridotite. On a small scale, the contacts are often extremely intricate (Fig. 4.2 A), in a manner which suggests the peridotite behaved plastically. On a large scale, contacts are stepped in section, showing that the gabbro magma prised off tabular slabs of peridotite up to 50 m. long (Fig. 4.2 B); this is best seen where the gabbro sheets thin and approach the limit of their lateral penetration into the ELS. In this area also, the gabbro is intercalated with the allivalites in the layered sequence, often brecciating them (GR 3742 9612 and 3772 9517), or, as at (GR 3758 9592), folding the allivalite and remobilising the overlying peridotite (section 3.5.2). Further in from this front, brecciated peridotite is concentrated into sub-horizontal zones, where the gabbroic matrix is coarsely poikilitic, which alternate with peridotite-free, finely layered granular gabbro. While some of the peridotite blocks are quite unaffected, others are hornfelsed to a fine-grained, rusty, compact rock with anastomosing veinlets of plagioclase and pyroxene. The hornfelsed blocks are often

rimmed by gabbro enriched in pyroxene with repect to the matrix. Hornfelsed peridotite also forms important screens over much of the area. While the evidence for gabbro intruding peridotite is overwhelming, at many localitites, peridotite intrudes (or re-intrudes) olivine gabbro, most spectacularly so on the south-facing cliffs at (GR 3765 9507; Plate 4.3). The peridotite is unbanded and bears significant biotite; it will be recalled from section 3.5, that most allivalites in the area consist of a mélange of troctolite blocks in a structureless peridotite matrix. Gabbro brecciated by peridotite is also described at the end of section 3.5.5.

4.2 The East Trallval Gabbro.

Form: A dyke-like body with numerous subsidiary sheets, it levels at about 600 m. of altitude. The subsidiary sheets are sub-parallel and at the head of Glen Dibidil, near the southern contact of the ultrabasic complex, the extension of the peridotite / olivine gabbro complex by sheets of this later, leucocratic gabbro exceeds 100 % (Plate 4.4): over a 100 m. section, measured normal to the inclina - tion of the sheets (50^{o} to the north), 58 m. of leucogabbro in 10 sheets was injected into 42 m. of peridotite, olivine gabbro and earlier dolerite dykes.

Field Characteristics.

A pale, fine to medium-grained gabbro, it is essentially free of olivine, while biotite and oxides are common. The plagioclase is not laminated, the rock is homogeneous and unbanded, and the pyroxene subophitic. The main dyke, 80 m. thick, brecciates peridotite and the older gabbro extensively. This intrusive breccia has less than 10 % of leucogabbro matrix and forms some of the subsidiary sheets.

4.3 The West Trallval Gabbro.

Form: A number of scattered elongate bodies, from flattened pipes to dykes, almost all intruded along faults demonstrably associated with the CS / ELS contact. The largest body is in fact intruded along this contact over at least 1.5 km., reaching a width of 130 m. to the south, but on average 15 m. wide.

Field Characteristics.

A coarse melagabbro, it does not chill against the peridotite of either series. Ophitic pyroxene is very abundant and reaches a length of 15 cm.(including subhedral plagioclase 1.5 cm. long) where the gabbro is thickest. Olivine is present but inconspicuous.

4.4 The Glen Harris Gabbro.

Harker (1908) described the contact relations of this mass as extremely complex. Wadsworth (1958) named it the Glen Harris Eucrite, describing the contacts as intrusion breccias and noting that it is unlayered but includes pieces of peridotite throughout and patches of a fine-grained facies.

Form: A vertical-sided boss east of the Long Loch Fault, with a wedge-shaped southwards extension, it consists of a couple of thick sheets (50 to 100 m. thick) to the west of the fault. The northern sheet is sub-horizontal and the southern one forms an elongate inclined mass which thins southwards to a dyke. As the west side has been down-faulted by 200 to 400 m. (section 2.3.2), the boss to the east probably branched into thick sills and sheets above the present level of exposure (Fig. 4.2 D). The dyke-like extensions to the south may be relics of original feeder dykes along fractures parallel to the Long Loch Fault (Fig. 4.1).

Field Characteristics.

Coarse-textured, this olivine gabbro weathers to rough surfaces and a gravelly soil (Plate 4.5) and supports a relatively luxuriant vegetation. The main facies is medium- to coarse-grained (pyroxene up to 10 cm. long, usually 1 to 3 cm.) with ophitic to subophitic pyroxene, common plagioclase segregations and no lamination. Layering is rare and only developed near contacts with peridotite. The uneven pyroxene distribution makes for a heterogeneous rock. It is often cut by a finer facies, modally layered at the contacts, with a granular texture, conspicuous oxides and scattered large plagioclase crystals (1 to 2 cm. long vs. an average size of 1 to 3 mm.). This rock is more homogeneous and poorer in olivine than the coarse facies. Neither facies show a chill at peridotite contacts.

Contact Relations.

To the east of the Long Fault, most contacts with peridotite are

vertical, and both the stoped masses of peridotite within the gabbro and the adjacent country peridotite are heavily injected with dykes, sheets and veins of the coarse olivine gabbro, up to 10 m. thick, which locally brecciate the peridotite (a greater block / matrix ratio correlates with a larger block size). Compact, rusty-orange hornfelsed peridotite occurs, but is not as widespread as the hornfelses associated with the Atlantic Corrie Gabbro. The main contact to the north is sharp, with modally layered gabbro up to 10 m. in from the contact; to the west, the layered gabbro borders 10 to 20 m. of peridotite breccia, with slabs grading from 6 m. across at the outer contact to an average of 20 cm. near the banded zone. The intrusive breccia is superbly developed at (GR 366 949), where it is 90 m. wide and forms the SW shoulder of Trallval. Block-free channels are sharply juxtaposed to the breccia (Fig. 4.2 C and Plate 4.6). Blocks are of all sizes up to 10 m. across (on average 30 cm.), angular to subrounded, consisting of dunitic peridotite and ultrabasic breccia. In the block-bearing parts, the percentage of gabbroic matrix varies from 10 to 50 %. The sheet west of Loch Fiachanis has numerous vertical zones bearing plastically deformed blocks of peridotite, sheared parallel to the margins of the zones. There is no discontinuity between the adjacent block-free zones and the matrix of the block-bearing zones, as with the contact breccias. Elsewhere, the gabbro is relatively free of blocks, though an occasional isolated xenolith does occur.

4.5 Other Gabbros Intruded into the Central Series.

Bosses, sheets and pipes of medium to coarse olivine gabbro, without chills, are scattered over the whole area. The most prominent are:

(1) The coastal gabbro complex which extends from Papadil to north of Rudha Sgorr an't Snidhe, which are all intruded into ultrabasic breccias. They have not been investigated in detail, but include bosses up to 300 m. wide and 20 m. thick sills. A xenolithic facies at Papadil includes fragments of dolerite, pure magnetite and hypersthene gabbro (GR 3620 9187).

(2) Several small, cylindrical plugs north of this complex.

(3) A 30 m. sill halfway up the NW face of Ruinsival, with promi-

nent, undulating banding (Plate 4.7), poikilitic pyroxene and xenoliths of hornfelsed peridotite. The upper contact consists of 10 m. of intrusion breccia. A branching dyke, also strongly banded, just west of the summit is probably an offshoot from the sill.

(4) A thick dyke of granular olivine gabbro on the Ruinsival - Ainshval col, cut by the Long Loch Fault.

(5) A remarkably plagioclase-rich sheet at Leac a Chaisteil.

(6) Similarly plagioclase-rich and pyroxene-poor gabbro forms a small outcrop on the slopes of Trallval. This may be a local facies of the Glen Harris Gabbro.

(7) Finally, a variety with a remarkable harrisitic texture. A boss exposed at the mouth of the Fiachanis River (GR 3423 9487), where it is cut, in part assimilated by an ultrabasic breccia (some of the brecciated blocks have extensive spinel rims, section 3.8.2) and has radiating clusters of extremely elongate olivine near the contact with the breccia. The gabbro is plagioclase-rich, low in oxides and has small subpohitic pyroxenes away from the contact. Autobrecciation is a common feature of this gabbro.

4.6 Marginal Gabbros.

Harker (1908) mapped a discontinuous ring of undifferentiated gabbro around the ultrabasic complex, which included the Papadil Gabbro. Brown (1956) described it as a continuous dyke-like body, around Hallival and Askival, of ophitic-textured, quick-weathering gabbro. Hughes (1955) interpreted the contact of marginal gabbro with the Southern Mountains Complex to plunge to the south at 40^{o} to 50^{o} and noted its compositional variability: at Sandy Corrie it is a hypersthene-olivine gabbro with amphibole, while it lacks olivine at Papadil and is much coarser. Also, while back-veining of felsite into the marginal gabbro is extensive on the Trallval-Ainshval col, it is absent at Papadil. This, and the petrological evicence for reheating of the gabbro, led Hughes to deduce that the Papadil Gabbro predates the adjacent granophyre. Dunham and Emeleus (1967), however, pointed out that this gabbro cuts the Main Ring Fault and found that the granophyre has also been reheated. The emplacement of the CS into the Papadil Gabbro, which postdates the granopyre, explains all these features, as suggested by Forster (1980)

on the basis of McClurg's (1982)hypothesis for the evolution of the ultrabasic complex.

In the Trallval area, marginal gabbro is exposed in isolated pockets at Papadil, Leac a Chaisteil and the Trallval - Ainshval col. Each gabbro is petrologically distinct (Chapter 6). The Leac a Chaisteil gabbro, however, closely resembles the West Trallval Gabbro associated with the CS contact, which strengthens the suggestion that the Papadil Gabbro predates the emplacement of the CS with its own, discontinuous, marginal gabbro. The Leac a Chaisteil gabbro is pyroxene-rich, medium-grained, unlayered and brecciates the peridotite and olivine gabbro. A pocket of similar gabbro occurs along the contact just north of the Papadil Gabbro. On the Trallval - Ainshval col, olivine gabbro (part of the Atlantic Corrie Gabbro) is brecciated by a fine-grained, olivine-free, leucocratic gabbro which chills against the Southern Mountains felsite and looks similar to the East Trallval Gabbro. The Papadil Gabbro is melanocratic, homogeneous, medium-grained, olivine-free. and weathers easily. All appear distinct from the marginal gabbro to the WLS at Harris Bay (Wadsworth, 1958) or that below Hallival and Askival (Brown, 1956).

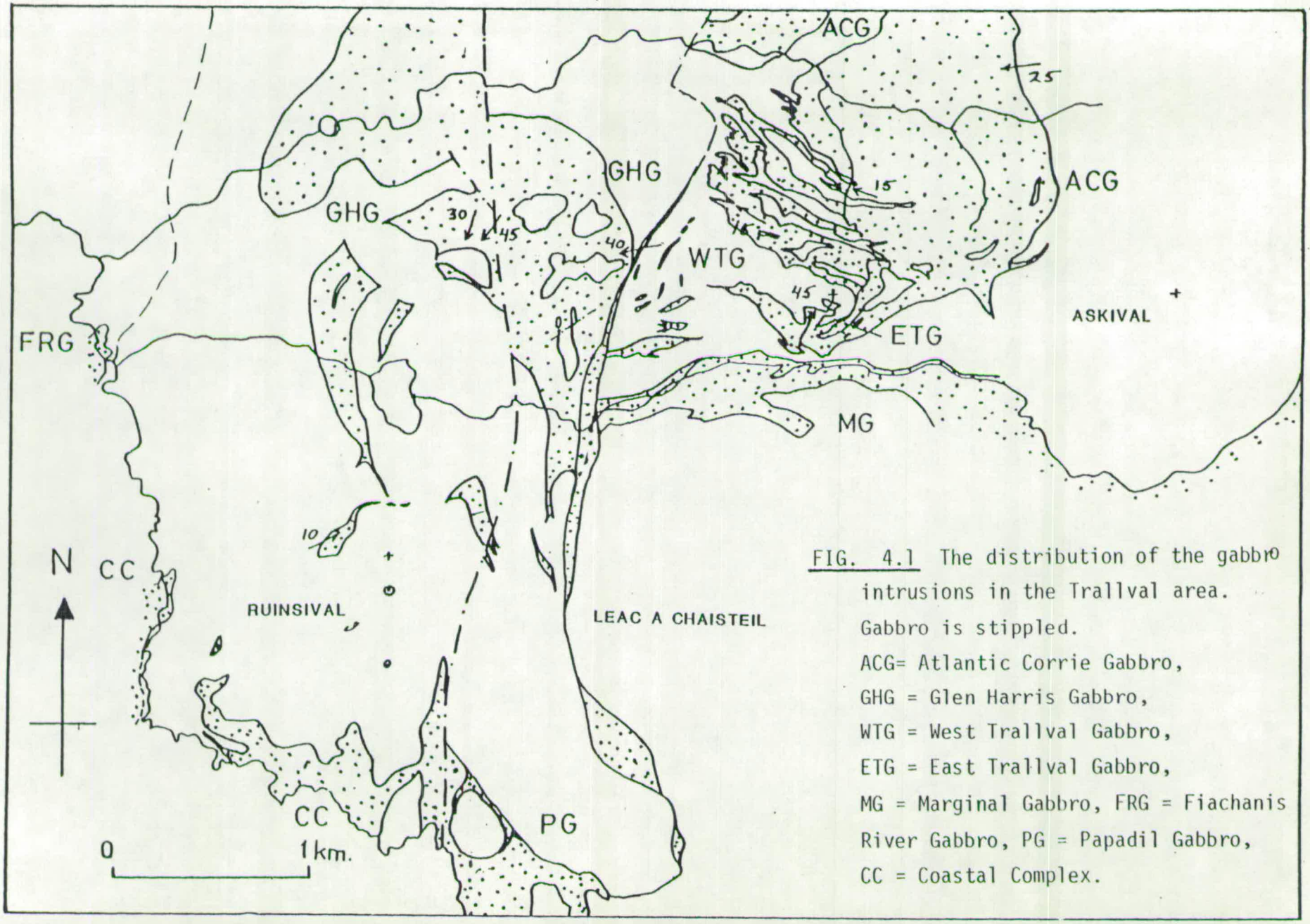

FIG. 4.1 The distribution of the gabbro intrusions in the Trallval area. Gabbro is stippled.
ACG= Atlantic Corrie Gabbro,
GHG = Glen Harris Gabbro,
WTG = West Trallval Gabbro,
ETG = East Trallval Gabbro,
MG = Marginal Gabbro, FRG = Fiachanis River Gabbro, PG = Papadil Gabbro,
CC = Coastal Complex.

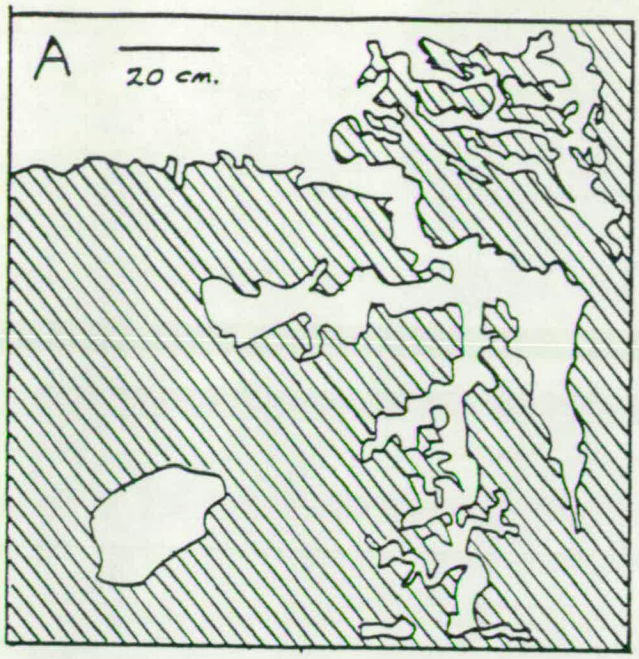

A- Gabbro/peridotite contact, N. Trallval.

B- Stepwise stoping of peridotite by gabbro, on a large scale, N. Trallval.

C- Intrusion breccia at the contact of the Glen Harris Gabbro with peridotite, W. Trallval.

D- schematic section illustrating the relationship of the Glen Harris Gabbro east of the Long Loch Fault to the body west of the fault.

FIG. 4.2 Peridotite (hatched)/Gabbro (blank or stippled) relations.

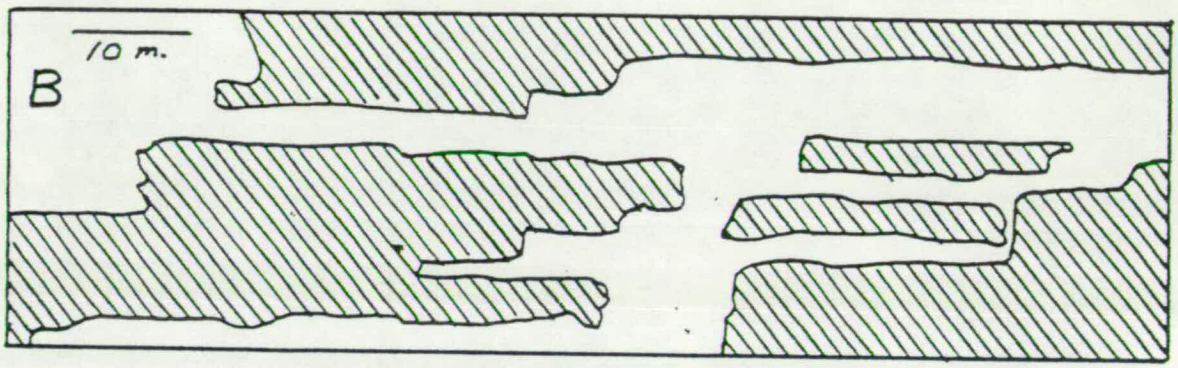

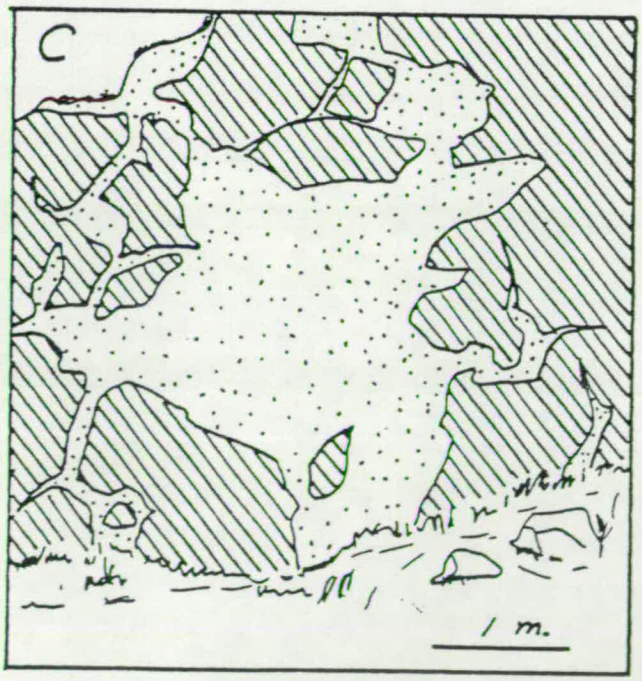

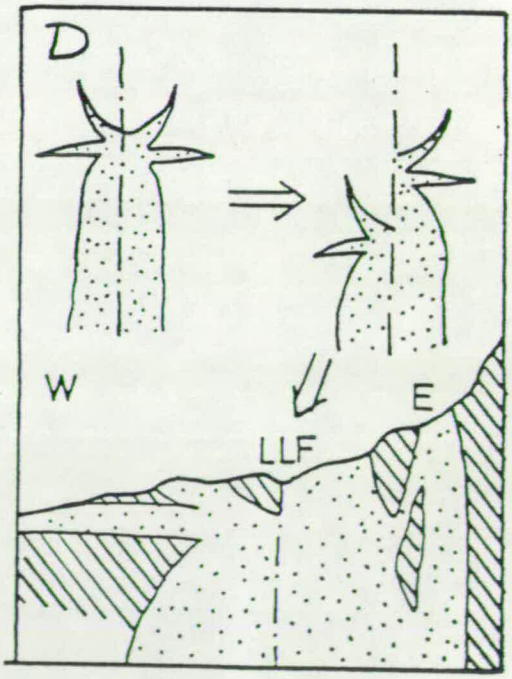

PLATE 4.1 Slump structures in the Atlantic Corrie Gabbro. The deformed lenses are rich in pyroxene. Atlantic Corrie.

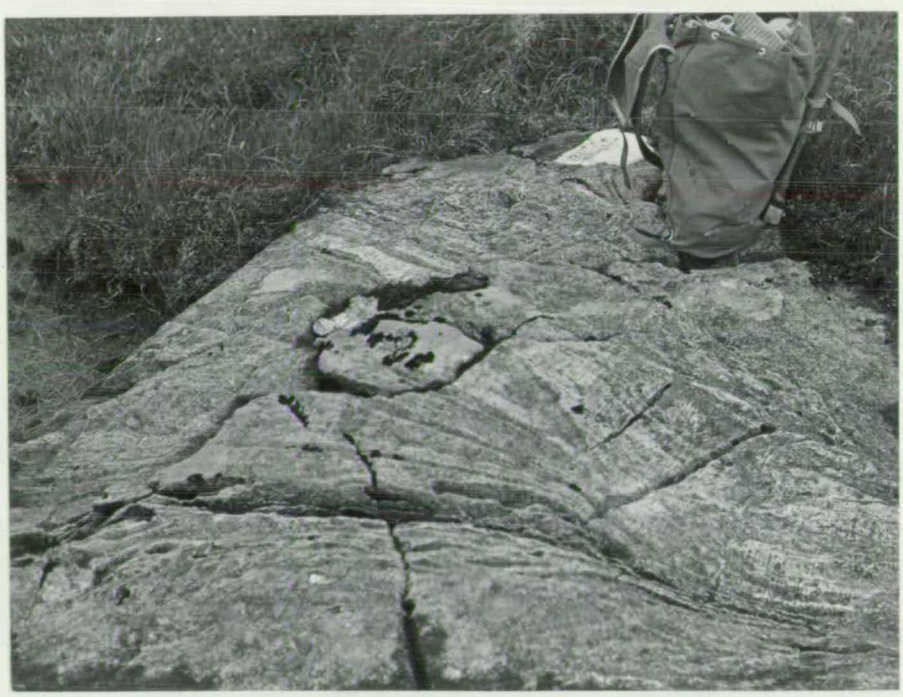

PLATE 4.2 Flow-banding in the Atlantic Corrie Gabbro, Atlantic Corrie. Plan view.

PLATE 4.3 Plagioclase-rich facies of Atlantic Corrie Gabbro on East Trallval (Harris Buttress) partly brecciated by intrusive peridotite.

PLATE 4.4 Parallel, inclined sheets of the East Trallval Gabbro (arrowed) intruding the Atlantic Corrie Gabbro. The view is to the NE along the head of Glen Dibidil.

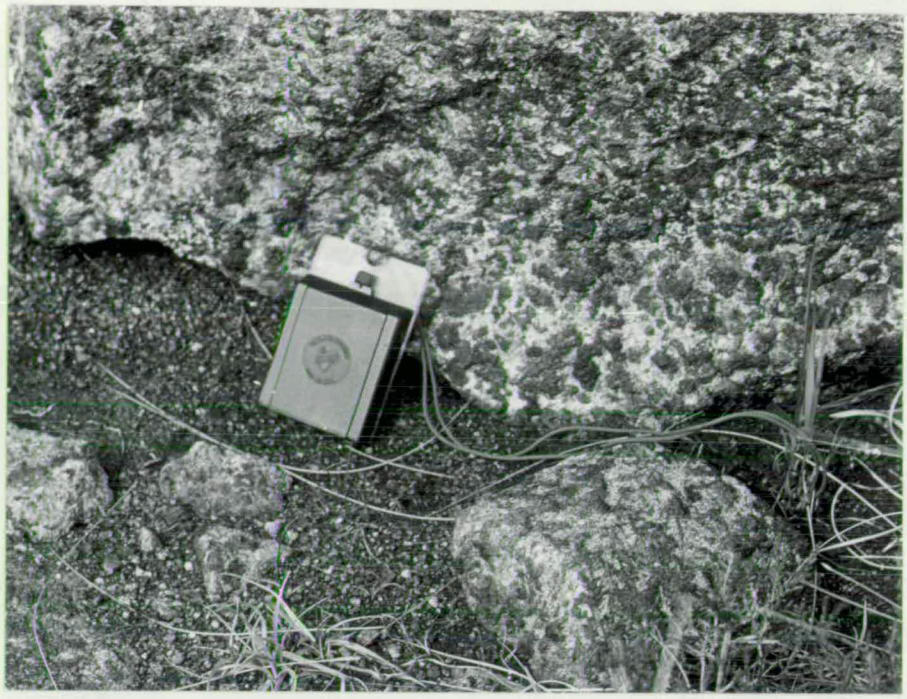

PLATE 4.5 Coarse-textured olivine gabbro. Glen Harris Gabbro near the Harris river.

PLATE 4.6 Intrusion breccia at the eastern contact of the Glen Harris Gabbro, SW shoulder of Trallval.

PLATE 4.7 Modal, undulatory layering in an olivine gabbro forming the cliffs of NW Ruinsival.

CHAPTER 5

PETROGRAPHY AND MINERAL CHEMISTRY OF THE ULTRABASIC ROCKS.

The ultrabasic rocks of the layered series have been collected along 12 traverses normal to the layering (Fig. 5.1), in addition to reconnaissance collecting of the layered series and sampling of most of the ultrabasic breccia zones, plugs and chromitite laminae encountered in the field. Thin sections were cut, and for each, the modes were measured, textures described, sulphide content and grain-size estimated and the various phases analysed by electron microprobe. This chapter presents the range in these parameters and their distribution in terms of stratigraphical and lateral variation within each layered series; the ultrabasic plugs and breccia matrices are compared with the layered series. A petrogenetic analysis of the results is given in chapter 7.

5.1 Cumulus Textures.

Typical textures are described first, followed by an account of specific textural features from the layered rocks, each of which may occur in a variety of rock types. "Cumulus" is applied descriptively to a texture which consists of a touching framework of euhedral to subhedral crystals of one or more phases (cumulus crystals) partially to wholly enclosed by poikilitic crystals which make up the intercumulus fraction of the rock (Wager et al., 1960). The distribution and textural relations of the exclusively intercumulus hydrous phases, the spinel laminae and sulphides are treated separately (sections 5.3 and 5.6)

5.1.1 Dunite and Dunitic Peridotite.

Chromite and olivine are the cumulus phases, with a minor amount of intercumulus pyroxene and plagioclase. Olivines are roughly subhedral, often with irregular lobate extensions. Some recrystallisation may be indicated by the equi-angular junctions of 3 or more crystals (Plate 5.1). Where spinel is abundant,"net textures" develop (Plate 5.2).

5.1.2 Feldspathic Peridotite.

These rocks best illustrate cumulus texture, with the same mine-

ral relationships as in the dunite, though cumulus plagioclase is abundant towards the top of the peridotite of some units and cumulus pyroxene occurs occasionally. Olivine occurs in three environments (Plate 5.3):

(1) As inclusions in pyroxene oikocrysts.

(2) Partially or wholly enclosed by smaller plagioclase oikocrysts.

(3) In dunitic aggregates free of intercumulus phases.

Whereas the dunitic aggregates and the crystals in plagioclase form a touching framework, those in the pyroxene are"matrix supported".

5.1.3 Allivalite.

Cumulus olivine, plagioclase, spinel and pyroxene may all occur. As the intercumulus material also consists of these phases, a clear distinction is difficult, though inclusion patterns or a different optical orientation can identify definite intercumulus overgrowths, as for pyroxene in Plate 5.4.

5.1.4 Ultrabasic Breccia Matrices and Plugs.

While the olivine and spinel appear similar to the cumulus crystals from the layered series, these rocks have a characteristic texture as they lack oikocrysts:

(1) The olivine forms an irregular framework hemming in interconnecting conduits occupied by plagioclase (Plates 5.5 and 5.6). The conduits stand out on weathered surface (Plates 3.33 and 3.44).

(2) The conduit-occupying plagioclase is usually devoid of spinel; spinel does occur as inclusions in the olivine, forms part of the aggregated olivine framework or adheres to the margin of the conduits, forming a "sprinkling" on the olivine.

(3) Clinopyroxene is less abundant than in the layered series and makes a partial outer lining to the olivine (Plate 5.7), sometimes cementing the olivine aggregates.

This texture has not been described before and will be referred to as "conduit texture".

5.2 Specific Textural Features and Microfabrics from the ELS and CS.

Textures which deviate from those described above are described below together with an interpretation, which attempts to recognise the imprint of the operation of some of the following processes:

(1) Crystal settling - the separation of crystals from melt by gravity.

(2) In situ crystallisation - crystals nucleate and grow without segregation of the melt.

(3) Deformation of the crystal mush - by current drag, slumping or tectonic shear.

(4) Compaction of the crystal cumulate under its own weight with filter-pressing of the interstitial magma and recrystallisation of the cumulus crystals.

Varying the order of operation and importance of these processes in conjunction with crystal nucleation and growth can explain most of the textures reported below. Irvine (1982) used the terms crystal mush, cumulate and porosity of igneous cumulate as follows: a crystal suspension or crystal mush is melt supported. With an increase in the crystal / liquid ratio, an uncompacted cumulate is obtained consisting of touching cumulus crystals with initial porosity defined as the volume fraction of intercumulus liquid. The final porosity is the volume fraction of postcumulus phases upon complete consolidation of the cumulate.

5.2.1 Melt-supported Texture.

This is illustrated by the olivine-gabbro of Plate 5.8, where cumulus crystals cannot have formed a touching framework. This texture is also found in the layered ultrabasic rocks:

(1) In the ELS, it occurs in the peridotites of the E. Trallval mélange zones (section 3.5.5), especially where the peridotite fills in fractures in the troctolite blocks.

(2) In the Dornabac Member of the CS, at Leac a Chaisteil, melt-supported textures are common in the peridotite and correlate strongly with a lack of olivine lamination (section 5.2.3).

(3) In the Ruinsival Group of the CS, 10 to 20 cm. thick layers consisting entirely of large poikilitic pyroxene plates with melt-supported distributions of olivine inclusions and some discrete cumulus olivine are found in the dunitic peridotite sections. The olivines are concentrated towards the core of the oikocrysts and, while sorting is good within each oikocryst, the average size of the included olivines varies considerably from one oikocryst to another (Plate 5.9).

Interpretation: in the first two instances, the lack of compaction and the fine grain-size of the cumulus phases indicate rapid cooling with respect to the rest of the layered series. That this is associa-

ted with mobilisation of the mush is suggested by the fracture infills in the ELS and the commonly associated conduit texture in the Dornabac Member. The rocks of the Ruinsival Group may represent early pyroxene oikocrysts which grew freely in the crystal suspension prior to compaction and were then compacted together with the olivines.

5.2.2 Conduit Texture.

Typical of the intrusive peridotites, this is locally observed in the layered series:

(1) In the ELS, it occurs commonly in the peridotites within 100 m. of the contact with the CS, e.g. in U11 and U12 samples on traverse 1 (Fig. 5.1).

(2) In the lower unit of the Long Loch Group at Rubha Sgorr an't Snidhe (LLG1, an't Snidhe) and the Dornabac Member in all outcrops, it occurs throughout the peridotite.

Interpretation: the texture is believed to result from mobilisation of the peridotite mush, by analogy with the clearly intrusive matrix of the breccias.

5.2.3 Mineral Lamination.

Lithologies with cumulus minerals of a pronounced tabular shape, from dunite (Plate 5.10) to anorthosite (Plate 5.11) almost invariably show a foliation parallel to the rhythmic layering. Such a lamination is best developed in layers where all the cumulus crystals have a tabular shape. Exceptions include the"melt-supported" rocks, those with conduit texture and layers of proto-harrisite in which the skeletal olivine is either randomly oriented or perpendicular to the layering. In peridotite, the olivine lamination is less clear in the pyroxene oikocrysts. Several peridotites show the imbrication of a number of olivines with respect to the main lamination (Plate 5.12)

Interpretation: The preferred explanation is compaction rather than current deposition, as the lamination is best developed in those rocks with the least intercumulus material. Pre-compaction growth of the pyroxene oikocrysts explains the poorer lamination of the included olivines. The isolated cases of imbrication may be due to shear within the mush (currents, slumping).

5.2.4 Modal Cumulus Phase Layering.

In laminae less than 5 mm. thick, repeated rhythmic concentrations of variable intensity of spinel relative to olivine occur in peridotite throughout both the ELS and CS (Plates 5.13, 5.14 and 5.15) and relative to plagioclase in the upper parts of allivalites in the ELS (Plate 5.16). These may be gradual or abrupt, and in the latter case often correlate with an abrupt increase in the size of the olivine. Modal layering of cumulus plagioclase with respect to olivine is found at the top of the peridotite of U14 on the W. Trallval traverse (GH24, U14, W Tr). Within the allivalites, rhythmic concentrations of any one of the cumulus plases relative to one or both of the others occurs on a very fine scale, 1 to 3 mm. (Plate 5.17). Some laminae in allivalite (e.g. U15 on Trallval) are mineral-graded with olivine at the bottom and plagioclase towards the top. All types of layering may occur without an accompanying mineral lamination, though the inverse is more common.

Interpretation: the lack of associated size sorting and the hydraulic incompatibility of tiny spinels and large olivines (Jackson, 1961) suggest an oscillatory chemical phenomenon controlled the rhythmic spinel layering (McBirney and Noyes, 1979). Current-sorting is an alternative explanation for the rhythmic cumulus layering in allivalite (Irvine, 1980).

5.2.5 Modal Intercumulus Phase Layering.

This includes layering due to modal variations in the total intercumulus fraction and the segregation into layers of intercumulus pyroxene and plagioclase. The former is seen as dunite laminae as little as 8 mm. thick in dunitic or feldspathic peridotite (GH32, U15, W Tr; HC7, LLG2, Coast.), and in association with textural layering where the intercumulus material is more abundant in the coarser laminae. In feldspathic peridotite, poikilitic pyroxene may be rhythmically concentrated into laminae one oikocryst thick (2 to 10 mm.), occasionally to the exclusion of plagioclase. In cumulus-layered allivalite, intercumulus pyroxene is often restricted to the olivine-rich laminae. In spinel laminae, the only interstitial phase is usually plagioclase, where it is strongly concentrated, in the case of laminae in the CS, with respect to the enclosing peridotite.

Interpretation: while the rhythmic concentration of pyroxene may be

controlled by a rhythmic distribution of cumulus nuclei (above section) or oscillatory intercumulus nucleation, the absence of pyroxene from spinel laminae may reflect a reaction relationship. The variation of total intercumulus material indicates the entrapment of intercumulus liquid at a specific horizon either by variations in the rate of accumulation or trapping of upward-moving liquid at levels marking a permeability decrease (Donaldson, 1982).

5.2.6 Textural Layering.

Sharp changes in cumulus crystal habit, size and lamination result in flat laminae as little as one crystal thick. These laminae, especially common in the CS, may consist of small olivines in an otherwise coarse rock (HD10, RG1) or coarse olivines in an otherwise fine rock (Plate 5.18). Single-crystal horizons occur of coarse spinel (Plate 5.15), foliated olivine in an isotropic host (FE9, LLG2, Pap.), imbricated olivine in a rock with an otherwise planar foliation HC4, LLG1, Coast.) and protoharrisitic olivine in a granular peridotite (GH20, U14, W Tr.). Fine layering in allivalite also often involves abrupt changes in olivine grain-size to form laminae as little as 5 mm. thick (Plate 5.17; GH1, U10, W Tr.). In many thin sections, both from the ELS and CS, only the interface between two layers is seen, again showing abrupt changes in olivine or spinel grain size, coarse over fine and vice versa. Olivine size changes often correlate with intercumulus layering and/or the appearance of lamination - sometimes in the coarse, sometimes in the fine olivine -(Plate 5.15). The appearance of an olivine lamination also coincides with changes in the spinel content in either sense (GN14, U14, E Tr.; LB3, U10, S Tr.)

Interpretation: the size separation may have been effected by gravity sorting, though this is unlikely because of the rarity of grading (see next section), or by shear of a crystal mush (flow-banding), or by in situ variations in growth and diffusion rates, which certainly produced the laminae of protoharrisitic olivine. Deposition from currents of variable flow regime may produce the thin foliated laminae, or compaction may have produced a lamination only in those layers with pronounced tabular olivines (again due to variable growth conditions in the mush, which may also be responsible for the changes in spinel concentration).

5.2.7 Graded Layering.

Only one sample showed upward-fining of olivine (CF10, U9, W Tr). Size and abundance grading of spinel is more common: upward-fining and a modal decrease are associated in an ELS allivalite (Plate 5.19) and in a chromitite lamina in the WLS (HK6). In a peridotite (GN11, U13, E Tr.), a gradual modal decrease in spinel occurs over an interval including a horizon marking an abrupt change in olivine grain size.

Interpretation: the association of an upwards modal decrease with size-fining in spinel laminae is due to the increase in frequency of spinel recrystallisation with increasing concentration. Elsewhere, upwards size-fining may reflect slow gravity-sorting or size segregation by shear dispersive forces in the crystal suspension before the crystallisation of olivine.

5.2.8 Clasts, Cross-layering and Convolute Layering.

Clasts of peridotite up to a few cm. across with a lamination oblique to that of the host occur in allivalite (M16, U14, S Tr) and in peridotite (GN15, U14, E Tr.). In one case (AD7, U11, Hallival), a peridotite includes rounded clasts of a coarse plagioclase aggregate. Slumping is occasionally seen in thin sections of ELS allivalites as these have fine enough layering. The lamination is only partly preserved, but the highly variable distribution of spinel picks out the contorted foliation (H4, U8, E Tr.). Cross-layering is seen as layers with distinct laminations, one of these terminating at the interface between the two. Such features are common at allivalite/peridotite contacts, sometimes with a spinel lining (Plates 5.20 and 5.21) and they are also found in texturally layered peridotite. In a rarer type of cross-layering, disconformable fabrics for different phases are superimposed. E.g., in one allivalite (HL7, U10, Ask.), olivine laminae are oblique to the feldpar lamination; olivine laminations oblique with respect to modal spinel layering (HD14, RG1) or intercumulus layering (GH24, U14, W Tr.) also occur occasionally. Finally, the spinel distribution in some allivalites suggests the presence of spinel-free channels (Plate 5.22).

Interpretation: the clasts represent brecciation and reworking of earlier layers. As cross-layering is so rarely seen in the field, the small-scale features seen here are probably the result of dif-

ferential loading or slumping with a rotational component, layers responding differently according to their viscosity. The disconformable superimposed fabrics may be due to slumping of a finely-layered one-phase crystal suspension followed by nucleation of the second phase with its associated fine-scale layering, or they may be due to slight shearing of the crystal mush with re-orientation of tabular crystals only. The spinel-free channel is probably erosional.

5.2.9 Unlayered Spinel Fabrics.

In many well-foliated feldspathic peridotites, the spinel crystals are strongly concentrated along the upper surfaces of the tabular olivines, with a corresponding depletion of spinel along the lower surfaces and between the olivines (Plates 5.23 and 5.24). "Upper" and "lower" describe the orientation of surfaces with respect to a palaeohorizontal parallel to the macro-layering. This texture is found in peridotites of both the ELS and the CS. Over the entire thin section, the distribution of spinel is often heterogeneous: commonly, spinel forms synneutic chains or rings (Plate 5.25), and, less commonly, it is distributed as isolated, sub-spherical spinel-bearing patches in an otherwise spinel-poor rock (Plate 5.26; GH21, U14, W Tr.; HD 25, RG2).

Interpretation: the geopetal texture is interpreted as resulting from crystal settling of spinel through the intercumulus liquid onto the olivine. The localised spinel concentrations may be produced by heterogeneous nucleation in the crystal mush or by shearing and boudinage of spinel-rich horizons.

5.2.10 Exotic Cumulus Crystals.

Within one lamina, most cumulus crystals have the same habit and size or else are completely unsorted. This section describes the intermediate cases with bimodal populations which may be due to one or two exotic grains, such as olivines full of spinel inclusions amongst spinel-free crystals (HL8, U10 and HL1, U14, Ask.; HD2, LLG3, Ruins.; GG4, DM, LaC), harrisitic olivine amongst granular olivine (LB3, U9, S Tr.; UU1, U11, Hall.; GG3, DM, LaC), olivine with abundant dendritic magnetite inclusions among clear olivines (HD29, RG2). Bimodal size distributions for spinel (LB8, U9, S Tr.) and olivine (FE6;LLG2,Pap) are uncommon.

Interpretation: The presence of a few crystals of "exotic" habit in an otherwise uniform rock is attributed to reworking of a layered sequence with horizons of exotic crystals. Rocks with a bimodal size distribution may be due to this process, to incomplete granulation or to separate nucleation episodes producing different generations of the same phases

5.2.11 Intercumulus Pyroxene Textures.

In peridotite, pyroxene oikocrysts, while commonly subspherical, are occasionally elongate, and may parallel the layering (GH15, U13, W Tr; HD17, RG1). Alternatively, they may form discordant vein-like fabrics oblique to normal to the layering and these are found in peridotite from both the ELS and CS. Elongate, perpendicular intercumulus pyroxene is more common in the allivalites, as in Plate 5.27 where a pyroxene oikocryst spans an entire spinel lamina. Oikocrysts of highly irregular shape and extent, sponge-like in 3-D, cement the cumulus crystals in rocks such as anorthosite and dunite, which have little intercumulus material.

Interpretation: pyroxene is a late phase to finish crystallising and in the case of dunite anorthosite does so after considerable compaction of the cumulus crystals. It is therefore suggested that the distribution of intercumulus pyroxene may be used as a tracer for the late movement of intercumulus liquid. The elongate oblique and perpendicular pyroxenes suggest the concentration of interstitial liquid into fractures oblique and normal to the layering in a semi-rigid cumulate.

5.2.12 Growth Interference Effects.

Compared to olivines in plagioclase oikocrysts, the olivines entirely enclosed in pyroxene are less concentrated (i.e.fewer crystals per unit area) and distinctly smaller, the average radius reaching only about 0.5 that of olivine in plagioclase, in some rocks (GH16, U13, W Tr; HD9, RG1; HD34, RG2). The average radius of cumulus plagioclase inclusions in pyroxene is as little as 0.25 that of discrete plagioclase in certain allivalites (GH39, U15, W Tr). Some pyroxene oikocrysts have an outer rim free of inclusions (Plate 5.9;GG11, DM, LaC) or a large central inclusion of plagioclase (Plate 5.28; GL3, U16, W Tr). Cumulus phases also overgrow earlier phases or fabrics. Olivine often encloses cumulus plagioclase in allivalite over the

outer 0.5 to 0.3 of its radius (Plate 5.11) and the enclosed plagioclases have the same lamination as those outside the olivine. In a few spinel laminae, olivine includes spinels over as much as 0.8 of its radius with the spinels gradually increasing in size from the olivine core outwards to approach that of spinels outside the olivine (Plate 5.29). Where spinels form localised clusters or concentrated laminae, they are often indiscriminately distributed between cumulus olivine and intercumulus feldspar, forming inclusions in the core of the olivine in the spinel-rich lamina or cluster while the olivine outside is spinel-free (Plate 5.26; GH21, U14, W Tr; HC22, LLG1, an't Snidhe; HD8, RG1). This texture is also observed for localised concentrations of sulphides, though sulphide inclusions have been observed only over the outer 0.6 of the cumulus olivine radius (GH10, U12, W Tr; GG6, DM, LaC; HD11, RG1). Such local sulphide concentrations are also found in allivalites, where they are distributed as inclusions over several neighbouring plagioclases, occurring over the outer 0.6 of the plagioclase radius.

Interpretation: upon entrapment by a later phase, the growth of the earlier phase is arrested and, in the case of many such crystals, an early fabric is preserved. If the cumulus crystals did accumulate, inclusions in pyroxene give an idea of their maximum size at the time of accumulation, and also of the porosity of the crystal mush (as much as 80 % in the case of samples with melt-supported texture). The overgrowth of cumulus olivine and plagioclase over localised fabrics suggests in situ growth of 100 to 80 % of the olivine in at least some peridotites and in situ growth of 60 to 70 % of the plagioclase in at least some allivalites.

5.2.13 Recrystallisation Fabrics.

Samples close to faults (LLG2, an't Snidhe), in strongly disturbed layers (U16, W Tr; DM and LLG1, LaC) or close to ultrabasic breccia zones in the CS often have a marked bimodal olivine population. Large, subhedral crystals with strain lamellae are surrounded by small, unstrained, polygonal crystals often in aggregates with equiangular junctions. The large crystals sometimes partly consist of polygonal domains of a different optical orientation. The intercumulus pyroxene usually forms normal oikocrysts, but the plagioclase may also consist of a fine-grained aggregate; a little intercumulus

phlogopite is commonly associated with this texture. Where spinels are highly concentrated, they may recrystallise to form large sub- to euhedral crystals with faint internal boundaries (Plate 5.30). This sintering texture is common in the CS, but is seen in the ELS only where the spinel has reacted extensively at gabbro contacts or where a chromitite lamina is displaced by a micro-fault, the sintering occurring at an intersection of lamina and fault (Plate 5.31). Finally, some chromitite/peridotite contacts are very sharp, with granulitised olivine on the contact.

Interpretation: tectonic stress associated with the movement of mushes and faults was high enough to granulate olivines producing recrystallised fabrics. Granulation always occurred before the crystallisation of intercumulus pyroxene and sometimes before that of plagioclase. The association of spinel sintering with microfaults suggests a fluid phase may be involved. The shearing at chromitite/peridotite contacts suggests the two had differing viscosities, the spinel suspension or cumulate behaving less rigidly.

5.3 The Mineralogy of the Layered Series.

The ultrabasic rocks consist of three anhydrous silicates (olivine, plagioclase and clinopyroxene), oxides of the chrome-spinel and magnetite-ilmenite series and minor amounts of sulphides and hydrous silicates. The rocks are exceptionally fresh and the minerals have been extensively described by Brown (1956), Wadsworth (1961), Donaldson (1975,1977) and McClurg (1982). McClurg (1982) also gives comprehensive electron microprobe analyses for the minerals of the ELS on Barkeval and the CS in the Long Loch area. Only brief descriptions of the minerals are presented below, together with mineral analyses, as they are strictly comparable with those of McClurg (1982). New data are, however, given for the hydrous minerals which occur both as intercumulus phases and as inclusions in spinels and olivines.

5.3.1 Olivine.

Grain shapes are rounded to subhedral-tabular; in harrisite and protoharrisite, skeletal and hopper shapes dominate (Plate 5.32), which have been attributed by Donaldson (1977) to growth in a supercooled magma. Skeletal olivine has been found in all units of the

ELS and CS. One characteristic feature is a "backbone" of included spinels (Plate 5.33). In allivalite, crystals tend to be smaller and more elongate, with anhedral extensions and sometimes poikilitic rims (Plate 5.11) and often form synneutic chains. Anhedral extensions are also well developed in dunitic peridotite and dunite. Inclusions of euhedral spinel, hydrous silicates (section 5.5), dendritic magnetite and linear arrays of thin platelets of a translucent brown material, possibly exsolved spinel (Wadsworth, 1961) are common throughout the layered series, while inclusions of rounded plagioclase are restricted to olivine in rocks with cumulus plagioclase. Strain lamellae are occasionally developed, especially in elongate olivine, with dislocation planes normal to the axis of elongation of the olivine. Alteration of the olivine is restricted to serpentinisation along edges and cracks in most rocks with a more pervasive alteration in the olivine-rich peridotites, where chlorite and carbonate occur commonly in small amounts. Where the Long Loch Fault crosses the Ruinsival - Ainshval col, up to 50 % of the CS dunite is serpentinised, the serpentine occurring both as veins cutting the rock fabric and as pseudomorphs after the olivine.

5.3.2 Plagioclase.

In peridotites, plagioclase forms intercumulus patches with inclusions of spinel, olivine and sulphides. Where a crystal is wholly or partly enclosed by intercumulus pyroxene, it shows euhedral terminations. Slight, continuous marginal zoning is common and is either normal or reverse. The tabular cumulus plagioclase of the allivalites also occurs commonly at both the top of the peridotite (HL1, U14,Ask.; GH8, U11, and GH24, U14, W Tr; DM; FG6, LLG2, Seag.) and in the bottom few metres (GH2, U11 and GH31, U15, W Tr; FG8, LLG2, Seag.). The twin lamellae of cumulus plagioclase are often strained.

5.3.3 Clinopyroxene.

Section 5.2 describes the shapes and textural relations of intercumulus pyroxene. Exsolution of a Ca-poor phase does not occur, although some crystals have a mesh of finely crystalline magnetite due to oxidation. The poikilitic crystals include rounded olivine, subhedral plagioclase and spinels which are usually smaller and with more irregular edges than those in intercumulus plagioclase. Cumulus pyroxene tends to be equidimensional and forms rounded crystals. In

the ELS, it is restricted to allivalite and peridotite just overlying allivalite (H4, U9, E Tr; GH2, U11 and GH15, U13, W Tr), while in the CS, it occurs in addition at the top of the peridotite (HC4, LLG1, Coast; FG12, LLG2, Seag.; HD15, RG1) and is characteristically abundant in the allivalite of the Dornabac Member. Alteration to biotite occurs sporadically.

5.3.4 Oxides

The terms chromite and Cr-spinel are here used sensu lato for spinels with more than 15 % by weight of Cr_2O_3. Disseminated chromite is nearly always euhedral and occurs as inclusions in olivines, cumulus and intercumulus plagioclase, intercumulus pyroxene, or at the boundaries between these phases. Spinels from chromitites are described in section 5.6. Synneusis is not uncommon, especially in the intrusive peridotites, the spinels forming chains, clusters or complex loops in intercumulus plagioclase (Plate 5.25). Spinel occurs in all rock types, except for some thin layers in allivalite. The abundance varies from ca. 1 % in allivalite, increasing through feldspathic peridotite to ca. 2 to 4 % in dunitic peridotite. The spinel itself includes sulphide grains and rounded silicate inclusions (section 5.5). Spinels in feldspathic peridotite have fine exsolution lamellae of ilmenite which tend to become coarser in the allivalites and develop into bleb-type exsolution, due to oxidation at moderate temperatures of ca. 600 ^{o}C (Putnis and Price, 1979). Ilmenite exsolution also occurs in some pyroxene oikocrysts, while primary interstitial ilmenite occurs in a few allivalites.

5.3.5 Sulphides.

Disseminated sulphides occur throughout both layered series, exceeding 1 volume % in some chromitite laminae. They occur as:

(1) Two to three phase (pyrrhotite-pentlandite, or po-pn, and chalcopyrite-pyrrhotite-pentlandite, or ccp-po-pn) globules in all of the cumulus phases except pyroxene, or adhering to the edge of the cumulus phases and the hydrous silicate inclusions in spinel and olivine (section 5.5).

(2) Magnetite-pentlandite, mt-pn, grains disseminated among and included in the intercumulus phases.

(3) Complex oxidised assemblages of Cu-Fe sulphides and Cu-sulphides, again as intercumulus phases.

(4) Reduced pn-mt-native Cu assemblages in the dunite and the dunitic peridotite of the CS.

The 3-phase globules are most common as inclusions in spinel and olivine. Ni-Fe sulphides are subordinate in the globules and in the intercumulus sulphides of the ELS, only dominating the Cu-Fe and Cu-sulphides in the intercumulus assemblages of some of the CS peridotites. The spinel-rich laminae with a high sulphide content are especially rich in Cu-Fe sulphides, which are also unusually abundant in the intrusive peridotite layer of U14 on Trallval (section 7.1.2.4). Native Cu is locally common in the CS and occurs rarely in the ELS (U11 and U15, W Tr). In the allivalites, sulphides are typically concentrated into scattered patches less than 1 mm. across.

Interpretation: the globular 2- to 3-phase assemblages are probably produced by exsolution from a monosulphide solid solution droplet, formed as an immiscible liquid at the time of its incorporation into or its adhesion onto the cumulus crystal (Gill, pers. comm.;Kullerud et al., 1969). The intercumulus Cu- and Ni-rich phases were precipitated later as sulphur was concentrated into the residual liquid until saturation was reached. The complex assemblages were produced at sub-magmatic temperatures by oxidation-reduction reactions.

5.3.6 The Hydrous Silicates.

Phlogopite and kaersutite with their alteration products are restricted to specific environments. In the ELS, they occur as:

(1) Small, primary intercumulus plates.

(2) A replacement of pyroxene.

(3) More widely, as rims on Cr-spinel.

(4) Inclusions in spinel and olivine (section 5.5).

Primary phlogopite in measurable amounts (more than 5 %) is seen in some of the protoharrisite layers where it is associated with the olivine, in peridotites for which there is evidence for remobilisation, such as the "sandwich" peridotite of U14, the mélange peridotites and peridotite veins intrusive into the East Trallval gabbro (section 3.5.5), and some of the heterogeneous peridotites affected by fault-drag. The dunitic peridotite near the bottom of U15 also has significant phlogopite. In the CS, combined modal abundances of 0.5 to 1.5 % for phlogopite and kaersutite (rare in the ELS, it is here sometimes dominant over phlogopite) are not uncommon in the dunitic

peridotite and also occur in the feldspathic peridotite of the Dornabac Member.

Interpretation: Assuming a low halogen content for the primary hydrous silicates, they attest to the substantial water activity during the intercumulus crystallisation of the layered series. Water was trapped and incorporated into crystalline lattices only under special circumstances related to thickening of the crystal mush and/or its accelerated cooling.

5.3.7 Mineral Size Relations for Non-Harrisitic Rocks.

Table 5.1 lists maximum and average sizes for the cumulus and intercumulus phases of the TLS and the CS. Average sizes are based on detailed measurements on a representative sample of 30 rocks from each series, while the maximum sizes reported are based on minerals from all rocks sectioned during this study. Where they occur together, olivine is larger than spinel by a factor of 8 (cf. 10 in the Stillwater intrusion, Jackson (1961)) and olivine is about the same as plagioclase. In peridotite, cumulus sizes are larger in the CS, although they are similar for allivalites in the two series. Intercumulus plagioclase oikocrysts are significantly larger in the ELS than in the CS; pyroxene oikocrysts are generally larger than plagioclase and of a similar size for the two series. The differences between the two series can be related to tock types: in dunitic peridotite, cumulus olivine , spinel and intercumulus pyroxene all form coarse crystals and intercumulus plagioclase only small patches. Dunitic peridotite is dominant in the CS and feldspathic peridotite in the ELS, which probably explains the above size differences. Size variation of olivine and spinel with stratigraphical height and rock type is presented in section 5.7.

5.4 Mineral Chemistry.

Mineral analyses were performed by a WDS electron microprobe technique (see Appendix A for details and accuracy levels). Selected analyses of each of the minerals in all the major rock types are presented in Tables 5.2 to 5.4. Compositions of the hydrous minerals and oxides are given in sections 5.4.4 and 5.4.5, respectively. The analyses in Tables 5.2 to 5.4 were selected from about 700 analyses on 60 rocks. These data show a broad overlap with those of McClurg

(1982) from the ELS and CS in the Long Loch - Barkeval area. Her results are summarised for each mineral and complemented with those obtained in the present study.

5.4.1 Olivine

McClurg (1982) found the following:

(1) Fo content ranges from 89.4 to 78.1 for both the ELS and CS. Zoning was not found.

(2) CaO contents range from 0.16 to 0.02 wt% and show little change with fractionation. This is attributed to diffusional loss of Ca to surrounding silicates during sub-solidus re-equilibration in the peridotite, while the Ca is retained in the olivine of the highly calcic allivalites.

(3) MnO content increases linearly with fractionation from 0.17 wt% at Fo_{89} to 0.33 wt% at Fo_{79}.

(4) NiO content ranges from 0.40 wt% at Fo_{89} to 0.22 wt% at Fo_{79} for the CS. For the ELS, the variation is less ordered but ranges from 0.37 to 0.12 wt%. The difference is attributed to equilibration of olivine with sulphur-saturated and sulphur-undersaturated magmas for the ELS and CS, respectively, as precipitation of Ni sulphides will deplete the magma and thus the olivine crystallising from it, in NiO. A rough calculation indicates that an average content of 7 ppm pentlandite in the ELS would cause the observed Ni depletion in olivine. Measured sulphide concentrations commonly exceed 50 ppm in the ELS, but rarely exceed 10 ppm in the CS (section 5.7.1).

Results from this study differ as follows:

(1) Fo ranges 87.7 to 78.3 for the ELS and 90.7 to 79.1 for the CS. Most olivines show slight reverse zoning of 0.1 to 0.5 % Fo. This becomes apparent only when hundreds of core - rim pairs consistently yield slightly higher Fo contents in the rim (Fig. 5.2).

(4) The NiO data are compared with McClurg's (1982) data in Fig. 5.3, in which wt% NiO is plotted against the Fo content of the olivine. For the CS, a regression line to the data from this study is parallel to but between the curves obtained by, (i), McClurg (1982) and, (ii), Duke and Naldrett (1978) for olivines in equilibrium with a sulphur-undersaturated magma. An increase in the Ni content of the magma with respect to that of the theoretical determination (based on 1600 ppm) will displace the curve upwards. McClurg's samples are unrepre-

sentative of the CS since only the lower two units outcrop in the northern part of the complex. The steep curve for the ELS confirms McClurg's (1982) hypothesis of its crystallisation from a sulphur-saturated magma.

5.4.2 Plagioclase.

McClurg reported that:

(1) Cumulus plagioclase is more calcic in the ELS (An_{90-81}) than in the CS (An_{83-79}).

(2) Intercumulus plagioclase cores show a similar range for both series ($An_{87.5-74}$).

(3) Zoning extends compositional ranges down to An_{64} and An_{53} for cumulus and intercumulus crystals and may be reversed.

(4) Within-sample variation of up to 6 mol % An is common in the intercumulus plagioclase.

From this study:

(1) Cumulus compositional ranges are similar except that the ELS plagioclase only reaches $An_{88.8}$, while $An_{86.6}$ is the most calcic plagioclase in the CS.

(3) Zoning of cumulus and intercumulus crystals extends the range to An_{59} and An_{56}, respectively, for the ELS and to An_{61} and An_{52} for the CS. Reverse zoning is as common as normal zoning.

(4) Within-sample variation of up to 10 mol % An is not uncommon.

5.4.3 Clinopyroxene.

. From McClurg (1982):

(1) Cumulus and intercumulus crystals from both series are diopsides. At constant Ca:Mg, the atomic ratio of Fe with respect to Ca and Mg varies from 5.5 to 10 %, while Ca varies from 49 to 44 % at constant Fe:Mg.

(2) Fractionation occurred by replacement of Ca at constant Fe by Mg, or at constant Fe by Mg. Zoning in single crystals is less than 1.3 % Ca and less than 3 % Fe or Mg.

(3) Cr_2O_3 contents decrease linearly from 1.44 wt% at an Mg-number of 89 to 0.10% at an Mg-number of 80 for both series. The decrease in Cr_2O_3 is complemented by an increase in TiO_2 from 0.20 to 2.05 wt%. TiO_2 contents vary by up to 0.4 % within one sample in both allivalite and peridotite.

(4) Na_2O content varies from 0.25 to 0.60 wt%.

(5) CS pyroxenes have a higher content of Al_2O_3 than those of the ELS (3.0 - 4.7 wt% vs. 2.2 - 3.5 wt%) suggesting that the CS pyroxene crystallised from a liquid supercooled with respect to plagioclase, i.e. pyroxene in the CS crystallised earlier than in the ELS with respect to plagioclase.

This study shows in addition that:

(1) The compositional range of the CS pyroxenes is more extensive than that of ELS pyroxenes: at constant Ca:Mg, Fe varies from 4.9 to 10.5 % in the CS and from 5.5 to 8.5 % in the ELS whereas Ca varies from 43.5 to 49.5 % in the CS and from 43.6 to 49.0 % in the ELS, at constant Fe:Mg.

(2) Two trends may be postulated (Fig. 5.6): an increase in Fe at constant Ca:Mg and a decrease in Ca at constant Fe:Mg. Most ELS pyroxenes plot along the Ca trend, while those of the CS lie along the Fe trend.

(3) The range in Cr_2O_3 extends from 1.69 to 0.54 wt% in the CS and from 1.32 to 0.46 wt% in the ELS (Fig. 5.4).

(4) The average CS pyroxene has a higher content of Na_2O (Fig. 5.5).

5.4.4 Histograms of Compositional Ranges.

Fig. 5.2 shows that:

(1) While the compositional parameters follow a skew Gaussian distribution in both the ELS allivalite and peridotite, as expected from a single-stage fractionation process, they show a marked bimodal distribution in the CS peridotite in the case of olivine, pyroxene and spinel, though not for plagioclase.

(2) There is a much wider separation between the median compositions of olivine in allivalite vs. the median in peridotite for the CS ($Fo_{82.9-86.9}$) than for the ELS ($Fo_{84.4-85.4}$). This is also true for the $MgCr_2O_4$ content of spinel, (0.17 - 0.31) vs. (0.22 - 0.28), to a lesser extent for pyroxene Mg-number, but not for the An content of plagioclase.

(3) Combined histograms for core and rim compositions show slight reverse zoning in the ELS olivines to be ubiquitous, although it is less common in the CS. Rim analyses were measured less than 30 microns from the edge of the crystal.

5.5 Hydrous Inclusions in Olivine and Spinel.

Sub-spherical inclusions of hydrous silicates with lesser amounts of anhydrous silicates, oxides and sulphides occur in a small proportion of the olivine and disseminated spinel throughout both series, although the most spectacular examples are in the spinels of the chromitite laminae. Similar inclusions have been observed in spinel (but not in olivine) from the Stillwater (Jackson, 1961), the Bushveld (McDonald, 1965) and Muskox (Irvine, 1975) intrusions, while McClurg (1982) noted their occurrence on Rhum, emphasising their greater abundance in chromitites within peridotite with respect to those at allivalite / peridotite contacts.

5.5.1 Textural Relations.

Four end-member types can be distinguished:

(1) Spinels with a single, large central inclusion (up to 350 microns across, commonly 50-100 microns), see Plate 5.34.

(2) Spinels or olivines with one or more off-centre inclusions, up to 600 microns in olivine and 200 microns in spinel, commonly 150-400 microns in olivine and 20-80 microns in spinel (Plates 5.35 to 5.38).

(3) Spinels with minute inclusions in a narrow zone along the rim, 5 to 30 microns across (Plate 5.39).

(4) Spinels with inclusions of crystalline outline, restricted to the ELS.

Any one spinel may show a combination of these types. The number of inclusions per spinel can reach into the 100's, but is usually under 10 per cut surface; the inclusions may form up to a third of the volume of the spinel. The presence of inclusions, their number and size correlate positively with the size of the hosting olivine or disseminated spinel. Inclusion-bearing spinels may themselves form inclusions in olivine, and in some rocks, these are the only inclusion-bearing spinels in the sample. Type 3 spinels, however, occur only discretely or as inclusions at the margins of olivine crystals. In a given sample, the ratio of hydrous-inclusion-bearing to inclusion-free crystals is as high as 1 : 2 for olivine, 4 : 5 for spinel in the CS and 1 : 20 for spinels in the ELS, and as low as 1 : 4000^{+}. Inclusion-bearing spinel occurs in all rock types, with inclusion-bearing olivine restricted to peridotite. In chromitite laminae, where the spinels have locally recrystallised to form massive aggregates, inclusions are either very

large or absent, while those in non-sintered spinels are more abundant and smaller. The ratio of inclusion-bearing to inclusion-free spinels is up to 9 : 1 in CS chromitites and 1 : 3 in ELS chromitites.

5.5.2 Mineralogy of Hydrous Inclusions.

Kaersutite, phlogopite, Na- and Na/K- phlogopite, enstatite and calcic feldspar all occur commonly but are listed in decreasing order of abundance. More unusual phases include albite, potassic feldspar, tremolite, hornblende, apatite, diopside and olivine; sphene has been identified in isolated probe analyses. Common alteration minerals found especially in inclusions in olivine are serpentine, calcite and chlorite. The various phases are all compatible with one another (except for the different types of phlogopite), although phlogopite and plagioclase have not been found together in a single inclusion. Electron-microprobe analyses, selected from 280 analyses on inclusions in 180 crystals from 75 rocks, are presented in Tables 5.5 and 5.6. Low totals are due to dispersion on soft silicates, which are difficult to polish since they are imbedded in Cr-spinel. The Mg-number of the inclusion silicates is compared with that of the olivine in the host rock in Fig. 5.8, which shows they bear a consistent relationship to each other: the fractionation trend for the host rock is paralleled by the fractionation trends for the individual inclusion minerals. The data are averaged in Table 5.6 for kaersutite and phlogopite and compared with the Mg-number of the corresponding intercumulus silicates; especially in the ELS, phlogopite and kaersutite behave in markedly parallel fashion. Relative to the intercumulus phases, inclusion phases have a lower TiO_2 content (Fig. 5.10) and a distinctly lower K_2O content (Fig. 5.11); the latter being slightly more pronounced in the CS when rocks of similar Mg-number are compared.

Textural relations within the globules are illustrated in Fig. 5.13 in which the sub-hedral outline of the enstatite and the rounded appearance of the sphene may be seen. Table 5.8 compares the Mg-number of phases which occur as inclusions in both olivine and spinel hosts within the same sample; in each case, the compositions are nearly identical (for complete analyses,compare phases 1 and 2, and 21 and 22 in Table 5.5). In addition to silicates, many inclusions have tiny (5 to 50 microns), spherical pn-po-ccp assemblages, representing unmixing of a monosulphide solid-solution immiscible droplet (section 5.4.5).

While many inclusion-bearing spinels occur in chromitites with a high content of sulphides, the inverse relationship does not hold.

5.5.3 Variation in the Mineralogy of the Inclusions through the ELS and CS.

Kaersutite and phlogopite occur throughout both layered series. Phlogopite is more common in olivine-hosted inclusions, in disseminated rather than chromitite spinels and in feldspathic peridotite (ELS and DM) rather than in dunitic peridotite. The distribution of enstatite is random, while diopside is restricted to the lower parts of the LLG overlying the DM (note the low Al_2O_3 contents of the inclusion pyroxene, also typical of the cumulus pyroxene in the DM; cf. analyses 24 and 25 in Table 5.5 with analysis 7 in Table 5.4). The distribution of the less common phases is given in Fig. 5.14 where their concentration along the margin of the present ultrabasic complex may be noted.

5.5.4 The Origin of the Inclusions

The varied mineralogy, the compositional similarity of phases included in both spinel and olivine, the lack of inclusions in sintered chromitite laminae, the common association with immiscible sulphide droplets, the compositional contrast with intercumulus phases and the common occurrence of inclusion-bearing spinels within olivines all suggest the inclusions represent a discrete phase, on which olivine or spinel nucleated, or which was entrapped by the growing host crystal.

As such, the low crystallisation temperature of the hydrous silicates suggests this phase was a liquid, probably an immiscible bubble with a high content of volatiles, alkalis, aluminium and silica. The parallelism of the Mg-numbers for olivine from the host-rock and for the hydrous inclusion phases is probably due to sub-solidus re-equilibration of Fe and Mg, though the identical compositions of phases included in both olivine and spinel in the same sample suggests this may have been limited and the parallelism of compositions is a primary phenomenon. The textures of the chromitite laminae suggest that the larger inclusions may have formed by migration of the smaller inclusions towards the centre and coalescence to produce the large inclusion by a process of annealing. During subsequent crystallisation of the globule, the subhedral orthopyroxene probably crystallised first, followed by outward diffusion of excess volatiles and crystallisation of the hydrous silicates.

The source of the volatile-rich immiscible globules may lie in

the country rocks as suggested by the concentration of exotic phases towards the margin of the complex; the occurrence, however, of the common hydrous phases in inclusions throughout the complex suggests the volatile-rich globules were part of the intercumulus fluid expulsed from below by the compacting pile of cumulates (see Irvine, 1980 and section 7.1.2). Some phases, such as high-Al enstatite (Fig. 5.12), may represent partly resorbed xenocrysts from the wall-rocks. Olivine and plagioclase may have been derived from earlier cumulates, and it is suggested that the low-Al diopside was derived from the Dornabac Member allivalites. The sphene, hornblende, apatite, albite and K-feldspar may represent incomletely equilibrated globules of granitic melt from the wall-rocks, as suggested for the inclusions in the spinels of the Muskox intrusion by Irvine (1974).

5.6 Chromitite Laminae.

Fig. 5.15 shows the location of chromitites in the Trallval area. Field relations are given in Chapter 3 and laminae are classified as follows:

(1) At contacts between peridotite and allivalite (Plates 5.20 and 5.31).
(2) Round blocks of allivalite or gabbro in peridotite.
(3) Associated with layers of harrisite or proto-harrisite.
(4) Along contacts between feldspathic and less feldspathic peridotite (Plate 5.15).
(5) In dunitic peridotite and dunite (Plate 5.30).
(6) In the top metre of allivalite layers (Plate 5.27).

All types may be deformed by loading or slump folding, often leading to boudinage. The concentration of the spinel is highly variable (Plates 5.40 and 5.41) and may be up to 90 % in recrystallised laminae; size-sorting is poor, nearly all laminae have some spinels with silicate inclusions, the intercumulus material is plagioclase and, sometimes, olivine. As in disseminated spinel, exsolution of ilmenite is common, especially in the ELS and best developed in type 6 concentrations, although in CS laminae in dunitic peridotite, it is restricted to a fine dusting of ilmenite around the crystal edges.

5.6.1 The Composition of Spinels.

McClurg (1982) analysed spinels from the ELS and CS, both those included in cumulus and intercumulus phases, and chromitite spinels

from the ELS. Her results, confirmed by a reconnaissance study of spinels from the Trallval area, are summarised below. Additional data on disseminated and chromitite spinels from the ELS and CS are presented afterwards.

(1) Spinels have re-equilibrated continuously with the intercumulus liquid and adjoining silicates during postcumulus crystallisation until trapped by intercumulus phases or the extensions of cumulus phases, after which some sub-solidus re-equilibration took place.

(2) Spinels closest to their liquidus compositions are found as inclusions in cumulus olivine, and these compositions are taken to represent primary variation in the trivalent cations. Sub-solidus re-equilibration of Fe^{2+} and Mg between olivine and spinel depends on the modal proportions of the two phases (Irvine , 1965 and 1967); no exchange of trivalent cations happens as the olivine lattice does not accept these. Bevan (1982) found partial orthopyroxene rims on spinels included in olivine, which she interpreted as products of a sub-solidus oxidation reaction between the two phases and fluid. Such rims are rare on layered series spinels and were identified in one instance only during this study (HL1, U14, Askival).

(3) The composition of all other spinels (and also some spinels close to the olivine rim) were modified by two competing processes:

I - Reaction with the adjoining silicates and the reservoir of intercumulus liquid in the uncompacted cumulate in an open system leading to an increase in Al, at the expense of Fe^{3+} and Cr; the "Al" trend.

II - Reaction with locally trapped intercumulus liquid in a closed system, leading to an increase in Ti and Fe at the expense of Al and Cr; the Fe trend.

The relative importance of these two processes depends on the degree of compaction of the cumulate and the growth rate of the cumulus phases.

(4) Chromitite types do not correlate with specific compositional ranges, although the intensity of compositional variation across a seam is highest for seam types 1 and 2. The overall variation in chromitite spinel composition parallels that of spinel disseminated in the intercumulus phases. This range is far greater than that for any other layered intrusion.

(5) There is no stratigraphic variation in chromitite spinel composi-

tion, although McClurg (1982) found a westwards increase in Fe, Ti and Cr with a decrease in Mg and Al over 1 km. for a seam of type 1 at the U7 / U8 contact on Barkeval.

Disseminated spinels included in olivine analysed in this study are plotted in Figs. 5.16 to 5.18. They define a wider range of compositional variation than McClurg's data (Table 5.9), partly because of more extensive sampling of the CS. The greater range for the CS relative to the ELS is attributed to a greater range of liquid compositions with which the spinel came in contact before entrapment, probably due to more extensive in situ overgrowth of the olivine over spinels which have reacted with intercumulus liquid.

Figs. 5.16 and 5.17 suggest that, for a given Mg-number, the CS spinels have a higher Fe^{3+} / Fe^{3+} + Cr + Al ratio and a lower Cr/Cr+Al ratio than the ELS spinels which suggests a higher oxygen fugacity and greater supersaturation of the CS liquid with respect to plagioclase.

Compositional trends for spinels in chromitites from the Trallval area are plotted in the trivalent cation field of Fig. 5.19. These data confirm McClurg's (1982) and Henderson's (1975) Al and Fe trends. Some chromitites from the CS (AG7 and HD16, both RG1), however, fall on the Fe-poor side of their Al trend, which implies a minimal effect of the Fe trend on these chromitites and suggests very effective expulsion of intercumulus liquids which is confirmed by the massive textures. For the chromitites at the extreme of the Al trend, there is field evidence for a close association with the forked ultrabasic breccia zone for GG19, while HG4 and AE12 are from an area intensively intruded by sheets of olivine gabbro. Chromitite HD31, at the extreme of the Fe trend was injected by a coarse pyroxene-rich gabbro vein. No recrystallisation textures are evident in chromitites HG4 and AE12, suggesting that the gabbroic liquid changed the composition of the intercumulus liquid from the layered series either by local mixing or by diffusion, while the layered series was still unconsolidated. Table 5.10 lists the effects of sub-solidus re-equilibration between spinel and olivine on the composition of the olivines near and within chromitite, resulting in a higher Fo content of the olivine. The intensity of this effect decreases with distance away from the chromitite and decreasing modal abundance of the spinel, as suggested by Irvine (1965 and 1967).

5.7 Stratigraphic Variation in the Layered Series.

Variations in mineral chemistry, modes, sulphide content and grain-size are presented in Figs. 5.19 to 5.30 for the traverses normal to the layering shown in Fig. 5.1

5.7.1 Techniques.

5.7.1.1 Mineral Modes

For each polished thin section, the silicate and oxide modes were determined by point-counting on a grid of 300 to 400 points over an area 5 to 8 cm^2. Precision is within 2.0 %. A semi-quantitative measurement of disseminated sulphide concentration was recorded by examining ten 0.64 $mm.^2$ areas, regularly spaced over the entire thin section, under a magnification of X125, estimating the fraction of the field of view covered by the sulphides, averaging these ten values and converting the area average into a bulk ppm figure. Precision depends on the grain-size of the sulphides, their concentration and uniformity of distribution, but is usually less than 100 ppm.

5.7.1.2 Grain-size.

For each section, the average of the maximum diameter and the diameter normal to it have been determined for the largest grains of olivine and spinel. The main weakness of only measuring the largest grains is a sampling problem: the coarser the grain-size, and the lower the concentration of the measured grain type, the less meaningful the procedure becomes. On the other hand, as many of the cumulates have a pronounced olivine foliation, comparison of average grain sizes between laminated and non-laminated olivine rocks or between sections at different orientations to the lamination in highly inequidimensional olivines is meaningless, while the lamination is never so good that, in a rock with perfect size-sorting, a single section at random does not have several grains with their maximum diameter in the plane of the thin section.

5.7.1.3 Mineral Chemistry.

The chemical mineralogy for each sample was determined by a WDS electron microprobe technique. Crystals of each phase were analysed from both ends and the middle of the polished section. For olivine and pyroxene, the within sample variation of core composition is generally small; see Table 5.11 for the range in standard deviations. Extreme within-sample variation of olivine core composition has been

found in and close to chromitites (Table 5.8), across allivalite/peridotite contacts (up to 4 mol % Fo) and in finely layered allivalites, such as the one shown in Plate 5.15 in which the olivine composition varies from lamina to lamina by up to 2.5 mol %Fo. In a texturally homogeneous sample, however, olivine core composition varies by less than 0.5 % Fo, provided the sample is not affected by metasomatism, as is the case close to gabbroic veins (Butcher, pers. comm.). Slight reverse zoning is common in olivine (Fig. 5.2). For intercumulus plagioclase, the range of core compositions is much wider and on Figs. 5.19 to 5.30, the whole range is plotted rather than just the average as for olivine and pyroxene.

5.7.2 Cryptic Variation.

This was documented along a number of traverses for each layered series to pursue the following objectives:

(1) To correlate the sets of traverses and test the structure of the series as suggested by the mapping (Chapter 2).

(2) To test the hypotheses advanced by previous workers (Chapter 7) for the petrogenesis of the ELS by supplying data for higher units in the series (McClurg (1982) gives data for U6 to U11 on Barkeval and Dunham and Wadsworth (1978) for U10 on Hallival) and on lateral variation within the units.

(3) To provide a similar data set for that part of the CS in the Trallval area.

From this study and data from McClurg (1982), the following compositional parameters show the largest variations with fractionation: Fo and NiO content in olivine, An content of plagioclase, Mg-number and Cr content of clinopyroxene. In this section, the systematic stratigraphic variation (if any) of these parameters is described.

5.7.2.1 The Eastern Layered Series. (Figs. 5.21 to 5.24)

The most comprehensive data (Fig. 5.21) were collected for that part of the ELS, U11 to U16, above the area of intense gabbro veining, along traverse 1 (Fig. 5.1). Samples were collected at intervals of 10 to 20 m. in peridotite decreasing gradually to 1 to 5 m. close to and within allivalite, as the strongest variation in the ELS occurs within 5 to 10 m. of lithological contacts (McClurg, 1982; Dunham and Wadsworth, 1978). From U11 to U16, only plagioclase shows a slight overall evolution. In general, there is none, the pattern of variation

showing a progressive trend towards evolved compositions followed by a sharp reversal back to primitive compositions. These reversals are found both near the bottom and within units (intra-peridotite reversals), the precise level varying from phase to phase and unit to unit. The sharpness of the reversals is partly a function of the sample spacing and, indeed, there may be hidden cycles of evolution followed by reversals: because of the staggering of reversals between the various phases, this is not likely, however. The strongest reversals are at the base of the U11 and U15.

Wt% NiO in Olivine: this is the simplest pattern. Major reversals occur across the contacts between units (except for U11/U12). These are initiated 2 to 6 m. below the top of the allivalite and terminated within 1-2 m. into the peridotite, except at the base of U14 and U16, where the most nickeliferous oivine occurs 7-8 m. above the base of the peridotite. Minor reversals occur halfway up within U14 and U15 and at the U11/U12 contact (5 m. below the top of the allivalite). Reversals, poorly defined due to inadequate sampling, occur within U12. Wt% NiO ranges for each unit are listed in Table 5.12, as are the ranges for the other compositional parameters.

Fo Content of Olivine: the pattern is similar to that of Ni in olivine (with a more important reversal at the U11/U12 contact). U11 and U15, however, show very little evolution towards fayalitic olivine and reversals are displaced upwards for all units by a maximum of 20 m. and a minimum of 7 m. at the bases of U13 and U16, respectively, except above the thick allivalite at the U14/U15 contact. Minor intra-peridotite reversals occur in U12, U15 and possibly U14, although they are displaced upwards with respect to the Ni reversals by a minimum of 4 m. for U14 and maxima of 42 m. for U12 and 13 m. for U15, as determined from the sample spacing constraints. In addition, minor reversals occur in the lower 1-2 m. of each allivalite.

Mg-number of Pyroxene: this pattern is almost identical to that of Fo in olivine, although neither of the intra-peridotite reversals in U12 were identified and, whereas the range of variation is more marked in U15, it is less so in U14.

Wt% Cr_2O_3 in Pyroxene: with the qualification that reversals at the base of allivalites are at least as important as those at the base of peridotite, the pattern is similar to that of the Mg-number of pyroxene.

The intra-peridotite reversals of U12 and U14 are more strongly marked and that of U15 less so.

An Content of Plagioclase: there is a good correlation between the major reversals and the appearance of cumulus plagioclase in each unit (at the base of the allivalite). Only a slight increase in Na accompanies the termination of cumulus plagioclase, as the evolution of intercumulus plagioclase in the peridotite continues a trend which starts within the allivalite. Minor reversals mimic the lower of the two intra-peridotite reversals in U12, those in U14 and possibly U15. Zoning of the intercumulus plagioclase is stronger just below reversals. A comparison of the most calcic plagioclase compositions in each unit indicates a slight upward increase in An content over the series.

Variation of Grain-size and Sulphide Content: in general, there is a positive correlation between variation in the Fo content of the olivine and the grain-size of olivine and spinel. Grain-sizes fine upwards to below the main allivalite of each unit, followed by a little increase at the base of the allivalite and a sharp increase at the base of the peridotite. Sulphides are scarce in the lower half of the peridotite of most units (except for a basal concentration in U15) with abundance peaks occurring in the peridotite just below allivalite layers; these level off gradually to the base of the overlying peridotite.

5.7.2.2 Stratigraphic Variation in U8 to U10 of the ELS.

Due to the intense injection of gabbro in this area, cryptic variation data are incomplete (Figs. 5.23 and 5.24). However, the patterns are similar to, but less regular than, those in the overlying units. It is worth noting that:

(1) The reversals in the Fo in olivine and Mg-number in pyroxene patterns coincide with the NiO reversals at the base of the peridotites.

(2) Only one unit, U10, has an intra-peridotite reversal.

(3) The Fo reversals at the base of U9 and U10 are small compared with that at the base of U11 (Fo 84 to 85 and 82 to 86 vs. 80.5 to 87.5).

5.7.2.3 Lateral Variation in the Eastern Layered Series.

The East Trallval traverse (3 on Fig.5.1) is compared with the W. Trallval traverse, described above, for U13 and U14, and also with a few samples from the bottom of each unit from the West Askival traverse, in Fig. 5.22. The variation patterns match very well for Ni in olivine and Cr in pyroxene when the 7 m. difference in thickness of U13 is

taken into account (the datum level for all sections and variation traces is the U12/U13 contact). The Fo and the pyroxene Mg-number patterns are displaced towards more Fe-rich compositions for East Trallval by 1 to 3 mol%, though the pattern shapes are unchanged. The sparse data for Askival match the E. Trallval curve. The sub-allivalite sulphide peaks coincide for the E. and W. Trallval sections, although the E. Trallval abundances are up to 1200 ppm. Intercumulus pyroxene is also more abundant over this traverse.

Figs. 5.23 and 5.24 compare the Trallval data for Fo and NiO contents in olivine with McClurg's (1982) cryptic variation on Barkeval and data for Hallival (Dunham and Wadsworth, 1978; Palacsz, pers. comm.) and suggest the following:

(1) Ni variations for both pairs of units for which data available on Trallval and Barkeval (base of U10, S. Tr. and Bark.; U11, W. Tr. and Bark.) are virtually identical when the Barkeval units are expanded to the same thickness as the Trallval units.

(2) Both the Trallval and Barkeval traverses show little variation in Fo content through the peridotite of U11, whereas this is strong for all other units. Intra-peridotite reversals for U8 and U10 on Barkeval are matched on W. Trallval, although the Barkeval variations are more extreme. The variation across the U9/U10 contact on Barkeval is better matched in the S. Trallval traverse than on W. Trallval.

(3) A compositional shift of 2 mol% Fo (towards fayalite) can be inferred for the Hallival section with respect to Trallval but is less than 1% for Barkeval.

Figs. 5.25 and 5.26 illustrate lateral variation in Fo content on a smaller scale along the ridge of Trallval, for 9 traverses spaced at 100 to 300 m. By comparing samples collected at precisely the same stratigraphical level, it can be concluded that the variation is not a gradual phenomenon. Instead, the Trallval series is partitioned into domains with vertical boundaries: traverses 1 and 6 have high-Mg olivines compared with traverses 2, 3, 4, 7 and 9, while traverse 5 has significantly more Fe-rich olivine, the disparities being of the order of 2 to 4 mol% Fo.

5.7.2.4 Cryptic Variation in the Central Series.

As no single traverse encompasses all the units in the series, a

composite profile (see paragraph on lateral variation) for the Fo and NiO contents of the olivines is presented to indicate the evolution of compositions over the entire series (Fig. 5.27). The behaviour of the remaining compositional parameters is described from the Seagull traverse (6 on Fig. 5.1) for the Dornabac Member and the Long Loch Group, and from the Ruinsival traverse (8 on Fig. 5.1) for the Ruinsival Group (Figs. 5.28 and 5.29).

As for the ELS, there is no overall evolution of olivine composition with respect to Fo content over the ca. 900 m. thick section across the CS (Fig. 5.27). A slight decrease in NiO content from the LLG1 unit upwards is indicated, however. The pattern of gradual evolution for each unit or sub-unit followed by a sharp reversal is repeated here in the Dornabac Member (DM), the lower unit of the Long Loch Group (LLG1) and the upper two units of the Ruinsival Group (RG1 and RG2). The remaining units either show slight reverse cryptic variation or none at all over most of their thickness, with a sharp drop in Fo or NiO content near the top, followed by a sharp reversal. While sub-cycles are defined only in the middle unit of the Long Loch Group (LLG2), many of the reversals in the coastline and lower Ruinsival traverses are of intra-peridotite type as the units in these areas lack an allivalite cap. As on the ELS traverses, samples were collected at smaller intervals (1 to 4 m.) close to peridotite/allivalite contacts and within allivalite, but the sampling interval was gradually increased to about 90 m. in the middle of the thickest cyclic units.

Wt% NiO in Olivine: all major reversals take place across contacts between units. They are usually initiated 1 m. below the contact, although this may be up to 10 m. for the DM/LLG1 and LLG2/LLG3 contacts, the former contact showing the strongest reversal in the CS. A maximum Ni content is attained within the lower 14 to 30 m. of each unit, except for RG2, after which there is a sharp drop followed by an upward-invariant or stepped reverse trend. Ranges in Ni content of the olivine for each unit of the CS are shown in Table 5.12 along with the ranges for the other compositional parameters.

Mol% Fo in Olivine: the pattern is similar to that of Ni, though the changes to more evolved compositions are more gradual. Reversals coincide with those of the Ni pattern, except that their initiation precedes that of the Ni reversals at some contacts (LLG1/LLG2, LLG3/RG1, RG1/

RG2) and maxima are attained within the bottom 28 to 50 m. of each unit, before a sharp drop. RG2 appears to follow an ELS pattern, although this may be due to the widely spaced sampling. Most of the stepped reversals of the Ni pattern are displaced upwards in the Fo pattern by less than 30 m. for RG1 and probably more than 14 m. with respect to the main Ni reversal within LLG2.

Variation in Pyroxene Composition: these traverses (Figs. 5.28 and 5.29) are incomplete due to the preponderance of dunitic rocks in the CS. The Mg-number variation follows that of Fo in olivine and the Cr_2O_3 content variation is analogous to that of Ni in olivine.

An Content of Plagioclase: again, a lack of feldspar-bearing rocks produces an incomplete pattern. Major reversals occur at the base of the allivalite, maximum An content is reached 5 to 10 m. below the top of the unit and the most evolved plagioclase occurs at about a third of the way up into the unit. As in the ELS, zoning in intercumulus crystals is most pronounced towards the top of the peridotite.

Sulphide Content and Grain-size: as for the ELS, sulphides are associated with the allivalites, especially their lower parts and also the peridotite just below. Grain-size generally shows little correlation with the cryptic variation, although there is an upward-fining trend in most units, with a marked reversal in RG1.

5.7.2.5 Lateral Variation in the Central Series.

Lateral lithological variation in the CS is strong (section 3.6), e.g. the 16 m. thick allivalite cap of LLG3 on the Seagull traverse is not seen at all on the coastline traverse through LLG3 and it is the cryptic variation which defines the top of the unit. Therefore, variation along a horizon mappable in the field must be established first in order to estimate the reliability of the compositional parameters for correlating the allivalite-free traverses.

Variation along the DM/LLG1 contact: Fig. 5.30 shows three traverses across the contact. The NiO and Fo variation patterns correlate well for the Seagull and An't Snidhe sections. The NiO pattern for the Leac a Chaisteil traverse, where the DM consists of a number of thin allivalites in feldspathic peridotite (it is correlated with the other two traverses on the Cr-spinel horizon and the allivalite of LLG1), fits the variation pattern for the other two traverses except that the magnitude of the reversal is smaller. Fo variation in the DM is more

marked, the reversal is more gradual and displaced upwards by 7 m., and the olivines are in general more Fe-rich by about 1 mol% Fa. There appears to be some correlation of sulphide contents: all three traverses have high sulphides towards the top of the allivalite, although the Leac a Chaisteil and Seagull traverses have a yet higher sulphide content at the bottom of LLG1, whereas there are none in LLG1 on the An't Snidhe traverse.

Lateral Variation in Olivine Composition for the Rest of the CS:

from the previous sections, the laterally least variable parameter is the NiO content of the olivine. Thus, the allivalite-free units of the LLG along the coastline traverse are correlated with those of the Seagull section on the Ni reversals at the base of the overlying units (Fig. 5.31). From Fig. 5.31, there appears to be no general lateral variation in the NiO content of olivine, as was the case for the ELS. Fo contents do vary (Fig. 5.32) from traverse to traverse, with those of Papadil and Ruinsival being the most forsteritic, followed by McClurg's (1982) traverse for the Long Loch area. On average, these have 2 to 3 mol% Fo more than the Seagull traverse, while the Leac a Chaisteil section has 1 to 2 mol% less. The NE Ruinsival and Trallval traverses have a similar Fo level to that of the Seagull traverse. The composite profile of Fig.5.27 was constructed by superposition of the patterns, after standardising unit thickness and shifting the Fo level of each section by the appropriate amount to obtain a profile at the Seagull traverse "Fo level".

5.8 The Mineralogy of the Ultrabasic Breccia Zones and Plugs.

Representative chemical analyses for the anhydrous minerals are presented in Tables 5.2 to 5.4. Compositional ranges for all phases fall within those of the layered series (Figs. 5.3, 5.4, 5.5 and 5.6), although the high end of the Fo range (Fo 88.0) lies just outside the range for the ELS but well within that of the CS. The breccia matrix minerals group towards the more evolved compositions. Within-sample variation of the olivine compsition is,on average, higher than that in either the ELS or the CS peridotite (Table 5.9). The NiO/Fo relations for olivine (Fig 5.3) suggest that those from the breccia matrices lie along the trend defined by the CS analyses, for olivine in equilibrium with a sulphur-undersaturated magma; the data for the plugs are incon-

clusive. The more Fe-rich intercumulus pyroxenes of the breccias show a similar compositional range to those of the CS (Fig. 5.4). In the pyroxene quadrilateral (Fig. 5.6), the breccia compositions define a trend of Ca-impoverishment, while the plug pyroxenes cluster close to the Fe-enrichment curve defined by the CS pyroxenes. Spinels included in the olivine (Figs. 5.16 to 5.18) have a generally low Cr / Cr + Al ratio and a high Mg / Mg + Fe^2 ratio, similar to those of the CS. Modally, these rocks are similar to the feldspathic peridotites of the layered series, with a lesser amount of intercumulus pyroxene and a high content of primary, intercumulus kaersutite and phlogopite (Plate 5.42), varying between 1 to 3 vol % for the breccia matrices and 1 to 6 vol % for the plugs.

	ELS peridotite		ELS allivalite		CS peridotite		CS allivalite	
	Max.	Avg.	Max.	Avg.	Max.	Avg.	Max.	Avg.
Olivine	7.2	1.2	5.1	1.0	20.0	2.1	5.3	1.0
Spinel	0.75	0.15	0.38	0.08	1.12	0.25	0.39	0.10
Cumulus pyroxene			3.3	1.5			2.8	1.3
Intercumulus pyroxene	17.2	5.5	12.0	5.0	20.1	4.5		
Cumulus plagioclase			4.4	1.0			9.0	1.5
Intercumulus plagioclase	11.1	3.7			8.4	1.8		

TABLE 5.1 Grain size data for the Layered Series. Figures are in mm.

		Mol % Fo	Wt % minor element oxides							Wt % major element oxides			Analysis Total
			Ni	Ca	Mn	Na	Ti	Al	Cr	Si	Fe	Mg	
ELS	dunitic peridotite	85.6	.326	.072	.235	.018	.020	.030	.020	39.78	14.06	45.75	100.32
	feldspathic perid.	84.4	.270	.029	.242	.008	.029	.030	.059	38.69	15.34	45.78	100.48
	mafic allivalite	82.1	.222	.061	.220	.011	.010	.05	.005	38.27	17.00	43.90	99.75
	anorthosite	85.3	.255	.047	.234	.025	.011	.062	.011	39.61	13.90	45.64	99.81
CS	dunite	88.8	.364	.099	.253			.019	.029	40.68	10.81	48.02	100.27
	feldspathic perid.	83.5	.215	.045	.217			.027	.012	39.59	15.63	44.42	100.17
	allivalite	86.6	.257	.102	.241				.018	41.03	12.41	45.77	99.83
Papadil plug		84.1	.238	.080	.229	.009	.012	.052	.009	40.03	14.31	44.84	99.80
Papadil plug core		83.4	.255	.036	.252	.007	.016	.050	.019	39.46	15.88	44.26	100.25
Trallval breccia zone		82.1	.244	.056	.269				.010	39.05	16.83	43.19	99.65
Ruinsival breccia zone		83.8	.278	.086	.275				.016	39.93	15.12	44.46	100.18
Average peridotite		84.4	.274	.064	.246	.011	.019	.035	.023	39.65	14.75	45.09	100.14
Average allivalite		84.7	.245	.070	.227	.018	.011	.056	.011	39.64	14.44	45.11	99.80

TABLE 5.2 Representative olivine analyses.

		Mol% An	Wt % Minor Element Oxides				Wt % Major Element Oxides				Analysis Total
			K	Fe	Mg	Ti	Si	Ca	Na	Al	
ELS	dunitic peridotite	66.3	.093	.211	.059	.089	51.28	13.42	3.77	30.71	99.63
	feldspathic peridotite	73.5	.094	.284	.048	.070	49.76	14.98	2.99	31.83	100.05
	mafic allivalite	83.1	.048	.426	.052	.036	46.99	16.51	1.75	33.34	99.16
	anorthosite	88.2	.072	.251	.050	.050	47.00	17.22	1.27	34.12	100.44
CS	dunitic peridotite	84.0	.034	.270	.046	.034	46.53	17.20	1.80	33.94	99.85
	feldspathic peridotite	83.7	.100	.252	.047	.057	47.07	17.25	1.86	33.43	100.07
	allivalite	85.3	.035	.479	.060	.066	47.56	17.87	1.70	32.32	100.08
Trallval intrusive peridotite		85.1	.059	.273	.038	.052	47.09	17.27	1.67	33.99	100.44
Papadil plug		80.7	.036	.303	.040	.027	48.28	16.49	2.20	32.16	99.88
Trallval breccia zone		82.7	.085	.290	.053	.064	47.55	16.93	1.96	33.50	100.43
Papadil breccia zone		77.6	.210	.381	.071	.094	48.89	15.76	2.52	31.45	99.37
Average peridotite		79.2	.089	.283	.050	.061	48.31	16.16	2.35	32.63	100.02
Average allivalite		85.8	.052	.385	.054	.051	47.18	17.20	1.57	33.26	99.89

TABLE 5.3 Representative plagioclase analyses.

			Cation Fraction			Wt % Minor Element Oxides						Wt % Major Element Oxides				Analysis Total
			Ca	Mg	Fe	Cr	Na	Al	Ti	K	Ni	Si	Fe	Mg	Ca	
1	ELS	dunitic peridot.	42.3	48.7	9.0	0.99	.365	3.50	0.64	.003		52.07	5.54	16.81	20.33	100.25
2		Feldspathic per.	44.2	47.3	8.5	1.00	.396	3.42	0.91	.031	.029	51.74	5.11	16.14	21.39	100.17
3		mafic allivalite	44.2	45.6	10.2	0.69	.405	3.16	1.29	.015		50.92	6.34	15.80	21.35	99.97
4		anorthosite	48.5	44.0	7.5	1.03	.432	3.42	1.01	.018		51.26	4.61	15.24	23.35	100.36
5	CS	dunite	50.8	42.8	6.4	0.90	.448	5.36	1.01		.026	50.67	3.82	14.32	23.67	99.78
6		feldspathic per.	44.9	46.8	8.3	1.07	.366	4.46	1.19			49.86	4.95	14.84	23.19	99.56
7		allivalite	48.4	44.7	6.9	1.12	.459	3.61	0.86		.054	51.86	3.95	15.40	23.20	100.06
8	Barkeval plug		46.2	47.3	6.5	1.20	.448	4.18	1.47			50.39	3.90	16.13	21.91	99.63
9	Seagull plug		46.8	47.7	5.6	1.23	.324	3.70	0.87			51.94	3.38	16.38	22.36	100.18
10	Papadil breccia zone		44.8	47.6	7.6	1.14	.395	3.07	.735		.061	51.70	4.77	16.82	21.58	99.88
11	Trallval breccia zone		46.8	44.8	8.4	0.86	.423	3.60	.908	.035		50.93	4.81	15.25	23.22	100.04
12	Average peridotite		45.8	46.6	7.6	1.05	.417	3.88	.968			51.09	4.54	15.84	22.21	99.94
13	Average peridotite		47.1	44.8	8.2	0.95	.432	3.40	1.05			51.35	4.97	15.48	22.63	100.13

TABLE 5.4 Representative Clinopyroxene analyses.

	KAERSUTITE	Mg no.	SiO_2	Al_2O_3	FeO	MgO	CaO	Na_2O	K_2O	TiO_2	Total
1	δp, O, LLG2	84.1	41.61	11.70	5.32	15.78	12.07	3.36	0.11	5.23	97.19
2	01, O, LLG2	83.4	41.88	12.98	6.22	16.47	11.96	2.73	0.12	4.21	96.57
3	δp, O, RG1	85.9	42.50	15.27	4.48	18.06	10.61	3.42	0.21	1.78	96.34
4	δp, O, RG1	83.9	46.44	8.77	5.50	21.56	9.10	2.49	0.26	2.56	96.69
5	δp, O, LLG1	83.3	41.22	12.75	5.64	15.56	11.99	3.91	0.21	5.00	96.26
6	δp, O, U11	84.1	44.00	11.25	5.35	16.70	11.67	3.38	0.15	5.35	96.82
7	01, θ, U14	78.1	43.22	10.12	7.65	15.85	10.07	4.25	0.23	5.48	96.87
8	Intercumulus, RG2	82.0	41.18	12.03	5.92	15.11	12.13	3.34	0.86	5.14	95.69
	PHLOGOPITE										
9	δp, θ, LLG2	90.9	38.00	14.74	3.68	20.58		3.22	5.80	7.72	93.75
10	01, θ, U11	87.0	38.29	14.42	5.63	21.15	0.01	1.65	7.74	5.21	94.08
11	01, O, U14	87.6	38.08	15.53	5.31	21.02		2.11	7.10	4.43	93.56
12	01, O, BD1 picrite	84.9	38.13	13.80	6.47	20.42		1.28	8.32	5.21	93.64
13	Intercumulus, DM	84.2	38.60	13.90	6.56	19.57	0.05	0.62	8.98	5.81	94.07
14	Intercumulus, LLG2	84.4	38.35	13.95	6.63	20.14		1.39	7.81	6.56	94.83
	NA - PHLOGOPITE										
15	δp, O, LLG2	90.9	38.74	15.11	3.68	20.62	0.24	5.84	1.79	8.89	94.91
16	δp, θ, RG1	91.4	38.27	15.20	3.37	20.09	0.18	6.71	0.31	9.89	94.00
17	δp, θ, WLS	90.8	38.20	16.17	3.88	21.55	0.20	7.20	0.14	6.55	93.89
18	δp, O, U11	89.2	37.91	16.70	4.09	21.84	0.14	5.75	1.92	5.29	93.64
	ENSTATITE										
19	δp, O, LLG2	88.4	56.13	1.18	7.66	32.68	1.08	0.20	0.02	0.19	99.13
20	δp, θ, WLS	91.5	57.16	1.07	5.59	35.10	0.45	0.05	0.01	0.14	99.57
21	δp, O, U11	84.8	55.24	1.08	10.20	32.05	0.70	0.02	0.02	0.29	99.60
22	01, θ, U11	84.9	55.35	0.62	10.10	31.92	0.83	0.02	0.01	0.21	99.07
23	01, θ, U14	86.0	56.21	0.55	8.98	33.46	0.28	0.05		0.07	99.60
	DIOPSIDE								Cr_2O_3		
24	δp, θ, LLG1	91.0	54.30	1.20	3.05	17.23	23.34	0.37	0.71	0.53	100.01
25	δp, O, LLG1	88.1	50.22	3.60	3.86	16.08	22.58	0.66	0.82	1.33	98.32

TABLE 5.5 Analyses of common minerals in hydrous inclusions in spinel or olivine. Explanation of symbols: δp = spinel host, 01 = olivine host, (no. of dots = no. of inclusions), O = single-phase inclusion, θ, θ = 2, 3-phase inclusions. Analyses from the same rock sample are bracketed together.

ALBITE	SiO_2	Al_2O_3	FeO	MgO	CaO	Na_2O	K_2O	TiO_2	Total	Cation Fractions
Sp, O, LLG2	59.39	24.53	1.88	0.63	0.23	13.92	0.02	0.15	100.75	An 0.9, Ab 99.1
Pl, θ, U10	68.08	18.40	0.65	0.14	0.34	9.08	0.57	0.02	99.08	An 2.1, Ab 97.9
K-FELDSPAR										
Pl, O, U10	65.49	18.05	0.82	0.47	1.43	6.62	2.84	0.16	98.86	An 10, Ab 69, Kf 21
TREMOLITE										
Pl, θ, U15	55.10	1.58	3.11	24.25	10.73	0.74	0.04	0.28	95.82	
Pl, θ, U12	52.75	0.70	7.29	23.12	9.91	0.44		0.08	94.29	
HORNBLENDE										
Sp, O, RG1	50.22	6.30	4.87	25.74	6.75	1.98	0.03	3.08	98.98	
Pl, θ, U13	50.59	6,74	4.71	26.10	8.65	0.82	0.13	0.35	98.09	
SPHENE										
Sp, θ, LLG1	30.63	0.61	0.62	0.03	27.86	0.05	0.04	40.11	99.96	
CALCITE										
Sp, θ, LLG3	0.01,	0.03	0.24	0.01	57.99	trace			58.28	

TABLE 5.6 Analyses of unusual inclusions in spinel or olivine.

		Average D	No. of samples	Standard dev'n
Intercumulus phlogopite	CS	+ 1.0	10	± 1.8
Intercumulus kaersutite		- 3.8	4	± 1.3
Intercumulus phlogopite,	ELS	+ 1.2	3	± 0.8
Pholgopite in spinel	CS	+ 1.5	19	± 1.2
Kaersutite in spinel		- 3.6	38	± 1.8
Phlogopite in spinel	ELS	+ 2.5	14	± 1.7
kaersutite in spinel		- 2.6	23	± 2.1

TABLE 5.7 compositions of hydrous phases in spinel compared with intercumulus phases. D = (Mg no. of hydrous phase) - (Mg no. of olivine in host rock.

	Mc Clurg (1982)	This study:	
		ELS	CS
$Mg / Mg + Fe^{2+}$	0.10 - 0.60	0.14 - 0.48	0.10 - 0.65
Cr / Cr + Al	0.48 - 0.82	0.49 - 0.75	0.37 - 0.75
$Fe^{3+} / Fe^{3+} + Cr + Al$	0.10 - 0.50	0.17 - 0.58	0.08 - 0.73
Ti / Ti + Cr + Al		0.006- 0.09	0.002 - 0.105

TABLE 5.9 Compositional ranges of spinels included in olivine.

TABLE I

Sample	Phase	01	&p
HD13	ka	86.5	87.9
HC23	ka	84.8	84.7
GH31	ka	85.5	86.2
DG1	ka	83.4	84.1
HD30	en	85.4	85.0
H3	en	84.9	84.8
HG3	en	84.9	84.8
HD12	di	92.3	90.9
GN2	chl	94.6	94.2

TABLE II

Sample	Phase	&p, 0	&p, 0 or θ	associated phase if θ
HD10	ka	83.7	83.7	-
HC5	ka	83.1	83.7	-
FE10	ka	84.2	85.7	-
GM2	ka	87.4	86.0	phlogopite
HL2	ka	84.7	84.1	plagioclase
GM2	en	89.9	89.0	ka
GM2	en	89.9	88.9	plagioclase
HC1	phlog	86.3	89.4	diopside
HC9	di	87.4	87.4	-

TABLE 5.8 I Mg numbers of phases occurring both in olivine-inclusions (01) and in spinel-inclusions (&p) within the same rock sample.

TABLE 5.8 II Mg numbers of phases occurring in different inclusions in spinel in the same rock. At least one of the phases compared in each pair is from a single-phase inclusion. Symbols as in table 5.5. Abbreviations: ka = kaersutite, en = enstatite, di = diopside, chl = chlorite, phlog = phlogopite.

Sample no.	chromitite type	spinel concentration (%)	lamina thickness (in cm.)	$Mg/Mg+Fe^2$ of spinel	Fo content of olivine: peridotite cores	peridotite rims	chromitite cores	chromitite rims	maximum D
H3 (ELS)	1	65	1.1	0.64	84.1		87.0		2.9
AA0 (ELS)	1	71	1.5	0.57	87.1		89.9		2.8
AB10 (ELS)	1	92	1.2	0.54	85.4		86.5		1.1
BD2 (ELS)	2	90	5.0	0.52	89.3		91.0		1.7
GN2 (ELS)	2	77	1.3	0.48	85.9		86.3		0.4
HL2 (ELS)	3	85	1.5	0.45	81.6	81.4	83.0	83.5	1.9
AE12 (ELS)	3	75	0.5	0.74	86.3		87.7		1.4
HG3 (ELS)	4	85	1.0	0.70	83.1		83.1	84.9	1.8
LB3 (ELS)	4	14	1.0	0.26	86.2	86.4	87.2	88.6	2.4
HG4 (ELS)	4	89	0.8	0.70	87.2	86.7	87.8	88.6	1.9
BK4 (ELS)	4	68	2.1	0.62	87.7		88.6		0.9
HD13 (CS)	4	8.4	20.0	0.48	89.1		89.9	91.1	2.0
HD31 (CS)	4	45	3.0	0.33	78.9		81.1	82.4	3.5
HD16 (CS)	4	70	5.0	0.66	89.0	89.3	91.9	93.4	4.4
GG19 (CS)	4	76	3.0	0.82	88.6	89.2	91.4	91.5	2.9
GM2 (CS)	4	87	10.4	0.64	88.3	88.5	91.0	92.3	4.0
CC1 (CS)	5	32	0.6	0.52	87.5		88.7		1.2
HD6 (CS)	5	65	2.5	0.44	87.0		87.7	88.5	1.5
B03 (CS)	5	72	1.0	0.60	88.8		91.1	91.4	2.5
GB1 (CS)	5	84	2.6	0.56	88.0		90.4	92.3	4.3
FE10 (CS)	5	87	1.2	0.49	87.8		88.6	89.9	2.1

TABLE 5.1C Mg - enrichment of olivines in chromitite laminae.
D = variation in Fo content of olivine near and within chromitite.

	ELS		CS		ultrabasic breccias and plugs
	perid.	alliv.	perid.	alliv.	
No. of samples	70	35	91	14	24
$\sigma < 0.10$	.51	.40	.49	.36	.50
$0.10 < \sigma < 0.20$	.23	.29	.26	.14	-
$0.20 < \sigma < 0.40$	.11	.17	.16	.29	.17
$0.40 < \sigma < 0.60$	.10	.09	.05	.14	.25
$\sigma > 0.60$	.03	.06	.02	.07	.08
maximum σ	0.78	0.91	2.08	1.40	0.77

TABLE 5.11 Within-sample variation of olivine composition. Figures give the fraction of the samples in each rock-type category for which the standard deviation (σ) for the analysed olivines falls in the ranges indicated.

ELS	OLIVINE		CLINOPYROXENE		PLAGIOCLASE
	Mol % Fo	Wt % NiO	Mg number	Wt % Cr_2O_3	Mol % An
U11	86.8 - 85.0	.33 - .24	88.0 - 87.1	1.16 - .92	85.7 - 70.9
U12	86.5 - 83.5	.36 - .25	88.8 - 85.0	.97 - .54	84.4 - 78.3
U13	87.7 - 83.5	.37 - .17	89.4 - 84.9	1.17 - .55	87.7 - 75.8
U14	86.6 - 83.1	.33 - .14	87.4 - 86.0	1.17 - .46	88.2 - 68.6
U15	87.5 - 85.3	.38 - .17	88.9 - 86.1	1.32 - 1.08	88.8 - 72.4
U16	87.1 - 83.2	.35 - .22	88.0 - 84.3	1.18 - 1.01	82.2 - 76.3
CS					
DM	- 81.8	- .17	- 83.0	- 1.15	- 81.8
LLG1	89.1 - 82.3	.42 - .29	89.2 - 83.8	1.57 - .55	87.6 - 64.2
LLG2	89.8 - 81.3	.38 - .27	89.9 - 83.1	1.44 - 1.14	87.5 - 72.7
LLG3	89.3 - 85.9	.39 - .27	88.2 - 84.3	1.48 - .90	85.8 - 71.6
RG1	90.1 - 84.6	.37 - .22	90.5 - 82.6	1.47 - .53	85.5 - 77.3
RG2	87.2 - 82.9	.37 - .25	88.1 - 82.8	1.25 - .99	85.1 - 72.9

TABLE 5.12 Compositional ranges for the minerals in the units described in sections 5.7.2.1.1 to 5.7.2.1.5 and 5.7.2.2.1 to 5.7.2.2.4.

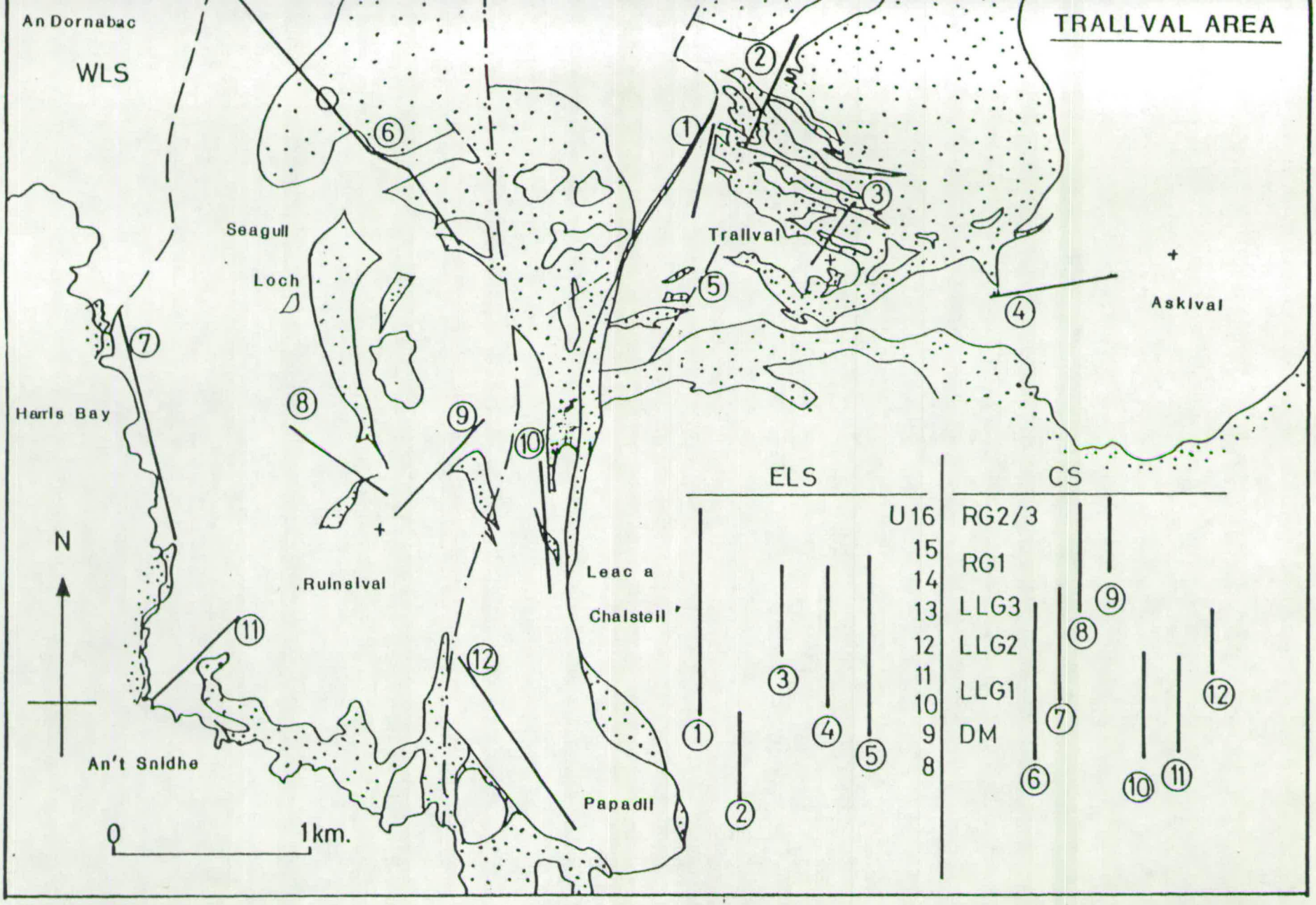

FIG. 5.1 Location of sampling traverses across the layered series and sections sampled by each. Gabbro intrusions are stippled. The numbered traverses are: 1 Upper W. Trallval (W. Tr.), 2 Lower W. Trallval (W. Tr.), 3 E. Trallval (E. Tr.), 4 Askival (Ask.), 5 S. Trallval (S. Tr.), 6 Seagull (Seag.), 7 Coastline (Coast.), 8 Ruinsival (Ruins.), 9 NE Ruinsival (NE Ruins.), 10 Leac a Chaisteil (LaC), 11 An't Sndhe, 12 Papadil (Pap.)

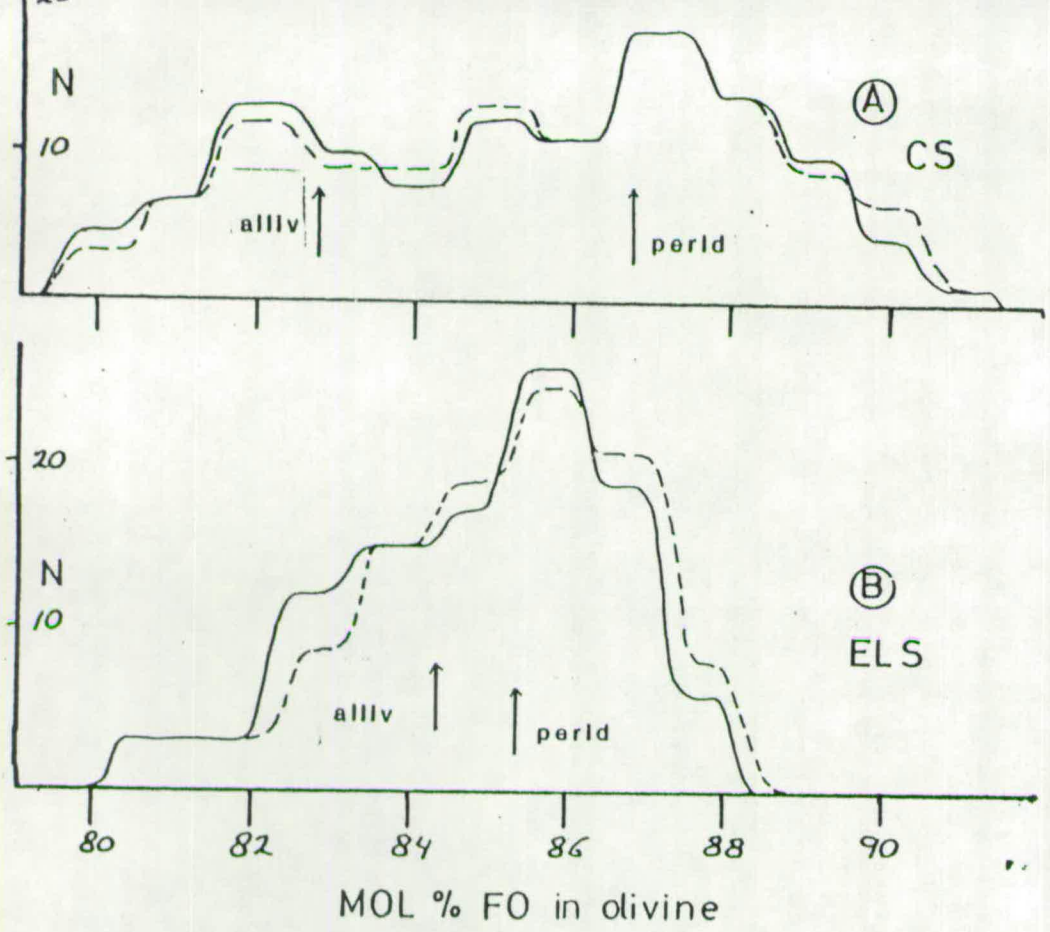

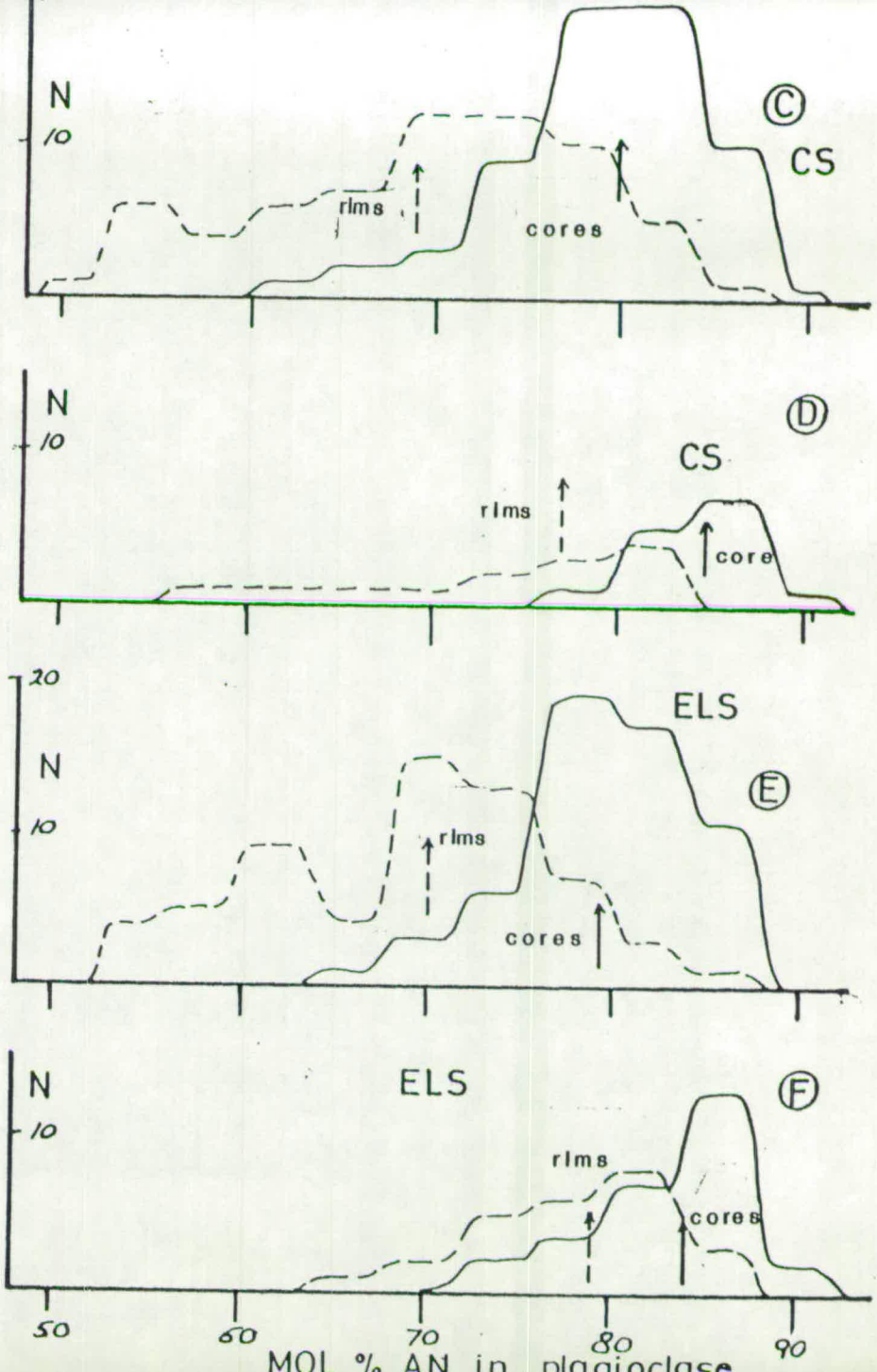

FIG. 5.2 Histograms for compositional ranges of minerals from the layered series:

A, B - Fo content of olivine in the CS, the ELS.

C to F - An content of plagioclase in peridotite and allivalite for the CS and the ELS.

The arrows give median values; solid lines are for core compositions and dashed lines for rim compositions of each phase.

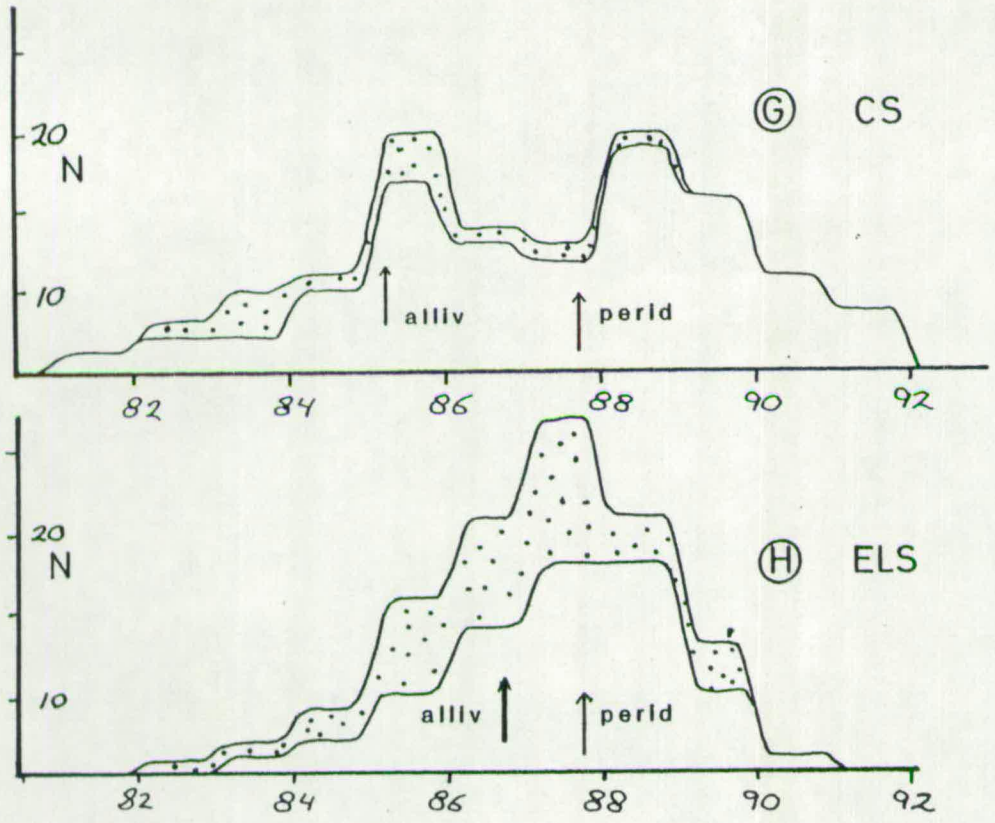

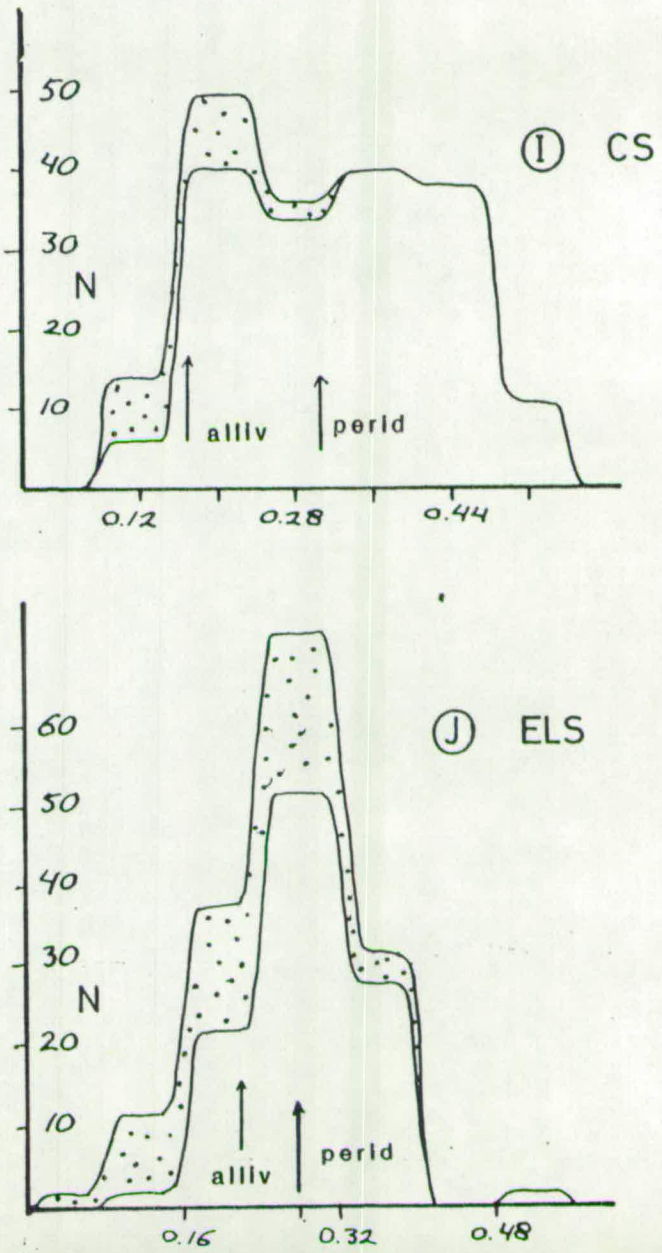

FIG. 5.2 (Ctd.) Histograms for mineral compositions.

G, H - Mg-number of pyroxene for the CS, the ELS.

I. J - Fraction of $MgCr_2O_4$ in chrome-spinel in the CS, the ELS.

Stippled areas represent phases counted in allivalite and unornamented areas those in peridotite.

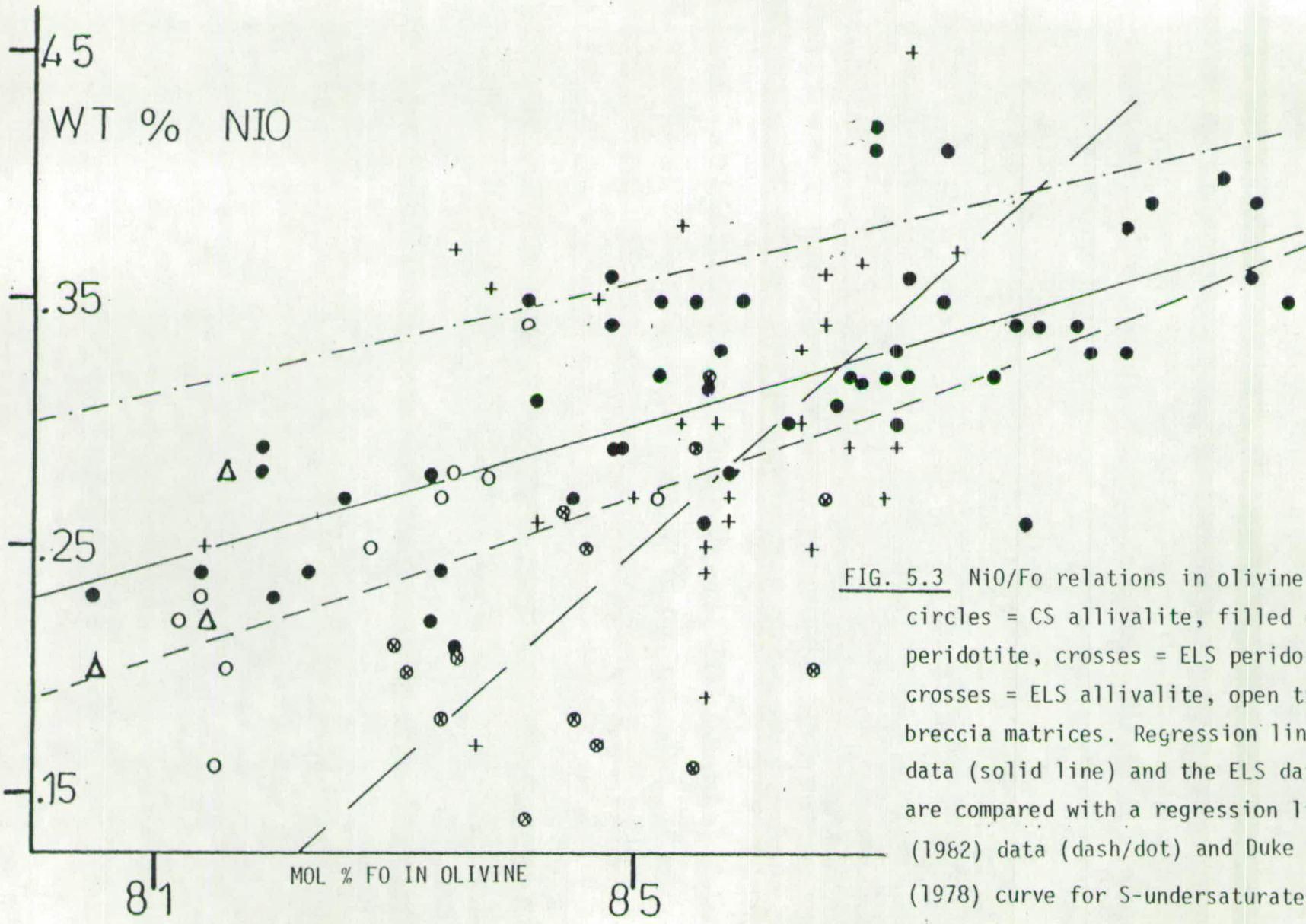

FIG. 5.3 NiO/Fo relations in olivine. Key: open circles = CS allivalite, filled circles = CS peridotite, crosses = ELS peridotite, circled crosses = ELS allivalite, open triangles = breccia matrices. Regression lines to the CS data (solid line) and the ELS data (long dashes) are compared with a regression line for McClurg's (1982) data (dash/dot) and Duke and Naldrett's (1978) curve for S-undersaturated magmas (short dashes).

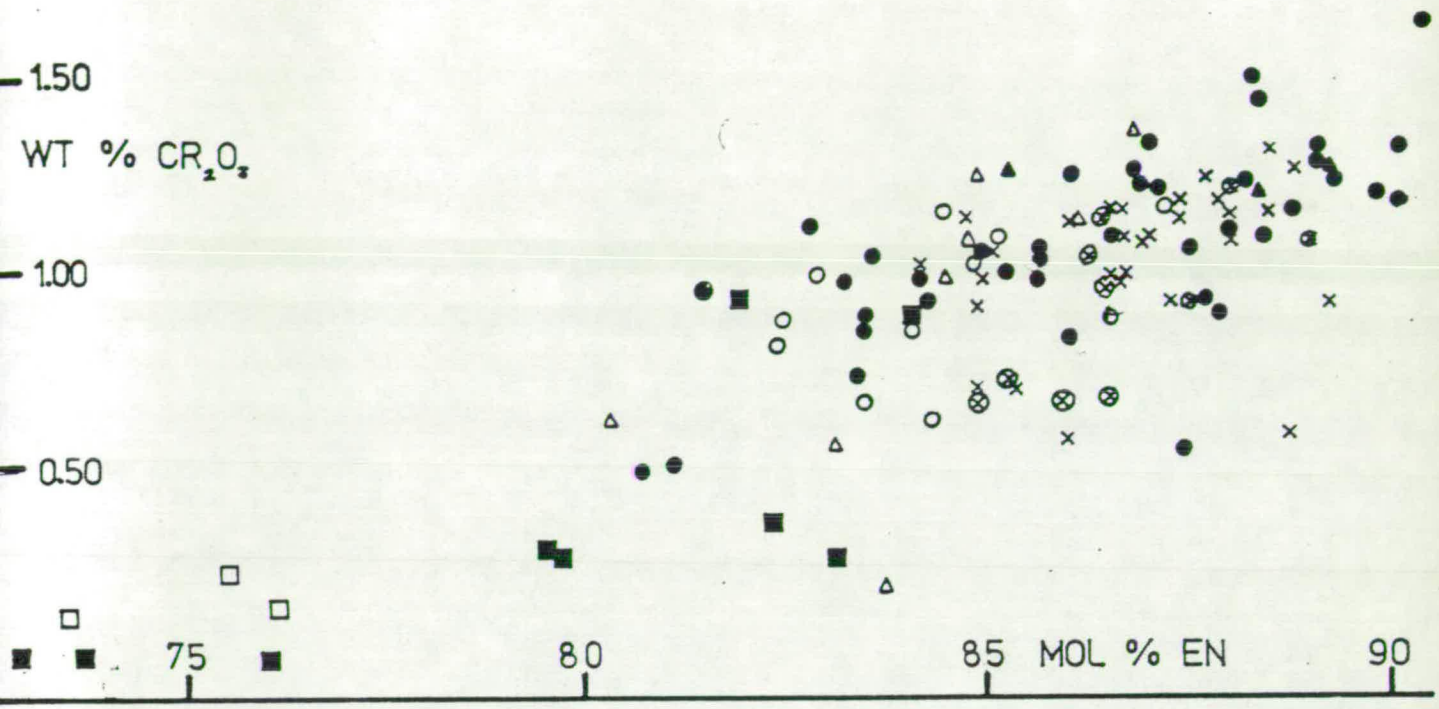

Fig. 5.4

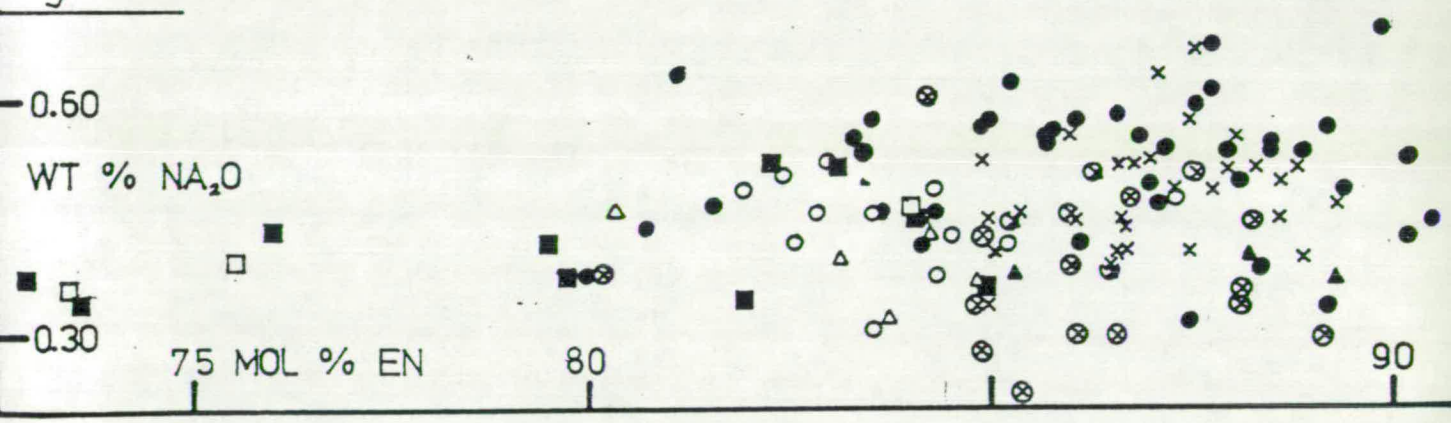

Fig. 5.5

FIG 5.4 Cr_2O_3 content of pyroxene. Symbols as in fig. 5.3; in addition, filled triangles = ultrabasic plugs, open squares = dykes, filled squares = gabbros.

FIG 5.5 Na_2O content of pyroxene. Symbols as in fig. 5.4.

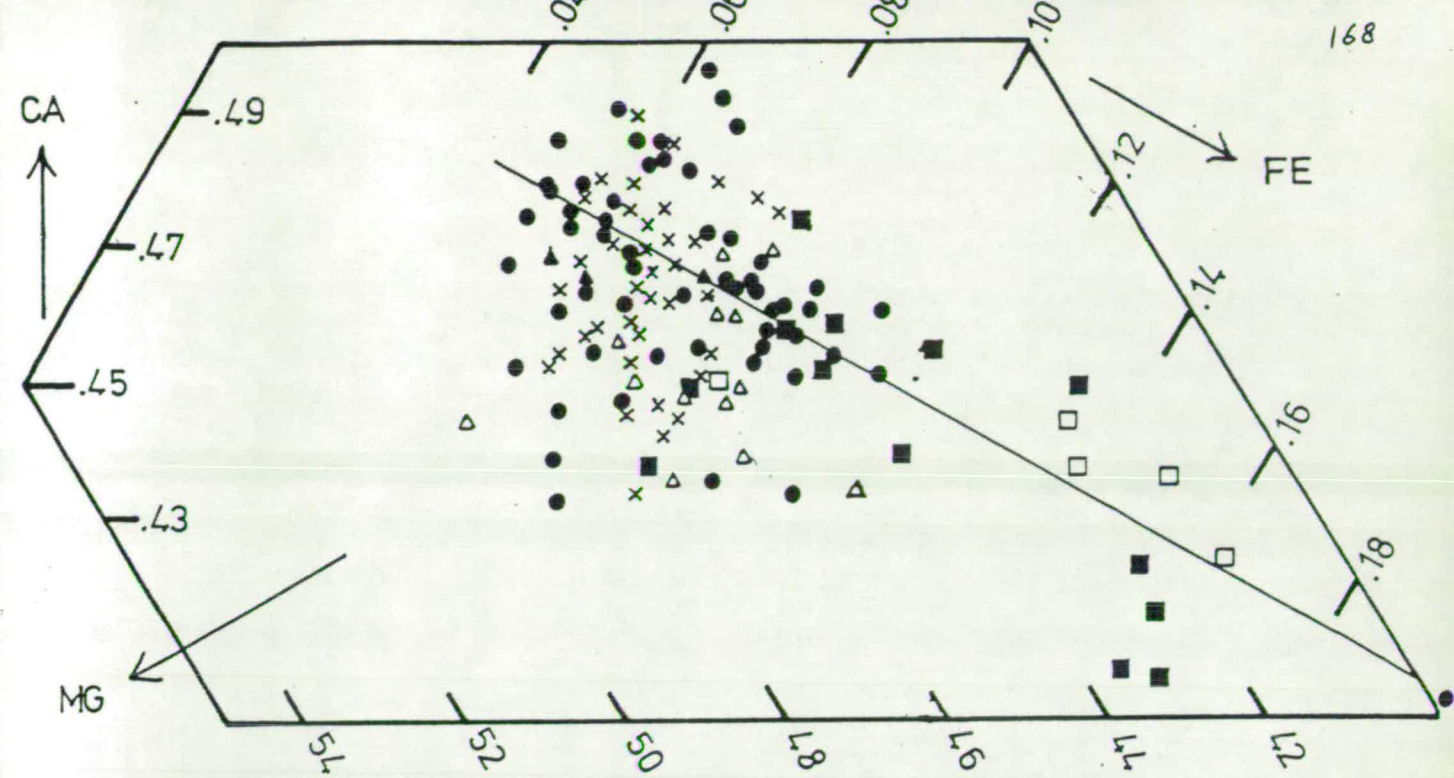

Fig. 5.6. Pyroxene compositions plotted on the Ca:Mg:Fe surface. The
The solid line is a regression line for the gabbro and dyke data

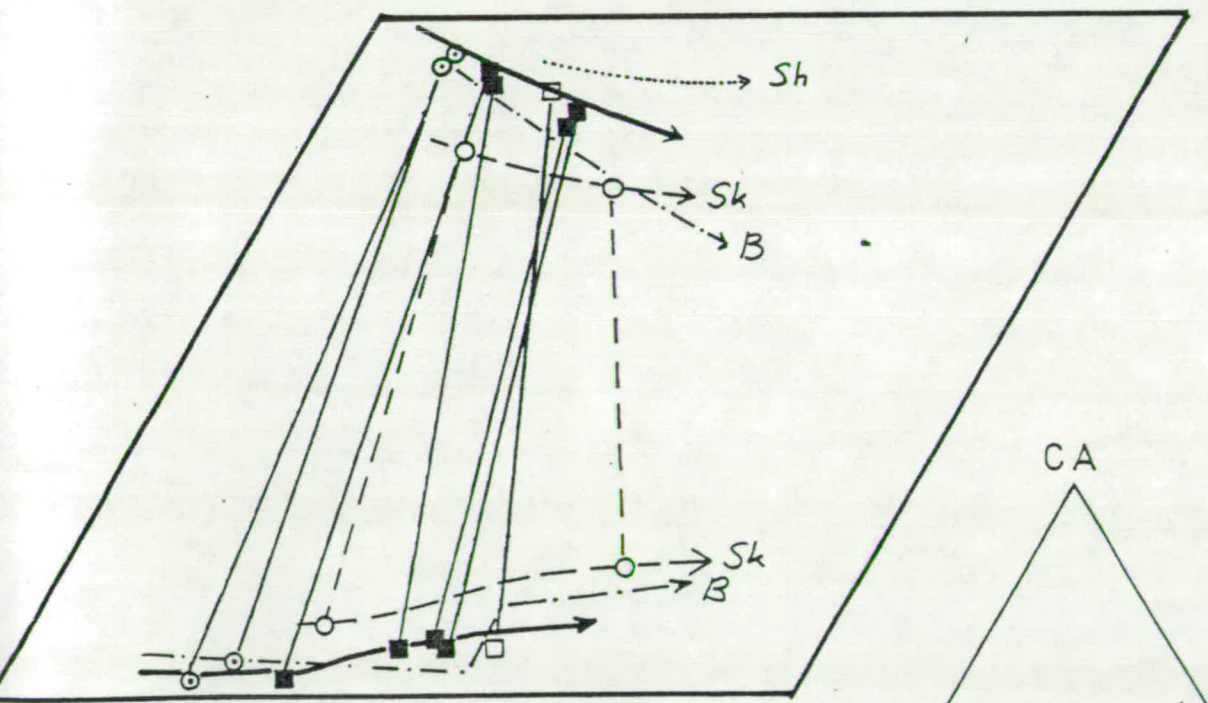

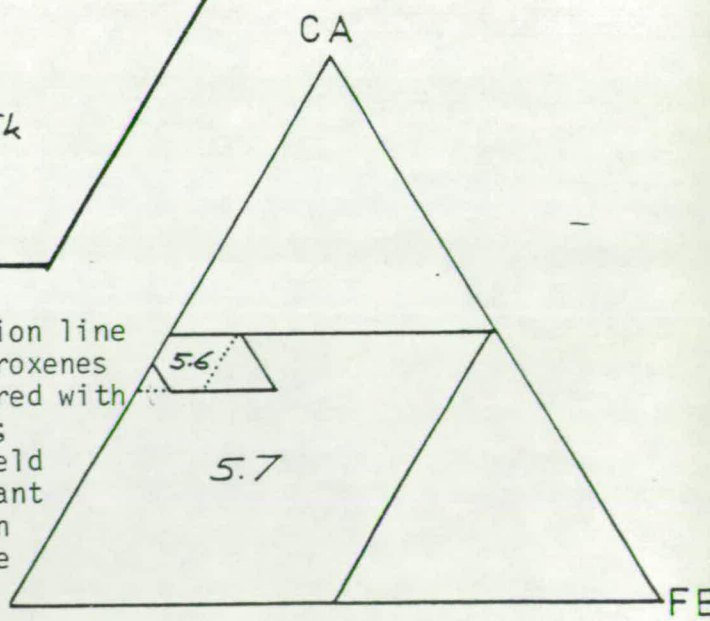

Fig. 5.7 Evolution of Ca-rich (regression line from fig. 5.6) and Ca-poor pyroxenes from Rhum (thick lines) compared with that from the Skaergaard (Sk.; Deer et al., 1966), the Bushveld (B; Atkins, 1969) and the Shiant Isles (Sh.; Gibb, 1973). Thin solid lines connect 2-pyroxene assemblages from inclusions in spinel (dotted circles, gabbros (filled squares) and the microdiorite hybrid dyke (chapter 6, open squares).

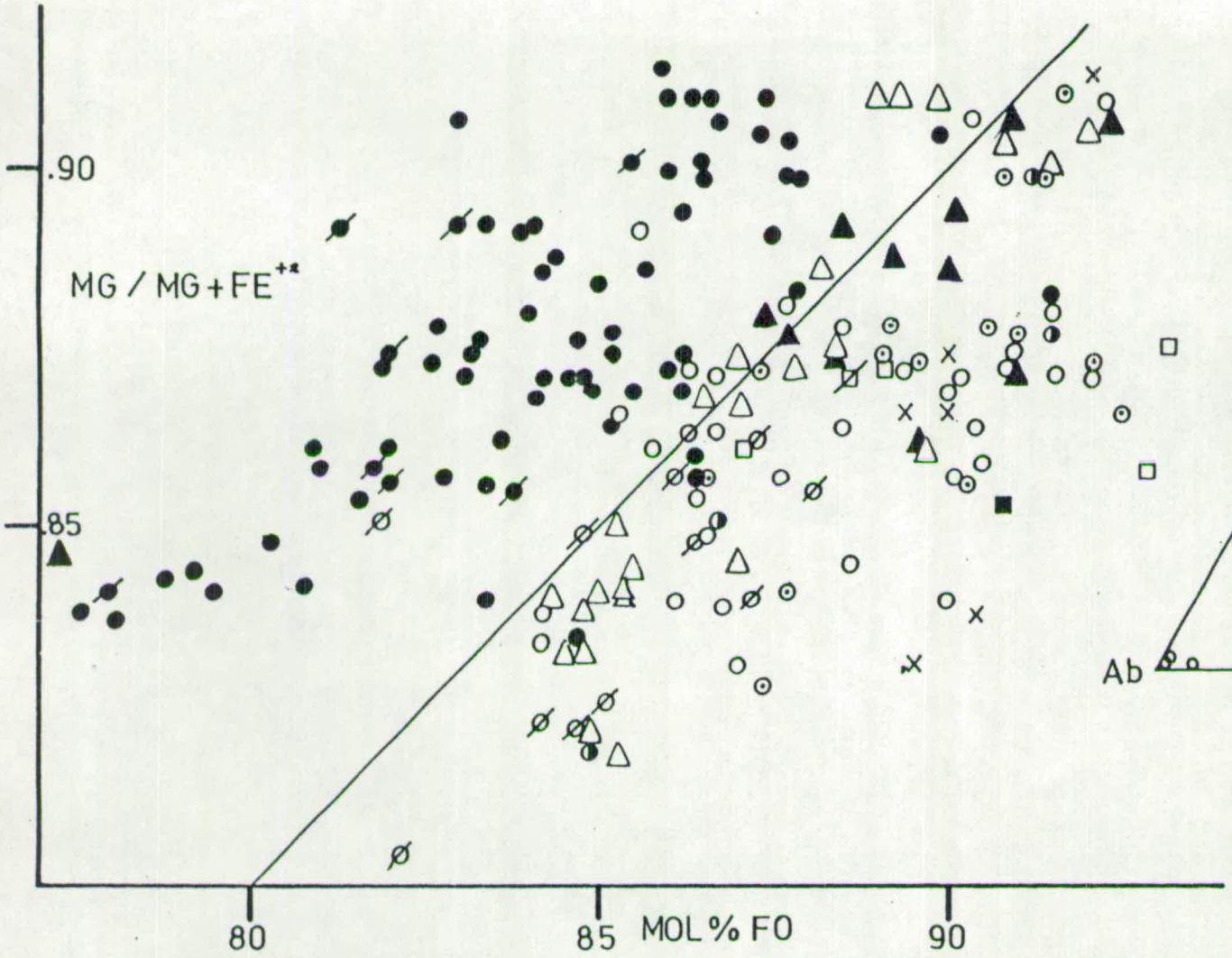

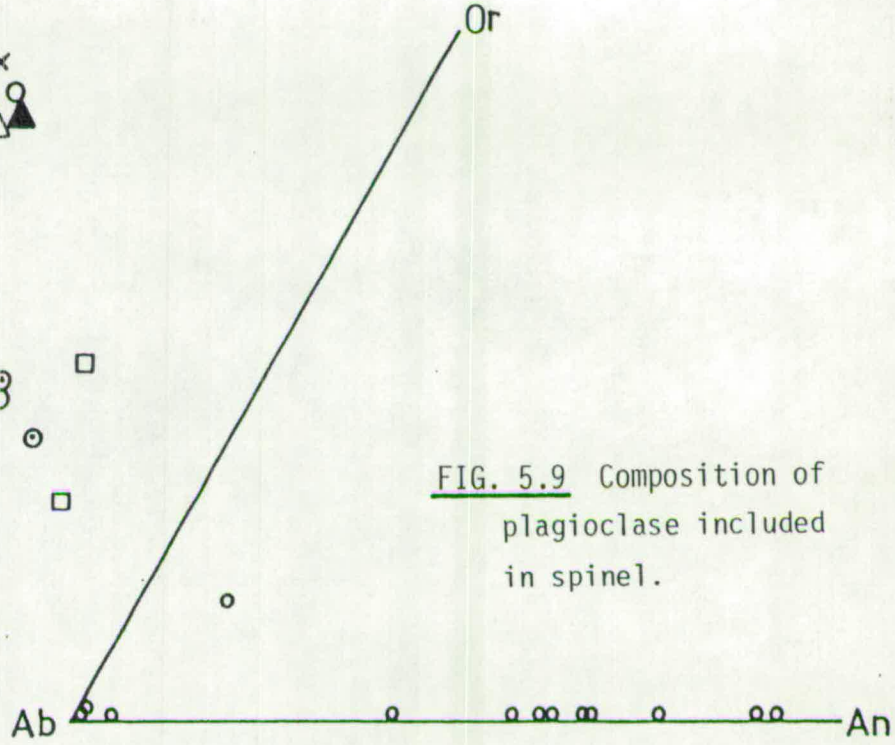

FIG. 5.9 Composition of plagioclase included in spinel.

FIG. 5.8 Mg-number of inclusion phase vs. that of olivine in host-rock. Key: filled circles = kaersutite, open circles = phlogopite, dotted circles = Na-phlogopite, half-filled circles = Na/K-phlogopite, open triangles = enstatite, filled triangles = diopside, open squares = tremolite-actinolite, filled squares = hornblende, crosses = olivine; symbols with superimposed oblique indicate intercumulus phases.

FIG. 5.10 Wt % TiO_2 vs. Mg-number of silicate phases in spinel. Filled circles = kaersutite, open circles = phlogopite, dotted circles = Na-phlogopite, half-filled circles = Na/K-phlogopite.

FIG. 5.11 Wt % K_2O vs. Mg-number for kaersutite in inclusion spinel. Filled circles = CS, open circles = ELS., symbols with a superimposed oblique indicate intercumulus phases.

FIG. 5.12 Al_2O_3 content of enstatites included in spinels. High-aluminium contents (2-3 % or more) are typical of enstatite from granulite-facies gneisses (Deer et al., 1966).

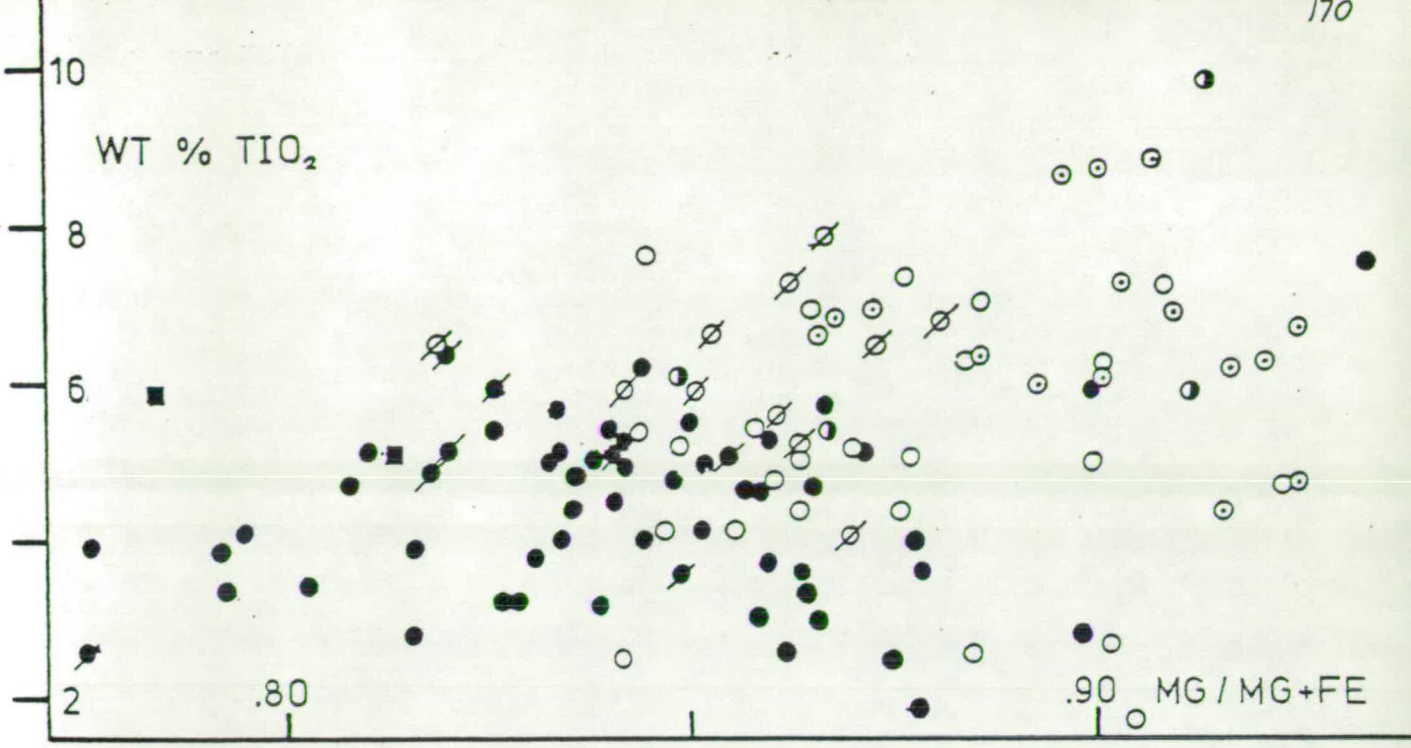

Fig 5.10

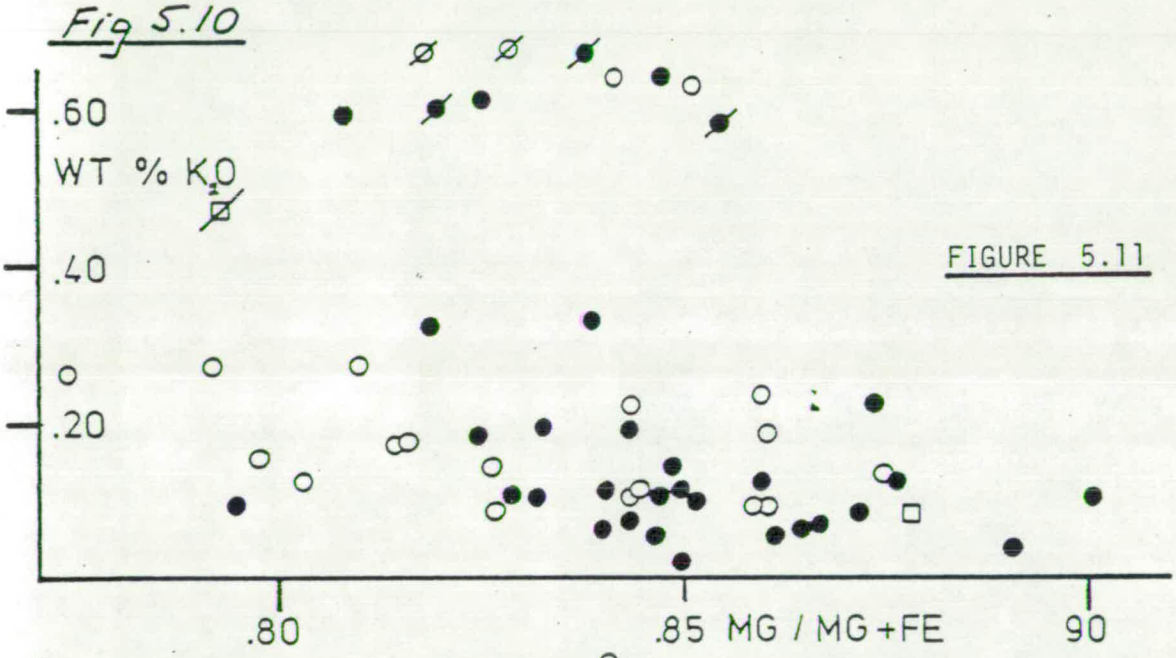

FIGURE 5.11

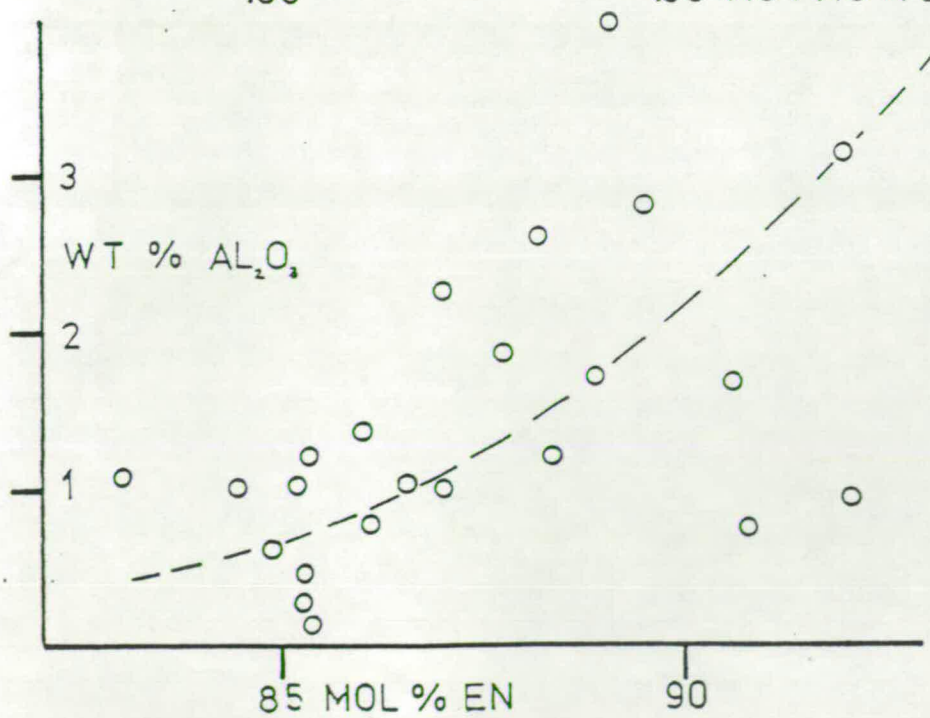

FIGURE 5.12

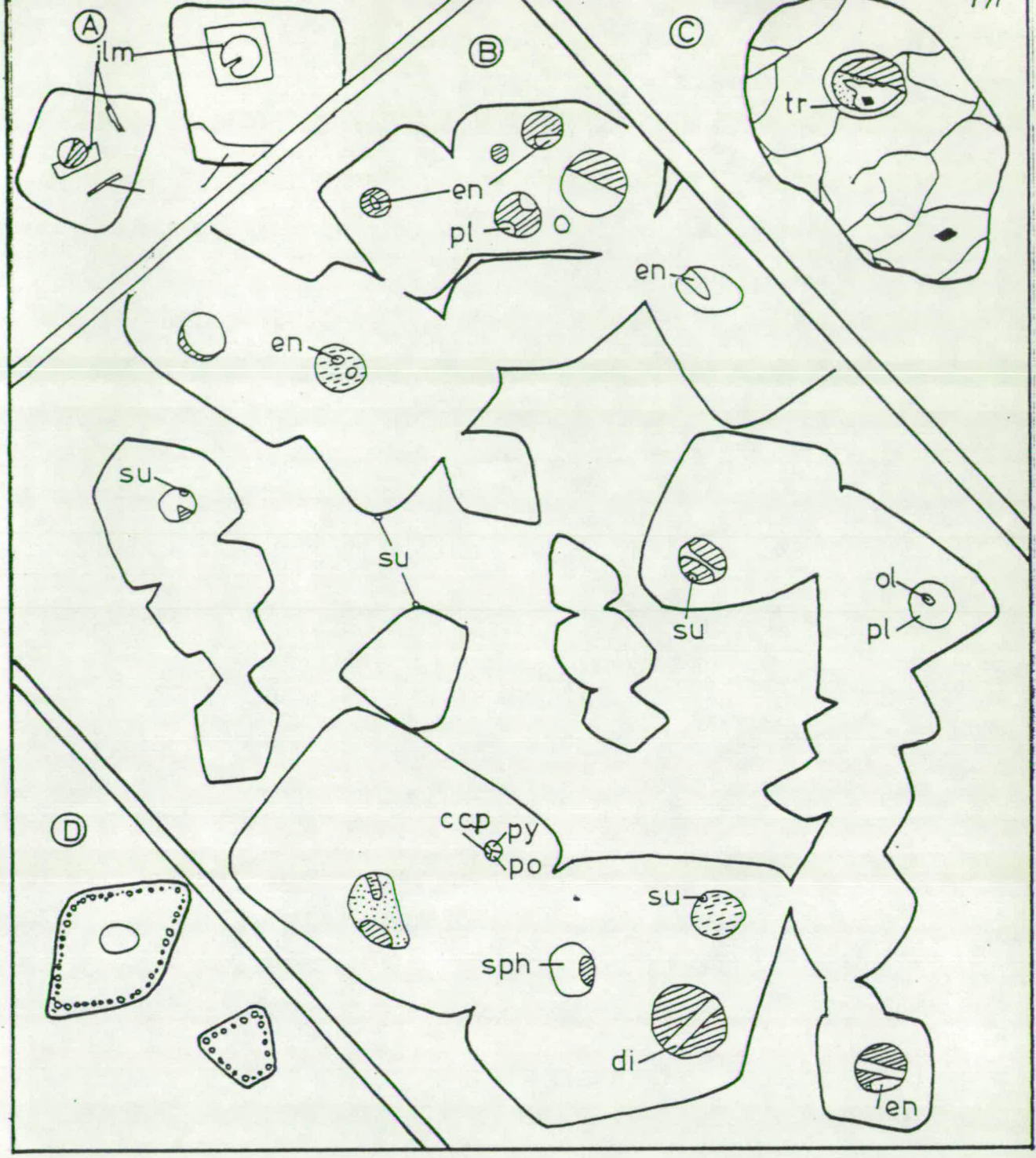

FIG. 5.13 Textural relations of silicate, oxide and sulphide phases included in spinel or olivine: A = spinels in ELS allivalite, B = spinels in a CS chromitite, C = inclusions in olivine from the ELS, D = type 3 spinel inclusions, disseminated in CS. Key: phlogopite inclusions are hatched, those of kaersutite unornamented, chlorite dashed, calcite stippled and other phases are identified as follows: ilm = ilmenite, su = sulphide, en = enstatite, pl = plagioclase, ol = olivine, tr = tremolite, di = diopside, and sph = sphene.

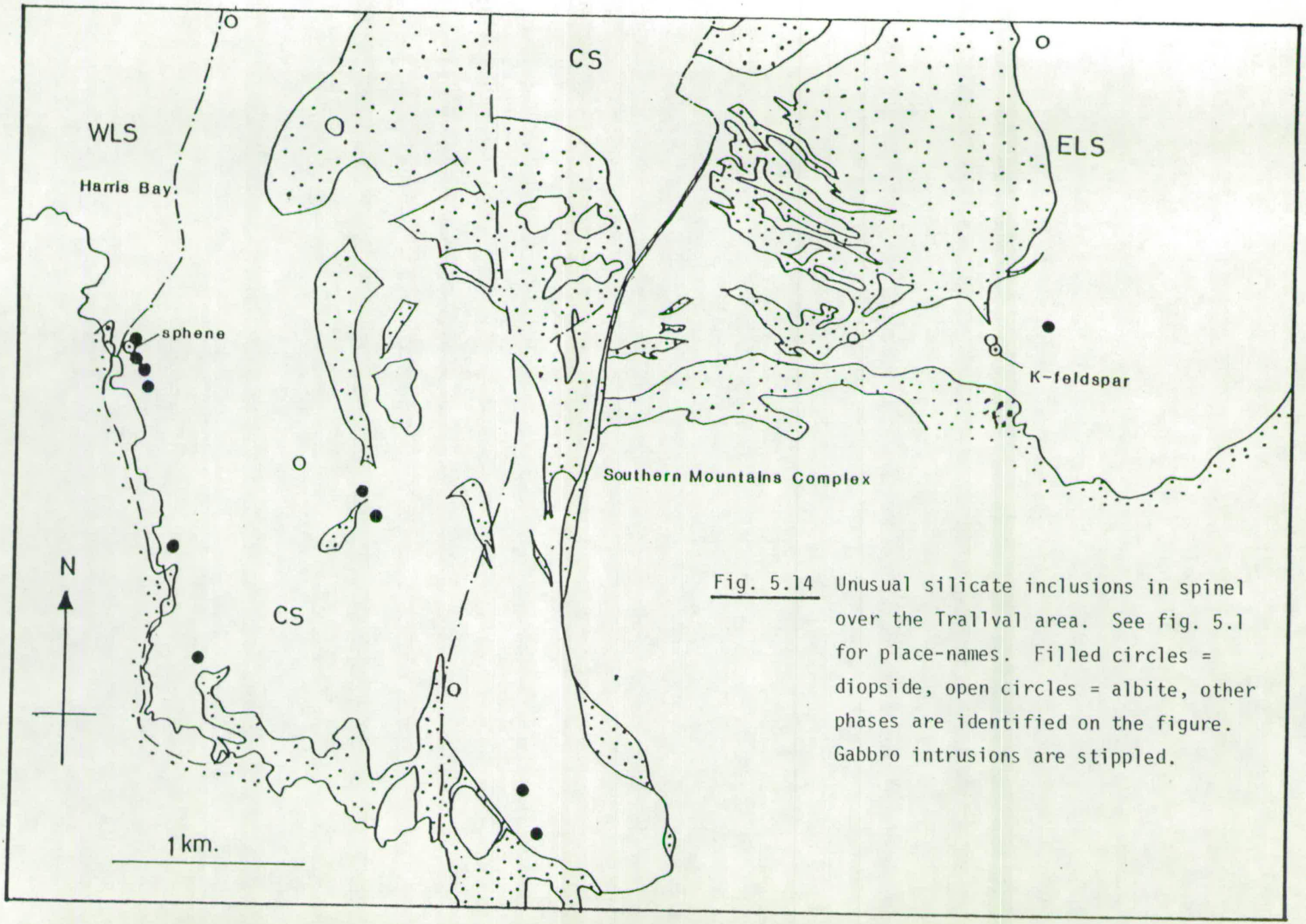

Fig. 5.14 Unusual silicate inclusions in spinel over the Trallval area. See fig. 5.1 for place-names. Filled circles = diopside, open circles = albite, other phases are identified on the figure. Gabbro intrusions are stippled.

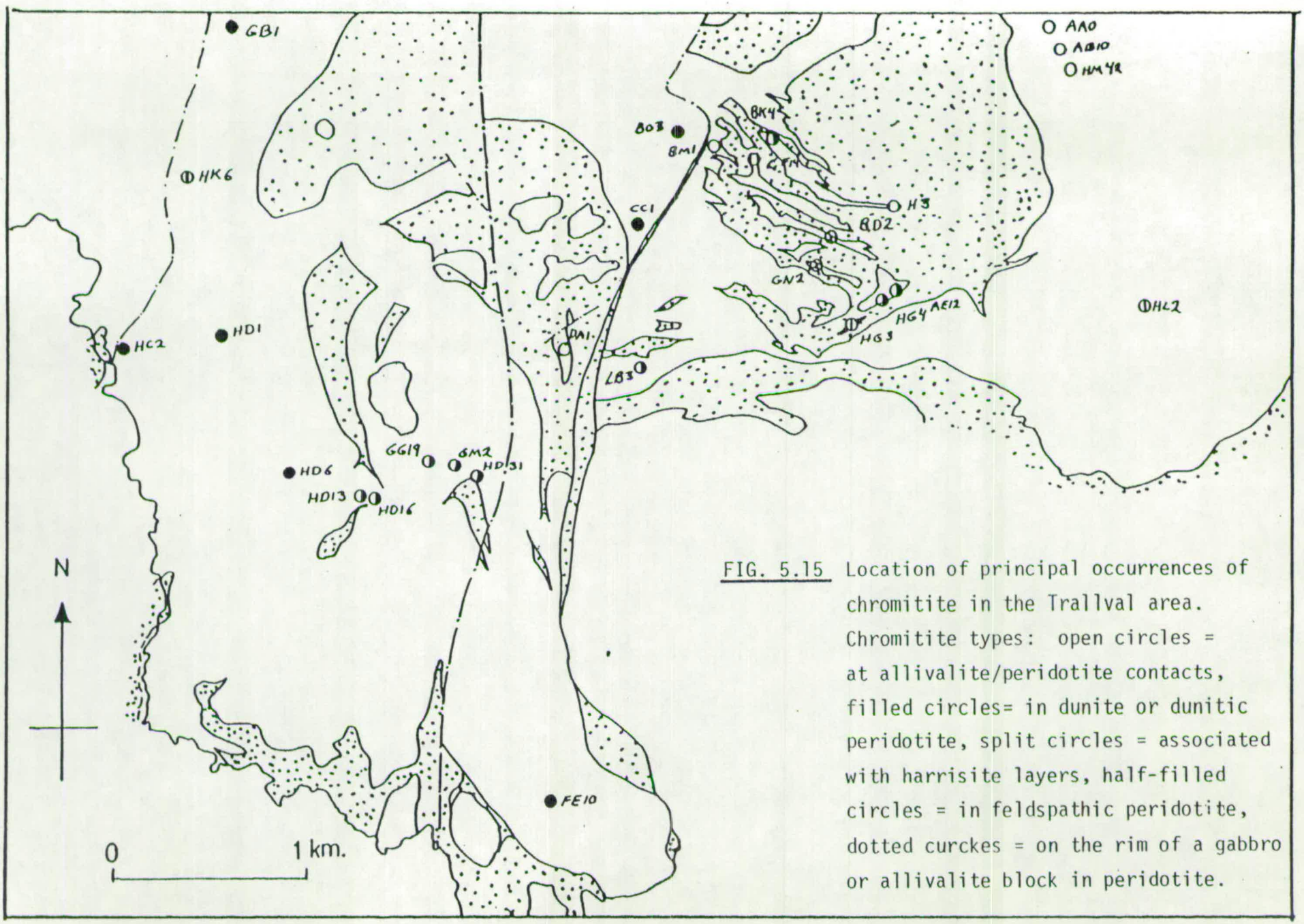

FIG. 5.15 Location of principal occurrences of chromitite in the Trallval area. Chromitite types: open circles = at allivalite/peridotite contacts, filled circles= in dunite or dunitic peridotite, split circles = associated with harrisite layers, half-filled circles = in feldspathic peridotite, dotted curckes = on the rim of a gabbro or allivalite block in peridotite.

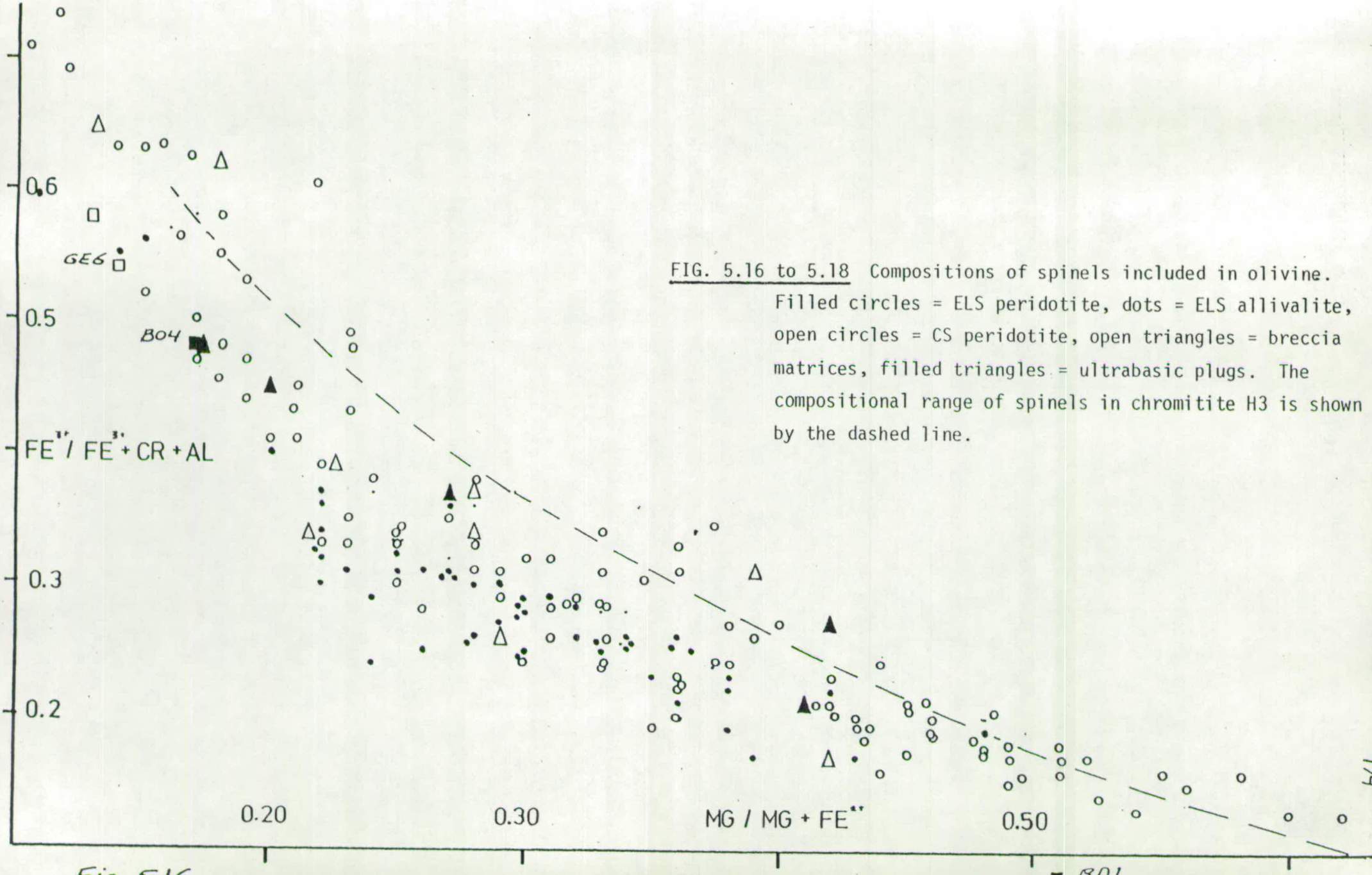

FIG. 5.16 to 5.18 Compositions of spinels included in olivine. Filled circles = ELS peridotite, dots = ELS allivalite, open circles = CS peridotite, open triangles = breccia matrices, filled triangles = ultrabasic plugs. The compositional range of spinels in chromitite H3 is shown by the dashed line.

Fig. 5.16

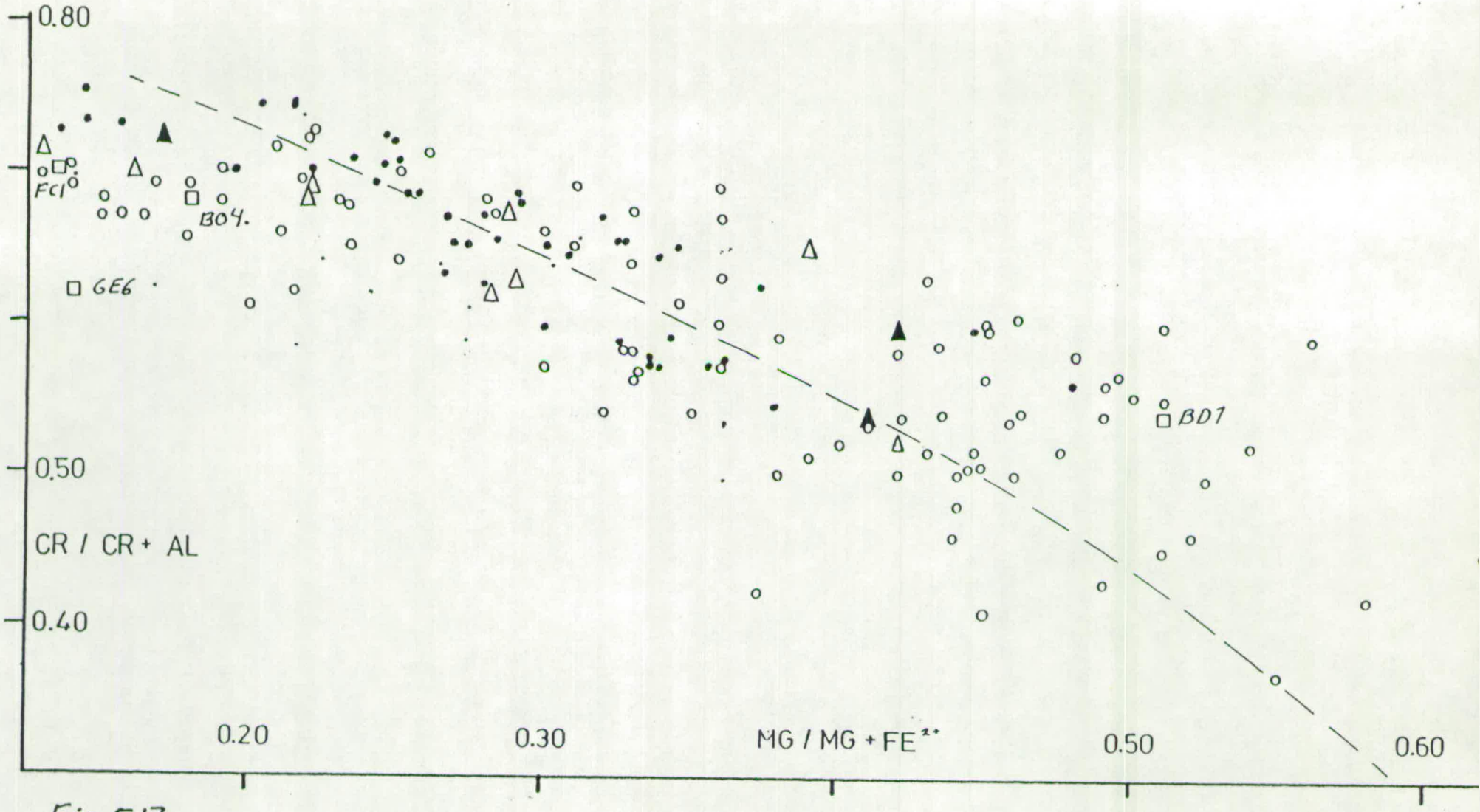

Fig 5.17

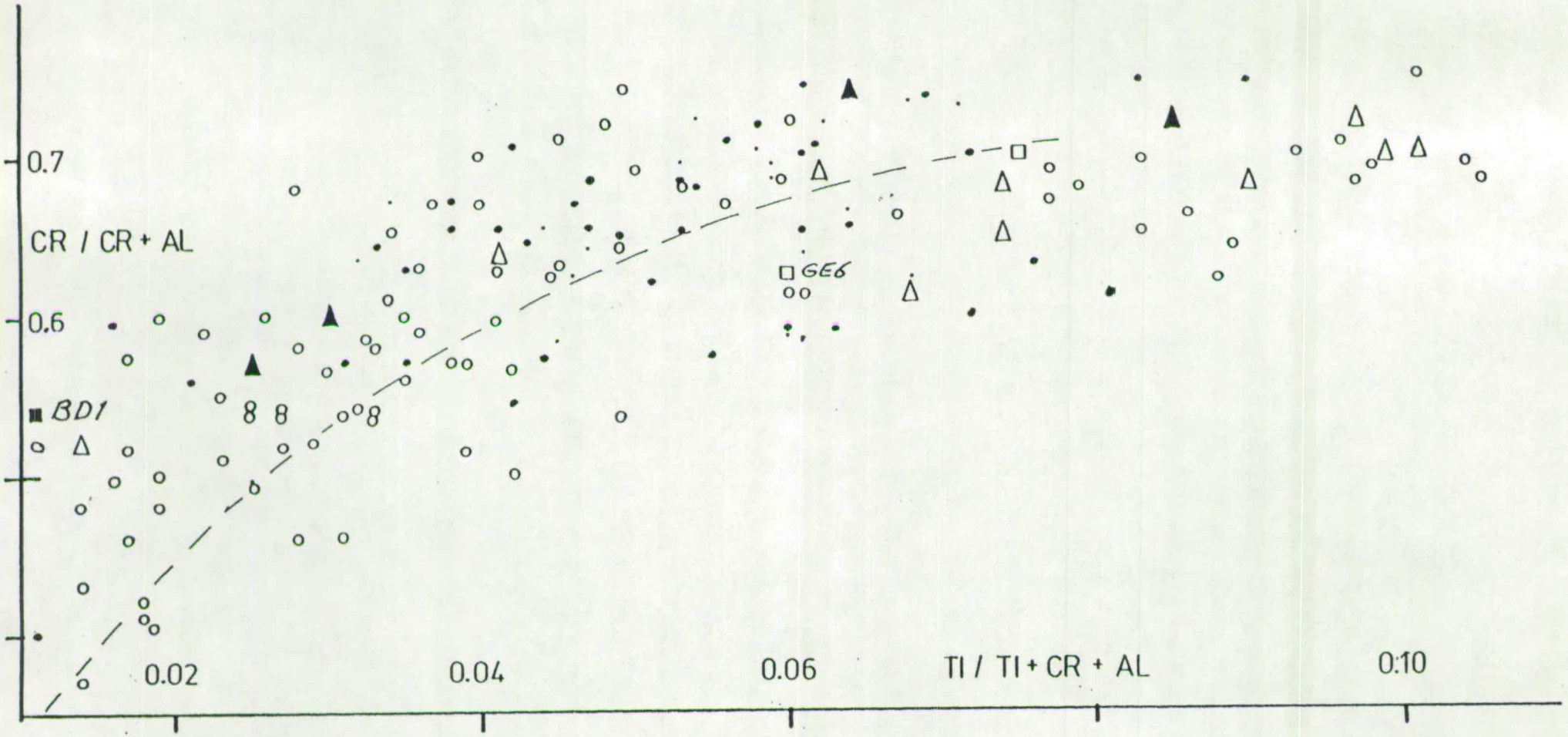

Fig. 5.18

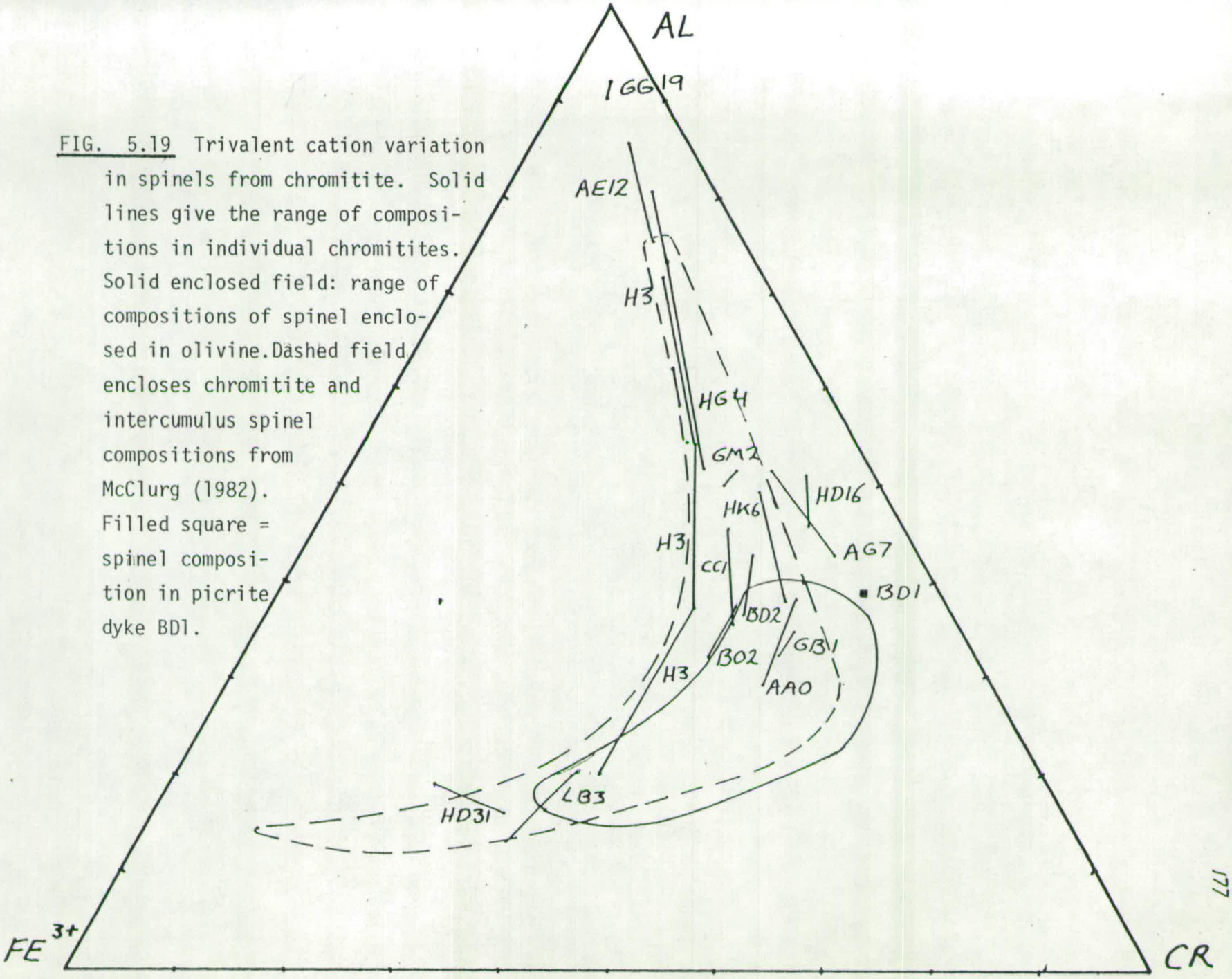

FIG. 5.19 Trivalent cation variation in spinels from chromitite. Solid lines give the range of compositions in individual chromitites. Solid enclosed field: range of compositions of spinel enclosed in olivine. Dashed field encloses chromitite and intercumulus spinel compositions from McClurg (1982). Filled square = spinel composition in picrite dyke BD1.

FIG. 5.21 Cryptic variation in the ELS, over the W. Trallval traverse. Left-hand column gives modes of analysed samples: spinel (black), pyroxene (stippled) leave an unornamented area which consists of olivine to the left and plagioclase to the right of the line. The variation traces are, from left to right, sulphide abundance, maximum spinel size, maximum olivine size, Fo content of olivine, Wt % NiO in olivine, the range in An content in plagioclase, the Mg-number of pyroxene and the Wt % Cr_2O_3 in pyroxene.

FIG. 5.22 (next page) Cryptic variation over Units 13 and 14 in 3 different sections: 1 W. Trallval, 2 E. Trallval, 3 Askival. The datum level for the alignment of the variation traces is the U12 / U13 contact; the solid trace is for the W.Trallval section, the dashed trace for the E. Trallval section and the crosses for the Askival section. For further explanation of the diagram, see the caption for fig 5.21.

FIG. 5.23 (2 pages on) Lateral cryptic variation in the ELS, in Wt % NiO in olivine (reference line for all sections: 0.40 Wt % NiO). Barkeval data are from McClurg (1982) and the Hallival data from Dunham and Wadsworth (1978).

FIG 5.24 (3 pages on) Lateral cryptic variation of the Fo content of olivine in the ELS (reference for all sections: Fo 87.5). Crosses indicate chromitite laminae. Data for Barkeval from McClurg (1982) and for Hallival from Dunham and Wadsworth (1978) and Palacsz (pers. comm.).

FIGURE 5.21

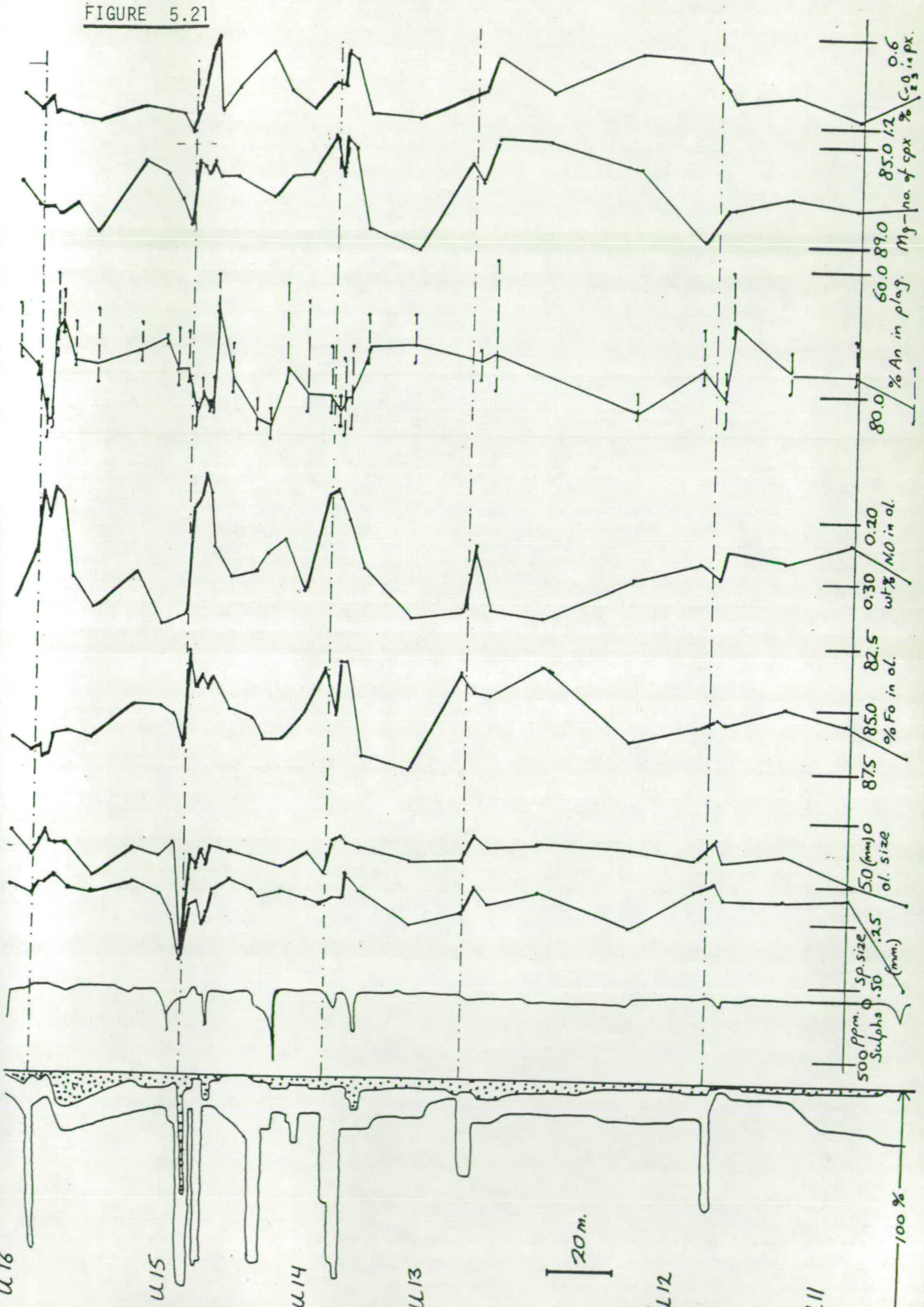
U16
U15
U14
U13
U12
U11
20m.
100 %
500 ppm. Sulphs
.50 Φ sp. size .25 (mm.)
5.0 (mm) ol. size
87.5 85.0 % Fo in ol.
0.30 0.20 wt% NiO in ol.
82.5
60.0 80.0 % An in plag.
89.0 85.0 Mg-no. of cpx
1.2 0.6 % Cr2O3 in px.

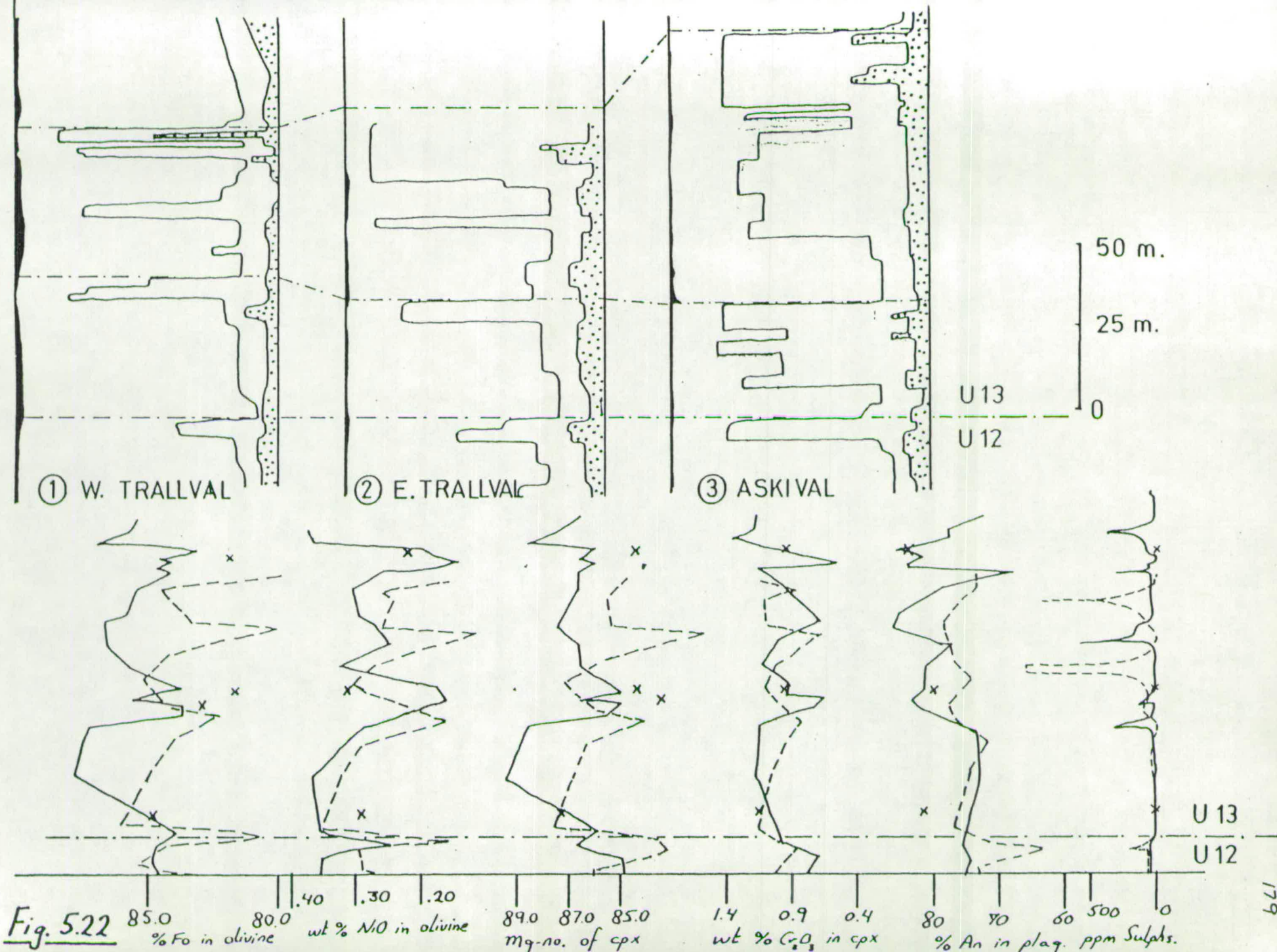
50 m.
25 m.
0
U13
U12
① W. TRALLVAL
② E. TRALLVAL
③ ASKIVAL
U13
U12
85.0
80.0
% Fo in olivine
.40
.30
.20
wt % NiO in olivine
89.0
87.0
85.0
mg-no. of cpx
1.4
0.9
0.4
wt % Cr2O3 in cpx
80
70
60
500
0
% An in plag.
ppm Sulphs.

Fig. 5.22

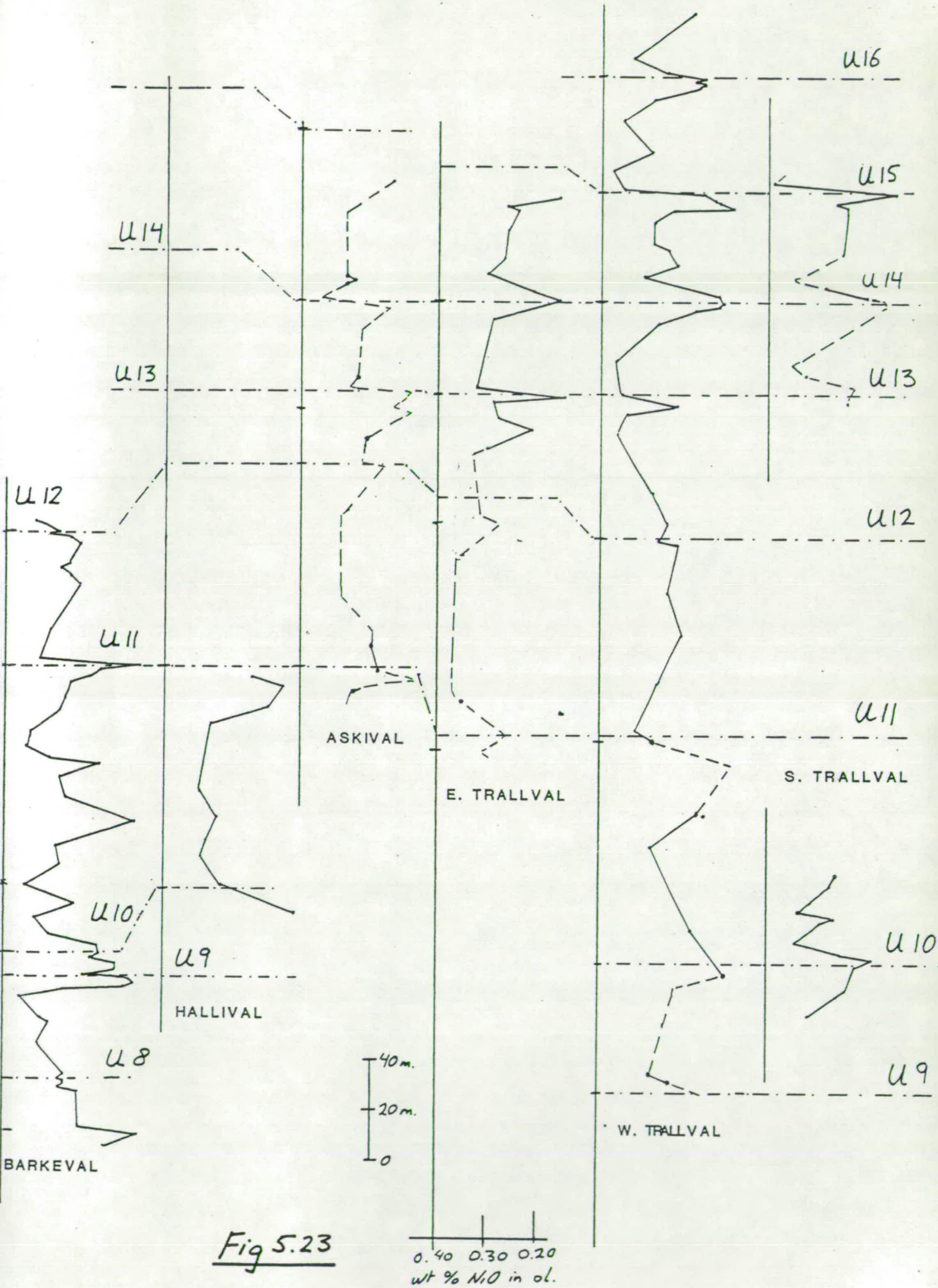
U16
U15
U14
U14
U13
U13
U12
U12
U11
U11
U10
U10
U9
U9
U8
ASKIVAL
E. TRALLVAL
S. TRALLVAL
HALLIVAL
W. TRALLVAL
BARKEVAL
40m.
20m.
0
0.40 0.30 0.20
wt % NiO in ol.

Fig 5.23

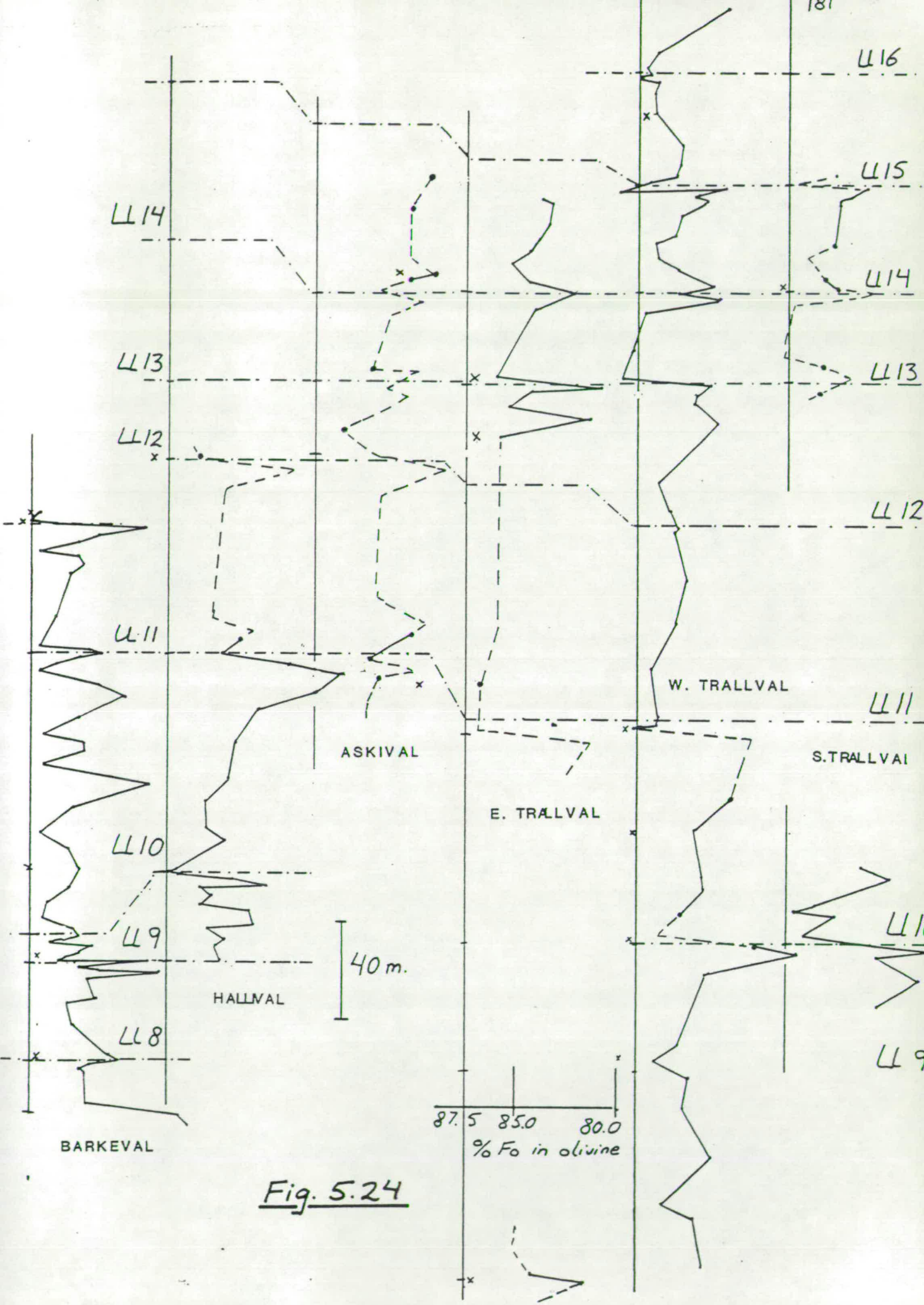
181
LL16
LL15
LL14
LL14
LL13
LL13
LL12
LL12
LL11
LL11
W. TRALLVAL
S.TRALLVAL
ASKIVAL
E. TRALLVAL
LL10
LL9
40 m.
HALLVAL
LL8
BARKEVAL
87.5 85.0 80.0
% Fo in olivine

Fig. 5.24

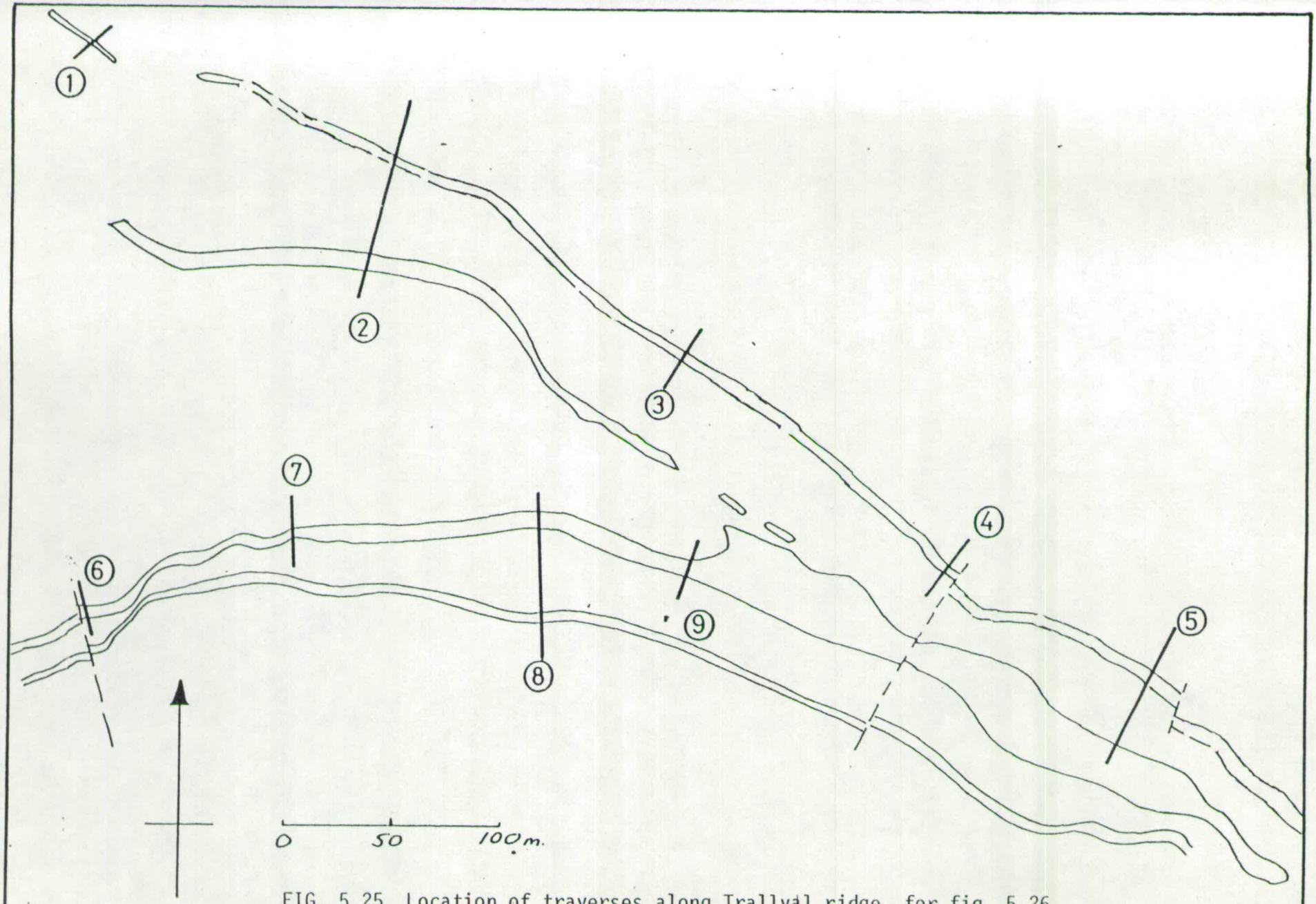

FIG. 5.25 Location of traverses along Trallvål ridge, for fig. 5.26.

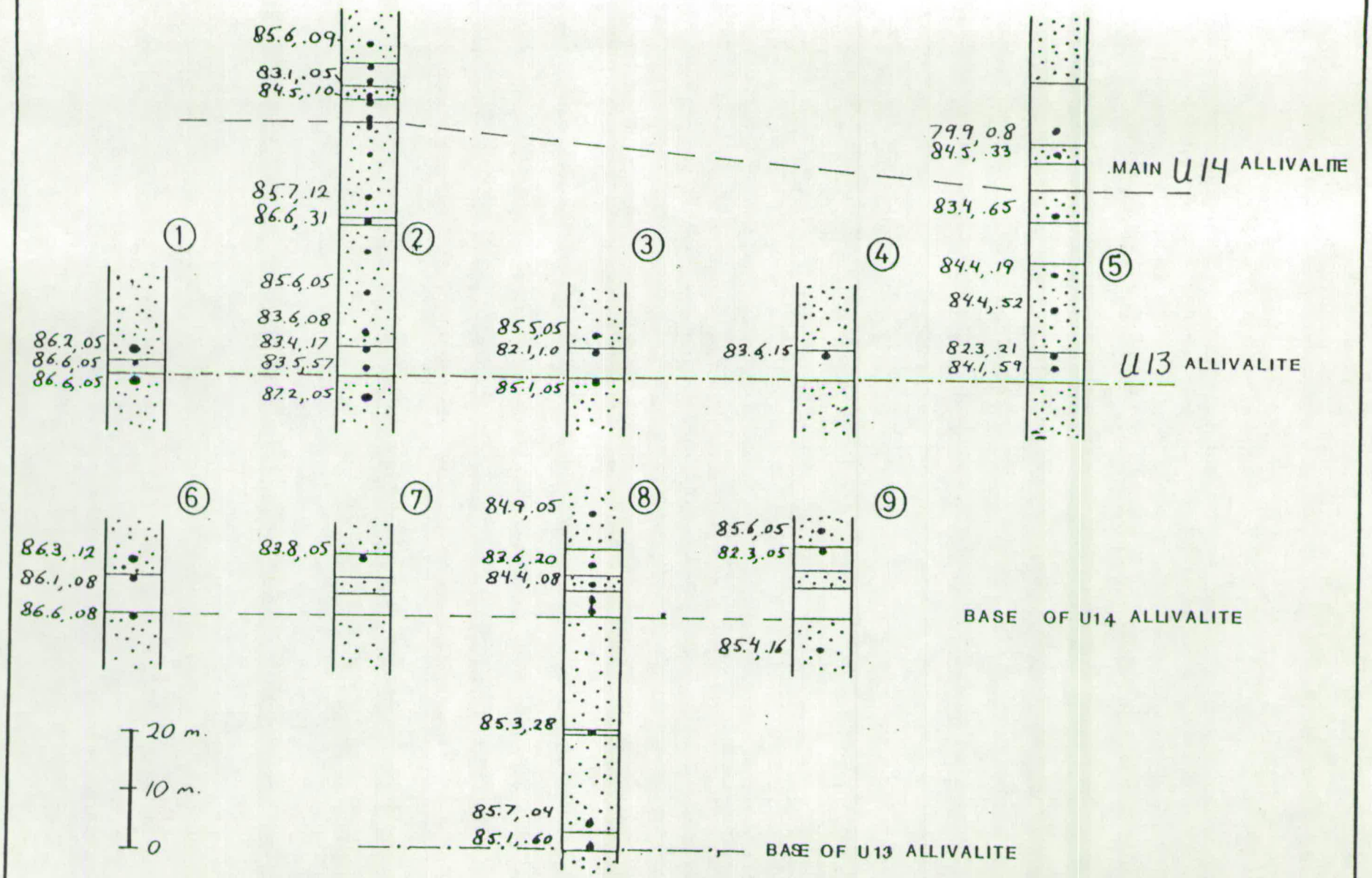

FIG. 5.26 Lateral variation of mole % Fo in olivine along Trallval ridge for the sections shown in fig. 5.25 (the second figure is the standard deviation for the analyses).

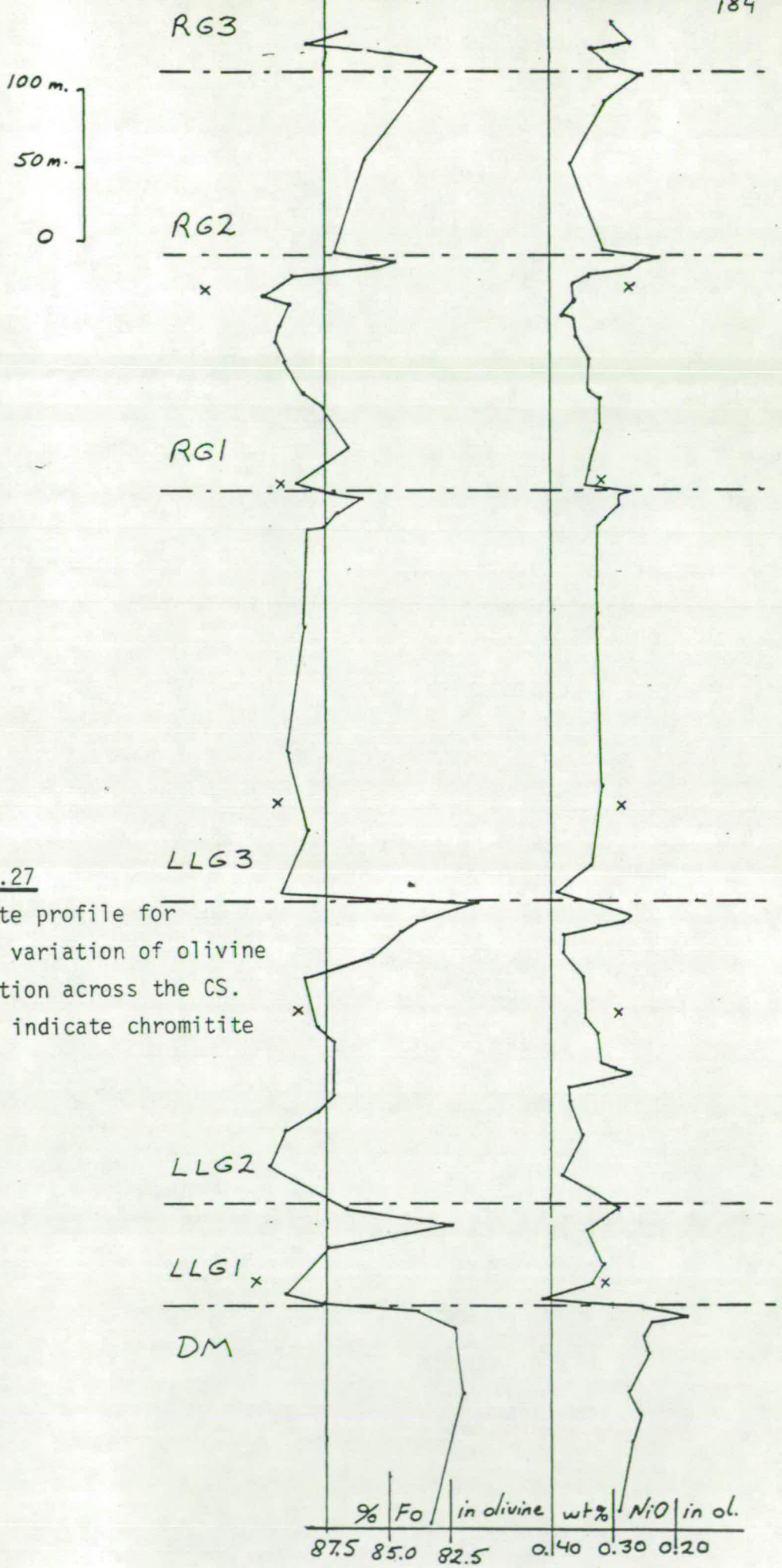

FIG. 5.27

Composite profile for cryptic variation of olivine composition across the CS. Crosses indicate chromitite layers.

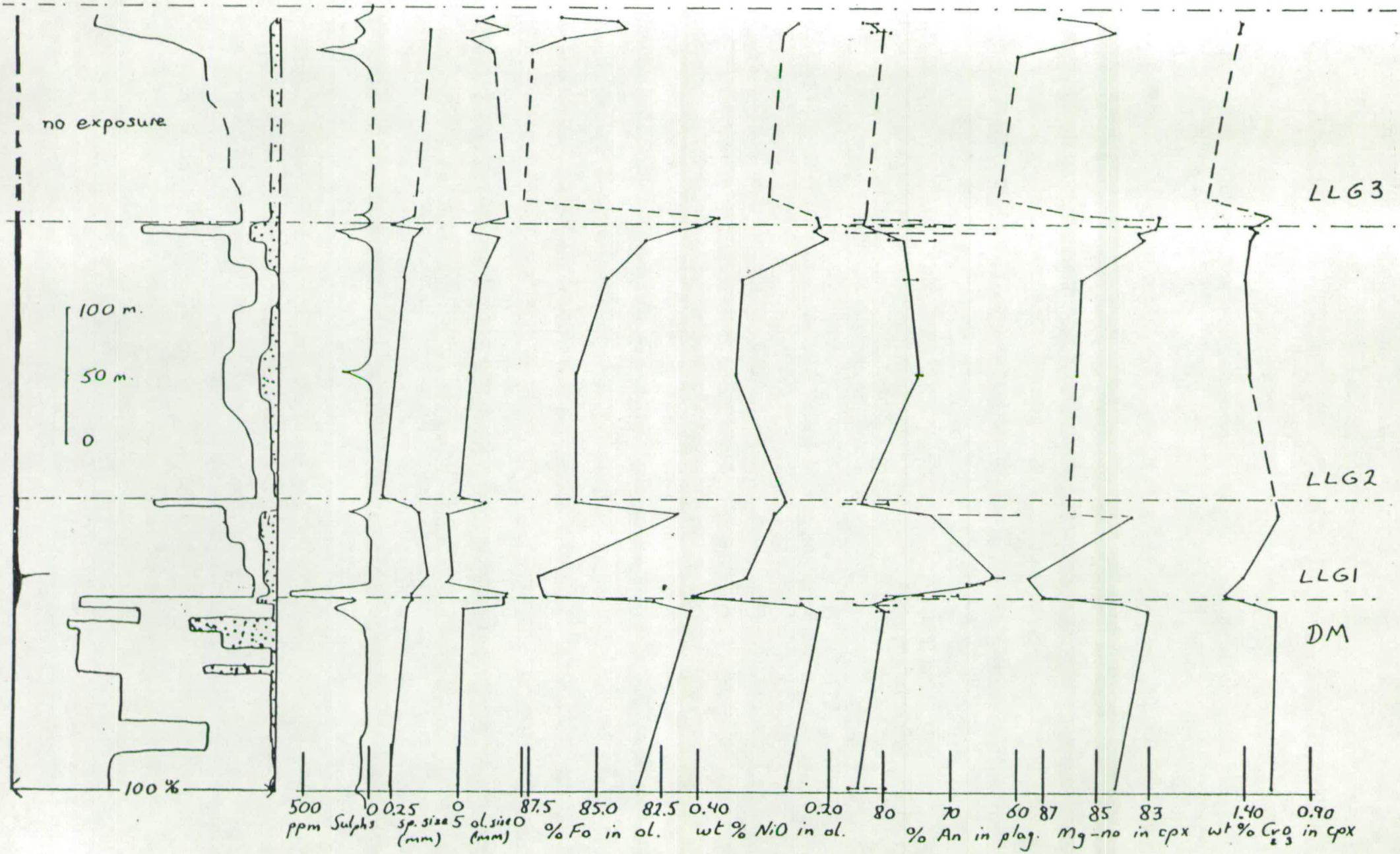

FIG. 5.28 Cryptic variation along the Seagull traverse through the CS. For diagram explanation, see fig. 5.21

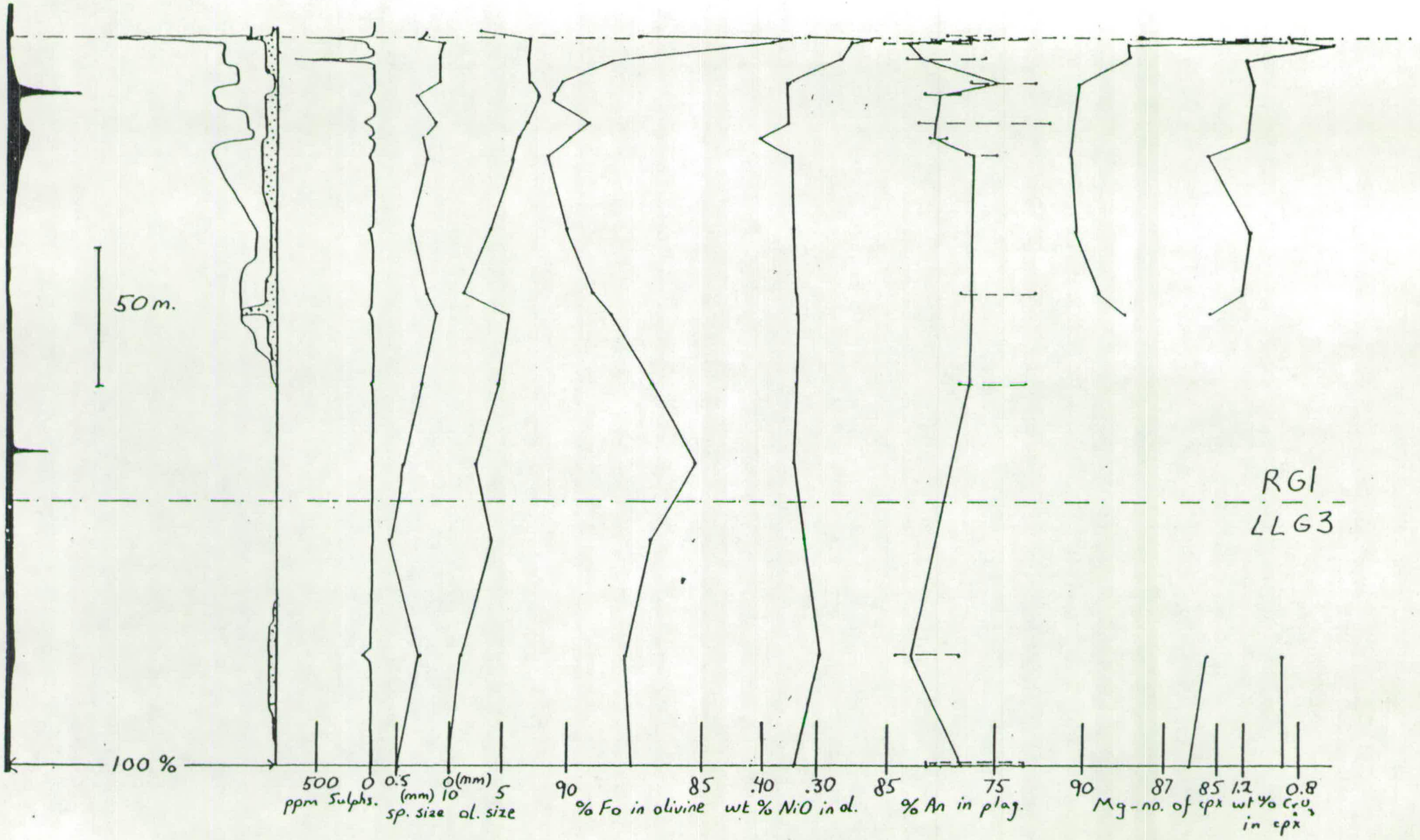

FIG. 5.29 Cryptic variation along the Ruinsival traverse. See fig. 5.21 for an explanation of the diagram.

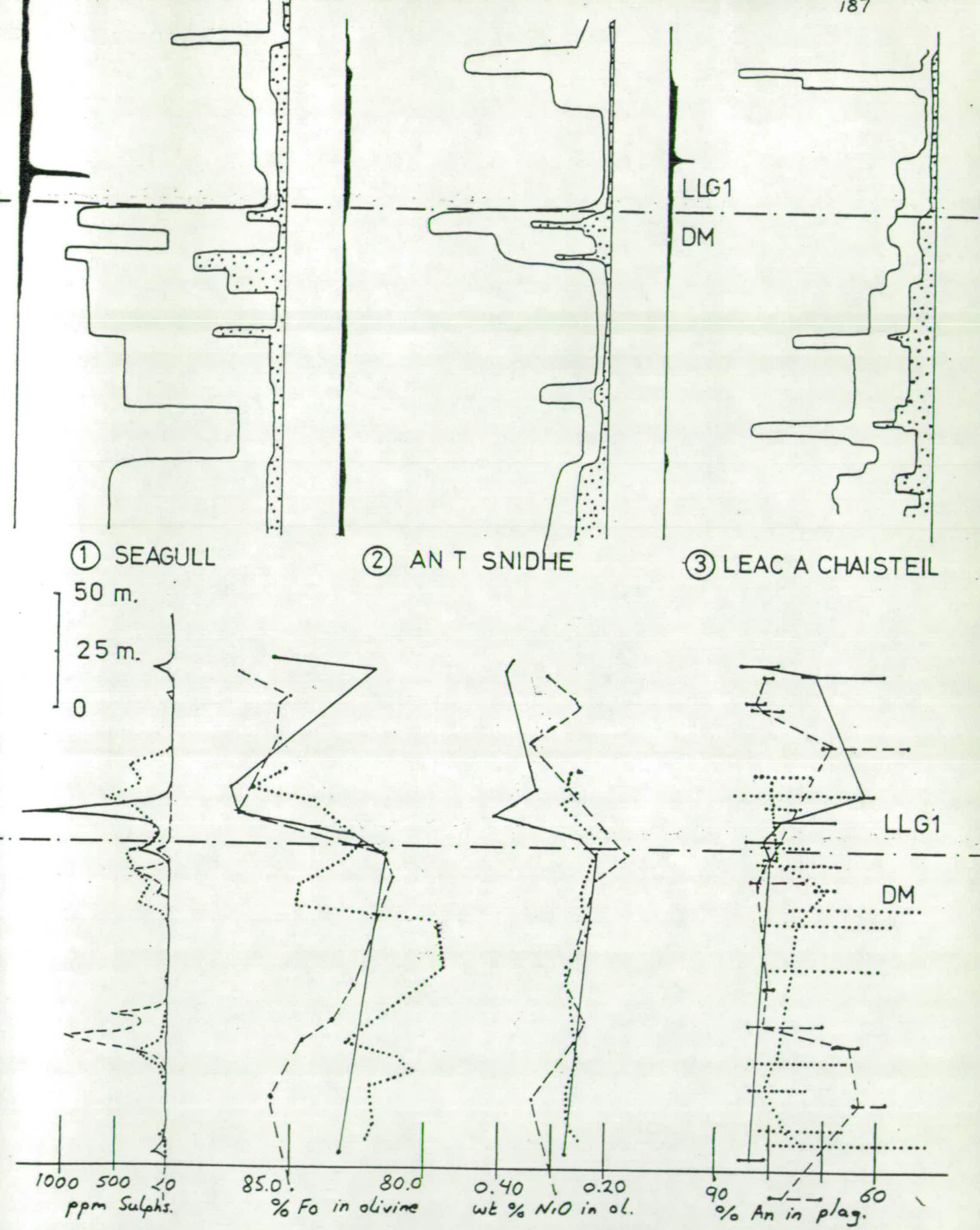

FIG. 5.30 Lateral cryptic variation across the DM/LLG1 contact (the datum level for all logs shown). The 3 logs at the top show lithological variation with stratigraphic height for 3 different traverses located on fig. 5.1 and the lower diagrams show the variation of cryptic parameter over the same interval. Key: 1 = Seagull traverse (solid variation trace), 2 = An't Snidhe traverse (dashed trace), 3 = Leac a Chaisteil traverse (dotted trace).

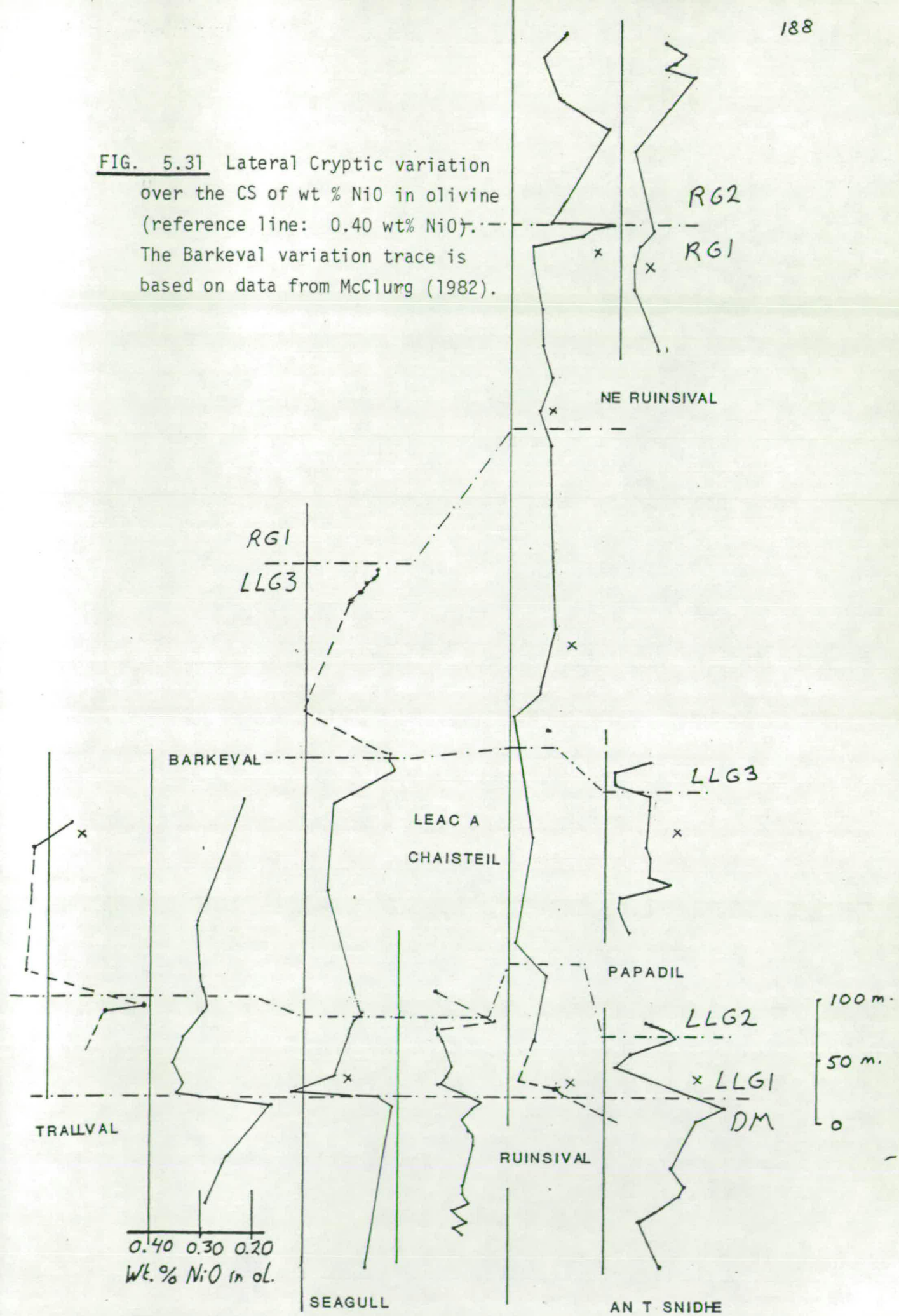

FIG. 5.31 Lateral Cryptic variation over the CS of wt % NiO in olivine (reference line: 0.40 wt% NiO). The Barkeval variation trace is based on data from McClurg (1982).

FIG. 5.32 Lateral cryptic variation of mole % Fo in olivine for the CS. (reference line : Fo 87.5). The variation trace for Barkeval is based on data from McClurg (1982).

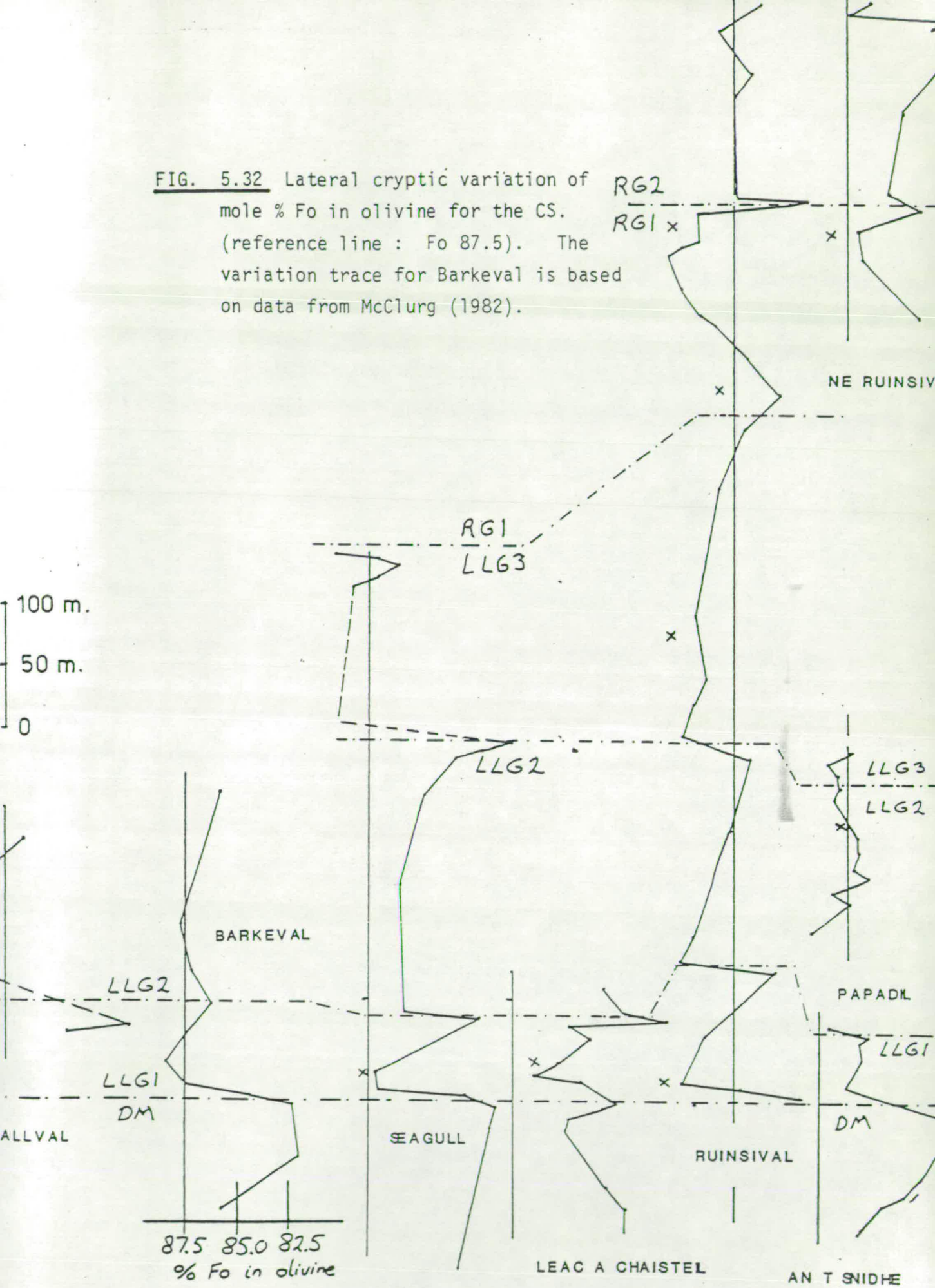

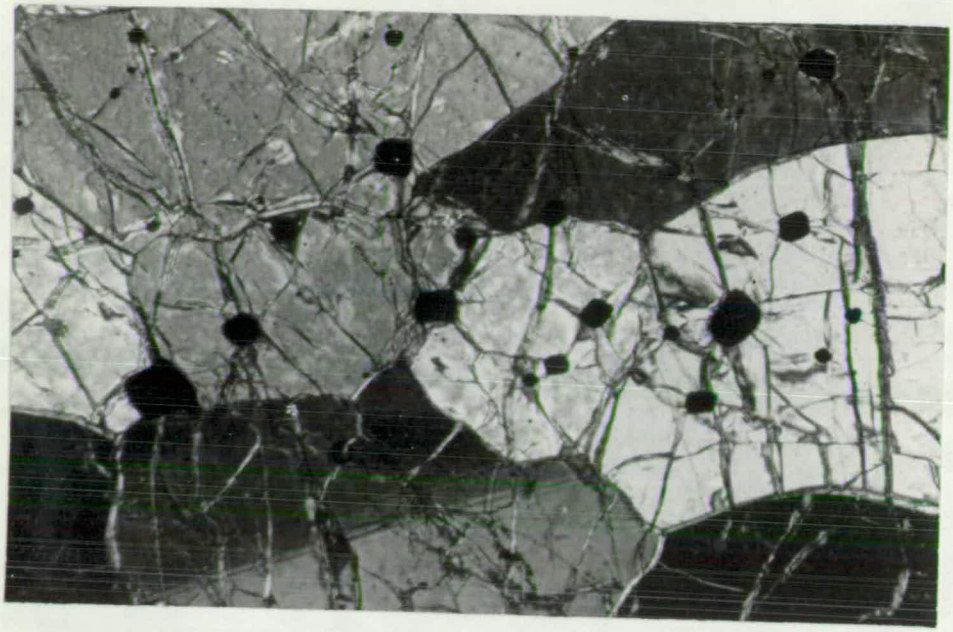

1 mm.

PLATE 5.1 Cumulus olivine and spinel in dunite. BK5, LLG2, CS, W. Trallval (sample number, unit number, series, locality).

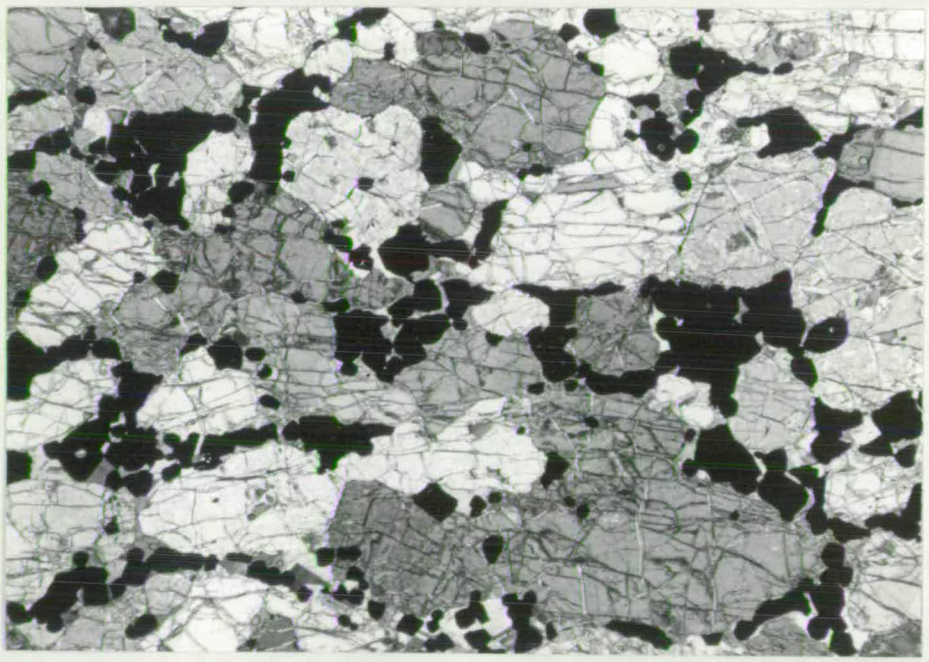

1 mm.

PLATE 5.2 Net texture in dunite. CC1, LLG2, CS, W. Trallval.

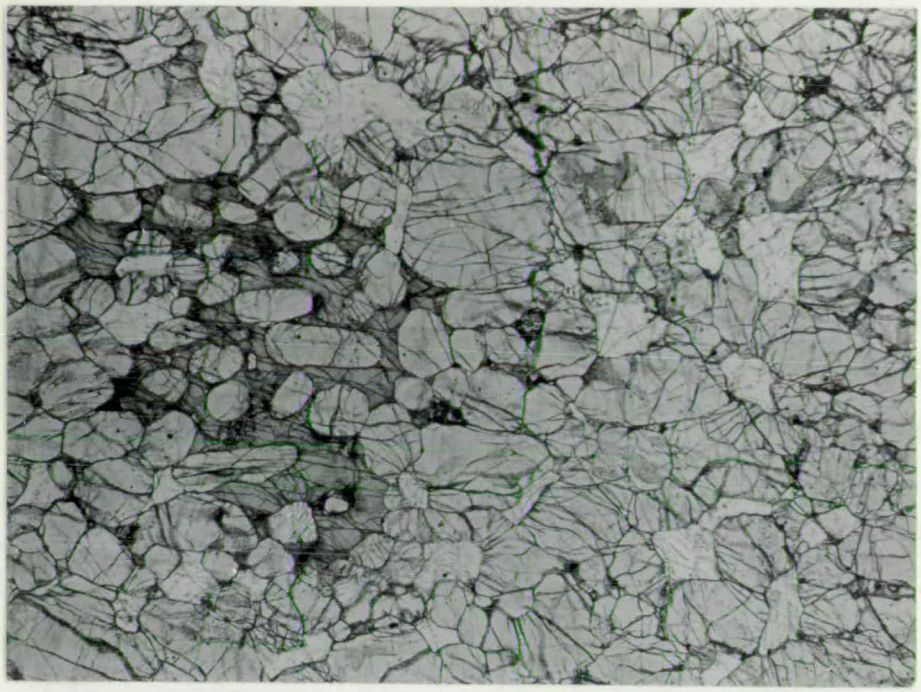

2 mm.

PLATE 5.3 Cumulus texture in a feldspathic peridotite. CF7, U9, ELS, W. Trallval. Dark crystal = pyroxene oikocryst, low relief crystals = intercumulus plagioclase, high relief cumulus crystals = olivine.

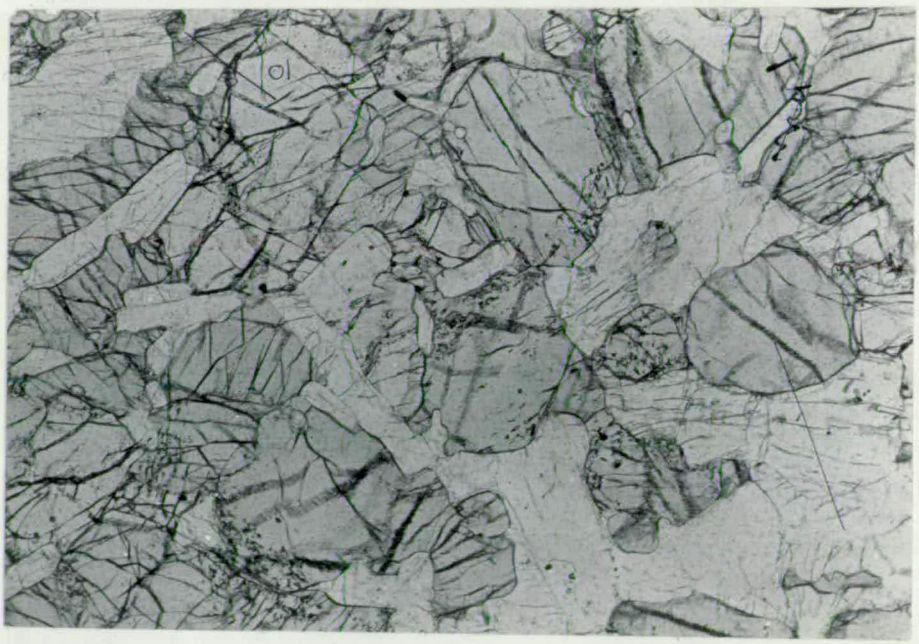

1 mm.

PLATE 5.4 Cumulus pyroxene, plagioclase and olivine in an allivalite . Note the intercumulus pyroxene. GH30, U14, ELS, W Trallval.

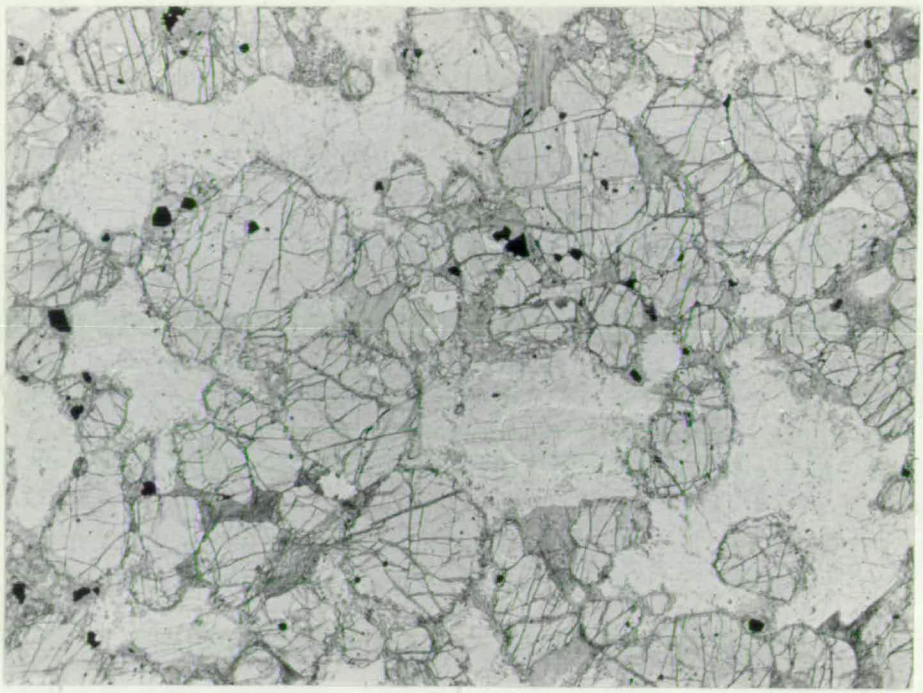

—— 1 mm.

PLATE 5.5 Conduit texture in feldspathic peridotite. Pyroxene forms the dark cement between the olivines. K7, Papadil plug, Papadil.

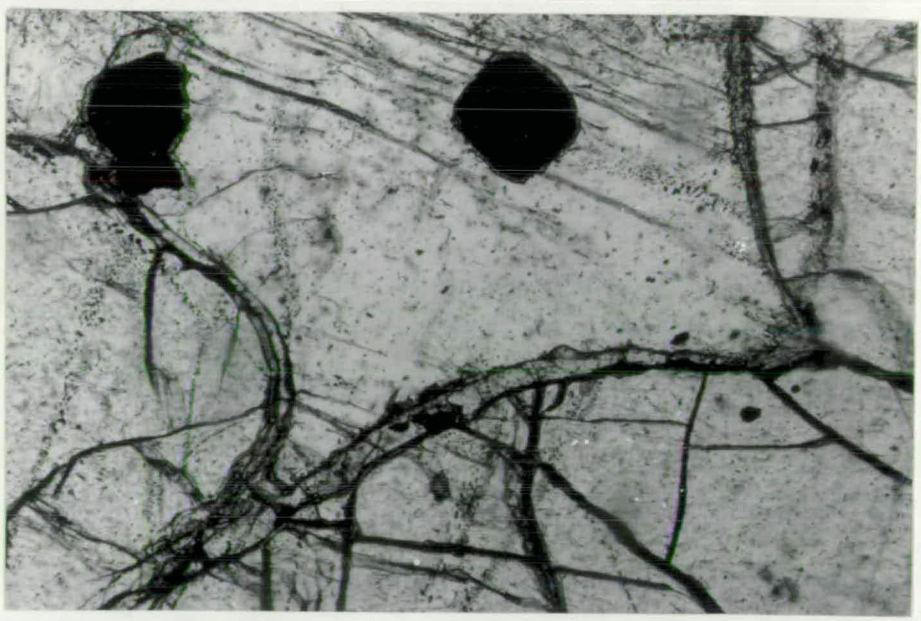

—— 100 microns

PLATE 5.7 Clinopyroxene fringe on olivine in peridotite. The low relief plagioclase includes spinel crystals. HK5, Trallval ELS breccia zone (X on fig. 3.5).

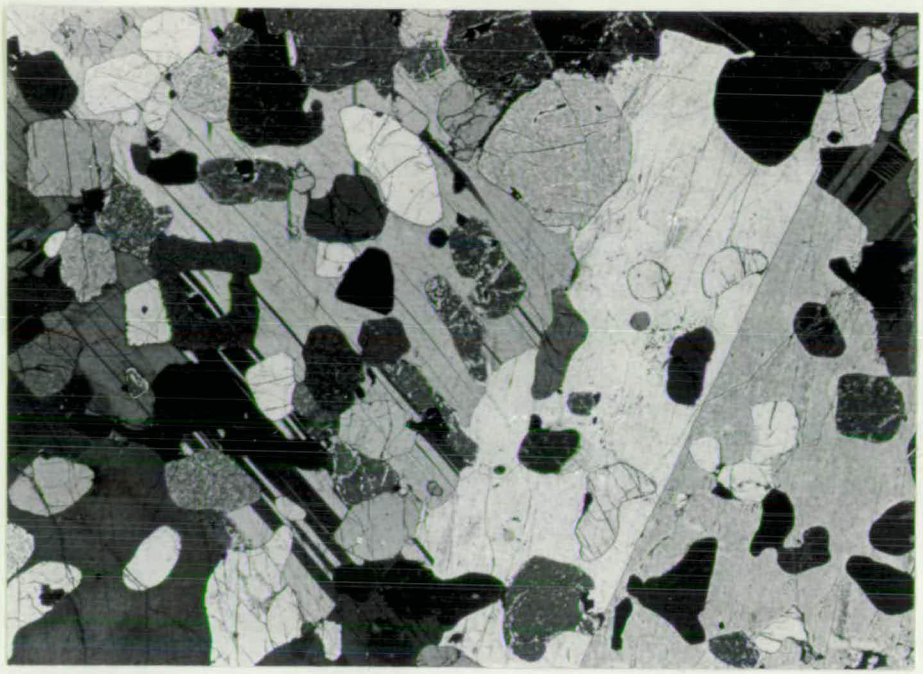

1 mm.

PLATE 5.8 Matrix-supported texture in an olivine gabbro. Plagioclase oilocryst to left, twinned pyroxene to right. All cumulus crystals are olivine (some have a skeletal habit). AD7, Atlantic Corrie Gabbro, E Trallval.

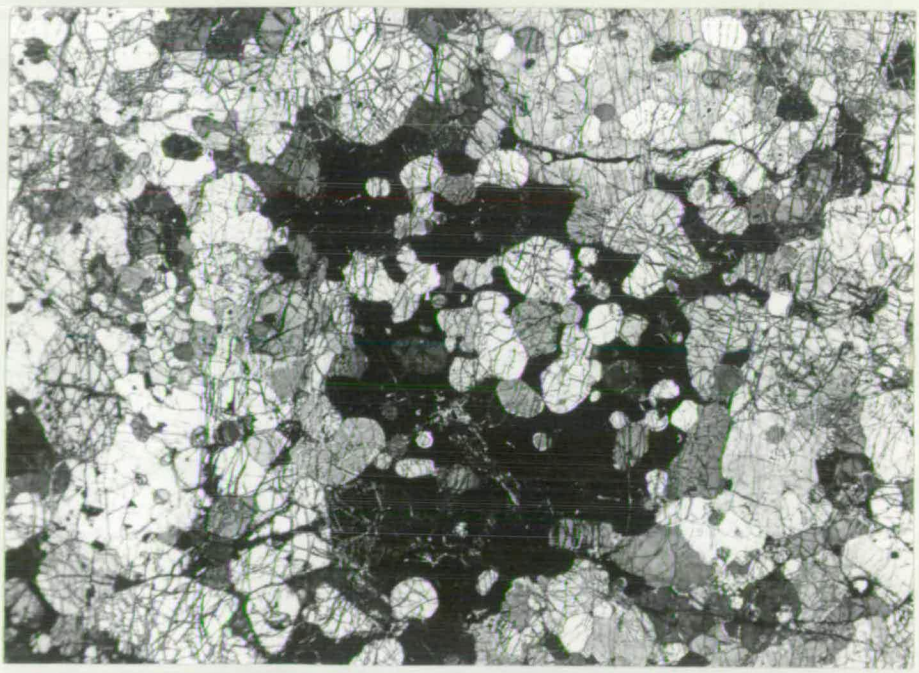

1 mm.

PLATE 5.9 Matrix-supported texture in plagioclase-free peridotite (central pyroxene oikocryst is in extinction). HD27, RG1, CS, NW Ruinsival.

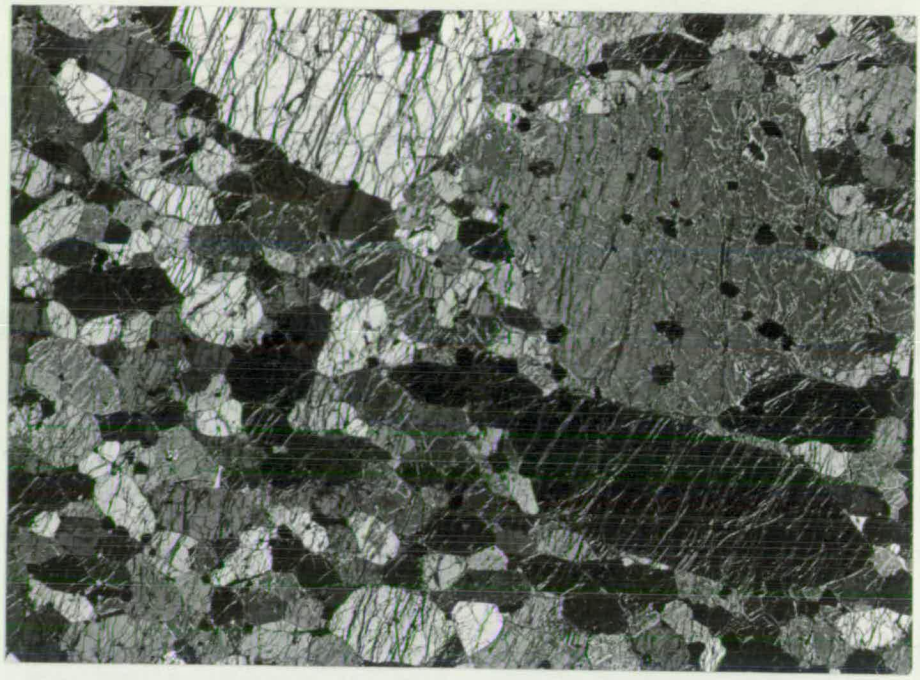

1 mm.

PLATE 5.10 Olivine foliation in poorly sorted dunite. FE6, LLG2, CS, Papadil.

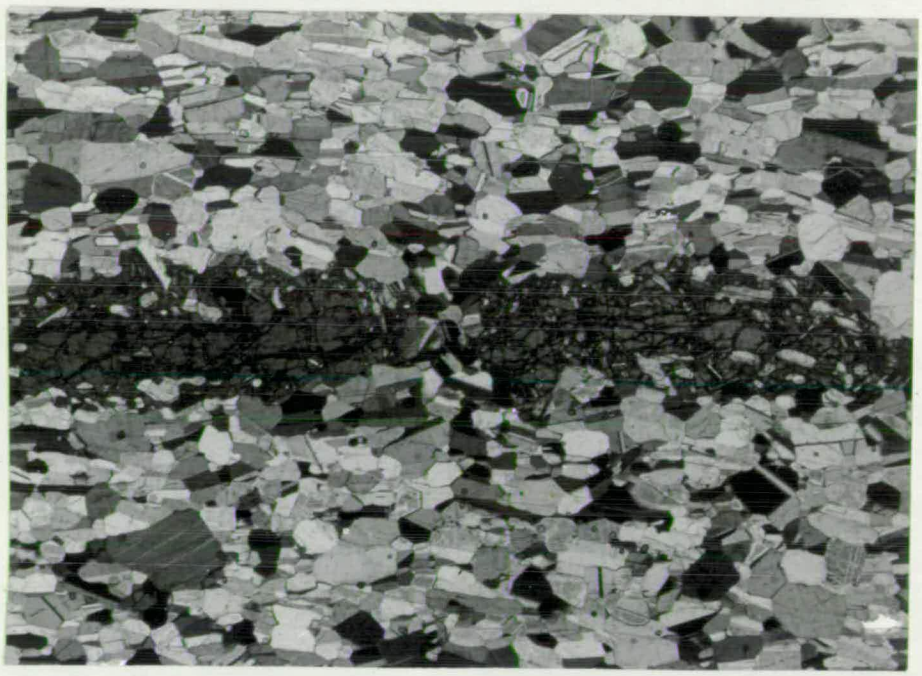

1 mm.

PLATE 5.11 Plagioclase foliation in anorthosite. The two olivine crystals have subophitic rims. HB1, U9, ELS, Hallival.

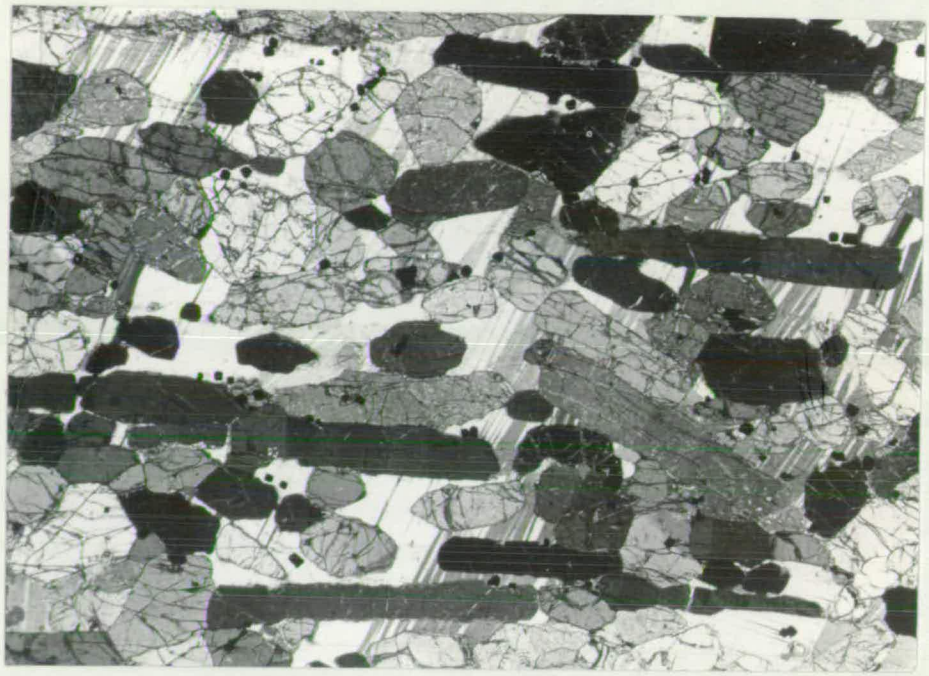

1 mm.

PLATE 5.12 Olivine foliation is feldspathic peridotite. HC4, LLG1, CS, Coastline traverse.

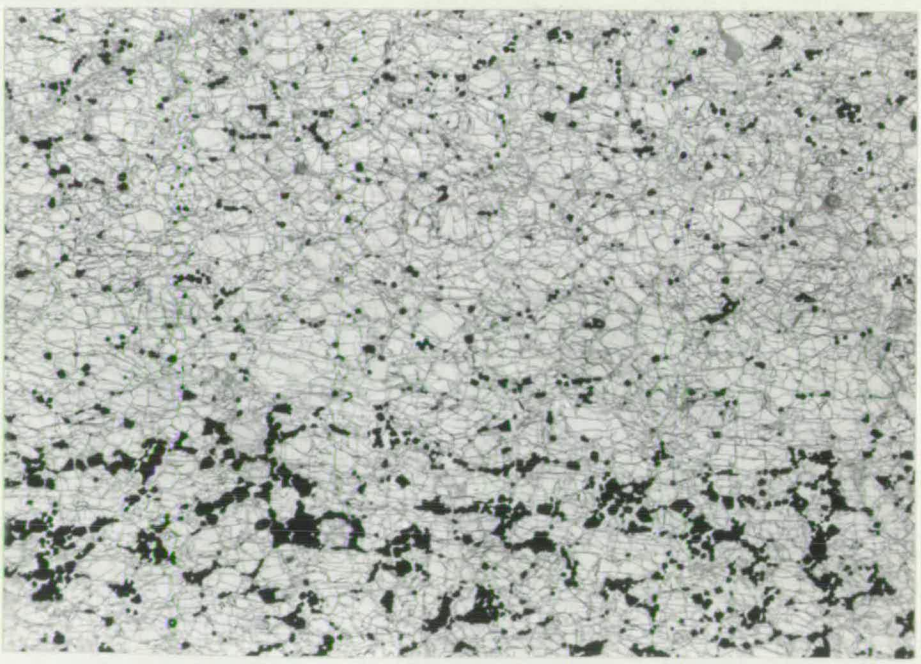

4 mm.

PLATE 5.13 Rhythmic spinel concentrations (arrows) in dunite. CC1, LLG2, CS, W Trallval.

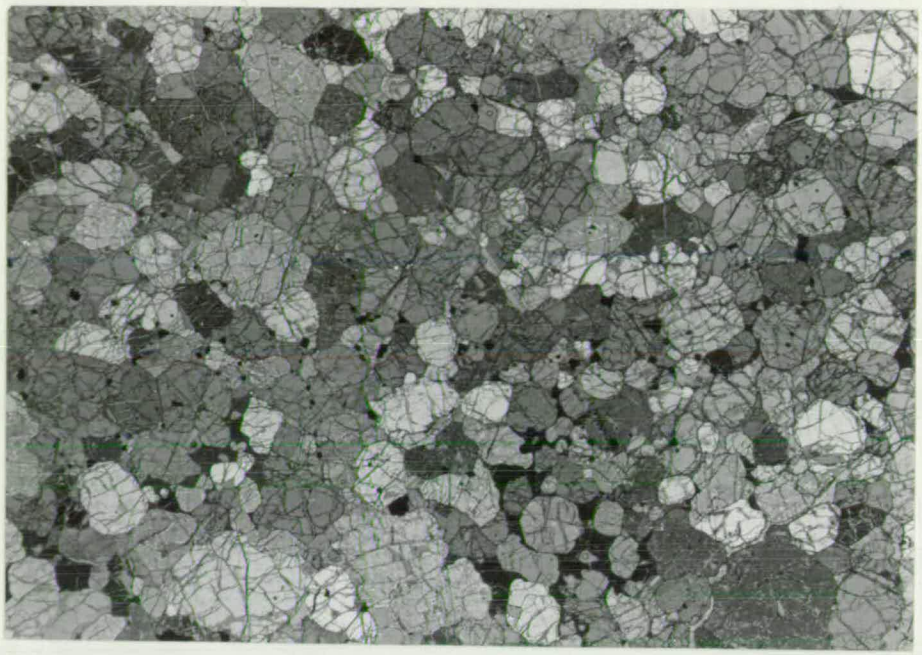

2 mm.

PLATE 5.14 One-crystal thick lamina of spinel in peridotite (arrows). HC22, LLG 1, CS, An't Snidhe.

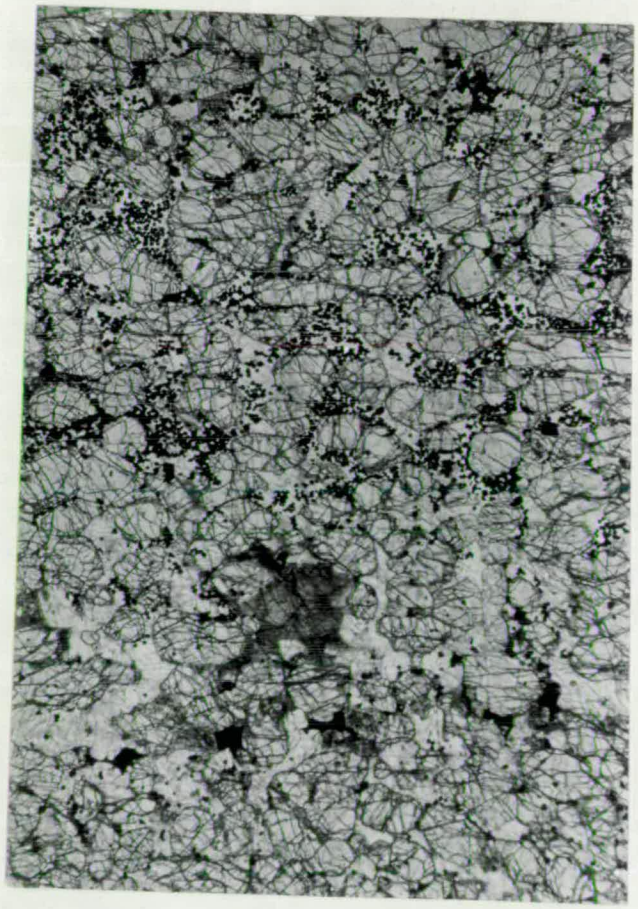

PLATE 5.15 Cr-spinel rich lamina in feldspathic peridotite, underlain by one-crystal thick lamina of coarse spinel (arrows). Note elongate, foliated olivine in spinel-rich lamina and the lamina rich in intercumulus material below. LB3, U10, ELS, S Trallval.

4 mm.

PLATE 5.16 Rhythmic spinel concentrations in allivalite. GH23, U14, ELS, W Trallval.

—— 1 mm.

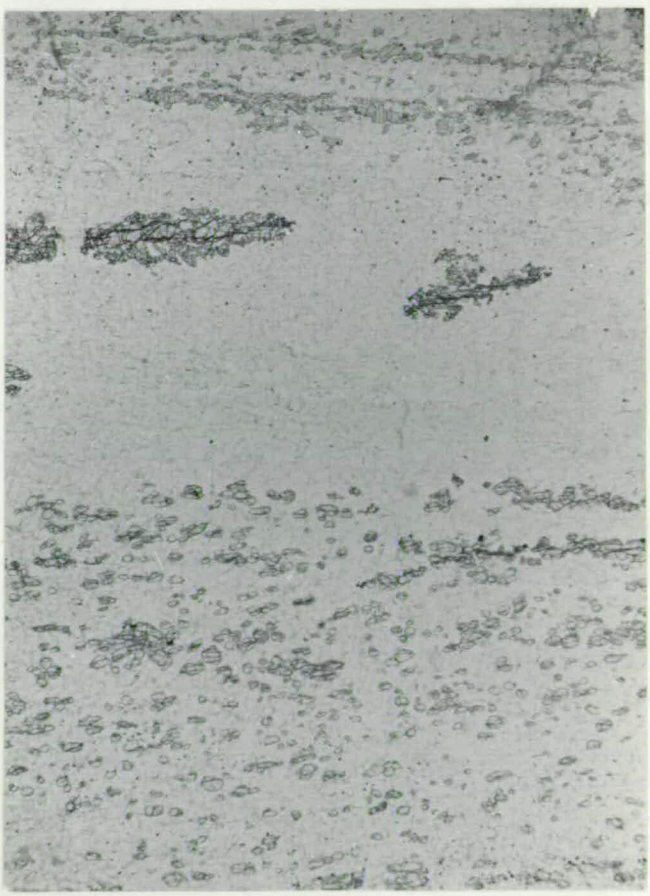

PLATE 5.17 Finely-layered allivalite:
4 - cumulus plagioclase, pyroxene and spinel

3 - anorthosite with large subophitic olivine

2 - cumulus olivine, spinel and plagioclase with intercumulus pyroxene

1 - cumulus olivine, spinel and plagioclase

—— 2 mm.

1 mm.

PLATE 5.18 Textural (grain-size) layering in dunite. Coarse olivines form a one-crystal layer (bracketed) in dunite. HC7, LLG2, CS, Coastline traverse.

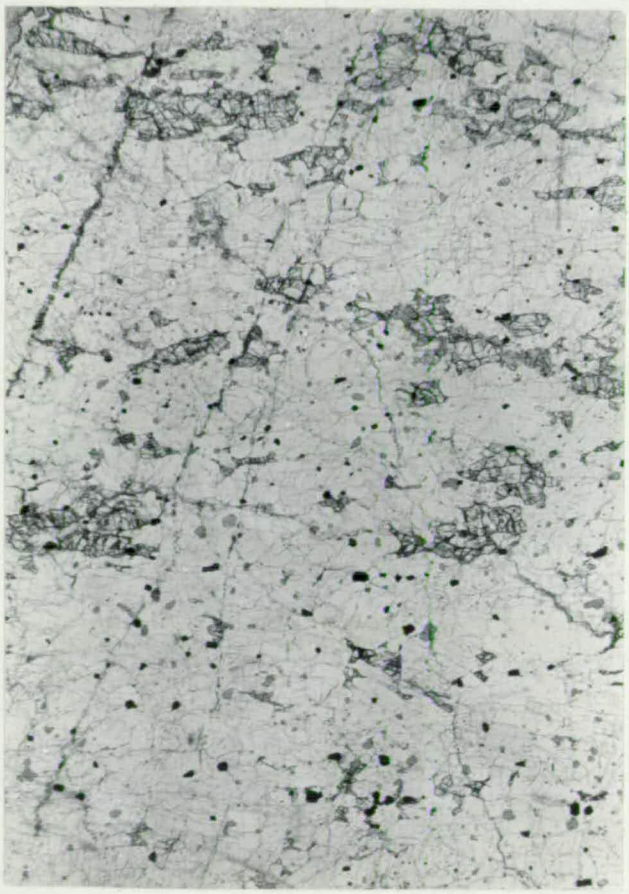

PLATE 5.19 Graded layering in allivalite. Spinel gradually fines upwards, followed by a return to coarse spinel. GH1, U10, ELS, W Trallval.

1 mm.

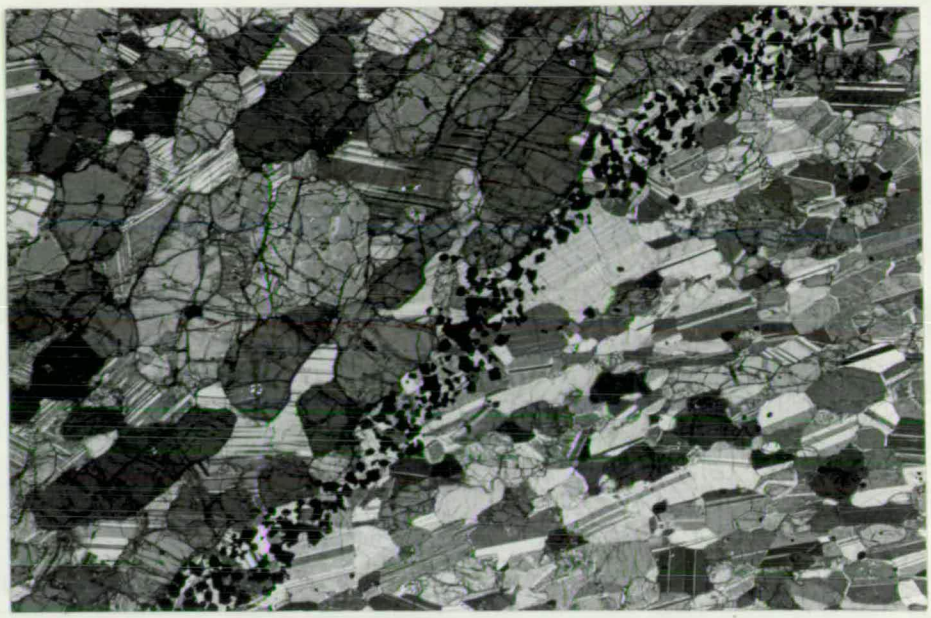

1 mm.

PLATE 5.20 Unconformable plagioclase and olivine foliations across a chromitite lamina. Section perpendicular to the layering. B02, U10, ELS, W Trallval.

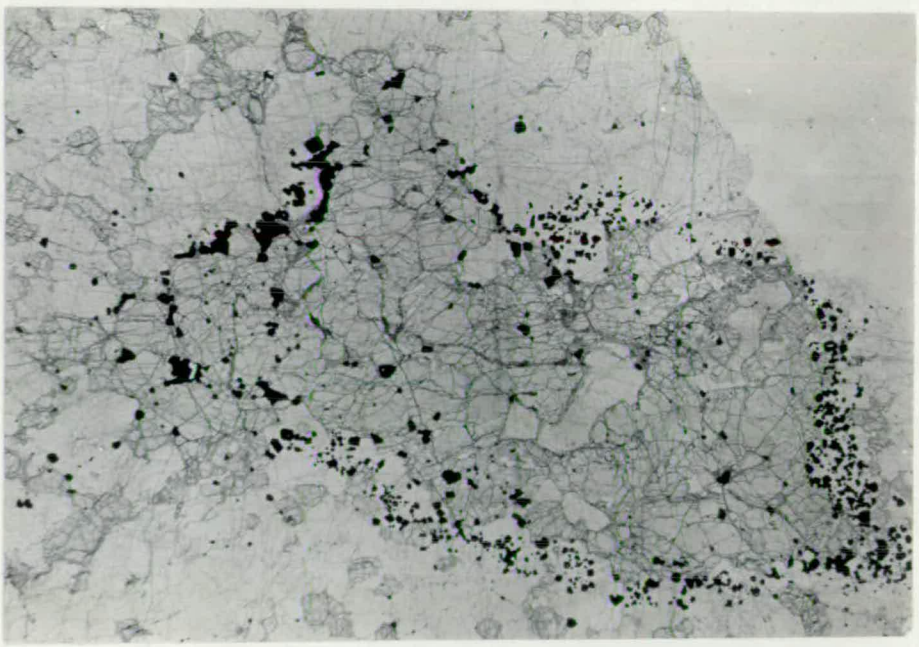

3 mm.

PLATE 5.21 Section parallel to the layering of the sample in plate 5.20, showing a peridotite loading structure. The loading explains the unconformable foliations.

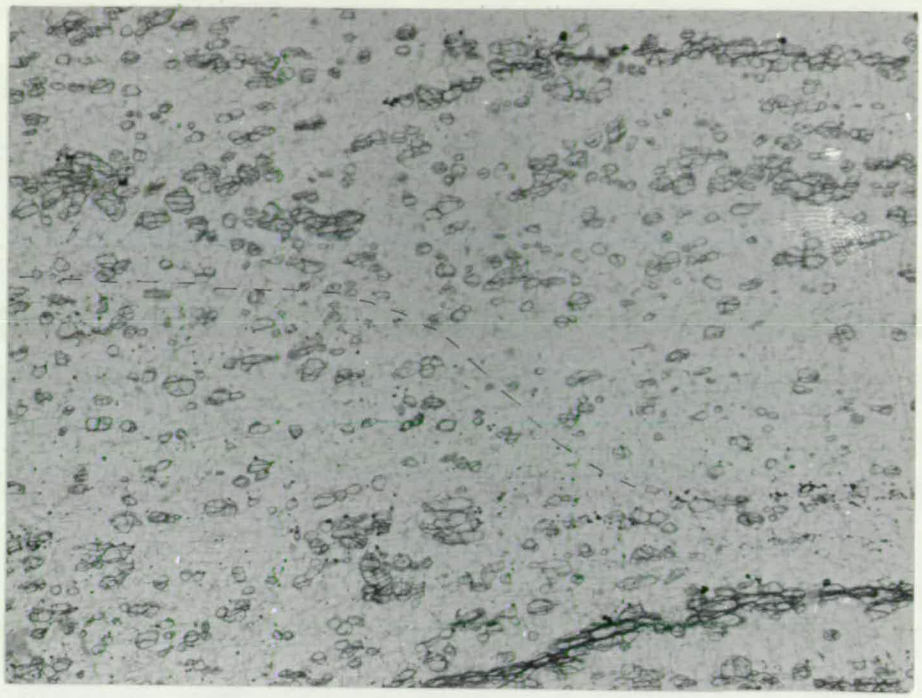

1 mm.

PLATE 5.22 Concentration of fine spinel defines a spinel-free channel feature (dashed) with concentrated spinel at the bottom. Plagioclase foliation is parallel to the length of the photograph. HB1, U9, ELS, Hallival.

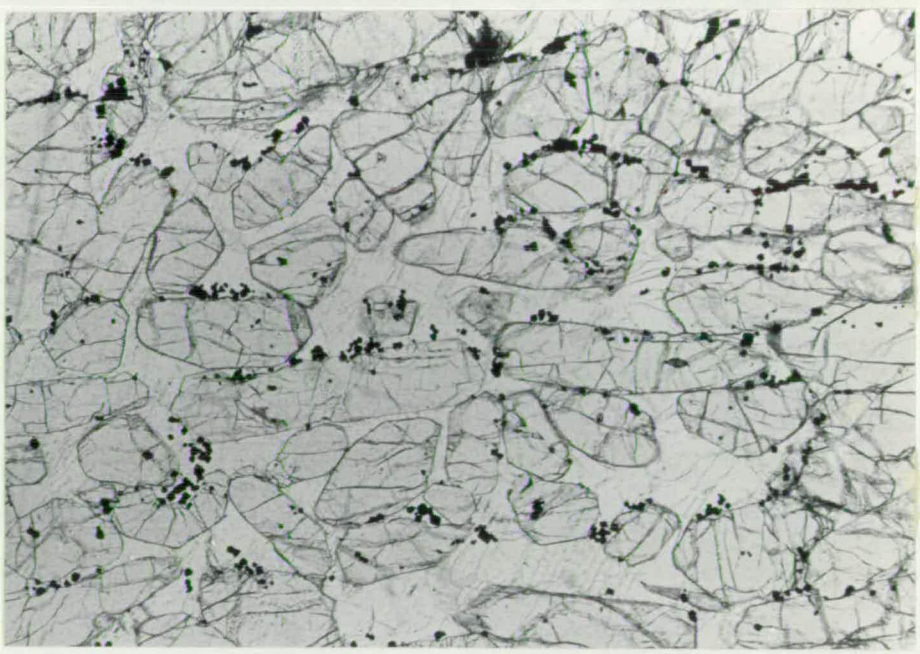

1 mm.

PLATE 5.23 Geopetal spinel structure in feldspathic peridotite. The intercumulus material is plagioclase. CE2, U9, ELS, W Trallval.

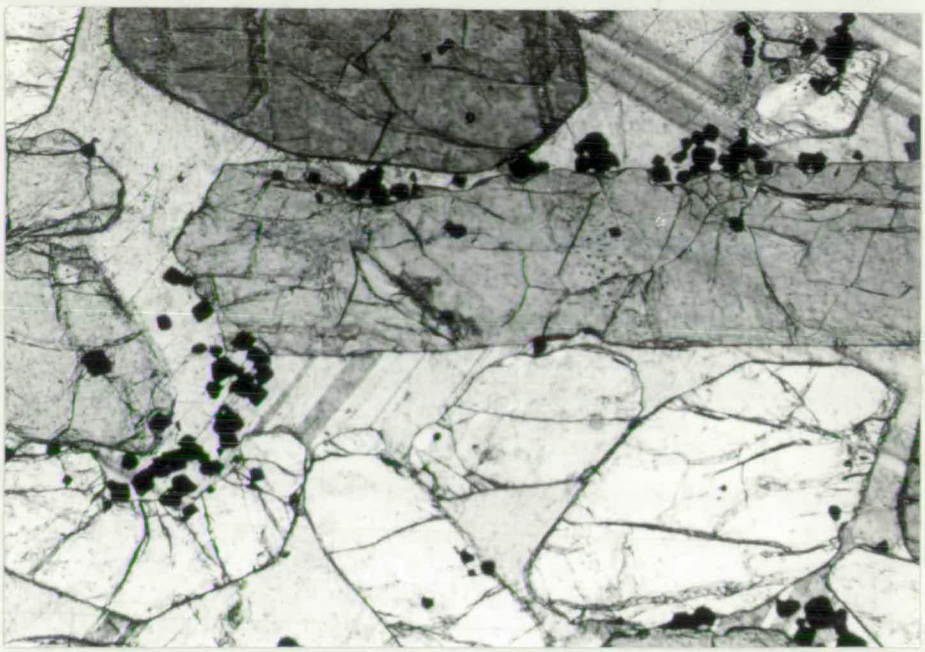

1 mm.

PLATE 5.24 Detail of plate 5.23.

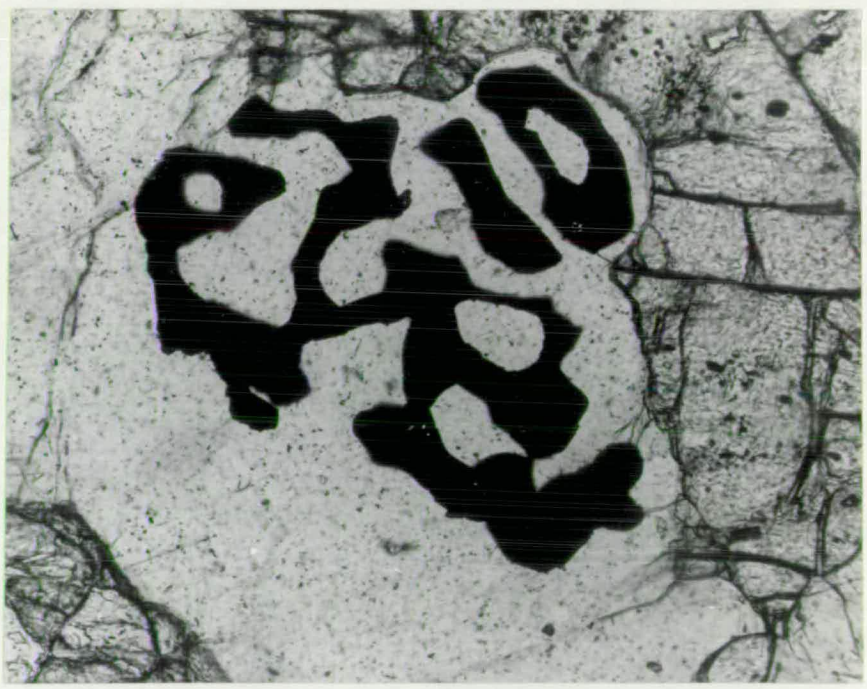

100 microns

PLATE 5.25 Recrystallised spinel loops. G6, Ruinsival breccia Zone, NW Ruinsival.

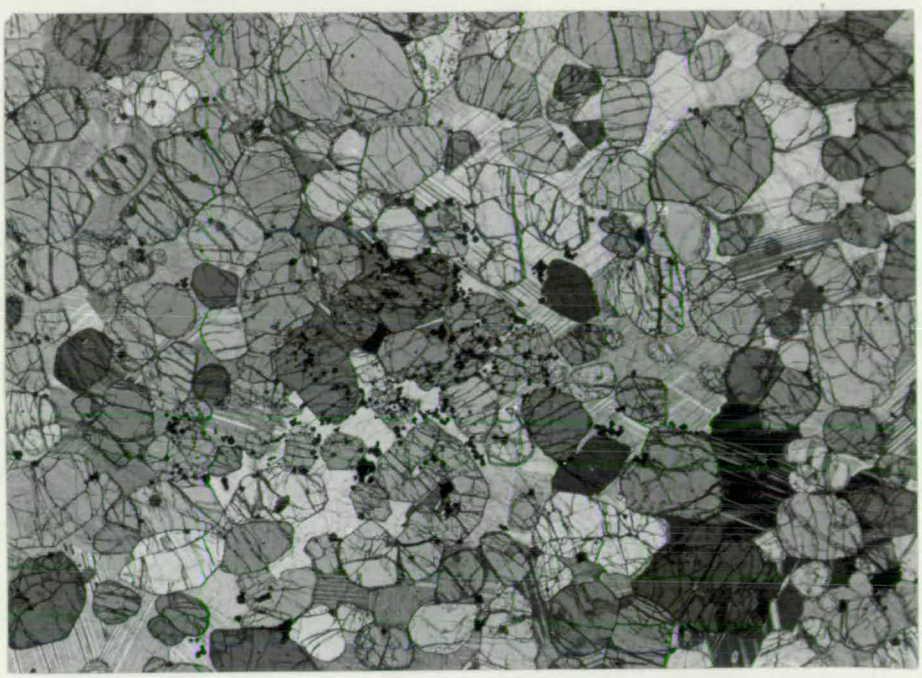

——— 1 mm.

PLATE 5.26 Local concentration of spinel disseminated in cumulus olivine as well as in intercumulus plagioclase, indicating *in situ* growth of cumulus olivine. GN 12, U14, ELS, E Trallval.

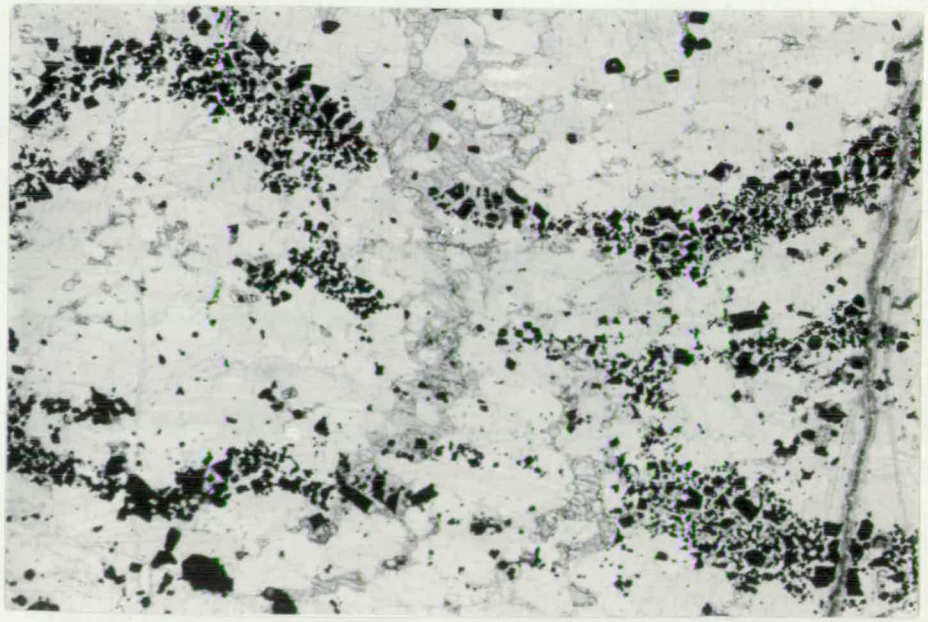

——— 1 mm.

PLATE 5.27 Elongate pyroxene oikocryst perpendicular to chromitite layering in the allivalite. DE5, U10, ELS, W Trallval.

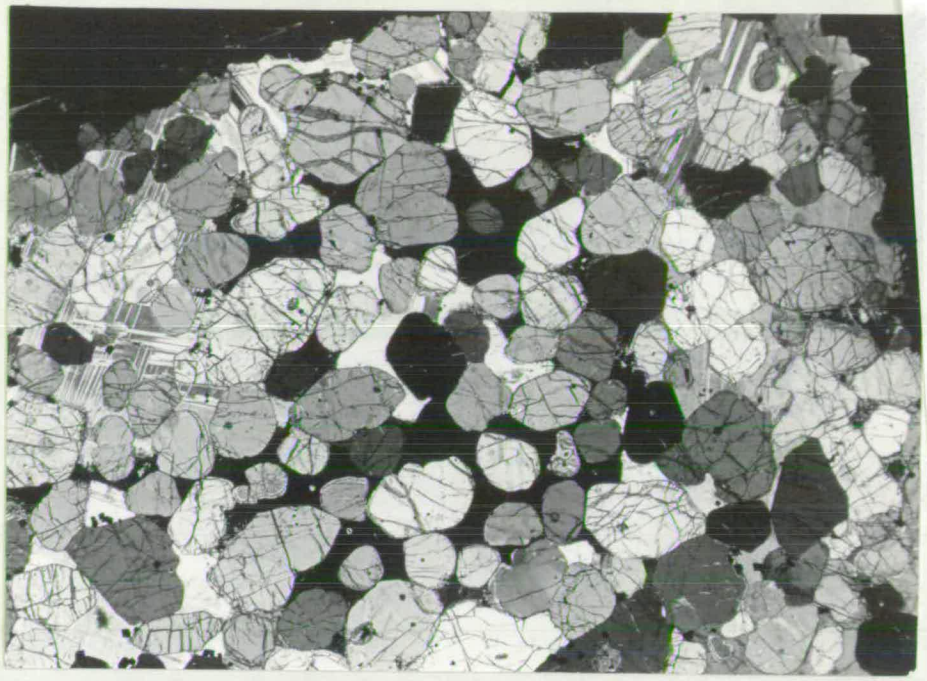

1 mm.

PLATE 5.28 Section through doughnut-shaped pyroxene oikocryst (in extinction with plagioclase at centre) in feldspathic peridotit GN12, U14, ELS, E Trallval.

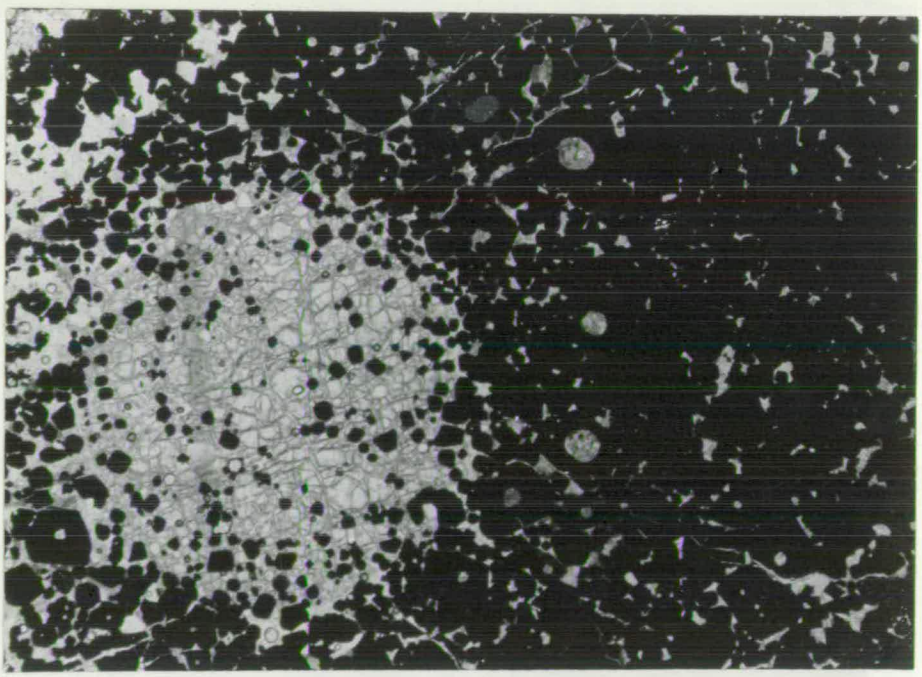

1 mm.

PLATE 5.29 Chromitite near bottom of the LLG1 unit (on the Seagull traverse) illustrating in situ simultaneous growth of olivine and spinel. GB1, LLG1, CS, An Dornabac.

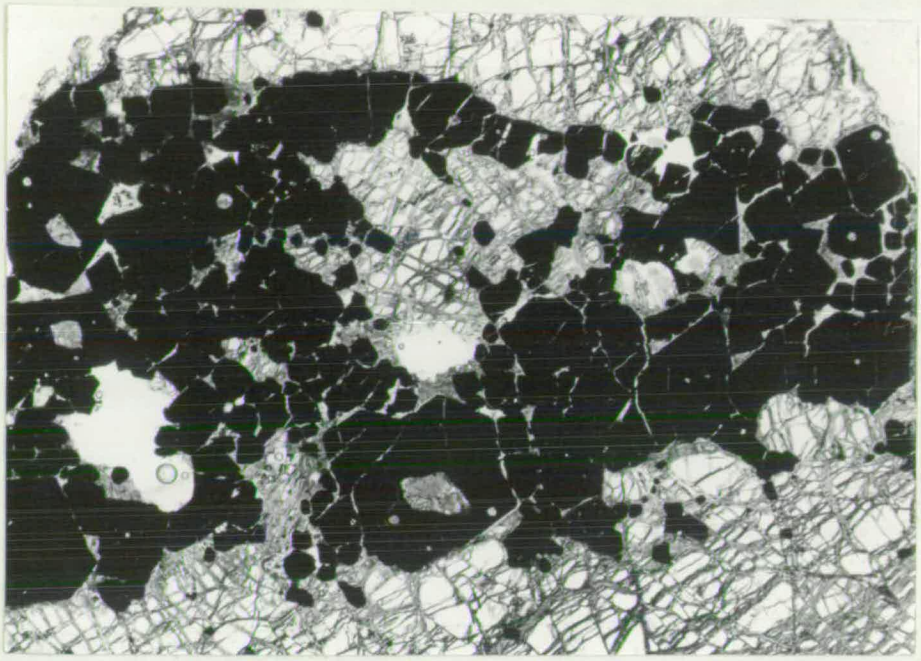

1 mm.

PLATE 5.30 Recrystallised chromitite in dunite. FE10, LLG2, CS, Papadil.

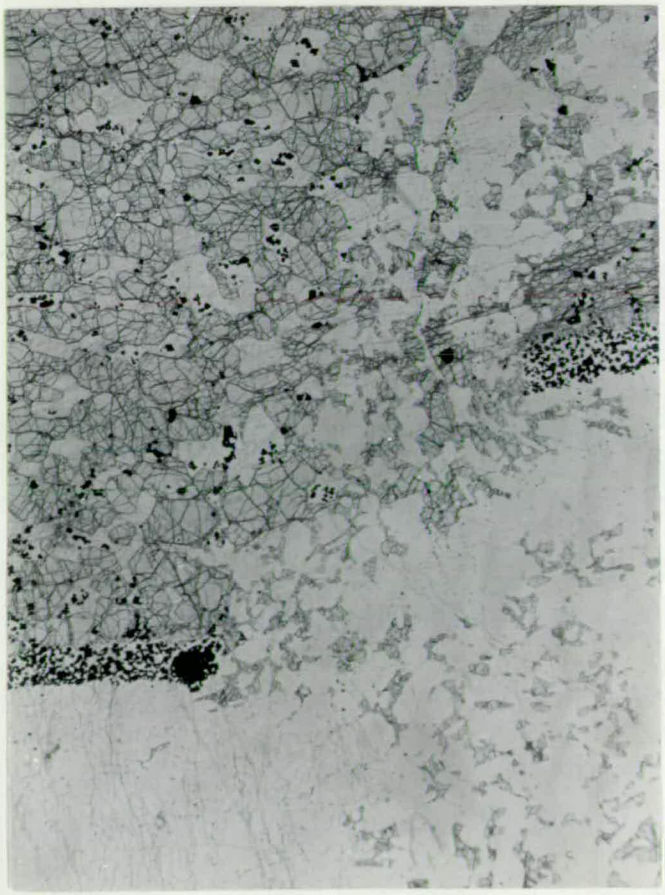

PLATE 5.31 Microfault displacing chromitite at the base of U10. Note the recrystallised spinel at the fault edge and the entrainment of plagioclase into the peridotite. BM1, U10, ELS, W Trallval.

1 mm.

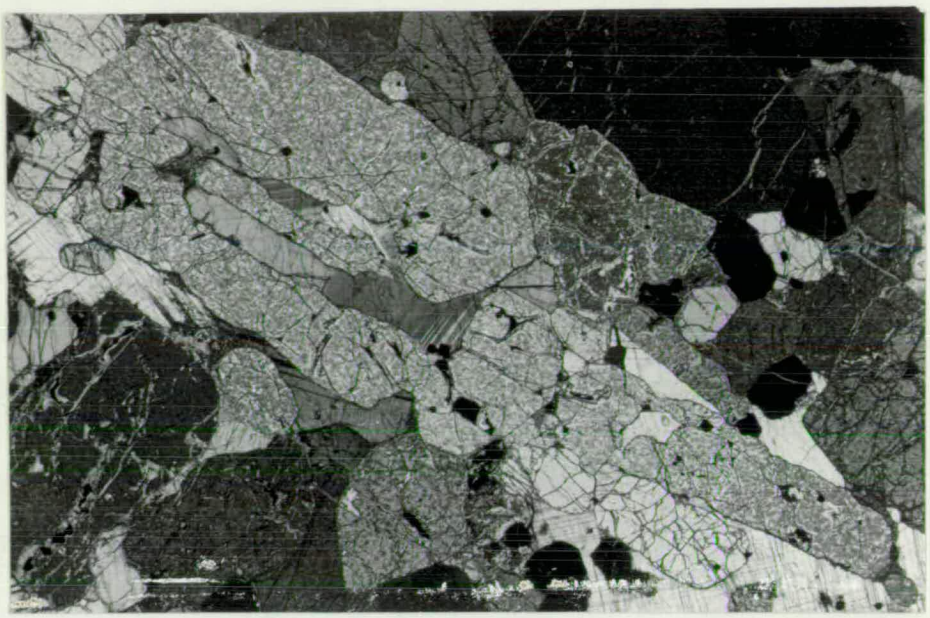

1 mm.

PLATE 5.32 Skeletal olivine in protoharrisite. M21, U15, ELS, W Trallval.

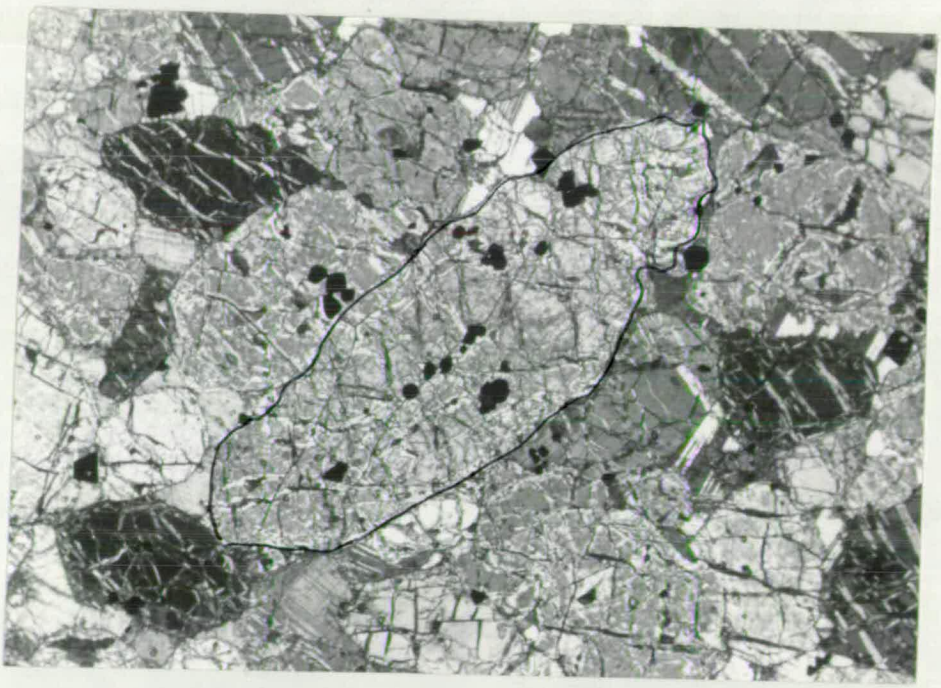

1 mm.

PLATE 5.33 Spinel backbone in protoharrisitic olivine. HD21, RG2, CS, NW Ruinsival.

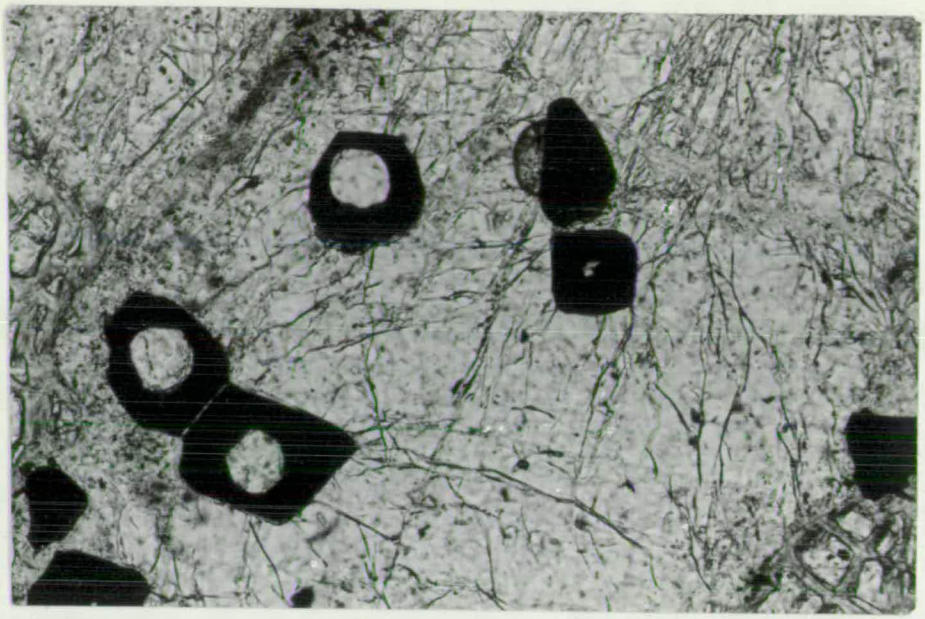

——100 microns

PLATE 5.34 Large central silicate inclusions in spinel (type 1). HD17, RG1, CS, NW Ruinsival.

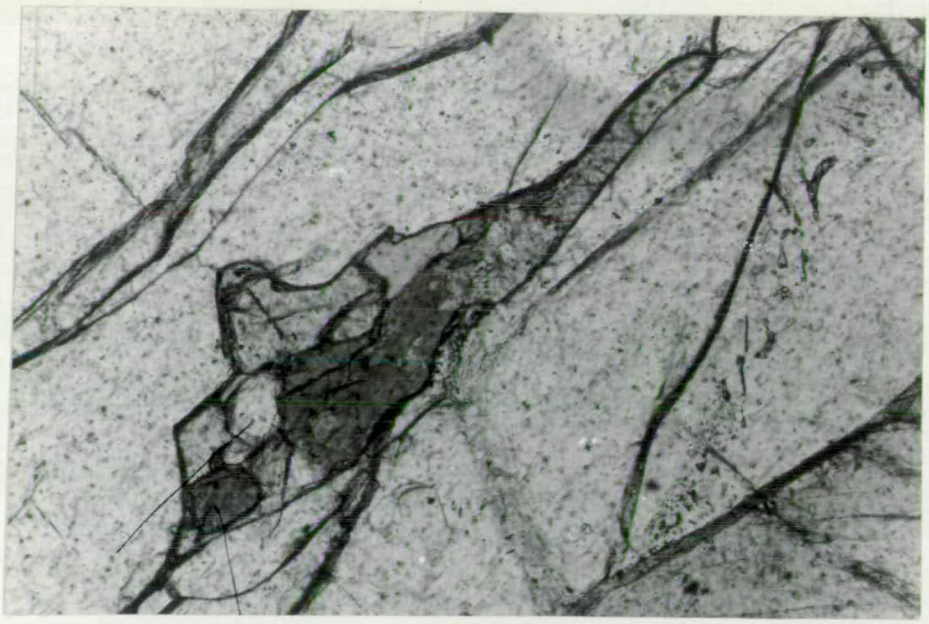

——100 microns

PLATE 5.35 Inclusion of enstatite and phlogopite in olivine. M15, U14, ELS, S Trallval.

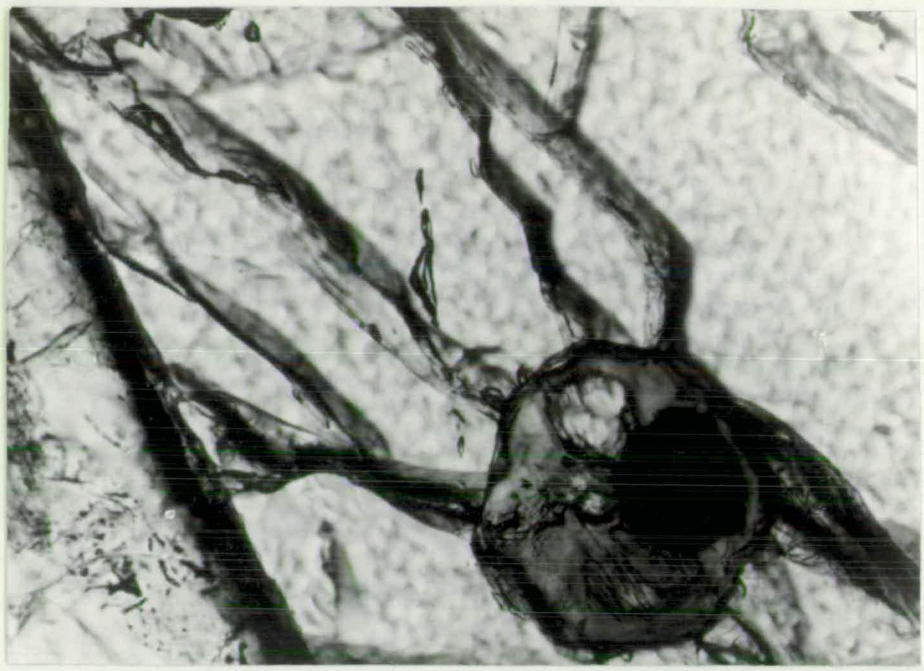

——— 100 microns

PLATE 5.36 Enstatite, spinel and phlogopite in olivine. The round inclusion shape is characteristic. HL6, U11, ELS, Askival.

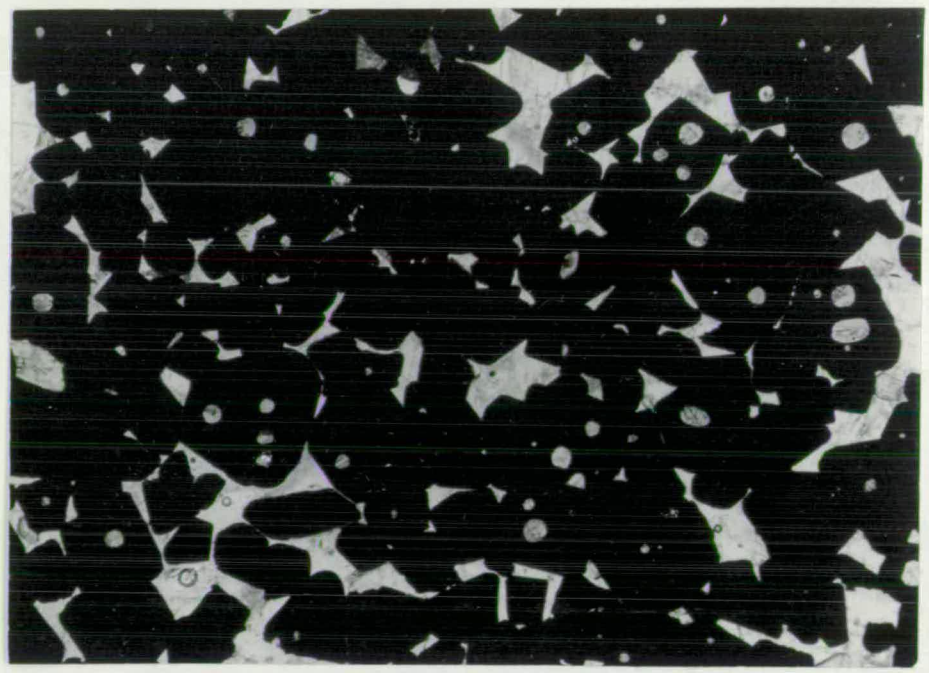

——— 1 mm.

PLATE 5.37 Inclusion-spinel chromitite. GM2, RG1, CS, NW Ruinsival.

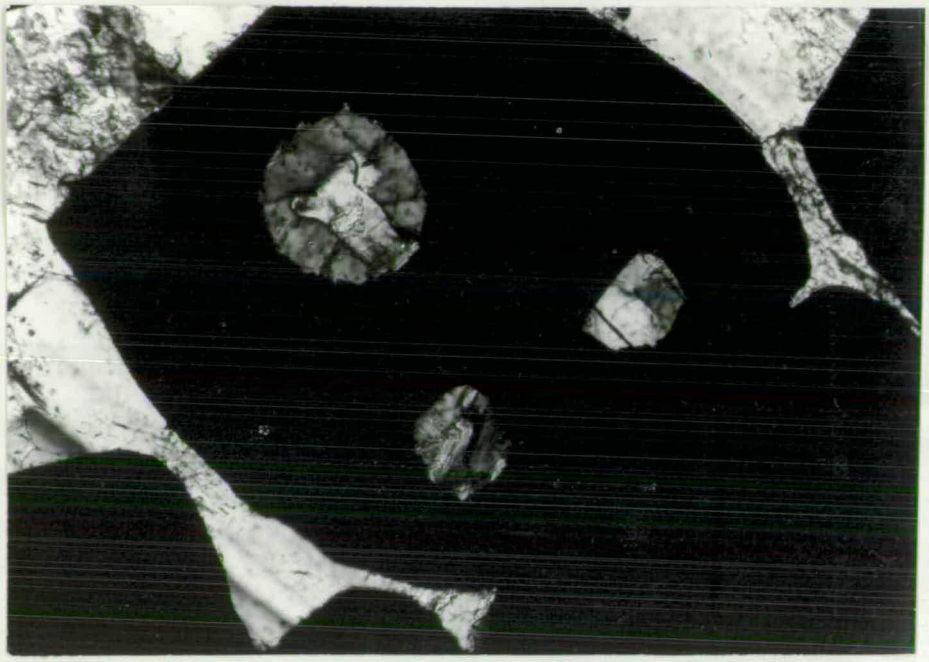

——100 microns

PLATE 5.38 Detail of plate 5.37; right-hand inclusion has enstatite and kaersutite.

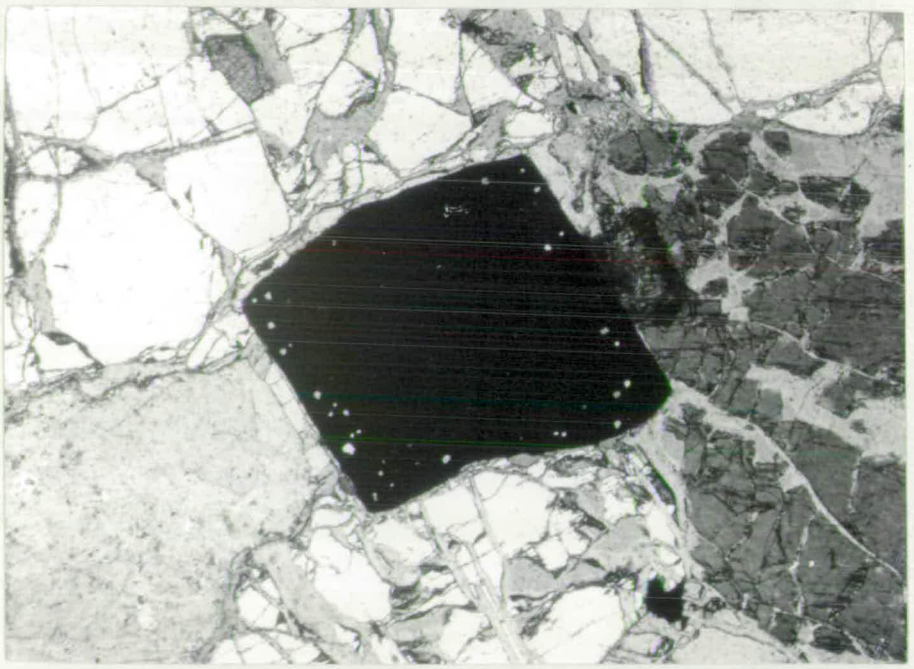

——200 microns

PLATE 5.39 Type 3 inclusion spinel. The inclusions are of kaersutite. The spinel is a disseminated grain in dunite. HC5, LLG2, CS, Coastline.

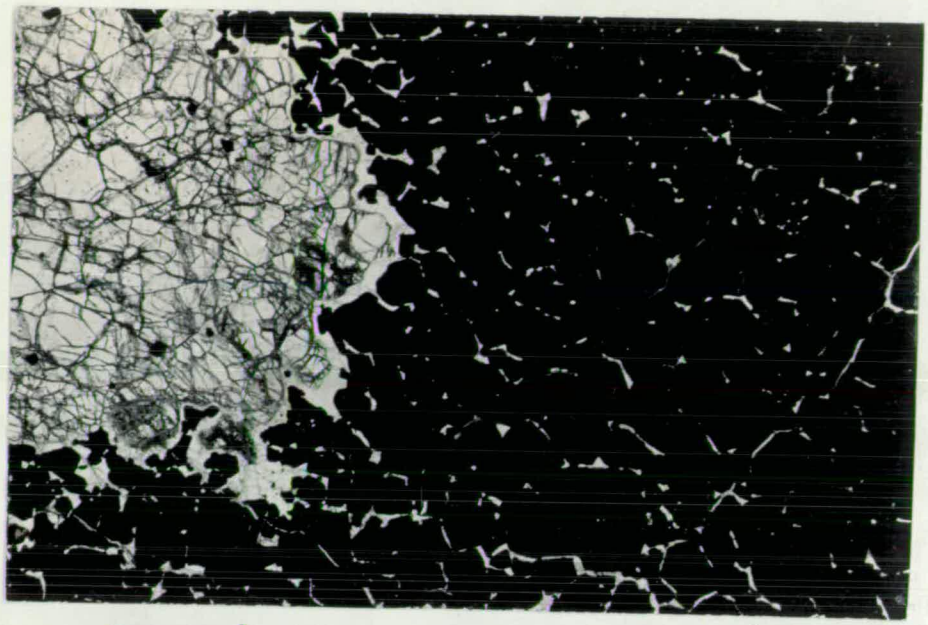

——— 1 mm.

PLATE 5.40 Highly concentrated chromitite. Spinels have recrystallised margins. Size-sorting is good. BO3, LLG2, CS, W Trallval.

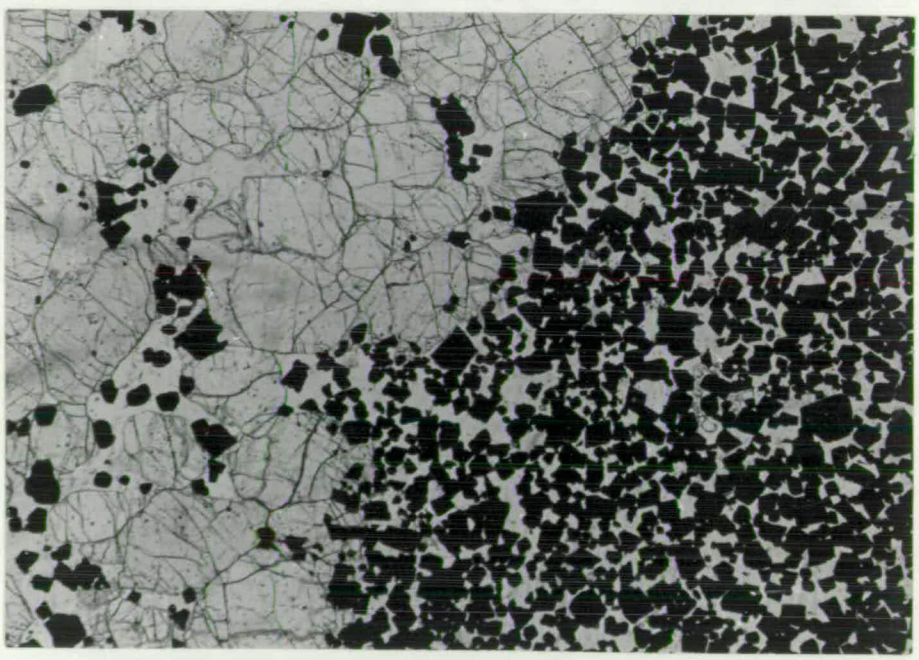

——— 1 mm.

PLATE 5.41 Poorly-sorted chromitite with low spinel density compared to the chromitite in plate 5.40. Intercumulus Plagioclase and olivine (arrow). BK4, U9, ELS, W Trallval.

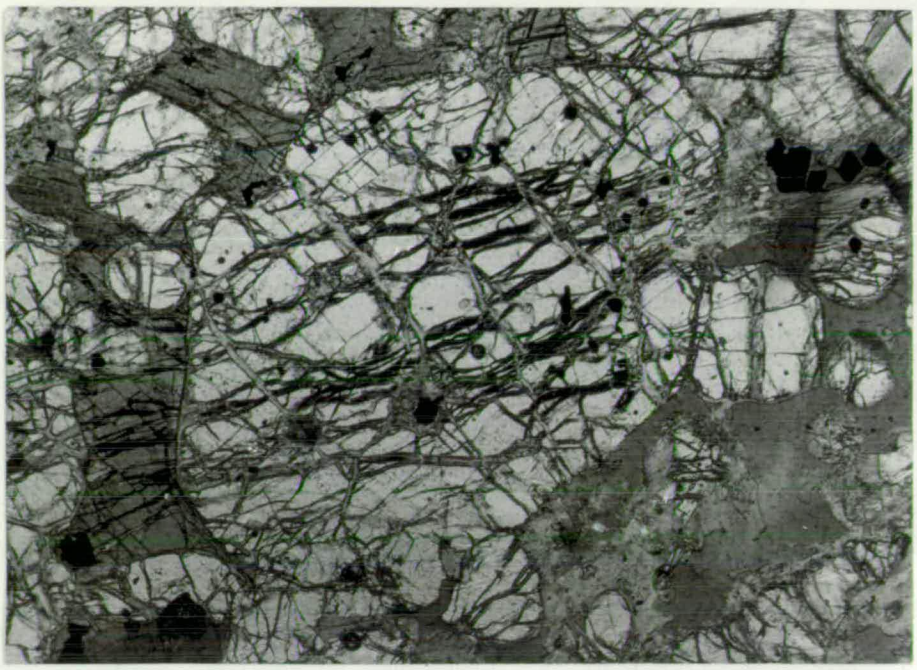

1 mm.

PLATE 5.42 Intercumulus kaersutite (top left) and phlogopite (bottom right) in feldspathic peridotite from the Papadil plug. AH1, Papadil plug, Papadil.

CHAPTER 6

THE PETROGRAPHY, MINERAL CHEMISTRY AND GEOCHEMISTRY OF THE DYKES AND GABBROS.

Whole-rock analyses have been obtained for the dykes and gabbros in the Trallval area in an attempt to estimate the range of liquids available during the formation of the layered series and to complement McClurg's (1982) work on the dykes and gabbros of the Barkeval-Long Loch area. These data are preceded by an account of the petrography and mineral chemistry of analysed samples. In addition, a variety of ultrabasic rock-types from both layered series, the ultrabasic breccias and the intrusive plugs has been analysed to compare trace element ratios with those of the dykes and gabbros.

6.1 The Dykes: Petrography.

The distribution of the dykes is given in section 2.3.1. McClurg (1982) classified the dykes in the Barkeval-Long Loch area as follows:

Group A - Picrites, which are usually brown-weathering and have 5 to 60 % of olivine phenocrysts. These are subdivided by their petrography:

- A1 - Euhedral to rounded, fresh olivine phenocrysts and euhedral spinel phenocrysts in a fine-grained groundmass of rounded olivine, brownish clinopyroxene, plagioclase and opaque minerals (including abundant sulphides) in an intersertal texture. Greenish amphibole and mica (up to 2 modal %) are common in the groundmass.
- A2 - Differ from Group A1 in the absence of hydrous phases, and the skeletal habit of the olivine in the selvedges.
- A3 - Black-weathering, with clouded, brown olivine phenocrysts (although the olivine is clear around included spinels, see Plate 6.1). Olivine is rare in the groundmass, commonly quenched with radiating sheaves of acicular plagioclase and interstitial clinopyroxene.

Group B - Basalts, which are fine-grained, grey and have less than 10 % of phenocrysts (plagioclase $\pm$ olivine $\pm$ clinopyroxene). Most have chilled margins. Only plagioclase occurs in all dykes

as phenocrysts, while the groundmass of intergranular to granular texture contains clinopyroxene, plagioclase, oxides, accessory Cu-sulphides, rarely olivine and up to 2 % biotite.

Group C - Aphyric aplites with saccharoidal texture and less than 5 % of mafic minerals.

Representatives of each of these groups (except group C) have been found in the Trallval area. A1 and A2 picrites, oriented NE-SW and about 0.1 to 0.5 m. wide, form a small swarm in Atlantic Corrie. Only one dyke, 1.0 m. wide, found on N. Trallval, belongs to group A3. Olivine and spinel phenocrysts in all dykes commonly have rounded inclusions of hydrous silicates and plagioclase (Plate 6.1), and hopper-type olivines with hollow interiors occur commonly. One dyke has an annealed, granular groundmass with poikilitic biotite plates (Plate 6.2) and is probably a slowly cooled variant of group A1, as it is emplaced, into a gabbro, parallel to the A1/A2 trend. A 0.15 m. thick dyke, which cuts all structures in the main breccia zone of the Trallval system, has the conduit texture typical of the olivine-rich breccia matrices, lacks a fine-grained groundmass and probably represents an intrusive, remobilised cumulate (Plate 6.3).

Most basalt dykes are 0.5 to 2.0 m. thick and have an intersertal texture with micro-phenocrysts of plagioclase and occasionally olivine or clinopyroxene. Some dykes have chlorite + magnetite pseudomorphs after larger phenocrysts of olivine, and quench rosettes of acicular plagioclase in the groundmass. On N. Trallval, a 1.0 m. thick dolerite dyke has about 40 % of skeletal plagioclase phenocrysts (Plate 6.4).

A particularly thick doleritic dyke (2.0 to 5.5 m. wide), runs parallel to and south of the Trallval ridge, is medium-grained in the centre, weathers to a pale-grey and has a prominent chill. In thin section, this rock has a spherulitic texture with globular masses consisting entirely of a subophitic intergrowth of clinopyroxene and plagioclase, surrounded by altered crypto-crystalline material with micro-phenocrysts of plagioclase, clinopyroxene and olivine (partly altered to iddingsite), oxides and sulphides (Plate 6.5). Because of these distinctive features, this dyke and a similar one outcropping in NW Trallval are classified together in Group D.

A poorly exposed, N-S striking, pale-weathering microdiorite hybrid dyke, 3.1 m. wide, outcrops on Ruinsival. It is composite with a coarse

eastern facies and a fine western one with a chilled margin against the peridotite. It has a hypidiomorphic texture with abundant euhedral micro-phenocrysts of orthopyroxene and a few of biotite in plates of sodic plagioclase and clinopyroxene, and interstitial patches of alkali feldspar,granophyre and quartz. Apatite is abundant and pale-green fibrous cummingtonite pseudomorphs about one out of 4 orthopyroxene crystals (Plate 6.6). This dyke is classed separately as Group E.

6.2 Mineral Chemistry of the Dykes.

McClurg (1982) gave data on the mineral chemistry for a range of dykes in each group. Her results are summarised below, followed by a presentation of mineral chemistry data on selected dykes from the Trallval area:

(1) Olivine compositions range $Fo_{83.8-79.9}$, $Fo_{77.0-72.5}$, $Fo_{92.5-83.0}$ and $Fo_{79.0-69.9}$ for groups A1, A2, A3 and B, respectively. CaO contents range 0.02 - 0.20 wt% for all groups except A3, discussed below. Maximum NiO contents range 0.49 wt% to 0.22 wt% from $Fo_{92.5}$ to $Fo_{79.9}$; some dykes have up to 0.18 wt% less NiO at a given Fo content, which McClurg (1982) attributed to depletion of the liquid in Ni by simultaneous precipitation of Ni-sulphides. The CaO contents are typical of olivines in equilibrium with a basaltic liquid.

(2) Plagioclase compositions range An_{89-85} for the phenocrysts, and groundmass compositions range An_{76-43}, which overlap with compositions from gabbros and intercumulus plagioclase from the layered series.

(3) Clinopyroxene compositions overlap with those of the cumulus pyroxene in the layered series and cover the range rom diopside to salite and subcalcic augite.

(4) Spinels fall into two groups: translucent brown Al-rich picotite and pleonaste which crystallised at high pressure and opaque, Fe^3-rich spinels which formed at low pressures according to McClurg (1982). Spinels as Cr-rich as those in the layered series are not found in the dykes, which is attributed by McClurg to a combination of the following:

(i) Crystallisation of layered series spinel with plagioclase on liquidus also, leading to an impoverishment of the liquid in in Al and consequent enrichment in Cr of the spinel.

(ii) Higher oxygen fugacity in the dyke liquid which favoured entry

of Fe^{3+} into the spinel.

(5) The Si-poor and Ti-rich nature of the kaersutite and phlogopite (5.16 to 6.15 wt% TiO_2 in the kaersutite) suggests crystallisation from a Si-poor and Ti-rich interstitial liquid prior to the crystallisation of the oxides (the Ti content of the kaersutite increases with decreasing Mg content, i.e. with fractionation).

Representative mineral analyses from dykes in the Trallval area are given in Tables 6.1 to 6.4. In view of the petrographic similarity of the Trallval area dykes to those of the Long Loch-Barkeval area (McClurg, 1982), the mineral chemistry of only a few samples was investigated; the results are summarised in Table A.3.

Sample BD1 is an A3 picrite directly comparable to sample M9 considered by McClurg (1982) as a possible parental liquid for the layered series and thus of great petrological importance. Whereas sample M9 occurs as thin, discontinuous veins 0.1 to 0.2 m. wide over an area 2 m. square, BD1 comes from a 1.0 m. thick dyke which can be traced over 100 m. This study confirms McClurg's results (1982) on mineral chemistry of this dyke type. The olivine-phyric rock probably represents a liquid as the Fe/Mg partitioning coefficient obtained by dividing the Fe/Mg ratio of the phenocrysts by that of the whole-rock analysis (section 6.3) works out at 0.34, within the crystal-liquid equilibrium range (Cawthorn et al., 1974). NiO-Fo relations for analysed dyke olivines are plotted in Fig. 6.1. The zoning of olivine in BD1 consists of a sharp decrease in Ni content followed by a more gentle decrease with more extensive evolution of the Fe/Mg ratio. This 2-stage evolution reflects the drop in pressure upon intrusion of the dyke liquid into high crustal levels (D_{Ni}^{ol-lq} increases with decreasing pressure; Mysen and Kushiro, 1979) followed by continued growth in a sulphur-undersaturated residual liquid (section 5.4.1). The presence of both Al-rich translucent spinels and opaque Fe^{3+}-rich spinels supports such a 2-stage crystallisation process. The olivine of Group D basalt BE3 also plots on the sulphur-undersaturated NiO/Fo fractionation curve, while the remobilised cumulate, BO4, plots in the field of layered series olivines. Other compositional parameters of the dyke minerals are presented in Figs. 5.4 to 5.9, which are discussed, together with those of the gabbros, in section 6.5.

6.4 The Gabbros: Petrography.

The gabbros have been classified according to their olivine and orthopyroxene content into 5 groups. The distribution, age relations and correlation with the history of the ultrabasic complex of each of these groups is summarised in Fig. 6.2. See Table 6.6 for modal analyses of representatives from each of these groups.

Group 1: Olivine-Gabbro (5 -30 % olivine, no orthopyroxene).

The major outcrops are in Atlantic Corrie, East Trallval, Glen Harris and along the eastern contact of the CS; smaller bodies form early veins in the ELS and late plugs cutting the CS, as well as a partial sheath round the intrusive peridotite plug at Papadil. Olivine is subhedral to anhedral, often forms clusters and commonly includes plagioclase $\pm$ spinel $\pm$ mica. Some alteration of the rims to chlorite, iddingsite and magnetite is common. The clinopyroxene varies from euhedral, discrete crystals to subophitic and ophitic plates with many tiny (less than 1 mm.) inclusions of olivine. The Atlantic Corrie Gabbro has a few layers with laminated cumulus clinopyroxene (sample BA1). The coarse, interpenetrating habit of the plagioclase, together with the complex zoning and twinning patterns, and the lack of a lamination distinguish gabbros from olivine-rich allivalite. Oxides are often scarce, but include at least some interstitial ilmenite (Plate 6.7). The East Trallval Gabbro has a locally developed biotite-rich facies; the biotite forms up to 5% of the rock in large ophitic plates, similar to the clinopyroxene, which it probably replaces (Plate 6.8). Accessory apatite is found in some samples.

Group 2: Transitional Cumulates. (more than 30 % olivine)

This group includes those rocks with euhedral spinel and a high modal content of apparently cumulus olivine, yet associated with discrete, strongly zoned plagioclase crystals (not forming "conduit texture", section 5.5.2), discrete clinopyroxene and sometimes orthopyroxene. Olivine displays the features typical of the ultrabasic rocks: coarser than in the olivine gabbros, it rarely includes plagioclase but commonly has chrome-spinel and spherical inclusions of hydrous silicates. In some samples (B2, B9 and FC1), the olivine has the skeletal habit typical of harrisites and proto-harrisites. Spinel enclosed in olivine also has hydrous inclusions, although these are

not found in the discrete spinels which often show signs of resorption and are partly enclosed by ilmenite. Brown mica is usually present in substantial amounts (more than 1 %) and some of the rocks are partly granulitised. Where the clinopyroxene forms poikilitic plates, these rocks are texturally transitional towards feldspathic peridotiwith an increase in olivine content. Two samples have substantial orthopyroxene (B2 and B9, Table 6.6). Both come from the matrix of ultrabasic breccia zones in the CS within a few metres of the contact with the granophyre of the Southern Mountains Complex. The large plates of orthopyroxene include resorbed olivine crystals, which it replaces and B9 is exceptionally rich in phlogopite, some of which is secondary after the clinopyroxene(Table 6.6). The intrusive feldspathic peridotite of the breccia adjacent to this transitional cumuis also rich in mica and Plate 6.11 shows a zircon crystal found in one interstitial occurrence of phlogopite. The abundant secondary orthopyroxene, hydrous minerals and the zircon all suggest extensive contamination of the breccia matrix by silicic, volatile-rich materials derived from the Southern Mountains Complex (section 7.11). Such contamination is also likely to have affected the peridotite of the CS where it intrudes the Southern Mountains Complex, as at Leac a Chaisteil. All other members of Group 2 are closely associated in space and time with Group 1 olivine gabbro (Fig. 6.2).

Group 3: Olivine - Hyperstene Gabbro. (5 to 30 % olivine and a little less than 5 % orthopyroxene)

This small group of gabbros occurs as veins and thin sheets cutting the Atlantic Corrie Gabbro. They are often closely spaced and may merge in anastomosing fashion to locally form the bulk of the outcrop. Many samples show signs of deformation and metamorphism (Plate 6.9). Orthopyroxene is strongly associated with olivine either as rims or as crystals partly enclosing the olivine and varies in habit from anhedral to subhedral; the olivine is similar to that of the olivine gabbro, although commonly more heavily altered along edges and cracks. Clinopyroxene has a subophitic habit, partly enclosing plagioclase. The tabular plagioclase is moderately zoned and may define a lamination, while anhedral, interstitial plagioclase is strongly zoned. Oxides are scarce and apatite is a common accessory phase.

Group 4: Hyperstene Gabbros. (more than 5 % orthopyroxene, little or no olivine).

Among this group are the marginal gabbro lining the contact of the ELS with the Southern Mountains Complex and a number of, probably contemporaneous, thin sheets and stocks cutting the ELS and the Atlantic Corrie Gabbro, the large body at Papadil which predates the emplacement of the CS (section 2.2.4), and some veins and thin sheets which cut the early olivine gabbro intruded along the eastern contact of the CS. The rock weathers to a lustrous, dark grey colour; euhedral to subhedral hypersthene, augite and cloudy plagioclase occur in about equal proportions. The orthopyroxene forms the largest grains and exsolves thin lamellae of clinopyroxene (Plate 6.10). Opaque oxides,mostly ilmenite, are abundant, forming both intergrowths with clinopyroxene and anhedral interstitial crystals. Olivine, when present, is often entirely pseudomorphed by iddingsite and subsidiary magnetite. Accessory biotite and apatite are ubiquitous. Some samples have a little quartz and alkali feldspar in mesostasis patches. One gabbro, sample DB1, from a sheet cutting olivine gabbro at Leac a Chaisteil (Fig. 6.2), has numerous fragments of both peridotite and troctolite, with reaction rims of orthopyroxene and amphibole around the former and clinopyroxene + opaque aggregates around the latter; the gabbro itiself has abundant large crystals of apatite (0.05 x 0.5 mm.), and much biotite.

Group 5: Ilmenite Gabbro. (more than 10 % opaques, trace of olivine, no orthopyroxene).

The largest body lies along the western fault bounding the An't Snidhe wedge of layered CS cumulates and it occurs elsewhere as thin, unchilled dykes and as thin sheets on Trallval and Barkeval. The only mafic silicate is an augite (except in a few samples which have relic, altered olivine) which is subhedral, equant, pale-green to brown (colour zoning sometimes defines hour-glass shapes within the crystal) and includes opaques; the latter are very abundant throughout the rock and dominated by ilmenite. Plagioclase is strongly zoned with a moderately zoned core and oscillatory-zoned margins. Accessories include apatite, biotite and a little sphene.

6.5 Mineral Chemistry of the Gabbros.

Mineral compositions for the gabbros in each group are given in Tables 6.1 to 6.4. The more primitive compositions overlap with the more evolved compositions of the minerals in the ultrabasic rocks as noted in section 4.1 for the field characteristics and in the previous section for the textures and petrography. McClurg (1982) reported similar evidence for the gabbros of the Long Loch - Barkeval area. While sample FC1 was classed as a gabbro in the field, its mineral chemistry indicates an ultrabasic composition and it may be considered as an intrusive allivalite.

Clinopyroxene compositions of the dykes and gabbros are plotted together with those of the ultrabasic rocks in Figs. 5.4 to 5.7. Cr_2O_3 contents of dyke pyroxenes lie on a trend defined by the peridotites and the CS allivalites and extend it to 0.15 wt% Cr_2O_3 at an Mg-number of 73. Gabbro pyroxenes have consistently lower Cr_2O_3 contents, like those of the ELS allivalites (Fig. 5.4). The Na_2O content of the pyroxene in the basic rocks follows the trend set by those in the CS peridotites and extends it to 0.35 wt% Na_2O at $Mg/Mg + Fe^2 = 0.73$ (Fig. 5.5). Together with the pyroxenes from the CS peridotites, those from the basic rocks define an evolutionary trend for the Rhum pyroxenes in the pyroxene quadrilateral (Fig 5.6). Fig. 5.7 compares this trend with those of the alkali-olivine basalt series of the Shiant Isles and the tholeiitic layered intrusions of Skaergaard and Bushveld; coexisting pyroxene compositions from the hypersthene gabbros, the microdiorite hybrid dyke and hydrous silicate inclusions in spinel and olivine (section 5.5) are also plotted in the figure and indicate a wider solvus between Ca-rich and Ca-poor pyroxene than those of the Skaergaard or Bushveld intrusions, probably due to lower P and/or higher water activity during crystallisation (Atkins, 1969). The compositions of spinels included in olivine from the picrite dyke BD1, the peridotite dyke B04 and the intrusive allivalite FC1 are plotted in Figs. 5.16 to 5.18; they are analogous to those in the CS peridotites. The kaersutite in the silicate inclusions in olivine and spinel of picrite BD1 has a similar K_2O content to that of those in the layered series, but a distinctly lower TiO_2 content (Figs. 5.10 and 5.11).

6.6 Geochemistry of the Dykes.

XRF analyses of 17 dyke samples are presented in Fig. 6.5 for major elements and Fig. 6.6 for trace elements. The technique is described in Appendix B, which also gives precision estimates determined for this study for each element analysed. The rocks are generally fresh with no petrographic evidence for hydrothermal alteration; only in some dunitic peridotites is the olivine partly serpentinised (leading to maximum "Loss On Ignition" value of 6.7 wt% due to evaporation of the volatiles). McClurg (1982) analysed a similar suite of dykes from the Barkeval - Long Loch area and concluded that:

(1) Most of the dykes are transitional basalts (less than 9 % MgO), defining a liquid line of descent controlled by fractionation of the observed phenocrysts, i.e. olivine, high-Fe spinel, plagioclase and clinopyroxene, in that order, at low pressure.

(2) Picrites (more than 9 % MgO), though few in number, form a chemically continuous series with the basalts and also contain mildly ne- and mildly hy-normative members. The more magnesian samples are direct evidence of the presence of a primitive liquid on Rhum with more than 20.5 % MgO, which McClurg (1982) identified as the parental liquid for both the dyke suite and the layered ultrabasic complex.

6.6.1 Classification.

Seven samples have more than 9 % MgO and are classed as picrites; the remaining samples have more than 5 % MgO and alkali/silica relations indicate that they from a suite of mildly alkaline (transitional) basalts (Fig. 6.3). The normative An content of the microdiorite hybrid samples averages at An 22.7, which classifies the dyke as an intermediate rock together with the Group D samples (BE3: normative An 48.2 and KB1: An 45.7), which may be called basaltic hawaiites, while all Group B samples are basalts (normative An greater than 50). In a plot of the Thornton-Tuttle Differentiation Index against silica saturation (Fig.6.4), group A and B dykes straddle the critical plane of silica undersaturation, suggesting a high-pressure origin for the suite (deeper than 25 km., O'Hara, 1968). With increasing D.I., there is a slight tendency towards silica undersaturation in groups A and B- group D and E depart strongly from this trend towards silica oversaturation.

6.6.2 Major Elements.

Major oxides are plotted against MgO in Fig. 6.5. Group A and B samples plot close to the fractionation trend established by McClurg (1982) for the suite. This trend is especially clear for the Fe plot: fractionation of olivine and Al-spinel produces a slow increase in Fe in the liquid up to 14 % MgO, followed by a sharp drop as plagioclase and clinopyroxene are fractionated. The inflection in the Ca diagram corresponds to the appearance of plagioclase at 9 % MgO and is matched in the Al plot by a levelling off of the steady increase over the five picrites. Other elements increase steadily with differentiation.

The microdiorite hybrid samples (Group E) differ markedly: relative to McClurg's (1982) fractionation trend, they are strongly enriched in Si, K, and P, slightly enriched in Mn, have similar Na contents and are strongly depleted in Fe, Ca, Al and Ti. For Group D, the discrepancies are of a similar nature but less extreme. The characteristic geochemistry of Groups D and E is attributed to contamination of picritic liquid with crustal material (section 6.6.4).

Other samples also deviate from the low-pressure liquid fractionation curve. These include the magnesian picrite BO4 (at 33.3 % MgO) which is low in Ti, P, K and Na suggesting enrichment in cumulus olivine $\pm$ spinel, supported by the high Fe content, the Fe-rich nature of its phenocryst olivine (Fo 81.0, Table 6.4) and confirmed by its cumulus texture. Sample BB6 (least magnesian basalt, at 5.4 % MgO) is high in Ca and Al and depleted in Fe, Mn and Ti as expected from its anomalously high content of plagioclase phenocrysts.

6.6.3 Trace Elements.

Abundances are plotted as ppm against wt% MgO in Fig. 6.6. The fractionation trend established for the major elements is reflected by a parallel behaviour of Sr with Ca with an inflection near 9 % MgO; the steady increase in Sc and V (which partition strongly into pyroxene, Thirlwall, 1980) with differentiation, though it is linear rather than hyperbolic, suggests that the fractionation of clinopyroxene was dominated by that of olivine and plagioclase. The decrease in Ni and Cr correlates closely with the decrease in MgO, irrespective of the distribution of MgO between phenocrysts and groundmass, indicating a strong fractionation couple between Cr-spinel

and olivine. Zn and Cu concentrations reach peaks at 7 % and 10 % MgO, respectively, suggesting saturation of the liquid in, followed by precipitation of, Cu- and then Cu-Zn-sulphides (Thirlwall, 1980; McClurg, 1982). Incompatible elements (Ba, Zr, Y, Nb, Rb, La, Ce and Nd) increase slowly with differentiation, although the increase is almost insignificant for Rb. The concentrations are low compared to other suites of mildly alkaline basalts, a characteristic shared by Tertiary lavas from Skye and Mull. It is attributed to depletion of the Upper Mantle in highly incompatible elements by the removal of a nephelinite fraction from the mantle, emplaced as swarms of lamprophyre dykes during the Permian (Thompson, 1981). Y/Zr and Ti/Zr ratios (Fig. 6.7) are fairly constant and average at 150 and 0.24, respectively, slightly higher than the values of 120 and 0.15 obtained by McClurg (1982) but nonetheless support her conclusion that the suite cutting the layered series is similar in its trace geochemistry to the transitional basalts of the Mull Plateau Group (Table 6.7). Over the range of analysed samples, K/Ba and K/Rb (only plotted for samples with more than 5 ppm Rb) are approximately constant, suggesting fractionation of either calcic plagioclase (for An greater than 75, the K/Rb coefficient of distribution exceeds unity; Philpotts and Schnetzler, 1970) or a small amount of phlogopite (Thirlwall, 1980). The former is corroborated by the mineral chemistry of plagioclase phenocrysts in sample BB6 (An 80.5), while the latter may explain the lack of Rb enrichment over the dyke suite.

The plagioclase-phyric dyke BB6 is enriched in Sr, as expected; it is also strongly depleted in Sc, V, Cu and Zn with respect to the rest of the suite, suggesting a higher degree of clinopyroxene and sulphide fractionation. The cumulus olivine-enriched sample, B04, is depleted in incompatible elements relative to picrite BD1. The microdiorite hybrid samples are strongly enriched in most incompatible elements (Ba, Rb, La, Nb, Ce and Nd), slightly enriched in Y, Zr and Zn, similar to the basalt suite in Ni, Cr and Sc content, and depleted in Sr, V and Cu; K/Ba is high (75) and Ti/Zr low (40).

6.6.4 Sr Isotope Ratios and Minor Element Patterns.

From the preceding sections, it is clear that the Group E and D dykes are anomalously enriched in many, although not all, incompatible elements which cannot have been produced by fractional crystalli-

sation of the mildly alkaline magma parental to the basalts. An alternative origin, contamination of a picrite by silicic crustal material, is suggested by the substantial interstitial alkali-feldspar, granophyre and quartz and the abundant apatite in the orthopyroxene-rich microdiorite. The replacement of orthopyroxene by cummingtonite is typical of hybrid rocks (Deer et al., 1966). The chemical heterogeneity of the microdiorite hybrid (samples KA1 and FI2 in Table 6.10 are from the same dyke) and the globular texture of the basaltic hawaiites suggest incomplete mixing of chemically contrasting melts. Cox and Clifford (1982) similarly attributed anomalous enrichment in Si, K, Rb and Ba and depletion in Mg, Fe, Ca and Ti in the Mahabaleshwar suite of basalts, after allowing for fractionation of olivine, plagioclase and clinopyroxene, to contamination of basalt by bulk melting of granitic crust.

A crude mixing model for the microdiorite involving a picrite and a leucocratic pegmatite from the amphibolite-facies Lewisian Gneiss (Tilley, 1944) in the Southern Mountains Complex is presented in Table 6.9 and compared with the microdiorite analysis. Lewisian Gneiss forms the sialic basement beneath the Inner Hebrides and consists of amphibolite-facies and granulite-facies units; it is the most likely contaminant of Tertiary magmas passing through the crust. These gneisses have characteristic Pb and Sr isotopic compositions. Thompson et al. (1982) presented a review of the minor element and Sr-isotopic compositions of the transitional lava suites of the Mull and Skye Plateau type, from which they concluded as follows:

(1) Basalts with initial Sr^{87}/Sr^{86} ratios of 0.7029 to 0.7031, considered free of isotopic contamination, i.e. of mantle isotopic composition, have normalised minor element abundances as illustrated in Fig. 6.8 A. The normalised patterns form a smooth, downward-facing curve. Depletion of strongly incompatible elements is attributed to the extraction of a very small melt fraction from the mantle during the Permian.

(2) Basalts with $(Sr^{87}/Sr^{86})_{60}$ between 0.7036 and 0.7049 contain a high fraction of Lewisian crustal Pb from a granulite-facies source and have minor element patterns (Fig. 6.8 A) characterised by a straightening to the left of Sr, with strong Ba, Rb and K peaks, Ba being more enriched than Rb relative to isotopically uncontaminated

basalts.

(3) Basalts with $(Sr^{87}/Sr^{86})_{60}$ greater than 0.7052 have a minor element composition (Fig. 6.8 A) which differs from that of the basalts with a granulite isotopic signature by greater enrichment in Rb, Th and Nb, with slightly lower enrichment in Ba. These basalts have an isotopic Pb composition contaminated by amphibolite-facies Pb.

$(Sr^{87}/Sr^{86})_{60}$ ratios for one of the basaltic hawaiites and the microdiorite hybrid from the Trallval area are presented in Table 6.8. Normalised minor element patterns have been calculated for these and a selection of the other dykes and compared with the "contamination fingerprints" of Thompson et al. (1982). The patterns for the two Lewisian Gneiss samples from the Southern Mountains Complex analysed in this study are similar to those presented by Thompson et al. (1982) for the Lewisian Gneiss from the mainland (Fig. 6.8 B). Assuming that these rocks form the crust below Rhum, and the mantle below that is of a similar composition to that below Skye and Mull, it may be concluded:

(1) Minor element patterns of Group A and B picrites and basalts show no strong Ba, Rb and K peaks and are closest to Thompson et al.'s (1982) uncontaminated lavas (Fig. 6.8 C). In comparing minor element patterns, it should be noted that Thompson et al.'s (1982) Th concentrations were determined by INAA. These authors suggest that XRF determinations, as used in this study, may yield spuriously high values at low concentrations. Note also that low-pressure fractionation of the basalts may superimpose Sr and Ti troughs on the minor element patterns, due to removal of plagioclase and oxides.

(2) Group D and E dykes show enrichment in Ba and Th, and especially in Rb and K, forming a pattern similar to that of the amphibolite-contaminated basalts of Thompson et al. (1982), see Fig. 6.8 D. The $(Sr^{87}/Sr^{86})_{60}$ ratios are high (Table 6.8), and lie on a mixing line between uncontaminated basalt and amphibolite-facies Lewisian Gneiss (see Dickin, 1981). The gabbro samples B9, DB1 and, to a lesser extent, AE8 have similar minor element patterns.

6.7 The Geochemistry of the Gabbros.

Major and trace elements are plotted against MgO in Figs. 6.9 and 6.10. Fractionation trends defined by the dyke chemistry in

Figs. 6.5 and 6.6 have been transferred directly onto the diagrams of Figs. 6.9 and 6.10. Relative to the dyke suite, the olivine gabbros have low or slightly low contents of most elements except for high Ca, Sr, Al and slightly high Si, indicating cumulus enrichment in plagioclase. The Group 4 hypersthene gabbros have a high Si, K and Rb content relative to the dyke suite; other elements are present in similar abundances. The transitional orthopyroxene- and olivine-rich cumulate B9 (at 27.4 % MgO) and the apatite-rich hypersthene gabbro DB1 (at 7 % MgO) have exceptionally high contents of Si, K, Ba, Zr, Rb, Nb, Ce, Nd and La and low Fe, Ca, Al, Ti, V and Cu; this deviant pattern is similar to that of the microdiorite hybrid dyke (see Fig. 6.8 for the minor elements), suggesting substantial contamination by crustal material (section 6.4.4). Hypersthene gabbro AE8 shows similar , though less extreme, deviations for the elements K, Ba, Rb, Ce and La, probably due to a smaller degree of contamination. The Group 5 ilmenite gabbro FD1 (at 7.8 % MgO) has much Fe, Ca, Ti, Sc and Cu relative to the dyke suite and low Si, Na, P, Mn and La, suggesting cumulus enrichment in oxides and clinopyroxene, confirmed by the petrography. Group 2 and 3 gabbros have a geochemistry similar to that of the olivine gabbros of Group 1.

6.8 The Geochemistry of the Ultrabasic Rocks.

The major element compositions of the ultrabasic breccia matrices and of the ultrabasic intrusive plugs plot in the narrow field of the peridotites and allivalites of the layered series,near a line joining plagioclase (An 84) and olivine (Fo 88), the deviation being proportional to the amount of interstitial material (Fig. 6.9). The breccia matrices have a slightly higher Al content than the plugs. Relative to the layered series and the breccia matrices, the plugs are distinctly enriched in the elements incompatible with olivine and plagioclase: mainly Na, K, Ti, P, Sc, V, Ba Rb, Zr, Y, Nb, Ce, Nd and La (Fig. 6.10). The Papadil plug samples (K7 and AH1, at 28.1 % MgO and 36.6 %) are especially high in alkalis, P and Ba, whereas the Barkeval plug (GC2, at 39.7 % MgO) has high Ti, Zr, and La. The variable enrichment in different incompatible elements of different plugs is ascribed to variable amounts of contamination by crustal material of different trace element composition. Samples GE3 (at

38.3 % MgO) and GE6 (at 24.4 % MgO) which have high contents of V, Sc, Nb and La relative to the other breccia matrices are both from later sheets of breccia cutting earlier breccias; sample GE3 has a trachytoid texture (section 3.8.2). Note that sample GE7 (at 15.5 % MgO) which is from a late vein cutting a Ruinsival System breccia zone has a composition almost identical to that of allivalite HC17 (15.7 % MgO) from the Dornabac Member. Y/Zr, Ti/Zr, K/Ba and K/Rb ratios (Fig. 6.11) for the breccia matrices and the intrusive plugs with measurable contents of these elements cluster close to the averages for the dyke suite and the gabbros, suggesting a common parental magma for the dykes, gabbros and the ultrabasic rocks.

Average values for Zr/Nb, Y/Nb and Ti/V are given in Table 6.17 for the dykes, gabbros, layered series peridotites and allivalites, ultrabasic breccias and plugs, based on all analysed samples. These ratios are all within one standard deviation of each other for the 4 classes of ultrabasic rocks and support the possibility of a common parental magma.

The data show the dykes and gabbros are co-genetic; the ratios are high compared with those of the ultrabasic rocks. The low-P phases into which Zr and Nb partition are amphibole, biotite and Fe-Ti oxides, and Zr/Nb can only increase in the liquid with evolution (Thirlwall, 1980). Y, Ti and V all partition into amphibole and clinopyroxene. The low Zr/Nb, Y/Nb and Ti/V ratios of the ultrabasic rocks may be compatible with a parental magma common with the basic rocks provided a hydrous assemblage ($\pm$ clinopyroxene and oxides) has fractionated from the liquid which gave rise to the minor intrusions but not from the magma which produced the ultrabasic rocks. The fractionation of a hydrous assemblage may have occurred at low pressure, despite the lack of hydrous cumulates in the complex, if the assemblage were removed from the cumulates during the post-depositional compaction stage (see section 7.10).

Melting and mixing of Lewisian Gneiss wall-rock, with its high Zr and low Ti and Y content (Table 6.9), with the evolving liquid will not produce the observed discrepancies.

Table 6.18 compares the Zr/Nb, Y/Nb and Ti/V ratios of the picrites with more than 20 % MgO with the average values for the dyke suite and suggests that sample BA3 is the most likely candidate for the

parental magma as, e.g., Zr/Nb ratios cannot decrease with evolution.

Table 6.10 presents 5 chromitite analyses. After recalculation of ppm Cr in terms of wt% Cr_2O_3, totals still remain low and Cr_2O_3 contents are considered unreliable as they fall well outside the calibration range of the XRF machine. All samples have high V and Zn contents but otherwise have trace element contents within the range of the layered series peridotites, except sample BD2, which is from a chromitite rim around a gabbro xenolith in peridotite (section 3.5.5) and has high contents of K, Ba, Th and La, comparable to those of gabbro. Other chromitite samples are from thin laminae which form part of the layered sequence.

6.9 Conclusions

(1) Picritic rocks are common in the Trallval area and include a thick dyke of a highly magnesian composition, which McClurg (1982) considered as representing a liquid with more than 20.5 % MgO, parental to the dyke suite and the layered ultrabasic complex.

(2) Basaltic dykes represent a mildly alkaline transitional suite which evolved by low-pressure fractionation of olivine, spinel, plagioclase and clinopyroxene, as established for the dykes of the Barkeval area by McClurg (1982).

(3) Evidence is presented which suggests that a large, composite microdiorite hybrid dyke from Ruinsival, of a type not recognised on Rhum before, represents a picritic or basaltic liquid strongly contaminated with amphibolite-facies Lewisian Gneiss.

(4) A small group of thick, late dykes from Trallval also has distinctive petrography and geochemistry and forms a group not described before, related to the picrites and basalts by a lesser amount of contamination than that postulated for the microdiorite dyke.

(5) The gabbros crystallised from magmas similar to those of the basaltic dykes: the geochemistry is related to that of the dyke suite by cumulus enrichment in plagioclase and, in some cases, by crustal contamination.

(6) The ultrabasic breccias, like the peridotites and allivalites of the layered series, are strongly depleted in incompatible elements. Trace element ratios indicate that the dykes, gabbros, layered peridotites, allivalites, ultrabasic breccias and plugs may have formed

from a common parental magma. The "trachytoid" breccia matrices of the Ruinsival system are slightly enriched in incompatible elements. This is more pronounced in the intrusive peridotites of East Trallval and the late intrusive plugs cutting the CS.

	Mol %	Wt % Minor Element Oxides							Major Element Oxides			Total
	Fo	Ni	Ca	Mn	Na	Ti	Al	Cr	Si	Fe	Mg	
phenocryst, BD1, picrite	92.3	.477	.430	.110		.010	.152	.148	40.60	7.47	50.30	99.70
Microphenocryst, BD1	85.5	.356	.325	.218		.022	.127	.112	40.14	13.58	45.13	100.01
Microphenocryst, BE3, basalt	64.8	.156	.282	.476		.000	.060		37.12	30.83	31.80	100.58
B2, Gp 2 olivine gabbro	80.5	.196	.073	.210	.010	.039	.055	.058	38.92	18.97	41.69	100.23
LB7, Gp 1 olivine gabbro	80.5	.204	.030	.257			.018		39.18	18.22	42.24	100.15
H1, olivine-hypersthene g.	68.5	.076	.049	.467			.026		37.36	28.04	34.26	100.29
FD 1, Gp 5 ilmenite gabbro	73.0	.060	.057	.494			.037		38.21	24.09	37.07	100.02

TABLE 6.1 Representative olivine analyses from the dykes and gabbros.

	Mol %	Wt % Minor Element Oxides				Wt % Major Element Oxides				Total
	An	K	Fe	Mg	Ti	Si	Ca	Na	Al	
BD1, picrite groundmass	67.6	.023	.429	.106	.106	49.91	13.97	3.69	30.64	98.88
BE3, basalt	61.0	.235	.807	.140	.075	53.76	12.12	4.29	28.16	99.60
FI2, microdiorite hybrid	38.2	.451	.330	.032	.051	58.60	7.32	7.16	25.25	99.20
B2, gp 2 olivine gabbro	60.2	.252	.405	.056	.138	51.39	12.60	4.60	29.11	98.46
LB7, olivine gabbro	72.8	.112	.364	.030	.073	49.38	15.04	3.11	31.37	99.57
H1, olivine-hypersthene g.	56.0	.272	.362	.089	.103	53.83	11.51	5.01	28.56	99.73
K8, hypersthene gabbro	64.2	.377	.382	.034	.076	53.29	12.16	3.76	30.02	100.10
FD1, Gp 5 ilmenite gabbro	72.3	.157	.423	.057	.055	49.54	14.94	3.15	31.44	99.76

TABLE 6.2 Representative plagioclase analyses from the dykes and gabbros.

CLINOPYROXENE	Cation fractions			Wt % minor element oxides						Wt% major element oxides				Total
	Ca	Mg	Fe	Cr	Na	Al	Ti	K	Mn	Si	Fe	Mg	Ca	
BE3, dolerite	41.0	40.8	18.2		.030	3.26	.905		.212	49.75	11.16	14.00	19.59	98.87
FI2, microdiorite	43.5	41.5	15.0	.010	.385	1.24	.518		.340	52.28	9.34	14.47	21.05	99.63
B2, Gp 2 olivine gabbro	43.2	45.6	11.2	.405	.436	4.67	1.13	.027	.618	49.48	6.71	15.06	21.59	99.51
LB7, olivine gabbro	45.7	45.1	9.2	.256	.514	2.76	.921	.151		51.87	5.46	15.60	22.57	100.43
H1, olivine-hypersthene g.	38.0	43.4	18.6	.013	.366	1.89	.858		.265	50.85	11.55	15.17	18.44	99.41
K8, hypersthene gabbro	44.3	43.0	12.7	.314	.360	3.79	1.30	.021	.224	48.52	7.82	14.82	21.25	98.41
FD1. Gp 5 ilmentite gabbro	44.9	41.9	13.2	.006	.427	2.70	1.11		.208	51.67	7.65	15.11	21.55	100.43
BD1, picrite	42.2	42.6	15.3		.337	1.06	.267			51.77	10.72	14.85	20.82	99.85
ORTHOPYROXENE														
BC5, olivine-hypersthene g.	1.7	80.5	17.8	.066	.029	1.21	.352		.286	54.87	11.99	30.23	.977	100.02
H1, olivine-hypersthene g.	3.3	69.7	27.0		.054	1.08	.456		.475	53.35	17.36	25.04	2.09	99.99
K8, hypersthene gabbro	2.1	71.2	26.7		.031	1.08	.382	.011		54.51	16.93	26.02	1.13	100.09
FI2, microdiorite hybrid	3.0	66.8	30.2	.038	.035	.762	.326		.543	52.85	19.35	24.07	1.50	99.48

TABLE 6.3 Representative pyroxene analyses from the dykes and gabbros.

K-FELDSPAR	Cation Fraction			Wt% Minor Element Oxides				Wt% Major Element Oxides				Total
	An	Ab	Or	Ca	Fe	Mg	Ti	Si	K	Na	Al	
FI2, microdiorite hybrid	1.1	42.2	56.7	.223	.205	.021	.019	65.81	9.84	4.82	18.62	99.56

BIOTITE	Mg number	Wt% Minor Element Oxides					Wt% Major Element Oxides					Total
		Na	Ti	Mn	Ca	F	Si	Fe	Mg	Al	K	
FI2, microdiorite hybrid	72.0	0.42	4.99	0.06	0.02	1.51	38.10	11.84	17.07	12.43	9.27	95.71
DM2, olivine gabbro	64.9	0.23	6.74	0.06		0.21	35.48	14.17	14.71	13.20	9.69	94.48
BC5, olivine-hypersthene g.	67.7	0.33	5.90	0.07		0.22	35.62	13.28	15.61	14.26	9.70	95.00

KAERSUTITE	Mg number	Wt% Minor Element Oxides			Wt% Major Element Oxides					Total
		K	Na	Ti	Si	Fe	Mg	Ca	Al	
BD1, picrite	45.6	0.09	3.07	0.57	38.62	19.53	8.77	11.88	13.18	95.71

CUMMINGTONITE	Mg number	Wt% Minor Element Oxides						Wt% Major Element Oxides			Total
		Ca	Na	Ti	Cr	Mn	Al	Si	Fe	Mg	
FI2, microdiorite hybrid	69.5	0.12	0.17	0.64	0.03	0.17	1.15	55.98	15.62	19.21	93.10

TABLE 6.4 Mica, amphibole and K-feldspar analyses from the dykes and gabbros.

Group	Sample	Oliv.	Opx.	Cpx.	Plag.	Opaques	Other
1	I9	14.9		27.7	56.7	0.7	
1	AE6	10.8		35.8	50.4	1.9	1.0 biotite
1	AG1	18.6		7.0	74.4	trace	
1	BA1	3.9		63.1	29.9	trace	
1	CB1	12.7		22.3	65.0	trace	trace biotite
1	CH1	5.5		38.2	56.3	1.0	
1	XO	9.6		19.1	71.3	trace	
2	B2	34.0	3.5	31.2	28.1	2.1	1.1 biotite
2	CH2	38.3		21.7	37.8	2.2	
2	B9	31.5	5.0	23.6	35.1	1.5	3.3 biotite
2	FC1	48.3		5.0	54.1	1.4	1.2 kaersutite
2	D3	50.5		13.7	34.9	0.9	
3	M3	12.8	3.6	35.0	48.6	trace	
3	E5	15.0	trace	22.4	61.5	1.1	
3	H1	5.6	0.2	42.9	46.5	4.7	
3	LB7	11.8	0.7	11.1	75.7	0.7	
3	DM2	13.0	0.7	19.3	62.4	2.2	2.4 biotite
4	K8		20.3	33.8	34.2	9.9	1.8 biotite
4	AD5		8.9	12.0	73.1	8.0	
4	BB1	trace	23.1	28.0	41.4	5.5	1.0 biotite
5	FD1	1.9		41.1	42.1	14.9	

TABLE 6.6 Modal analyses of selected gabbros.

	Fairy Bridge type	Preshall Mhor type	Skye Main Lava Series	Mull Plateau group	Rhum dykes Barkeval area	Rhum dykes
	Mattey et al. (1977)	Mattey et al. (1977)	Thompson et al. (1980)	Morrison et al. (1980)	McClurg (1982)	This study
Ti / Zr	160	110	70	120	120	150
Y / Zr	0.40	0.50	0.15	0.15	0.15	0.22

TABLE 6.7 Minor Element ratios of Tertiary basaltic suites from Skye, Mull and Rhum.

	Rb (ppm)	Sr (ppm)	Rb/sr	Sr^{87}/Sr^{86}	Rb^{87}/Sr^{86}	$(Sr^{87}/Sr^{86})_{60}$
BE3, dolerite	18.0	223	0.0978	0.7062	0.2829	0.7059
KA1, microdiorite	80.1	86.0	0.930	0.7087	2.691	0.7064

TABLE 6.8 Sr-isotope ratios of selected dykes from the Trallval area.

	Lewisian Gneiss		Picrite	Model	Microdiorite
	F3	HH3	BA3	BA3+HH3/2	KA1
SiO_2	62.1	74.0	43.1	58.6	59.6
Al_2O_3	18.0	14.0	9.26	11.6	10.0
FeO*	5.04	0.73	12.5	6.64	8.96
MgO	1.63	0.14	24.7	12.4	8.21
CaO	4.54	0.90	7.37	5.15	5.46
Na_2O	3.11	3.24	1.30	2.27	2.94
K_2O	3.01	5.79	0.06	2.93	2.05
TiO_2	0.69	0.08	0.88	0.48	0.66
MnO	0.06	0.01	0.18	0.10	0.20
P_2O_5	0.42	0.01	0.07	0.04	0.42
Total	98.61	99.08	99.42	100.21	98.50
Ni	19.0	6.4	1105	556	169
Zn	47.2	3.3	70	36.7	92.8
Pb	6.7	19.4	8.0	13.7	13.6
Th	24.0	0.2	0.8	0.5	1.8
Rb	62.5	144	1.1	73.0	63.0
Sr	718	576	138	357	165
Y	13.5	4.0	12.5	8.3	31.0
Zr	427	84.4	53.5	69.0	141
Nb	6.7	2.7	2.6	2.7	5.8
Cr	18.0	53.7	1891	971	233
Ce	252	17.6	2.8	10.2	63.0
Nd	76.5	8.6	3.0	5.8	34.1
Sc	4.4	0	25.7	13.0	30.2
V	84.2	9.4	217	113	138
Cu	33.7	13.7	99.6	62.3	66.5
Ba	2912	875	26.9	450	296
La	139	7.7	0	3.9	24.9

TABLE 6.9 Crude mixing model of Lewisian Gneiss and picrite. F3 is amphibolite facies gneiss, HH3 from a sheet of pegmatite cutting it. Major elements are in % and trace elements in ppm.

	BD2	GM2	HM42	GG19	CF10B
type of chromitite	2	4	1	4	3
SiO_2	18.31	11.35	20.36	25.62	39.89
Al_2O_3	23.64	22.31	15.67	30.55	6.23
Fe_2O_3	19.48	20.49	19.77	10.03	13.27
MgO	12.91	16.43	22.62	24.88	32.62
CaO	4.40	2.09	2.48	4.48	5.26
Na_2O	0.96	0.32	0.19	0.27	0.62
K_2O	0.06	0.03	0.00	-	.007
TiO_2	0.82	1.46	0.79	0.31	0.24
MnO	0.09	0.12	0.10	0.08	0.18
P_2O_5	0.01	0.01	-	-	0.01
Cr_2O_3	12.31	11.93	11.79	1.59	2.40
Total	92.99	86.53	93.77	97.82	100.31
Ni	1091	1125	1866	1426	1909
Zn	234	250	229	162	81.3
Pb	10.2	11.3	11.0	7.5	9.3
Th	3.2	-	-	0.8	1.6
Rb	2.2	-	-	0.1	1.2
Sr	84.3	44.1	41.3	137	83.9
Y	3.7	3.2	3.0	3.5	3.5
Zr	12.4	12.5	5.3	10.3	2.2
Nb	2.7	2.5	1.9	2.2	0.9
Cr	84164	81570	80732	10894	16371
Ce	2.3	-	1.3	-	-
Nd	3.2	-	1.1	-	-
Sc	13.2	10.4	7.9	5.6	11.6
V	658	1050	851	205	164
Cu	19.0	30.9	1432	28.7	83.8
Ba	61.7	29.6	35.2	26.3	26.3
La	-	-	-	1.5	-

TABLE 6.10 Major and trace element analyses of chromitites.

Group	B	D	B	D	B	B	B	E	B	E	A	A	A	A	A
	BB6	BE3	CH3	KB1	AC2	KA2	H8	KA1	G3	FI2	QQ2	H2	BA3	BD1	B04
SiO_2	46.26	49.37	46.30	50.71	46.47	45.49	46.98	59.58	47.13	59.30	45.56	46.38	43.10	42.01	39.94
Al_2O_3	19.11	14.11	15.22	14.70	14.26	14.70	15.64	10.00	15.00	7.00	15.00	14.67	9.26	6.32	5.93
Fe_2O_3	10.31	14.04	14.66	11.94	12.79	13.03	12.82	8.96	13.11	9.71	12.85	12.37	12.54	11.32	16.48
MgO	5.44	6.11	6.25	6.49	7.66	7.90	8.08	8.21	9.92	10.06	10.91	11.21	24.67	33.09	33.29
CaO	11.69	10.52	12.01	1041	11.83	12.08	11.91	5.46	11.09	7.22	11.89	12.07	7.37	4.93	3.12
Na_2O	2.80	2.95	2.89	3.40	2.77	2.79	2.95	2.94	2.68	1.93	2.07	2.05	1.30	.698	.506
K_2O	.189	.682	.220	.203	.197	.165	.157	2.05	.256	2.08	.041	.092	.060	.052	.022
TiO_2	1.54	1.67	2.06	1.79	1.84	3.25	1.93	.657	2.05	.679	1.42	1.07	.877	.564	.166
MnO	.137	.224	.216	.179	.198	.157	.187	.204	.185	.265	.192	.173	.175	.153	.199
P_2O_5	.107	.182	.100	.198	.146	.006	.172	.422	.221	.530	.077	.015	.066	.044	.012
Total	99.08	99.88	99.92	100.05	99.16	99.46	100.83	99.49	99.76	99.72	100.00	100.09	99.41	99.18	99.68
CIPW NORMS (wt% Fe_2O_3 / FeO = Fe_2O_3 = 0.180)															
Q	-	-	-	-	-	-	-	10.66	-	1.70	-	1.49	-	-	-
Or	1.12	4.02	-	1.18	-	1.01	.945	12.11	1.48	12.06	.236	.532	.355	.295	.118
Ab	23.69	24.96	22.68	28.77	23.35	19.00	21.24	24.88	17.30	.5.99	16.88	-	10.68	5.92	4.32
An	39.01	23.25	28.56	24.26	26.25	27.08	28.96	8.04	27.05	4.21	31.52	39.76	19.25	13.96	13.83
Ne	-	-	.959	-	-	2.50	2.02	-	2.45	-	.345	-	.172	-	-
Cpx Wo	7.63	11.66	12.68	10.89	13.02	13.67	12.12	6.81	10.21	11.71	11.25	8.35	7.04	4.28	.660
Cpx En	4.14	5.74	5.28	5.97	7.37	8.36	7.00	4.24	6.27	7.52	6.99	5.23	5.16	3.29	.480
Cpx Fs	3.22	5.70	6.15	4.52	5.11	4.67	4.56	2.16	3.36	3.41	3.60	2.61	1.21	.536	.119
Opx En	.053	4.82	-	7.68	.294	-	-	16.21	-	17.04	-	22.69	-	2.03	2.57
Opx Fs	.041	4.78	-	5.81	.204	-	-	8.26	-	7.73	-	11.32	-	.331	.637
Fo	6.56	3.27	6.51	1.76	8.00	8.00	9.20	-	12.26	-	14.15	-	39.44	54.02	55.96
Fa	5.62	3.58	7.02	1.47	6.12	4.99	6.60	-	7.26	-	8.03	-	10.23	9.70	15.31
Mt	2.47	3.36	3.51	2.86	3.06	3.12	3.07	2.14	3.01	2.28	3.07	2.96	3.00	2.71	3.94
Ilm	2.93	3.17	3.91	3.40	3.50	6.17	3.67	1.25	3.74	1.27	3.70	2.03	1.67	1.06	.323
Ap	.255	.417	.232	.463	.348	.023	.394	.973	.487	1.02	.185	.046	.162	.093	.023

TABLE 6.11 Major element analyses of the dykes (in wt%).

	BB6	BE3	CH3	KB1	AC2	KA2	H8	KA1	G3	FI2	DQ2	H2	BA3	BD1	B04
Ni	75.5	53.1	52.8	101	129	212	111	169	150	184	264	242	1105	1754	1587
Zn	64.6	88.1	79.0	82.3	81.2	54.7	82.1	92.8	69.9	95.4	72.7	64.6	70.0	59.1	92.5
Pb	9.7	6.7	9.7	8.6	8.5	6.8	10.1	13.6	6.0	10.6	10.1	8.7	8.0	6.0	7.2
Th	1.0	2.3	1.8	-	1.5	1.2	-	1.8	-	3.3	-	-	0.8	0.9	1.6
Rb	4.6	18.5	1.5	0.5	2.2	1.5	2.4	63.0	2.4	80.1	1.2	0.5	1.1	2.9	1.1
Sr	347	217	327	262	240	27.9	289	165	344	86.0	197	219	138	79.2	101
Y	17.L	37.9	23.4	30.0	23.5	15.2	23.5	31.0	23.1	40.6	18.6	10.7	12.5	8.7	2.6
Zr	82.6	123	52.8	114	116	47.8	122	141	55.7	172	45.1	15.7	53.5	29.2	4.1
Nb	3.6	5.2	3.5	5.6	3.4	3.1	3.2	5.8	3.6	6.8	2.7	1.6	2.6	0.8	0.4
Cr	119	102	923	228	307	189	220	233	233	259	450	640	1891	2618	2410
Ce	10.5	20.5	5.5	35.1	9.3	0.7	11.4	63.3	15.9	70.4	-	-	2.8	0.1	-
Nd	8.9	12.9	8.8	22.2	9.9	2.7	11.8	34.0	13.6	42.2	3.0	0.4	3.0	2.2	-
Sc	30.2	46.1	39.7	33.3	41.0	40.0	37.5	29.5	35.9	38.7	35.7	40.5	25.7	17.0	7.4
V	356	400	464	389	430	722	466	138	386	153	364	384	217	157	57.9
Cu	70.0	136	80.9	76.3	161	181	163	66.5	89.2	59.1	154	201	99.6	66.2	239
Ba	66.9	281	149	259	21.6	64.6	24.6	296	183	256	19.9	54.9	26.9	21.2	31.2
La	1.3	11.0	2.3	13.8	3.5	-	3.2	24.9	8.2	27.2	1.3	-	-	1.9	0.1
Zr/Nb	23	24	15	20	34	16	38	34	33	35	17	10	31	36	10
Y/Nb	4.7	7.3	6.6	5.4	7.1	4.8	7.5	5.3	8.8	6.0	7.0	6.9	5.0	11	6.5
Ti/V	25.9	25.0	26.5	27.5	25.6	27.0	25.9	28.6	31.9	26.6	23.4	16.7	24.2	21.5	17.2

TABLE 6.12 Trace element analyses of the dykes (in ppm), and selected trace element ratios.

Group	DB1 4	X6 3	FD1 5	XO 1	AE8 4	DM2 3	AE6 3	BE2 3	CH1 1	K8 4	F6 1	X9 1	I9 1	FC1 2	CH2 2	B2 2	B9 2
SiO_2	65.30	49.04	44.48	49.42	51.81	48.79	46.65	52.12	48.42	49.65	49.36	44.39	47.09	42.70	42.90	43.70	45.95
Al_2O_3	13.96	15.88	13.47	18.44	15.10	18.41	14.80	16.73	16.16	13.40	12.71	20.18	16.74	18.28	8.71	8.16	7.54
Fe_2O_3	9.45	10.77	14.80	5.86	9.08	8.17	13.07	6.28	7.20	12.08	7.36	7.77	5.97	7.76	15.92	14.59	10.63
MgO	7.02	7.48	7.81	8.62	8.84	9.09	9.70	9.87	10.49	10.74	11.88	13.14	14.28	17.43	23.99	25.23	27.44
CaO	7.41	11.40	14.35	15.81	11.48	11.20	12.31	11.92	14.48	12.11	15.48	12.10	14.28	10.06	7.27	6.91	4.78
Na_2O	2.85	2.74	1.91	1.82	2.52	2.62	2.24	2.53	2.01	2.13	1.62	1.32	1.13	0.98	1.19	0.86	1.25
K_2O	1.32	0.42	0.14	0.05	0.45	0.27	0.18	0.18	0.07	0.22	0.16	0.05	0.05	0.11	0.10	0.11	0.51
TiO_2	1.31	1.42	2.99	0.61	0.96	0.83	1.68	0.46	0.59	1.43	0.28	0.30	0.25	0.32	1.05	0.48	0.66
MnO	0.15	0.17	0.17	0.10	0.16	0.12	0.19	0.11	0.10	0.16	0.16	0.11	0.11	0.11	0.20	0.16	0.16
P_2O_5	0.13	0.13	0.01	0.02	0.06	0.07	0.04	0.01	0.01	0.05	0.02	0.02	0.01	0.02	0.06	0.02	0.06
Total	97.89	99.43	100.14	100.74	100.45	99.57	100.85	100.22	99.53	101.99	99.05	99.91	99.90	97.77	101.38	100.26	98.97
CIPW NORMS (Fe_2O_3 / FeO + Fe_2O_3 = 0.180)																	
Q	5.35	-	-	-	-	-	-	-	-	-	-	-	-	-	-	-	-
Or	7.80	2.49	-	.295	2.69	1.60	1.06	.768	.414	1.30	.945	.284	.295	.650	.591		3.04
Ab	24.12	23.19	12.51	15.40	21.32	22.17	18.16	21.83	16.50	18.02	13.71	11.14	9.56	-	-		10.54
An	21.40	29.77	28.18	42.00	28.59	37.68	29.80	35.76	34.87	26.36	26.94	49.02	40.46	49.55	23.47		13.47
Ne	-	-	1.98	-	-	-	.429	-	.278	-	-	-	-	-	-		-
Cpx Wo	6.06	10.84	17.93	15.16	11.68	7.28	12.95	9.93	15.41	13.95	20.76	4.55	12.66	.093	5.10		4.11
Cpx En	3.67	6.40	10.07	10.66	7.59	4.83	7.80	6.92	10.75	8.80	14.58	3.23	9.47	.069	3.57		3.12
Cpx Fs	2.07	3.90	7.13	3.21	3.41	1.92	4.46	2.19	3.37	4.28	4.43	.924	1.93	.015	1.10		.567
Opx En	13.82	4.71	-	2.30	12.89	4.54	-	13.45	-	7.90	1.93	1.26	2.12	16.34	17.17		13.08
Opx Fs	7.79	2.87	-	.692	5.86	1.81	-	4.25	-	3.86	.585	.360	.433	3.51	5.30		2.38
Fo	-	5.27	6.58	5.97	1.14	9.30	11.47	1.66	10.77	7.04	9.17	19.80	16.80	18.92	27.34		36.53
Fa	-	3.54	5.14	1.98	.569	4.08	7.23	.578	3.72	3.78	3.07	6.25	3.78	4.48	9.31		7.32
Mt	2.26	2.58	3.54	1.40	2.17	1.95	3.13	1.50	1.73	2.89	1.76	1.86	1.43	1.86	3.81		2.54
Ilm	2.49	2.70	5.68	1.16	1.82	1.58	3.19	.931	1.12	2.72	.532	.570	.418	.608	1.99		1.25
Ap	.301	.292	.023	.046	.139	.162	.093	.046	.023	.116	.046	.037	.023	.046	.139		.139

TABLE 6.13 Major element analyses of the gabbros and CIPW norms.

	DB1	X6	FD1	XO	AE8	DM2	AE6	BE2	CH1	K8	F6	X9	I9	FC1	CH2	B2	B9
Ni	168	121	324	123	124	253	307	132	284	174	218	376	410	516	979	1006	1403
Zn	76.7	68.0	60.2	22.3	62.1	44.9	67.1	31.5	30.1	69.2	43.5	38.5	26.8	36.2	96.5	82.7	69.3
Pb	15.9	7,8	9.9	7.4	9.1	7.4	6.5	8.0	9.2	6.4	6.9	5.2	10.8	10.0	6.8	7.5	10.0
Th	2.5	-	0.2	-	0.9	0.4	-	1.1	0.3	1.1	-	-	-	0.6	0.7	-	-
Rb	37.4	7.0	3.3	1.3	9.9	5.1	3.0	3.2	2.1	6.0	4.2	1.1	1.5	4.0	1.9	2.0	15.9
Sr	256	245	261	283	228	233	246	291	276	221	188	261	231	229	176	133	113
Y	2319	21.8	18.7	9.4	19.5	13.5	15.6	7.8	8.5	18.0	10.0	6.7	4.8	6.5	9.4	6.6	13.2
Zr	150	129	68.5	18.1	79.6	51.1	57.5	10.9	13.6	46.5	17.5	15.5	6.5	23.4	32.9	24.8	80.6
Nb	6.1	4.1	3.4	0.7	3.3	2.2	2.7	0.3	0.6	1.7	1.7	1.7	1.1	2.5	2.3	1.7	3.6
Cr	380	266	660	714	259	528	358	501	527	332	849	431	694	731	1599	1458	2305
Ce	39.9	18.2	4.0	1.3	16.7	10.9	-	0.1	0.6	5.5	2.4	0.7	-	2.4	-	-	18.0
Nd	21.9	12.3	6.7	2.9	10.3	7.4	3.0	1.8	3.2	4.6	1.6	2.5	1.1	3.8	0.7	-	8.6
Sc	27.5	34.7	58.3	49.3	41.9	21.4	40.5	31.7	48.7	49.5	55.3	13.9	33.0	7.0	23.6	21.4	17.7
V	254	315	775	231	289	170	441	143	197	503	195	80.6	94.1	61.8	228	133	143
Cu	113	140	436	33.4	74.6	144	160	62.8	140	204	9.9	80.0	43.2	81.4	125	110	57.3
Ba	343	116	5417	25.1	168	109	51.0	66.2	25.3	70.9	94.8	20.3	19.9	26.1	62.2	52.9	165
La	17.2	7.2	-	-	4.0	5.0	0.1	-	-	0.2	0.9	-	-	-	2.0	3.4	9.7
Zr/Nb	25	31	20	26	24	23	21	36	22	27	10	9.1	5.8	9.4	14	15	22
Y/Nb	3.9	5.3	5.5	13	5.9	6.1	5.8	26	14	11	5.9	3.9	4.4	2.6	4.1	3.9	3.7
Ti/V	30.9	27.0	23.1	15.8	19.9	29.3	22.9	18.0	18.0	17.0	8.6	22.3	15.9	31.1	27.6	21.7	27.7

TABLE 6.14 Trace element analyses of the gabbros and selected element ratios.

	Layered series peridotites										layered series allivalites					breccia matrix
	AG7	CF4	CF15	CF112	FG1	GG9	HC4	HC11	HM41	HK4	DE5	BL1	HG17	HM1	HH2	GE7
Ni	3009	3105	1963	1140	1372	1375	2072	1737	2140	2273	263	227	484	258	260	580
Zn	55.4	77.4	62.2	65.7	99.7	92.7	77.3	68.5	56.1	76.7	38.9	9.4	27.4	12.6	16.2	34.2
Pb	6.0	12.2	7.5	7.2	13.6	7.7	10.8	6.9	7.2	7.8	6.8	8.3	7.0	6.6	6.3	6.3
Th	1.3	o.4	o.3	-	-	-	-	-	-	0.3	0.9	0.5	-	0.4	-	-
Rb	0.7	1.6	0.9	-	1.0	1.7	2.4	0.5	0.3	0.3	1.9	0.8	-	0.5	-	0.5
Sr	11.9	68.7	98.2	75.0	107	98.8	67.7	70.8	85.8	8.9	299	448	273	204	369	260
Y	1.6	3.4	3.6	3.6	2.6	5.0	4.7	3.6	2.5	4.5	2.7	3.0	4.3	6.2	2.9	5.6
Zr	2.0	4.5	3.6	2.4	3.7	10.4	16.3	6.3	6.6	8.2	3.8	4.1	9.1	8.8	6.3	11.0
Nb	1.3	1.1	0.6	0.6	0.9	1.1	1.8	2.5	1.9	1.5	1.7	1.4	1.4	1.2	1.0	1.1
Cr	4078	2556	6047	2076	1880	2430	3323	3108	4478	6928	17697	286	500	2290	264	935
Ce	-	-	-	-	-	-	2.2	-	1.3	1.3	4.0	0.3	0.2	2.4	2.0	-
Nd	-	-	-	-	-	-	-	-	1.1	1.9	2.8	1.7	0.7	2.3	1.4	1.2
Sc	7.5	12.7	13.4	23.1	7.9	143	9.7	14.6	6.8	18.1	3.6	4.5	13.9	38.4	-	29.2
V	45.2	74.8	102	74.1	59.4	100	60.3	66.7	44.5	153	202	21.4	49.5	118	5.7	97.6
Cu	11.1	38.7	65.9	123	49.8	49.9	42.9	287	740	74.9	127	173	279	19.0	9.0	51.1
Ba	27.1	31.3	29.7	15.3	29.8	46.0	49.7	33.9	22.7	20.0	22.6	24.3	22.1	14.9	24.6	21.1
La	-	-	2.8	-	-	0.7	1.2	-	-	0.9	-	-	-	-	-	-
	CS RG1	ELS U10	ELS U10	CS DM	CS LLG1	CS DM	CS LLG1	CS DM	ELS U12	ELS U14	ELS U10	ELS U9	CS DM	ELS U14	CS LLG1	Ruinsival
Zr/Nb	1.5	4.1	6.0	4.0	4.1	9.5	9.1	2.5	3.5	5.5	2.2	2.9	6.5	7.3	6.3	10.0
Y/Nb	1.2	3.1	6.0	6.0	2.9	4.5	2.6	1.4	1.3	3.0	1.6	2.1	3.1	5.2	2.0	5.1
Ti/V	14.6	15.2	12.4	14.6	16.1	18.6	17.9	16.2	10.8	12.2	10.1	39.2	16.9	15.8	7.7	20.3

TABLE 6.15 Trace element analyses of the ultrabasic rocks and selected element ratios.

	ultrabasic breccia matrices								intrusive peridotites								
	DK2	GE6	AG81	DN1	DK1	DN2	GE3	DG4	K7	BF1*	GF1	FG16	FI4	DQ1*	DH1	AH1	GC2
Ni	663	1057	1393	1202	1221	1838	1868	1923	1183	1050	1562	1734	1651	1452	1840	1605	2373
Zn	50.6	59.6	61.5	62.7	7.3	64.5	83.5	61.1	65.2	84.8	54.8	49.6	69.7	75.6	65.6	74.1	58.9
Pb	6.6	6.9	10.3	6.5	9.8	7.5	6.7	8.8	8.8	6.2	6.9	6.8	6.9	7.0	10.8	5.3	7.8
Th	-	1.1	1.9	-	1.7	-	-	3.7	-	2.3	-	0.6	0.2	-	1.3	0.8	1.0
Rb	-	2.6	1.0	0.9	-	0.1	0.3	1.2	3.2	3.9	1.3	1.8	2.4	0.2	0.5	2.2	1.4
Sr	210	172	219	130	115	68.8	53.4	56.7	245	86.7	111	118	85.9	92.5	78.2	112	44.6
Y	4.5	5.4	2.4	3.4	2.0	2.0	4.1	2.3	5.9	6.6	5.3	5.6	7.3	5.8	3.6	5.4	4.6
Zr	2.8	12.2	3.9	3.1	2.4	0.9	6.4	-	17.0	10.8	12.8	10.6	29.9	9.9	7.9	10.9	16.8
Nb	1.2	2.4	1.6	0.9	1.4	1.5	1.7	0.7	2.0	0.9	2.5	1.8	2.3	1.7	0.8	1.4	1.8
Cr	998	1918	1459	1982	2102	2762	3229	2880	2072	1248	2845	2558	2192	2401	2248	2561	3256
Ce	-	-	-	-	-	-	-	-	-	-	-	3.1	3.3	-	-	-	0.1
Nd	-	-	-	-	-	-	-	-	0.1	-	-	-	0.9	-	-	-	0.8
Sc	17.0	25.7	6.6	15.4	8.7	8.6	11.0	8.0	11.2	18.4	13.8	14.1	11.7	19.1	11.5	11.4	11.6
V	72.2	138	43.4	66.1	54.4	52.2	92.7	41.7	76.7	130	83.7	75.3	111	104	75.1	76.7	74.0
Cu	76.4	128	50.0	75.5	29.1	106	154	52.6	20.9	188	57.7	37.8	35.7	93.7	45.7	20.8	43.8
Ba	15.1	25.6	38.6	22.7	23.2	24.3	22.8	24.9	100	33.4	25.4	27.0	34.1	19.9	19.6	77.2	26.2
La	-	5.6	-	-	-	-	3.2	-	0.2	2.2	o.4	-	4.0	-	-	-	1.7
	Ruinsival System (RS)			Trallv. RS System		TS	RS	Papad. System	P	*	B	S	P	*	R	P	B
Zr/NB	2.3	5.1	1.6	3.4	1.7	0.6	3.8	-	8.5	12.0	5.1	5.9	13.0	5.8	9.9	7.8	9.3
Y/Nb	3.8	2.3	1.5	3.8	1.5	1.3	2.4	3.3	3.0	7.3	2.1	3.1	3.2	3.4	4.5	3.9	2.6
Ti/V	19.1	17,8	22.1	17.3	16.5	13.7	14.2	14.4	24.3	15.7	17.3	19.1	24.9	16.7	20.0	21.1	21.1

TABLE 6.15 (Ctd.) Trace element analyses of ultrabasic rocks. * = the intrusive (into gabbro) peridotites of East Trallval (see section 3.4.1)- all other intrusive peridotites analysed are vertical plugs cutting the CS: P = Papadil plug, S = Seagull plug, B = Barkeval plug, R = Ruinsival plug.

	AG7	CF4	CF15	CF112	FG1	GG9	HC4	HC11	HM41	HK4	DE5	BL1	FG4	HC17	HM1	HH2	GE7
SiO_2	39.76	41.60	41.56	42.28	39.96	41.30	40.70	40.17	39.51	38.82	42.16	47.56	45.17	43.94	47.41	45.31	45.99
Al_2O_3	1.22	4.78	6.78	6.69	6.89	5.51	5.20	4.66	7.61	1.18	28.36	28.63	21.63	18.80	17.51	27.32	16.48
Fe_2O_3	11.58	13.58	11.42	13.46	15.16	14.99	12.92	12.95	11.41	14.38	5.00	3.07	5.53	7.53	4.36	3.79	7.43
MgO	46.62	36.72	34.65	29.50	32.03	32.65	36.89	35.41	34.94	39.94	5.34	4.00	12.16	15.75	11.64	8.77	15.51
CaO	0.48	3.47	4.25	6.62	3.71	4.11	3.05	3.75	3.96	2.71	14.03	14.87	12.87	11.22	16.94	13.89	12.27
Na_2O	.01	.40	.74	.53	.76	.45	.32	.25	.29	-	1.58	2.16	1.49	1.14	.94	1.25	1.51
K_2O	-	.03	.011	-	.026	.046	.070	.025	-	-	.017	.059	.068	.025	.012	.016	.01
TiO_2	.11	.19	.21	.18	.16	.31	.18	.18	.08	.31	.34	.14	.17	.14	.31	.06	.33
MnO	.15	.18	.14	.19	.20	.21	.17	.18	.14	.18	.01	.05	.08	.11	.07	.06	.12
P_2O_5	.004	.011	.012	.010	.005	.011	.009	.009	.019	.008	.012	.006	.009	.003	.002	.001	.010
Total	99.92	100.95	99.78	99.44	98.90	99.57	99.51	97.47	97.95	97.50	98.86	100.55	99.17	98.65	99.18	100.45	99.65

	DK2	GE6	AG81	DN1	DK1	DN2	GE3	DG4	K7	BF1	GF1	FG16	FI4	DQ1	DH1	AH1	GC2
SiO_2	44.17	43.00	42.61	42.12	41.01	39.09	39.86	40.84	41.76	41.50	40.75	41.23	39.17	41.23	40.97	41.48	39.29
Al_2O_3	15.13	9.75	13.42	9.93	8.60	5.87	2.97	5.77	10.48	7.12	7.62	7.61	5.24	6.65	5.59	6.00	3.33
Fe_2O_3	9.26	12.65	10.85	12.19	13.57	12.90	15.44	11.51	11.42	15.51	10.94	9.49	13.01	14.31	13.29	13.81	11.35
MgO	19.86	24.40	26.53	28.67	31.42	35.29	38.33	39.01	28.09	28.34	30.30	32.10	33.25	31.18	36.00	36.62	39.69
CaO	10.17	8.40	6.46	6.62	5.02	3.57	2.56	3.12	5.73	5.89	5.53	5.78	3.27	5.58	3.94	3.17	2.54
Na_2O	1.21	1.01	1.06	.62	.53	.28	.21	.27	.94	.74	.70	.56	.80	.56	.51	.68	.21
K_2O	.01	.02	.08	.01	-	-	-	.01	.12	.06	.02	.02	.10	-	-	.06	.02
TiO_2	.23	.41	.16	.19	.15	.12	.22	.10	.31	.34	.24	.24	.46	.29	.25	.27	.26
MnO	.12	.16	.15	.17	.18	.16	.21	.16	.15	.22	.15	.13	.18	.20	.18	.18	.16
P_2O_5	.01	-	.01	.01	-	.01	.01	.01	.06	.02	.01	.01	.05	.01	.02	.03	.01
Total	100.17	99.80	101.3	100.51	100.47	97.27	99.82	100.88	99.05	99.75	96.26	97.17	95.52	100.02	100.73	101.3	96.86

TABLE 6.16 Major element analyses of the ultrabasic rocks.

	Zr / Nb			Y / Nb			Ti / V		
	Average	standard deviation	N	Average	standard deviation	N	Average	standard deviation	N
Dykes	22.3	± 8.2	15	6.7	± 1.6	15	24.8	± 3.8	15
Gabbros	19.0	± 7.3	16	6.2	± 3.4	16	22.4	± 6.1	16
Layered Series peridotite	5.0	± 2.5	10	3.2	± 1.7	10	14.9	± 2.4	10
Layered Series allivalite	5.0	± 2.1	5	3.0	± 1.2	5	18.5	± 10.3	6
Ultrabasic breccias	2.6	± 1.4	7	2.5	± 1.0	8	16.9	± 2.7	8
Ultrabasic plugs	8.6	± 2.6	9	3.7	± 1.4	9	20.0	± 3.0	9

TABLE 6.17 A comparison of selected trace and minor element ratios for the major rock types in the Trallval area. N gives the number of samples.

Group	Sample	Wt% MgO	Zr/Nb	Y/Nb	Ti/V
A2	BA3	24.7	21	5.0	24.2
A3	BD1	33.1	36	11	21.5
A4	BO4	33.3	10	6.5	17.2

TABLE 6.18 A comparison of selected trace and minor element ratios between the 3 highly magnesian dykes (more than 20 % MgO) analysed from the Trallval area.

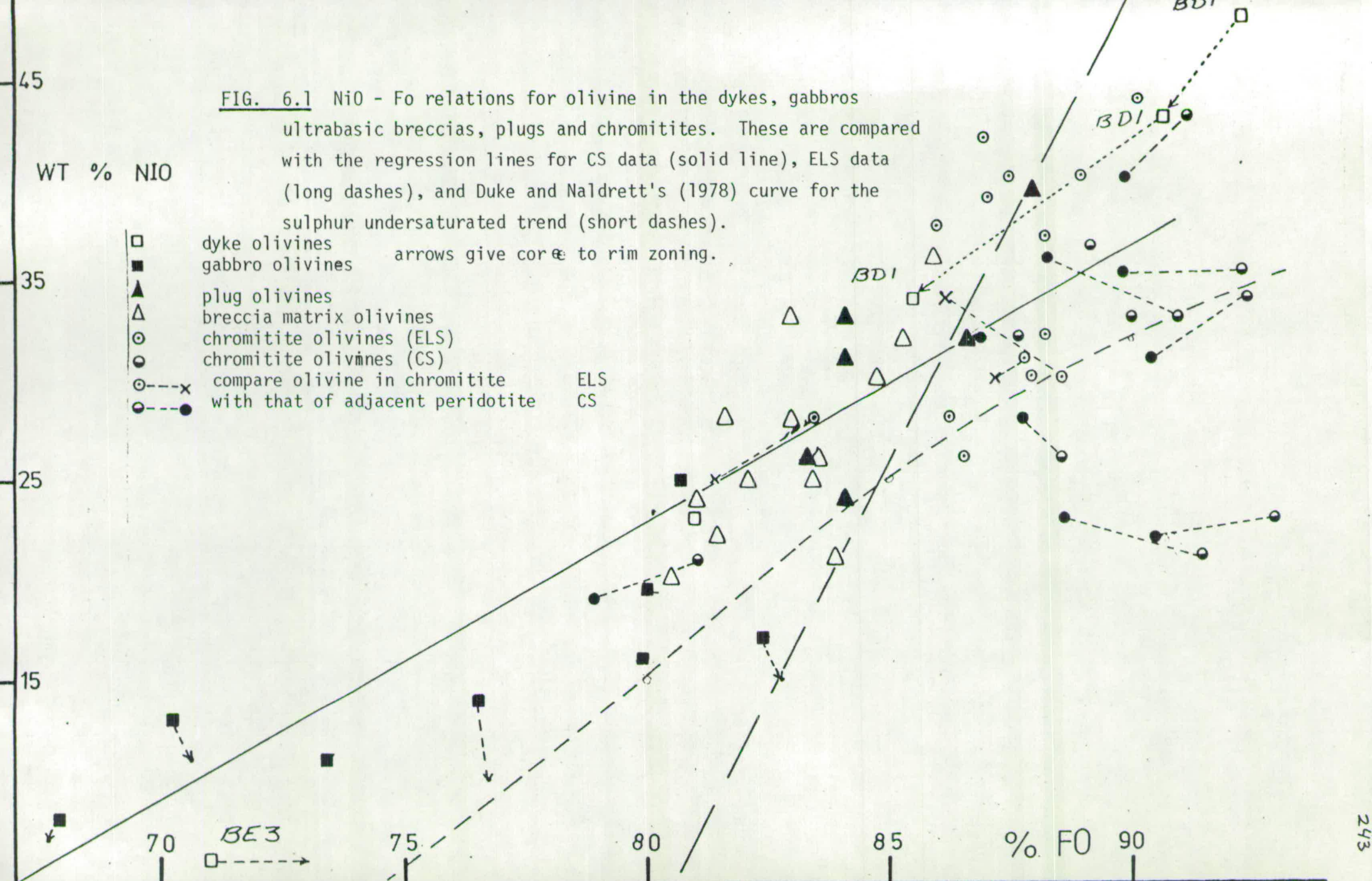

FIG. 6.1 NiO - Fo relations for olivine in the dykes, gabbros ultrabasic breccias, plugs and chromitites. These are compared with the regression lines for CS data (solid line), ELS data (long dashes), and Duke and Naldrett's (1978) curve for the sulphur undersaturated trend (short dashes).

arrows give core to rim zoning.

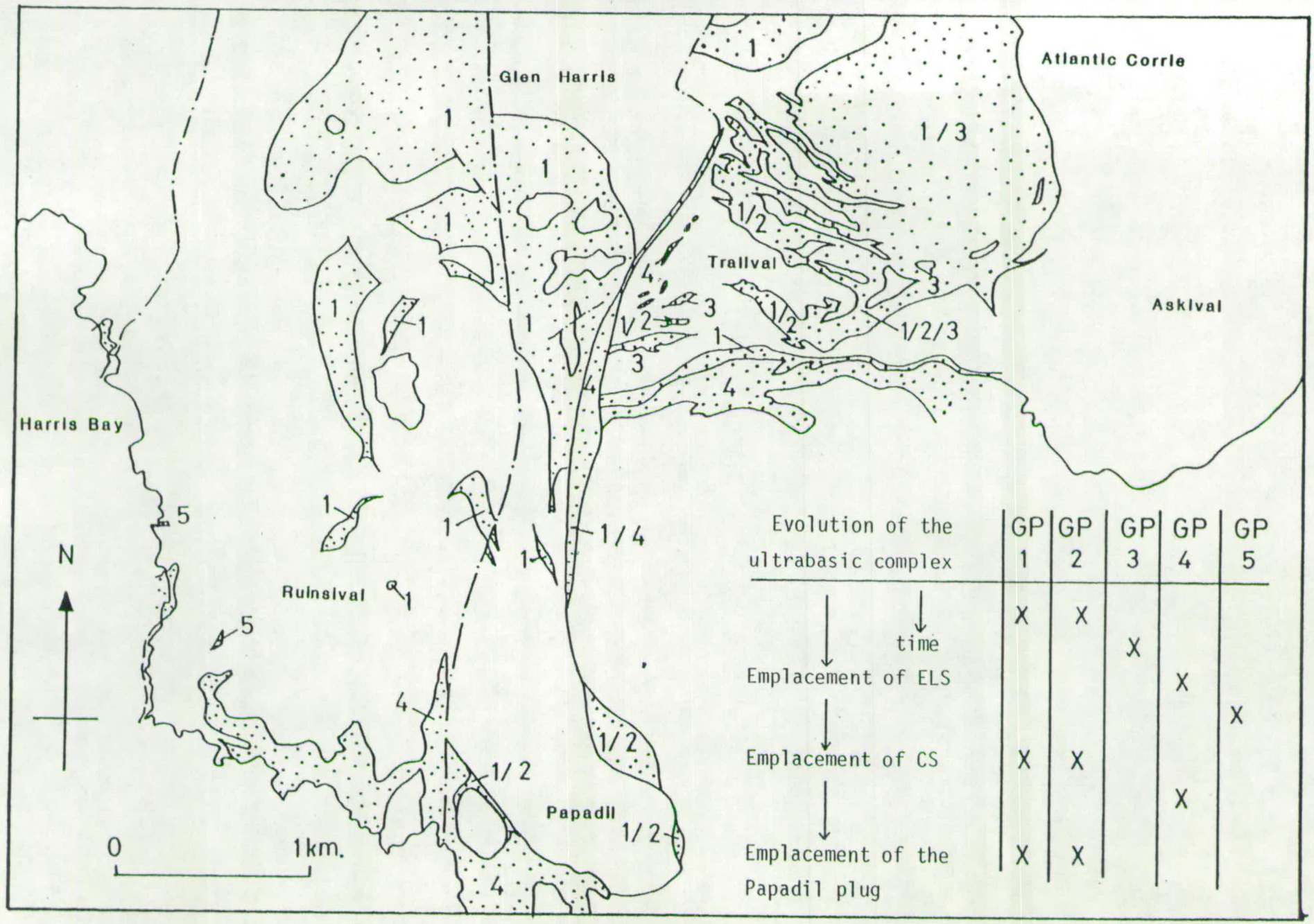

FIG. 6.2 The distribution of gabbro groups 1→5 and their age relationships.

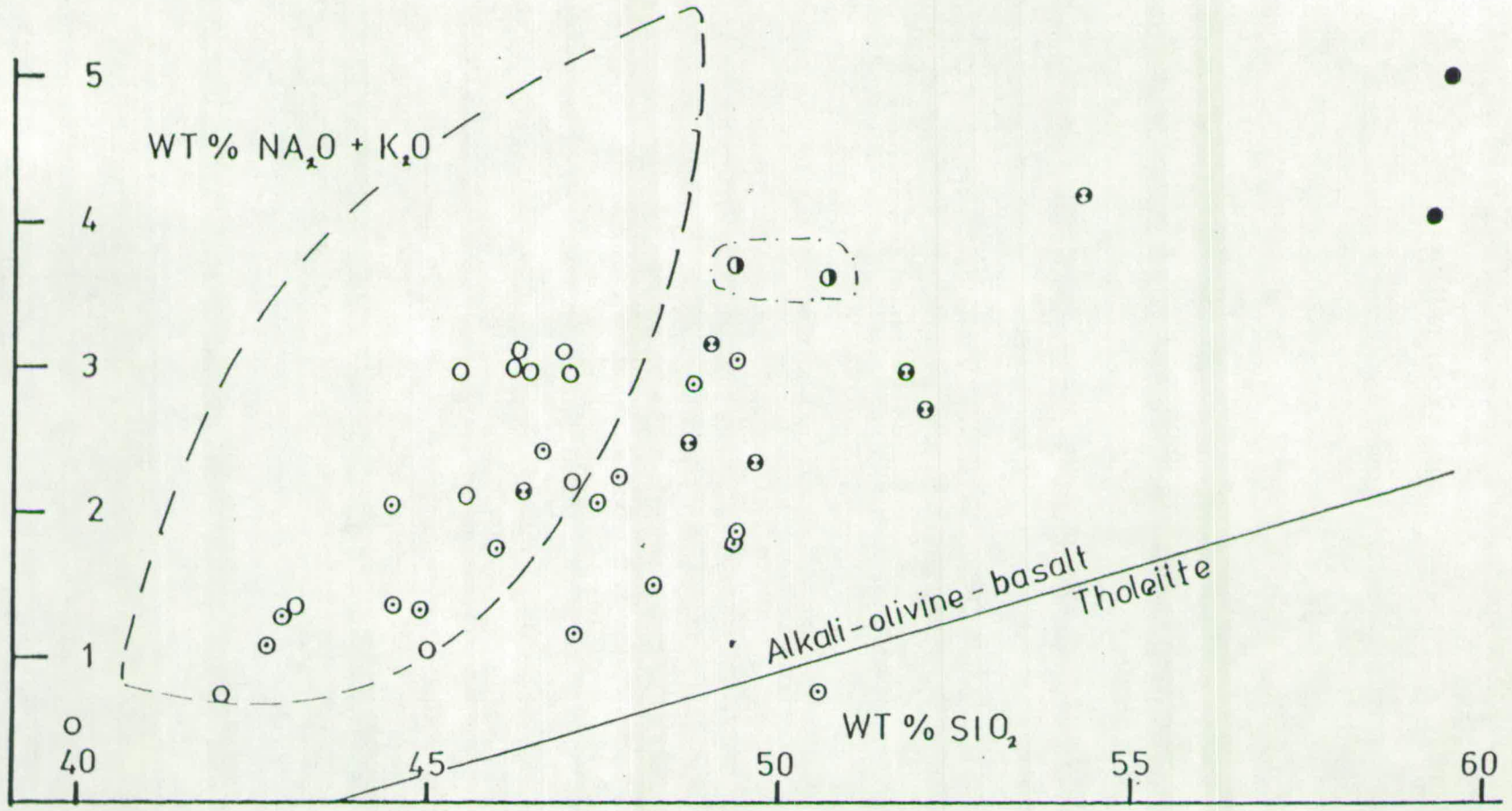

FIG 6.3 Alkali - silica plot for dykes and gabbros. Dashed field encloses Group A and B dykes from McClurg (1982), and dot-dashed field, group D dykes. The dividing line is from Irvine and Baragar (1971). Open circles = group A and B dykes, half-filled circles = group D dykes., filled circles = group E dykes, circles with single dot = all gabbros except those in group 4 (circles with 2 dots).

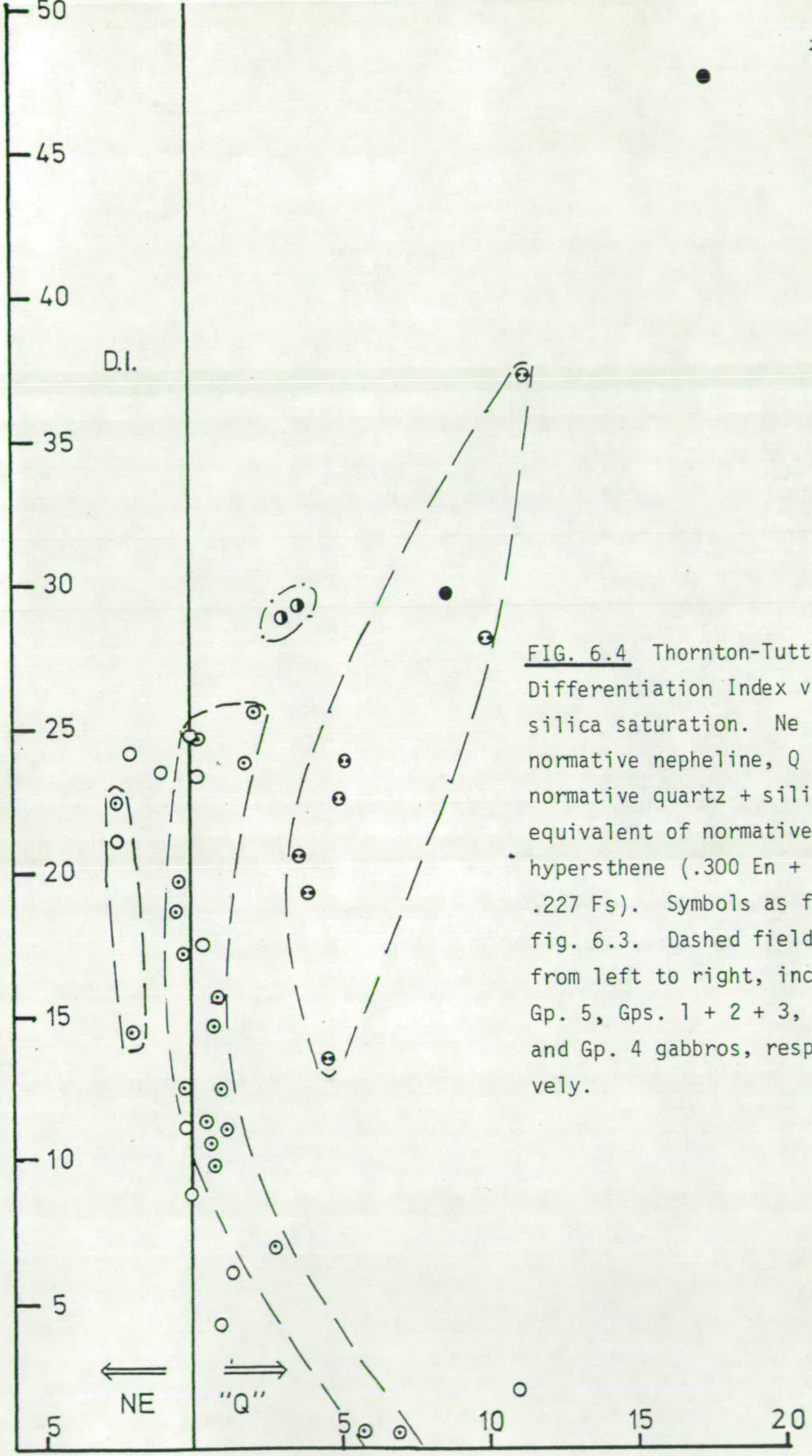

FIG. 6.4 Thornton-Tuttle Differentiation Index vs. silica saturation. Ne = normative nepheline, Q = normative quartz + silica equivalent of normative hypersthene (.300 En + .227 Fs). Symbols as for fig. 6.3. Dashed fields, from left to right, include Gp. 5, Gps. 1 + 2 + 3, and Gp. 4 gabbros, respectively.

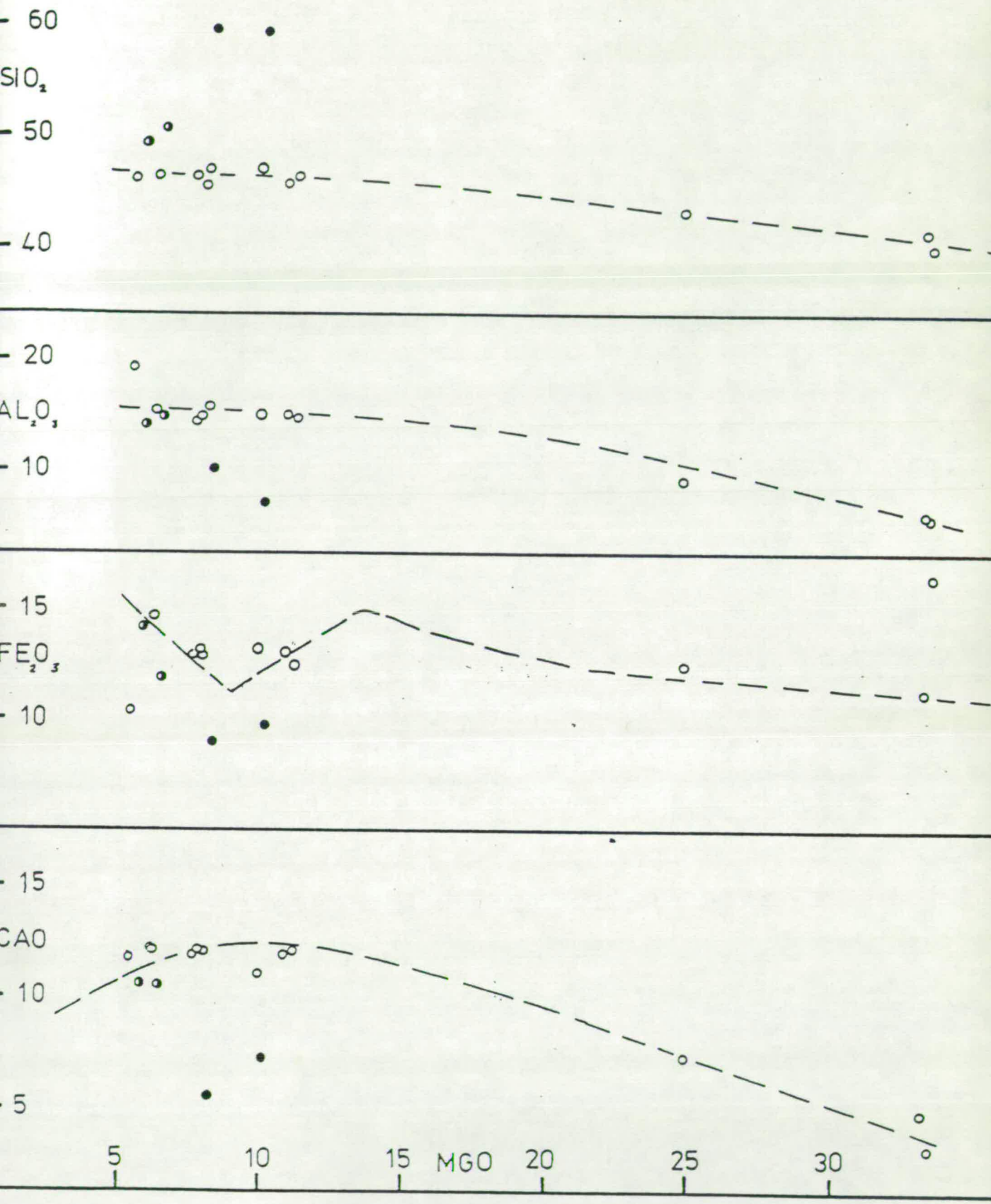

FIG. 6.5 Major elements of the dykes plotted against wt% MgO. Symbols as in fig. 6.3. Dashed line is the magma fractionation line for Rhum dykes determined by McClurg (1982).

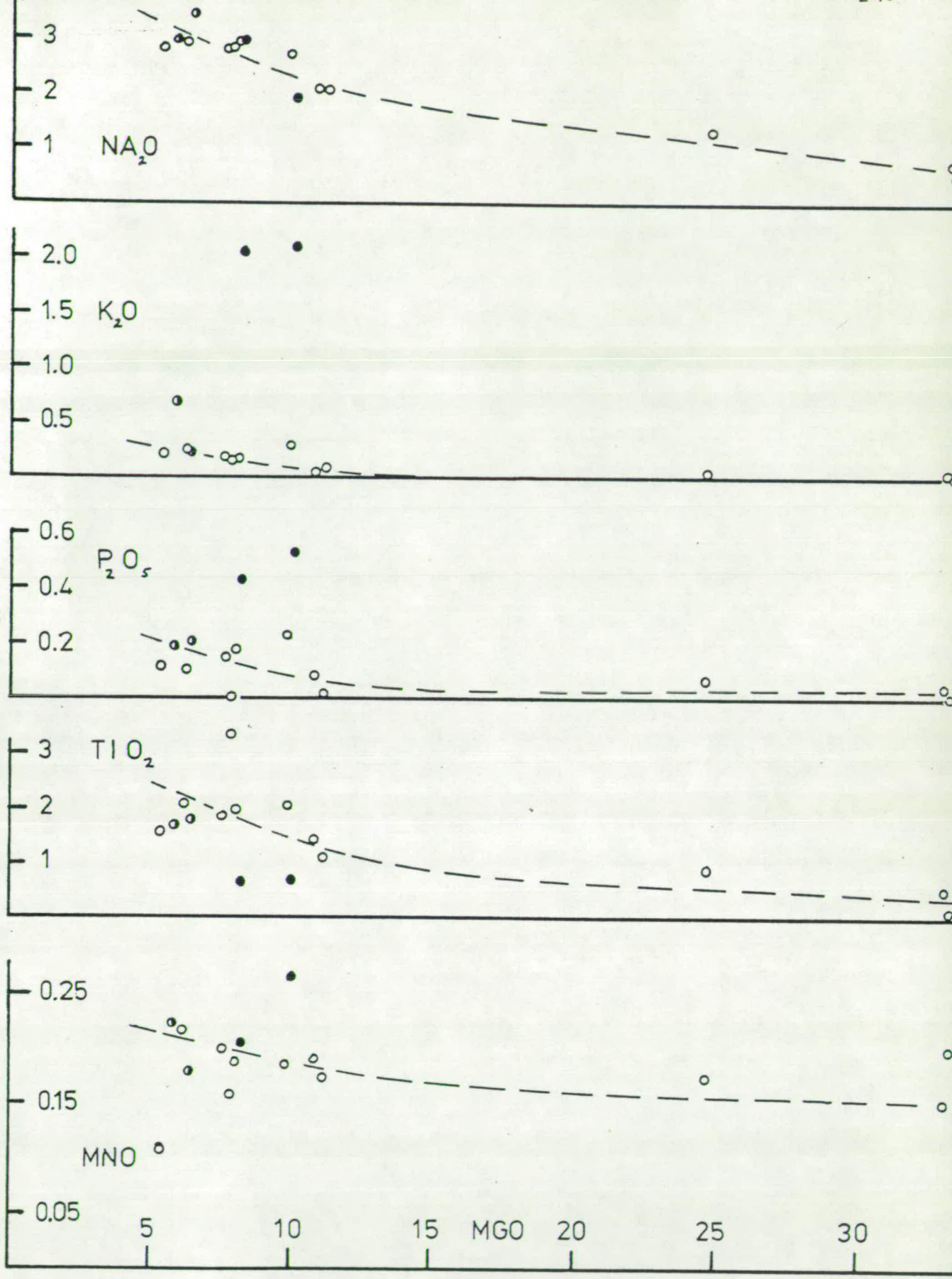
3
2
1
NA2O
2.0
1.5
K2O
1.0
0.5
0.6
P2O5
0.4
0.2
3
TIO2
2
1
0.25
0.15
MNO
0.05
5
10
15
MGO
20
25
30

Fig 6.5 (Ctd.)

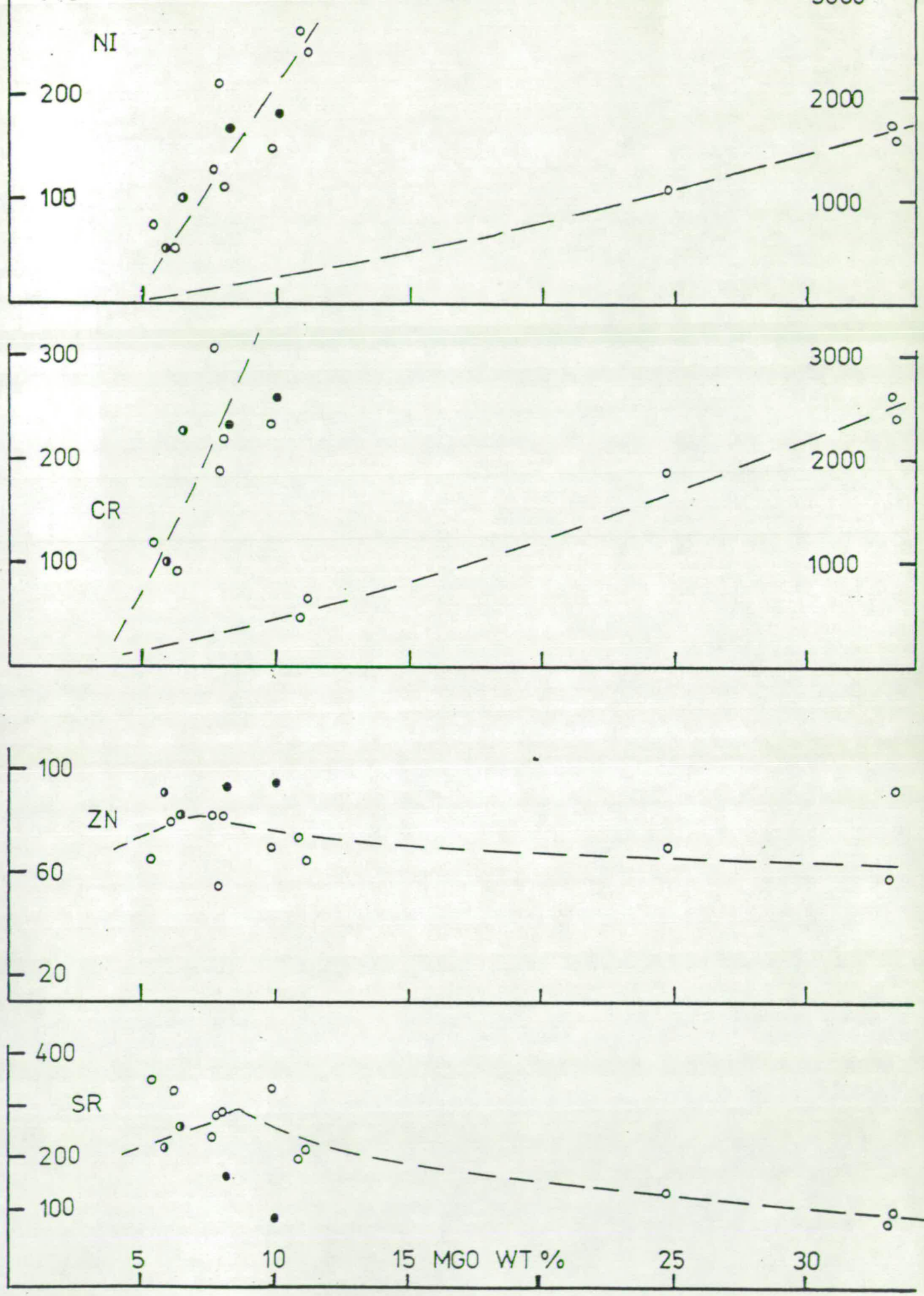

FIG. 6.6 Trace elements of the dykes plotted as ppm vs. wt% MgO. Symbols as for fig. 6.3. Dashed line is a regression line to Trallval data on Gp. A and B dykes, except for Zn, Sr, and Cu, which are after McClurg (1982).

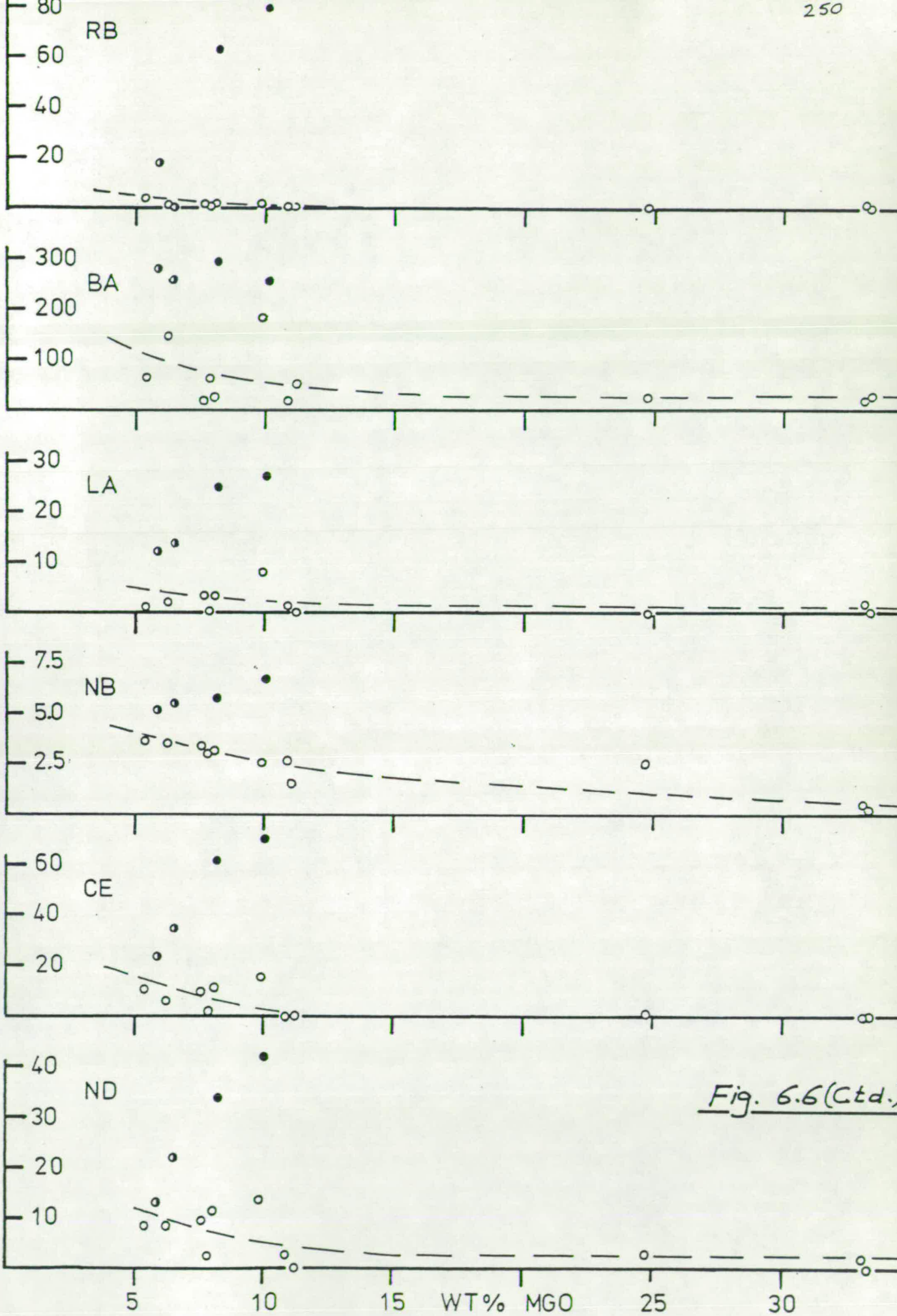
250
80
RB
60
40
20
300
BA
200
100
30
LA
20
10
7.5
NB
5.0
2.5
60
CE
40
20
40
ND
30
20
10
5
10
15
WT% MGO
25
30

Fig. 6.6 (Ctd.)

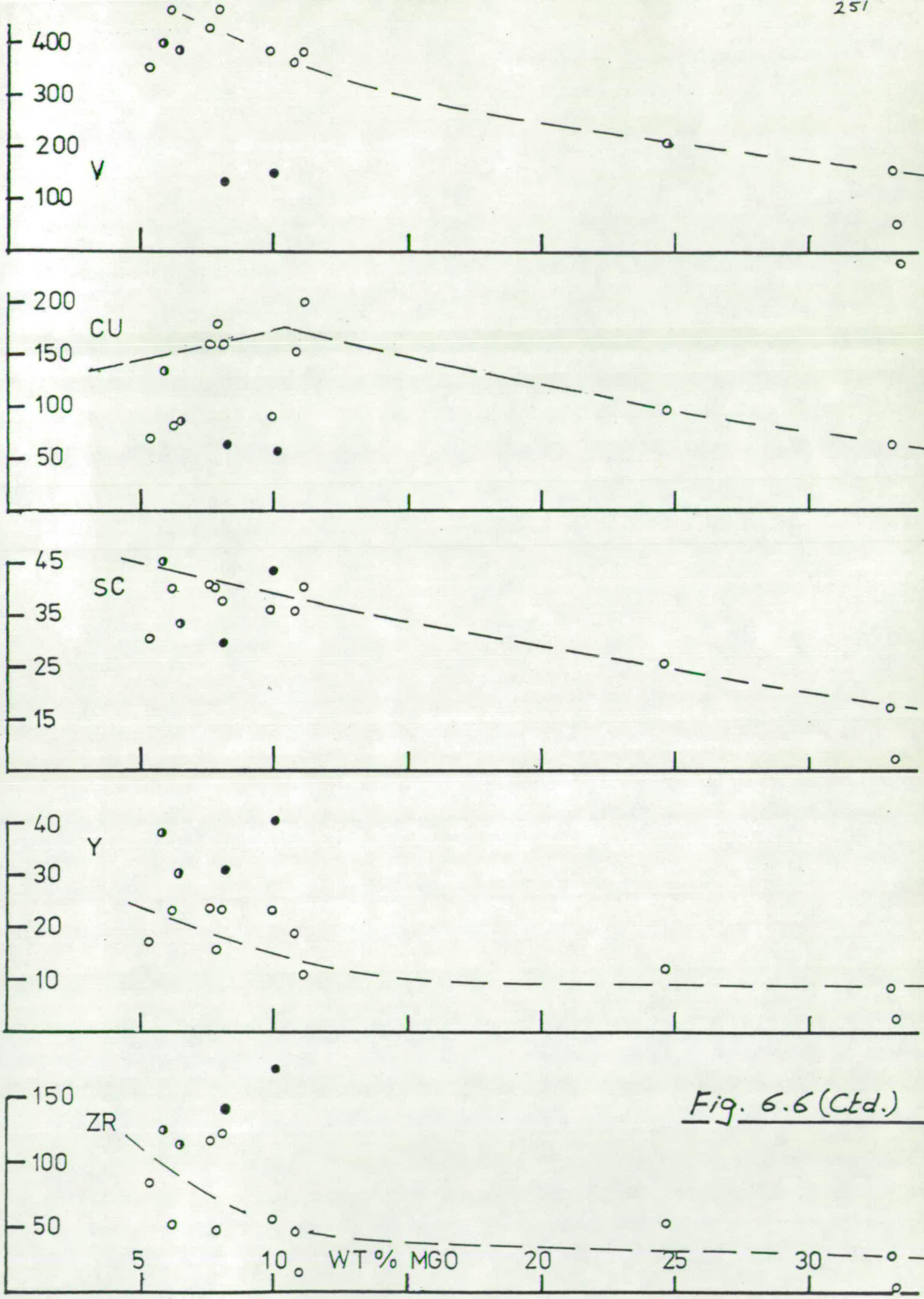
400
300
200
V
100
200
CU
150
100
50
45
SC
35
25
15
40
Y
30
20
10
150
ZR
100
50
5
10
WT % MGO
20
25
30

Fig. 6.6 (Ctd.)

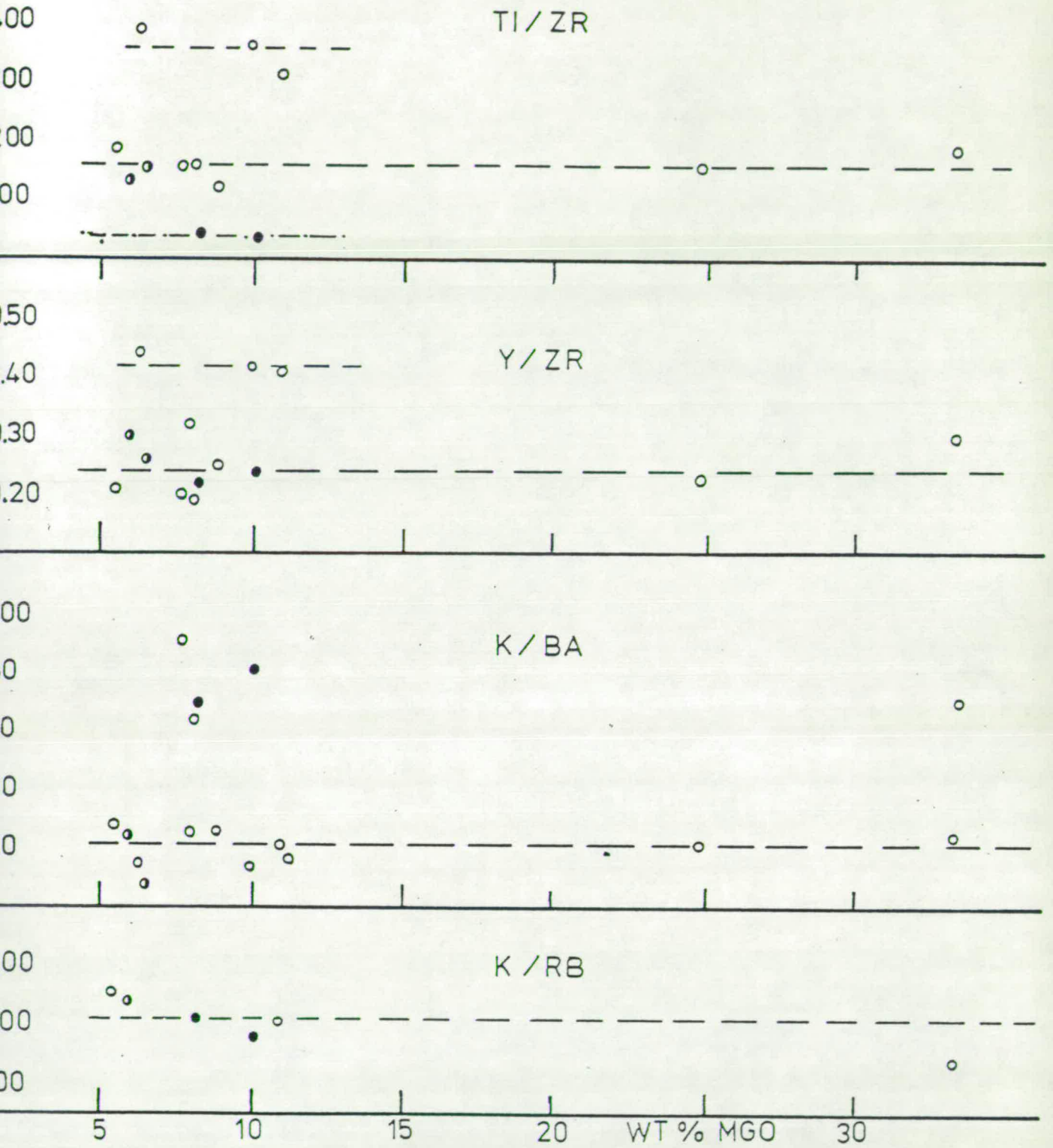

FIG. 6.7 Minor element ratios for the dykes. Dashed line is the average for Gp. A and B dykes; dot-dashed line is the average for Gp. E dykes, where it differs from the average for the Gp. A and B dykes.

FIG. 6.8 Normalised minor element patterns (modified after Thompson et al., 1982) for:

A - Isotopically uncontaminated lavas (stippled field), amphibolite-contaminated lavas (dashed line) and granulite facies Lewisian Gneiss-contaminated lavas (solid line); all are from the Skye and Mull Plateau-type lava series (Thompson et al., 1982).

B- Lewisian Gneiss:(i)from Thompson et al. (1982) - the stippled field, (ii) a pegmatite cutting Lewisian Gneiss in the Southern Mountains Complex (solid line), and, (iii) amphibolite facies Lewisian Gneiss from the SMC (dashed line).

C - Relatively uncontaminated dykes from the Trallval area: a picrite BD1, an aphyric basalt AC2, and a plagioclase-phyric basalt BB6. Stippled field = uncontaminated lavas of Thompson et al. (1982).

D - Contaminated dykes from the Trallval area. KA1 = micro-diorite hybrid; BE3 and KB1 = basaltic hawaiites of Gp. D.

FIG. 6.9 (next page) Major elements of the gabbros and ultrabasic rocks. Open squares = Gp 1 + Gp 2 + Gp 3 gabbros (more than 5% olivine), filled squares = Gp. 4 gabbros (more than 5 % orthopyroxene), half-filled squares = Gp 5 gabbros (no olivine or orthopyroxene but abundant opaques), open triangles = ultra-basic breccia matrices, filled triangles = plugs of intrusive peridotite, dots = layered series peridotite and allivalite. The dashed line is the low-pressure fractionation trend established for the dykes (figs. 6.5 and 6.6).

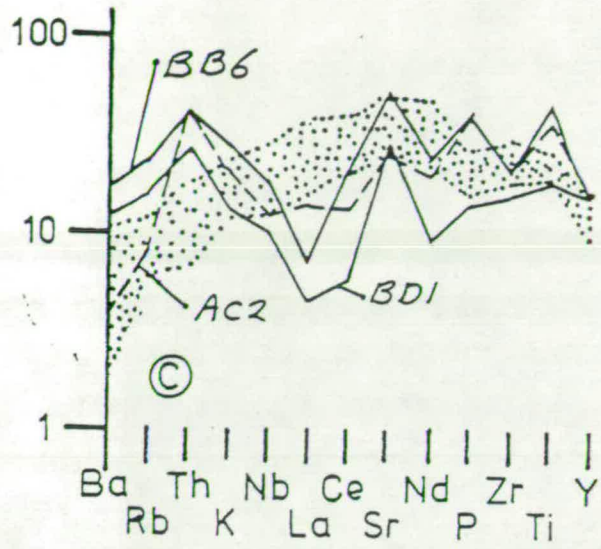
100
10
1
BB6
AC2
BD1
C
Ba Th Nb Ce Nd Zr Y
Rb K La Sr P Ti

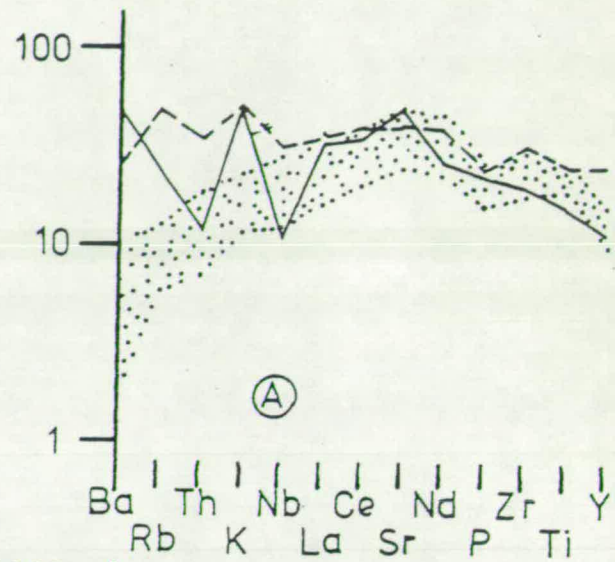
100
10
1
A
Ba Th Nb Ce Nd Zr Y
Rb K La Sr P Ti

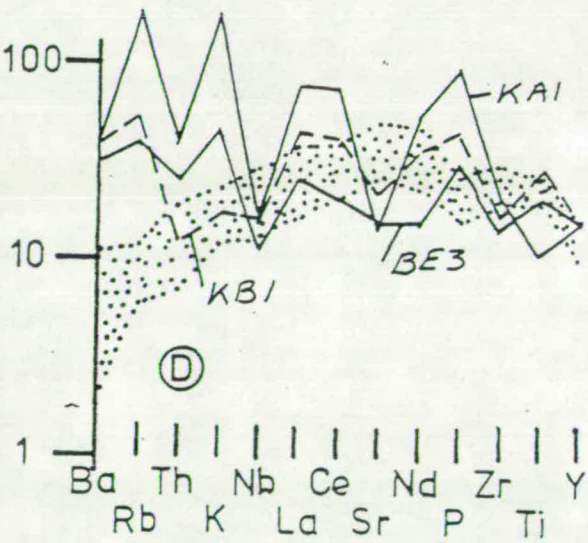
100
10
1
KA1
KB1
BE3
D
Ba Th Nb Ce Nd Zr Y
Rb K La Sr P Ti

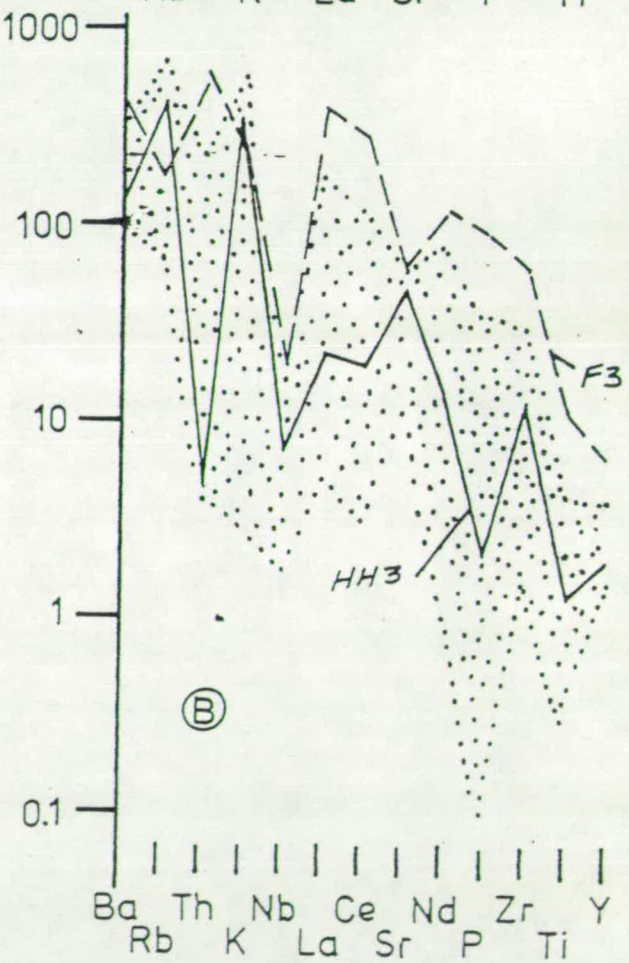
1000
100
10
1
0.1
F3
HH3
B
Ba Th Nb Ce Nd Zr Y
Rb K La Sr P Ti

FIGURE 6.8

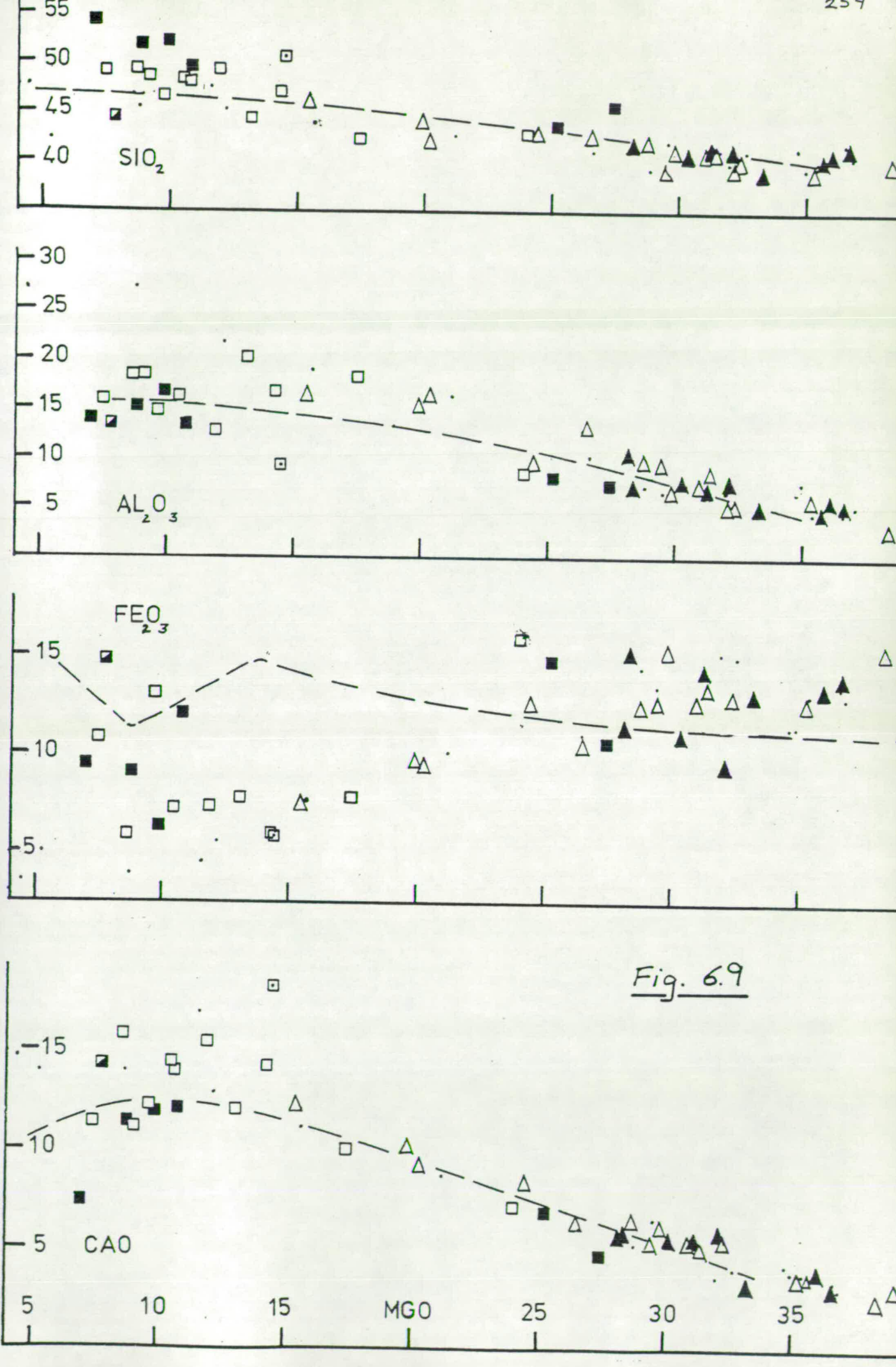
55
50
45
40
SIO2
30
25
20
15
10
5
AL2O3
FEO23
15
10
5
15
10
5
CAO
5
10
15
MGO
25
30
35

Fig. 6.9

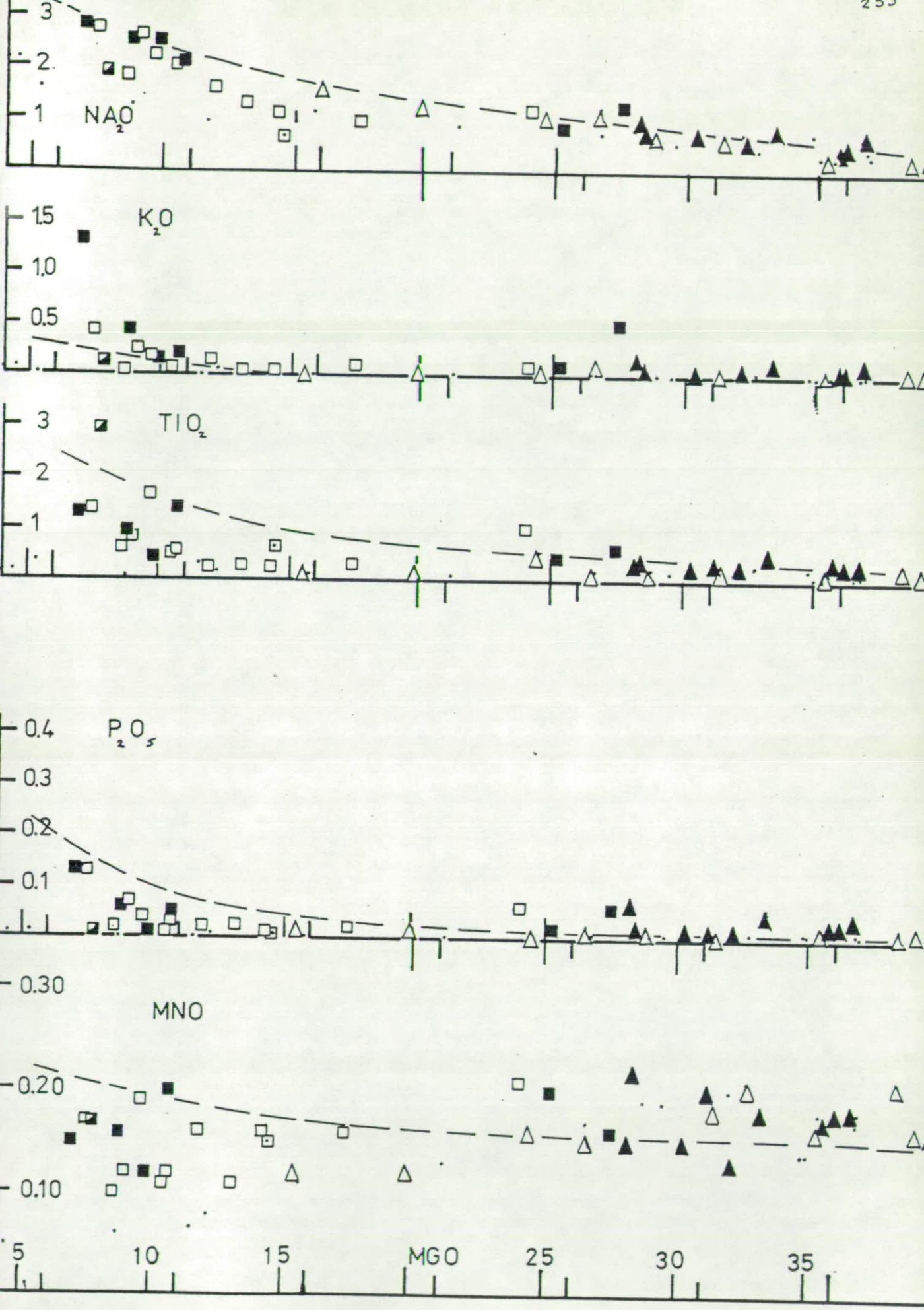
3
2
1
NA2O
1.5
K2O
1.0
0.5
3
TIO2
2
1
0.4
P2O5
0.3
0.2
0.1
0.30
MNO
0.20
0.10
5
10
15
MGO
25
30
35

Fig. 6.9 (Ctd.)

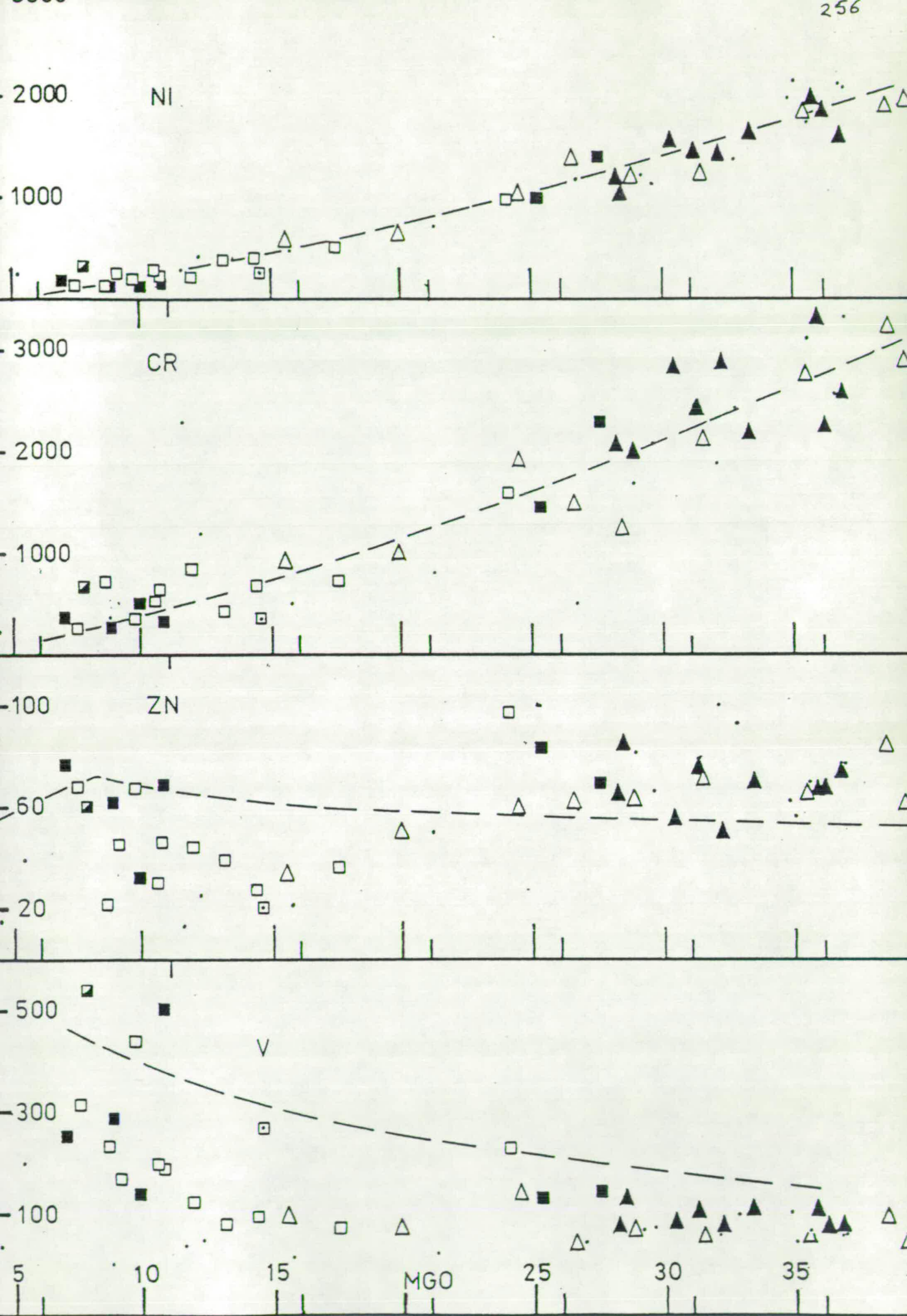

FIG. 6.10 Trace elements for the gabbros, symbols as for fig. 6.9.

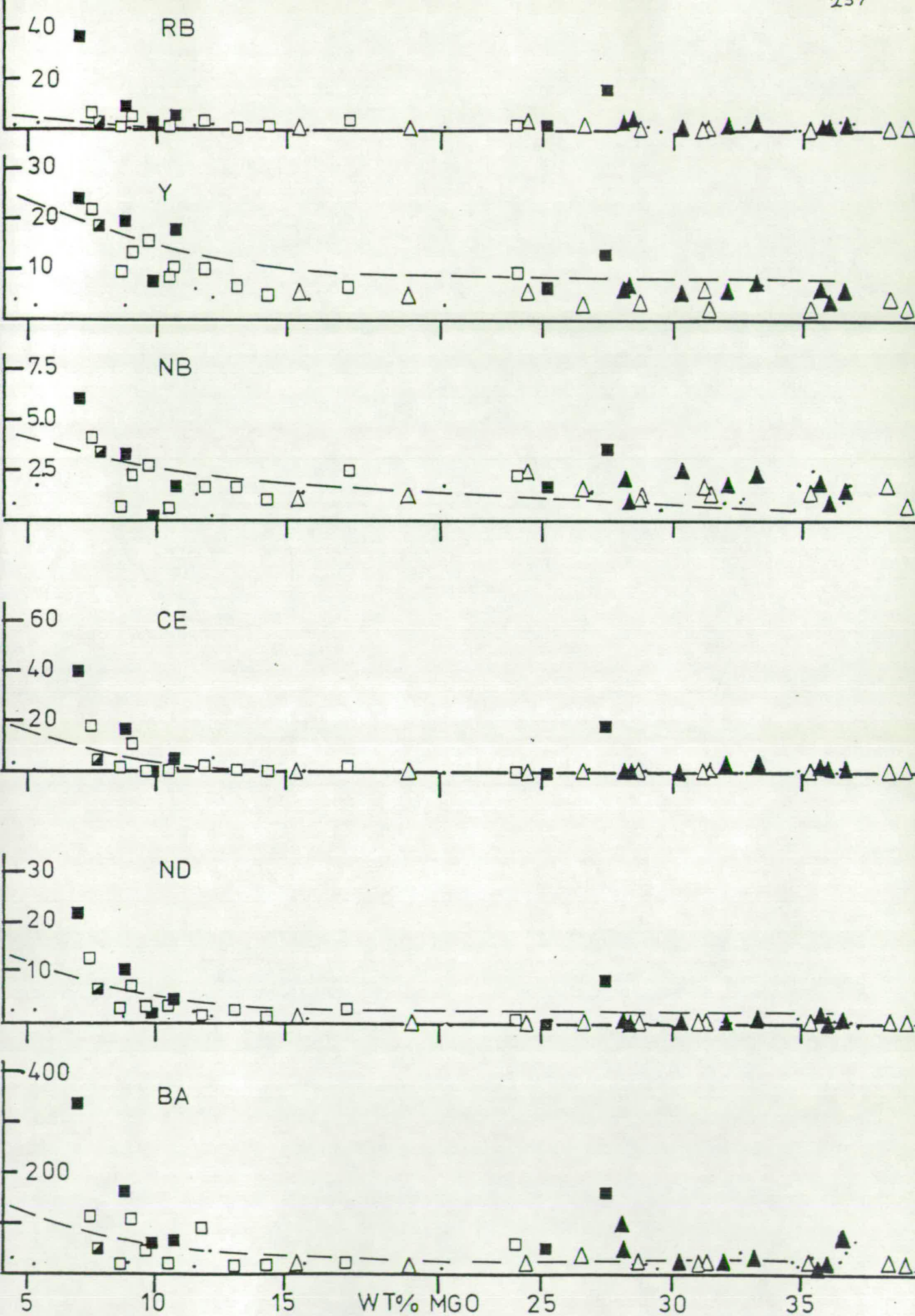
40
RB
20
30
Y
20
10
7.5
NB
5.0
2.5
60
CE
40
20
30
ND
20
10
400
BA
200
5
10
15
WT% MGO
25
30
35

Fig. 6.10 (Ctd.)

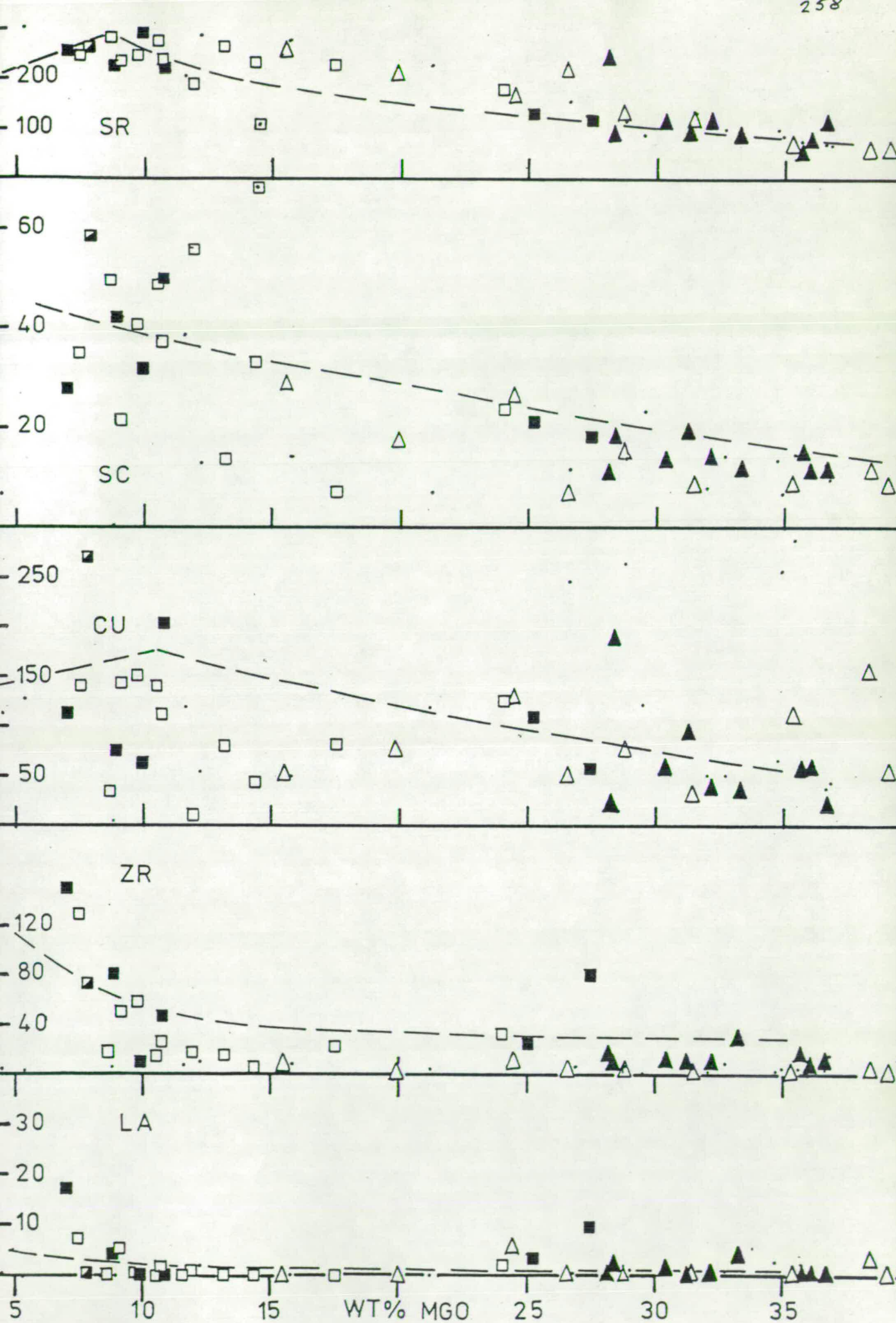
200
100
SR
60
40
20
SC
250
CU
150
50
ZR
120
80
40
30
LA
20
10
5
10
15
WT% MGO
25
30
35

Fig 6.10 (Ctd.)

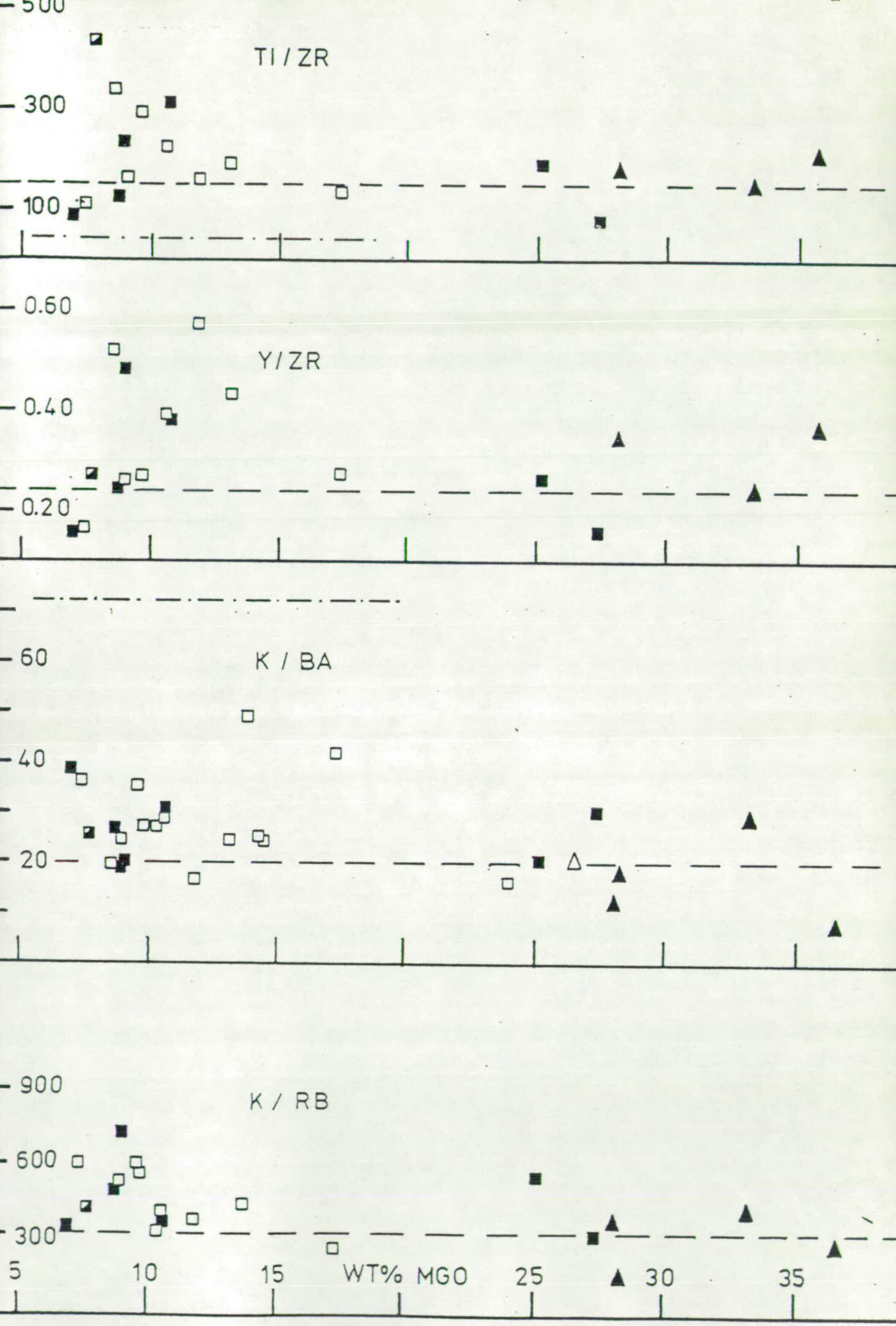

FIG . 6.11 Minor element ratios of the gabbros and ultrabasic rocks. Symbols as for fig. 6.10. Dashed and dot-dashed lines from fig. 6.7.

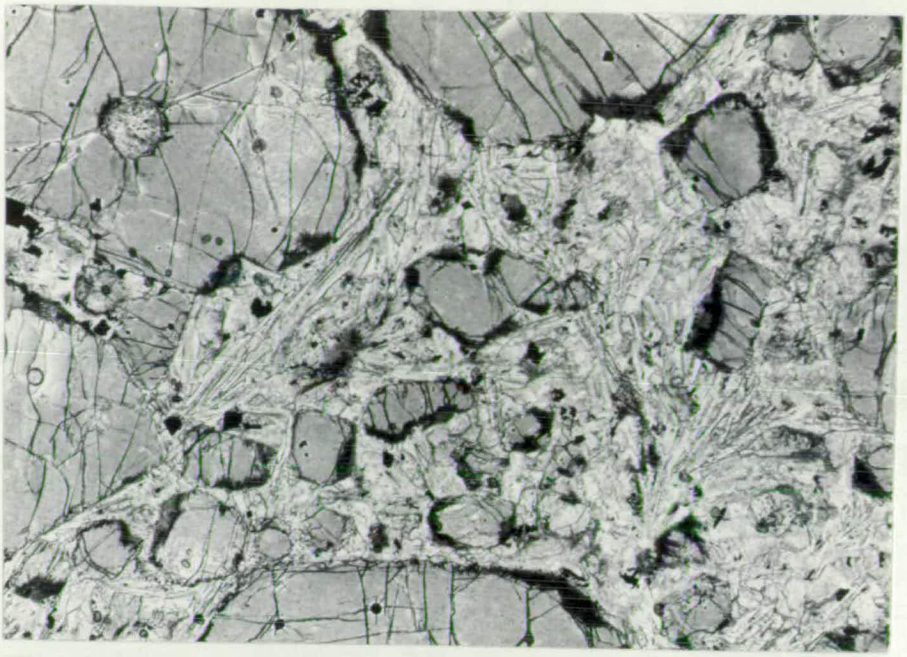

0.5 mm.

PLATE 6.1 Picrite with abundant olivine phenocrysts in quenched groundmass. Note silicate inclusion in olivine (top left) and the clear rims around the spinels included in these brown olivines. BD1, N Trallval.

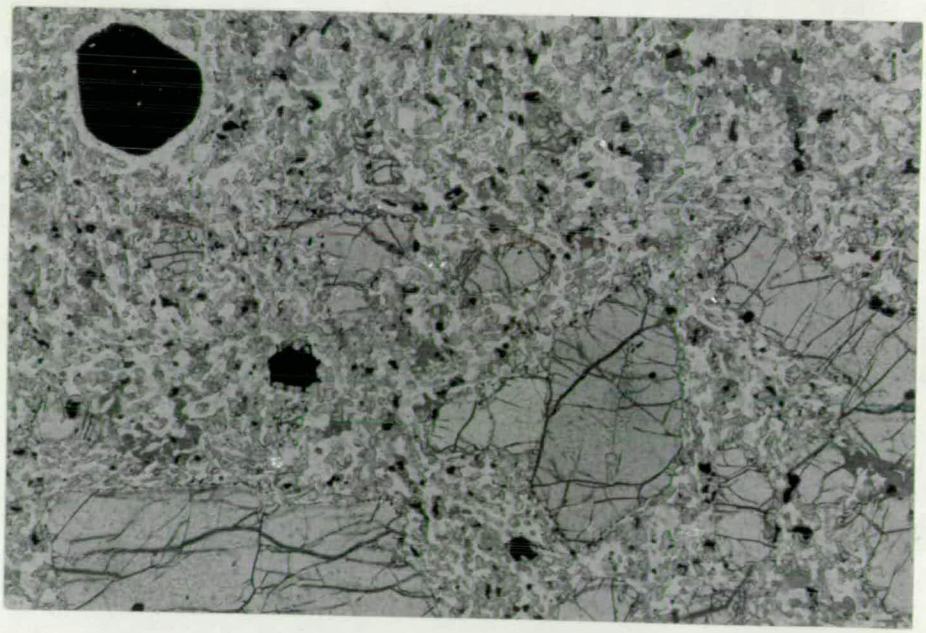

1 mm.

PLATE 6.2 Picrite with olivine and spinel phenocrysts in recrystallised groundmass. BA 3, Atlantic Corrie.

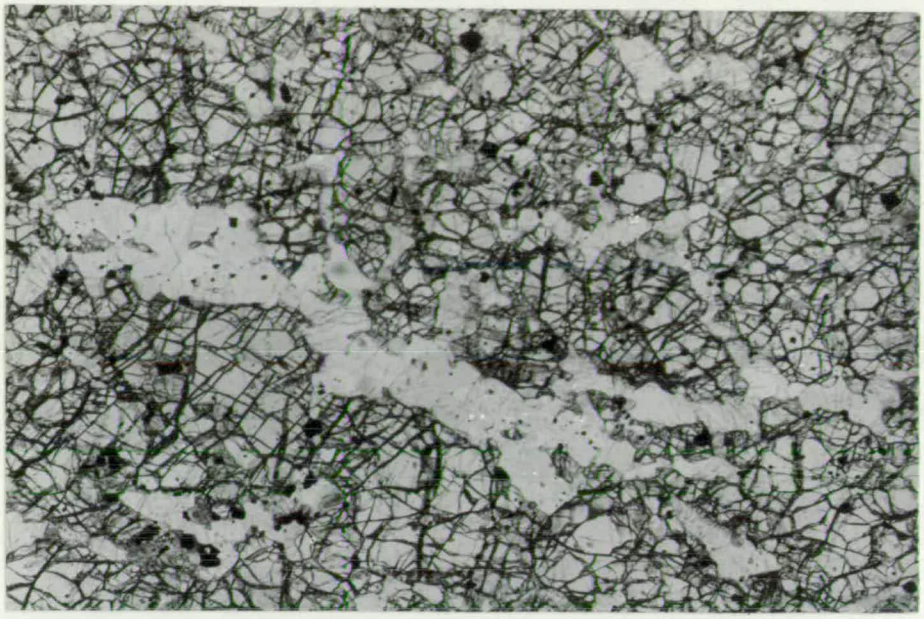

1 mm.

PLATE 6.3 Picrite showing conduit texture and high olivine content typical of remobilised peridotite. B04, NW Trallval.

1 mm.

PLATE 6.4 Feldparphyric basalt (Group B). The plagioclase phenocrysts are partly resorbed. BB6, E Trallval.

0.3 mm.

PLATE 6.5 Group D basalt: an altered cryptocrystalline groundmass with microphenocrysts of olivine, plagioclase and oxides surround clear, subophitic-textured patches of clinopyroxene and plagioclase. BE 3 , S Trallval.

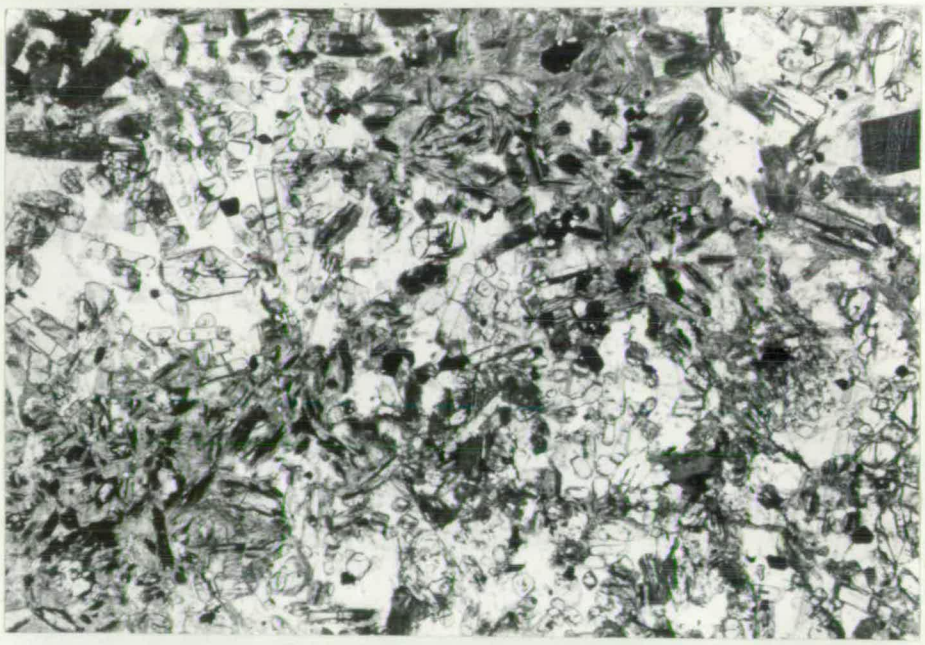

1 mm.

PLATE 6.6 Microdiorite hybrid with euhedral orthopyroxene microphenocrysts (some have reacted to fibrous cummingtonite) set in plates of plagioclase, alkali-feldspar and quartz. The rock has a few euhedral biotite microphenocrysts (upper right). KA1, N Ruinsival.

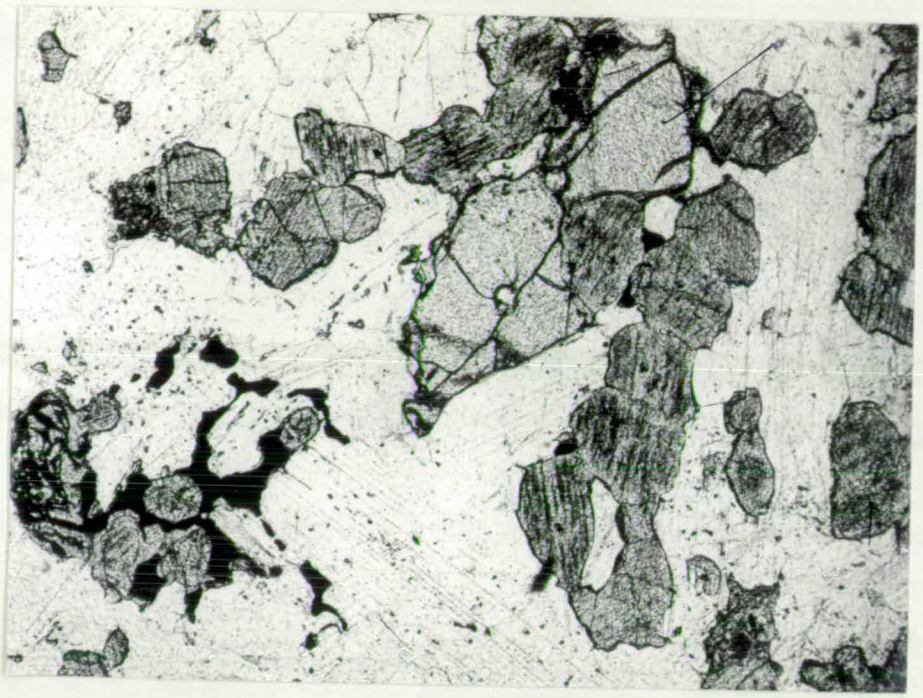

PLATE 6.7 Olivine gabbro. Olivine, clinopyroxene, plagioclase and interstitial ilmenite in a granular texture. E5, Trallval-Ainshval col.

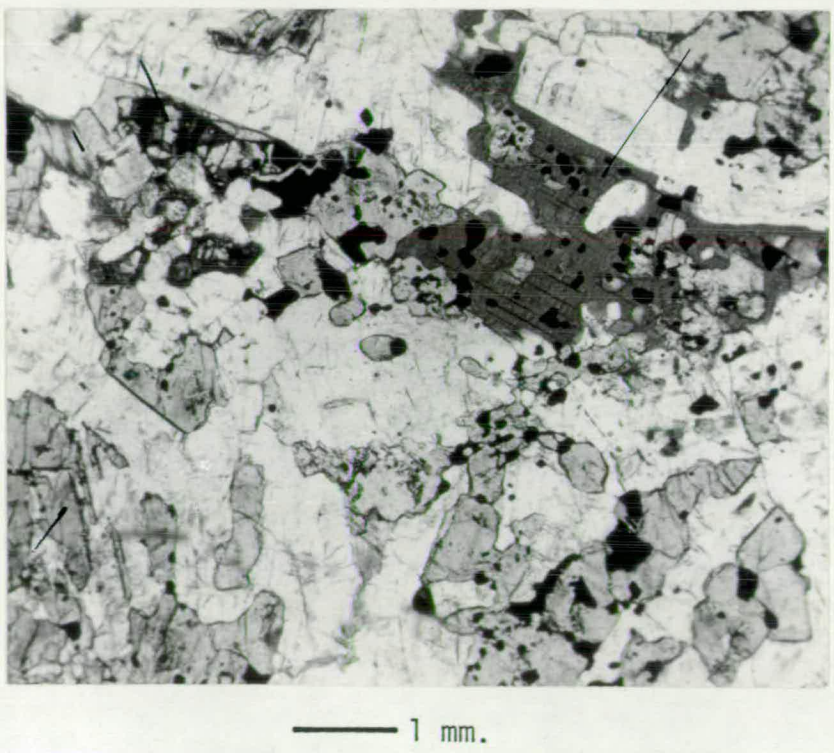

PLATE 6.8 Olivine-hypersthene gabbro. Poikilitic clinopyroxene plates partly replaced by biotite. H5, N Trallval.

clino-
pyroxene

olivine

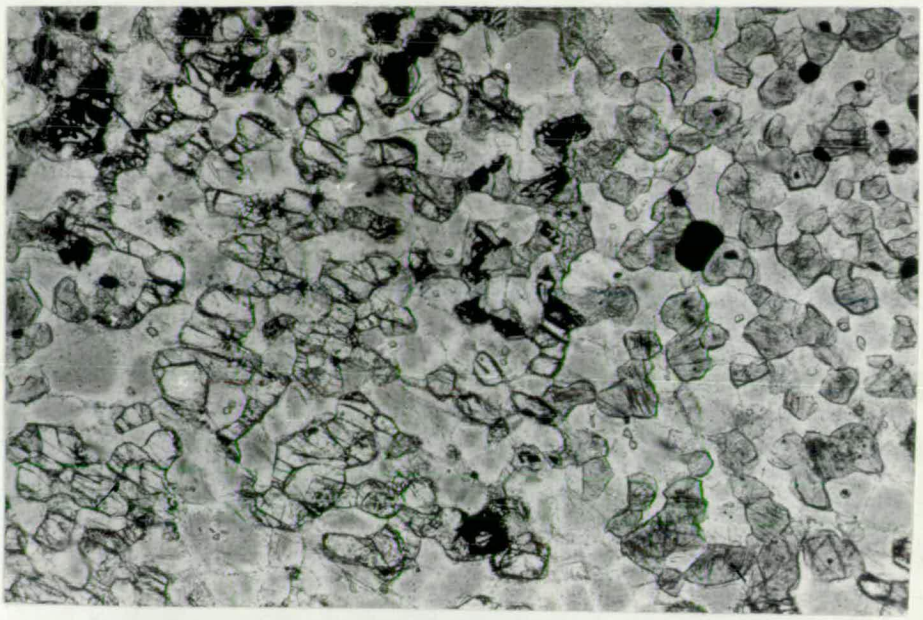

hypersthene

0.5 mm.

PLATE 6.9 Granular, annealed texture in hornfelsed olivine-hypersthene gabbro. M2, S Trallval.

hypersthene

clino-
pyroxene

1 mm.

PLATE 6.10 Hypersthene gabbro: hypersthene (altered), subcalcic augite, plagioclase and ilmenite in a granular texture. K8, Papadil Gabbro, Papadil.

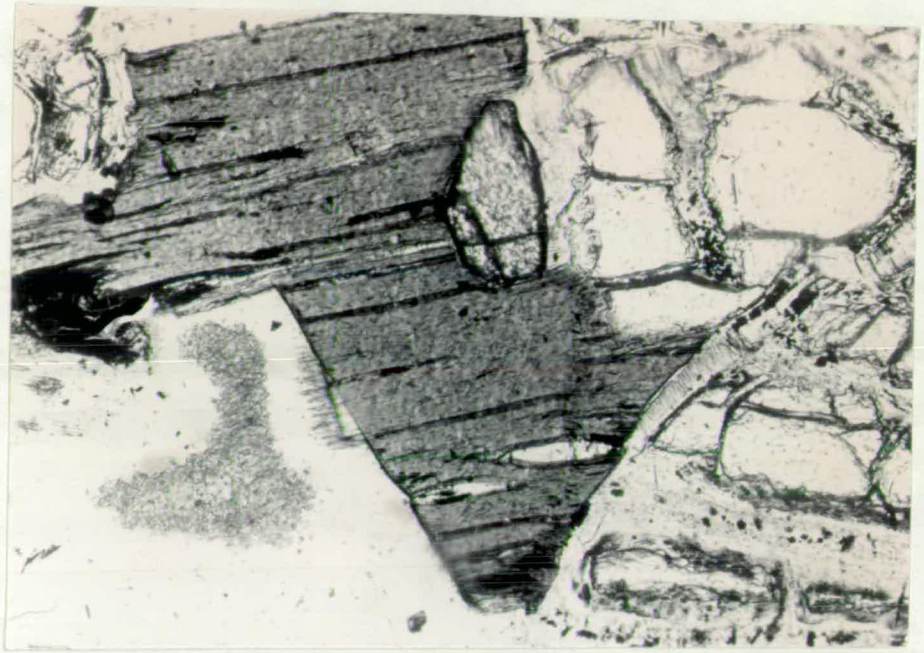

——— 0.5 mm.

PLATE 6.11 Partly serpentinised olivine and intercumulus phlogopite enclosing a subhedral zircon crystal. From a marginal ultrabasic breccia zone in the CS. B4, Papadil.

CHAPTER 7

PETROGENESIS OF THE ULTRABASIC ROCKS

The data from previous chapters are summarised and interpreted below. This is followed by discussion of the magma processes that may have operated (sections 7.8 to 7.11). No quantitative modelling has been attempted.

7.1 Summary and Interpretation of the Field Observations on the ELS.

7.1.1 General Features.

The set of ELS units exposed on Trallval differs from the classic Hallival and Askival sections (Brown, 1956) as follows:

(1) Over the W. Trallval sections, feldspathic peridotite is always much more abundant than troctolite in each unit. The allivalite of U10, U12, U13 and U14 consists of two or more troctolite layers separated by highly feldspathic peridotite layers commonly with irregularly shaped inclusions of troctolite. Thin (less than 1 m.) allivalite layers consist mostly of anorthosite as do the top and bottom of thicker layers. If the layers of feldspathic peridotite are included in the estimate of allivalite thickness, the Trallval allivalites compare closely with those of Askival and Hallival. These features suggest either a volume for volume replacement of allivalite by peridotite, the more anorthositic layers and those protected by anorthosite being relatively unaffected, or a primary lateral facies variation from allivalite to peridotite. A combination of the two is likely.

(2) Coarse cluster textures are common and especially so in the higher units. These are similar to textures found in the plugs and breccia zones intruded as mushes into the CS, and their development on Trallval is attributed to the formation of similarly large thicknesses of unconsolidated cumulates. This is supported by the occurrence of texturally layered concentric shells up to 6 m. in diameter around peridotite blocks in U13, a texture also seen in ultrabasic breccias (section 3.8.2.1). The upward flux of intercumulus liquid, expected from the compaction of unconcolidated cumulates (Irvine, 1980), is suggested by the feldspathic streamers developed e.g. at the base of U14.

(3) Allivalite layers, coherent on W. Trallval become layers of mélange

(troctolite blocks in feldspathic peridotite) on E. Trallval. In the lower units, internal brecciation of feldspathic peridotite is common near gabbro contacts and so is local folding of allivalite. Layering in peridotite is only poorly developed in E. Trallval, which is the area most intensively intruded by gabbro; the intrusion of peridotite into gabbro is also common in this area (sections 3.5.5 and 4.1). The homogenisation of peridotite and the brecciation of both allivalite and peridotite in this area is associated with gabbro intrusions which have extremely irregular contacts with the peridotite (Fig. 4.2 A). This suggests that the layered series was unconsolidated at the time of intrusion and that the gabbroic liquid or volatiles derived from it may have mixed with intercumulus liquid, resulting in an unlayered crystal mush which re-intruded the more brittle allivalites and earlier gabbros. (4) Within 200 m. of the faulted contact with the CS, the layering steepens rapidly, the allivalite thins and breaks up into gently warped slabs. The modal layering of peridotite is preserved in only a few large blocks in a matrix of structureless peridotite. This matrix has an extremely coarse texture due to the segregation of intercumulus pyroxene and plagioclase, as in some of the ultrabasic breccia matrices and plugs. The textures support the suggestion (section 2.2.3) that most of the ELS close to the CS contact was unconsolidated at the time of emplacement of the CS. The proportion of intercumulus liquid required to remobilise the cumulates by a process analogous to fluidisation in sediments (e.g. Doe and Dotts, 1980) may have been increased in this area as a result of flow of liquid from the unconsolidated CS cumulates across the fault-plane into the ELS.

7.1.2 Textures and Structures.

Many of these are novel both for Rhum and worldwide, or have not been described in detail before and interpreted below.

Structures at the Base of the Unit: U16 has irregular schlieren of troctolite in the basal layer of feldspathic peridotite which is succeeded upwards by layers of dunite. The bases of U10 and U11 grade up into less feldspathic rock and include lenses of pyroxene cumulate and troctolite probably derived from reworking of the underlying unit. The higher content of feldspar at the base suggests either some assimilation of allivalite or crystallisation from plagioclase-rich intercumulus liquid expelled from below. Basal dunite layers are more common and

thicker on Hallival.

Chromitite Layering (sections 3.5.2 and 3.5.7): this may be found at any level in the peridotite of a macro-rhythmic unit: it occurs near the bottom of U14, halfway up U9 and U11, and near the top of U8, U10 and U11. Such chromitite zones are also found in U9 on Barkeval (McClurg, 1982) and U10 on Hallival. Chromitite laminae also occur in these zones, thus suggesting a higher than average spinel content (not merely a segregation of spinel into thin laminae), and the regular and continuous nature of the layering suggests that it is a primary phenomenon. Absence of mineral or size sorting and the lack of hydraulic equivalence between olivine and spinel (Jackson, 1961) indicate that the process is one of *in situ* oscillatory nucleation rather than current sorting. The apparent abundance of chromitite zones in the Trallval section compared with those of Barkeval and Hallival may only be a function of the much better exposure of the Trallval peridotite layers.

Slumps: asymmetric convolute layering is attributed to slumping. It is best seen in allivalite with fine-scale modal layering; it may be restricted to the troctolite or, more rarely, involve adjacent layers of peridotite which often become fragmented. Layers composed of anorthosite fragments in mafic troctolite may be due to high strain rates achieved during slumping, leading to the brecciation of thin brittle layers. The thickest slumped layer (8 m.) occurs in the allivalite of U14 on the west face of Askival. The ubiquity of slumps and the rarity of graded bedding suggest that apparent laminar cross-bedding in allivalites (section 3.5.8) is in reality due to localised slumping.

Loading Structures: the most spectacular structures occur along the contact between the lower troctolite layer and the "sandwich peridotite" of the main allivalite of U14 (section 3.5.10). They are interpreted as a response to the sudden injection of a thick layer of dense peridotite musn into the allivalite (as suggested by the intrusive contacts of the peridotite layer with allivalite where it terminates to the west, see Fig. 3.7) followed by partial assimilation of the allivalite (see 2 pages on). Loading elsewhere is less pronounced, suggesting not only that a reverse density contrast is required to form these structures but that it must be established rapidly. The source of the mush must have lain to the east, and it may have been peridotite remobilised by the intrusion of gabbro in E. Trallval (section 7.1.1). Other loading struc-

tures occur between layers of contrasting mode in the allivalites, such as contacts of pyroxene-rich allivalite over troctolite (section 3.5.10), troctolite over mafic troctolite (section 3.5.2) and olivine-rich peridotite over feldspathic peridotite (section 3.5.4). In these cases, the present density contrasts are either slight reversed or mormal, and the loading may be explained by a mechanism suggested for the Bushveld (Lee, 1981): the strong reverse density contrasts required were produced by the upward concentration of volatiles below a relatively impermeable horizon. There is some support for this hypothesis on Trallval: the coarsening of the texture within troctolite flames up into pyroxene-rich allivalite (Plate 3.12) is attributed to higher diffusion and growth rates of crystals at the top of the flames due to the concentration of volatiles. A similar texture at a loaded contact in the Klokken syenite intrusion has been so explained by Parsons and Butterfield (1981). Also, the only occurrence of zeolites on Trallval is below a relic fragment of allivalite along the spectacularly loaded contact in the U14 allivalite.

Graded Layering: where a layer shows size grading of olivine (section 3.5.2), it is invariably associated with modal intercumulus layering so that the coarse olivine occurs in feldspar-rich laminae. The coarser layers grade into protoharrisite which has yet more intercumulus feldspar. An explanation for this close association of olivine coarsening and increasing content of intercumulus phases is given below.

Harrisite and Protoharrisite: a recent paper by Donaldson (1982) attributed the formation of these layers to the trapping of hydrous intercumulus liquid below relatively impermeable horizons within a pile of unconsolidated cumulates, forming layers of supercooled liquid free of nuclei. This trapping is analogous to the formation of water-sills during the diagenesis of sediments (Fyfe et al., 1978). Previous work (Wadsworth, 1961; Donaldson, 1974) suggested that harrisite layers form at the cumulate/magma interface from supercooled magma. Data from this study supporting the recent concept of a water-sill origin include the common occurrence of irregular harrisite and protoharrisite in sub-spherical pockets in feldspathic peridotite and their common occurrence in remobilised peridotite where the thickness of uncompacted cumulate was great and the upward movement of intercumulus liquid to be expected. The strong association of the increasing coarseness and tendency to-

wards a harrisitic habit of olivine with increasing amounts of intercumulus phases also supports this hypothesis. More support comes from the chromitite and/or dunite laminae frequently found at the bottom of a harrisite layer (e.g. section 3.6.2), presumably due to the gravity settling of olivine or spinel through a thickness of low-viscosity, volatile-rich liquid.

Cluster-layering: by analogy with the poikilo-macro-spherulitic feldspars of Donaldson et al. (1973), the clusters described here probably grew from a liquid supersaturated in plagioclase. The downward orientation of the branches suggests that the source of the supercooled liquid was below the nucleation horizon and that the clusters formed within the cumulate pile. The observed gradation (section 3.5.5) from feldspathic peridotite to allivalite via cluster-layered peridotite is probably a consequence of the "seeding" of the upper layers of peridotite with laminae rich in plagioclase nuclei which increase in frequency as the allivalite is approached. The appearance of cumulus plagioclase in peridotite (not cluster-layered), below the allivalite is observed in some of the lower units (section 3.5.2). The underplating process described in section 3.5.10 reflects the lateral equivalent of this phenomenon. In this apparently primary facies change, troctolite passes laterally into feldspathic peridotite with a few nuclei of cumulus plagioclase.

Assimilation of Troctolite: field evidence for this process includes (i), the irregular, partly resorbed lower surface of allivalite, with truncation of the lamination in the allivalite. These finger-like structures have been partly described by Brown (1956) and Robins (1983) and are at present under investigation by Butcher (pers. comm.; see section 3.5.1), (ii) the east to west gradual replacement of slumped allivalite by peridotite with relic fragments of allivalite which still retain their slump structures (Fig. 3.7, Plate 3.28) and (iii), the westward transition of the allivalite of Ul2 into isolated anorthosite schlieren and then dendritic peridotite (section 3.5.5). The resorption of only the lower surfaces of allivalite suggests that volatiles played an important role in the process by their upward concentration below the impermeable, platy troctolite layers. The other examples of assimilation involve intrusive peridotite (sections 7.1.2.4 and 7.1.1) with, it is suggested, a high volatile content (section 7.10). That here has been a

lack of chemical equilibrium between troctolite inclusions and the peridotite host is also suggested by the modal intercumulus layering developed concentrically and close to the block in an otherwise unlayered peridotite (sections 3.5.5 and 3.5.8) and similar layering which follows the rim of ball-and-pillow structures of peridotite in troctolite breccia (Plate 3.19).

Pipe-like Vertical Features: regularly spaced feldspathic streamers are developed in peridotite (i) at the bottom of U14 (section 3.5.7), (ii) above diapiric loading structures of troctolite (section 3.5.10) and (iii) above troctolite blocks in mélange layers (sections 3.5.1 and 3.5.10). They are attributed to the upward infiltration of peridotite by intercumulus liquid from a troctolitic source. Late pipe-like bodies rich in intercumulus pyroxene locally replace feldspathic peridotite and are best seen where they cut chromitite-layered sequences without distortion of the layering (sections 3.5.2, 3.5.4 and 3.5.7). Their irregular distribution suggests that they represent a later phase of intercumulus liquid expulsion through restricted, irregular channels. The metasomatic replacement of plagioclase by pyroxene may be explained by the addition of water to the intercumulus liquid (section 7.10).

Sulphide Concentrations: these are associated with allivalites in the ELS, being especially common in the lower half and in the peridotite just below (section 5.7.2.1), and similarly for the CS (section 5.7.2.4). The crystallisation of plagioclase and pyroxene would have been expected to inhibit sulphide precipitation due to the concentration of Fe^{2+} into the residual liquid, increasing the solubility of sulphides (Haughton et al., 1974). A secondary rather than a primary origin is thus suggested for these concentrations. Irvine (1982) suggested that upward moving intercumulus liquid redistributes sulphides, as intercumulus liquid exchanges Fe^{2+} for Mg at the bottom of a unit and vice versa at the top. Sulphides may thus have dissolved into the liquid from the lower half of the unit and reprecipitated in the upper half.

7.2 Summary of Field Observations on the CS.

(1) Dunite and dunitic peridotite are the dominant lithologies in most of the units, except the Dornabac Member (DM) at Leac a Chaisteil which has dominant feldspathic peridotite. The units of the Long Loch Group are the most olivine-rich.

(2) Textures observed in the feldspathic peridotite of the ELS (including chromitite-layering, harrisite and protoharrisite layers and cluster-layering) also occur in the relatively thin feldspathic peridotite layers which occur as a lateral and vertical transition between dunitic peridotite and troctolite.

(3) Features attributed to the activity of intercumulus liquids in the ELS, such as feldspathic streamers, internal brecciation and loading structures, are uncommon in the CS. Evidence for the assimilation of troctolite, however, is abundant in the form of partly resorbed lower contacts and especially the occurrence of separated slabs of troctolite with strongly embayed margins,which truncate slump structures, along particular horizons (section 3.6.2). Allivalite caps are not present in the units along the SW coast where the units are thickest and most olivine-rich.

(4) Disruption of earlier cumulates is indicated by the inclusion of troctolite fragments at the base of LLG1 and LLG2 (where LLG1 has an allivalite) and within LLG2 at Papadil by the scattered olivines characteristic of the underlying "black olivine" layer.

(5) The CS is rich in spinel. As in the ELS, spinel forms laminae at the base of harrisite layers (section 3.6.2), but more commonly it occurs as disrupted laminae in dunitic peridotite, especially near contacts with dunite, feldspathic peridotite or troctolite. In LLG1 on Trallval and in the lower unit of the Ruinsival Group (RG1), the spinel content increases upwards sympathetically with intercumulus plagioclase, forming chromitite zones near the top with chromitite layering and chromitite laminae. In RG1, laminae show loading at a contact of feldspathic peridotite with overlying olivine-rich peridotite, foundering as much as 10 m. down (section 3.6.5). In LLG1 on Trallval, there is a thick chromitite lining along the bottom surface of the allivalite.

(6) Allivalites throughout the CS were strongly deformed by contemporaneous faulting, and shearing resulted in folding, boudinage, sigmoidally shaped peridotite inclusions and the sudden attenuation and truncation of layers. Loading structures are infrequent and this is attributed to the efficient filter-pressing by deviatoric stress acting on a crystal mush, due to the rapid segregation of the liquid to regions of lower stress (Propach, 1976; Spera, 1980).

(7) At Rudha Sgorr an't Snidhe, layers below the troctolite of the DM and LLG1 show reverse modal gradation from troctolite at the bottom to dunitic peridotite at the top (section 3.6.1). As there is no size-grading, the reverse grading is probably an in situ oscillatory phenomenon.

7.3 Interpretation of Observations on the Ultrabasic Breccia Zones.

The features interpreted below are shared by most of the breccia zones in the Trallval area:

(1) The vertical contacts and internal structures such as flow-banding, defined by block distribution and modal variations in the matrix and contacts between matrices of different composition, indicate that the breccias were intrusive.

(2) The injection of sub-parallel, closely spaced anorthosite veinlets into the country-rock flanking the breccia zones is interpreted as the initial stage of the brecciation process, immediately preceding the loss of coherence of the country rock as it breaks into angular fragments which then constitute the breccia together with injected matrix.

(3) More rarely, sub-horizontal anorthosite veinlets form a converging system which drains laterally into larger veins and breccia zones (section 3.8.2.2) suggesting possibly transfer and concentration of intercumulus liquid from the layered series into narrow zones where it forms the matrix of the breccia together with any entrained cumulus olivines. Such a mechanism explains the highly variable olivine content of the breccia matrices.

(4) The variety in shape, size and lithology of blocks correlates positively with the size and complexity of the breccia zone. Blocks tend to be small (less than 1 m. across), angular and lithologically indentical to the country rock in thin, immature breccia zones and at the margins of the bigger, mature zones. The latter have blocks 25 m. across or more, sometimes defining screens attributed to the convergence of two or more zones, and include blocks of all lithologies adjacent to the zone and, in some cases, additional types not exposed but inferred to intersect the breccia at depth. Troctolite, which is a subordinate rock-type in the CS is occasionally the dominant lithology in individual breccia sheets (Plate 3.37) within the zones, suggesting either a concentration by a density-selective mechanism or preferential disaggregation of peridotite blocks into their constituent cumulus crystals.

(5) Blocks with disequilibrium textures are common in the mature zones, suggesting long residence in a "foreign" matrix unlike the blocks in immature zones, which appear to be in equilibrium with the matrix. These textures include dunitic margins to feldspathic peridotite blocks, partial troctolite coatings to peridotite blocks, spinel linings around blocks of troctolite and gabbro and concentric modal banding in the matrix around slabs of feldspathic peridotite. Plagioclase supersaturation textures, analogous to the poikilo-macro-spherulitic feldspars reported by Donaldson et al. (1973) from the Dornabac System are common in the Ruinsival System and occasionally have a nucleus of dunitic peridotite.

(6) The sense of shear deduced from the plastic deformation of blocks and the distribution of a brecciated marker horizon indicate upward and lateral movement of matrix with respect to blocks in the Trallval Zone and subsidence of the CS along the southern contact at Papadil. Part of the Trallval Zone has sub-horizontal flow-banding below a roof-contact and the flattening out of structures in the Ruinsival Zone upward also suggests a roof contact and upward intrusion of the breccias. Lateral movement of matrices with respect to blocks is also suggested by the development of a "shadow" coating of troctolite on one side only of peridotite blocks. In the Forked Zone, there is evidence (from shear sense at the margins and the general widening upward of the zone) of the downward movement of matrix with respect to blocks and walls.

(7) The late "trachytoid" breccia sheets in the Ruinsival area (section 3.8.2.2) and the late, thin, olivine-rich sheets cutting the Trallval and Ruinsival zones probably formed by the process outlined in paragraph 3 above but involving intercumulus liquid of a lower viscosity which allowed greater concentration of entrained olivines, probably as a result of higher volatile activity (section 7.10).

(8) It was suggested in section 3.3 that the breccia zones represent systems of cracks. Propach (1976) stated that, upon dilatational deformation of a crystal mush, the pressure relief in the liquid will result in the opening of fractures (but only if the entire chamber is filled with the mush), filled in by the liquid, simultaneously with plastic folding of the unconsolidated residuum. It is suggested that, upon subsidence of the CS into a graben separating the ELS from the WLS (McClurg, 1982), cracks formed due to pressure relief (their location

and morphology being defined by the differential subsidence), and filled in with the intercumulus liquid from the CS, together with entrained olivines and blocks, leaving a dunitic residuum. With repeated episodic tectonism, these buoyant liquids were forced up and brecciated the overlying cumulates in a number of separate events to yield the present complex structure of the zones. The similarity, though slightly more evolved nature, of the mineral chemistry to that of the layered CS supports the hypothesis of a local derivation of the breccia matrices.

7.4 Interpretation of Observations on the Ultrabasic Plugs.

The sharply bounded cylindrical shape of the plugs indicates that the layered series was rigid at the time of intrusion. The general homogeneity and the concentric, vertical, modal intercumulus banding suggest that the plugs were intruded as crystal mushes. A horizontal temperature gradient and/or the escape of volatiles at the margin which established a compositional gradient probably produced the banding; the same factors may also have produced the remarkable fining towards the margin of the coarse plagioclase supersaturation textures in the Ruinsival Plug. Blocks are rare in the centre of the plugs; where they do occur, they are rounded, while angular blocks are common at the margins. McBirney (1959) suggested that the intrusion of basaltic volcanic necks was sustained by convection within the plug. Any blocks broken off at the margins (because of the expansion of pore fluid on heating and of the rock itself) cool the mush, increase its density and entrain it downwards while hot crystal mush rises up the centre of the plug. Blocks in the rising currents are expected to be small and rounded due to exfoliation during further expansion of the blocks. Such a convection mechanism is supported by the plagioclase-rich cylindrical core with rounded, low-density anorthosite fragments which would be expected to have been concentrated in the rising current. The gabbro sheath around the Papadil Plug suggests that some of the peridotite plugs followed earlier basic plugs or that their emplacement was lubricated by basic liquid, as suggested by Brown (1956) for the ELS. The local segregation of intercumulus liquid which produced the rootless anorthositic veins may be due to late internal shear of the mush. The irregular distribution and large size of blocks in the Barkeval Plug

suggests that the mush was locally derived and not emplaced over a large vertical distance. A possible source would be the northward continuation of the Ruinsival Group (intruded downwards). In view of the characteristic trace element abundances of the plugs (section 6.8) and their late position in the history of the complex (Table 2.1), the plugs are not considered as possible feeders for the layered series. The high content of intercumulus hydrous minerals (section 5.8) suggests that volatiles were trapped within the plugs. The high volatile pressure would have aided the diapiric intrusion of these bodies by decreasing their viscosity and density (section 7.10).

7.5 A Model for the Crystallisation of Crystal Mush.

The following model is suggested to explain the textures described in sections 5.1 and 5.2, and bears on the processes occurring within the crystal mush of the boundary layer at the interface of magma and uncompacted cumulate (McBirney and Noyes, 1979), and those within the uncompacted cumulate.

7.5.1 The Boundary Layer.

Nucleation and growth of one or more phases produces a one-phase or multi-phase mush. Thermal and compositional gradients exist across this layer which may procude a chemical and density stratification in the liquid (Rice, 1976; McBirney and Noyes, 1979) and volatile-rich buoyant intercumulus liquid from the compaction of the cumulates below may percolate up through the mush (Irvine, 1980). This mush may be deformed by down-slope slumping or drag due to convection outside the boundary layer. These shear-dispersive forces may concentrate crystal nuclei into planar horizons as well as segregating the constituents of the melt (e.g. polymerised and depolymerised domains, H_2O, etc.) into separate laminae, thus producing a chemical micro-stratification (Barriere, 1981).

7.5.2 Crystal Settling.

A silicate melt at its liquidus temperature has a structure, consisting of poorly polymerised silica tetrahedra, which gives it strength and a rheological behaviour intermediate between that of a liquid and a solid. This yield strength (McBirney and Noyes, 1979) must be overcome before a crystal of greater density can sink through it; this happens for a given yield strength when a crystal reaches a critical size.

Therefore, a crystal mush eventually collapses to a cumulate due to crystal growth and/or a decrease in yield strength of the melt. The yield strength or degree of polymerisation of the melt is reduced by an increase in Mg, Fe^{2}, H_2O and alkalis, while increasing Si, Fe^{3}, Al and P has the opposite effect; H_2O has the most dramatic effect (Shaw, 1963; Watson, 1981).

7.5.3 Intercumulus Crystallisation.

This process begins once the cumulus crystals have formed a touching framework and takes the form of overgrowths on cumulus crystals or nucleation and growth of new phases. As the cumulate pile grows, the loading causes compaction by rotation and recrystallisation of the cumulus crystals, expelling the intercumulus liquid which mixes with the liquid in the overlying cumulate as it moves up (Irvine, 1980). Crystallisation in the uncompacted pile may produce a buoyant residual hydrous liquid which moves up, even without loading, setting up a convection system in which primitive liquid from above the cumulate pile sinks down to take its place, helped by the 3 % loss of volume on crystallisation (Hess, 1980). This convection system may be one of double-diffusive convection (Rice, 1976; McBirney and Noyes, 1979). Upward moving liquid is likely to encounter layers of low permeability and to accumulate below such layers. Fluid pressure may then build up and eventually lift the overlying cumulates to form a layer of liquid analogous to the water-sills produced during the diagenesis of sedimentary rocks (Donaldson, 1982). As the amount of intercumulus liquid decreases, the upward-moving fraction is expected to concentrate into irregularly distributed channels or fracture zones in the solidifying pile (Irvine, 1980).

7.6 Interpretation of Micro-textures in the Ultrabasic Rocks.

The interpretations given in sections 5.1 and 5.2 are summarised below and integrated with the models presented above.

7.6.1 Crystallisation of the Mush.

The lack of mineral or size-grading indicates that the settling distance of crystals must have been short. Direct evidence of settling over probably less than 1 cm. is given by the spinel geopetal texture (section 5.2.9). The lack of mutual growth interference suggested by spinel-olivine net textures (section 5.1.1) indicates that some mushes

crystallised at least two phases before settling. Oscillatory nucleation (McBirney and Noyes, 1979) in the mush can produce the primary alternations of cumulus minerals, such as chromitite layering.

7.6.2 Deformation of the Mush.

Shearing of the mush may have produced the fine mineralogical layering of some allivalites (section 5.2.4), especially as settling is not expected due to the low density contrast of plagioclase with the melt and the viscous nature (high yield strength) of a melt crystallising plagioclase (McBirney and Noyes, 1979). There is independent evidence for current activity (which would shear the mush) in the form of current scour (section 5.2.8), fragmental layers in allivalite and peridotite (section 5.2.8) and bimodal grain populations which suggest the local reworking of earlier cumulates (section 5.2.10). The occasional size grading of spinel (section 5.2.7) may be due to slow settling or size-sorting by current shear (Irvine, 1980_b). The unconformable superimposed fabrics for different phases (section 5.2.8) suggest deformation of a layered one-phase mush (by slumping, current-drag or loading) followed by *in situ* nucleation of a second phase in laminae which transgress the deformed early layering. Similarly, the size-graded spinels associated with ungraded cumulus plagioclase (section 5.2.7), suggest that the latter nucleated *in situ*, within a one-phase spinel mush. Deformation of a spinel-bearing mush may have produced the localised concentrations of spinel (section 5.2.10) by boudinage.

7.6.3 The Uncompacted Cumulate.

Melt-supported textures (section 5.2.1) indicate that some mushes did not collapse to form a cumulate, while those rocks with evidence for extensive mutual growth interference between two minerals (section 5.2.12) suggest collapse of the mush at an early stage, followed by *in situ* crystallisation of most of the cumulate. To reconcile *in situ* crystallisation textures with the chemically divergent nature of cumulates such as chromitite and anorthosite requires either extreme segregation of the liquid by a process such as double-diffusive convection (McBirney and Noyes, 1979) or the continued growth of the cumulus crystals in a one-phase mush from a flux of liquid through the layer without nucleation of other phases. The latter mechanism would operate once the cumulus crystals form a touching framework and would require less extreme differentiation of the magma by liquid/liquid stratification; it is sug-

gested by the evidence for the upward movement of liquid (section 7.1.5).

7.6.4 Compaction of the Cumulate.

Mineral lamination was probably largely a result of compaction (section 5.2.3) which also explains the strain lamellae in elongate sub-horizontal olivines (section 5.3.1) and recrystallisation textures (section 5.2.13) in the highly compacted dunitic peridotites. Parallel orientation is not observed in the melt-supported rocks which represent uncompacted cumulate or mush (section 5.2.1), in olivines included in pyroxene oikocrysts grown in uncompacted cumulate (section 5.2.3) and the remobilised peridotites with conduit texture from E. Trallval and the drag zone of the ELS close to the contact with the CS. Compaction is aided by:

(1) Rapid loading of the cumulate due to slow cooling of the cumulate pile relative to cooling of the magma at the roof to produce a large thickness of uncompacted cumulate (Hess, 1972).

(2) Decreasing viscosity of the intercumulus liquid due to the concentration of H_2O into residual liquid during intercumulus crystallisation (section 7.10). This factor may explain the higher concentration of hydrous minerals in the dunitic peridotite compared with feldspathic peridotite (section 5.3.6). The associated larger olivine sizes may also be due to the increased diffusivitites and higher growth rates in hydrous melts.

7.6.5 Upward Movement of Intercumulus Liquid.

As clinopyroxene is the last phase to finish crystallising, its distribution can be used as a tracer for the movement of intercumulus liquid (section 5.2.11); elongate oblique and perpendicular pyroxenes suggest movement of liquid along fractures transverse to the layering. Entrapment of such a liquid below relatively impermeable horizons probably produced the harrisite and protoharrisite laminae (sections 5.2.6 and 7.1.2). These show no lamination in the thicker layers, suggesting that the permeability contrast was maintained until the cumulate had entirely crystallised, which is supported by the abundance of hydrous minerals in these layers (section 5.3.6). Entrapment of liquid below horizons marking a permeability decrease is also suggested by modal intercumulus layering (section 5.2.5).

7.6.6 Deformation of the Cumulate.

The conduit texture (section 5.2.2) is interpreted as a segregation

of intercumulus liquid into narrow channels by the action of deviatoric stress on the uncompacted cumulate (Propach, 1976). This is supported by the intrusive nature of (and evidence of shearing in) the conduit textured ultrabasic breccia matrices. The abundance of plagioclase in these channels reflects the troctolitic nature of the liquid. Clinopyroxene forms thin fringes on olivine, suggesting that the final fraction of intercumulus liquid moved along the interfaces between olivine and plagioclase. Granulation of olivine before the crystallisation of intercumulus phases also indicates deformation of an unconsolidated cumulate and the wide development of this texture along the margins of the CS at Leac a Chaisteil supports the intrusion of the CS as a mush with shearing along the margins (section 2.2.3). Annealed micro-faults (section 5.2.1) suggest brittle deformation at a late stage.

7.7 Interpretation of the Mineral Chemistry of the Ultrabasic Rocks.

The primary mineral compositions attained during growth in the suspension of crystals in the boundary layer put constraints on the composition of, and the conditions of crystallisation in, the magma above the cumulate pile. Continued growth, re-equilibration with the intercumulus liquid and the nucleation of new phases occurred in the zone of cumulate compaction. Finally, sub-solidus processes locally altered the mineral compositions. A qualitative estimate of these various controls on composition is attempted in this section after an appraisal of the evidence for the composition of the parental magma.

7.7.1 The Parental Magma for the Layered Ultrabasic Rocks.

Various compositions have been suggested:

(1) Basalt with less than 10 % MgO (Brown, 1956; Wadsworth, 1961).

(2) Basalt of the Preshall Mhor type with more than 12 % CaO (Donaldson et al., 1973; Dunham and Wadsworth, 1978).

(3) Hydrous picrite with more than 10 % MgO (Donaldson, 1975; Gibb, 1976).

The most recent work (Foster, 1980; McClurg, 1982; Chapter 6, this study) favours a highly magnesian (more than 20 % MgO), hydrous magma for the following reasons:

(1) A picritic magma can precipitate a great thickness of olivine cumulates showing little cryptic variation, as required by the narrow

range of olivine composition in the peridotite (McClurg, 1982; section 5.4).

(2) Such liquids are found as fine-grained dykes intruded at a late stage (Foster, 1980; McClurg, 1982; Chapter 6). At an earlier stage, picritic liquids would be expected to pond at the base of any existing magma chambers below more evolved liquid (Huppert and Sparks, 1980), assuming a slow rate of input (Campbell et al., 1983).

(3) For basaltic magma to precipitate 100 m. of olivine cumulate, requires a 500 m. high liquid column and a large volume of extruded lavas (Dunham, 1970). The near-surface position of the magma chamber (section 1.8) together with evidence for rapid erosional unroofing of the layered complex (Dunham and Emeleus, 1967) suggest a small magma chamber which produced few differentiates, thus favouring a picritic parent.

(4) The abundance of supersaturation textures for olivine and plagioclase suggests a hydrous magma (Donaldson, 1975; Donaldson et al., 1973; McClurg, 1982). A high volatile content would also decrease the magma density and facilitate its emplacement at high crustal levels (Rast, 1970).

(5) Chondrite-normalised LREE abundances for plagioclase (Henderson and Gijbels, 1976) and clinopyroxene (Palacsz, pers. comm.) are slightly enriched, unlike those for the Preshall Mhor magma type, which also has plagioclase on the liquidus before olivine. The other suggested parents are slightly LREE-enriched and have olivine on the liquidus first, followed by plagioclase and then pyroxene (Foster, 1978, 1980; McClurg, 1982) which is the sequence of appearance of the cumulus phases in the layered series.

7.7.2 The Bearing of the Mineral Chemistry on the Magma Composition.

The ranges of mineral chemistry for all phases of the ELS and CS cumulates are similar (section 5.4) suggesting a common parental magma; this is confirmed by the similar trace element ratios (Table 6.14). There are, however, significant differences between the magmas for the two series:

(1) NiO-Fo relations for olivine indicate that the ELS was saturated with sulphides while the CS was undersaturated (section 5.4.1).

(2) The crystallisation of pyroxene was earlier with respect to plagioclase in the CS than in the ELS. The evidence for this is:

(i) The maximum Cr content of CS pyroxene is higher than that for ELS pyroxene (1.69 vs. 1.32 wt% Cr_2O_3; section 5.4.3).
(ii) Na_2O and Al_2O_3 contents of CS pyroxenes are higher than those for the ELS (section 5.4.3)
(iii) Textural relations (sections 5.2.1 and 5.3.3).

The evidence suggests the inhibition of plagioclase growth, leading to a plagioclase-supersaturated liquid. This may have been effected by an increase in water content or total pressure (Irvine, 1979). The subsidence of the CS with respect to the ELS suggests that the effect was probably due to higher water activity, as confirmed by the greater abundance of hydrous minerals in the CS (section 5.3.6). The "Ca-trend" defined for the ELS pyroxene on the pyroxene quadrilateral (section 5.4.3) probably reflects a change in the shape of the pyroxene solvus due to fluctuation in total P or P_{H_2O} (Atkins, 1969), with the latter again being more likely.

(3) At a given Mg-number, CS spinels included in olivine have higher Fe^{3+}/Fe^{3+}+Cr+Al and lower Cr/Cr+Al, also suggesting growth from a plagioclase-saturated liquid with a high oxygen fugacity.

(4) Cumulus plagioclase in the ELS is more calcic than that of the CS which is attributed to the simultaneous crystallisation, in the CS, of Ca-rich pyroxene. This supports the expansion of the liquidus field of pyroxene with respect to that of plagioclase in the CS, as suggested above, at least for the cumulus stage of crystallisation.

7.7.3 Compositional Effects of Intercumulus Processes.

These are difficult to separate from primary compositional parameters, but the following features suggests that they must have been important (see also sections 7.11, 7.7.5 and 7.7.6):

(1) Intercumulus "core" compositions are highly variable and strong reverse zoning is common (section 5.4.2). This suggests that plagioclase nucleated against cumulus crystals (heterogeneous nucleation; Campbell, 1978) which it partly enclosed, and gradually grew into the pore spaces from evolving intercumulus liquid. Zoning of the cumulus plagioclase is usually normal (McClurg, 1982).

(2) The wide range in composition of spinels compared to that for other layered intrusions suggests re-equilibration with intercumulus liquid of changing composition over a long period (Henderson, 1975; section 5.6). The wider compositional range of CS spinels included

in olivines with respect those of the ELS suggests the olivine was a stable intercumulus phase for longer than in the ELS, which would be expected from the expansion of the Fo field with decreasing P and increasing water activity (above section and section 7.10).

7.7.4 Sub-solidus Re-equilibration.

Highly localised diffusional exchange between minerals may be suggested for:

(1) Ca between olivine and plagioclase (section 5.4.1).

(2) Mg and Fe^{2+} in olivine within or close to chromite concentrations (Irvine and Smith, 1967; Table 5.8). A similar process involving olivine rims and spinels disseminated between the olivines is probably responsible for the slight reverse zoning of olivine (sections 5.4.1 and 5.4.4) which is supported by the relative lack of such zoning in the dunitic peridotite of the CS, where most disseminated spinel is actually included in olivine.

(3) Mg and Fe^{2+} between spinel and mafic silicate inclusions (section 5.5.2).

(4) Ti between spinel and hydrous mafic silicate inclusions (section 5.5.2); this explains the higher Ti content of the latter compared with the intercumulus occurrences.

7.7.5 Cryptic Variation over the ELS.

The main points to arise from the data presented in section 5.7.2 are as follows:

(1) There is no overall stratigraphic variation except that cumulus plagioclase tends to be more calcic in the upper units.

(2) Variations in the Ni content of the olivine correlate most closely with the lithological variation and show little lateral variation over the outcrop of each series. Sharp reversals in the variation mark the base of most units, followed by slow evolution. Reversals are displaced upward (by a maximum of 7 to 8 m.) only at the base of U14 and U16 and minor reversals occur within the peridotite layer of U10, U12, U14 and U15. The variation may reflect the primary Ni content of the magma, reversals being produced by replenishment of the chamber in picritic liquid (section 7.8; McClurg, 1982). The strongest reversals occur at the base of U11 and U15.

(3) The Fo content of the olivine and the Mg-number of the pyroxene vary sympathetically, sugesting late-stage Fe/Mg equilibration between

these phases. The variation patterns are similar to those of Ni in olivine but basal reversals are displaced upward by 7 to 20 m., except for U15, which overlies the thickest allivalite layer on Trallval; intra-peridotite reversals are displaced 4 to 43 m. up with respect to the Ni reversals. The upward displacement of reversals in mineral chemistry with respect to lithological contacts has been attributed for the Muskox intrusion (Irvine, 1980) to upward expulsion of intercumulus liquid from the underlying, more evolved cumulates. Irvine showed that the reversal in Fo variation is displaced more strongly than the Ni reversal due to the higher crystal/liquid partitioning coefficient of Ni. The strongest field evidence for the upward movement of intercumulus liquid is (i), the feldspathic streamers at the base of U14 and (ii), the deformation zone at the base of U16, which lies in the fault-drag zone near the CS contact (section 7.7.4). It is only at the base of these units that the Ni reversals are displaced. The lack of a displacement of even the Fo reversal at the base of U15 is attributed to the relative impermeability of the thick allivalite of U14, while the strong displacement of intra-peridotite reversals points to the permeability of the peridotite.

(4) The Cr content of pyroxene shows equally strong reversals at the base of a unit as at the base of allivalite layers. This is attributed to the abrupt cessation of Cr-spinel crystallisation at the base of allivalite layers.

(5) Reversals in the An content of plagioclase occur near the base of the unit, followed by a gradual evolution to the base of the next allivalite layer. The strong reversal is attributed to the change in the order of nucleation of the mineral phases: the transition to a more evolved liquid (section 7.8) marking the base of the allivalite is more than compensated by the early formation of the cumulus plagioclase. At the base of the next unit, the crystallisation order reverts so that intercumulus plagioclase crystallises late from a liquid into which alkalis have been concentrated by the fractionation of olivine.

(6) The Fo content of olivine on the W. Trallval section is higher by ca. 1 %, 2 % and 1-3 % than on Barkeval, Hallival and E. Trallval, respectively. This lateral variation is not gradual and by analogy with the 2-4 % variation on Trallval Ridge, it is suggested that the

ELS is partitioned into a number of domains, 50 to 100 m. across (section 7.9.3).

7.7.6 Cryptic Variation over the CS.

The data (section 5.2) differ from those for the ELS as follows:

(1) Through large thicknesses of dunitic perisotite (e.g. LLG2), there is no variation in olivine composition. Over the RG1 unit, this composition shows a continuous reverse trend. Both the invariant and reverse trends are explained in section 7.12.

(2) At unit contacts (except DM/LLG1), the initiation of reversals in the Fo pattern occurs below the lithological contact and precedes that of Ni; Fo reversals terminate higher than those for Ni (28 to 50 m. up vs. 14 to 32 m.). This suggests that magma or intercumulus liquid of a relatively high density from the overlying unit moved down to replace some of the upward moving liquid from the underlying cumulates. This process probably operated in the ELS as well, but is not seen because of the expected smaller scale of reversal displacement. The strongest reversal in the CS occurs at the base of the LLG1 unit, along which there is no displacement of cryptic reversals (except at Leac a Chaisteil). This is attributed to the relative impermeability of the thick allivalite layer of the DM (except at Leac a Chaisteil, where it consists of a few thin layers).

(3) The most evolved intercumulus plagioclase cores occur about a third of the way up into the unit, while zoning is strongest just below the allivalite: the base of the latter is marked by the major reversal in plagioclase composition, as in the ELS.

(4) There is little lateral variation of Ni content in olivine, except at the base of LLG1 where olivines in the Leac a Chaisteil section are Ni-poor and fayalitic. This is attributed to contamination of the magma by molten wall-rock from the Southern Mountains Complex (sections 6.4.2 and 7.11). The lateral variation in Fo again defines local domains within which the Fo content is about constant. Olivines of the southern Papadil, NW Ruinsival and Coastline sections and the northern Long Loch section are all richer in Fo than those in a central belt including the Seagull, Trallval and NE Ruinsival sections (lower by ca. 2-3 mole % Fo) and especially the Leac a Chaisteil section (lower by 3-5 mole % Fo). This belt coincides at Leac a Chaisteil with a structural dome (section 2.2.2.3), which may

be associated with locally accelerated cooling and the observed chemical phenomenon (section 7.9.3.3).

7.8 The Origin of the Macro-Layering.

Brown (1956) suggested that the repetition of peridotite/allivalite units, together with the apparent lack of cryptic variation, was produced by repeated injections of primitive magma on the olivine-plagioclase liquidus, accompanied by the eruption of evolved liquid. At first, only olivine crystallised (to give the peridotite layer) until the liquid was supersaturated to the required degree to nucleate plagioclase. In a more refined model, also devised for Rhum, Huppert and Sparks (1980) showed that upon entering a magma chamber, dense picritic liquid does not mix with the residual liquid in the chamber but underflows it to form a stratified liquid column. Crystallisation and separation of olivine brings the density of the newly injected liquid down to that of the overlying "old" liquid, at which point the two liquids mix to produce a hybrid magma crystallising plagioclase. Such a two stage process produces a layer of allivalite over peridotite. It is supported by data from McClurg (1982) and this study (section 5.7) on cryptic variation, which shows an abrupt change near peridotite/allivalite contacts and is stronger in the thin allivalite layer than it is over the peridotite layer. The strongest evidence for epidodic replenishment is the lack of chemical evolution from one peridotite layer to the next over the entire set of units. Indeed, only the allivalite layers would be expected to show such evolution with height in the series, as at least a fraction of the residual liquid from the crystallisation of each allivalite layer is retained in the reservoir of old liquid in the model of Huppert and Sparks (1980). The increasing anorthite content of plagioclase with height in the ELS may be due to the buil-up of volatiles in such a reservoir of old liquid.

Palacsz (pers. comm.) determined that the allivalites have a distinct, enriched Sr^{87}/Sr^{86} isotopic ratio compared with that of the peridotites. This suggests that the reservoir of residual liquid became contaminated with crustal material from the wall-rock, consistent with its long residence in the chamber, while the peridotite layers retained the low isotopic ratios of uncontaminated melts.

Between major injections, small pulses of picritic liquid may have entered the chamber to produce some of the intra-peridotite reversals in cryptic variation and the common, thin peridotite layers within the allivalites. Indeed, Huppert et al. (1982) suggested that major injections may be due to the continuous input of magma which will eventually rise through the early cumulates to produce the next injection. The escape of small batches of magma from this pool could produce the irregularities noted above.

7.9 Models for Lateral Variation.

Although individual units can be correlated over the entire outcrop of the ELS and CS, the series are both laterally partitioned into a number of small domains , each with distinct structural, lithological, textural and chemical features (sections 3.5, 7.1.1 and 7.5.5). This suggests a strong local control over the formation of the cumulates that is incompatible with an origin by homogeneous nucleation from a convecting magma, followed by settling to the bottom and crystallisation of intercumulus material within a few metres of the main, convecting body of magma (Brown, 1956; Wager and Brown, 1968). Models which explain strong lateral variation are discussed below, and illustrated in Fig. 7.1.

7.9.1 Slumping of Wall Cumulates.

Slump structures are conspicuous in the allivalites, which also have a laminar flow fabric (Brothers, 1964) and show some evidence for erosional scour (section 5.2.8). McBirney and Noyes (1979) demonstrated that the effective viscosity of magmas is high enough to allow the formation of wall cumulates and to stabilise the superposition of liquid layers of different density and composition. Irvine (1980_b) suggested that layers of unconsolidated wall cumulates become unstable and slide downward to form aprons at the foot of the wall which, upon over-steepening or fluidisation by rising intercumulus liquid from underlying bottom cumulates, periodically slump toward the centre of the intrusion. In the case of an evolved liquid layer overlying a picritic liquid (above section), the wall cumulates would be allivalitic and spread down and across over peridotitic cumulates which would continue to form in between and away from the slump deposits (Fig. 7.1 A). Such a model may explain the strong lateral variation in allivalite thickness seen in both the ELS and CS, despite

the approximately uniform thickness of the unit as a whole. However, grading is not as common as predicted by Irvine (1980_b) and the zone of feldspathic peridotite with some cumulus plagioclase in lateral as well as vertical transitions, or facies changes (sections 7.1.2 and 7.2.2), from peridotite to allivalite is not explained by this model.

7.9.2 Lateral Accretion.

Irvine (1981 and 1982) suggested that layered intrusions form by lateral accretion of the layer-like convection cells of a horizontally stratified liquid. It may be predicted that such a process would give rise to lateral chemical evolution of the cumulates and a discordance between the fine-scale layering parallel to the cooling surface and the lithological layering parallel to the liquid stratification. The latter feature has been observed in the Bay of Islands complex (Casey and Karson, 1981). In addition, repeated injection of picritic liquid (as suggested in section 7.8), if it occurs while the allivalite-forming cell has only partly accreted onto the walls, will displace this cell upward and produce a lateral transition to peridotite (Fig. 7.1 B). Over the entire series, allivalite layers are expected to reach their maximum development near the walls and dwindle in importance inwards. A minor discordance has been observed in Ul4 of the ELS between cluster layering and lithological layering (section 3.5.10), which supports the model although this is not seen in any of the other units. Also, lateral cryptic variation on Rhum is not gradual and systematic (section 5.7.2.3); therefore, other processes must be involved.

7.9.3 Crystallisation of Intercumulus Liquid.

The most powerful model for producing lateral cryptic variation is <u>in situ</u> crystallisation of the cumulate to produce a mush in which lateral circulation of the intercumulus melt is restricted, thus producing domains where crystallisation processes are locally controlled. With more efficient isolation of the reservoir of intercumulus liquid in such a domain from the body of convecting magma above the mush, a larger degree of lateral variation between the domains can be expected. Such isolation is controlled by the thickness of the uncompacted cumulate. Before considering specific local processes which operate in this compacting zone, the evidence for <u>in situ</u> crystallisation and thickness of the compacting zone is reviewed.

7.9.3.1 In Situ Crystallisation.

Alternatives for the formation of cumulates to Wager and Brown's (1968) theory of nucleation throughout the chamber (homogeneous nucleation), followed by crystal settling, include the processes of bottom crystallisation (Jackson, 1961) and heterogeneous nucleation (i.e. at liquid/solid boundaries; Campbell, 1978), based on, respectively, the inability of the settling theory to account for the size distribution of cumulus crystals, and the non-horizontal orientation of primary layering. Such concepts were strengthened by McBirney and Noyes' (1979) demonstration of the non-newtonian behaviour of basic magma at liquidus temperatures, which prevents the sinking of even dense, mafic cumulus minerals. Crystal settling can, however, occur in ultrabasic magmas of low viscosity and even hydrous, syenitic liquids (Parsons and Butterfield, 1981). Evidence from this study (section 5.2, 7.1.2, 7.2.7 and 7.6) suggests that some allivalites and chromitites crystallised almost entirely in situ together with most of the cumulus crystals (plus all the intercumulus phases) forming the peridotite. Cameron (1969) likewise suggested that at least half of the cumulates of the Bushveld formed in situ.

7.9.3.2 The Thickness of the Compacting Zone.

The maximum thickness of the slumped layers gives an absolute minimum for the thickness of the unconsolidated cumulate (Hess, 1960). For Rhum, this is about 8 m. (section 3.5.7). Only about 20 % crystals is necessary to form a rigid framework (Shaw, 1980), however, and thermal studies (Hess, 1972) have shown that unconsolidated cumulates must extend much further down. The exact thickness of such a compacting zone depends mainly on the ratio between the cooling rate at the bottom and that at the top of the chamber (the conductivity of the roof is generally much higher than that of the cumulates forming the floor) but is estimated to be about 0.75 of the unit's thickness (Hess, 1972), which is up to 75 m. for the ELS and 270 m. for the CS. These figures may be larger if the underlying unit is still unconsolidated and may be compared with an independently derived estimate of 300 m. for the compacting zone of the Muskox intrusion (Irvine, 1980). Sections 7.1 to 7.7 present detailed evidence for a considerable thickness of uncompacted cumulate, its compaction and the associated upward movement of intercumulus liquid.

7.9.3.3 Intercumulus Processes Leading to Lateral Variation.

McBirney (1975) suggested that lateral variations in the height of appearance of new phases in the Skaergaard intrusion was due to a combination of *in situ* crystallisation, a substantial compacting zone and differential cooling rates from one side of the intrusion to the other, depending on the differential influx of meteoric water as controlled by the permeability of the wall-rock. Casey and Karson (1981) similarly attributed lateral lithological variation in the Bay of Islands Complex to differential cooling rates produced by the fault-controlled influx of meteoric water. The lithological and chemical variations which define the partitioning of the layered series on Rhum may have been controlled by these processes (Fig. 7.1 C):

(1) Variation in chamber shape may increase cooling, *e.g.* through increasing the ratio of cooling surface area to volume of cumulate. This may explain the low-Mg belt of the CS (section 7.7.5) which coincides with a structural dome on the chamber floor. A higher cooling rate will lead to more efficient trapping and crystallisation of the evolved intercumulus liquid and thus to more Fe-rich olivine. This is supported by the greater importance of feldspathic peridotite with respect to the dunitic peridotite which makes up most of the CS to the south and north. This mechanism predicts that orthocumulates are most likely to form where cooling rates are highest such as close to the walls or bottom of the chamber. On Rhum, orthocumulates are found in the lower units towards the perimeter of the exposed complex (Brown, 1956 and Wadsworth, 1961), as predicted.

(2) Fault or fracture controlled influx of meteoric water may also locally accelerate the cooling rate. The effect on olivine composition is partly offset by oxidation of the magma which results in more Mg-rich olivine (section 7.10).

(3) Mixing or re-equilibration of intercumulus liquid with gabbroic liquid injected into the layered series. There is evidence that this may have been important in the E. Trallval section (sections 7.1.1 and 5.6.1). The chemical exchange with the more evolved gabbroic liquid would result in more Fe-rich olivine.

(4) Differential compaction may be due to unequal loading (*e.g.* by aprons of slumped wall cumulates near the walls of the chamber; section 7.9.1) or delayed crystallisation of the intercumulus liquid

due to slower cooling rates or possibly a high volatile content (section 7.10). The high proportion of dunitic peridotite in the coastline section of the CS is probably due to highly efficient compaction because of a combination of high loading (the CS is thickest here), slow cooling rates at the walls and floor (the chamber was widest here and the cooling effect of the walls was thus lessened) and a greater permeability of the compacting zone due to the virtual absence of "blocking" allivalite layers, thus allowing more complete expulsion of intercumulus liquid.

(5) Lateral chemical variation is expected due to the crystallisation of intercumulus phases from upward moving liquid of different composition. The composition of this liquid depends on the extent to which it fractionates by crystallisation as it moves up and the degree to which it re-equilibrates with the cumulates through which it passes. For instance, the passage of the liquid through a thick sequence of evolved allivalite cumulate will result in more Fe-rich overgrowths on the olivine in the overlying peridotite, while the efficient compaction in an allivalite-free sequence results in a scarcely more evolved upward moving liquid. The composition of the intercumulus liquid expelled at the interface of the cumulate pile with the magma may, in turn, affect the composition and even the nature of the nature of the primary cumulus phases. In section 7.1.5, it was suggested that the hydrous, upward moving intercumulus liquid may be partly responsible for the resorption of allivalite which varies laterally according to the flux of intercumulus liquid and its composition. Thus, the more efficient expulsion of liquid from the compacting zone at the centre of the intrusion, due to its delayed crystallisation, may be partly responsible for the scarcity of allivalite in this domain of the ELS.

7.10 The Importance of Water in the Magma Chamber.

Mildly alkaline basalts have 0.2 to 0.6 wt% H_2O (Moore, 1970; Aoki et al., 1981). Mildly alkaline picrites probably have even less, and K_2O contents of picrites analysed in this study (Table 6.10) suggest that mantle-derived water composes less than 0.05 wt% of the liquid (Aoki et al., 1981). Meteoric water contamination of shallow intrusions is considered general where country rocks allow access and

convection (Carmichael et al., 1974; Taylor and Forrester, 1971), or where the chamber lies close to or across fault-zones (MacLean, 1969). The Rhum layered series probably formed at P = 0.3 to 1.0 Kb (section 1.8), at which basalt is water-saturated for H_2O contents of 1.0 to 2.5 wt% (Williams and McBirney, 1979). Thus, it is likely that even if the magma overlying the cumulates is initially undersaturated, the intercumulus liquid in the compacting zone is water-saturated due to absorption of meteoric water through the walls (Donaldson, 1982). This is supported by the abundance of hydrous minerals in mesostasis patches representing trapped liquid, in the orthocumulates and harrisite layers (Williams, 1978; Donaldson, 1975). The effects of a high water pressure in the magma include:

(1) A lowering of the liquidus temperature by ca. 40 ^{o}C for every 1 % of H_2O (Zavaritsky and Sobolev, 1964). This counteracts the crystallisation effect of cooling and favours a thick compacting zone, where meteoric water is absorbed into the intercumulus liquid. Devolatilisation, by e.g. pressure relief, causes rapid supercooling and has been invoked to explain the origin of harrisite layers (Donaldson, 1974). A decrease in liquidus temperature results in more An-rich plagioclase (Loomis, 1982) and more Mg-rich olivine.

(2) An increase in oxygen fugacity, if the initial H_2 content of the liquid is low or H_2 can escape through the roof (MacLean, 1969). High oxygen fugacity, by oxidising Fe^{2}, increases the Mg/Fe^{2} ratio of the liquid which thus crystallises more Mg-rich olivine (Roeder and Emslie, 1970) and more Fe^{3}-rich spinel. Sulphide solubility decreases with increasing oxygen fugacity (Haughton et al., 1974).

(3) Depolymerisation of the silica groupings in the melt, at least for the first 2 wt% of H_2O dissolving into the liquid, which results in lower viscosities, higher element diffusivities and higher growth rates (Stolper, 1982). The viscosity of albite melt is lowered by a factor of 10^{5} by the incorporation of 6.4 wt% H_2O (Burnham, 1979). From the settling evidence of spinel grains 0.2 mm. across (section 5.2.9), it may be deduced that the yield strength (effective viscosity) of the probably water-saturated liquid was close to 20 dyne/$cm.^{2}$ (McBirney and Noyes, 1979), lower by a factor of 10^{3} than the 1000 dyne/$cm.^{2}$ estimated for anhydrous basaltic liquids at 1100 ^{o}C (Williams and McBirney, 1979). Depolymerisation also shifts the li-

quidus phase relations: increasing H_2O content expands the Di field in the An-Di system (Zavaritsky and Sobolev, 1964; Yoder, 1965) and the Di and Fo fields with respect to An in the Fo-An-Di-Si system (Irvine , 1979). Hydrous intercumulus liquid from peridotite may not be in equilibrium with troctolite, resorb plagioclase and crystallise pyroxene instead. Such a process is suggested by the replacement of troctolite by pyroxene-rich peridotite (section 7.1.2).

(4) The separation or vesiculation of a separate fluid phase upon ascent of water-saturated melt (Williams, 1978; Sparks, 1978). The adiabatic expansion of the water-saturated melt and vapour mixture supercools the liquid by 0.1 ^{o}C for every metre of height and may explain the importance of supercooling textures apparently formed within the compacting zone (Donaldson, 1982; section 7.1.2). The separate fluid phase, which consists mostly of H_2O in a supercritical liquid/gas state, absorbs elements such as Na, K, Rb, Al and Si which concentrate preferentially into the vapour phase (Williams, 1978; Sinton and Byerly, 1980; Hart and Allègre, 1980). This removal of alkalies from the intercumulus liquid favours the crystallisation of An-rich plagioclase (Jaques, 1981). The removal of a hydrous assemblage from the compacting zone may explain the discrepancy between the minor element ratios observed and those expected for the ultrabasic rocks if they formed from the magma parental to the dyke suite (section 6.8). Concentration of volatiles towards, eventually, the top of the chamber produces a liquidus temperature gradient which favours *in situ* bottom crystallisation (Elsdon, 1970). Vesiculation near the roof may result in indentation fracturing of the brittle crust (Sharpe, 1981), a process which may have played a role in the emplacement of the volatile-rich ultrabasic plugs.

7.11 Contamination of the Melt and the Origin of Chromitite.

O'Hara (1978) suggested that considerable assimilation of roof and wall rocks is necessary in sub-volcanic magma chambers to reconcile the evidence for crystal fractionation with the low heat flow above modern volcanoes. De Paolo (1981) believed that assimilation of wall rocks is necessary to absorb the latent heat of crystallisation in a compacting pile of cumulates. If the country rock is pre-heated (*e.g.* by repeated injection of basic magma , as on Rhum), basic magma

can melt and absorb up to 40 % of sialic material (Taylor, 1980) with olivine remaining on the liquidus, although the high intake of Si expands the liquidus volume of orthopyroxene (Irvine,1975). Thus, Irvine (1975) and Gray et al. (1981) suggested that the abundance of orthopyroxenite in the layered intrusions of Muskox, Stillwater, Bushveld and the Great Dyke reflects strong crustal contamination of basic liquid. In the shallower intrusion of Rhum, a higher level of sialic contamination would be required to produce orthopyroxenite due to the expansion of olivine and plagioclase liquidus volumes at the expense of Ca-poor pyroxene with decreasing pressure (Irvine, 1979). At least some bulk contamination is suggested by the inclusions in spinel (section 5.5.3). Maury (1978) and Watson (1982) have proposed that melting of the wall rock produces a liquid which does not mix with the magma but exchanges chemically with it by liquid/liquid diffusion, producing selective contamination of basic magma in K_2O, trace elements and possibly Na_2O and Al_2O_3 . The absorption of hydrous fluids from the country rock enriched in incompatible elements may also effect selective contamination of the magma, as suggested by Palacsz (pers. comm.) to explain the strong variation in Sr isotopic ratios of the ELS cumulates. An important effect of crustal contamination is the production of chromitite suggested by the shift of hybridised basic/acid liquids into the spinel liquidus volume in the Fo-An-Di-Pc-Si system (Irvine, 1975_b). Alternative origins for the chromitites are considered below:

(1) In recent reviews, an origin by current sorting and gravity settling (Wager and Brown, 1951) has been discounted, as Jackson (1961) demonstrated the lack of hydraulic equivalence between olivine and spinel in mixed layers and the lack of grading in chromitites.

(2) As chromitite layers, by their unsystematic positions within cyclic units often appear not to be related to fractionation cycles, many workers (Cameron and Desborough, 1969; Ridley, 1977; Cawthorn and McCarthy, 1980) appealed to sudden but temporary changes in total P (e.g. by roof collapse) or water activity (by periodic assimilation of water-rich country rock or devolatilisation by eruption) to explain their origin.

(3) Maaloe (1978) suggested that the build-up of latent heat released by intercumulus crystallisation periodically inhibits the crystallisa-

tion of all phases except spinel, thus forming spinel concentrates.
(4) Because of the curved forsterite/picotite cotectic in the system Fo-Di-An-Pc-Si, mixing of liquids on the cotectic puts the hybrid in the spinel liquidus volume; the greater the difference in degree of evolution of the liquids (separation along the cotectic), the more abundantly the hybrid will crystallise spinel before rejoining the cotectic (Irvine, 1981). As the cotectic wraps around an area in the system of non-ideal mixing above a sub-solvus liquid miscibility gap (Irvine, 1981), addition of H_2O to the system, which lowers the liquidus temperature, may result in a hybrid which plots in a two-liquid field. Such a composition may develop into an emulsion of one liquid within another, with spinel nucleating on the globules.
(5) Huppert and Sparks (1980) suggested that the reaction of evolved basaltic liquid and picritic magma $\pm$ melted allivalite also results in the formation of spinel, according to the model of Irvine (1977). The situation arises when a pulse of picritic liquid is injected into a chamber crystallising plagioclase from a more evolved liquid. The dense picritic liquid spreads over the floor, separated from the allivalite by a thin cushioning layer of old liquid, as suggested for the Great Dyke by Wilson (1982), who observed no evidence at the top of the allivalite of resorption or reverse zoning expected from the direct juxtaposition of allivalite and picrite.

No single model accounts for all chromitite layers (section 5.6) and chromitite-layered zones (section 7.1.2) on Rhum. Gravity settling of spinel over short distances has been demonstrated (section 5.2.9) and probably accounts for some of the chromitite laminae associated with harrisite or protoharrisite layers (section 7.1.2). The spinel rims around allivalite or gabbro xenoliths in peridotite or ultrabasic breccia matrix suggest a reaction mechanism such as that proposed by Irvine (1977), or may be due to the local increase in oxygen fugacity around the highly oxidised blocks (with respect to peridotite). For such a reaction to occur, or oxidation front to develop, it is suggested that intercumulus liquid in equilibrium with the plagioclase-rich rock, of internal or external origin, must be available. The sporadic development of such spinel coatings on xenolith margins suggests it often was not. The basal chromitites (at allivalite/peridotite contacts) found in some units may have a similar origin rather than

represent accumulation of liquidus spinels.

The abundance of silicate inclusions in the spinels from some chromitite layers (section 5.5) suggests that they may be linked with the origin of the chromitites. These inclusions are either derived from earlier cumulates or wall-rock, or consist of hydrous, alkali- and silica-rich minerals. They suggest liquid blending (Irvine, 1981) involving (i) melted allivalite and/or wall-rock and a basic liquid which nucleates spinel on xenocrysts from the allivalite or remnant globules of granitic melt from the wall-rock, or (ii) evolved water-saturated intercumulus liquid with a vesiculated phase into which alkalis and silica have preferentially partitioned (section 7.10) which mixes with more primitive liquid as it moves upward, the spinel nucleating on or enclosing the incompatible element enriched globule. The second process of liquid mixing may occur throughout the compacting zone (as suggested by the ubiquitous inclusion-bearing spinels) but is likely to have the strongest effect at the interface of the cumulate pile and the magma, especially when crystallisation of phases other than spinel is inhibited by the latent heat of crystallisation carried up by the intercumulus liquid (Maaloe, 1978). When other phases did crystallise simultaneously, chromitite-layered zones (section 7.1.2) may develop, especially in peridotite just overlying allivalite, which yields much evolved intercumulus liquid. Section 7.9 emphasises the local controls on the behaviour of intercumulus liquid however, and it is possible that chromitites which are laterally continuous over the many domains of the ELS may represent chamber-wide fluctuations in water activity or oxygen fugacity, especially when associated with sulphide concentrations which also form on rapid oxidation of the magma (MacLean, 1969). If the Huppert and Sparks (1980) model for the macro-layering on Rhum applies, chromitites would be expected where the residual picritic liquid and the "old" evolved liquid mix, i.e. just below the allivalite. Some units of the ELS have chromitite-layered zones in just such a position (section 7.1.2) and in unit RG1 of the CS, chromite concentrations at the top of the peridotite also suggest an origin by liquid mixing (section 7.2).

7.12 The Formation of the Central Series.

McClurg (1982) concluded that the parent for the CS was a mush with up to 50 % olivine crystals, injected into a chamber of a shape and position similar to that of the outcrop of the CS. This is supported by the large cumulate thickness of stratigraphically invariant mineral chemistry, which may represent the deposition of crystals from a vigorously convecting, homogenised mush (Huppert and Sparks, 1980). That the entire chamber should be filled with crystal mush is also a requirement for the mechanism of ultrabasic breccia formation suggested in section 7.3. Finally, the almost instantaneous formation of such a large thickness of incompacted cumulate (unconstrained by cooling rates within the chamber) favours rapid compaction and the efficient expulsion of intercumulus liquid, thus leading to thick layers of dunite and dunitic peridotite. The abundance of hydrous intercumulus minerals (section 5.3.6) suggests that the intercumulus liquid had a low yield strength which aided compaction. The high water activity also delayed the nucleation of plagioclase with respect to that of olivine and clinopyroxene (section 7.7.2), leading to a smaller volume of more evolved differentiates with respect to the ELS (section 5.4.4) which collected to form a "pool" of evolved liquid by the ascent of intercumulus liquid, and then crystallised to produce allivalite. Each unit represents a new injection of crystal mush, with the intercumulus liquid moving upward and collecting at the top of the chamber to form the troctolite layer; irregularities in the shape of the roof may be partly responsible for the strong lateral variation of allivalite thickness.

The strong deformation of the cumulates can be attributed to the tectonic activity required to emplace a pulse of crystal mush and the stronger drag effect associated with the convection of a crystal mush compared with that of a liquid. The reverse cryptic variation for both Ni and Fo content of olivine in unit RG1, associated with a reverse, upward increase in modal spinel may represent a normal evolutionary trend in cumulates within a lower reservoir (where the mush formed) which has been inverted by slow injection into the new chamber. The slow rate of injection would prevent the convective homogenisation of cryptic variation as in the mushes which crystallised to form the other units. The inversion of a lower reservoir may explain the formation of the thick allivalite which composes the DM, at the

base of the CS. The DM cumulates may have crystallised from the reservoir of evolved liquid which had accumulated at the top of the lower chamber and formed the first injection of material into the "CS chamber".

7.13 Conclusion

The cumulus crystals of the ELS formed by *in situ* nucleation at the margins of the magma body. Repeated replenishment, which produced the macro-layering, also produced a stratified magma, as fresh injections of picritic liquid underflowed a layer of residual liquid from the fractionation of previous primitive injections. The lateral accretion of plagioclase cumulates from this upper layer may have led to the observed facies change to olivine cumulates; thickening of allivalite layers towards the margin of the intrusion was accentuated by the formation of aprons of slumped cumulates near chamber walls. The layer of picritic liquid crystallised olivine and as each new injection increased the heat build-up around the chamber, cooling rates at the bottom decreased to produce thick mushes and compacting zones, especially towards the centre of the chamber. The upward streaming of intercumulus liquid from these zones and its collection as a layer of evolved liquid is thought to be a major factor in the fractionation of the picritic liquid to form ultrabasic cumulates.

Textures, shared by the peridotites of the plugs and breccia zones, characteristic of unconsolidated cumulates, developed and also those indicative of the ascent of intercumulus liquid. These unconsolidated cumulates were locally deformed, mobilised and intruded into adjacent parts of the cumulate pile. A similar process, on a larger scale, produced the peridotite plugs and was responsible for the formation of the CS, which may represent an inverted stratigraphy developed in a lower reservoir. As most of the growth of the cumulus crystals and the nucleations and growth of intercumulus phases took place in the compacting zone, the final textures and mineral compositions of both series were largely determined by secondary processes in this zone of unconsolidated cumulates.

These processes include the chemical exchange with intercumulus liquid and rates of cooling and compaction, which are themselves controlled by the chamber shape, local controls on the absorption of

meteoric water and tectonic and chemical effects associated with the intrusion of gabbro and, in the case of the ELS, the emplacement of the CS.

The ultrabasic breccia zones are considered to represent the segregation of intercumulus liquid into large cracks which opened in the compacting zone and mush during tectonic emplacement and subsidence of the CS. The variation in the processes affecting cumulates in the compacting zone produced strong lateral variation in composition and textures, resulting in the partitioning of each series into a number of domains. The importance of lateral variation on Rhum is attributed to the small size of the intrusion, with the consequent predominance of boundary effects, and its complex tectonic history.

FIG. 7.1 Models for lateral variation in cumulates. Dishes = olivine cumulates, stipples = plagioclase cumulates, circles = orthocumulate, cross-hatches = gabbro, R or r = residual liquid, P or p = picritic liquid.

A- Variation in allivalite thickness by slumping. 1 = slump deposits from laterally accreting layer of residual liquid, 2 = laterally accreting layer of uncompacted olivine cumulate, 3 = compacted allivalite, 4 = compacted peridotite.

B- Attenuation of allivalite by combined lateral accretion and repeated picrite injection. 1 = first picrite injection, 2 = second injection, 3 = the products of the process shown on a more realistic scale.

C- Lateral variation due to intercumulus processes. 1 = laterally accreting layers from stratified magma, 2 = orthocumulates at the bottom and walls of the chamber, produced by rapid cooling, 3 = plagioclase cumulates thin towards the centre due to processes as suggested in A or B above; the thickness of the allivalite near the walls inhibits the ascent of intercumulus liquid and where it does occur, the liquid composition is changed considerably, 4 = thick compacting zone near middle of chamber with efficient expulsion of intercumulus liquid and the assimilation of allivalite, 5 = variation in shape of floor and local influxes of meteoric water near fault-zones influence cooling rates and volatile content of intercumulus liquid, 6 = juxtaposition of another set of unconsolidated cumulates results in the exchange of intercumulus liquid across the fault-plane, 7 = gabbro injection into uncompacted cumulates also results in heat, volatile and possibly liquid exchange with the intercumulus liquid.

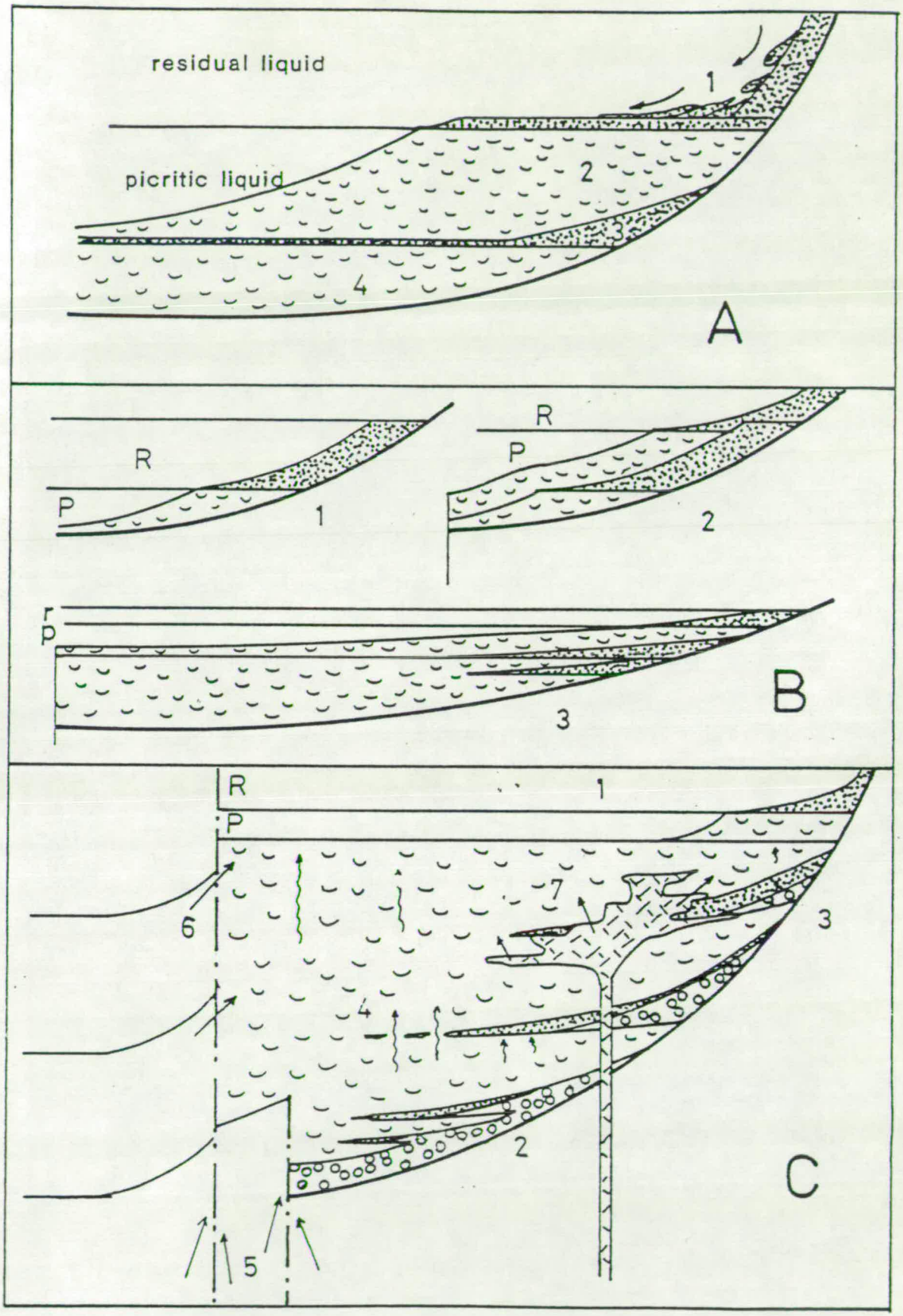
residual liquid
picritic liquid
1
2
3
4
A
R
P
1
R
P
2
r
p
3
B
R
P
1
6
7
3
4
2
5
C

FIGURE 7.1

APPENDIX A

ELECTRON MICRO-PROBE ANALYSIS.

All mineral analyses reported in this thesis were determined with a Cambridge Instruments Microscan 5 electron microprobe at the Grant Institute of Geology, Edinburgh. Operating conditions were as follows:

(i) Gun potential of 20 Kv.
(ii) Beam current of 30 nA.
(iii) Beam diameter of 1.5 micron.

The X-rays produced were analysed by wavelength-dispersive spectrometry (WDS). Two elements were determined simultaneously and automation of the system, introduced in the summer of 1981, allowed the full analysis of each mineral phase from a single spot by computer controlled resetting of the spectrometers for each new pair of elements. Analyses were printed out on the spot, within minutes, after reduction of apparent concentrations of elements relative to standards. Correction for the atomic number, absorption and fluorescence were incorporated into the computer programs written by D. J. Humphries and based on the procedures of Sweatman and Long (1969). Table A.1 lists the operating conditions for the WDS analyses. Precision of the analyses and dectection limits are given in Table A.2.

Samples were prepared in batches of 15 polished thin sections and carbon-coated together with the standards. Mineral compositions reported in this thesis for the cryptic variation traverses represent calculated averages of:

(i) 3 core and 2 rim analyses for 3 different olivine crystals.
(ii) 3 analyses for pyroxene crystals.
(iii) 3 analyses for spinel crystals.

The reported ranges for plagioclase composition are based on analyses of 6 different crystals.

Compositional data for all samples probed are summarised in Table A.3. These compositions are plotted on the traverses discussed in Chapter 5. The samples analysed for these traverses are identified in Fig. A.2, while traverses discussed but not illustrated in Chapter 5 are shown in Fig. A.1. Full representative analyses are given in Chapters 5 and 6.

ELEMENT	LINE	CRYSTAL	ANGLE 2θ degrees	B'GRND	COUNTING TIME (s) peak	background	STANDARD
Ca	Kα	LiF	113.35	±2	40	40	wollastonite
Si	Kα	RAP	31.47	+1.5	40	40	wollastonite
Fe	Kα	LiF	57.34	±2	40	40	Fe metal
Mg	Kα	RAP	44.35	+1.5	40	40	olivine
K	Kα	PET	50.43	±1.75	40	40	orthoclase
Na	Kα	RAP	54.20	+1.5	40	40	jadeite
Ti	Kα	PET	36.42	±2	40	40	Ti metal or rutile
Al	Kα	RAP	37.21	+1.5	40	40	corundum
Ni	Kα	LiF	48.42	±2	40	40	Ni metal
Mn	Kα	quartz	36.42	±2	40	40	Mn metal
Cr	Kα	quartz	40.06	±2	40	40	Cr metal

Flow counters used for all elements

Accelerating potential of 20kV used throughout

TABLE A.1 Wavelength-dispersive analytical conditions.
(Taken from Table A.1, McClurg, 1982).

OLIVINE M50 Analysis 1

oxide	analysis	precision ± 2	detection limit
SiO_2	40.34	0.202	0.021
TiO_2	0.05	-	0.022
Al_2O_3	0.05	0.009	0.009
Cr_2O_3	0.05	0.014	0.025
FeO	13.94	0.160	0.024
MgO	45.26	0.194	0.028
CaO	0.22	0.014	0.022
MnO	0.17	0.033	0.021
NiO	0.25	0.028	0.029

PYROXENE M50 Analysis 4

oxide	analysis	precision ± 2	detection limit
SiO_2	50.78	0.252	0.022
TiO_2	0.75	0.033	0.029
Al_2O_3	4.07	0.051	0.011
Cr_2O_3	1.26	0.030	0.020
FeO	4.14	0.111	0.030
MgO	15.91	0.117	0.012
CaO	21.30	0.296	0.044
MnO	0.13	0.033	0.023
NiO	0.02	0.027	0.035
Na_2O	0.25	0.034	0.011

PLAGIOCLASE M50 Analysis 2

oxide	analysis	precision ± 2	detection limit
SiO_2	52.24	0.266	0.021
TiO_2	0.11	-	0.041
Al_2O_3	28.36	0.192	0.019
FeO	0.60	0.069	0.040
MgO	0.09	0.028	0.013
CaO	12.34	0.322	0.029
Na_2O	4.41	0.043	0.020
K_2O	0.21	-	0.015

Formula used:

$$\text{detection limit} = S \times \frac{3\sqrt{C_B}}{(C_{SP} - C_{SB})} \text{ wt \%}$$

$$\text{precision} = S \times \frac{\sqrt{C_P}}{(C_{SP} - C_{SB})} \text{ wt \%}$$

S = Standard composition in wt %

C_{SP} = Total counts on standard peak

C_{SB} = Total counts on standard background

C_P = Total counts on sample peak

C_B = Total counts on sample background

TABLE A.2 Precision and detection limits of typical wavelength-dispersive electron microprobe analyses. (Taken from Table A.2, McClurg, 1982).

Sample	Type	Locality	Olivine				Plagioclase		Clinopyroxene		Spinel			
			Fo(c)	Fo(r)	wt% NiO	2D(c)	An(max)	An(min)	En(c)	% Cr_2O_3	Mg/Mg+Fe^2	Fe^3/ Fe+Cr+Al	Ti/ Ti+Al+Cr	Cr/Cr+Al
B2	Ol G.	Pap.	80.5		.210	3.0	79.4	66.4	80.0					
C4	UBM	Pap.	84.8		.296	0.18	81.4		86.2	1.14	.291	.261	.04	.632
D5	UBM	LaC	86.6		.342	0.08					.435	.174	.03	.503
E5	Ol G.	S Tr	72.7			0.52	76.4	60.3						
G6	Per	Ruins	83.8		.349	0.08	75.9	67.4			.318	.281	.06	.635
G9	Per	Ruins	83.5	83.7	.258	0.20	75.7		86.9	1.36	.221	.332	.06	.688
G12	Per	Ruins	83.0	83.1	.280	0.16	80.7		85.3		.217	.394	.09	.678
G13	Hybrid	Ruins	Plag (An/Ab/Or): 35.2/62.2/2.6(core), 20.8/76.2/3.0 (rim). K-Fsp.: 1.8/44.0/54.2 (core), 1.1/											
	Dyke		35.5/63.4 (rim). Cpx (Ca/Mg/Fe): 43.5/41.5/15.0(core), 45.5/41.2/13.3 (rim), Cr_2O_3: .11%(C), .03%(r)											
G17	Per	Ruins	84.0	84.9	.409	0.60			86.0					
G21	Per	Ruins	83.0		.332	0.8	82.2		84.9	1.24	.282	.340	.07	.675
H1	Gab	A.C.	67.9	67.8	.083	0.66	61.9	54.3	73.7	0.01	.024	.912	.559	.176
M5	Per		86.0	86.1	.250	0.38	75.6	59.4	86.5	1.15	.244	.355	.06	.711
M6	Per		85.7		.325	0.40			85.4		.197	.484	.05	.784
M7	All		85.1		.210	1.20	84.6							
M11	Per		85.5	85.8	.293	0.16	87.5	77.9	86.5					
M14	All		85.3				82.5							
M16	Per		84.8				84.7							
M17	All		84.9				80.3							
M18	Per		84.4		.270	0.16	78.6		85.8					
M19	All		83.5		.150	0.86	81.4							
M20	Per		85.2		.419	0.38	53.8	52.1	85.7		.215	.292	.07	.751

TABLE A3. Synopsis of Microprobe analyses. c = core, r = rim, D = standard deviation, G or Gab = Babbro, Per = peridotite, All = allivalite, UBM = ultrabasic breccia matrix, Chr = chromitite, dol = dolerite, pic = picrite.

Sample	Type	Locality	Olivine				Plagioclase		Clinopyroxene		Spinel			
			Fo(c)	Fo(r)	wt% NiO	2D(c)	An(max)	An(min)	En(c)	% Cr_2O_3	Mg/Mg+Fe	Fe^3/ Fe+Cr+Al	Ti/ Ti+Cr+Al	Cr/Cr+Al
K7	plug	Pap	83.4				79.7							
K8	hy G	Pap	Opx:	En72.7			64.2	55.5	77.5					
L1	Per	Seag	87.6	87.7	.311	0.16	70.9		88.2	1.21	.374	.230	.04	.611
L2	Per	Seag	86.4		.292	.08	84.9	78.5			.301	.287	.08	.629
L5	All	Seag	86.5	86.3	.256	0.21	85.3	85.0	86.7	1.16	.331	.342	.07	.567
XO	Ol G	Seag	70.2	70.6	.127	1.70	72.4	59.1	79.7	0.26				
AAO	Chr	Hall	88.3		.330	2.4								
AB10	Chr	Hall	86.0		.360	1.0								
AE12	Chr	E Tr	87.1			1.2								
AG2	Per	Ruins	86.8	86.8	.364	.030	85.0		87.4	1.06	.306	.279	.04	.635
AG3	UBM	Ruins	83.9		.214	0.21	81.2	72.1			.284	.374	.07	.617
AH1	plug	Pap	84.1				65.0							
AH3	Per	Pap	87.4			0.4	57.0				.368	.198	.04	.678
BA2	Ol G	A.C.	76.5	76.7	.136	0.96	85.3	60.5	79.5	.279	.049	.936	.670	.180
BB6	Dol	N Tr	Groundmass Plag:An 40.0, Phen.:				80.6	68.9	68.8	0.55				
BC5	Gab	E Tr	64.4	65.1	.025	1.02	54.6	44.2	72.9	.012	.068	.902	.615	.055
BD1	pic	N Tr	90.7	85.8	.431		67.8	59.6	75.5	0.22	.513	.98	.01	.543
BD2	Chr	N Tr	90.1			0.9								
BE3	Dol	S Tr	65.0		.150	0.3	59.6		77.7	0.19				
BK3	Chr	W Tr	86.6		.260	0.4								
BK4	Chr	W Tr	88.3		.370	0.8								
BK5	Per	W Tr	86.6		.347	0.14	84.2		87.0	0.90	.508	.119	.02	.450
BO2	Chr	W Tr	87.5		.400	0.6								
BO3	Chr	W Tr	90.0			2.2								
BO4	Per Dy.	W Tr	81.0			1.2	74.9				.179	.484	.14	.679
CC1	Chr	W Tr	88.0		.304	0.90	80.7				.523	.156	.03	.462
CE1	Per	E Tr	81.6			0.10	71.8		84.0					
CE2	Per	E Tr	84.3			0.10	63.8		85.8					
CE3	Per	Tr	85.5	85.7		0.10			86.7					
CE4	All	Tr	82.1				84.9							
CER4	All	W Tr	83.6				77.8							
CER5	Per	W Tr	85.1			0.10	83.2	58.3						
CER6	Per	Tr	86.2	85.9		0.10	78.8							
CER7	All	Tr	86.6			0.10	58.9							

TABLE A3 (Ctd.).

Sample	Type	Locality	Olivine				Plagioclase		Clinopyroxene		Spinel			
			Fo(c)	Fo(r)	wt% NiO	2D(c)	An(max)	An(Min)	En(c)	% Cr_2O_3	Mg/Mg+Fe	Fe^3/ Fe+Cr+Al	Ti/ Ti+Al+Cr	Cr/Cr+Al
CER8	Per	Tr	86.6				82.8							
CF3	All	E Tr	79.5			0.60	84.5		81.7					
CF4	Per	Tr	84.1			0.20	81.6		86.0					
CF5	UBM	Tr	84.6			0.80	73.3		87.0					
CF6	Per	W Tr	83.6			0.10	66.3		87.2					
CF7	Per	W Tr	85.1			0.20	74.1		86.2					
CF8	All	W Tr	84.8			0.40	86.8							
CF9	Per	W Tr	85.1			0.20	77.6		84.7					
CF10	Per	W Tr	85.3			0.24	81.0		86.9					
CF12	Per	W Tr	84.2			0.60	74.6		89.5					
CF13	Per	W Tr	82.6		.312	0.40	73.6		84.8					
CF14	Chr	W Tr	81.6			0.20	83.6		85.0					
DA1	Chr	W Tr	81.4		.196	4.0	85.3	67.2	81.0	.397				
DE5	All	W Tr	87.7			0.60	88.2		85.4					
DG1	UBM	Pap	89.2				76.7				.424	.173	.01	.525
DH1	plug	Ruins	84.1			0.8	74.0							
DK4	All	Fiach	83.6			0.2			81.6					
DM2	Ol G	E Tr	73.4	73.8	.114	3.4	70.5	52.5	81.9	0.93	.059	.917	.445	.119
DN1	UBM	W Tr	82.1			0.10	80.1		84.2					
DN2	UBM	W Tr	85.3			0.4	83.5							
DN4	Per	W Tr	85.3	85.3	.315	0.6	81.4				.341	.295	.05	.580
DQ1	Per	Bark	81.0			0.10	83.9							
FB1	Dun	H.B.	89.4	89.6	.379	0.16					.541	.131	.01	.515
FC1	Ol G	H.B.	82.4	82.8	.169	0.44	87.8	77.0	84.1	0.86	.133	.584	.08	.698
FD1	Ilm G	Ruins	71.0	73.0	.056		72.3	57.1	76.0	0.01	.052	.934	.469	.146
FE1	Per	Pap	86.5	86.5	.350	.08	78.9	77.2	87.4	1.19	.476	.184	.02	.517
FE2	Per	Pap	87.3	87.5	.366	.10	81.9	62.5	87.3	1.19	.458	.213	.03	.536
FE3	Dun	Pap	88.3	88.2	.374	.24	76.1	67.8	88.2	1.23	.480	.173	.02	.542
FE4	Per	Pap	86.5	86.3	.267	.38	76.2	69.0			.422	.203	.05	.573
FE5	Dun	Pap	87.6	87.7	.318	.10			91.0		.471	.139	.04	.515
FE6	Dun	Pap	87.2	87.5	.312	.24	73.5	68.6	87.6	0.96	.462	.191	.03	.541

TABLE A3 (Ctd.).

Sample	Type	Locality	Olivine				Plagioclase		Clinopyroxene			Spinel		
			Fo(c)	Fo(r)	wt% NiO	2D(c)	An(max)	An(min)	En(c)	% Cr_2O_3	Mg/Mg+Fe	Fe^3/ Fe+Cr+Al	Ti/ Ti+Al+Cr	Cr/Cr+Al
FE7	Dun	Pap	87.2	87.6	.310	0.20			89.4	1.10	.435	.194	.03	.539
FE8	Dun	Pap	87.0	87.2	.310	.10			86.7	1.19	.431	.193	.03	.515
FE9	Dun	Pap	87.1	87.3	.319	0.14			84.6	0.95	.374	.238	.04	.596
FE10	Chr	Pap	87.8	89.9	.279		78.9	59.7			.491	.180	.03	.539
FE11	Per	Pap	88.1	88.0	.310	0.10	79.5	77.1	88.4	0.94	.450	.172	0.03	.564
FE12	Dun	Pap	87.9	87.9	.314	0.08			87.8	1.34	.434	.184	0.03	.585
FE13	Dun	Pap	88.0	88.3	.382	0.09	85.9	84.9	88.3	1.23	.525	.141	0.02	.498
FE14	Per	Pap	88.4	88.6	.384	0.18	81.5	76.8	89.1	1.24	.495	.157	0.03	.567
FG1	Per	Seag	81.6	81.0	.280	0.58	77.0		83.7	0.20	.129	.652	.101	.698
FG2	All	Seag	83.4	84.6	.270	.18	85.4	80.0	84.3	0.61	.179	.456	.07	.656
FG3	All	Seag	81.4	81.3	.219	0.18	81.6	79.6	83.1	0.55	.105	.708	.10	.707
FG4	All	Seag	82.8	83.1	.251	0.50	85.0	78.6	84.1	0.84	.164	.563	.06	.669
FG5	Dun	Seag	87.0	87.3	.415	0.34	80.0	64.7	87.1	1.33	.362	.222	.02	.575
FG6	Per	Seag	87.2	87.4	.334	0.10	63.8	61.5	87.6	1.05	.218	.607	.08	.698
FG7	All	Seag	81.9	82.7	.292	0.94	75.0	53.4	81.1	0.50	.117	.733	.148	.623
FG8	Per	Seag	85.8	85.9	.277	0.16	86.3	79.8			.374	.345	.04	.422
FG9	Per	Seag	85.9	86.1	.349	1.22	75.8	55.9	85.8	0.97	.346	.304	.08	.348
FG10	Per	Seag	84.8	84.9	.344	0.24	77.7	75.9	85.7	1.06	.331	.259	.04	.565
FG11	Per	seag	83.3	83.2	.216	0.76	80.0	72.7	83.3	0.97	.208	.423	.06	.714
FG12	Per	Seag	82.0	82.5	.234	0.78	86.6	64.0	83.5	0.84	.168	.625	0.10	.692
FG13	All	Seag	81.4	81.5	.226	2.8	86.6	70.4	82.9	0.99	.157	.633	.135	.670
FG131	Per	Seag	80.5	80.7	.229	0.34	85.1	75.0	80.7	0.49	.139	.631	.129	.703
FG14	All	Seag	83.8	84.0	.278	0.34	82.8	77.9	84.5	1.15	.233	.432	.08	.650
FG15	All	Seag	84.4	84.5	.260	0.16	84.3	82.1	85.2	1.10	.233	.479	.08	.678
FG16	Plug	Seag	86.6	86.8	.320	0.09	80.8	64.2	89.3	1.25	.422	.274	.03	.621
GB1	Chr	An D	90.4	92.3	.312	0.18	67.4	65.6			.510	.173	.02	.595
GC2	Plug	Bark	88.0	88.1	.394	0.10	81.6	64.1	88.3	1.19	.405	.206	.01	.540
GE6	UBM	Ruins	80.7	80.9	.253	0.18	71.8	65.0	82.3	0.35	.140	.538	.06	.624
GG1	Per	LaC	82.1	81.7	.248	0.42	80.8	52.4	84.8	0.75	.165	.498	0.10	.727
GG2	Per	LaC	81.9	81.9	.268	0.32	82.1	66.6	84.6	1.07	.177	.480	.08	.719
GG3	Per	LaC	82.3	82.4	.239	0.42	81.8	50.2	84.9	1.06	.188	.465	.09	.719
GG4	Per	LaC	82.0	82.1	.267	0.18	84.6	73.0	83.1	0.91	.247	.328	.05	.667
GG5	Per	LaC	80.4	80.5	.235	0.32	82.4	68.3	84.2	0.94	.183	.547	.143	.674
GG6	Per	LaC	81.0	80.9	.248	0.82	84.0	61.0	82.9	1.03	.167	.570	0.10	.704
GG7	Per	LaC	82.9	83.0	.250	0.10	82.7	69.6	84.6	1.06	.196	.446	.08	.698

TABLE A3 (Ctd.).

sample	Type	Locality	Olivine				Plagioclase		Clinopyroxene			Spinel		
			Fo(c)	Fo(r)	wt% NiO	2D(c)	An(max)	An(min)	En(c)	% Cr_2O_3	Mg/Mg+Fe	Fe^3/ Fe+Al+Cr	Ti/ Ti+Al+Cr	Cr/Cr+Al
GG8	All	LaC	79.3	79.5	.278	0.90	80.6	59.0	84.5	0.99	.124	.690	.08	.687
GG9	Per	LaC	81.5	81.5	.225	0.00	78.6	57.6	82.8	0.73	.280	.487	.143	.681
GG10	All	LaC	79.6	79.8	.227	0.28	82.1	57.9	82.4	0.69	.146	.560	.12	.699
GG11	Per	LaC	84.9	85.1	.241	1.56	77.0	52.7	87.1	1.26	.286	.294	.07	.693
GG12	Per	LaC	84.7	84.9	.247	0.26	72.1	68.6	85.7	0.90	.275	.376	.08	.678
GG13	Per	LaC	83.1	83.1	.225	4.2	83.0	67.4	84.3	0.99	.268	.347	.07	.695
GG14	Per	LaC	82.5	82.7	.211	1.08	81.8	73.0	84.1	0.98	.215	.412	.09	.705
GG15	Per	LaC	84.2	84.4	.285	0.24	81.6	75.5	85.6	0.93	.242	.382	.09	.688
GG16	Per	LaC	86.5	86.6	.263	0.10	83.7	62.7	87.6	1.12	.285	.305	.06	.700
GG17	Per	LaC	86.2	86.4	.278	.48	86.5	82.2	86.4	0.98	.329	.282	.04	.657
GG18	Per	LaC	85.3	85.3	.271	0.34	83.6	73.1	86.0	0.93	.254	.341	.07	.741
GG19	Chr	Ruins	88.6	91.5	.233	90.1	79.3				.816	.049	.00	.046
GH1	All	W Tr	86.5	86.5	.196	1.0	86.9	81.1	86.0	1.03	.217	.332	.05	.583
GH2	Per	W Tr	86.4	86.5	.333	0.34	85.7	78.7	88.1	1.15	.326	.251	.06	.588
GH3	Per	W Tr	86.8	86.8	.292	0.10	83.7	75.1	87.3	0.92	.338	.259	.04	.571
GH4	Per	W Tr	85.6	85.7	.237	0.10	78,1	72.5	87.5	1.13	.357	.208	.03	.571
GH5	Per	W Tr	85.0	85.2	.266	0.10	79.7	73.3	87.1	1.09	.336	.257	.06	.573
GH7	Per	W Tr	85.6	85.9	.254	0.34	70.9	60.9	87.6	1.03	.343	.281	.06	.573
GH8	All	W Tr	85.5	85.5	.294	0.24	85.3	76.6	87.6	0.92	.377	.226	.02	.486
GH9	Per	W Tr	85.8	86.0	.272	0.10	78.3	69.8	88.8	0.60	.389	.171	.02	.496
GH10	Per	W Tr	86.4	86.3	.302	0.18	84.3	80.1	86.0	0.63	.355	.264	.05	.577
GH11	Per	W Tr	83.5	83.7	.365	0.18			85.0	0.97	.302	.248	.05	.598
GH12	Per	W Tr	84.7	84.8	.353	0.10	80.1	59.2	84.9	0.70	.272	.306	.06	.617
GH13	All	W Tr	84.6	84.6	.250	0.62	78.4	73.5	86.7	0.97	.238	.289	.04	.638
GH14	Per	W Tr	83.8	83.8	.355	0.34			85.4	1.01	.275	.359	.08	.610
GH15	Per	W Tr	87.7	87.7	.367	0.16	75.9	68.3	89.3	1.18	.345	.232	.05	.650
GH16	Per	W Tr	87.2	87.2	.288	0.10	76.0	65.6	88.6	1.15	.281	.262	.05	.686
GH17	All	W Tr	83.5	83.7	.214	1.14	86.7	73.2	85.3	0.72	.141	.656	.05	.695
GH18	All	W Tr	83.4	83.7	.177	0.34	87.6	75.6	84.9	0.65	.145	.558	.07	.732
GH19	All	W Tr	85.5	85.5	.163	0.38	86.5	81.5	86.5	0.95	.304	.278	.04	.601
GH20	Per	W Tr	83.7	83.7	.172	0.16	84.0	73.8	84.9	0.90	.220	.342	.06	.716
GH21	Per	W Tr	85.6	85.8	.324	0.10	83.8	66.7	86.5	1.13	.274	.308	.05	.652
GH22	Per	W Tr	86.5	86.5	.245	0.44	79.8	62.7	86.8	0.99	.292	.297	.05	.680

TABLE A3 (Ctd.).

Sample	Type	Locality	Olivine				Plagioclase		Clinopyroxene		Spinel			
			Fo(c)	Fo(r)	wt% NiO	2D(c)	An(max)	An(Min)	En (c)	$\%Cr_2O_3$	Mg/Mg+Fe	$Fe^3/Fe^3+Al+Cr$	Ti/Ti+Al+Cr	Cr/Cr+Al
GH23	All	W Tr	86.6	86.7	.269	0.62	88.2	83.7	87.4	0.69	.344	.263	.03	.593
GH24	Per	W Tr	85.7	85.7	.299	0.24	86.6	82.1			.267	.317	.05	.670
GH25	Per	W Tr	85.4	85.8	.303	0.16	80.9	73.5	86.7	1.09	.257	.309	.05	.685
GH26	Per	W Tr	84.2	84.5	.262	0.38	68.2	62.7	86.7	1.16	.282	.262	.o4	.622
GH27	All	W Tr	84.1	84.3	.142	0.50	84.3	82.8	86.8	0.66	.243	.365	.06	.693
GH28	All	W Tr	84.7	84.7	.174	0.34	84.3	78.9	86.0	0.64	.199	.449	.05	.661
GH29	All	W Tr	84.5	84.7	.182	0.20	82.4	79.0	86.3	1.04	.285	.265	.06	.621
GH30	All	W Tr	83.1	83.5	.199	0.10	86.2	83.4	86.1	1.14				
GH31	Per	W Tr	86.9	86.9	.363	0.10	79.3	71.5	88.6	1.31	.325	.261	.05	.654
GH32	Per	W Tr	85.6	85.8	.193	0.18	80.1	71.2	87.5	1.18	.284	.299	.06	.654
GH33	Per	W Tr	85.4	85.6	.381	0.18	73.7	72.6	86.6	1.16	.301	.292	.06	.651
GH34	Per	W Tr	85.3	85.3	.465	76.3	76.3	70.5	86.1	1.13	.354	.329	.06	.685
GH35	Per	W Tr	86.6	86.6	.361	0.16	79.9	68.7	88.9	1.26	.327	.299	.03	.635
GH36	Per	W Tr	86.4	86.7	.308	0.62	77.4	70.8	87.8	1.22	.323	.260	.04	.647
GH37	Per	W Tr	86.5	86.9	.457	0.16	72.3	65.5			.319	.294	.04	.678
GH38	Per	W Tr	87.3	87.6	.451	0.10	74.1	63.2	88.3	1.18	.327	.278	.04	.655
GH39	All	W Tr	87.4	87.7	.398	0.24	87.3	84.6	88.1	1.21	.312	.291	.04	.657
GH40	All	W Tr	86.9	87.0	.370	0.34	88.8	83.2	88.1	1.08	.303	.291	.03	.637
GH41	Per	W Tr	87.1	87.3	.268	0.20	79.2	77.3	88.0	1.18	.300	.282	.02	.596
GH42	Per	W Tr	86.6	86.8	.344	0.10	76.3	66.9	87.0	1.07	.269	.358	.04	.653
GL3	Per	W Tr	83.0	83.0	.221	0.10	82.2	79.2	84.2	1.01	.168	.576	.07	.622
GM2	Per	Ruins	88.3	88.5	.362	81.3	74.7				.584	.160	.018	.420
GM2	Chr	Ruins	91.0	92.3	.326						.644	.126	.018	.414
GN2	Chr	E Tr	85.9	86.3	.300	0.24	84.3	61.1	85.1	1.06	.483	.193	.02	.561
GN3	Per	E Tr	81.3	81.3	.205	0.80	82.7	68.7	85.9	1.10	.219	.317	.05	.740
GN4	All	E Tr	84.2	84.2	.294	0.24	72.2	60.8	83.2	0.84	.144	.543	.14	.752
GN5	All	E Tr	80.7	80.7	.149	0.10	77.8	75.9	83.6	0.98	.155	.565	.136	.717
GN6	Per	E Tr	85.4	85.2	.289	0.82	81.0	71.1	86.0	1.00	.246	.312	.05	.721
GN7	Per	E Tr	86.0	86.0	.315	0.34	84.8	73.7	87.5	1.16	.248	.332	.05	.719
GN8	Per	E Tr	84.1	84.4	.293	1.18	79.4	70.3	86.3	0.93	.204	.405	.09	.743
GN9	All	E Tr	82.3	82.4	.161	0.34	85.7	72.6	84.1	0.82				
GN10	Per	E Tr	84.4	85.0	.208	0.42	86.3	70.2	86.1	0.98	.245	.329	.06	.704
GN11	Per	E Tr	85.3	85.6	.304	1.04	81.7	72.9	87.2	1.10	.258	.246	.05	.701
GN12	Per	E Tr	84.4	84.2	.268	0.38	83.0	79.0	86.0	1.03	.230	.309	.o7	.737

TABLE A3 (Ctd.).

Sample	Type	Locality	Olivine				Plagioclase		Clinopyroxene		Spinel			
			Fo(c)	Fo(r)	wt% NiO	2D(c)	An(max)	An(min)	En(c)	% Cr_2O_3	Mg/Mg+Fe	Fe^3/ Fe+Al+Cr	Ti/ Ti+Al+Cr	Cr/Al+Cr
GN13	All	E Tr					85.0	80.6	81.8	0.67				
GN14	All	E Tr	83.4	83.4	.257	1.29	84.7	80.6	85.4	1.09	.215	.355	.06	.742
GN15	Per	E Tr	84.4	84.6	.257	0.70	81.1	76.6	85.4	1.11	.221	.369	.06	.701
GN16	Ol G	E Tr	79.9	80.4	.161	1.6	82.9	74.1	84.8	1.02				
HB1	All	Hall	83.7	83.7	.148	0.10	83.6		86.6	0.71	.185	.337	.131	.733
HB1	Anorth	Hall	85.9	86.0	.153	0.10	86.4	83.8	87.6	0.98	.318	.184	.02	.660
HC1	Per	Coast	87.2	87.4	.299	0.18	81.8	71.0	89.2	1.29	.359	.224	.05	.630
HC3	Per	Coast	88.8	88.8	.341	0.28	82.9	78.4	89.2	1.32	.432	.197	.04	.632
HC4	Per	Coast	85.3	85.3	.324	1.28	80.6		87.5	0.54	.261	.277	.05	.712
HC5	Per	Coast	87.6	87.8	.351	0.32	72.7	71.7			.486	.168	.01	.433
HC6	Dun	Coast	89.3	89.3	.386	0.16					.492	.154	.04	.564
HC7	Dun	Coast	88.7	88.8	.344	0.32			89.9	1.20	.455	.188	.03	.504
HC8	Dun	Coast	89.1	89.1	.328	0.62					.438	.157	.02	.479
HC9	Per	Coast	88.0	88.0	.322	0.10	71.6	66.6	87.8	0.93	.420	.207	.o2	.504
HC10	Per	Coast	84.8	85.0	.293	0.18	79.4	78.5	85.3	1.06	.315	.287	.03	.537
HC11	Per	An't S	84.9	85.1	.287	0.10	81.3	69.4	86.3	0.83	.217	.330	.05	.717
HC12	Per	An't S	85.7	85.6	.331	0.28	64.1	57.8	86.6	1.09	.248	.304	.o4	.695
HC13	Per	An't S	84.5	84.6	.267	0.10	68.0	62.8	85.0	1.08	.220	.390	.06	.718
HC14	Per	An't S	83.4	83.7	.238	0.18	84.3	70.2	81.5	0.95	.197	.412	.06	.607
HC15	Per	An't S	82.6	82.6	.273	0.50	81.5	60.0	83.4	0.73	.172	.466	.08	.747
HC16	All	An't S	81.2	81.1	.221	0.42	83.7	74.3	82.4	0.81	.140	.574	.08	.678
HC17	All	An't S	81.5	82.3	.160	0.10	79.8	76.8	83.5	0.66				
HC18	Per	An't S	85.5	86.1	.346	1.14	71.1	55.3	87.8	0.93	.227	.327	.03	.676
HC19	All	An't s	85.6	85.8	.256	0.34	84.1	78.2	86.9	1.26	.303	.242	.04	.572
HC20	All	An't S	85.2	85.5	.266	0.34	85.2	82.0	86.6	0.88				
HC21	Per	An't S	87.3	87.3	.318	0.28	80.2	77.2	87.5	0.94	.363	.195	.04	.567
HC22	Per	An't S	83.3	83.3	.280	.000	69.5	57.9	84.9	1.01	.213	.449	.04	.667
HC23	Per	An't S	87.1	87.3	.347	0.52	75.8	68.4	88.9	1.11	.334	.243	.o4	.667
HC24	All	An't S	84.1	84.2	.338	0.66	83.3	75.5	87.3	1.17	.253	.327	.05	.643
HC25	Per	An't S	87.4	87.5	.291	0.18	81.3	76.0	88.5	1.09	.364	.224	.03	.596
HD2	Per	Ruins	87.6	87.6	.410	0.74					.402	.272	.03	.522
HD4	Dun	Ruins	86.9	87.0	.323	0.34					.452	.207	.02	.411
HD5	Dun	Ruins	85.2	85.2	.341	0.28					.391	.246	.02	.506
HD6	Dun	Ruins	86.9	87.2	.320									

TABLE A3 (Ctd.).

Sample	Type	Locality	Olivine				Plagioclase		Clinopyroxene		Spinel			
			Fo(c)	Fo(r)	wt% NiO	2D(c)	An(max)	An(min)	En(c)	% Cr_2O_3	Mg/Mg+Fe^2	Fe^3/ Fe+Al+Cr	Ti/ Ti+Al+Cr	Cr/Cr+Al
HD6	Chr	Ruins	87.7	88.5	.320						.444	.240	.03	.455
HD8	Dun	Ruins	86.8	86.7	.322	0.38					.382	.270	.04	.500
HD9	Per	Ruins	88.4	88.5	.337	0.10			88.5	1.44	.416	.225	.04	.584
HD10	Per	Ruins	89.2	89.1	.381	0.10	78.2	66.1	89.4	1.23	.361	.314	.05	.710
HD11	Dun	Ruins	90.0	90.1	.344	0.62			90.3	1.16	.461	.196	.03	.611
HD12	Per	Ruins	90.7	90.6	.351	0.16	77.9		90.5	1.48	.514	.156	.02	.556
HD13	Per	Ruins	89.9	90.2	.403	1.64	81.3	74.0	90.2	1.18	.482	.179	.03	.576
HD14	Per	Ruins	89.2	89.5	.355	0.66	82.2	51.5	90.2	1.32	.451	.184	.03	.606
HD15	Per	Ruins	90.2	90.4	.356	0.10	77.5	71.5	90.2	1.14	.447	.205	.o4	.600
HD16	Chr	Ruins	90.5	90.3	.217	0.10	81.8	78.6			.655	.084	.01	.484
HD17	Per	Ruins	88.3	88.4	.258	0.42	83.3	76.2	88.3	1.20	.357	.230	.04	.671
HD18	Per	Ruins	82.3	82.4	.240	0.10	85.8	77.6	88.4	0.56	.178	.578	.10	.692
HD19	Per	Ruins	86.7	86.7	.307	0.34	75.6	62.3	87.2	1.21	.313	.258	.03	.648
HD20	All	Ruins	81.6	81.7	.201	0.42	78.6	72.5	82.5	0.87	.149	.627	.12	.668
HD21	Per	Ruins	87.3	87.3	.319	0.17	79.6	75.7	88.0	0.89	.352	.188	.03	.536
HD22	Per	Ruins	83.5	83.8	.214	0.42	82.6	75.9	84.2	0.92	.186	.525	,10	.699
HD23	Per	Ruins	88.2	88.0	.338	0.16	82.3	76.7	88.4	1.50	.376	.238	.04	.592
HD24	Per	Ruins	86.3	86.5	.296	0.48	78.6	69.2	87.0	1.22	.278	.325	.05	.681
HD25	Per	NE Rui	87.3	87.4	.356	0.10	79.6	55.6	88.1	1.10	.314	.314	.06	.688
HD26	Per	NE Rui	81.9	81.8	.277	0.24	72.9	64.7	82.8	1.11	.190	.438	.10	.675
HD27	Per	NE Rui	81.4	81.4	.242				83.6	1.04	.231	.354	.09	.630
HD28	Per	NE Rui	84.8	84.8	.355	0.16	85.1	82.3	86.1	1.25	.331	.239	.03	.576
HD29	Per	NE Rui	85.6	85.7	.318	0.00	84.0	65.6	85.7	1.03	.331	.385	.09	.639
HD30	Per	NE Rui	84.1	83.9	.349	0.94	79.2	59.2			.276	.305	.08	.673
HD31	Per	NE Rui	78.9	78.9	.190		75.3	69.3	80.0	0.54	.151	.523	.105	.677
HD31	Chr	NE Rui	81.1	82.4	.212	1.40					.333	.563	.243	.579
HD32	Per	NE Rui	84.2	84.2	.310	0.58	84.3	58.6	85.3	1.00	.303	.316	.07	.662
HG3	Per	E Tr	87.2	86.7	.300		88.4	85.8			.428	.171	.01	.395
HG3	Chr	E Tr	87.8	88.6	.311						.695	.073	.00	.174
HG4	Chr	E Tr	83.1	84.9	.351	0.74	82.4	67.0	84.2	1.01	.195	.398	.08	.697
HK4	Per	W Tr	85.5	85.6	.333	0.16			85.3	1.11	.340	.261	.06	.606
HK5	UBM	W Tr	81.0	81.2	.237	1.54	75.0	72.7	84.8	1.09	.158	.615	.10	.698
HK6	Chr	WLS	89.9	92.3	.348	0.10	82.2	78.4			.619	.127	.02	.457
HL1	All	Ask	81.8	82.1	.219	0.18	86.5	83.6	84.4	0.93	.174	.381	.08	.669

TABLE A 3 (Ctd.).

Sample	Type	Locality	Olivine				Plagioclase		Clinopyroxene			Spinel		
			Fo(c)	Fo(r)	wt% NiO	2D(c)	An(max)	An(min)	En(c)	% Cr_2O_3	Mg/Mg+Fe	Fe^3/ Fe+Al+Cr	Ti/ Ti+Al+Cr	Cr/Cr+Al
HL2	Chr	Ask	81.6	81.4	.281	0.18	78.4	62.6	84.3	0.92	.452	.242	.07	.603
HL3	Per	Ask	82.8	83.0	.314	1.56	83.1	60.4	83.5	0.93	.241	.400	.07	.717
HL4	Per	Ask	84.8	84.9	.292	0.34	86.6	78.4			.248	.339	.06	.763
HL5	Per	Ask	86.1	86.2	.267	0.10	85.9	76.6	87.3	1.18	.297	.265	.04	.691
HL6	Per	Ask	82.8	83.1	.263	1.14	73.1	56.0	86.2	1.15	.206	.437	.09	.695
HL7	All	Ask	84.9	85.2	.248	0.16	79.7	72.2			.270	.270	.03	.668
HL8	Per	Ask	84.4	84.5	.304	0.58	64.7	55.8	85.6	1.00	.247	.317	.06	.703
LA1	Per	W Tr	85.6	85.6	.445	0.10	79.2	68.9	87.3	1.12	.283	.273	.04	.676
LA2	All	W Tr	82.3	82.4	.226	0.48	83.6	80.1	84.1	0.85	.068	.762	.14	.718
LA4	All	W Tr	85.4	85.4	.271	0.32	82.5	71.7	87.0	0.86	.227	.379	.05	.715
LA6	All	W Tr	83.8	84.3	.205	0.10	83.3	78.6						
LA8	Per	W Tr	86.3	86.4	.419	0.24	74.8	63.9	87.3	1.23	.314	.244	.03	.623
LA9	All	W Tr	86.1	86.3	.201	0.16	85.4	79.9	88.2	0.91				
LA11	Per	W Tr	86.6	86.6	.312	0.16	80.9	74.9			.322	.252	.03	.647
LB1	All	S Tr	83.8	83.8	.274	0.14	87.4	69.4	85.1	0.95	.183	.416	.09	.657
LB2	Per	S Tr	82.4	82.8	.284	0.44	75.3	58.4	84.5	0.87	.194	.527	.10	.572
LB3	Per	S Tr	86.2	86.3	.337	0.20	81.4	58.4	86.8	o.99	.244	.441	.06	.681
LB4	Per	S Tr	86.7	87.0	,348	0.34	78.8	51.6	86.7	1.05	.503	.196	.02	.497
LB6	All	S Tr	83.1	83.3	.261	0.28	81.0	70.6	86.4	0.50	.249	.429	.02	.603
LB7	01 G	S Tr	8o.0	80.4	.203	0.10	76.6	66.9	83.1	0.25	.043	.998	.25	.333
LB8	Per	S Tr	83.1	83.3	.232	0.16	87.2	69.2	85.6	0.66	.151	.738	.17	.638
LB10	Per	S Tr	80.9	81.1	.252	1.02	79.6	63.9	83.9	0.77	.321	.387	.04	.617
LB11	Per	S Tr	83.1	83.3	.315	1.18	87.3	64.4	85.4	1.41	.192	.552	.11	.702

TABLE A3 (Ctd.).

A.1 Cryptic variation for traverses through the layered series. Left-hand column identifies the data points. Columns to the right give the average Fo content and wt% NiO in olivine, the range of An content in plagioclase, the wt% Cr_2O_3 in clinopyroxene and, for some traverses, the Mg-number of the pyroxene, ppm. sulphides in the sample and maximum olivine and spinel sizes. The Traverses are as follows (number in bracket refers to traverse number on Fig. 5.1):

A.1 (i) South Trallval (5).

A.1 (ii) East Trallval (3).

A.1 (iii) Askival (4).

A.1 (iv) An't Snidhe (11).

A.1 (v) Leac A Chaisteil (10).

A.1 (vi) Coastline (7).

A.1 (vii) Papadil (12).

A.1 (viii) NE Ruinsival (9).

A.2 Sample identification keys for the data points on cryptic variation traverses, presented in Chapter 5, based on the variation pattern for the Fo content of olivine . The keys refer to the following traverses:

A - South Trallval (Figs. 5.23 and 5.24, traverse 5 on Fig. 5.1).

B - Lower West Trallval (Figs. 5.23 and 5.24, traverse 2).

C - Seagull (Fig. 5.28, traverse 6).

D - Upper West Trallval (Fig. 5.21, traverse 1).

E - Ruinsival (Fig. 5.29, traverse 8).

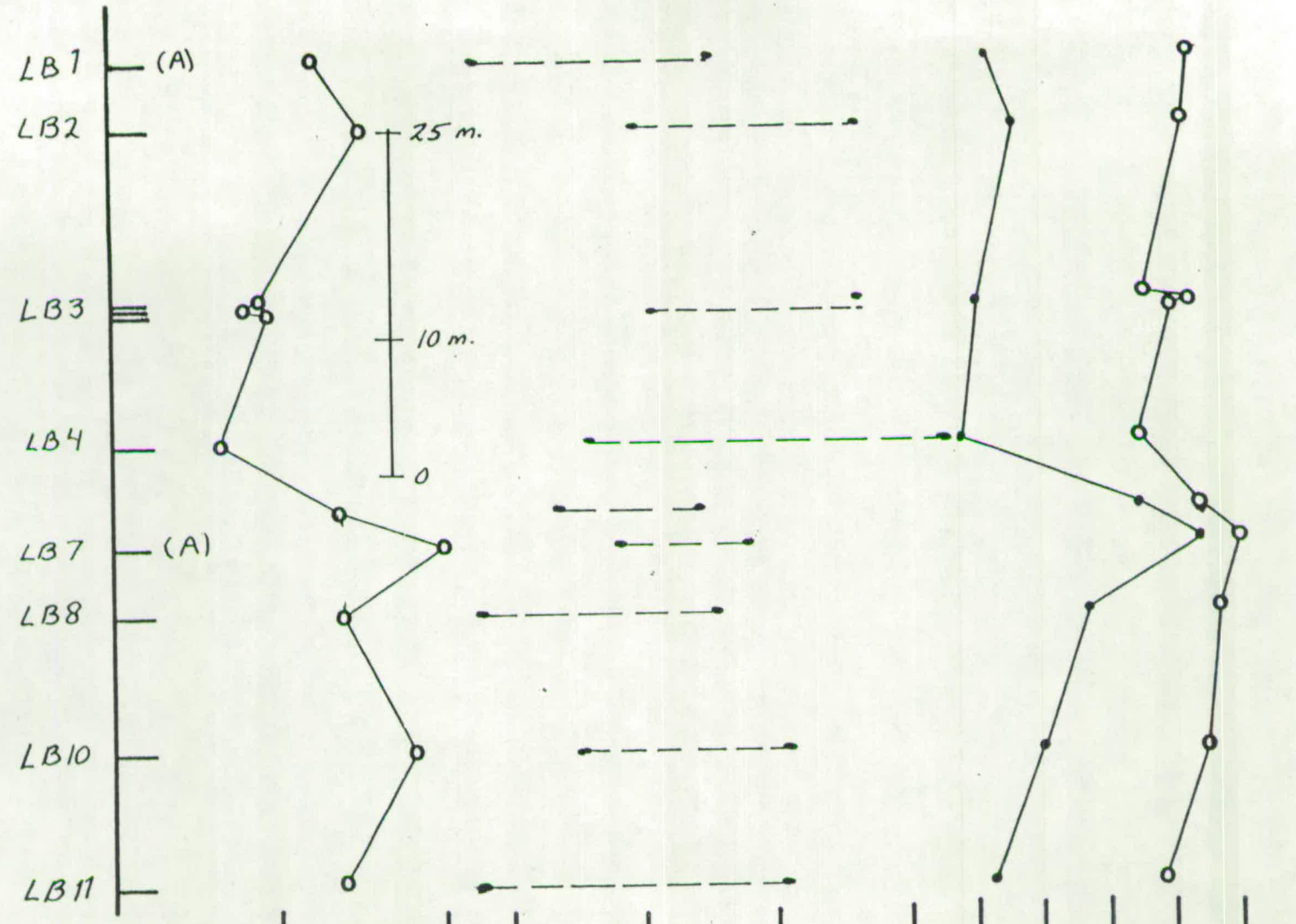
LB1
(A)
LB2
LB3
LB4
LB7
(A)
LB8
LB10
LB11
25 m.
10 m.
0
85.0
80.0
Mol % Fo in olivine
85
75
65
Mol % An in plagioclase
1.2
1:0
0.8
Wt. % Cr_2O_3 in cpx
0.40
0.30
0.20
Wt % NiO in ol.

Fig A.1 (i)

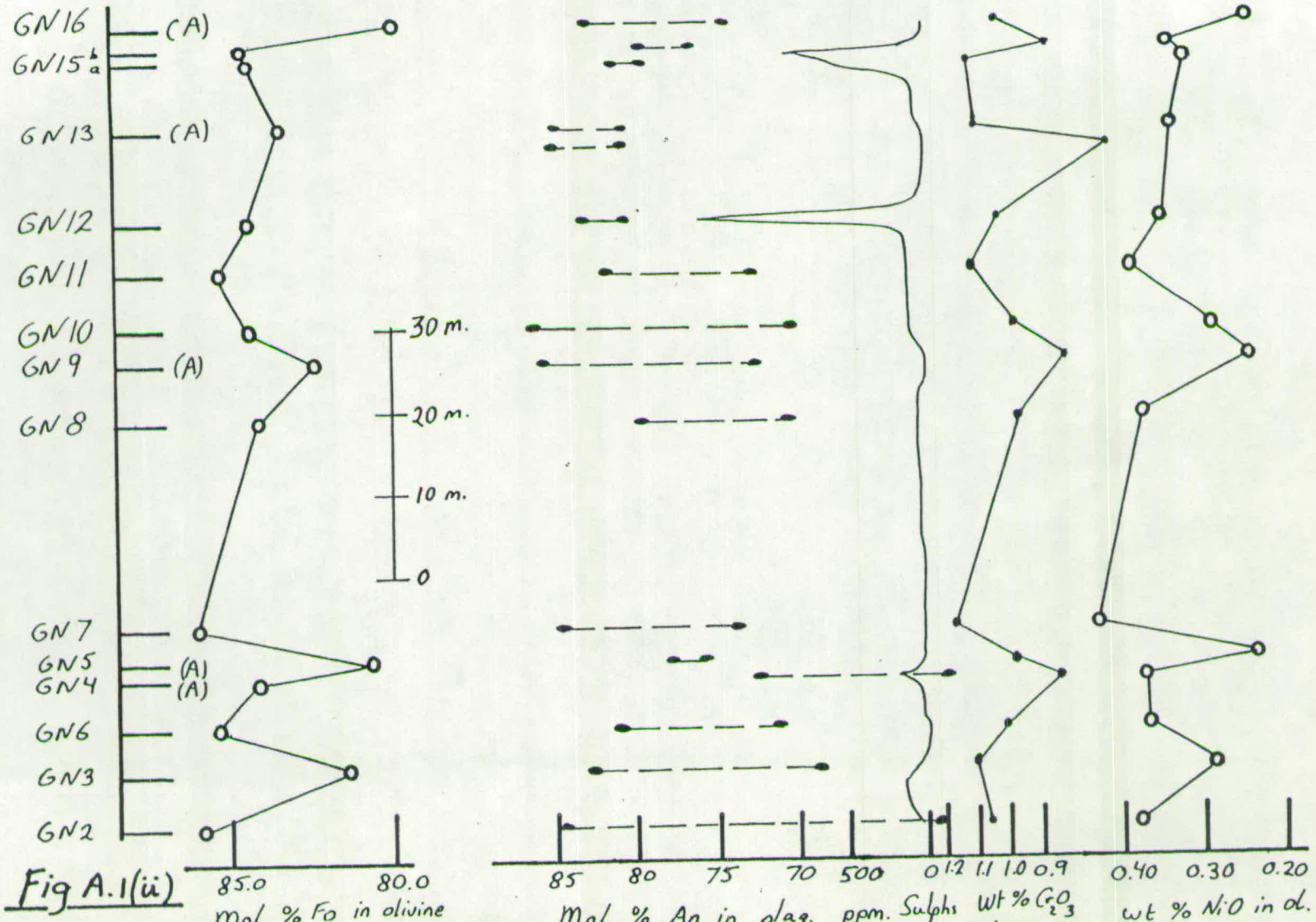
GN16
(A)
GN15 b a
GN13
(A)
GN12
GN11
GN10
GN9
(A)
GN8
GN7
GN5
(A)
GN4
(A)
GN6
GN3
GN2
30 m.
20 m.
10 m.
0
85.0
80.0
Mol. % Fo in olivine
85
80
75
70
500
0
1·2
1.1
1.0
0.9
Mol. % An in plag.
ppm. Sulphs
Wt % Cr_2O_3 in cpx.
0.40
0.30
0.20
wt % NiO in ol.

Fig A.1(ii)

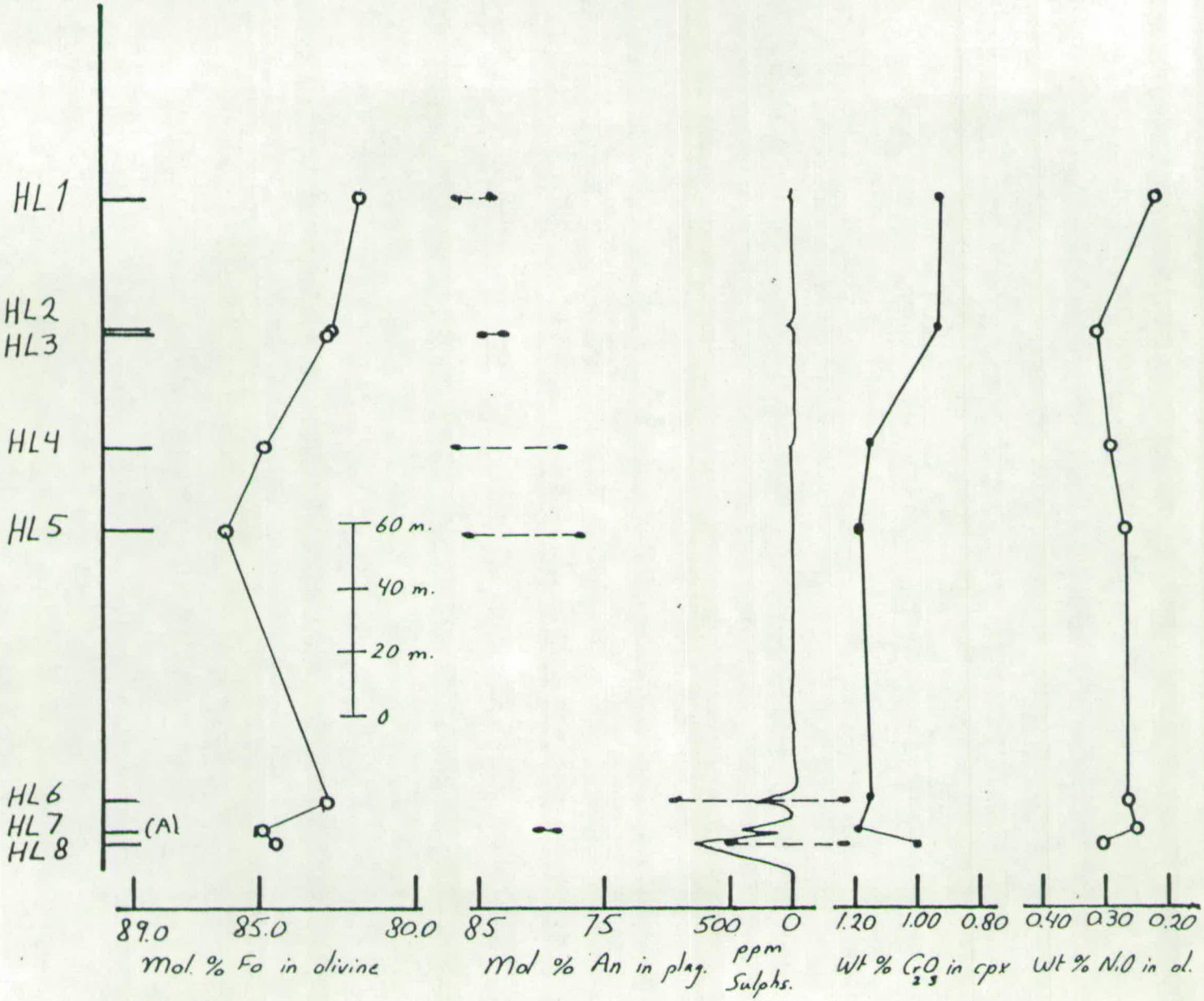
HL1
HL2
HL3
HL4
HL5
HL6
HL7
HL8
(A)
60 m.
40 m.
20 m.
0
89.0
85.0
80.0
Mol. % Fo in olivine
85
75
500
0
Mol % An in plag.
ppm Sulphs.
1.20
1.00
0.80
Wt % Cr_2O_3 in cpx
0.40
0.30
0.20
Wt % NiO in ol.

Fig A.1(iii)

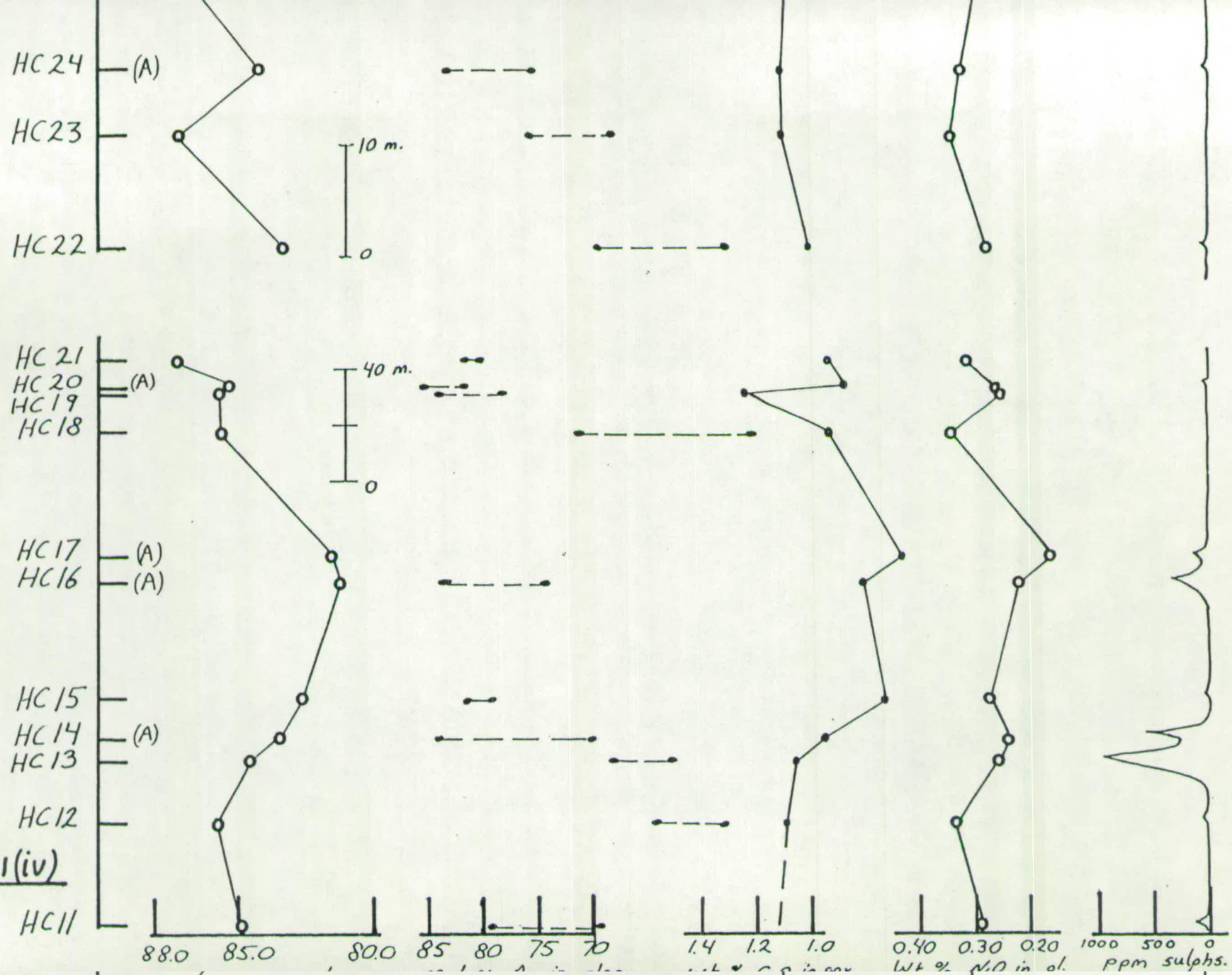
HC 24
(A)
HC 23
HC 22
10 m.
0
HC 21
HC 20
(A)
HC 19
HC 18
40 m.
0
HC 17
(A)
HC 16
(A)
HC 15
HC 14
(A)
HC 13
HC 12
HC 11
88.0
85.0
80.0
85
80
75
70
1.4
1.2
1.0
0.40
0.30
0.20
1000
500
0
ppm sulphs.

Fig A.1(iv)

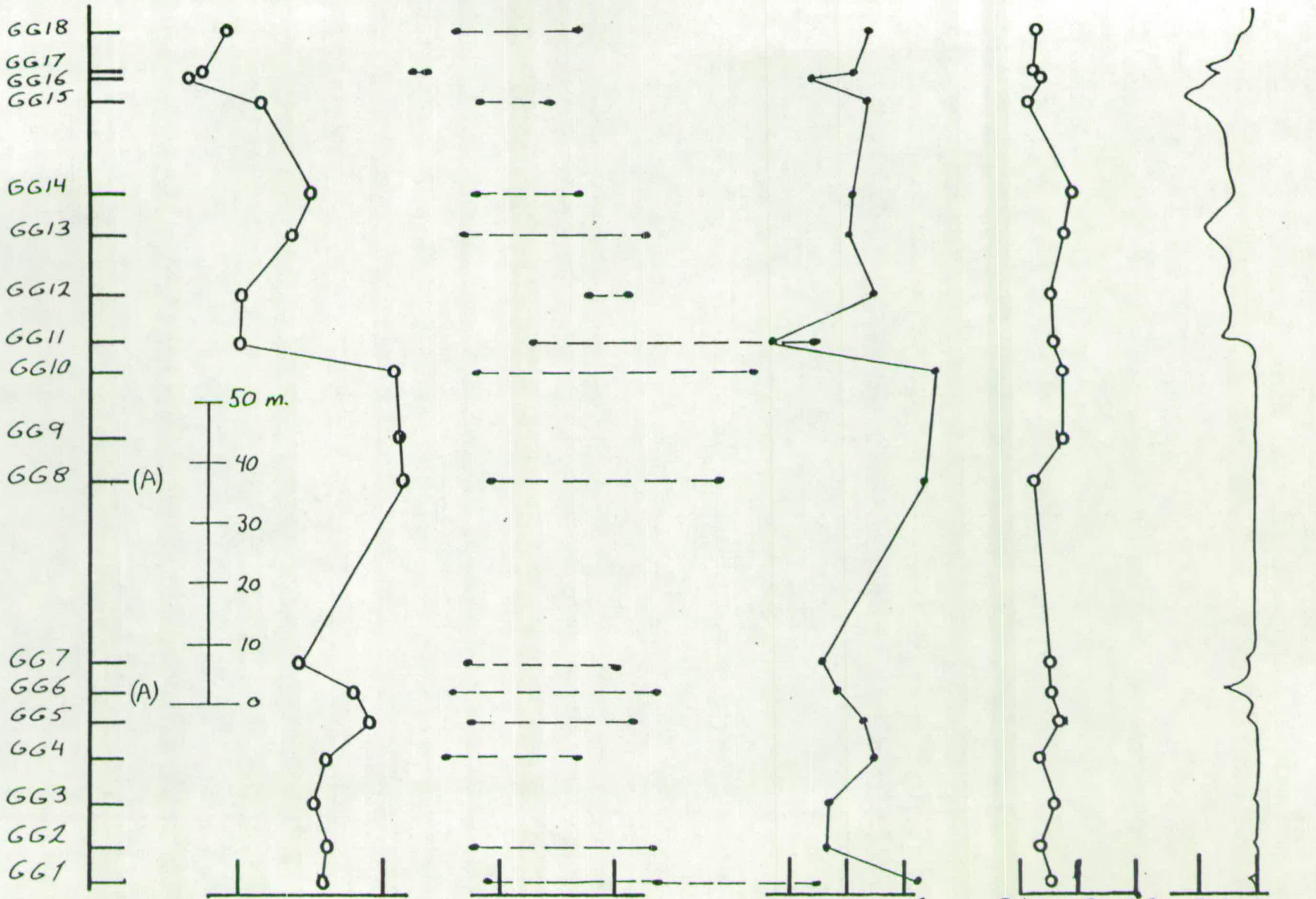
GG18
GG17
GG16
GG15
GG14
GG13
GG12
GG11
GG10
GG9
GG8
(A)
GG7
GG6
(A)
GG5
GG4
GG3
GG2
GG1
50 m.
40
30
20
10
0
85.0
80.0
Mol. % Fo in olivine
80
60
mol. % An in plag.
1.4
1.0
0.6
Wt % Cr_2O_3 in cpx
0.40
0.30
0.20
500
0
Wt % NiO in ol. ppm Sulphs.

Fig A.1 (v)

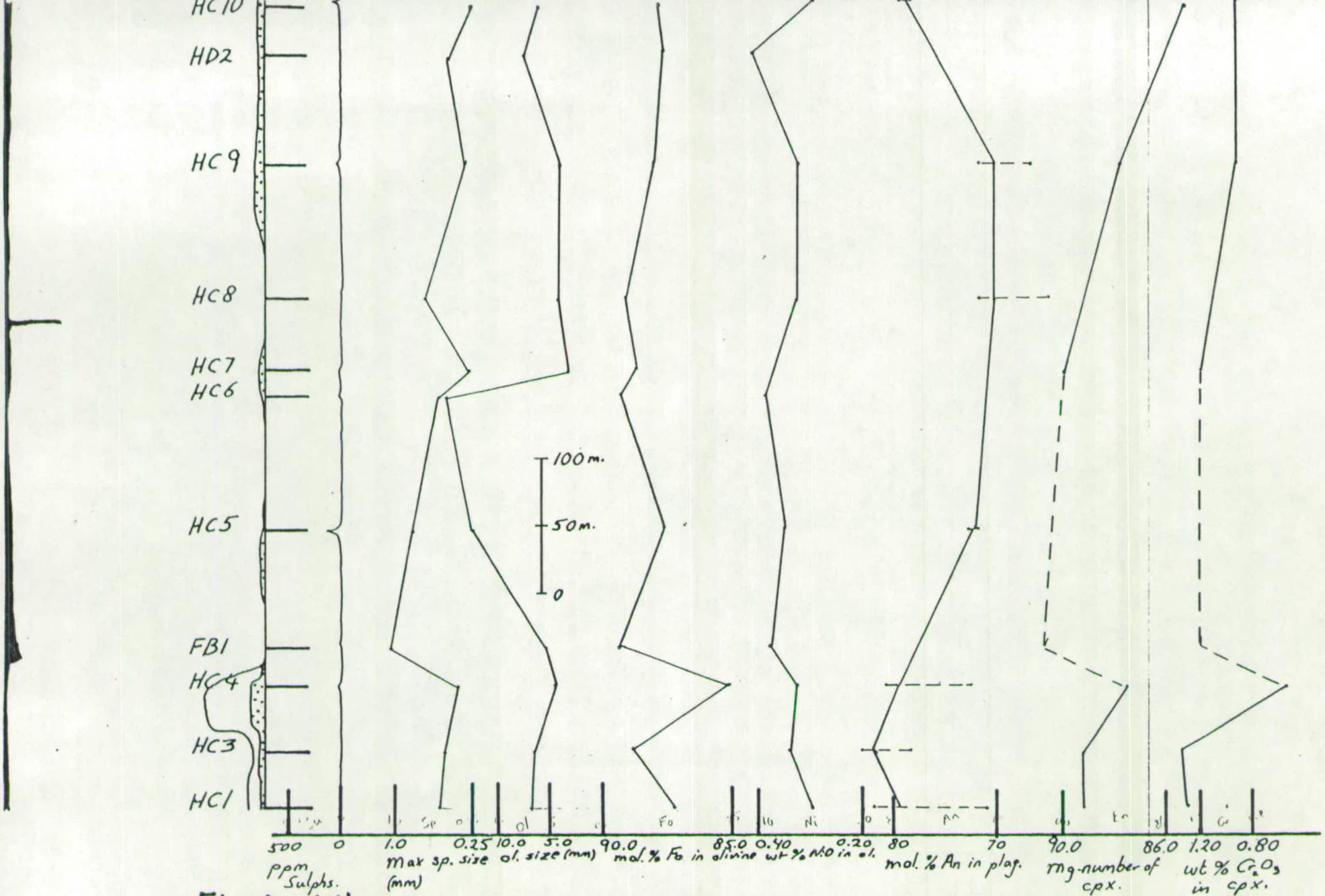
HC10
HD2
HC9
HC8
HC7
HC6
HC5
FB1
HC4
HC3
HC1
100m.
50m.
0
500
0
1.0
0.25
10.0
5.0
90.0
85.0
0.40
0.20
80
70
90.0
86.0
1.20
0.80
ppm Sulphs.
Max sp. size (mm)
ol. size (mm)
mol. % Fo in olivine
wt % NiO in ol.
mol. % An in plag.
mg-number of cpx.
wt % Cr2O3 in cpx.

Fig. A.1 (vi)

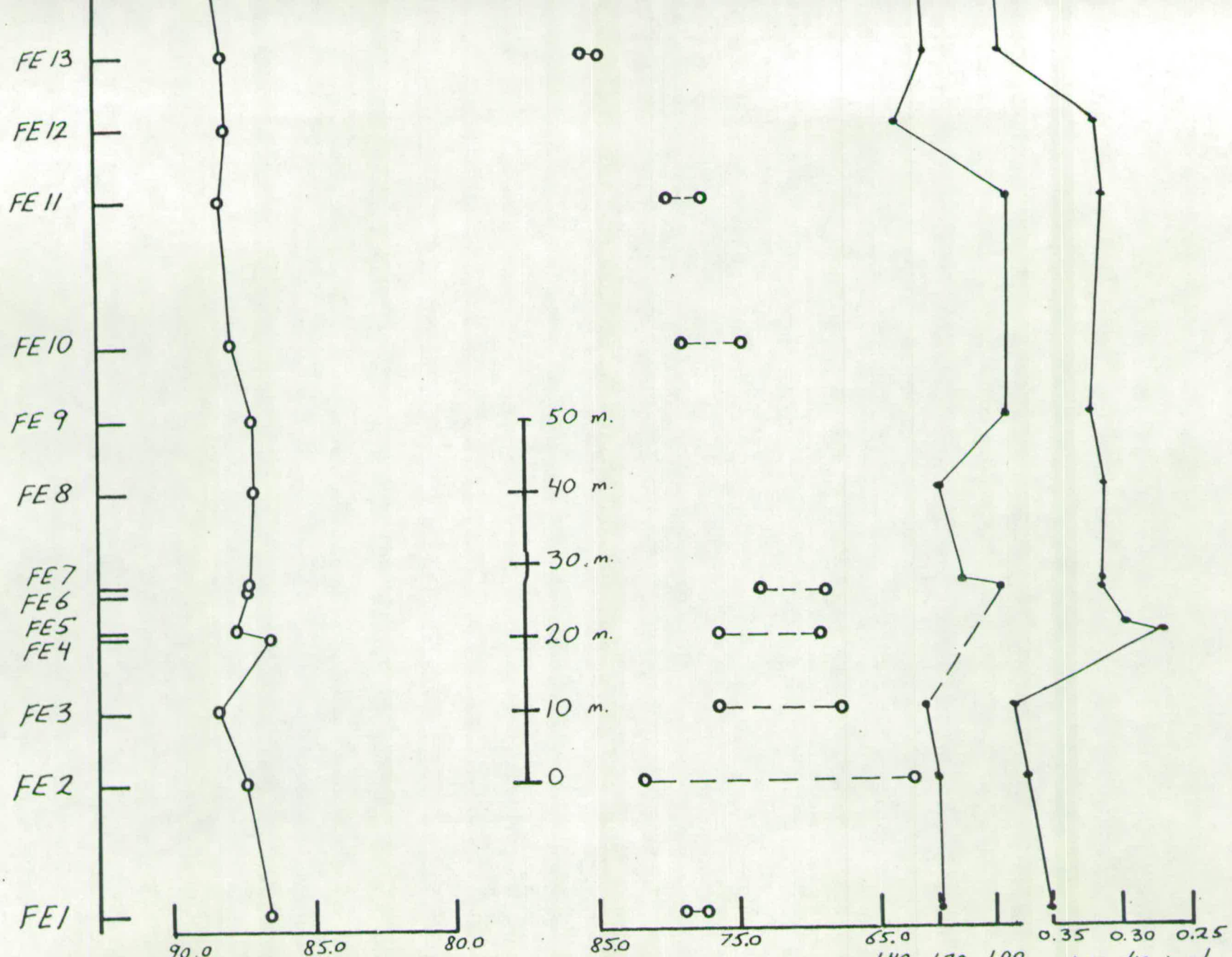

Fig. A.1 (vii). mol % F in olivine mol % An in plag.

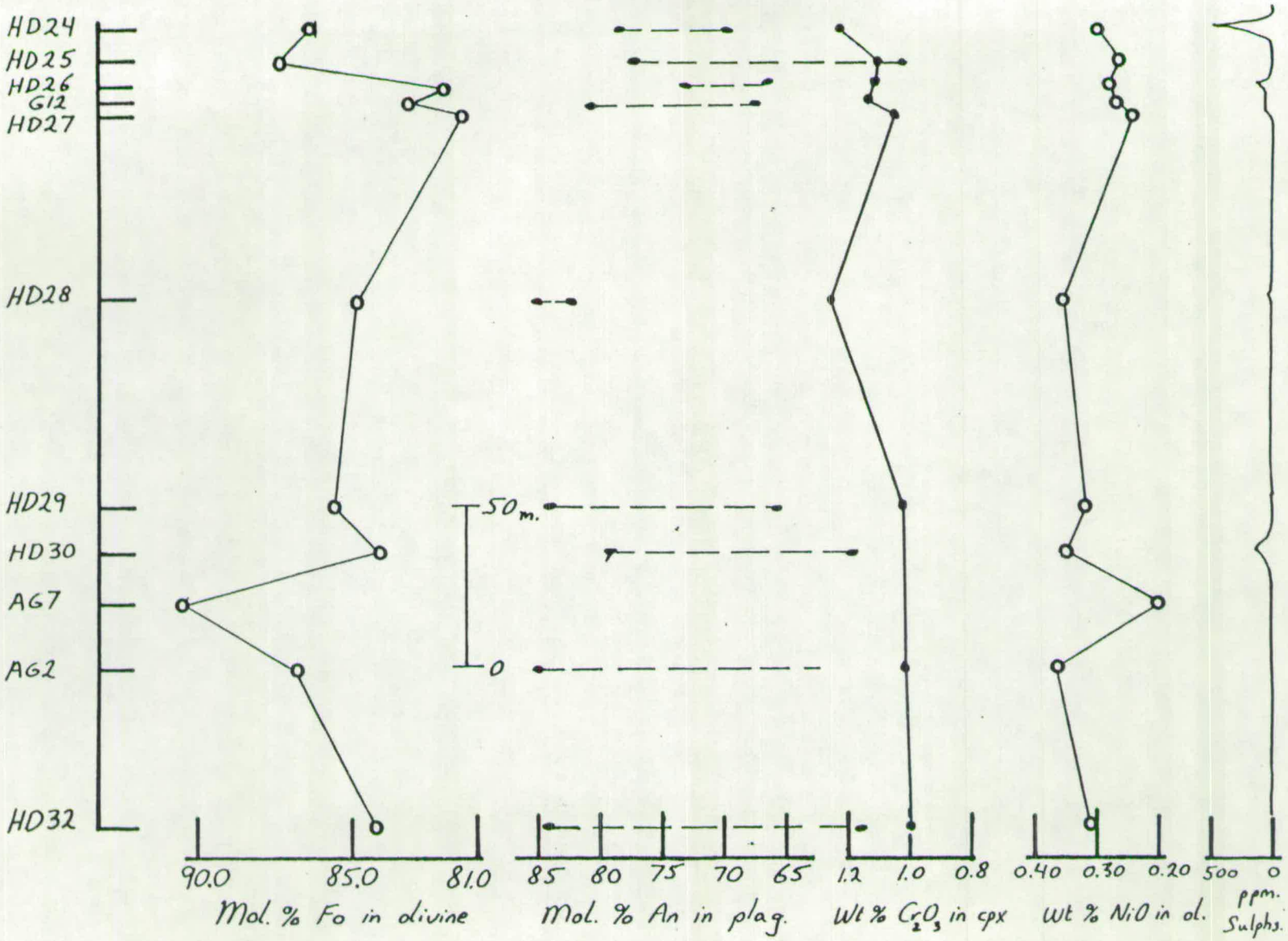
HD24
HD25
HD26
G12
HD27
HD28
HD29
HD30
AG7
AG2
HD32
50 m.
0
90.0
85.0
81.0
Mol. % Fo in olivine
85
80
75
70
65
Mol. % An in plag.
1.2
1.0
0.8
Wt % Cr2O3 in cpx
0.40
0.30
0.20
Wt % NiO in ol.
500
0
ppm. Sulphs.

Fig. A.1 (viii)

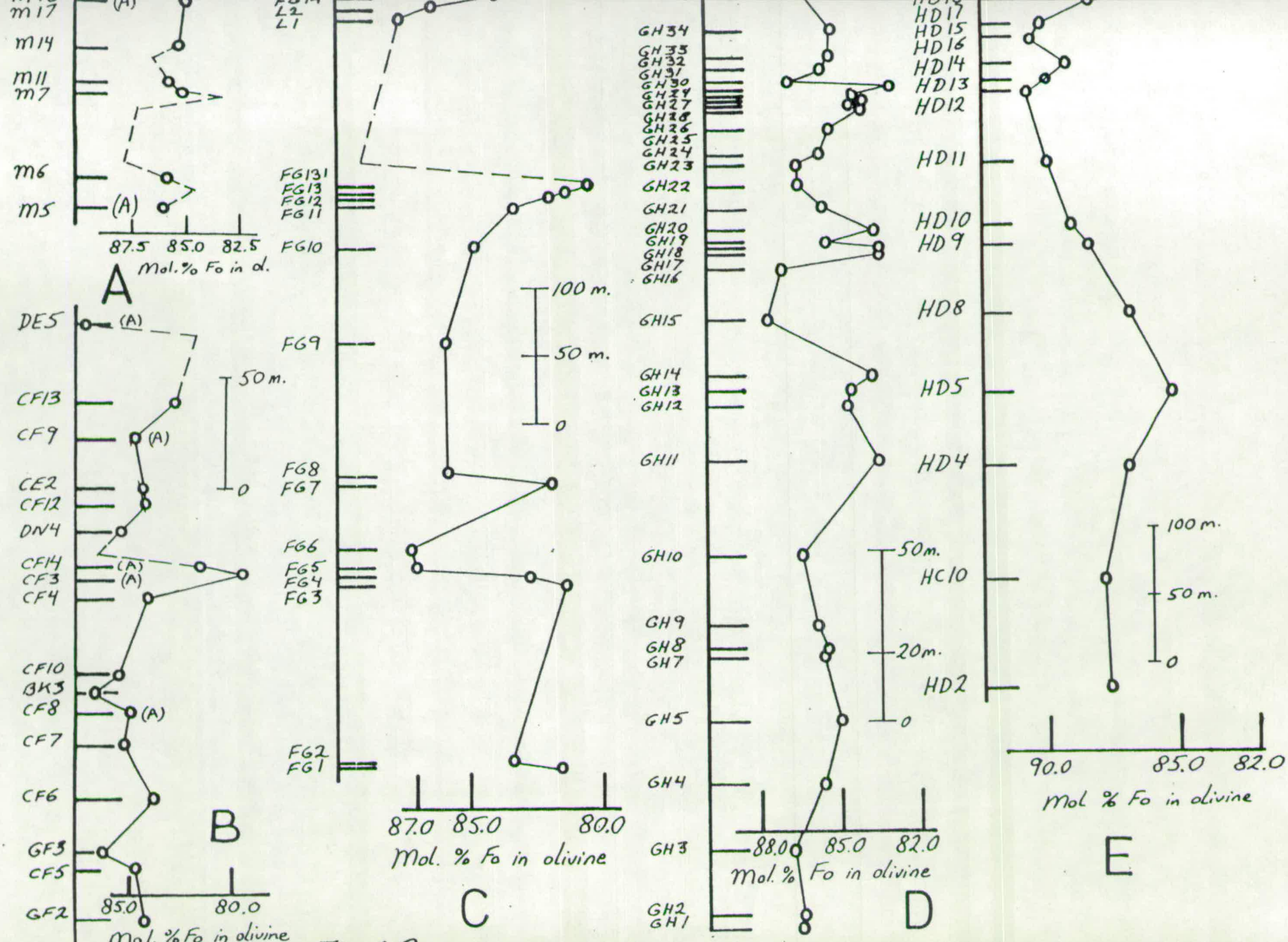
m17
m14
m11
m7
m6
m5
(A)
87.5 85.0 82.5
Mol.% Fo in ol.
A
DE5
CF13
CF9
CE2
CF12
DN4
CF14
CF3
CF4
CF10
BK3
CF8
CF7
CF6
GF3
CF5
GF2
50 m.
0
85.0 80.0
Mol. % Fo in olivine
B
L2
L1
FG131
FG13
FG12
FG11
FG10
FG9
FG8
FG7
FG6
FG5
FG4
FG3
FG2
FG1
100 m.
50 m.
0
87.0 85.0 80.0
Mol. % Fo in olivine
C
GH34
GH33
GH32
GH31
GH30
GH27
GH26
GH25
GH24
GH23
GH22
GH21
GH20
GH19
GH18
GH17
GH16
GH15
GH14
GH13
GH12
GH11
GH10
GH9
GH8
GH7
GH5
GH4
GH3
GH2
GH1
50m.
20m.
0
88.0 85.0 82.0
Mol. % Fo in olivine
D
HD17
HD15
HD16
HD14
HD13
HD12
HD11
HD10
HD9
HD8
HD5
HD4
HC10
HD2
100 m.
50 m.
0
90.0 85.0 82.0
Mol % Fo in olivine
E

Fig. A2

APPENDIX B

BULK ROCK X-RAY FLUORESCENCE ANALYSIS.

For bulk rock analysis, at least 500 gm of unweathered sample material was collected. Samples were processed at the Grant Institute of Geology, Edinburgh, as follows:

(i) Crushing in a Sturtevant jaw crusher to 0.5 mm. fragments.

(ii) Grinding in a Tema mill to less than 100 mesh.

(iii) Fusing of ca. 1 gm. of the powder to produce glass discs with the help of a flux.

Ultrabasic samples were held in a furnace at 1200 ^{o}C for 45 mn. to melt all phases including spinel, while other samples dissolved entirely at 1100 ^{o}C after about 20 mn. Samples were not ignited prior to flux addition as potential weight losses on ignition - the LOI value - were less than 5 %. The detailed procedure described in the internal report of Fitton et al. (1982) was closely followed.

(iv) Pressing of about 7 gm. of powder at a pressure of 10 ton/in.^{2} to powder pellets, again according to the procedure of Fitton et al. (1982).

(v) Major elements (Si, Al, Fe, Mg, Ca, Na, K, Ti, Mn and P) were analysed on the glass discs on an automated Philips PW 1450/20 spectrometer fitted with a Cr-anode X-ray tube.

(vi) Powder pellets were analysed for the trace elements Sc, V, Cu, Ba and La on the same system and for Ni, Zn, Th, Cr, Rb, Sr, Y, Zr, Nb, Ce and Nd on the Philips PW 1450/20 with a tungsten anode X-ray tube.

The reproducibility of discs and pellets produced as in steps (iii) and (iv) is given in Table B.1. For steps (v) and (vi), analytical conditions and the significance of interference on the chosen analytical lines are tabulated in,respectively, Tables B.2 and B.3. Thirlwall (1979) wrote the computer programs for the data processing and their use is detailed in the report by Fitton et al. (1982). Thirlwall (1979) also tested the accuracy of the system (Table B.4) and the precision obtained in this study is given in Table B.5. Data from this study are presented in the tables and diagrams of Chapter 6. The data points on these diagrams are identified by sample number in Fig. B.1.

DISCS

	SiO2	Al2O3	Fe2O3	MgO	CaO		
Mean	54.529	15.589	8.248	6.743	8.023		
± 2-sigma	0.342	0.114	0.101	0.069	0.025		
	Na2O	K2O	TiO2	MnO	P2O5	LOI	
Mean	3.317	1.356	1.281	0.115	0.347	1.542	
± 2-sigma	0.104	0.011	0.007	0.016	0.004	0.100	

PELLETS

	Sc	V	Cu	Ba	La	TiO2CR	Ni	Zn	Th
Mean	24.4	167.0	49.9	543.6	31.1	1.309	138.3	67.9	10.6
± 2-sigma	0.4	4.6	1.2	8.5	2.1	0.036	0.8	1.1	2.3

	Rb	Sr	Y	Zr	Nb	Cr	Ce	Sm	Nd	TiO2W
Mean	17.3	601.1	25.8	249.1	12.4	289.8	73.3	8.8	34.1	1.331
± 2-sigma	0.9	4.5	0.8	1.5	0.9	4.0	2.3	4.6	1.7	0.016

TABLE B.1 Reproducibility of discs and pellets. (Taken from Tables B.1 and B.3, Thirlwall 1979).

ne	Crystal	kV	mA	Colli-mator	Counter	Background offset 2θ°	Lower Level	Windo
K_{α}	PE	50	45	C	F	+ 4.40	25%	60%
K_{α}	PE	60	45	C	F	- 5.75	25%	60%
K_{α}	LiF200	50	45	F	F	- 1.63	20%	60%
K_{α}	TlAP	60	45	C	F	+ 2.70	25%	50%
K_{α}	LiF200	50	30	F	F	- 3.00	25%	60%
K_{α}	TlAP	60	45	C	F	- 2.25	30%	50%
α	LiF200	50	45	F	F	- 4.55	25%	60%
K_{α}	LiF200	50	45	F	F	+ 4.74	30%	50%
K_{α}	LiF200	60	45	F	F	- 1.00	15%	70%
α	Ge	50	45	C	F	+ 3.14	35%	40%
K_{α}	LiF200	60	45	F	F	- 1.59	25%	60%
α	LiF220	60	45	F	F	- 2.62	30%	50%
K_{α}	LiF200	60	45	C	F	+ 1.01	39%	26%
L_{β_2}	LiF220	60	45	F	F	+ 1.75	15%	60%
L_{α_1}	LiF200	60	45	C	F	- 1.08	30%	50%
K_{α}	LiF200	60	45	F	F	+ 1.33	25%	50%
K_{α}	"	60	45	F	F	+ 0.80	25%	50%
L_{α_1}	"	90	30	F	FS	-	20%	60%
K_{α}	"	90	30	F	FS	+ 2.09	20%	60%
K_{α}	"	90	30	F	FS	-	20%	60%
α	"	90	30	F	FS	+ 0.48	20%	60%
K_{α}	"	90	30	F	FS	-	20%	60%
K_{α}	"	90	30	F	FS	- 0.40	20%	60%
K_{α}	"	60	45	F	F	+ 1.44 - 0.74	15%	60%
L_{β_1}	"	60	45	F	F	-	15%	60%
L_{α_1}	"	60	45	F	FS	- 0.48	20%	60%
L_{α_1}	"	60	45	F	F	- 1.34	15%	60%
K_{β}	"	60	45	F	F	- 1.54	30%	50%
K_{β}	"	60	45	F	F	-	25%	60%

Crystals

PE = Pentaerythritol, TlAP = Thallium acid phthalate
Ge = Germanium, LiF = Lithium Fluoride

Collimators

C = coarse, F = fine

Counters

F = gas flow proportional counter
FS = flow counter and scintillation counter

TABLE B.2 XRF analytical conditions. (Taken from Table B.6, Thirlwal 1979).

Line	Interference	Approx extent of Interference	Correction made
Mn K_α	Cr K_β	Unimportant for Cr <1500 ppm	None
P K_α	Ca K_β (2nd order)	Unimportant for CaO <20%	Narrow energy window
Mg K_α	Ca K_α (3rd order)	? 0.1% MgO for 20% CaO	None
Sc K_α	Ca K_β	1 ppm. Sc per % CaO	Regression
V K_α	Ti K_β	180 ppm. V per % TiO_2	Regression
La $L\alpha_1$	Ti K_α	5 ppm. La per % TiO_2	Regression
Ti K_β	Ba $L_{\beta 3}$	0.00004 % TiO_2 per ppm. Ba	Yes
	V K_α	0.0004 % TiO_2 per ppm. V	Yes
Ni K_α	Y K_α (2nd order)	Unimportant for Y <400 ppm.	Narrow energy window
Y K_α	Rb K_α	0.22 ppm. Y per ppm. Rb	Regression
Zr K_α	Sr K_α	0.07 ppm. Zr per ppm. Sr	Regression
Nb K_α	La K_α (2nd order)	0.01 ppm. Nb per ppm. La	Regression
	Y K_β	Unimportant for Y <1000 ppm.	None
	U $L_{\beta 2,4}$	Unimportant for U<50 ppm.	None
Cr K_α	V K_β	0.05 ppm. Cr per ppm. V	Regression
Ce L_{β_1}	Nd $L\alpha_1$	Probably unimportant?	None
Nd $L\alpha_1$	Ce $L_{\beta 1}$	0.01 ppm. Nd per ppm. Ce	Regression
Sm $L\alpha_1$	Ce $L_{\beta 2}$	0.02 ppm. Sm per ppm. Ce	Regression
Cu background	Hf $L\alpha_1$	Unimportant for Zr <800 ppm	None
	Zr K_α (2nd order)		
Y, Zr, Nb backgrounds	U, Th	Unimportant for <500 ppm U, Th	None
Ce, Nd background	Cr K_α	Unimportant for Cr <800 ppm	None

TABLE B.3 Interferences on chosen analytical lines and backgrounds. (Taken from Table B.5, Thirlwall, 1979).

Major elements: sample GS-N

	SiO_2	Al_2O_3	Fe_2O_3*	MgO	CaO	Na_2O	K_2O	TiO_2	MnO	P_2O_5
XRF	66.09	14.81	3.82	2.30	2.45	3.60	4.687	0.662	0.060	0.269
Abbey (1977)	65.98	14.71	3.75	2.31	2.51	3.78	4.64	0.68	0.06	0.28

	XRF						Abbey (1977)					
	DR-N	FK-N	UB-N	W1	SY2	TB	DR-N	FK-N	UB-N	W1	SY2	TB
Sc	34	0	14	37	6	21	-	-	-	?35	?7	13.5
V	224	2	68	264	50	121	220	-	75	240	50	105
Cu	44	4	20	102	3	32	52	?3	30	110	4	50
Ba	398	198	40	175	460	777	380	?210	?45	160	460	720
La	20	2	3	12	67	51	-	-	-	?12	?85	?56

		Ni	Zn	Th	Rb	Sr	Y	Zr	Nb	Cr	Ce	Sm	Nd
XRF	W1	74	84	2	22	196	24	107	9	128	19	3	11
	SY2	11	260	427	226	270	124	288	37	9	157	13	72
	TB	44	98	19	189	164	33	188	20	107	103	7	43
Abbey (1977)	W1	78	86	2	21	190	25	105	?10	120	?23	?4	15
	SY2	10	250	?370	220	270	130	270	?25	10	?210	?16	?70
	TB	40	95	?19	180	155	?39	175	-	80	?115	?9	-

TABLE B.4 Analytical accuracy (Analyses of samples run as unknowns, compared with values from Abbey, 1977)).
(Taken from Table B.7, Thirlwall, 1979). Major elements in wt%, trace elements in ppm.

	DN1 (analysed 6 times)		DO1 (analysed 3 times)	
	Avg.	2 D	Avg.	2 D
Si	41.36	0.68	49.36	0.20
Al	9.68	0.20	14.18	0.14
Fe*	12.25	0.08	14.13	0.04
Mg	27.84	0.74	5.71	0.08
Ca	6.64	0.06	10.66	0.04
Na	0.620	0.06	2.91	0.20
K	0.005	0.002	0.698	0.012
Ti	0.196	0.004	1.69	0.04
Mn	0.169	0.008	0.221	0.02
P	0.003	0.002	0.184	0.004
Ni	1183	15.2	53.1	2.0
Zn	64.7	2.0	88.1	2.0
Pb	5.0	2.4	6.7	2.9
Th			2.3	1.0
Rb	0.8	0.4	18.5	8.3
Sr	127	2.2	217	3.0
Y	3.5	0.6	37.9	0.3
Zr	4.6	3.6	123	3.0
Nb	1.4	0.4	5.2	1.0
Cr	1961	28.0	102	1.5
Ce			20.6	1.7
Nd			12.9	0.8
Sc	15.4	0.8	46.1	4.2
V	66.1	0.8	400	2.0
Cu	75.5	2.0	136	0.5
Ba	22.7	2.6	281	3.0
La			11.0	1.3

TABLE B.5 Precisions obtained for repeated analyses of the same rock samples during the course of this study. Major elements are expressed in wt% oxides and trace elements in ppm. D = standard deviation.

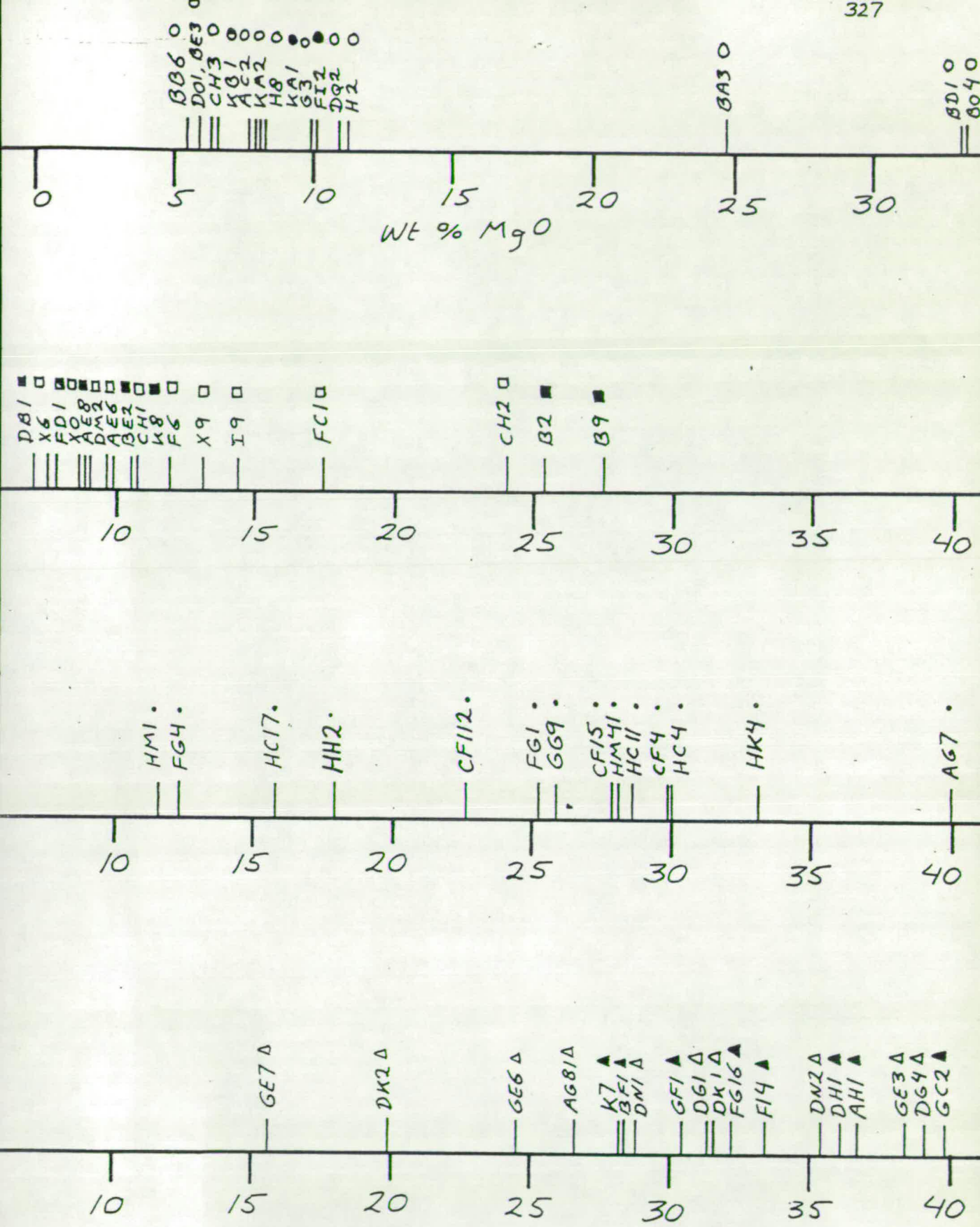

FIG. B 1 Identification of the points in the Harker variation diagrams of Figs. 6.5 to 6.7 and 6.9 to 6.11.

REFERENCES

AOKI, K., K. ISHIWAKA and S. KANISAWA, 1981. Fluorine geochemistry of basaltic rocks from continental and oceanic regions and petrogenetic applications. Contribs. Min. Pet. 76, 53-59

ATKINS, F. B. 1969. Pyroxenes of the Bushveld intrusion, South Africa. J. Petrol. 10, 222-249.

BAILEY, E. B. 1945. Tertiary igneous tectonics of Rhum, Inner Hebrides. Q. Jl. Geol. Soc. Lond. 100, 165-191.

BARRIERE, M. 1981. On curved laminae, graded layers, convection currents and dynamic crystal sorting in the Ploumanac'h (Brittany) subalkaline granite. Contr. Min. Pet. 77, 214-224.

BEVAN, J. C. 1982. Reaction rims of orthopyroxene and plagioclase around chrome-spinels in olivine from Skye and Rhum (NW Scotland). Contr. Min. Pet. 79, 124-129.

BLACK, G. P. 1954. The acid rocks of western Rhum. Geol. Mag. 91, 257-272.

BOTT, M. H. P. and J. TUSON, 1973. Deep structure beneath the Tertiary volcanic regions of Skye, Mull and Ardnamurchan, northwest Scotland. Nature Phys. Sci. 242, 114-116.

BROTHERS, R. N. 1964. Petrofabric analyses of Rhum and Skaergaard layered rocks. J. Petrol. 5, 255-274.

BROWN, G. M. 1956. The layered ultrabasic rocks of Rhum, Inner Hebrides. Phil. Trans. R. Soc. Lond. B240, 1-53.

BUCHANAN, D. L. 1979. A combined transmission electron microscope and electron microprobe study of Bushveld pyroxenes from the Bethal area. J. Petrol. 20, 327-354.

BURNHAM, C. W. 1979. The importance of volatile constituents. IN: The Evolution of the Igneous Rocks, Fiftieth Anniversary Perspectives, H. S. Yoder, Jr., (ed.), Princeton University Press, Princeton, New Jersey.

CAMERON, E. N. 1969. Postcumulus changes in the eastern Bushveld Complex. Am. Min. 54, 754-779.

CAMERON, E. N. and G. A. DESBOROUGH, 1969. Occurrence and characteristics of chromite deposits- eastern Bushveld Complex. Econ. Geol. Monogr. 4, 23-40.

CAMPBELL, I. H. 1978. Some problems with the cumulus theory. Lithos 11, 311-323.

CAMPBELL, I. H., A. J. NALDRETT and S. J. BARNES, 1983. A model for the origin of the platinum-rich sulfide horizons in the Bushveld and Stillwater complexes. J. Petrol. 24, 133-165.

CARMICHAEL, I. S. E., F. J. TURNER and J. VERHOOGEN, 1974. Igneous Petrology, McGraw-Hill, New York.

CASEY, J. F. and J. A. KARSON, 1981. Magma chamber profiles from the Bay of Islands ophiolite complex. Nature 292, 295-301.

CAWTHORN, R. G. and T. S. McCARTHY, 1980. Variations in Cr content of magnetite from the upper zone of the Bushveld complex: evidence for heterogeneity and convection currents in magma chambers. Earth Plan. Sci. Letts. 46, 335-343.

CAWTHORN, R. G., C. E. FORD, G. M. BIGGAR, M. S. BRAVO and D. F. CLARK 1974. Determination of the liquid composition in experimental studies: discrepancies between microprobe analyses and other methods. Earth. Plan. Sci. Letts. 21, 1-6.

COX, K. G. and P. CLIFFORD, 1982. Correlation coefficient patterns and their use in three basaltic suites. Contr. Min. Pet. 79, 268-278.

DEER, W. A., R. A. HOWIE and J. ZUSSMAN, 1966. An Introduction to the Rock-forming Minerals. Longman, London.

DE PAOLO, D. J. 1981. Trace element and isotopic effects of combined wall-rock assimilation and fractional crystallisation. Earth Plan. Sci. Letts. 53, 189-205.

DICKIN, A. P. 1981. Isotope geochemistry of Tertiary igneous rocks from the Isle of Skye, NW Scotland. J. Petrol. 22, 155-189.

DOE, T. W. and R. H. DOTT, Jr., 1980. Genetic significance of deformed crossbedding - with examples from the Navajo and Weber sandstones of Utah. J. Sed. Petrol. 50, 793-812.

DONALDSON, C. H. 1974. Olivine crystal types in harrisitic rocks of the Rhum pluton and in Archaean spinifex rocks. Bull. Geol. Soc. Am. 85, 1721-1726.

DONALDSON, C. H. 1975. Ultrabasic breccias in layered intrusions. The Rhum complex. J. Geol. 83, 33-45.

DONALDSON, C. H. 1977. Laboratory duplication of comb-layering in the Rhum pluton. Min. Mag. 41, 323-336.

DONALDSON, C. H. 1982. Origin of some of the Rhum harrisite by segregation of intercumulus liquid. Min. Mag. 45, 201-209.

DONALDSON, C. H., H. I. DREVER and R. JOHNSTON, 1973. Crystallisation of poikilo-macro-spherulitic feldspar in a Rhum peridotite. Nature Phys. Sci. 243, 69-70.

DUNHAM, A. C. 1962. The petrology and structure of the northern edge of the Tertiary igneous complex of Rhum. D. Phil. Thesis, Oxford.

DUNHAM, A. C. 1970. The emplacement of the Tertiary igneous complex of Rhum. IN: Geol. J. Spec. Issue 2, Mechanisms of Igneous Intrusion, N. Rast (ed.).

DUNHAM, A. C. and C. H. EMELEUS, 1967. The Tertiary geology of Rhum, Inner Hebrides. Proc. Geol. Assoc. 78, 391-418.

DUNHAM, A. C. and W. J. WADSWORTH, 1978. Cryptic variation in the Rhum layered intrusion. Min. Mag. 42, 347-356.

ELSDON, R. 1970. Crystallisation behaviour of mafic intrusions. Earth Plan. Sci. Letts. 9, 313-316.

EMELEUS, C. H. 1981. A thrust fault at Welshman's Rock, Isle of Rhum. Scott. J. Geol. 17, 1-6.

FITTON, J. G., D. E. JAMES and M. F. THIRLWALL, 1981. A User's guide to the X-ray fluorescence analysis of rock samples. Internal Report, Grant Institute of Geology, Edinburgh.

FORSTER, R. M. 1978. Preliminary atmospheric pressure melting relationships of some proposed Rhum parent magmas. Prog. Exp. Petrol. Report 3, 200-201, N. E. R. C.

FORSTER, R. M. 1980. A geochemical and petrological study of the Tertiary minor intrusions of Rhum, northwest Scotland. Ph. D. Thesis, Durham.

FYFE, W. S., N. J. PRICE and A. B. THOMPSON, 1978. Fluids in the Earth's Crust. Their Significance in Metamorphic, Tectonic and Chemical Transport. Elsevier, Amsterdam.

GEIKIE, A. 1897. The Ancient Volcanoes of Great Britain, volume 2. London.

GIBB, F. G. F. 1973. The zoned clinopyroxenes of the Shiant Isles sill, Scotland. J. Petrol. 14, 203-230.

GIBB, F. G. F. 1976. Ultrabasic rocks of Rhum and Skye: the nature of the parent magma. J. Geol. Soc. Lond. 132, 209-222.

GRAY, C. M., R. A. CLIFF and A. D. T. GOODE, 1981. Neodymium-strontium isotopic evidence for extreme contamination in a layered basic intrusion. Earth Plan. Sci. Letts. 56, 189-198.

HARKER, A. 1908. The Geology of the Small Isles of Inverness-shire. Mem. Geol. Surv. Scotland.

HART, S. R. and C. J. ALLEGRE, 1980. Trace element constraints on magma genesis. IN: Physics of Magmatic Processes, R. B. Hargreaves (ed.), Princeton University Press, Princeton, New Jersey.

HAUGHTON, D., P. L. ROEDER and B.J. SKINNER, 1974. Solubility of sulphur in mafic magmas. Econ. Geol. 69, 451-467.

HENDERSON, P. 1975. Reaction trends of chrome spinel on Rhum. Geoch. Cosmoch. Acta 39, 1039-1044.

HENDERSON, P. and R. GIJBELS, 1976. Trace element indicators of the genesis of the Rhum layered intrusion. Scott. J. Geol. 12, 325-333.

HENDERSON, P. and R.J. WOOD, 1981. Reaction relationships of chrome-spinels in igneous rocks - further evidence from the layered intrusions of Rhum and Mull, Inner Hebrides, Scotland. Contr. Min. Petrol. 78, 225-229.

HESS, G. B. 1972. Heat and mass transport during crystallisation of the Stillwater igneous complex. IN: Studies in Earth and Space Sciences, R. Shagam (ed.), Geol. Soc. Am. Mem. 132, 503-523.

HESS, H. H. 1960. Stillwater Igneous Complex, Montana, a Quantitative Mineralogical Study, Geol. Soc. Am. Mem. 80.

HESS, P. C. 1980. Polymerisation model for silicate melts. IN: Physics of Magmatic Processes, R. B. Hargreaves (ed.),Princeton University Press, Princeton , New Jersey.

HUGHES, C. J. 1955. Petrological and structural studies in south-east Rhum, Inverness-shire. D. Phil. Thesis, Oxford.

HUGHES, C. J. 1960. An occurrence of tilleyite-bearing limestone in the Isle of Rhum, Inner Hebrides. Geol. Mag. 97, 384-388.

HUPPERT, H. E. and R. S. J. SPARKS, 1980. The fluid dynamics of a basaltic magma chamber replenished by influx of hot, dense ultra-basic magma. Contr. Min. Petrol. 75, 279-289.

HUPPERT, H. E., J. S. TURNER and R. S. J. SPARKS, 1982. Replenished magma chambers: effects of compositional zonation and input rate. Earth Plan. Sci. Letts. 57, 345-357.

IRVINE, T. N. 1965. Chromian spinel as a petrogenetic indicator. I Theory. Can. J. Earth Sci. 2, 648-672.

IRVINE, T. N. 1967. Chromian spinel as a petrogenetic indicator. II Petrologic application. Can. J. Earth Sci. 4, 71-103.

IRVINE, T. N. 1975. Crystallisation sequences in the Muskox intrusion and other layered intrusions. I Origin of chromitite deposits and similar deposits of magmatic ores. Geoch. Cosmoch. Acta 39, 991-1020.

IRVINE, T. N. 1975b. Olivine-pyroxene-plagioclase relations in the system Mg_2SiO_4 - $CaAl_2Si_2O_8$ - $KAlSi_3O_8$ - SiO_2 and their bearing on the differentiation of stratiform intrusions. Carn. Inst. Wash. Yearbk. 74, 492-500.

IRVINE, T. N. 1977. Origin of chromitite layers in the Muskox intrusion and other stratiform intrusions: a new interpretation. Geology 5, 273-277.

IRVINE, T. N. 1979. Rocks whose composition is determined by crystal accumulation and sorting. IN: The Evolution of the Igneous Rocks, Fiftieth Anniversary Perspectives, H. S. Yoder (ed.), Princeton University Press, Princeton, New Jersey.

IRVINE, T. N. 1980. Magmatic infiltration metasomatism, double-diffusive fractional crystallisation and adcumulus growth in the Muskox intrusion and other layered intrusions. IN: Physics of Magmatic Processes, R. B. Hargreaves (ed.), Princeton University Press, Princeton, New Jersey.

IRVINE, T. N. 1980b. Magmatic density currents and cumulus processes. Am. J. Sci., Jackson volume, 280 A, 1-58.

IRVINE, T. N. 1981. A liquid-density controlled model for chromitite formation in the Muskox intrusion. Carn. Inst. Wash. Yearbk. 80, 317-324.

IRVINE, T. N. 1982. Terminology for layered intrusions. J. Petrol. 23, 127-162.

IRVINE, T. N. and W. BARAGAR, 1971. Chemical classification of common volcanic rocks. Can. J. Earth Sci. 8, 523-548.

IRVINE, T. N., D. W. KEITH and S. G. TODD, 1982. Formation of the Stillwater J-M reef by concurrent fractional crystallisation and liquid mixing in a stratified magma body. Carn. Inst. Wash. Yearbk. 81, 281-286.

IRVINE, T. N. and C. H. SMITH, 1967. The ultramafic intrusion of Muskox, Northwest Territories, Canada. IN: Ultramafic and Related Rocks, P. J. Wyllie (ed.), J. Wiley and Sons, New York.

JACKSON, E. D. 1961. Primary textures and mineral associations in the ultramafic zone of the Stillwater complex, Montana. U.S. Geol. Surv. Prof. Paper 358.

JAQUES, A. L. 1981. Petrology and petrogenesis of cumulate peridotites and gabbros from the Marum ophiolite complex, northern Papua New Guinea. J. Petrol. 22, 1-40.

JUDD, J. W. 1889. The Tertiary Volcanoes of the Western Isles of Scotland. Q. J. Geol. Soc. Lond. 45, 187-218.

KULLERUD, G., R. A. YUND and G. H. MOH, 1969. Phase relations in the Cu-Fe-S, Cu-Ni-S and Fe-Ni-S systems. Econ. Geol. Monogr. 4, 323-343.

LEE, C. A. 1981. Post-depositional structures in the Bushveld complex mafic sequence. J. Geol. Soc. Lond. 138, 327-341.

LEE, C. A. and M. S. SHARPE, 1980. Further examples of silicate liquid immiscibility and spherical agglomeration in the Bushveld complex. Earth Plan. Sci. Letts. 48, 131-147.

LOOMIS, T. P. 1982. Numerical simulation of crystallisation processes of plagioclase in complex melts: the origin of major and oscillatory zoning in plagioclase. Contr. Min. Petrol. 81, 219-229.

MAALOE, S. 1978. The origin of rhythmic layering. Min. Mag. 42, 337-345.

MAC INTYRE, R. M., T. McMENAMIN and J. PRESTON, 1975. K-Ar results from western Ireland and their bearing on the time and siting of Thulean magmatism. Scott. J. Geol. 11, 227-249.

MAC LEAN, W. H. 1969. Liquidus phase relations in the FeS-FeO-Fe_3O_4-SiO_2 system, and their application in geology. Econ. Geol. 64, 865-884.

McBIRNEY, A. R. 1959. Factors governing emplacement of volcanic necks. Am. J. Sci. 257, 431-448.

McBIRNEY, A. R. 1975. Differentiation of the Skaergaard intrusion. Nature 253, 691-694.

McBIRNEY, A. R. and R. M. NOYES, 1979. Crystallisation and layering of the Skaergaard intrusion. J. Petrol. 20, 487-554.

McDONALD, J. A. 1965. Liquid immiscibility as one factor in chromitite seam formation in the Bushveld igneous complex. Econ. Geol. 60, 1674-1685.

McQUILLIN, R. and P. E. BINNS, 1973. Geological structure in the Sea of the Hebrides. Nature Phys. Sci. 241, 2-4.

McQUILLIN, R. and J. TUSON, 1963. Gravity measurements over the Rhum Tertiary pluton. Nature 199, 1276-1277.

MAURY, R. 1978. La Contamination magmatique. IN: Les Roches Volcaniques: Pétrologie et Cadre Structural, M. Girod (ed.), Doin, Paris.

MOORE, J. G. 1970. Water content of basalt erupted on the ocean floor. Contr. Min Petrol. 28, 272-279.

MYSEN, B. O. and I. KUSHIRO, 1979. The effect of pressure on the partitioning of nickel between olivine and aluminous silicate melt. Earth Plan. Sci. Letts. 42, 383-389.

O'HARA, M. J. 1968. The bearing of phase equilibria studies in synthetic and natural systems on the origin and evolution of basic and ultrabasic rocks. Earth Sci. Revs. 4, 69-133.

O'HARA, M. J. 1978. Thermal history of magmas: the low-pressure reference point. Phil. Trans. R. Soc. Lond. A 288, 627-639.

PARSONS, I. and A. N. BUTTERFIELD, 1981. Sedimentary structures of the Nunarssuit and Klokken syenites, S Greenland. J. Geol. Soc. Lond. 138, 289-306.

PHILPOTTS, J. A. and C. C. SCHNETZLER, 1970. Phenocryst-matrix partition coefficients for K, Rb, Sr and Ba, with applications to anorthosite and basalt genesis. Geoch. Cosmoch. Acta 34, 307-322.

PROPACH, G. 1976. Models of filter differentiation. Lithos 9, 203-209.

PUTNIS, A. and G. D. PRICE, 1979. The nature and significance of exsolved phases in some chrome-spinels from the Rhum layered intrusion. Min. Mag. 43, 519-526.

RAST, N. 1970. The initiation, ascent and emplacement of magmas. IN: The Mechanisms of Igneous Intrusion, Newall and Rast (eds.), Geol. J. Spec. Issue 2.

RICE, A. 1981. Convective fractionation: a mechanism to provide cryptic zoning (macro-segregation), layering, crescumulates, banded tuffs, and explosive volcanism in igneous processes. J. Geoph. Res. 86, 405-417.

RIDLEY, W. I. 1971. The petrology of the volcanic rocks from the British Tertiary Province: the islands of Rhum, Eigg, Canna and Muck. Contr. Min. Petrol. 32, 251-266.

RIDLEY, W. I. 1977. The crystallisation trends of spinels in Tertiary basalts from Rhum and Muck and their petrogenetic significance. Contr. Min. Petrol. 64, 243-255.

ROBINS, B. 1983. Finger structures in the Lille-Kufjord layered intrusion, Finmark, northern Norway. Contr. Min. Petrol. 81, 290-295.

ROEDER, P. L. and R. F. EMSLIE, 1970. Olivine-liquid equilibrium. Contr. Min. Petrol. 29, 275-289.

SHARPE, M. R. 1981. The chronology of magma influxes to the eastern compartment of the Bushveld complex as exemplified by its marginal border groups. J. Geol. Soc. Lond. 138, 307-326.

SHAW, H. R. 1963. Obsidian - H_2O viscosities at 1000 bars and 2000 bars in the temperature range 700 ^{o}C to 900 ^{o}C. J. Geoph. Res. 68, 6337-6343.

SHAW, H. R. 1980. The fracture mechanisms of magma transport from the mantle to the surface. IN: The Physics of Magmatic Processes, R. B. Hargreaves (ed.), Princeton University Press, Princeton.

SINTON, J. M. and G. R. BYERLY, 1980. Silicic differentiation of abyssal oceanic magmas: evidence of late-stage vapour transport of potassium. Earth Plan. Sci. Letts. 47, 423-430.

SPARKS, R. S. J. 1978. The dynamics of bubble formation and growth in magmas. J. Volc. Geoth. Res. 3, 1-37.

SPERA, F. J. 1980. Aspects of magma transport. IN: The Physics of Magmatic Processes, R. B. Hargreaves (ed.), Princeton University Press, Princeton, New Jersey.

STOLPER, E. 1982. Water in silicate glasses: an infrared spectroscopic study. Contr. Min. Petrol. 81, 1-17.

SWEATMAN, T. R. and J. V. P. LONG, 1969. Quantitative electron-probe micro-analysis of rock-forming minerals. J. Petrol. 10, 332-379.

TAYLOR, H. P., Jr., 1980. The effects of assimilation of country rocks by magmas on O^{18}/O^{16} and Sr^{87}/Sr^{86} systematics in igneous rocks. Earth Plan. Sci. Letts. 47, 243-254.

TAYLOR, H. P., Jr., and R. W. FORRESTER, 1971. Low O^{18} igneous rocks from the intrusive complexes of Skye, Mull and Ardnamurchan, western Scotland. J. Petrol. 12, 465-497.

THIRLWALL, M. F. 1980. The petrochemistry of the British Old Red Sandstone volcanic province. Ph. D. Thesis, Edinburgh.

THOMPSON, R. N., A. P. DICKIN, I. L. GIBSON and M. A. MORRISON, 1982. Elemental fingerprints of isotopic contamination of hebridean Palaeocene mantle-derived magmas by Archaean sial. Contr. Min. Petrol. 79, 159-168.

TILLEY, C. E. 1944. A note on the gneisses of Rhum. Geol. Mag. 81, 129-131

WADSWORTH, W. J. 1958. An investigation of ultrabasic igneous rocks in southwest Rhum. D. Phil. Thesis, Oxford.

WADSWORTH, W. J. 1961. The layered ultrabasic rocks of south-west Rhum, Inner Hebrides. Phil. Trans. R. Soc. Lond. B 244, 21-64.

WADSWORTH, W. J. 1973. Magmatic sediments. Min. Sci. Eng. 5, 25-35.

WAGER, L. R. and G. M. BROWN, 1951. A note on rhythmic layering in the ultrabasic rocks of Rhum. Geol. Mag. 88, 166-168.

WAGER, L. R. and G. M. BROWN, 1968. Layered Igneous Rocks. Oliver and Boyd, Edinburgh.

WAGER, L. R., G. M. BROWN AND W. J. WADSWORTH, 1960. Types of igneous cumulates. J. Petrol. 1, 73-85.

WATSON, E. B. 1981. Diffusion in magmas at depth in the earth: the effects of pressure and dissolved H_2O. Earth Plan. Sci. Letts. 52, 291-301.

WATSON, E. B. 1982. Basalt contamination by continental crust: some experiments and models. Contr. Min. Petrol. 80, 73-87.

WILLIAMS, C. T. 1978. Uranium-enriched minerals in mesostasis areas of the Rhum layered pluton. Contr. Min. Petrol. 66, 29-39.

WILLIAMS, H. and A. R. McBIRNEY, 1979. Volcanology. Freeman and Cooper, Los Angeles.

WILSON, A. H. 1982. The geology of the Great Dyke, Rhodesia: the ultramafic rocks. J. Petrol. 23, 240-292.

YODER, H. S., Jr., 1965. Anorthite-diopside-water at five and ten kilobars: implications for explosive volcanism. Carn. Inst. Wash. Yearbk. 64.

ZAVARITSKY, A. N. and V. S. SOBOLEV, 1964. The Physico-chemical Principles of Igneous Petrology. Israel Progr. Sci. Translations, Jerusalem.

ACKNOWLEDGMENTS

I thank Professor Brian G. J. Upton for the suggestion of the project, encouragement at every stage and especially the prompt and meticulous reading of the final draft. I also thank Dr. Roy Gill for initial supervision in the field, much advice on photography and how to get the most out of a rock, imaginative discussions and sharp criticism. The receipt of a Science Faculty Scolarship for the duration of the project is gratefully acknowledged.

Peter Williamson introduced me to Rhum and Mrs. Janet Rainey to its geology. Logistical support from the Nature Conservancy on Rhum is acknowledged and I thank the people of the island for their hospitality.

Help from Dr. J. G. Fitton and Mrs. D. James with the preparation, XRF analysis and data processing for bulk rock samples is gratefully acknowledged. For instruction in the use of the electron microprobe and his tireless devotion to the efficient running of the probe unit, I thank Dr. Pete Hill. Dr. Alex Halliday, at the S.U.R.R.C., kindly measured the Sr isotopic ratios of the dyke samples discussed in section 6.6.4. Thanks also go to the technical staff of the Grant Institute of Geology and in particular to Mr. Kenneth Cameron for thin section preparation and Mrs. Diane Baty for the excellent printing of the photographs.

Finally, many friends and colleagues in the department and elsewhere have greatly sustained me. Among these, I particularly want to thank: Bruce Anderson, Alan Butcher, John Faithful, Omar Fridleifson, Haflidi Haflidason,John-Henry Looney, David Pattison, John Ridley and Ulrich Soffler. My parents are thanked for their support and tremendous patience and Miss C. Rostant I cannot thank enough.

KEY

TERTIARY

Minor Intrusions

I_{pb} picrite basalt matrix

Intrusion Breccia

I_p peridotite matrix

Gabbro plugs / sheets veining

Dunite

Peridotite

B 'Black' Peridotite

Central Series

R Ruinsival Member

LL Long Loch Member

D Dornabac Member

OB Outer Breccia Member

Eastern Layered Series

Peridotite

U_8 Allivalite (Unit 8)

Western Layered Series

AM Ard Mheall Member

A-B I — Acid-basic Intrusion Breccia

Gr — Granophyre

F — Porphyritic Felsite

E — Explosion Breccia

G — GABBRO Group 1

PRE-TERTIARY

T — TORRIDONIAN ARKOSE

L — LEWISIAN GNEISS

GEOLOGICAL BOUNDARIES

Certain

Inferred

IGNEOUS LAYERING

23 — Dip in degrees

MAP 1

SECTIONS

FAULTS

MAIN RING

INNER RING

LONG LOCH

minor

STREAM

ROAD

RIVER

TRACK

LOCH

MAP 2

▲ GABBROS

◆ PERIDOTITIC MINOR INTRUSIONS

⊙ DYKES

● EASTERN LAYERED SERIES

■ CENTRAL SERIES

X ARD MHEALL MEMBER

S_1 SECTION 1

T_1 TRAVERSE 1

THE GEOLOGY OF THE TRALLVAL AREA

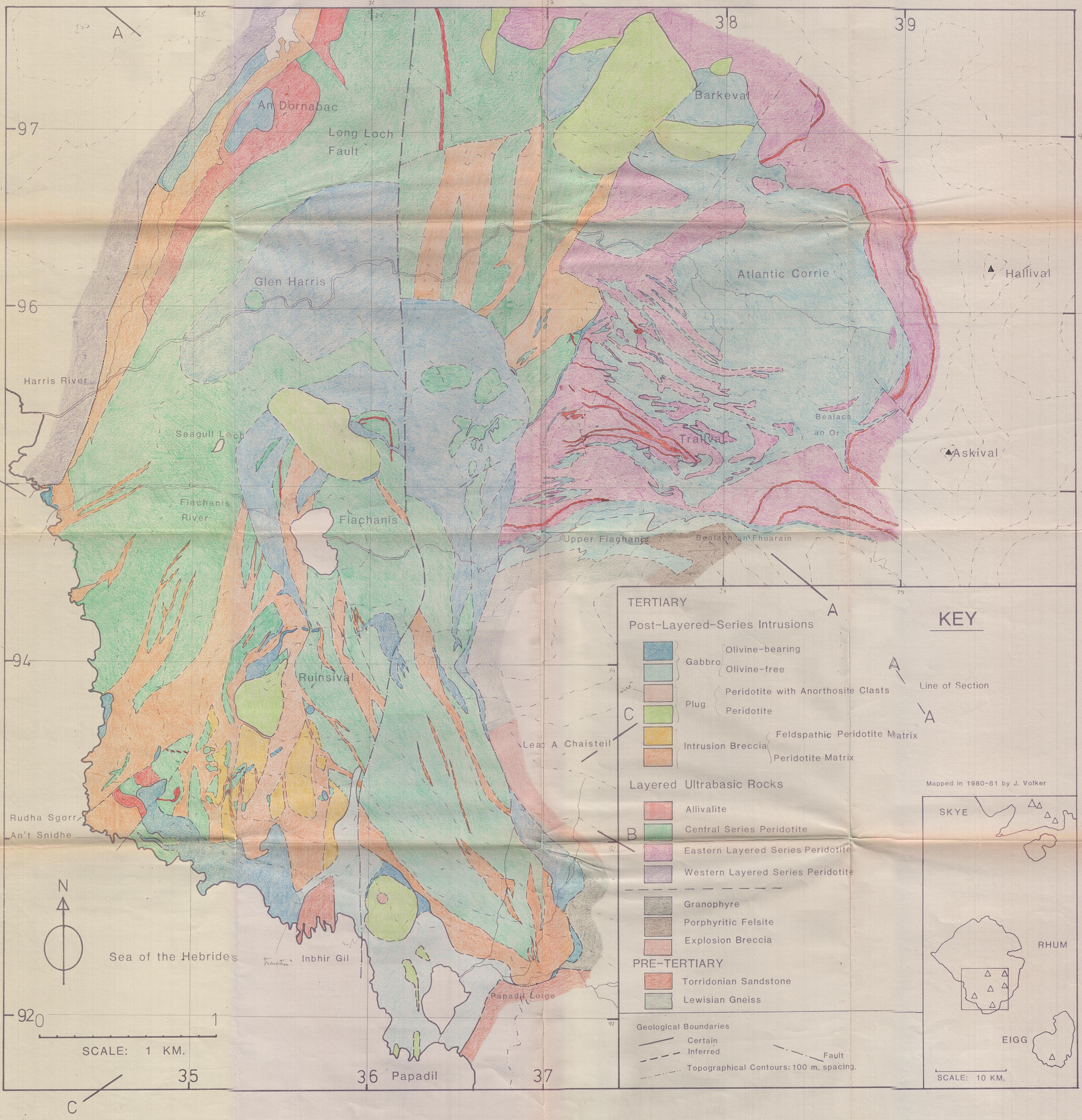

KEY

TERTIARY

Post-Layered-Series Intrusions

- Gabbro
  - Olivine-bearing
  - Olivine-free
- Plug
  - Peridotite with Anorthosite Clasts
  - Peridotite
- Intrusion Breccia
  - Feldspathic Peridotite Matrix
  - Peridotite Matrix

Layered Ultrabasic Rocks

- Allivalite
- Central Series Peridotite
- Eastern Layered Series Peridotite
- Western Layered Series Peridotite

- Granophyre
- Porphyritic Felsite
- Explosion Breccia

PRE-TERTIARY

- Torridonian Sandstone
- Lewisian Gneiss

Geological Boundaries

- Certain
- Inferred
- Fault
- Topographical Contours: 100 m. spacing.

A — A Line of Section

Mapped in 1980-81 by J. Volker

THE GEOLOGY OF THE TRALLVAL AREA

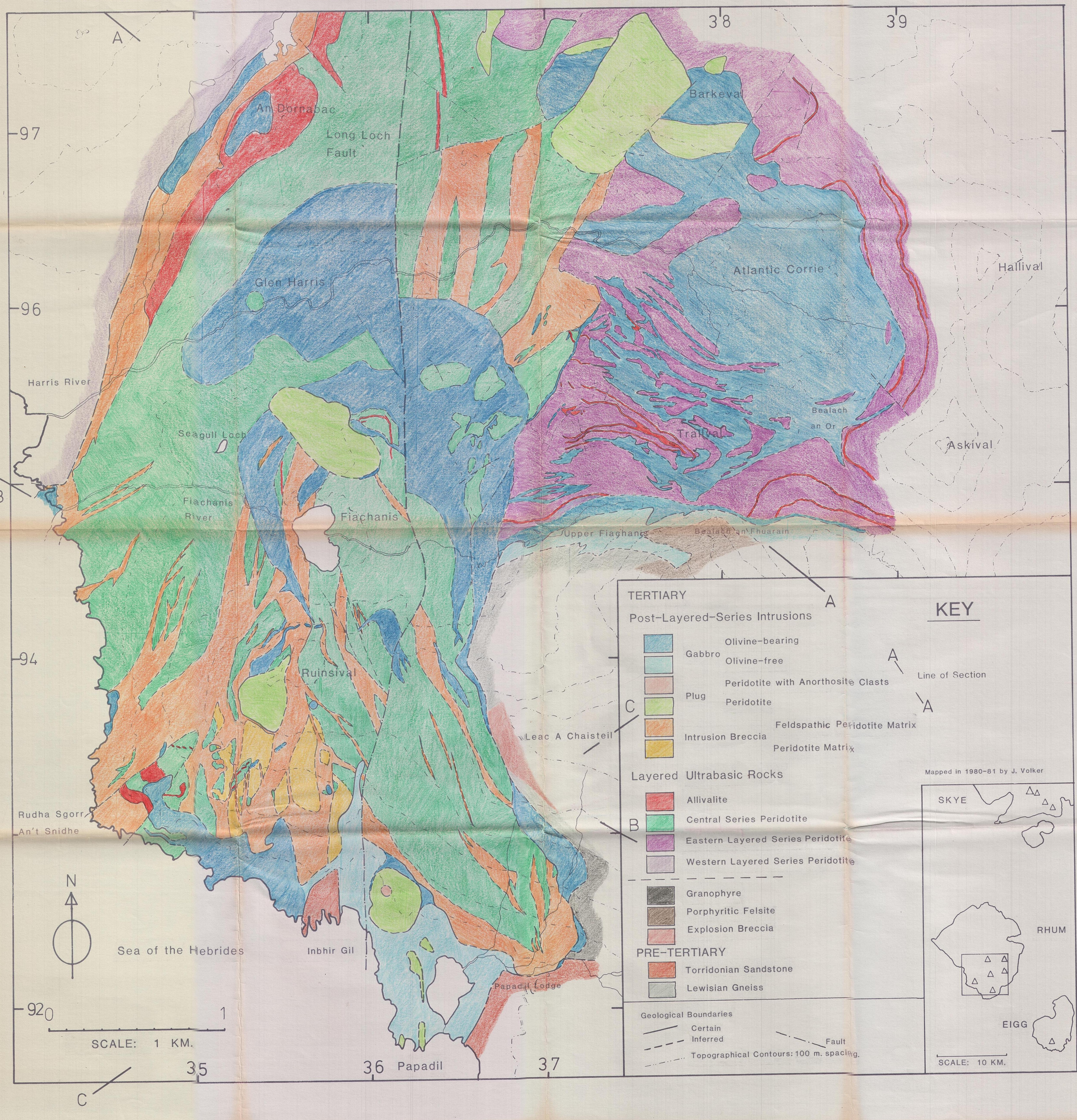

KEY

TERTIARY

Post-Layered-Series Intrusions

- Gabbro: Olivine-bearing
- Gabbro: Olivine-free
- Plug: Peridotite with Anorthosite Clasts
- Plug: Peridotite
- Intrusion Breccia: Feldspathic Peridotite Matrix
- Intrusion Breccia: Peridotite Matrix

Layered Ultrabasic Rocks

- Allivalite
- Central Series Peridotite
- Eastern Layered Series Peridotite
- Western Layered Series Peridotite

- Granophyre
- Porphyritic Felsite
- Explosion Breccia

PRE-TERTIARY

- Torridonian Sandstone
- Lewisian Gneiss

Geological Boundaries

- Certain
- Inferred
- Fault
- Topographical Contours: 100 m. spacing.

A — Line of Section — A

Mapped in 1980–81 by J. Volker

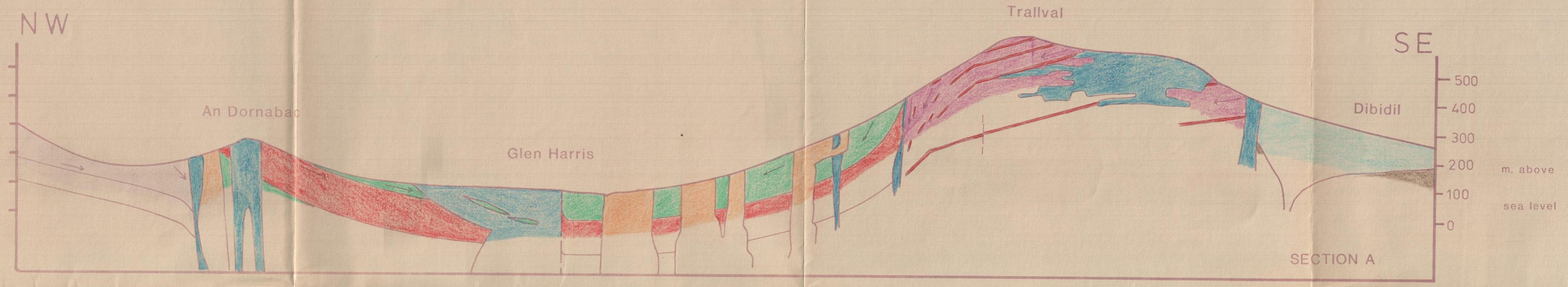
NW
An Dornabac
Glen Harris
Trallval
SE
Dibidil
500
400
300
200
100
0
m. above
sea level
SECTION A

NW
Harris Bay
Ruinsival
Leac a Chaisteil
SECTION B

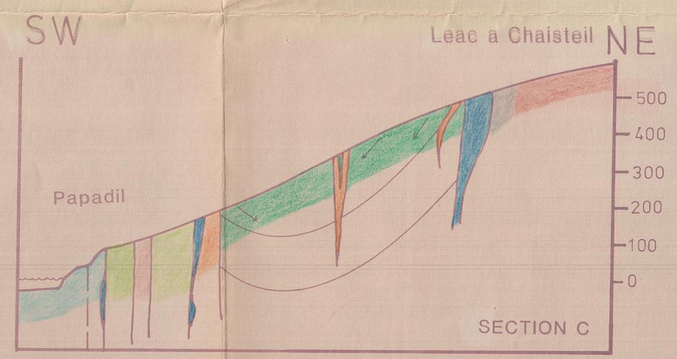
SE SW
Papadil
Leac a Chaisteil NE
500
400
300
200
100
0
SECTION C

THE GEOLOGY OF THE TRALLVAL AREA